



**Operational Issues related to the Integration of
Renewable Generation in Distribution
Networks**

Thesis presented for the degree of
Doctor of Philosophy
at the University of Strathclyde

by

FAHAD SAEED ALSOKHIRY

BSc. (Hons), MSc.

Supervisor: Professor K. L. Lo

Power System Research Group
Institute of Energy and Environment
Department of Electronic and Electrical Engineering
University of Strathclyde
2015

Declaration

This thesis is the result of the author's original research. It has been composed by the author and has not been previously submitted for examination which has led to the award of a degree.

The copyright of this thesis belongs to the author under the terms of the United Kingdom Copyright Acts, as qualified by University of Strathclyde Regulation 3.50. Due acknowledgement must always be made of the use of any material contained in, or derived from, this thesis.

Dedication

To my mother, my father, my wife, my brothers and sisters

Acknowledgements

First and foremost, all praise is to Allah the Almighty, the only one God, for lighting my way and directing me through each and every success and achievement I have ever reached or may reach. I humbly and sincerely thank Allah, the most gracious and merciful, who gave me the ability and means to accomplish this work.

Many thanks to my supervisor Professor K. L. Lo, Head of the Power Systems Research Group (PSRG) at the University of Strathclyde, Glasgow, for his valuable support, guidance and help throughout my PhD. I also appreciate his comments and suggestions during the writing of this thesis.

I would like to acknowledge King Abdulaziz University, Jeddah, Saudi Arabia, for offering me the full scholarship to complete my PhD studies.

I would also like to thank the staff and my colleagues at the Department of Electronic and Electrical Engineering at the University of Strathclyde for their valuable discussions during the years of my research.

Last but not least, heartfelt gratitude goes to my parents for their prayers, support and encouragement. I deeply appreciate all the sacrifices and endless support my wife has given throughout my PhD period. I also wish to extend my thanks to my brothers and sisters for their support and encouragement during this research work.

Fahad Alsokhry

October 2015

Abstract

With the dramatic increase in electricity demand and the need to tackle climate change by reducing greenhouse gas emissions such as CO₂, renewable generation has been increased in recent years in power systems. However, highly integrating renewable generation in distribution systems raises several issues and challenges that need to be addressed and some of these issues are investigated in this thesis.

This research focuses on investigating the fault ride through, the system transient stability, the system frequency response and the grid power factor of distribution systems with high renewable energy penetration based on wind and solar-photovoltaic (PV). Several proposed control techniques for wind generators and PVs are introduced in this research to solve these issues and mitigate the negative impact of these units on distribution systems. A modified control system of DGs based on wind and PV in different distribution systems is used to help to ride through faults and meet the low voltage ride through (LVRT) grid code requirements for voltage recovery. A three phase two stage transformerless PV grid connected system is proposed with a new technique to ride through faults and protect the power electronic converters. A DC chopper is added to the DC link of wind generators to enable wind generating units to ride through faults and protect their converters from overvoltages. The Transient Stability Index method is used to assess the impact of such renewable sources on the system transient stability of various distribution networks. Different frequency control methods published in literature are used for various DGs based on wind and PV to investigate the frequency response of different distribution networks with high renewable energy penetration, and a new frequency control technique is proposed for wind generators based on Doubly Fed Induction Generator (DFIG) to improve the system frequency response. The impact of high renewable energy penetration based on wind and PV with different power factor settings on grid power factor of various distribution systems is discussed in this research. A three phase two stage transformerless PV grid connected system with reactive power capability is proposed to operate under different solar irradiance conditions and improve the utility grid power factor. Simulation results validate the proposed systems in various distribution systems, including IEEE 13 bus, IEEE 37 bus and IEEE 123 bus systems.

Table of Contents

Declaration	i
Dedication	ii
Acknowledgements	iii
Abstract	iv
Table of Contents	v
List of Figures	x
List of Tables	xv
List of Abbreviations	xvi
List of Symbols	xix
CHAPTER 1 Introduction	1
1.1 Background.....	1
1.2 Investigated Issues	5
1.3 Motivation.....	11
1.4 Research Objectives.....	12
1.5 Original Contributions of the Thesis.....	13
1.6 Thesis Structure	14
1.7 Publications.....	17
CHAPTER 2 Solar Energy – Photovoltaic Systems	19
2.1 Introduction.....	19
2.2 Solar Energy Background.....	20
2.3 Solar Power Potential and Benefits.....	21
2.4 Environmental Impact of PV	22
2.5 Economic Potential of Photovoltaic Technology.....	23
2.6 Photovoltaic Technology Growth	24
2.7 Photovoltaic Technology in Europe and the United Kingdom	25
2.8 Current Photovoltaic Technologies.....	27
2.9 Photovoltaic Systems	30
2.10 Photovoltaic Cells, Modules and Array Characteristics	32
2.10.1 PV Cells Characteristics	33
2.10.2 PV Modules Characteristics	34
2.10.3 PV Arrays Characteristics	35
2.11 Solar Irradiance.....	38
2.12 Maximum Power Point Tracking (MPPT).....	39
2.13 Challenges of Photovoltaic Technology	41

2.13.1 Land for PV	42
2.13.2 PV Raw Materials.....	43
2.13.3 Reliability	43
2.13.4 PV System Efficiency.....	44
2.13.5 Grid Code Requirement for PV	47
2.13.6 PV Payback Time	49
2.14 Conclusions.....	50
CHAPTER 3 Wind Energy	51
3.1 Introduction.....	51
3.2 Wind Energy Background.....	52
3.3 Wind Power Potential and Benefits	54
3.4 Environmental Impact of Wind Power	57
3.5 Economic Potential of Wind Energy	58
3.6 Wind Power Growth	59
3.7 Wind Energy in Europe and the United Kingdom.....	61
3.8 Current Wind Power Technologies.....	63
3.9 Wind Power Systems	65
3.10 Wind Generation Characteristics	67
3.10.1 Fixed Speed Generators (Induction Machines)	70
3.10.2 Variable Speed Wind Turbine Generators.....	72
3.11 Wind Speed.....	84
3.12 Impact of Wind Speed Variations.....	88
3.13 Maximum Power Point Tracking (MPPT).....	89
3.14 Power Electronics Applications	90
3.15 Challenges of Wind Power	91
3.15.1 Land for Wind	92
3.15.2 Social Acceptance of Wind Power	93
3.15.3 Reliability	94
3.15.4 Wind Turbine Efficiency	96
3.15.5 Grid Code Requirements for Wind Power.....	97
3.16 Conclusions.....	100
CHAPTER 4 Fault Ride through of Distribution Systems with High Penetration of Renewable Energy	102
4.1 Introduction.....	102
4.2 Fault Ride through Background.....	103
4.3 Grid Code Requirements for FRT.....	103

4.4 Wind Generation Impact on FRT Requirements	105
4.5 Photovoltaic Generation Impact on FRT Requirements	109
4.6 Modelling and Control of a Renewable Energy System for FRT	110
4.6.1 DFIG Modelling and Control	110
4.6.2 Wind Turbine based on Synchronous Generator with Fully Rated Converters	111
4.6.3 Solar Energy based on Photovoltaic	111
4.7 Simulation Scenarios	114
4.7.1 IEEE 13 Bus Distribution System	114
4.7.2 IEEE 37 Bus Distribution System	129
4.7.3 IEEE 123 Bus Distribution System	141
4.8 Conclusions	149
CHAPTER 5 Transient Stability of Distribution Systems with High Renewable Energy Penetration	151
5.1 Introduction	151
5.2 Power System Stability Background	152
5.3 Transient Stability Analysis	154
5.4 Wind Generation Impact on Transient Stability	155
5.5 Photovoltaic Generation Impact on Transient Stability	156
5.6 Modelling and Control of Renewable Energy Systems	157
5.6.1 DFIG Modelling and Control	157
5.6.2 Wind Turbine based on Synchronous Generator with Fully Rated Converters	158
5.6.3 Solar Energy based on Photovoltaic	158
5.7 Simulation Scenarios	158
5.7.1 IEEE 13 Bus Distribution System	159
5.7.2 IEEE 37 Bus Distribution System	174
5.7.3 IEEE 123 Bus Distribution System	185
5.8 Conclusions	195
CHAPTER 6 Frequency Response of Distributed Generation based on Renewable Energy	196
6.1 Introduction	196
6.2 Frequency Control Background	198
6.3 Grid Code Requirements for Frequency Response	199
6.4 Wind Generation Impact on System Frequency	203
6.5 Photovoltaic Generation Impact on System Frequency	205
6.6 Modelling and Control of Renewable Energy Systems for Frequency Response	206
6.6.1 DFIG Modelling and Control	206

6.6.2 Wind Turbine based on Synchronous Generator with Fully Rated Converters	210
6.6.3 Solar Energy based on Photovoltaics	210
6.7 Simulation Scenarios	211
6.7.1 IEEE 13 Bus Distribution System	212
6.7.2 IEEE 37 Bus Distribution System	220
6.7.3 IEEE 123 Bus Distribution System	226
6.8 Conclusions	233
CHAPTER 7 Effect of Renewable Generation in Distribution Networks on Grid Power Factor.....	234
7.1 Introduction.....	234
7.2 Reactive Power Background.....	235
7.2.1 Conventional Synchronous Generators	235
7.2.2 Capacitor Banks.....	236
7.2.3 Static Var Compensator (SVC)	237
7.2.4 STATCOM (D-STATCOM).....	238
7.2.5 End User or Distributed Generation Owner	239
7.3 Grid Code Requirements for Reactive Power Support	239
7.4 Wind Generation Impact on Grid System Power Factor	242
7.5 Photovoltaic Generation Impact on Grid System Power Factor	243
7.6 Modelling and Control of Renewable Energy Systems for Reactive Power Support	244
7.6.1 DFIG Modelling and Control	244
7.6.2 Wind Turbine based on Synchronous Generator with Fully Rated Converters	245
7.6.3 Solar Energy based on Photovoltaics	245
7.6.4 Proposed Technique for PV Reactive Power Controllability	245
7.7 Simulation Scenarios	247
7.7.1 Proposed Technique for PV Reactive Power Controllability	248
7.7.2 IEEE 13 Bus Distribution System	251
7.7.3 IEEE 37 Bus Distribution System	260
7.7.4 IEEE 123 Bus Distribution System	268
7.8 Conclusions.....	277
CHAPTER 8 Conclusions	278
8.1 General Conclusions	278
8.2 Suggestions for Future Research.....	282
REFERENCES.....	284
Appendices.....	297
Appendix A: Commonly PV Modules in the UK Market.....	297

Appendix B: IEEE Distribution Systems Detailed Data.....	305
B1. IEEE 13 Bus Distribution System.....	305
B2. IEEE 37 Bus Distribution System.....	307
B3. IEEE 123 Bus Distribution System.....	311
Appendix C: Conventional Distributed Generation (CDG) Data	322
C1. Synchronous generator parameter (salient pole rotor)	322
C2. Automatic Voltage Regulator (AVR)	322
C3. CDG Governor (Diesel Engine Governor)	322
Appendix D: Renewable Energy Generating Units Modelling Parameters.....	323
D1. Three phase two stage transformerless PV grid connected system.....	323
D2. DFIG modelling parameters	324
D3. Synchronous generator with fully rated converter modelling parameters	324

List of Figures

Figure 1.1: Outlook of power generation by fuel type in Europe to 2030.....	2
Figure 1.2: Renewable energy generation in the UK, country by country, from 2003 to 2013.....	2
Figure 1.3: Future power system.	3
Figure 1.4: Renewable generation impact on grid power factor.	11
Figure 2.1: Evolution of global PV cumulative installed capacity 2000-2014.....	20
Figure 2.2: Evolution of global PV annual installations 2000-2014 (MW).....	22
Figure 2.3: PV cumulative installed capacity share in the world until year 2014.	25
Figure 2.4: Evolution of the PV cumulative installed capacity in MW by region from 2000 – 2014.....	25
Figure 2.5: The total PV cumulative installed capacity in the UK.....	26
Figure 2.6: Silicon solar cell band diagram.	27
Figure 2.7: PV cell, module and array.	28
Figure 2.8: PWM voltage source inverter.....	29
Figure 2.9: TLCI inverter.	29
Figure 2.10: Block diagram of DC load supplied by a stand-alone PV system.	31
Figure 2.11: Block diagram of AC load supplied by a stand-alone PV system.	31
Figure 2.12: Block diagram of single-stage grid-connected photovoltaic system.....	32
Figure 2.13: Block diagram of two-stage grid-connected photovoltaic system.	32
Figure 2.14: Photovoltaic array.	33
Figure 2.15: PV cell equivalent circuit.	33
Figure 2.16: The effect of solar irradiance on I-V and P-V curves.....	34
Figure 2.17: The impact of solar irradiance and temperature on P-V curves.....	35
Figure 2.18: I – V and P – V characteristics curves for one module at STC.....	36
Figure 2.19: I – V and P – V characteristics curves for one array at STC.	36
Figure 2.20: Open circuit condition.	37
Figure 2.21: Short circuit condition.	38
Figure 2.22: The flowchart of the hill climbing MPPT technique.....	40
Figure 2.23: Power converter duty cycle (D) using hill climbing MPPT technique.....	41
Figure 2.24: PV output power using hill climbing MPPT technique.....	41
Figure 2.25: Typical power supply and demand load curves.....	42
Figure 2.26: Best research solar cell efficiencies.....	46
Figure 3.1: Global cumulative wind power capacity.....	52
Figure 3.2: The increase in the size of wind turbines since 1985.....	53
Figure 3.3: Global cumulative installed wind capacity from 1997 to 2014.....	54
Figure 3.4: Global annual installed wind capacity from 1997 to 2014.....	55
Figure 3.5: Short term expected growth in wind power by region.....	55
Figure 3.6: Long term expected growth in wind power by region (advanced scenario).....	56
Figure 3.7: Specific cost reductions per kilowatt installed.....	58
Figure 3.8: The world’s cumulative installed wind capacity shares by the end of 2014.....	60
Figure 3.9: The world’s cumulative installed wind capacity shares in 2014.....	61
Figure 3.10: Leading countries in terms of wind energy penetration (%) in power systems from 2009 to 2011.....	62
Figure 3.11: Structural differences between HAWT and VAWT.....	64
Figure 3.12: Horizontal Axis Wind Turbines (upwind and downwind turbines).....	64
Figure 3.13: The $C_p - \lambda$ curve under various pitch angles β	68
Figure 3.14: The power curve of a typical wind turbine.....	69
Figure 3.15: Energy conversion stages in wind turbines.....	70
Figure 3.16: Fixed speed wind turbine generator.....	71
Figure 3.17: DFIG based on wind energy (general structure).....	73
Figure 3.18: d-axis DFIG dynamic model.....	74
Figure 3.19: q-axis DFIG dynamic model.....	74
Figure 3.20: Overall vector control scheme of the DFIG rotor side converter.....	76
Figure 3.21: Overall vector control scheme of the DFIG grid side converter.....	80
Figure 3.22: Synchronous generator with fully rated converters based on wind energy (general structure).....	81
Figure 3.23: Vector control of the rotor side converter (RSC).....	83
Figure 3.24: Vector control of the grid side converter (GSC).....	84
Figure 3.25: Variations in wind speed with a time resolution of 10 minutes over several months for a low wind speed site.....	86

Figure 3.26: Weibull probability density for a low wind speed site.....	86
Figure 3.27: Cumulative Weibull probability distribution for a low wind speed site.	86
Figure 3.28: Variations in wind speed with a time resolution of 10 minutes over several months for a high wind speed site.	87
Figure 3.29: Weibull probability density for a high wind speed site.	87
Figure 3.30: Cumulative Weibull probability distribution for a high wind speed site.	87
Figure 3.31: The wind turbine power output for different wind speeds as a function of rotor speed.....	89
Figure 3.32: Social acceptance for different sources of energy in Europe in 2011	93
Figure 3.33: Typical bathtub curve for wind turbines.....	95
Figure 3.34: Percentage of required maintenance and repairs for the main components of wind turbines according to AWEA.....	96
Figure 3.35: Frequency requirements for wind turbines in the UK.....	98
Figure 3.36: AC fault ride-through capability requirements for wind turbines in the UK.	99
Figure 3.37: Reactive power requirements for wind turbines in the UK.....	100
Figure 4.1: German LVRT requirements for distributed generators.	105
Figure 4.2: The crowbar protection scheme in the DFIG based on wind energy.	107
Figure 4.3: The DC chopper protection scheme in the DFIG based on wind energy.....	108
Figure 4.4: Wind turbine based on synchronous generator with fully rated converters and converter control in the dq synchronous frame.....	111
Figure 4.5: Simplified PV model.....	112
Figure 4.6: B lock diagram summarizing the three phase grid connected PV inverter.	112
Figure 4.7: The impact of a rapid change in solar irradiance on the PV output power for different PV systems.	113
Figure 4.8: IEEE 13 Node Test Feeder.....	116
Figure 4.9: Voltage recovery for the base case of the 13 bus system (the fault is applied on bus 650)	117
Figure 4.10: Voltage recovery for the base case of the 13 bus system (the fault is applied on bus 680)	117
Figure 4.11: Voltage recovery for the 35 % PV penetration case of the 13 bus system (the fault is applied on bus 650).....	119
Figure 4.12: Voltage recovery for the 35 % PV penetration case of the 13 bus system (the fault is applied on bus 680).....	119
Figure 4.13: Proposed three phase two stage transformerless PV grid connected system with FRT capability... ..	120
Figure 4.14: PV DC link voltage with and without protection when a fault is applied close to the PV system... ..	121
Figure 4.15: Voltage recovery for the case of 35 % wind based on DFIG penetration of the 13 bus system (the fault is applied on bus 650).....	122
Figure 4.16: Voltage recovery for the case of 35 % wind based on DFIG penetration of the 13 bus system (the fault is applied on bus 680).....	123
Figure 4.17: DFIG DC link voltage with and without protection when the fault is applied close to the DFIG. ..	124
Figure 4.18: Voltage recovery for the case of 35 % wind based on FRC penetration of the 13 bus system (the fault is applied on bus 650).....	125
Figure 4.19: Voltage recovery for the case of 35 % wind based on FRC penetration of the 13 bus system (the fault is applied on bus 680).....	126
Figure 4.20: DC Link voltage of the wind based on synchronous generator with fully rated converters with and without protection when the fault is applied on bus 680.....	127
Figure 4.21: Voltage recovery for the 35 % mixed renewables penetration case of the 13 bus system (the fault is applied on bus 650).....	128
Figure 4.22: Voltage recovery for the 35 % mixed renewables penetration case of the 13 bus system (the fault is applied on bus 680).....	129
Figure 4.23: IEEE 37 Node Test Feeder.	130
Figure 4.24: Voltage recovery for the base case of the 37 bus system (the fault is applied on bus 799)	131
Figure 4.25: Voltage recovery for the base case of the 37 bus system (the fault is applied on bus 741)	132
Figure 4.26: Voltage recovery for the PV case of the 37 bus system (the fault is applied on bus 799)	133
Figure 4.27: Voltage recovery for the PV case of the 37 bus system (the fault is applied on bus 741)	134
Figure 4.28: Voltage recovery for the 35 % wind based on the DFIG penetration case of the 37 bus system (the fault is applied on bus 799).....	135
Figure 4.29: Voltage recovery for the 35 % wind based on the DFIG penetration case of 37 bus system (the fault is applied on bus 741).....	136
Figure 4.30: Voltage recovery for the 35 % wind based on the FRC penetration case of the 37 bus system (the fault is applied on bus 799).....	137
Figure 4.31: Voltage recovery for the 35 % wind based on the FRC penetration case of the 37 bus system (the fault is applied on bus 741).....	138

Figure 4.32: Voltage recovery for the 35 % mixed renewables penetration case of the 37 bus system (the fault is applied on bus 799).....	139
Figure 4.33: Voltage recovery for the 35 % mixed renewables penetration case of the 37 bus system (the fault is applied on bus 741).....	140
Figure 4.34: IEEE 123 Node Test Feeder.....	141
Figure 4.35: Voltage recovery for the base case of the 123 bus system (the fault is applied on bus 150)	142
Figure 4.36: Voltage recovery for the base case of the 123 bus system (the fault is applied on bus 85)	143
Figure 4.37: Voltage recovery for the PV case of the 123 bus system (the fault is applied on bus 150)	144
Figure 4.38: Voltage recovery for the PV case of the 123 bus system (the fault is applied on bus 85)	144
Figure 4.39: Voltage recovery for the 35 % wind based on the DFIG penetration case of the 123 bus system (the fault is applied on bus 150).....	145
Figure 4.40: Voltage recovery for the 35 % wind based on the DFIG penetration case of the 123 bus system (the fault is applied on bus 85).....	146
Figure 4.41: Voltage recovery for the 35 % wind based on the FRC penetration case of the 123 bus system (the fault is applied on bus 150).....	147
Figure 4.42: Voltage recovery for the 35 % wind based on the FRC penetration case of the 123 bus system (the fault is applied on bus 85).....	147
Figure 4.43: Voltage recovery for the 35 % mixed renewables penetration case of the 123 bus system (the fault is applied on bus 150).....	148
Figure 4.44: Voltage recovery for the 35 % mixed renewables penetration case of the 123 bus system (the fault is applied on bus 85).....	149
Figure 5.1: Power system stability classification.....	153
Figure 5.2: CDG responses in 13 bus system to a fault on bus 650 (base case).....	160
Figure 5.3: CDG responses in 13 bus system to a fault on bus 680 (base case).....	161
Figure 5.4: Conventional DG and PV responses in 13 bus system to a fault on bus 650 (PV case).....	163
Figure 5.5: Conventional DG and PV responses in 13 bus system to a fault on bus 680 (PV case).....	164
Figure 5.6: CDG responses in the 13 bus system to a fault on bus 650 (DFIG case).....	165
Figure 5.7: DFIG responses in the 13 bus system to a fault on bus 650 (DFIG case).....	166
Figure 5.8: CDG responses in the 13 bus system to a fault on bus 680 (DFIG case).....	166
Figure 5.9: DFIG responses in the 13 bus system to a fault on bus 680 (DFIG case).....	167
Figure 5.10: CDG and wind based on FRC responses in the 13 bus system to a fault on bus 650 (FRC wind case).....	168
Figure 5.11: CDG and wind based on FRC responses in the 13 bus system to a fault on bus 680 (FRC wind case).....	169
Figure 5.12: CDG responses in 13 bus system to a fault on bus 650 (mixed renewables case).....	170
Figure 5.13: Renewable units' responses in 13 bus system to a fault on bus 650 (mixed renewables case).....	171
Figure 5.14: CDG responses in 13 bus system to a fault on bus 680 (mixed renewables case).....	172
Figure 5.15: Renewable units' responses in 13 bus system to a fault on bus 680 (mixed renewables case).....	173
Figure 5.16: CDG responses in 37 bus system to a fault on bus 799 (base case).....	175
Figure 5.17: CDG responses in 37 bus system to a fault on bus 741 (base case).....	176
Figure 5.18: CDG and PV responses in 37 bus system to a fault on bus 799 (PV case).....	177
Figure 5.19: CDG and PV responses in 37 bus system to a fault on bus 741 (PV case).....	177
Figure 5.20: CDG responses in 37 bus system to a fault on bus 799 (DFIG case)	178
Figure 5.21: DFIG responses in 37 bus system to a fault on bus 799 (DFIG case).....	179
Figure 5.22: CDG responses in 37 bus system to a fault on bus 741 (DFIG case)	179
Figure 5.23: DFIG responses in 37 bus system to a fault on bus 741 (DFIG case).....	180
Figure 5.24: CDG and wind based on FRC responses in 37 bus system to a fault on bus 799 (FRC wind case).....	181
Figure 5.25: CDG and wind based on FRC responses in 37 bus system to a fault on bus 741 (FRC wind case).....	181
Figure 5.26: CDG responses in 37 bus system to a fault on bus 799 (mixed renewables case).....	182
Figure 5.27: Renewable units' responses in 37 bus system to a fault on bus 799 (mixed renewables case).....	183
Figure 5.28: CDG responses in 37 bus system to a fault on bus 741 (mixed renewables case).....	183
Figure 5.29: Renewable units' responses in 37 bus system to a fault on bus 741 (mixed renewables case).....	184
Figure 5.30: CDG responses in 123 bus system to a fault on bus 150 (base case).....	185
Figure 5.31: CDG responses in 123 bus system to a fault on bus 85 (base case).....	186
Figure 5.32: CDG and PV responses in the 123 bus system to a fault on bus 150 (PV case).....	187
Figure 5.33: CDG and PV responses in the 123 bus system to a fault on bus 85 (PV case).....	188
Figure 5.34: CDG responses in the 123 bus system to a fault on bus 150 (DFIG case).....	189
Figure 5.35: DFIG responses in 123 bus system to a fault on bus 150 (DFIG case).....	189
Figure 5.36: CDG responses in the 123 bus system to a fault on bus 85 (DFIG case).....	190
Figure 5.37: DFIG responses in the 123 bus system to a fault on bus 85 (DFIG case).....	190

Figure 5.38: CDG and wind based on FRC responses in the 123 bus system to a fault on bus 150 (FRC wind case)	191
Figure 5.39: CDG and wind based on FRC responses in the 123 bus system to a fault on bus 85 (FRC wind case)	192
Figure 5.40: CDG responses in the 123 bus system to a fault on bus 150 (mixed renewables case)	193
Figure 5.41: Renewable units' responses in the 123 bus system to a fault on bus 150 (mixed renewables case)	193
Figure 5.42: CDG responses in the 123 bus system to a fault on bus 85 (mixed renewables case)	194
Figure 5.43: Renewable units' responses in the 123 bus system to a fault on bus 85 (mixed renewables case)	194
Figure 6.1: Germany's grid code requirements for renewable generators.	201
Figure 6.2: UK operational and statutory limits of power system frequency.	202
Figure 6.3: Frequency response in the UK's power system.	202
Figure 6.4: Inertia response control from DFIG.	207
Figure 6.5: Active power reduction technique for frequency response control from renewable generating units	208
Figure 6.6: Proposed frequency control in DFIG.	210
Figure 6.7: IEEE 13 bus system without renewable energy frequency response for under-frequency condition.	213
Figure 6.8: IEEE 13 bus system without renewable energy frequency response for over-frequency condition.	213
Figure 6.9: IEEE 13 bus system with renewable energy frequency response for under-frequency condition with different wind power penetration.	214
Figure 6.10: DFIG based wind energy performance during and after under-frequency condition with different wind power penetration.	215
Figure 6.11: IEEE 13 bus system with renewable energy frequency response for over-frequency condition with different wind power penetration.	215
Figure 6.12: DFIG based wind energy performance during and after over-frequency condition with different wind power penetration.	216
Figure 6.13: The frequency response of the IEEE 13 bus system with high renewable energy penetration using the active power reduction method for the under-frequency condition.	217
Figure 6.14: The frequency response of the IEEE 13 bus system with high renewable energy penetration using the active power reduction method for the over-frequency condition.	218
Figure 6.15: The proposed frequency response of the IEEE 13 bus system with high DFIG penetration for the under-frequency condition.	219
Figure 6.16: The proposed frequency response of the IEEE 13 bus system with high DFIG penetration for the over-frequency condition.	219
Figure 6.17: IEEE 37 bus system without renewable energy frequency response for under-frequency condition	221
Figure 6.18: IEEE 37 bus system without renewable energy frequency response for over-frequency condition.	221
Figure 6.19: IEEE 37 bus system with renewable energy frequency response for under-frequency condition with different wind power penetration.	222
Figure 6.20: IEEE 37 bus system with renewable energy frequency response for over-frequency condition with different wind power penetration.	223
Figure 6.21: The frequency response of the IEEE 37 bus system with high renewable energy penetration using the active power reduction method for the under-frequency condition.	224
Figure 6.22: The frequency response of the IEEE 37 bus system with high renewable energy penetration using the active power reduction method for the over-frequency condition.	224
Figure 6.23: The proposed frequency response of the IEEE 37 bus system with high DFIG penetration for the under-frequency condition.	225
Figure 6.24: The proposed frequency response of the IEEE 37 bus system with high DFIG penetration for the over-frequency condition.	226
Figure 6.25: IEEE 123 bus system without renewable energy frequency response for under-frequency condition.	227
Figure 6.26: IEEE 123 bus system without renewable energy frequency response for over-frequency condition.	228
Figure 6.27: IEEE 123 bus system with renewable energy frequency response for under-frequency condition with different wind power penetration.	229
Figure 6.28: IEEE 123 bus system with renewable energy frequency response for over-frequency condition with different wind power penetration.	229
Figure 6.29: The frequency response of the IEEE 123 bus system with high renewable energy penetration using the active power reduction method for the under-frequency condition.	230
Figure 6.30: The frequency response of the IEEE 123 bus system with high renewable energy penetration using the active power reduction method for the over-frequency condition.	231
Figure 6.31: The proposed frequency response of the IEEE 123 bus system with high DFIG penetration for the under-frequency condition.	232

Figure 6.32: The proposed frequency response of the IEEE 123 bus system with high DFIG penetration for the over-frequency condition.....	232
Figure 7.1: Synchronous generator block diagram.....	236
Figure 7.2: SVC configurations.....	238
Figure 7.3: STATCOM structure.....	239
Figure 7.4: Utility grid supplies a load with 0.9 p.f. lagging.....	241
Figure 7.5: Utility grid and renewable unit supply a load with 0.9 p.f. lagging.....	241
Figure 7.6: PV inverter P-Q capability curve.....	246
Figure 7.7: PV output power in (W & VAr) and grid voltage in (V) and current in (A) during sunny day conditions under different power factor settings.....	249
Figure 7.8: PV output power in (W & VAr) and grid voltage in (V) and current in (A) during cloudy weather under different power factor settings.....	250
Figure 7.9: PV output power in (W & VAr), grid voltage in (V) and current in (A) for night operation.....	251
Figure 7.10: IEEE 13 bus system without renewables - (a) grid power factor, (b) grid voltage and current.....	252
Figure 7.11: IEEE 13 bus system, PV with unity power factor impact on grid power factor.....	253
Figure 7.12: IEEE 13 bus system, PV with 0.9 lag power factor impact on grid power factor.....	253
Figure 7.13: IEEE 13 bus system, PV with 0.8 lag power factor impact on grid power factor.....	254
Figure 7.14: IEEE 13 bus system with PV penetration, grid power factor at various PV power factor settings.....	254
Figure 7.15: IEEE 13 bus system, DFIG based wind with unity power factor impact on grid power factor.....	255
Figure 7.16: IEEE 13 bus system, DFIG based wind with 0.9 lag power factor impact on grid power factor.....	256
Figure 7.17: IEEE 13 bus system, DFIG based wind with 0.8 lag power factor impact on grid power factor.....	256
Figure 7.18: IEEE 13 bus system with DFIG penetration, grid power factor at various DFIG power factor settings.....	257
Figure 7.19: IEEE 13 bus system, FRC based wind with unity power factor impact on grid power factor.....	258
Figure 7.20: IEEE 13 bus system, FRC based wind with 0.9 lag power factor impact on grid power factor.....	258
Figure 7.21: IEEE 13 bus system, FRC based wind with 0.8 lag power factor impact on grid power factor.....	259
Figure 7.22: IEEE 13 bus system with wind FRC penetration, grid power factor at various FRC power factor settings.....	259
Figure 7.23: IEEE 37 bus system without renewables - (a) grid power factor, (b) grid voltage and current.....	260
Figure 7.24: IEEE 37 bus system, PV with unity power factor impact on grid power factor.....	261
Figure 7.25: IEEE 37 bus system, PV with 0.9 lag power factor impact on grid power factor.....	262
Figure 7.26: IEEE 37 bus system, PV with 0.8 lag power factor impact on grid power factor.....	262
Figure 7.27: IEEE 37 bus system with PV penetration, grid power factor at various PV power factor settings.....	263
Figure 7.28: IEEE 37 bus system, DFIG based wind with unity power factor impact on grid power factor.....	264
Figure 7.29: IEEE 37 bus system, DFIG based wind with 0.9 lag power factor impact on grid power factor.....	264
Figure 7.30: IEEE 37 bus system, DFIG based wind with 0.8 lag power factor impact on grid power factor.....	265
Figure 7.31: IEEE 37 bus system with DFIG penetration, grid power factor at various DFIG power factor settings.....	265
Figure 7.32: IEEE 37 bus system, FRC based wind with unity power factor impact on grid power factor.....	266
Figure 7.33: IEEE 37 bus system, FRC based wind with 0.9 lag power factor impact on grid power factor.....	267
Figure 7.34: IEEE 37 bus system, FRC based wind with 0.8 lag power factor impact on grid power factor.....	267
Figure 7.35: IEEE 37 bus system with wind FRC penetration, grid power factor at various FRC power factor settings.....	268
Figure 7.36: IEEE 123 bus system without renewables - (a) grid power factor, (b) grid voltage and current.....	269
Figure 7.37: IEEE 123 bus system, PV with unity power factor impact on grid power factor.....	270
Figure 7.38: IEEE 123 bus system, PV with 0.9 lag power factor impact on grid power factor.....	270
Figure 7.39: IEEE 123 bus system, PV with 0.8 lag power factor impact on grid power factor.....	271
Figure 7.40: IEEE 123 bus system with PV penetration, grid power factor at various PV power factor settings.....	271
Figure 7.41: IEEE 123 bus system, DFIG based wind with unity power factor impact on grid power factor.....	272
Figure 7.42: IEEE 123 bus system, DFIG based wind with 0.9 lag power factor impact on grid power factor.....	273
Figure 7.43: IEEE 123 bus system, DFIG based wind with 0.8 lag power factor impact on grid power factor.....	273
Figure 7.44: IEEE 123 bus system with DFIG penetration, grid power factor at various DFIG power factor settings.....	274
Figure 7.45: IEEE 123 bus system, FRC based wind with unity power factor impact on grid power factor.....	275
Figure 7.46: IEEE 123 bus system, FRC based wind with 0.9 lag power factor impact on grid power factor.....	275
Figure 7.47: IEEE 123 bus system, FRC based wind with 0.8 lag power factor impact on grid power factor.....	276
Figure 7.48: IEEE 123 bus system with wind FRC penetration, grid power factor at various FRC power factor settings.....	276

List of Tables

Table 2.1: The top ten leading photovoltaic markets worldwide in 2014.	24
Table 2.2: PV module characteristics under STC.	37
Table 2.3: The maximum output voltage of the boost converter (V_{out}) dependent on D.	40
Table 2.4: Solar cell efficiency of different technologies.	45
Table 2.5: Highlights of IEEE 1547 and IEC 61727 regulation standards.	48
Table 2.6: UK distributed generation standards guide.	49
Table 3.1: Leading wind power markets in terms of added capacity in 2014.	60
Table 3.2: The cumulative offshore wind installed capacity in MW from 2011 to 2014.	63
Table 3.3: The global top ten wind turbines in terms of rated capacity.	65
Table 3.4: The main components of wind turbines and their percentage of overall cost.	66
Table 4.1: IEEE 13 Bus Network Data.	115
Table 4.2: Power generation sources' outputs and their locations (PV case).	118
Table 4.3: Power generation source outputs and their locations (DFIG case).	121
Table 4.4: Power generation source outputs and their locations (wind FRC case).	124
Table 4.5: Power generation sources outputs and their locations (mixed renewables case).	127
Table 4.6: IEEE 37 Bus Network Data.	130
Table 4.7: Power generation source outputs and their locations (PV case).	132
Table 4.8: Power generation source outputs and their locations (DFIG case).	134
Table 4.9: Power generation source outputs and their locations (wind FRC case).	137
Table 4.10: Power generation source outputs and their locations (mixed renewables case).	139
Table 4.11: IEEE 123 Bus Network Data.	142
Table 4.12: Power generation source outputs and their locations (PV case).	143
Table 4.13: Power generation source outputs and their locations (DFIG case).	145
Table 4.14: Power generation source outputs and their locations (wind FRC case).	146
Table 4.15: Power generation source outputs and their locations (mixed renewables case).	148
Table 5.1: Power generation source outputs and their locations (PV case) in the IEEE 13 bus system.	161
Table 5.2: The capacity of energy sources and their locations (DFIG case).	164
Table 5.3: The capacity and location of each generation source in the system (wind FRC case).	167
Table 5.4: Output power of each energy source and locations (mixed renewables case).	169
Table 5.5: Transient stability analysis of the IEEE 13 bus system using TSI in %, stable >0 , unstable <0	174
Table 5.6: Transient stability analysis of the IEEE 37 bus system using TSI in %, stable >0 , unstable <0	184
Table 5.7: Transient stability analysis of the IEEE 123 bus system using TSI in %, stable >0 , unstable <0	195
Table 6.1: DFIG active power reduction parameters.	208
Table 6.2: FRC active power reduction parameters.	210
Table 6.3: PV active power reduction parameters.	211
Table 7.1: Design circuit parameters and design specification.	248
Table 7.2: IEEE 13 bus system, power generation source outputs and their locations (PV case).	252
Table 7.3: IEEE 13 bus system, power generation source outputs and their locations (DFIG case).	255
Table 7.4: IEEE 13 bus system, power generation source outputs and their locations (FRC case).	257
Table 7.5: IEEE 37 bus system, power generation source outputs and their locations (PV case).	261
Table 7.6: IEEE 37 bus system, power generation source outputs and their locations (DFIG case).	263
Table 7.7: IEEE 37 bus system, power generation source outputs and their locations (FRC case).	266
Table 7.8: IEEE 123 bus system, power generation source outputs and their locations (PV case).	269
Table 7.9: IEEE 123 bus system, power generation source outputs and their locations (DFIG case).	272
Table 7.10: IEEE 123 bus system, power generation source outputs and their locations (FRC case).	274

List of Abbreviations

AAAS	American Association for the Advancement of Science
AC	Alternating Current
AM	Air Mass
APAC	Asia Pacific
ARMA	Autoregressive Moving Average
AVR	Automatic Voltage Regulator
AWEA	American Wind Energy Association
C	Coulomb (unit of charge)
CDG	Conventional Distributed Generation (based on fossil fuels)
CF	Capacity Factor
CIGRE	International Council on Large Electric Systems (in French: Conseil International des Grands Réseaux Électriques)
CO₂	Carbon Dioxide
CSI	Current Source Inverter
D	Duty Cycle
DC	Direct Current
DFIG	Doubly Fed Induction Generator
DG	Distributed Generation
DIN	German Institute for Standardization
DNO	Distribution Network Operator
d-q	Direct-Quadrature
DSTATCOM	Distributed Static Synchronous Compensator
DVR	Dynamic Voltage Restorer
EPIA	European Photovoltaic Industry Association
EWEA	European Wind Energy Association
FACTS	Flexible AC Transmission Systems
FF	Fill Factor
FIT	Feed In Tariff
FRC	Fully Rated Converters
FRT	Fault Ride Through
GSC	Grid Side Converter
GWEC	Global Wind Energy Council
HAWT	Horizontal Axis Wind Turbine
HCS	Hill-Climb Search
HVDC	High Voltage Direct Current
Hz	Hertz
IEA	International Energy Agency

IEA-PVPs	International Energy Agency-Photovoltaic Power Systems Programme
IEC	International Electrotechnical Commission
IEEE	Institute of Electrical and Electronics Engineers
IGBT	Insulated Gate Bipolar Transistor
IPCC	Intergovernmental Panel on Climate Change
IRENA	International Renewable Energy Agency
Isc	Short Circuit Current
ISE	Institute for Solar Energy
Ish	Shunt Current
J/K	Joule per Kelvin
kWh	kilo Watt hour
lag	lagging
lead	leading
LVRT	Low Voltage Ride Through
m/s	meter per second
MA	Moving Average
MCS	Microgeneration Certification Scheme
MEA	Middle East and Africa
MOSFET	Metal-Oxide Semiconductor Field-Effect Transistor
MPPT	Maximum Power Point Tracking
Ni-Cd	Nickel Cadmium
OECD	Organization for Economic Cooperation and Development
p.f.	Power Factor
p.u.	Per Unit
PCC	Point of Common Coupling
PI	Proportional Integral
PMSG	Permanent Magnetic Synchronous Generator
PR	Proportional Resonant
PSF	Power Signal Feedback
PV	Photovoltaic
PV-EPT	Photovoltaic-Energy Payback Time
PWM	Pulse Width Modulation
rad/s	radian per second
RES	Renewable Sources
RES	Renewable Electricity Standard
RMS	Root Mean Square
ROC	Renewable Obligation Certificate
RoW	Rest of the World

rpm	revelations per minute
RPS	Renewable Portfolio Standard
RSC	Rotor Side Converter
SCADA	Supervisory Control And Data Acquisition
SCIG	Squirrel Cage Induction Generator
SG	Synchronous Generator
Si	Silicon
SM	Synchronous Machine
SMA	German solar energy equipment supplier
STATCOM	Static Synchronous Compensator
STC	Standard Test Conditions
SVC	Static VAr Compensator
TCR	Thyristor Controlled Reactor
THD	Total Harmonic Distortion
TLCI	Thyristor based Line Commutated Inverters
TSC	Thyristor Switched Capacitor
TSI	Transient Stability Index
TSO	Transmission System Operator
TSR	Tip Speed Ratio
UK	United Kingdom
UNFCCC	United Nation Framework Convention on Climate Change
US	United States
VAr	Volt Ampere reactive
VAWT	Vertical Axis Wind Turbine
V_{DC}	DC Voltage
V_{DCmax}	Maximum limit of DC Voltage
VDE	Association for Electrical, Electronic and Information Technologies (in German: Verband der Elektrotechnik)
Voc	Open Circuit Voltage
VSC	Voltage Source Converter
VSI	Voltage Source Inverter
W	Watt
W/m²	Watt per meter squares
WEF	Wind Energy Foundation
WHO	World Health Organisation
WWEA	World Wind Energy Association

List of Symbols

S	Apparent Power
P	Active Power
Q	Reactive Power
I_{ph}	light generated current
I_o	reverse saturation current
q	electron charge which equals $1.6 \times 10^{-19} \text{C}$
A	junction material factor
T	junction temperature
k	Boltzmann constant which is $1.38 \times 10^{-23} \text{J/K}$
R_s	series resistance
R_{sh}	shunt resistance
I_{pv}	photovoltaic output current
V_{pv}	photovoltaic output voltage
I_{pva}	PV array output current
V_{pva}	PV array output voltage
n_p	number of parallel strings in the PV array
n_s	number of series PV modules in one string
E	photon energy
h	Plank's constant $6.63 \times 10^{-34} \text{ J.s}$
c	light speed $3 \times 10^8 \text{ m/s}$
λ	wavelength of radiation measured in m
η	solar cell efficiency
P_{MPP}	power at the maximum power point
E	solar irradiance
I_{MPP}	current at the maximum power point
V_{MPP}	voltage at the maximum power point
A_c	solar cell surface area
P_w	wind turbine output power
v_w	wind speed
ρ	air density (1.225 kg/m^3)
A	turbine swept area
C_p	power coefficient
λ	tip speed ratio
β	blade pitch angle
ω	rotational speed
R	rotor radius
ω_r	rotational speed of the rotor

ω_s	synchronous speed of the generator
s	machine slip
P_r	rotor power
P_g	total power generated
P_s	stator power
V_{ds}	stator voltage in the d-axis
I_{ds}	stator current in the d-axis
λ_{ds}	stator flux linkage in the d-axis
V_{qs}	stator voltage in the q-axis
I_{qs}	stator current in the q-axis
λ_{qs}	stator flux linkage in the q-axis
V_{dr}	rotor voltage in the d-axis
I_{dr}	rotor current in the d-axis
λ_{dr}	rotor flux linkage in the d-axis
V_{qr}	rotor voltage in the q-axis
I_{qr}	rotor current in the q-axis
λ_{qr}	rotor flux linkage in the q-axis
R_s	stator resistance
R_r	rotor resistance
L_{ls}	stator leakage inductance
L_{lr}	rotor leakage inductance
L_m	magnetising (mutual) inductance
L_s	self-inductance
ω_{rf}	frequency of the rotor current
T_e	electromagnetic torque
Q_r	rotor reactive power
Q_s	stator reactive power
K_i	PI integral gain
K_p	PI proportional gain
I_{gabc}	3 phase ac side of the GSC current
V_{gabc}	3 phase ac side of the GSC voltage
V_{sabc}	three phase stator voltage
r_g	ac side of GSC resistance
L_g	ac side of GSC inductance
λ_m	magnetic flux in the rotor
V_d	the equivalent stator voltage in the d-axis
V_q	the equivalent stator voltage in the q-axis
I_d	the equivalent stator current in the d-axis

I_q	the equivalent stator current in the q-axis
L_d	the equivalent inductance of the stator in d-axis
L_q	the equivalent inductance of the stator in q-axis
T_m	mechanical torque
J	the inertia of the rotating components
p	number of pole pairs
c	Weibull scale parameter
k	Weibull shape parameter
$f(v)$	the probability of occurrence of wind speed v ($v \geq 0$)
$CF(v)$	the probability of the wind speed exceeding the value v
$F(v)$	the cumulative probability density function
δ_{max}	maximum angle separation in degrees between any two generators
f	electrical frequency
P_m	mechanical power
P_e	electrical power
H	system inertia constant
df/dt	rate of change of frequency
ΔP	power change
P_L	load power
P_G	generation power
f_o	frequency at disturbance time
Q_{add}	additional reactive power required to correct the power factor
Φ	phase shift angle between the terminal voltage and current
Q_{old}	grid supplied reactive power
Q_{new}	total reactive power needed

CHAPTER 1 Introduction

1.1 Background

In recent years, electricity demand has increased dramatically in response to population and economic growth and it rapidly fluctuates in the short term in response to weather conditions and business cycles [1]. Long term forecasts show that electricity demand will continue to increase and satisfying future demand for electricity is therefore a significant and worldwide concern [2]. In general, fossil fuels have been used considerably as primary electricity generation sources to supply demand. However, these sources of energy produce greenhouse gas emissions that can affect the environment and future generations [3, 4]. Reducing greenhouse gas emissions is a global environmental concern and several countries have agreed to the Kyoto Protocol [5]. European countries, for instance, have set a target to decrease greenhouse gases by the year 2050 by 85-90 % compared to 1990 [6]. Due to the fast increase of electricity demand and the deficiency of fossil fuels such as petroleum products, renewable energy sources such as wind and solar have been utilised considerably in power systems as alternative sources of energy. Indeed, there has been a substantial interest in generating electric power using renewable resources in recent years due to their capability to reduce greenhouse gas emissions such as carbon dioxide (CO₂) and tackle climate change [7-10]. Increasing the share of renewable energy sources in the entire energy system boosts sustainability and renewable generating units are also becoming economically competitive compared to conventional energy sources in the long term. Greater use of renewable energy sources in power systems can also contribute to reducing the uncertainties associated with fossil fuels.

According to the International Energy Agency (IEA), 57 % to 71 % of global electricity will be supplied by renewable energy sources by the year 2050 for the “sustainable future” scenario [11]. In Europe, renewable power generation has increased rapidly in the last decade and it is expected to increase steeply in the next decade, as illustrated in Figure 1.1. Electricity production from fossil fuels and nuclear power plants is also expected to decrease in European countries in the next decade. Generation of electricity from

renewable energy sources has grown dramatically in the UK in the last few years, as shown in Figure 1.2.

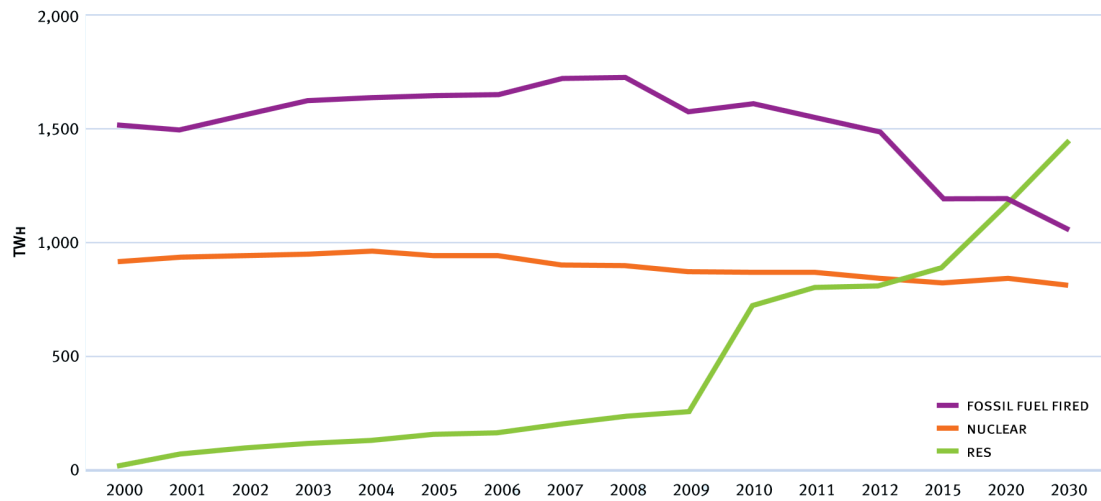


Figure 1.1: Outlook of power generation by fuel type in Europe to 2030 (RES: Renewable Sources) [12].

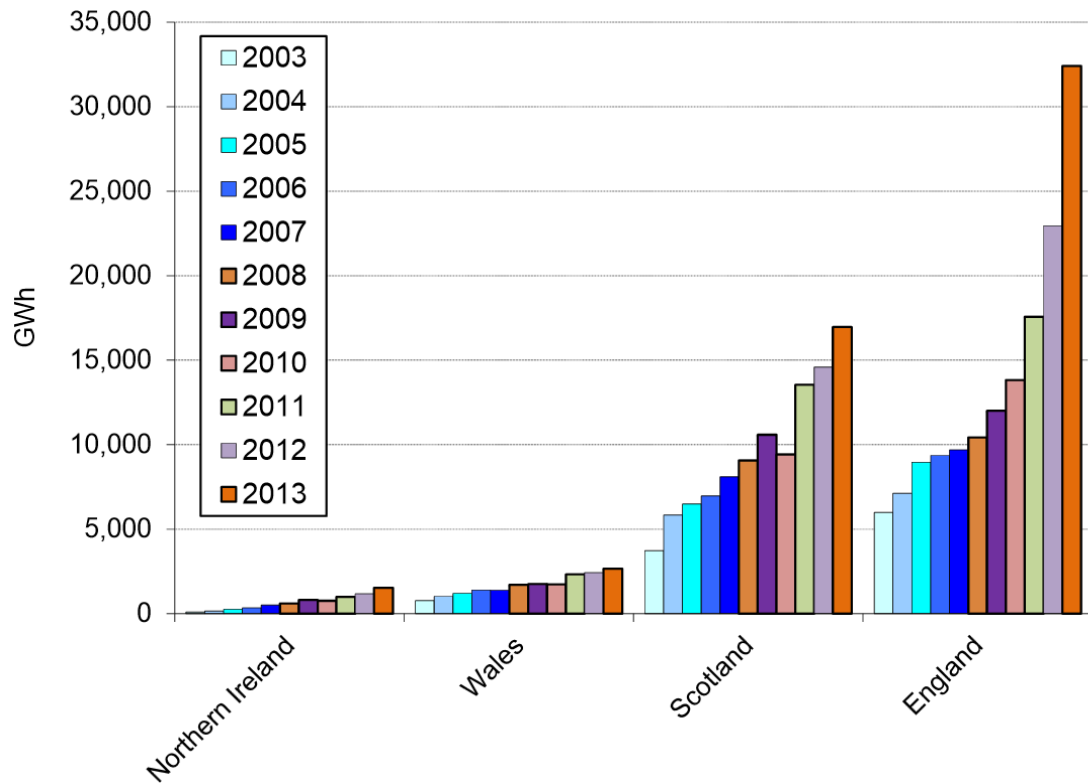


Figure 1.2: Renewable energy generation in the UK, country by country, from 2003 to 2013 [13].

In addition, massive changes to power system structures have been observed since electricity deregulation began in the late 1980s. Restructuring of electricity industries is very complicated and depends on the various policies and regulations linked to national energy strategies. Deregulating and privatizing the generation sector in liberalized electricity markets aims to decrease any restrictive regulatory frameworks to encourage companies to invest in the power sector and meet customer needs. Competition is encouraged to decrease costs, enhance the security of supply and increase efficiency [14]. Numerous electricity markets in different parts of the world are currently implementing plans for more competition in electricity markets. They have found that enhancing the security of supply and maintaining system stability are big concerns. Moreover, they recognize that generation and distribution networks should not be monopolized. They also realize that many economic benefits, such as making profits and reducing costs, can be obtained [15]. Competitive generation gives the market flexibility to sell power directly to large customers and can help transfer this power to distribution networks to sell ultimately to end users. These transitions are based on several transactions and contracts between buyers and sellers within certain timeframes. Future power systems may be complicated but they will improve operation, efficiency and resilience (as shown in Figure 1.3) according to the International Energy Agency (IEA).

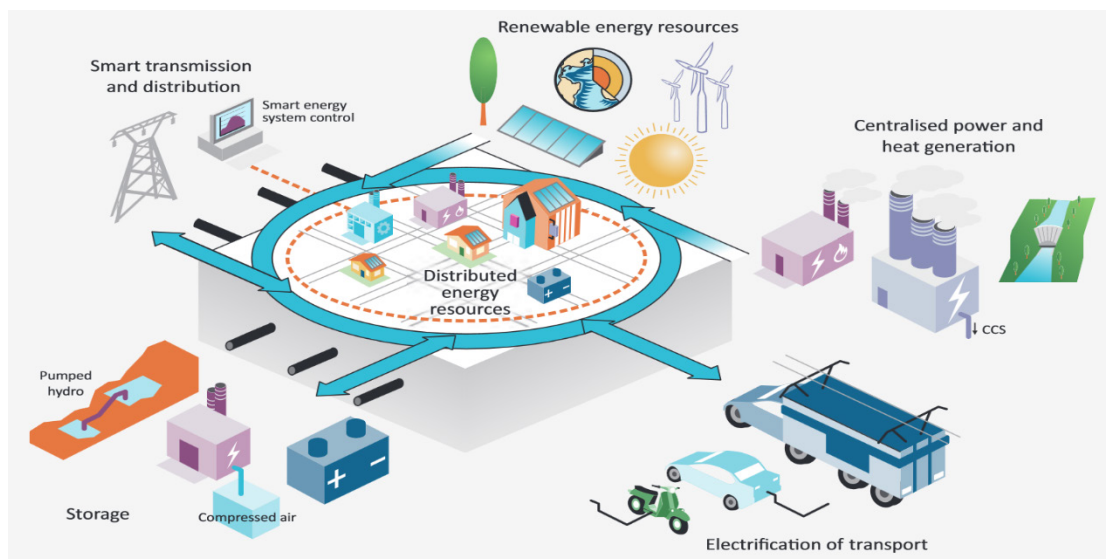


Figure 1.3: Future power system [16].

In recent years, power system deregulation and competition have been adopted in many parts of the world as a means to reduce consumer energy costs, enhance security of supply and increase efficiency [14, 15]. This has encouraged the increased penetration of distributed generations (DGs) in power systems and a subsequent reduction in greenhouse gas emissions through the use of renewable resources, as well as the start of a new industry valued at billions of dollars [17-20].

As mentioned earlier, the rapid increase in electricity demand necessitates solutions to increase generation capacity. One of the most useful solutions is increasing distributed generation (DG), called embedded generation in distribution systems. IEEE defines distributed generation as "the generation of electricity by facilities that are sufficiently smaller than central generating plants so as to allow interconnection at nearly any point in a power system" [21]. Several organizations depict DG by size and capacity; for example, CIGRE defines DGs as units that produce power on a customer site which have size smaller than 50 – 100 MW [22] and location is IEA's method of describing DGs [23].

There are many benefits to using distributed generation in numerous power systems around the world. These benefits can be classified as customer, supplier and social benefits. Ensuring the reliability of the power supply, providing the right energy solution in the right location, offering efficiency gains for onsite applications, providing the power quality needed, giving customers a choice in satisfying their particular electric energy services, and enabling savings on electric energy rates are all benefits of DG from a customer's perspective. The benefits of distributed generation from a supplier's viewpoint include avoiding unessential capital expenditure by closely matching generating capacity to demand growth, and avoiding investment in new transmission and distribution systems as the DGs are located close to customers. Moreover, there are public benefits to employing DG in power systems such as reducing greenhouse gas emissions through renewable resource usage.

Wind and solar energy are commonly used as distributed generation sources in small to medium-scale low and medium voltage micro or smart grids because they are located on

either the utility or customer side, they are a sustainable energy source and they are environmentally friendly [24]. In recent years, wind and solar energy have become the most attractive and fastest growing renewable energy technologies in power generation worldwide. According to the European Wind Energy Association (EWEA), a seven-fold growth in European wind power capacities is expected, from 34 GW in 2004 to 230 GW, by the year 2020 [6]. Additionally, more than 21.9 GW of new PV capacity was installed in Europe in 2011, which represents about 74 % of the total installation around the world according to the European Photovoltaic Industry Association (EPIA) [25].

However, there are several challenges and difficulties to integrating distributed generation in power systems [26] and it is not straightforward to solve these difficulties and challenges. Technical and economic issues related to the integration of renewable generation in power systems need to be addressed. Therefore, this thesis will discuss several technical issues related to the integration of renewable energy sources based on wind and PV in distribution systems as illustrated in section 1.2.

1.2 Investigated Issues

Highly integrating distributed generation based on renewable energy sources in distribution systems raises several issues and challenges that need to be addressed. These issues include stability, reliability, quality of supply, frequency control and system protection. The issues related to the fault ride through, transient stability, frequency response and the impact on the grid power factor of distribution systems are all investigated in this thesis, as described in the below points:

- **Fault ride through**

With the rapid increase in penetration levels of renewable energy sources in distribution networks, system operators need to maintain control of overall power generation interconnected to ac grids. Distributed generation units based on renewable energy have been required to be disconnected in the past for all fault conditions. This may lead to severe voltage and dynamic stability problems at high renewable penetration levels [27]. Disconnection of renewable generating units in

such a system could also cause a large imbalance between generation and load, and this jeopardises the security of supply. Therefore, Distribution Network Operators (DNOs) have introduced fault ride through requirements to prevent the consequences of disconnection of distributed generation units. Typically, when a power system is under abnormal conditions such as a fault, a short voltage sag will occur. During this short time, fault ride through (FRT) requirements ensure that generating units are connected to the system through a temporary fault condition and they are required to stay connected to the transmission or distribution systems to help maintain system security [28]. In fault scenarios close to renewable energy generating units based on wind and PV, these units may operate under high risk to its power electronic converters and DC link capacitors due to resulting overvoltages and/or overcurrents. Therefore, fault ride through is one of the significant issues that need to be investigated.

FRT requirements have been discussed in literature for wind turbines based on DFIG [29-33] and synchronous generator with fully rated converters [34-36]. These publications investigated the FRT issue for wind generators based on DFIG and synchronous generator with fully rated converters in small-scale transmission systems. Unlike the aforementioned works, this research uses a modified control design on distributed generation based on DFIG wind turbines and synchronous generator with fully rated converters in different distribution systems to help to ride through faults and meet the low voltage ride through (LVRT) grid code requirements for voltage recovery. For PV grid connected systems, fault ride through capability has been investigated in literature [37, 38]. However, there are few papers that investigate the FRT capability for a three phase two stage photovoltaic grid connected system. For this reason, this thesis proposes a three phase two stage transformerless PV grid connected system with FRT capability to protect the power electronic converters and the DC link of the PV system from overvoltages or overcurrents.

- **Transient stability**

Traditionally, a single renewable energy source has a small impact on power system stability as they were insignificant in power systems [39]. However, with the increase of renewable penetration levels in power systems, the dynamic performance of such systems can be affected [40]. Therefore, it is significant to study the impact of high renewable energy penetration on system transient stability and to investigate the behaviour of renewable generating units in relation to system disturbances such as faults. There are various renewable energy technologies and they may have different responses to fault conditions. This thesis considers three such technologies, a wind turbine based on the DFIG, a wind turbine based on a synchronous generator with fully rated converters, and photovoltaics based on solar energy.

The impact of integrating wind power based on DFIG on a power system's transient stability has been investigated in literature [41-43] and in [44, 45] for wind turbines based on synchronous generator with fully rated converters. The higher the penetration of wind energy in the system, the lower the stability of the system is [46]. Unlike these publications which consider transmission systems, this research investigates the impact of high penetration of wind power based on DFIG and synchronous generator with fully rated converters on the transient stability of different systems at the distribution voltage level, where no reactive power supporters or FACTS devices are in the system. The impact of small PV grid connected systems on the operation of distribution systems has been investigated in [47]. Power system transient stability for systems with high photovoltaic penetration has been assessed in [48, 49]. It has been shown in [50] that system transient stability in high PV grid connected systems can be affected by PV topologies and fault locations. This thesis investigates the transient stability of different modified generic distribution systems with high penetration levels of PV grid connected systems and it assesses the stability by using the Transient Stability Index method.

- **Frequency response**

The frequency of a power system is continuously varying but it should remain within acceptable limits as defined by the power system operator so as to enhance the power system's security. A sudden loss or increase of generation or load demand could lead to a frequency deviation from the nominal value because the system frequency is directly proportional to the balance between generation and load [51]. High renewable energy generation in power systems can affect frequency stability and this issue has become a significant concern for Transmission System Operators (TSOs) in recent years [52]. It is an issue in power dynamic operations, as some renewable energy sources have different characteristics from conventional synchronous generators in several respects. One important difference is that, some renewable generating units are connected to the grid via power electronic converters and this causes decoupling of the inertia of their generators from power system inertia, such as in variable speed wind turbines based on the DFIG or a synchronous generator with fully rated converters. Some other renewable units, such as photovoltaics based solar energy, do not contribute towards system inertia as there is no machine in their structures to contribute towards power system inertia. Therefore, it is significant to study system frequency response with high penetration of such renewable technologies when a system is subjected to a frequency disturbance such as a sudden increase or decrease in load demand.

Wind based on DFIG was discussed in terms of frequency response in [53-56]. However, these publications were based on wind turbines connected to large power systems. In this research, the frequency response of wind power based on DFIG is investigated for smaller power systems, i.e. distribution systems where the penetration of wind is significant. Different frequency responses for the DFIG are discussed to meet the grid code requirements, including active power reduction, inertia response and a proposed frequency control model to enhance the frequency response of the DFIG based on wind energy. The frequency control in wind turbines based on synchronous generator with fully rated converters has not

been considered much in literature and there are only a few papers such as [57] and [58] discussing this issue. For PV grid connected system, there are three different approaches to provide frequency responses: keep PV systems in the Maximum Power Point Tracking (MPPT) mode and install an energy storage system, as shown in [59, 60], install a dump load to absorb surplus energy and the PV active power curtailment approach [61]. [62], shows that the power curtailment approach is more cost effective than the other two approaches for providing frequency control via a PV system because there is no need to install a new hardware in the PV system. In this thesis, the active power curtailment approach is used for renewable generating units based on wind and PV to provide a frequency response to different generic distribution systems. The active power reduction approach is based on the German grid code requirements discussed in [63].

- **Impact on grid power factor**

The increase in renewable generating units based on wind and PV which operate at unity power factor and do not have reactive power controllability in distribution systems has also had a negative impact on the utility grid power factor, as illustrated in Figure 1.4. From Figure 1.4, a grid working on a 0.9 power factor (p.f.) to supply a load with 900 W active power and 435.9 VAr reactive power. The grid power factor will be affected if the renewable unit shown in Figure 1.4 works at the unity power factor (without reactive power controllability) is connected to the system and the utility grid power factor deteriorates to become 0.878. The higher the penetration of renewable energy without reactive power controllability in the system, the lower the grid power factor of the system is. Therefore, it is important to investigate the impact of renewable energy generation based on wind and PV on the grid power factor and to investigate the ability of such renewable sources to work at different power factor settings (non-unity) to improve the grid power factor.

The reactive power capability of wind turbines based on DFIG was discussed in [64-66]. There are few papers in literature that have investigated the reactive

power capability of wind turbines based on synchronous generator with fully rated converters (FRC), however, in [67], reactive power provision with technical and economic limitations from an FRC wind unit were discussed. The majority of research papers in literature have studied the reactive power capability of large-scale wind turbines in large power systems (transmission systems). In contrast, this thesis investigates the impact of high wind power penetration based on DFIG and synchronous generator with fully rated converters on the grid power factor and the possibility of providing reactive power and operating at non-unity power factor in various generic distribution systems. When a DG starts producing power into a low-voltage network, the voltage magnitude can change considerably because of the high resistance of the lines. In low-voltage distribution systems, the R/X ratio is larger than that in transmission systems and voltages rise near the point of DG connection. Therefore, DGs can use their power electronic converters to control the voltage at the point of connection and provide/absorb reactive power. Wind and photovoltaic generating units are competitive options for reactive power compensation, as they have a fast response when compared to traditional methods such as capacitor banks. PV penetration is increasing rapidly in distribution networks as there is no extra cost in using PV units as a reactive power supporter. There is promising potential to use PV inverters as reactive power supporters for local utility grids and they become essential to operate at non-unity power factor in recent years in power systems with high PV penetration [68, 69]. This thesis investigates the impact of high solar energy penetration based on PVs on the grid power factor and the capability to provide reactive power in different distribution systems. A three phase two stage transformerless PV grid connected system with reactive power capability is proposed in this research to operate under different solar irradiance conditions and improve the utility grid power factor.

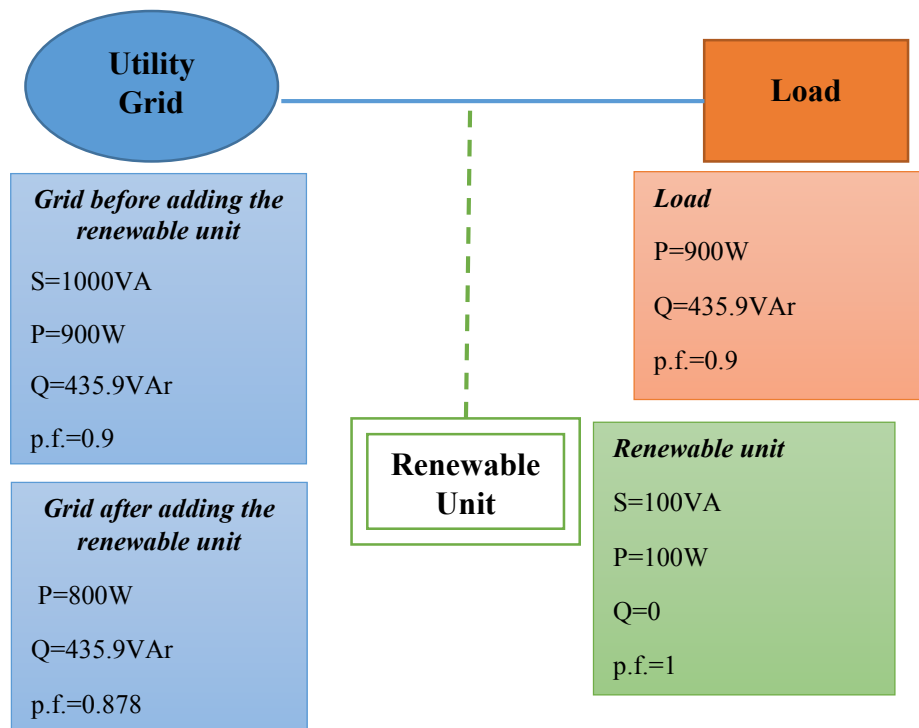


Figure 1.4: Renewable generation impact on grid power factor.

1.3 Motivation

Distributed generation based on renewable energy sources has increased rapidly, as discussed earlier, to mitigate climate change problems and decrease dependency on fossil fuels. Several countries have planned for their renewable energy portfolios to reduce greenhouse gas emissions, such as to reduce CO_2 by 80 % in comparison to a 1990 baseline in the UK [70]. Indeed, the UK's government has planned to increase renewable energy in the British power system to meet this target. Maximising the potential of local distributed generation based on renewable energy is highly encouraged in the UK to meet renewable targets and the government provides promotions and incentives to renewable source owners such as the Feed In Tariff (FIT) and Renewable Obligation Certificate (ROC) [71]. The FIT is mainly a support mechanism for small scale (less than 5 MW) renewable generation while the Renewable Obligation (RO) is one of the main support mechanisms for larger renewable projects [72]. As a result, research and investment on distributed generation based on renewable sources such as wind and solar energy has increased dramatically. However, there are several issues related to the integration of

renewable energy generation in distribution networks, as discussed earlier. The motivation behind this research can therefore be described in the following points:

- The integration of renewable generation in distribution systems benefits not only the power suppliers and customers but also society as a whole. Therefore, solving the problems of integrating high renewable energy sources in distribution systems can help to achieve these benefits.
- There is a need to study the impact of high integration of renewable generation in distribution systems on system voltages, frequency and stability.
- There is a need to understand the characteristics of various distributed generation technologies based on wind and solar energies to investigate their dynamic performance during various disturbances in distribution systems.
- There is a need to develop control techniques for renewable generating units based on wind and photovoltaic to investigate some technical issues related to the integration of such sources in distribution systems in order to ride through faults, improve frequency responses and enhance grid power factor.

1.4 Research Objectives

Due to the rapid increase in electricity demand and the need to reduce greenhouse gas emissions, distributed generation based on renewable energy sources has increased in recent years. However, there are some technical issues related to the integration of renewable energy generation based on wind and PV in distribution systems need to be investigated and these issues are fault ride through, transient stability, frequency response and grid power factor. The main objectives of this thesis can be summarised as follows:

- To conduct comprehensive reviews to understand the characteristics of various renewable generating units, including a wind turbine based on the DFIG, a synchronous generator with fully rated converters based on wind energy, and photovoltaics based on solar energy.
- To investigate the fault ride through of distribution systems with high renewable energy penetration based on wind and PV, and discuss the behaviour of wind and

PV generating units during faults. To modify a control design for wind generators and PVs to ride through faults and protect their power electronic converters from overvoltages.

- To discuss the main issues associated with the system transient stability of distribution networks with high renewable energy penetration based on wind and photovoltaics. To assess the system transient stability by using the Transient Stability Index with and without renewable energy penetration.
- To explore the frequency response of distribution systems with high penetration of renewable sources based on wind power and solar-photovoltaics. To propose a new frequency control technique for wind based on DFIG to improve the system frequency response when the system experiences an under or over-frequency conditions.
- To study the impact of integrating high renewable energy sources based on wind and PV in distribution systems on grid power factor. To improve the grid power factor by enabling DGs based on wind and PV to operate under various power factor settings (non-unity).

1.5 Original Contributions of the Thesis

The original contributions to fulfil the research objectives can be summarised in the following points:

- A modified control design on distributed generations based on wind and solar energy in different distribution systems is used to help to ride through faults and meet the low voltage ride through (LVRT) grid code requirements for voltage recovery. A DC chopper was added to the DC link of wind generators to protect them from overvoltages during fault, and a three phase two stage transformerless grid connected PV system was proposed with a new technique to protect the converters from faults.
- An investigation into different distribution networks with high penetration of renewable energy based on wind and PV to discuss the impact of such renewable

sources on system transient stability and using the Transient Stability Index method to assess their effects.

- A discussion on various frequency control methods published in literature for various DGs based on renewable energy, including wind turbine based on the DFIG, synchronous generator with fully rated converters based on wind energy, and photovoltaics based on solar energy to investigate the frequency response of different distribution systems with high renewable energy penetration. A new frequency control technique was proposed in this thesis for DFIG based wind energy in relation to various distribution systems. The simulation results have shown improvements in the system frequency response for both under- and over-frequency conditions.
- A design of a three phase two stage (back-to-back power electronic converters) transformerless PV grid connected system with reactive power capability to operate under different solar irradiance conditions and improve the utility grid power factor. The development of various distribution systems with high penetration of renewable energy generating units including photovoltaics, wind systems based on the DFIG and synchronous generator with fully rated converters operating under different power factor settings to study the impact of these sources on the grid power factor.

1.6 Thesis Structure

The work carried out in this thesis is organised into eight chapters. **Chapter 1** provides the introduction to the thesis and presents the motivation behind this work. It also provides the research objectives and identifies the original contributions of the thesis.

In **Chapter 2**, a background to solar energy is given as well as the evolution of the photovoltaic industry, and the potential and benefits of solar energy based on photovoltaic technology are investigated. Environmental and economic issues related to photovoltaics based on solar energy are also highlighted. Then, photovoltaic technology growth in power systems worldwide is discussed, such as in Europe and the United Kingdom. After that, current photovoltaic technology is investigated in detail and it is shown how solar

cells produce electricity. The differences between PV cells, modules and arrays are mentioned and PV power electronic inverters are discussed. Then, photovoltaic systems are discussed and the differences in PV structure to supply DC load or AC load are mentioned. Moreover, stand-alone and grid connected PV systems are highlighted. Then, a detailed discussion is given on the technical characteristics and mathematical equations of PV systems used to generate electric power. After that, the impact of solar irradiance on PV output power and the need for Maximum Power Point Tracking (MPPT) to generate the maximum power available from PV units are investigated. Finally, several challenges and limitations of large scale PV generation are discussed, such as how much land is needed, raw material availability, reliability problems, PV system efficiency and grid code requirements.

Chapter 3 presents the background to wind energy and discusses wind power's potential and benefits. Then, environmental and economic concerns related to the integration of wind power in power systems are highlighted. Next, wind power growth in the world, Europe and the United Kingdom is discussed. This is followed by a detailed presentation of current wind power technologies and the differences between the horizontal axis wind turbine (HAWT) and vertical axis wind turbine (VAWT) are discussed. The construction of wind turbines and the advantages of using the HAWT are mentioned. After that, wind generation characteristics are highlighted. Three wind generator concepts are investigated in this chapter, namely a fixed speed generator based on an induction machine, variable speed wind based on the DFIG, and a synchronous generator with fully rated converters. Then, a detailed review of the control and operation of a wind turbine based on the DFIG and a synchronous generator with fully rated converters is given. The impact of wind speed variations on the output power of wind generation and the need to track the maximum available power are highlighted. Then, power electronic applications in wind power generation are discussed. Finally, various challenges and barriers related to the integration of wind power in power systems are investigated in this chapter.

In **Chapter 4**, an explanation to fault ride through is given. The grid code requirements for FRT are discussed in this chapter and examples of these requirements are shown. Then,

the impact of wind power generation on fault ride through requirements is highlighted. Next, the impact of solar energy based on photovoltaic technology on fault ride through requirements is discussed. After that, modelling and control of renewable energy generation, such as a wind turbine based on the Doubly Fed Induction Generator (DFIG), a wind synchronous generator with fully rated converters, and solar energy based on photovoltaics, in order to ride through faults are investigated. Then, simulation scenarios used to investigate the fault ride through of distribution systems with high renewable energy penetration are discussed. Three distribution systems, namely IEEE 13 bus, IEEE 37 bus and IEEE 123 bus distribution systems, are used in this chapter to verify the methodology.

Chapter 5 gives an introduction to the transient stability analysis method. After that, the impact of wind energy generation and solar energy based on photovoltaics on system transient stability is investigated. Then, the control and modelling of wind power generation based on the DFIG and a synchronous generator with fully rated converters are included. The PV grid connected system's control and modelling in distribution systems is next discussed. Then, the transient stability of distribution systems with high renewable power generation in simulation scenarios is discussed. Finally, this chapter uses three different distribution systems, namely IEEE 13 bus, IEEE 37 bus and IEEE 123 bus distribution systems, to study the impact of renewable energy generation on system transient stability.

In **Chapter 6**, the concepts of frequency control is presented. Then, the grid code requirements for frequency response are highlighted. The impact of renewable energy generation based on wind and solar energy on the frequency response of a power system is discussed. Then, modelling and control of various renewable energy sources, such as wind based on the DFIG, a synchronous generator with fully rated converters, and solar based on photovoltaics, are investigated to improve the frequency response of distribution systems. Next, simulation scenarios to study the frequency response of various distributions systems with high renewable energy penetration are highlighted. This chapter also uses three different distribution systems to validate the proposed frequency

control techniques, namely IEEE 13 bus, IEEE 37 bus and IEEE 123 bus distribution systems.

Chapter 7 gives an introduction to reactive power requirement and the reactive power compensation devices discussed in literature. It also highlights the end user reactive power compensation in distribution systems based on inverter technologies. Then, grid code requirements for reactive power support are discussed. The impact of wind power generation and solar based on photovoltaics on the utility grid's power factor is investigated. After that, the proposed modelling and control of various renewable energy sources to operate under different power factor settings (non-unity) are discussed. Then, simulation scenarios used to investigate the impact of these renewable generating units in various distribution systems on the grid power factor are discussed. Three various distribution systems, namely IEEE 13 bus, IEEE 37 bus and IEEE 123 bus distribution systems, are used to validate the proposed models and verify the methodology.

Chapter 8 summarises the conclusions of this research and makes suggestions for future work.

1.7 Publications

During this research, lists of relevant published work by the author are summarised as follows:

- **F. Alsokhiry**, G. P. Adam, and K. L. Lo, "Contribution of distributed generation to ancillary services," in *Universities Power Engineering Conference (UPEC), 2012 47th International*, 2012, pp. 1-5.
- **F. Alsokhiry** and K. L. Lo, "Distributed generation based on renewable energy providing frequency response ancillary services," in *Power Engineering, Energy and Electrical Drives (POWERENG), 2013 Fourth International Conference on*, 2013, pp. 1200-1205.
- **F. Alsokhiry** and K. L. Lo, "Effect of distributed generations based on renewable energy on the transient fault - Ride through," in *Renewable Energy Research and Applications (ICRERA), 2013 International Conference on*, 2013, pp. 1102-1106.

- **F. Alsokhiry** and K. L. Lo, "Provision of reactive power support ancillary services from distributed generation based on renewable energy," in *Renewable Energy Research and Applications (ICRERA), 2013 International Conference on*, 2013, pp. 1018-1023.
- **F. Alsokhiry**, B. Alajmi and K. L. Lo, "Impact of distributed generation based on renewable energy on grid system power factor," *International Journal of Electrical Power & Energy Systems*, (Submitted).
- **F. Alsokhiry** and K. L. Lo, "Fault ride through capability of various renewable energy sources in distribution systems", (Under preparation for Journal Submission).
- **F. Alsokhiry** and K. L. Lo, "Frequency response of distribution systems with high renewable energy penetration", (Under preparation for Journal Submission).

CHAPTER 2 Solar Energy – Photovoltaic Systems

2.1 Introduction

Electricity demand has increased considerably over the past few years due to the rapid growth in populations and economies. The global demand for electric energy is expected to double by the year 2050, varying based on economic growth [73]. In low economic growth countries, electricity demand will increase by 18% from the year 2011 to 2040 compared with about 42% in high economic growth countries [74]. About 93% of total world energy generation was produced from fossil fuels in 2010; 38% from oil, 28% from coal, 21% from natural gas and 6% from nuclear plants [75]. Only 7% of our energy was produced from renewable resources in 2010.

The dependency on fossil fuels for energy production leads to a significant rise in greenhouse gas emissions such as carbon dioxide (CO₂). As a result, the penetration of renewable energy power generators should be increased, considering total power system security and reliability. Among many renewable resources, solar energy is one of the most promising renewable source of energy due to its sustainability and advanced technologies. There are three main solar energy technologies, namely photovoltaics (PV) which directly convert sun-light into electric energy, concentrated solar power (CSP) called concentrated solar thermal which converts the concentrated sun-light to heat (thermal energy) to drive a heat engine (usually steam turbines) and then produce electricity, and heating and cooling systems which collect thermal energy from the sun to provide hot water and air conditioning. Solar generating units based on photovoltaic (PV) systems have been growing in use substantially in recent years due to their availability and environmental friendly impact. 2014 was a historical year for the increase in photovoltaic generation since the world's PV cumulative installed capacity exceeded 178 GW, as shown in Figure 2.1. Around 141 GW of the globe's photovoltaic units were installed in the years 2011, 2012, 2013 and 2014. This growth trend is expected to increase in the future, with PV cumulative installed capacity forecast to be around 540 GW by the year 2019 [76]. Together with statistical data, this shows that photovoltaic systems are an important

renewable resource for the future of electricity generation. Photovoltaic systems are also suitable for use in a variety of different applications, such as in mobile systems, satellite applications and for distributed generation, which makes them one of the most promising and efficient renewable energy sources in the world.

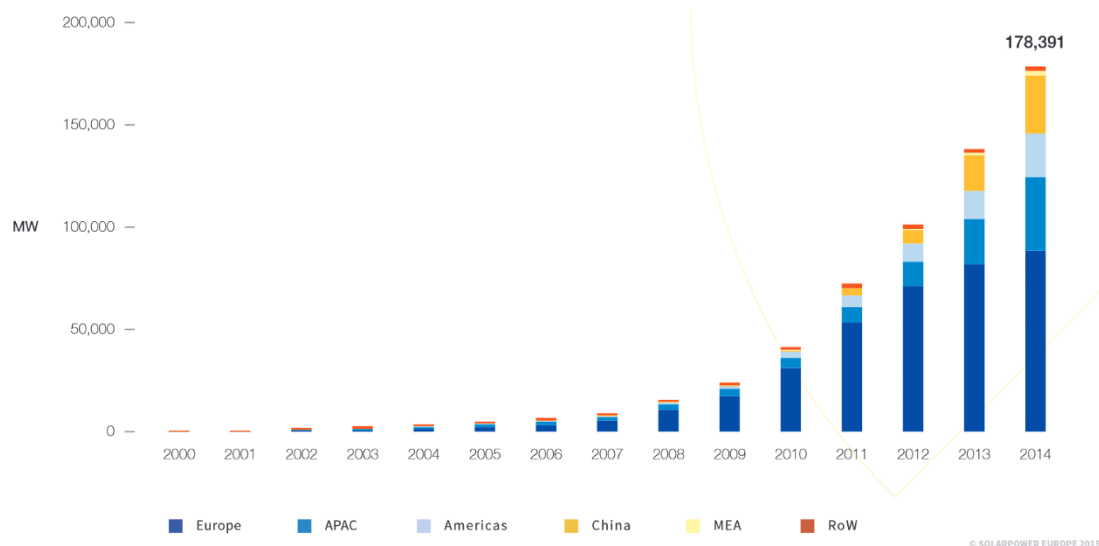


Figure 2.1: Evolution of global PV cumulative installed capacity 2000-2014, APAC: Asia Pacific, MEA: Middle East & Africa and RoW: Rest of the World (MW)[76].

2.2 Solar Energy Background

Solar energy is not a new technology and it has a history which goes back to the 16th century when a Swiss scientist named Horace-Benedict de Saussure created the first solar collector in 1767. In 1839, a French physicist, Edmond Becquerel, defined the photovoltaic effect. This was a major evolution in solar energy. Willoughby Smith discovered photo-conductivity of a material known as Selenium in 1873. An American inventor named Charles Fritts introduced the first solar cell in 1883 with efficiency of only 1%. Photovoltaic technology was then born in the United States in 1954 when Daryl Chapin, Calvin Fuller and Gerald Pearson invented the first crystalline silicon solar photovoltaic cell with 6% efficiency [77]. The term ‘photovoltaic’ is made up of two words, ‘photo’ which means light (from Greek) and ‘voltaic’ from ‘volt’ which is the unit used to measure electric voltage at a given point. Solar cells are used in a photovoltaic structure to convert solar radiation into electric power, measured in kilowatts (kW). A cell

is made from one or two layers of a semi-conducting material. Positive charge is placed on one layer and negative charge on the other layer. Semiconductor atoms absorb photons from sunlight when the PV cell is subjected to sunlight. Then, the atoms release electrons from the negative layer and the external circuit enables these electrons to flow back to the cell's positive layer, representing an electric current. An electric field is created across the layers when sunlight shines on the cell. Then, electricity can be produced. The first practical PV technology was used in the space satellite projects of 1958 and the 1960s. In the last 50 years, photovoltaic technology has improved considerably and scientists and researchers have contributed towards enhancing PV cell efficiency.

Successful use of PV in space satellite projects inspired researchers to use photovoltaic systems for electricity generation. In September 2013, the German Fraunhofer Institute for Solar Energy Systems (ISE), Soitec, CEA-Leti and the Helmholtz Center Berlin announced that they had accomplished a new world record for the conversion of sunlight into electric power using a new solar cell structure with four solar sub-cells. Their new world record was based on the development of a new solar cell with 44.7% efficiency [78]. The efficiency of a solar cell is the ratio of the power output in watts of this cell to the incident energy in the form of sunlight.

2.3 Solar Power Potential and Benefits

Use of solar units based on photovoltaic technology as a source of electricity has increased remarkably over the past decade. The increase in use of photovoltaic systems as an alternative to conventional power plants has resulted in a reduction in harmful greenhouse gas emissions such as CO₂. In recent years, new installed photovoltaic systems have saved the emission of more than 53 million tons of CO₂ per year. The world cumulative PV installed capacity exceeded 178 GW in 2014 and photovoltaic systems were the number one power generating source in terms of newly installed capacity. The European Union's countries became the world's leaders in terms of cumulative installed capacity, with about 70 GW in 2012. This represents approximately 70% of the world's new cumulative photovoltaic installed capacity. However, China was the PV market leader in the years

2013 and 2014 respectively and its new installed capacity exceeds 10.9 GW in 2014. Figure 2.2 shows that the potential of photovoltaic systems has been growing dramatically over the last 14 years, and the installed capacity of PV in the year 2014 represented around 137 times the installed capacity of the year 2000.

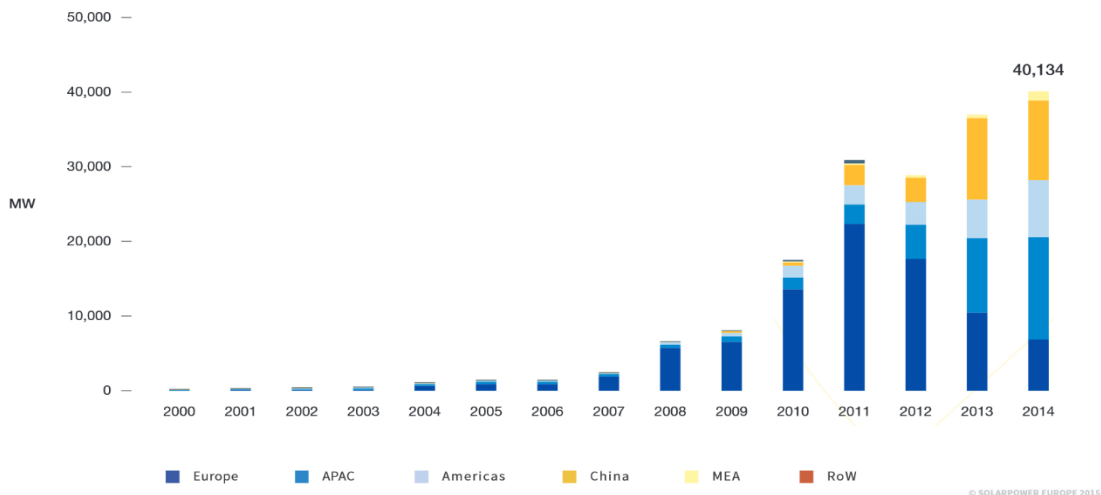


Figure 2.2: Evolution of global PV annual installations 2000-2014 (MW) [76].

Providing clean and sustainable electric energy could lead to a decrease of up to 4,047 million tonnes of CO₂ emissions every year by 2050 [79]. Photovoltaic systems have no emissions and this is one of the advantages of PV. It means there is no radioactive or combustion waste and this can help in meeting international targets to reduce greenhouse emissions and tackle climate change. PV systems have a vast fuel source which is widely accessible, as the most abundant source of free energy is sunlight. They also have a negligible environmental impact and can be installed anywhere. Photovoltaic units can be very easily integrated at any point of use and can be installed in existing or newly built roofs. PV systems also need no fuel and this results in low operating costs. The typical lifetime of a PV unit is at least 25 years, making them an efficient source of energy as they generate many times more energy than they cost.

2.4 Environmental Impact of PV

The sun provides an abundant resource for generating clean and sustainable electric energy; it releases no warming emissions or toxic pollutions. However, gas emissions can

result from the photovoltaic cell manufacturing process. The amount of emitted gases during the PV cell manufacturing process is much less than that of conventional power plants. A solar unit based on photovoltaic technology emits around 40 grams of CO₂ per kilo-watt-hour (kWh). Conversely, a conventional coal power plant emits 1000 grams of CO₂ per kWh [80]. This means that the production of carbon dioxide in a conventional coal power plant is 25 times that produced from a PV generating unit. Additionally, generating electricity from a photovoltaic system is safe for supplying domestic loads as they cause no noise or air pollution. A PV cell can also be recycled after the end of its lifetime and this may reduce the energy used to produce a new one.

2.5 Economic Potential of Photovoltaic Technology

Photovoltaic technology use in power systems has grown considerably over the past few years due to the reduction in PV costs. Government support and various financial incentives for its use, such as Feed in Tariff (FIT), have also contributed towards high integration of PV in power networks. According to the International Renewable Energy Agency (IRENA), the average price per watt of a PV module fell by 65-70% from 2009 to 2013. In Germany, the cost per PV system declined between 2009 and 2013 by 53%. New levels of competitiveness have emerged in terms of both utility and distribution. The fast growth of PV technology has continued even during economic crises and it is expected to become one of the major sources of power generation in the future [81].

PV price depends on economic incentives and the photovoltaic system manufacturers. PV manufacturers set a selling price which meets their profit margin and this depends mainly on manufacturing process costs. The process costs are related to the cost of raw materials need for a PV cell and the cost of the power electronics converters. Photovoltaic efficiency also plays a significant role in reducing overall PV costs. The larger the PV efficiency, the lower the overall PV costs. Unlike other power generation technologies, photovoltaic technology requires almost no maintenance and has a long lifetime.

2.6 Photovoltaic Technology Growth

At the end of 2000, the world's cumulative photovoltaic installed capacity was 1.3 GW. The growth in photovoltaic capacity was doubled in 2003 and this was followed by a steady increase until 2008. The world's cumulative PV capacity was around 16 GW in 2008 and one year later it was approximately 23 GW. Since 2009, PV capacity has dramatically increased, approaching a historic record of more than 100 GW in 2012. Photovoltaic systems are now becoming main power producers and they deliver clean and affordable energy to many parts of the world. In terms of new global renewable installed capacity, PV is the third most important renewable source after hydro and wind power. As mentioned above, PV is growing continually even during difficult economic periods, such as economic crises. PV installation capacities reached another record of 178 GW in 2014, and the new global added capacity reached around 40.13 GW. The top ten leading PV markets in the world in 2014 are summarised in Table 2.1. The global PV cumulative installed capacity share in 2014 by top PV markets is shown in Figure 2.3 and by region this is illustrated in Figure 2.4.

Table 2.1: The top ten leading photovoltaic markets worldwide in 2014.

Country		Installations in GW
China		10.6
Japan		9.7
USA		6.2
UK		2.3
Germany		1.9
Australia		0.9
France		0.9
South Korea		0.9
South Africa		0.8
India		0.6

Total PV Cumulative Capacity 178.4 GW

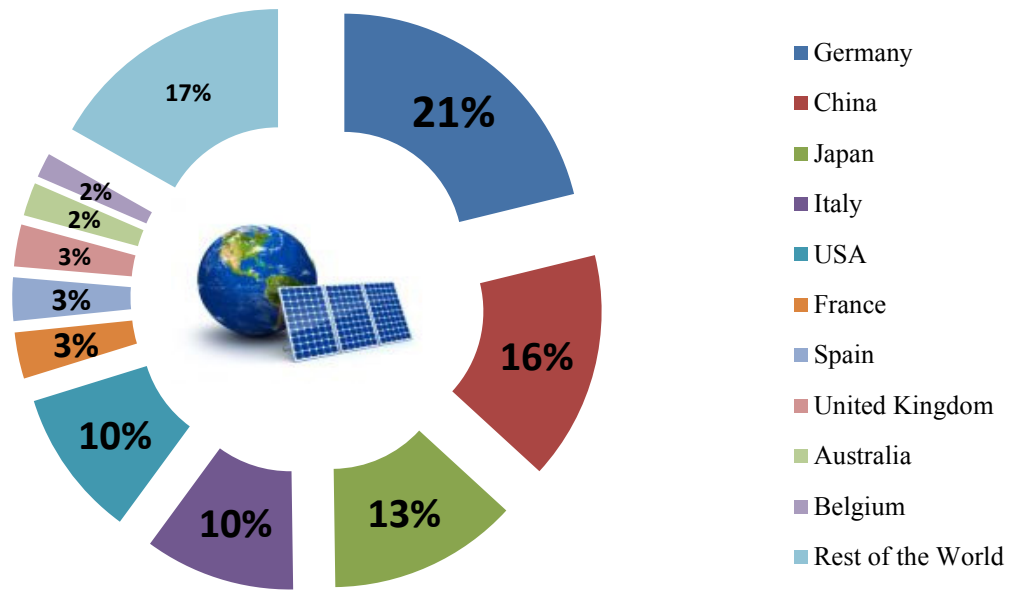


Figure 2.3: PV cumulative installed capacity share in the world until year 2014.

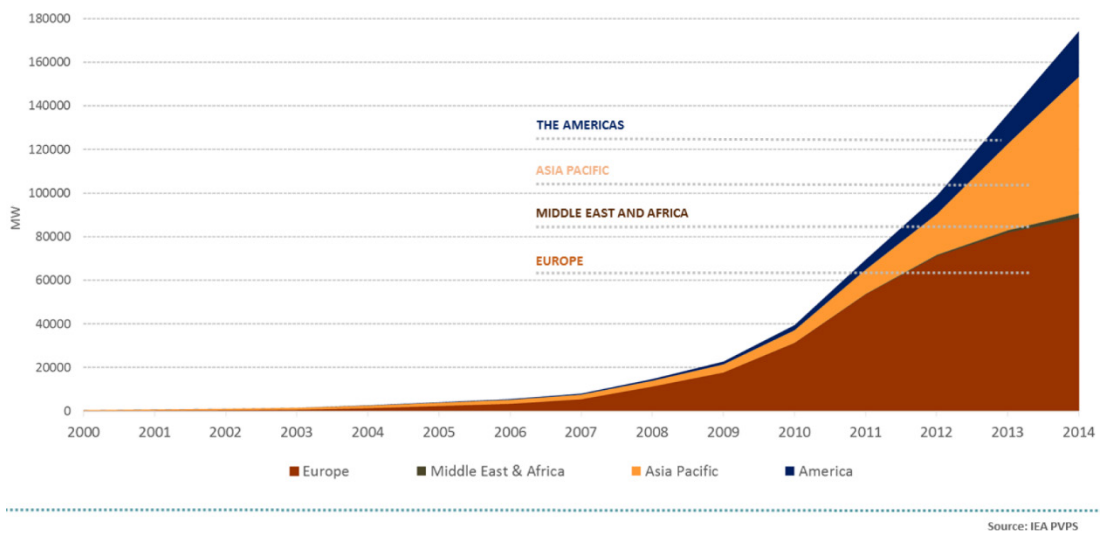


Figure 2.4: Evolution of the PV cumulative installed capacity in MW by region from 2000 – 2014, IEA-PVPS (International Energy Agency Photovoltaic Power Systems Programme [82]).

2.7 Photovoltaic Technology in Europe and the United Kingdom

Europe became the world's leading region in terms of cumulative photovoltaic installed capacity in 2007 with more than 5.3 GW. The growth of PV installed capacity has

continued in Europe in the last seven years and keeps Europe as the photovoltaic leader in terms of PV cumulative installed capacity, which represents around 50% of the total capacity as shown in Figure 2.4. Germany is the world's top PV market in terms of total cumulative installed capacity, representing around 21% of the global PV cumulative installed capacity share in 2014.

In the last few years, installation of photovoltaic systems has increased rapidly in the United Kingdom (UK) due to support from the UK Government and investment policy. The UK's cumulative PV installed capacity was 10.9 MW in 2005 and this has increased dramatically, reaching 1.9 GW in 2013 [83]. PV based on solar energy dominated installed capacity, with about 88.5% of the total installed capacity over the three years of the Feed in Tariff (FIT) scheme. The total PV installed capacity was 1585 MW in March 2013, whilst only 133 MW was wind installed capacity in the same period [84]. By the end of the third quarter of 2015, the total PV cumulative installed capacity reached 8.4 GW in the UK (see Figure 2.5) and in 2014 the UK became the seventh country in the world to reach 5 GW after Germany, China, Italy, Japan, the United States and Spain [85, 86].

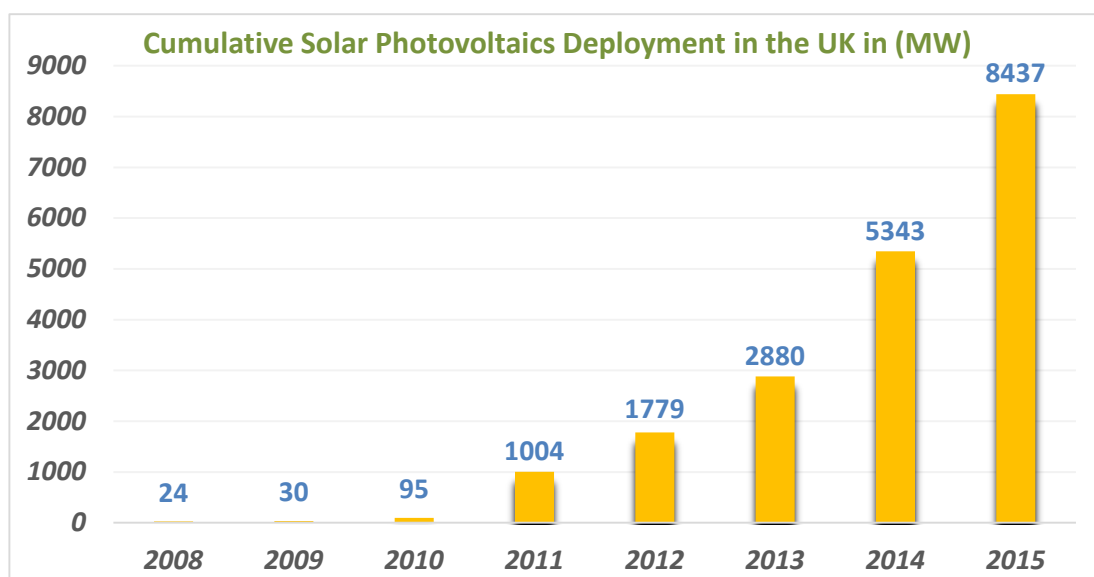


Figure 2.5: The total PV cumulative installed capacity in the UK.

2.8 Current Photovoltaic Technologies

Solar cells are used in a photovoltaic structure to convert solar radiation into electric power, measured in kilowatts (kW) and they are made from one or two layers of a semi-conducting material. The greater the intensity of the sunlight, the more electricity is generated. Silicon is the most common semi-conducting material used in photovoltaic systems because there is no limitations on silicon as a raw material and it is widely distributed in sand and dust. Silicon is also the second most abundant element in the earth's mass after Oxygen. The minority carrier transport in a silicon cell and electron-hole pair generation with an external circuit are illustrated in Figure 2.6.

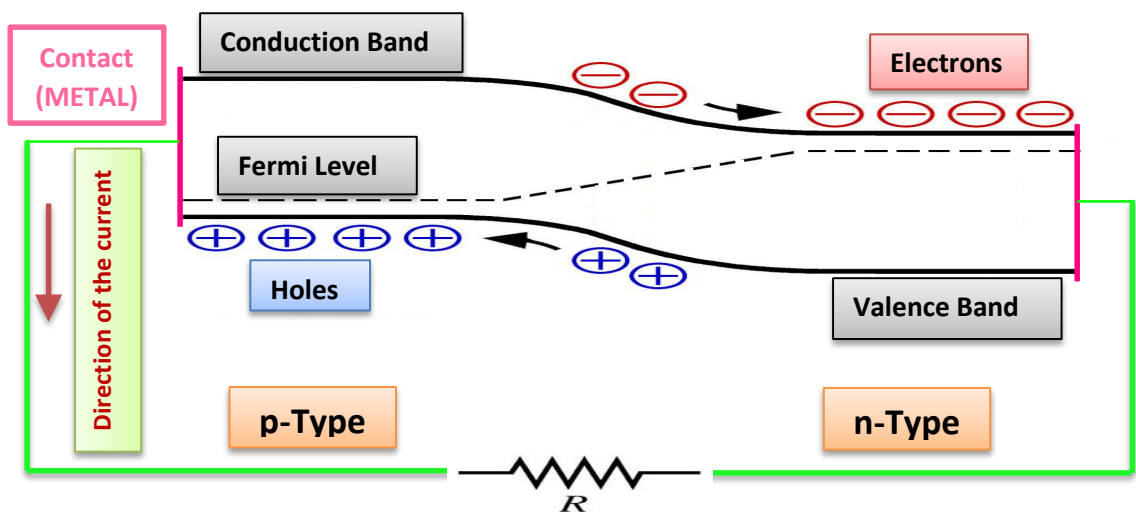


Figure 2.6: Silicon solar cell band diagram.

Solar energy generation based on a photovoltaic system involves four main components:

1. PV cells and modules.
2. A power electronic inverter to convert direct current (DC), which is obtained from PV modules, to alternate current (AC).
3. Storage devices such as batteries for stand-alone PV systems.
4. Support structures to adjust the photovoltaic modules toward the sun.

PV Cells and Modules

Crystalline silicon technology is the most common PV technology, representing around 90% of the photovoltaic market (according to the European Photovoltaic Industry

Association, EPIA). A crystalline silicon cell is made up of thin slices cut from a single crystal of silicon, which is called Monocrystalline, or created from a block of silicon crystals, which is called Polycrystalline. The efficiency of the crystalline silicon cells varies between 12% and 17%.

Another type of photovoltaic technology is called Thin Film technology. This is produced by depositing thin layers of photosensitive materials onto a low-cost support such as plastic, stainless steel or glass. Nowadays, several other types of photovoltaic technologies are available, such as concentrated photovoltaic technology which depends on the concentration of sunlight and collects as much sunlight as possible. The efficiency of concentrated photovoltaic technology is between 20% and 30%. Flexible cells and third generation photovoltaics are other types of photovoltaic technologies which enhance the flexibility of the solar cell.

Solar cells are connected together to structure larger units called modules. These modules can be connected to each other in a series known as an array to increase the voltage produced by the PV system. The arrays can be connected to each other in parallel to enhance the photovoltaic system current (see Figure 2.7).



Figure 2.7: PV cell, module and array.

Power Electronic Inverters

Inverters are an essential part of PV-grid connected systems and can convert PV array DC power to AC power to supply the connected network. This procedure makes PV systems compatible with distribution networks and the majority of electrical appliances. There are two main types of power electronic inverters, pulse width modulated (PWM) voltage

source inverters and thyristor based line commutated inverters (TLCI). Figures 2.8 and 2.9 show the differences between them.

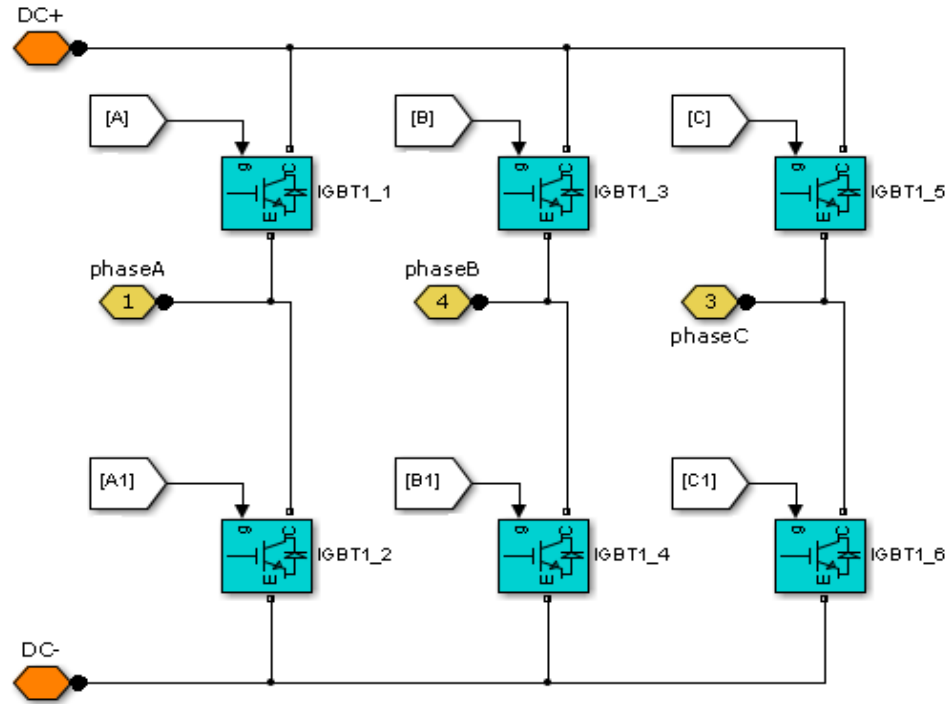


Figure 2.8: PWM voltage source inverter.

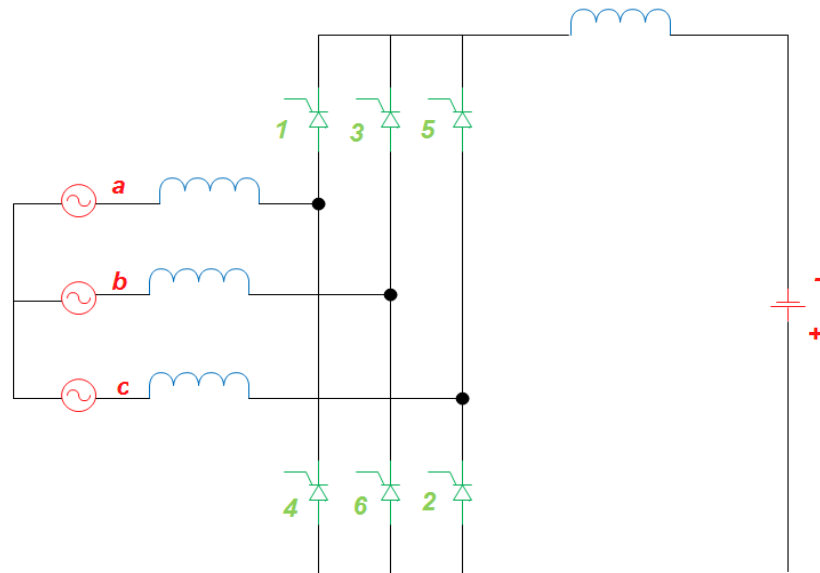


Figure 2.9: TLCI inverter.

The use of high quality sinusoidal PWM voltage source inverters has been increased in PV systems due to their fast real time control and the recent development of the MOSFET (Metal Oxide Semiconductor Field Effect Transistor) and IGBT (Insulated Gate Bipolar Transistor) to consider high power ratings. The magnitude of the input DC voltage is fixed in these types of inverters and the output voltage and frequency of the inverters can be controlled by pulse width modulation of the PWM inverter switches.

TLCIs (thyristor based line commutated inverters) are commonly used in many current PV systems due to their low cost and availability for high power levels. Changing the thyristor firing angle of this inverter can control the current drawn from the PV array and this helps in grid connected PV mode.

2.9 Photovoltaic Systems

Photovoltaic systems can provide clean energy for small or large utilities. PV systems can be classified as stand-alone and grid connected modes. Standalone PV systems are PV systems installed in isolated locations and operated independently of the utility grid. They are known as off-grid PV systems and are usually equipped with storage devices such as batteries. They can supply DC or AC loads with considering different control systems. The controller of a PV system which supplies a DC load uses a single stage DC/DC power electronic converter such as a buck, boost or buck-boost converter (see Figure 2.10). These converters also help in changing the voltage level and tracking the maximum power point (MPP). However, a two-stage control topology with storage devices is necessary to supply AC loads, as illustrated in Figure 2.11. The first stage consists of a DC boost converter to increase the PV voltage and track the MPP. A DC/AC inverter is used in the second stage to convert the DC power to AC power and it also enhances the AC power quality.

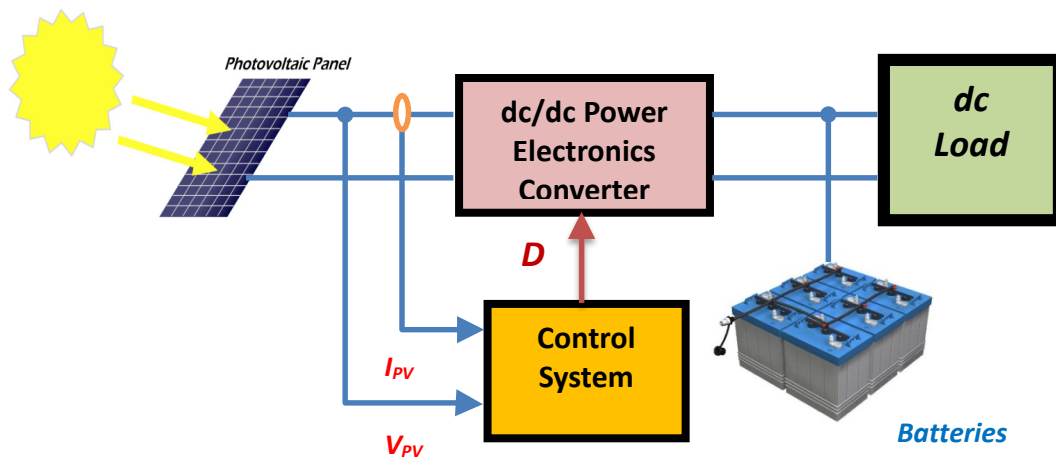


Figure 2.10: Block diagram of DC load supplied by a stand-alone PV system.

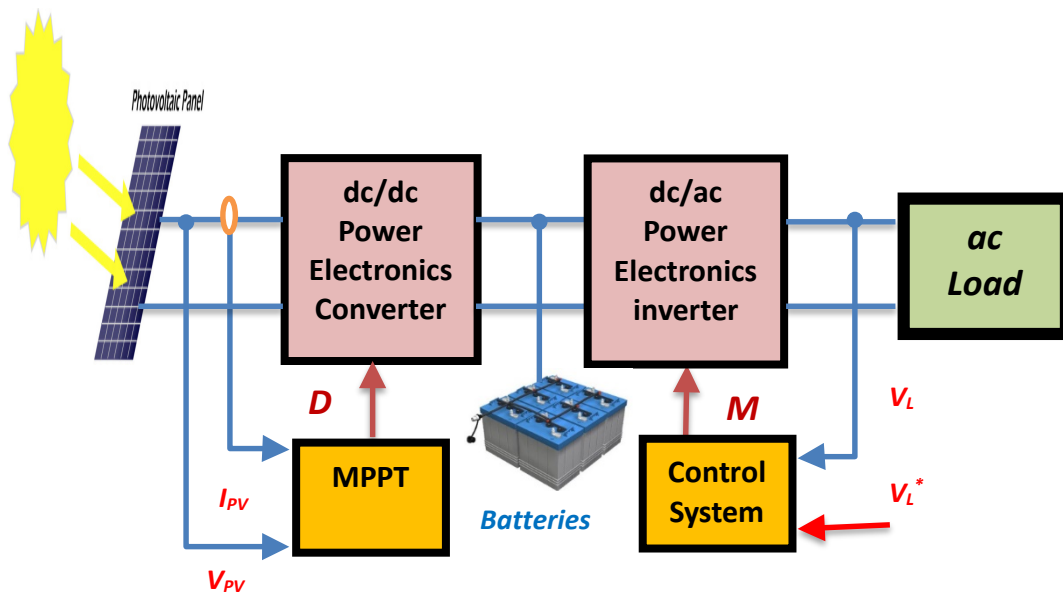


Figure 2.11: Block diagram of AC load supplied by a stand-alone PV system.

For grid-connected PV systems, single and two-stage topologies have been used. A single stage grid-connected PV system uses a single conversion unit known as a DC-AC inverter to obtain the MPP and connect the PV to the grid (see Figure 2.12). For this topology, a step up transformer is required to achieve the grid-requirements. This leads to a decrease in the efficiency and increase the cost. On the other hand, a two-stage grid connected PV system has two conversion steps, as shown in Figure 2.13, a DC/DC converter and a DC/AC inverter. The DC/DC converter could be buck, boost or buck boost and it is utilised to track the MPP and can change the PV output voltage. The second step is the

DC/AC inverter which regulates the DC link voltage and controls the power factor by synchronising the grid current and voltage.

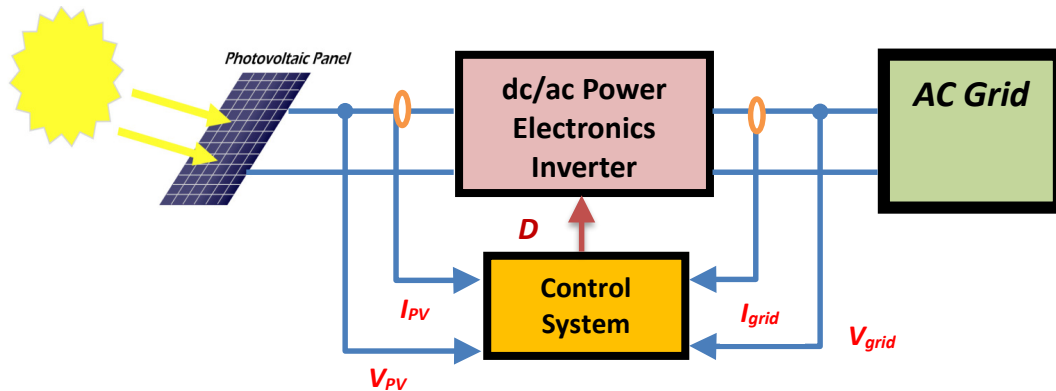


Figure 2.12: Block diagram of single-stage grid-connected photovoltaic system.

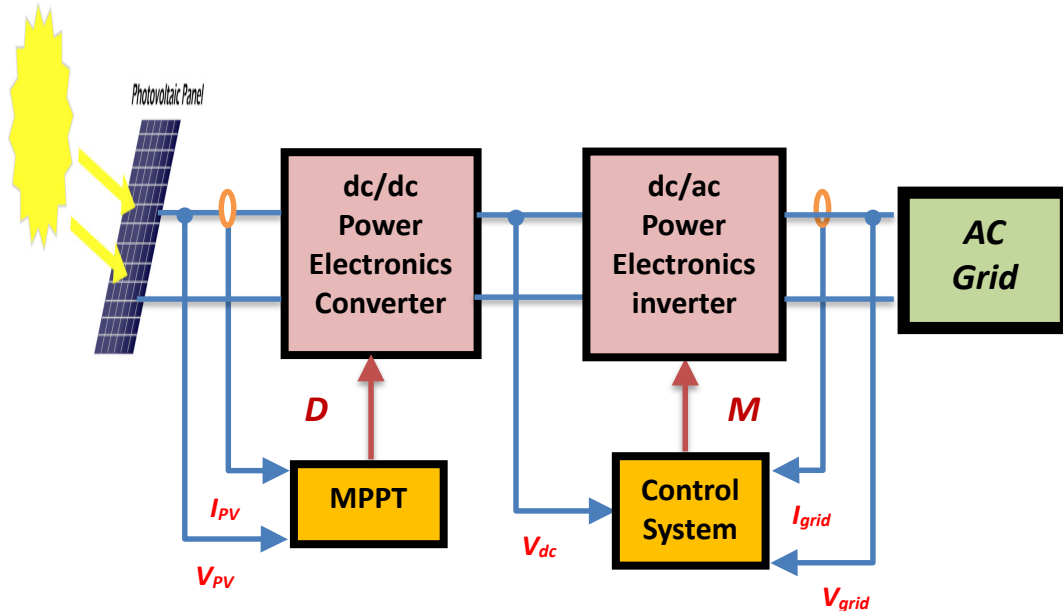


Figure 2.13: Block diagram of two-stage grid-connected photovoltaic system.

2.10 Photovoltaic Cells, Modules and Array Characteristics

A photovoltaic system consists of a solar array, which contains a set of series, and parallel connected modules. PV modules consist of groups of photovoltaic cells which are the basic components of PV systems. Figure 2.14 illustrates a photovoltaic array in detail.

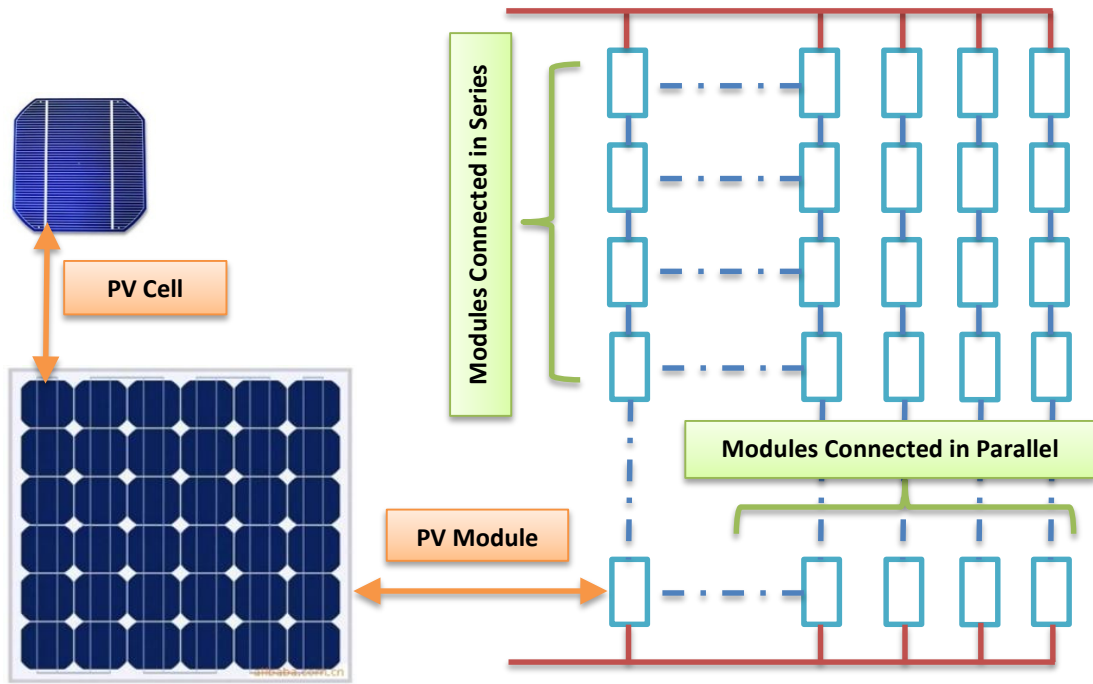


Figure 2.14: Photovoltaic array.

2.10.1 PV Cells Characteristics

The equivalent circuit of a solar cell is shown in Figure 2.15, consisting of a photocurrent, a diode, a series resistor to represent the internal resistance and a shunt resistor which models the leakage current.

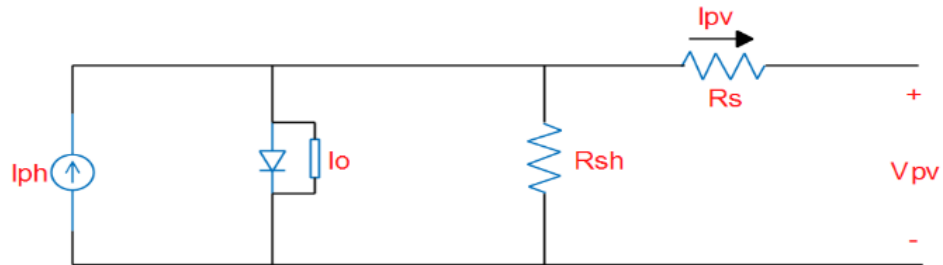


Figure 2.15: PV cell equivalent circuit.

From the photovoltaic cell equivalent circuit, a mathematical model of the generated PV current can be obtained as:

$$I_{pv} = I_{ph} - I_0 \left[e^{\left(\frac{q(V_{pv} + R_s I_{pv})}{AkT} \right)} - 1 \right] - \frac{(V_{pv} + R_s I_{pv})}{R_{sh}} \quad (2.1)$$

Where I_{ph} is the light generated current and the reverse saturation current is I_o . q is the electron charge which equals $1.6 \times 10^{-19} \text{C}$ and A is the junction material factor called the ideality factor, ranging from 1 to 2. T is the junction temperature measured in Kelvin and k is the Boltzmann constant which is $1.38 \times 10^{-23} \text{J/K}$. The solar cell series and shunt resistances are R_s and R_{sh} respectively. I_{pv} and V_{pv} are the photovoltaic output current and voltage respectively.

2.10.2 PV Modules Characteristics

To get a desired working voltage and current, a group of series solar and parallel cells should be connected together to form a PV array. The photovoltaic model rating is determined by its DC output power under standard test conditions (STC). Typically, the commercial STC is set at 25°C solar cell temperature and 1000 W/m^2 solar irradiance at a 1.5 (AM) spectral distribution of air mass [87]. Usually the current–voltage (I – V) and the power–voltage (P – V) characteristics are used for evaluating the performance of the PV system respectively. The characteristic curves (P – V and I – V) of the PV system are considerably influenced by the variations in solar irradiance and temperature, as shown in Figures 2.16 and 2.17.

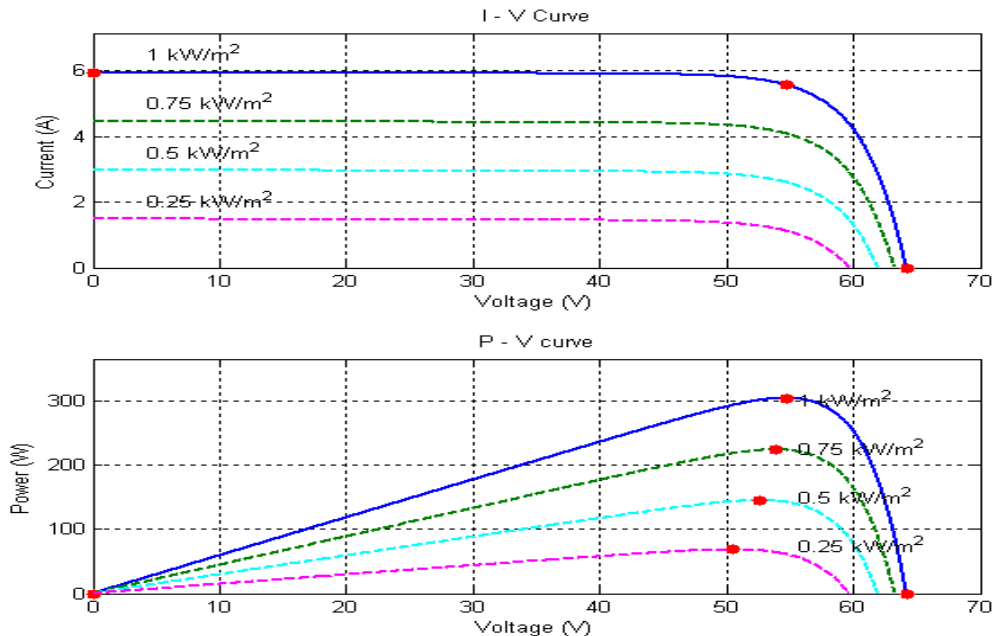


Figure 2.16: The effect of solar irradiance on I-V and P-V curves.

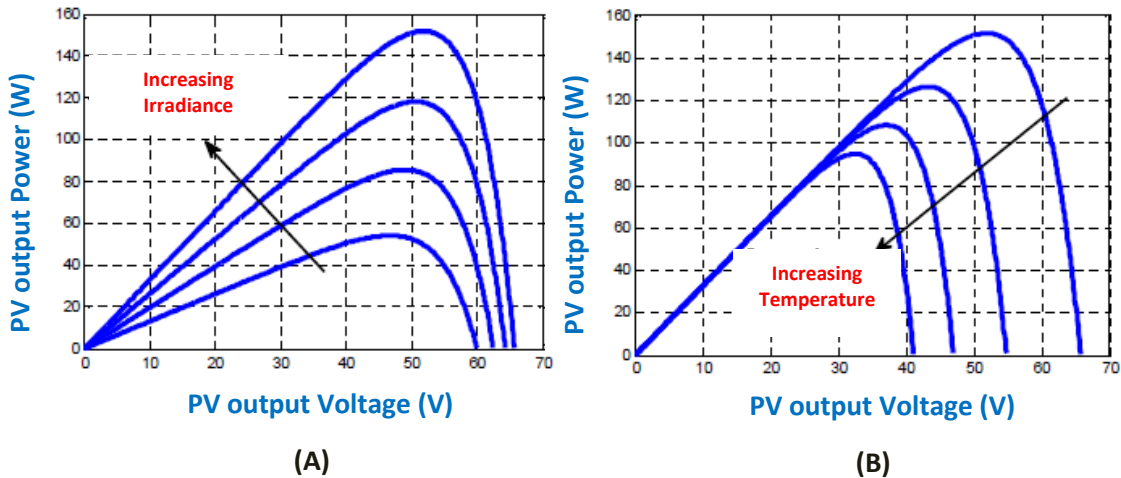


Figure 2.17: The impact of solar irradiance and temperature on P-V curves.

2.10.3 PV Arrays Characteristics

To get a sufficient voltage and current, a group of series and parallel PV modules should be connected, representing a photovoltaic array. The size of a PV array depends on the number of PV modules which are connected in a given PV system. Output current and voltage of the PV array can be determined by equations 2.2 and 2.3 respectively. The PV array characteristics can be evaluated by multiplying the PV module output current by the number of parallel strings and multiplying the PV module output voltage by the number of series modules in the individual string.

$$I_{pva} = I_{pv} * n_p \quad (2.2)$$

$$V_{pva} = V_{pv} * n_s \quad (2.3)$$

Where I_{pva} and V_{pva} are the PV array output current and voltage respectively. I_{pv} and V_{pv} are the PV module output current and voltage respectively. The number of parallel strings is n_p in the PV array and n_s is the number of series PV modules in one string.

Three important operating points should be considered - Open Circuit Voltage (V_{oc}) at point A, Short Circuit Current (I_{sc}) at point B, and Maximum Power Point (MPP) at point C - when designing a PV array, as shown in Figures 2.18 and 2.19. The PV module type and parameters are illustrated in Table 2.2.

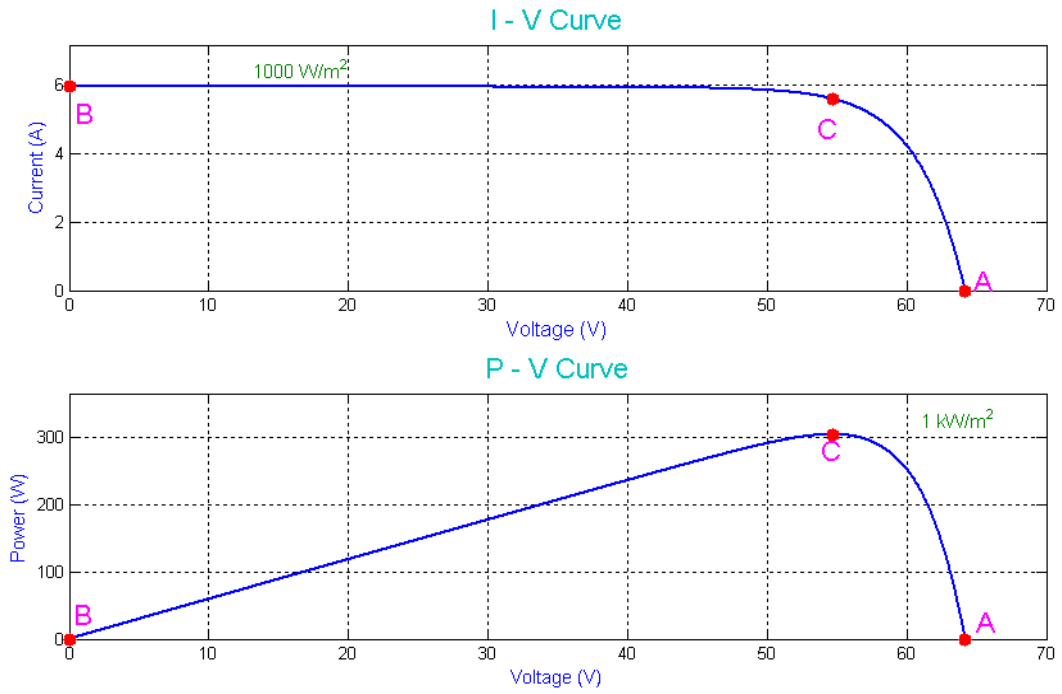


Figure 2.18: $I - V$ and $P - V$ characteristics curves for one module at STC.

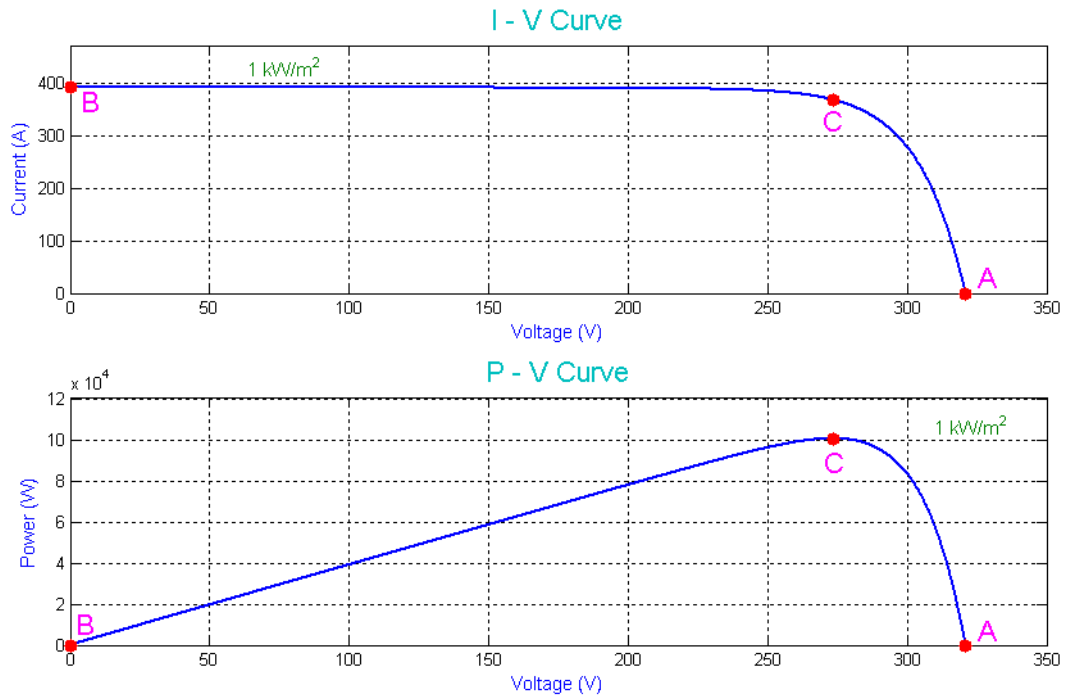


Figure 2.19: $I - V$ and $P - V$ characteristics curves for one array at STC.

Table 2.2: PV module characteristics under STC.

Module Type	SunPower SPR-305-WHT
Number of Cells per Module	96
Number of Series Connected Modules per String	5
Number of Parallel Strings	66
Open Circuit Voltage (V_{oc})	64.2 V
Short Circuit Current (I_{sc})	5.96 A
Voltage at Maximum Power Point (V_{mpp})	54.7 V
Current at Maximum Power Point (I_{mpp})	5.58 A
Series Resistance (R_s)	0.038 ohm
Shunt Resistance (R_{sh})	993.51 ohm
Saturation Current (I_0)	0.118 nA
The Light Generated Current (I_{ph})	5.96 A

Open Circuit Voltage (V_{oc})

The open circuit voltage is shown in Figure 2.18 at the operating point A. The open circuit voltage can be obtained by neglecting I_{sh} (shunt current) (see Figure 2.20).

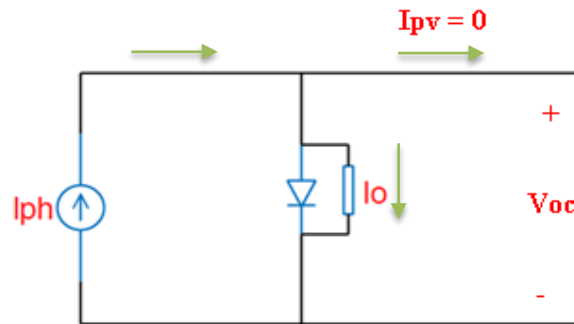


Figure 2.20: Open circuit condition.

From the above figure, the open circuit voltage can be calculated using equation 2.5 as:

$$I_{ph} - I_0 \left[e^{\left(\frac{q(V_{oc})}{AkT} \right)} - 1 \right] = 0 \quad (2.4)$$

Then,

$$V_{oc} = \frac{AkT}{q} \ln \left(\frac{I_{ph} + I_0}{I_0} \right) \quad (2.5)$$

Short Circuit Current (I_{sc})

In Figure 2.18, the short circuit current is shown at the operating point B. The short circuit condition can be obtained by neglecting (R_s) series resistance (see Figure 2.21) and it can be determined by equation 2.6.

$$I_{sc} = I_{ph} \quad (2.6)$$

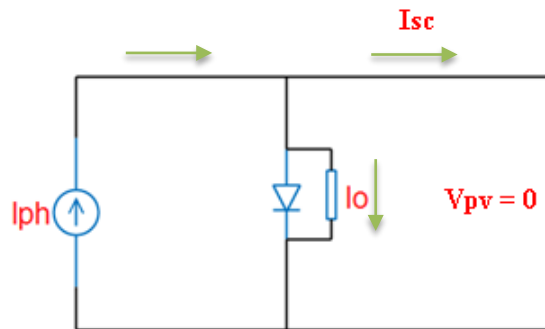


Figure 2.21: Short circuit condition.

2.11 Solar Irradiance

Solar irradiance can be defined as the radiant power incident per unit area on a specified surface and it is measured in W/m^2 . Radiant power is expressed as the rate of flow of electromagnetic energy and sunlight containing many electromagnetic waves of a wide spectrum. These waves include different photons with different energies which travel at a constant speed (c), represented as the speed of light. The photon energy can be calculated according to equation 2.7. The longer the wavelength, the smaller the amount of energy that can be obtained.

$$E = \frac{hc}{\lambda} \quad (2.7)$$

Where, E is photon energy measured in J, h is Plank's constant 6.63×10^{-34} J.s, c is light speed 3×10^8 m/s and λ is the wavelength of radiation measured in m.

The solar irradiance intensity on the earth's horizontal surface is approximately constant at 1350 W/m^2 when the entry point into the atmosphere is directly outside the earth. The entry point into the atmosphere is called AM or air mass.

2.12 Maximum Power Point Tracking (MPPT)

As shown in the previous sections, the characteristic curves ($P - V$ and $I - V$) of a PV system are considerably influenced by variations in solar irradiance and temperature, as shown in Figures 2.16 and 2.17. As a result, a maximum power point tracker (MPPT) is essential to solve these problems and ensure that the photovoltaic system generates the maximum available power.

There are several MPPT techniques that have been discussed in literature, such as simple panel load matching, incremental conductance, constant voltage, constant current, perturbation and observation, hill climbing, ripple correlation control, the fuzzy logic controller, and artificial intelligence techniques [88, 89]. These MPPT methods require algorithms to determine the maximum power point and they vary in accuracy, simplicity, time response and cost. There have also been several techniques proposed to solve partial shading problems using advanced optimization methods such as particle swarm [90].

Hill climbing is the most commonly used technique in tracking the maximum PV output power due to its low cost, simplicity and straightforward utilization. This thesis considers the hill climbing method as the MPPT technique in the model of the PV system, for the aforementioned reasons. Unlike Perturb and Observe (P&O) MPPT method which involves a perturbation in the operating voltage of the PV array, Hill climbing basically works by perturbing (changing) the PV power converter duty cycle (D) and observing the effect of this change on the output power of the PV system. After each perturbation/observation iteration the MPPT decides the new direction of the duty cycle (positive or negative) to track the maximum available power. If the output power $P(k)$ is greater than the pre-set value $P(k-1)$, the duty cycle is increased and vice versa (see the flowchart of the hill climbing MPPT technique in Figure 2.22). A comparison on photovoltaic array maximum power point tracking techniques was discussed in literature

such as [89] and explained in details how hill-climbing method works. The duty cycle of the power converter is the fraction of the commutation period T the switch is on and it depends on the ratio of input to output voltage as shown in equation 2.8. Table 2.3 illustrates the relationship between the maximum output voltage of the boost converter (V_{out}), the input voltage (V_{in}) and the duty cycle D . In real application, the duty cycle of the converter is less than 0.9 [91]. The impact of using the hill climbing MPPT technique on the power converter duty cycle and PV output power is shown in Figures 2.23 and 2.24 respectively.

$$D = 1 - \frac{V_{in}}{V_{out}} \quad (2.8)$$

Table 2.3: The maximum output voltage of the boost converter (V_{out}) dependent on D .

Duty cycle D	0.5	0.75	0.8	0.9
V_{out}	$2 \times V_{in}$	$4 \times V_{in}$	$5 \times V_{in}$	$10 \times V_{in}$

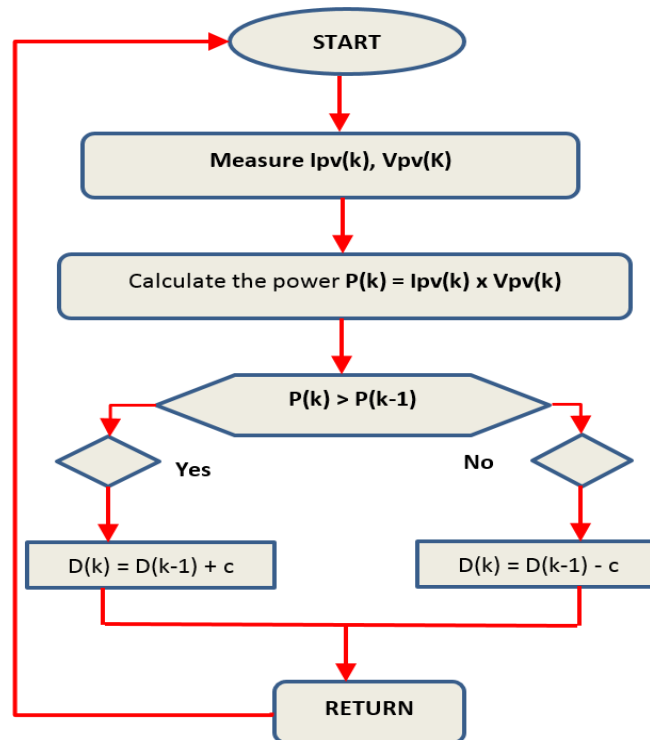


Figure 2.22: The flowchart of the hill climbing MPPT technique.

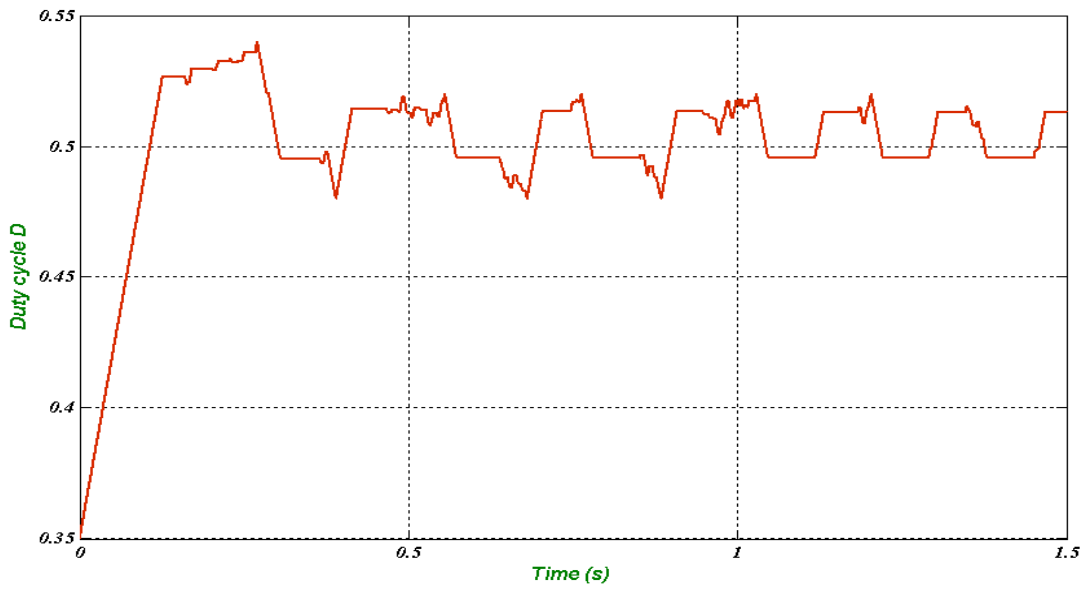


Figure 2.23: Power converter duty cycle (D) using hill climbing MPPT technique.

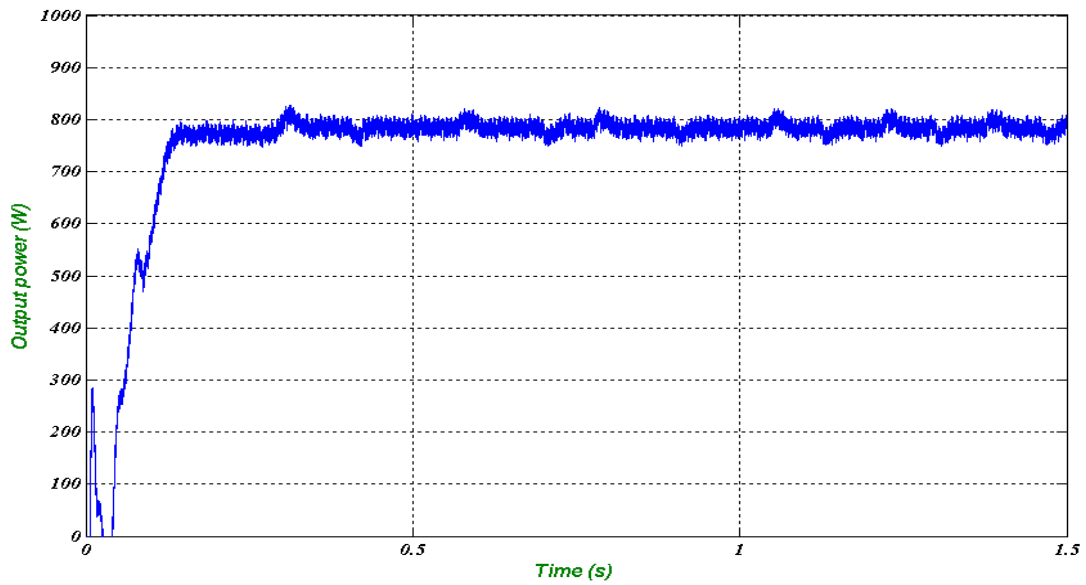


Figure 2.24: PV output power using hill climbing MPPT technique.

2.13 Challenges of Photovoltaic Technology

In this section, the requirements and limitations of large-scale PV energy generation will be discussed, such as the amount of land and raw materials needed, reliability, system efficiency, grid codes and payback time.

2.13.1 Land for PV

To calculate how much land is needed to install a PV system, the capacity factor concept of fossil-fuel power plants can be used. The capacity factor (CF) concept is the ratio of the energy actually produced by the power plant over the rated power times the number of hours per year, i.e. 8760 h, as illustrated in equation 2.9.

$$CF = \frac{\text{The energy actually produced}}{\text{Rated power} \times 8760} \quad (2.9)$$

For instance, if one MW generator generated 6000 MWh per year, its corresponding capacity factor would be 0.68. The capacity factor is usually less than one because the power plant may need to stop for certain periods for maintenance or as a management order from the system operator. In typical power systems, base load is usually supplied by power plants with relatively low fuel costs and they typically have 0.7 capacity factors or more. Renewable energy sources such as PV and wind usually have lower capacity factors depending on their locations due to their intermittent nature of operation and the fact that they can operate to supply peak demands (see Figure 2.25). In the UK, the average capacity factor of wind units is 28.42 per cent in the past five years [92], while 9.7 per cent is the typical annual capacity factor for photovoltaics based on solar energy [93].

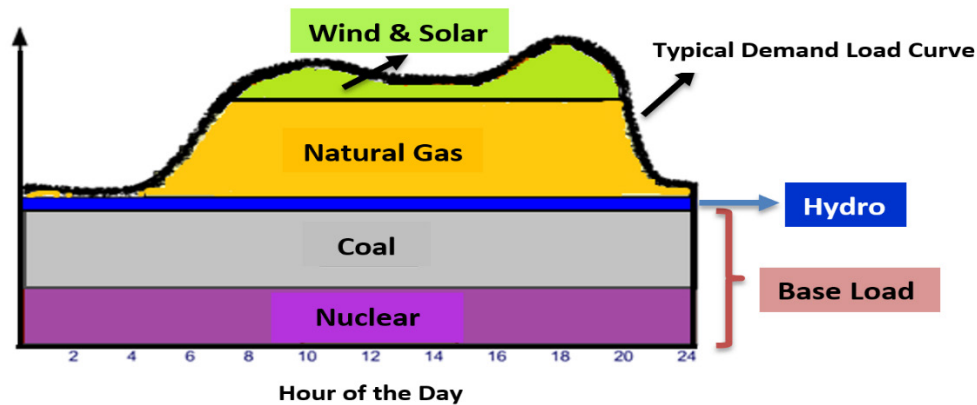


Figure 2.25: Typical power supply and demand load curves.

The capacity factor for PV units ranges from 8% (0.08) for fixed PV modules in Hamburg to 26% (0.26) in Albuquerque in Mexico with PV sun tracking [77]. In 2013, the average PV capacity factor was 0.102 in the UK [94] and EPIA analysis assumes the PV average

capacity factor to be 12-17%. In the UK, household electricity consumption is about 5.4 kWh/day/person, or 27 kWh/day per family of five. If the CF of the PV unit is 0.15, this household load demand can be met with a photovoltaic installation of $27 / (0.15 \times 24) = 7.5$ kW. For a rated PV module (panel) efficiency of 13% (0.13×1000 W/m²), land needed will be $7500 / 130 \approx 58$ m² of PV panels. Various common PV modules which are available in the UK market are listed in Appendix A.

2.13.2 PV Raw Materials

There should be enough raw materials on Earth to make PV panels to generate a significant fraction of global electricity needed in the future. Silicon has been the main material used to make solar cells in recent years. It is the second most abundant material on Earth, as mentioned in section 2.8. Therefore, there will be no shortage in finding silicon and the current production of silicon is around 50 times greater than that required for PV cell manufacturing. Also, non-silicon solar cells have several limitations and constraints.

2.13.3 Reliability

PV systems consist of four main components: a PV panel, power electronic devices (DC/DC converter and/or DC/AC inverter), a PV system controller and storage devices such as batteries. Failure in a PV system's components may occur similar to any other electrical equipment due to occasional failures or accidental events. These failures result in significant economic loss and show the importance of the reliability of PV systems to both utilities and customers. Over the past few years, the reliability of PV modules has been improved considerably and they now have a long lifetime (up to 30 years) [95]. However, power electronic devices have low reliability in PV systems as they can easily be influenced by any disturbances in the grid or during scheduled maintenance. Therefore, protection devices must be used to avoid any failure event of the electric power circuit.

Florida Solar Energy Centre [96] published reliability data from 1999-2003 on 103 grid-connected PV systems that used PV arrays from 9 manufacturers; 176 inverters from 4 manufacturers confirmed that most of the failure events were due to the inverters. Also, 213 reliability events had been recorded on these 103 PV systems indicating that 65% of these failures were caused by inverters. One of the main causes of an inverter failure event

is the inverter heat extraction mechanisms for semiconductors switches and thermal management systems. Inverter components such as switches and capacitors are very sensitive to temperature and this makes inverter thermal management one of the main reliability issues for PV inverters. However, the reliability of new inverters has been steadily improving as inverter manufacturers have solved some of the above problems. They have tried to extend inverter lifetimes and ensure that inverters work adequately over their warranty period [97].

Energy storage would solve the problem of PV intermittency, which depends on solar irradiance. Storage devices such as batteries are essential components in PV systems to supply a continuous and high quality electricity in many PV application systems with critical loads, such as medical and telecommunication systems. Lead acid batteries are the most commonly used storage devices in PV systems due to their low cost and availability. In extreme weather conditions, particularly cold, and for smaller applications, lead acid and nickel (Ni-Cd) batteries are highly preferred. These storage devices should be selected and managed properly in PV systems to increase their lifetime, thus resulting in great overall PV system reliability [98].

2.13.4 PV System Efficiency

To study the overall efficiency of a PV system, the efficiency of the main PV components should be considered: the PV module efficiency, the efficiency of the DC/AC inverter and the MPPT controller. In a grid-connected PV system, transformer efficiency should also be considered. Solar cell efficiency was 1-2 % in the past to convert sunlight into electricity because most of the sunlight was reflected or dissipated by the cell's materials. The efficiency of a PV cell is the ratio of the power output in (W) of a PV cell to the incident energy in the form of sunlight. Equation 2.10 describes this relationship.

$$\% \eta = \frac{P_{output}}{P_{input}} = \frac{P_{MPP}}{E \times AC} \quad (2.10)$$

$$\% \eta = \frac{I_{MPP} \times V_{MPP}}{P_{input}} = \frac{I_{sc} \times V_{oc} \times FF}{P_{input}} \quad (2.11)$$

Where, η is solar cell efficiency, P_{MPP} is the power at the maximum power point in W, E is solar irradiance (input light in W/m^2) and A_c is solar cell surface area in m^2 . I_{MPP} and V_{MPP} are the current and voltage at the maximum power point in Ampere and Volt respectively. I_{sc} and V_{oc} are the short circuit current and open circuit voltage in Ampere and Volt respectively. FF is defined as the ratio of the maximum power from the solar cell to the product of open circuit voltage (V_{oc}) and short circuit current (I_{sc}). It is directly affected by the series resistance (R_s) and shunt resistance (R_{sh}) of the PV circuit. Typical commercial solar cells has a fill factor greater than 0.7. Solar cells with a high fill factor have a low series resistance and a high shunt resistance of the PV circuit to decrease internal losses [99]. Increasing R_{sh} and decreasing R_s leads to a higher FF, thus resulting in great efficiency.

In recent years, the solar cell industry has developed considerably and the efficiency of solar cells varies from one technology to another. Cost and efficiency of solar cells are directly linked. Highly efficient cells require expensive single-crystal semiconductor material and they use advanced structures to decrease energy losses. Around 91% of the global PV market uses single-crystal Si cells [100]. Thin film solar cells use less material and they are cheaper; however, they have low efficiency conversion. Table 2.4 and Figure 2.26 illustrate the cell conversion efficiency of current PV cell technologies [101].

Table 2.4: Solar cell efficiency of different technologies.

Solar Cell Technology	Cell Efficiency %
Multi-junction cells	31.1 – 44.7
Single junction GaAs	26.4 – 29.1
Crystal Silicon cells	20.4 – 27.6
Thin Film	13.4 – 23.3
Emerging PV such as Organic	8.6 – 17.9

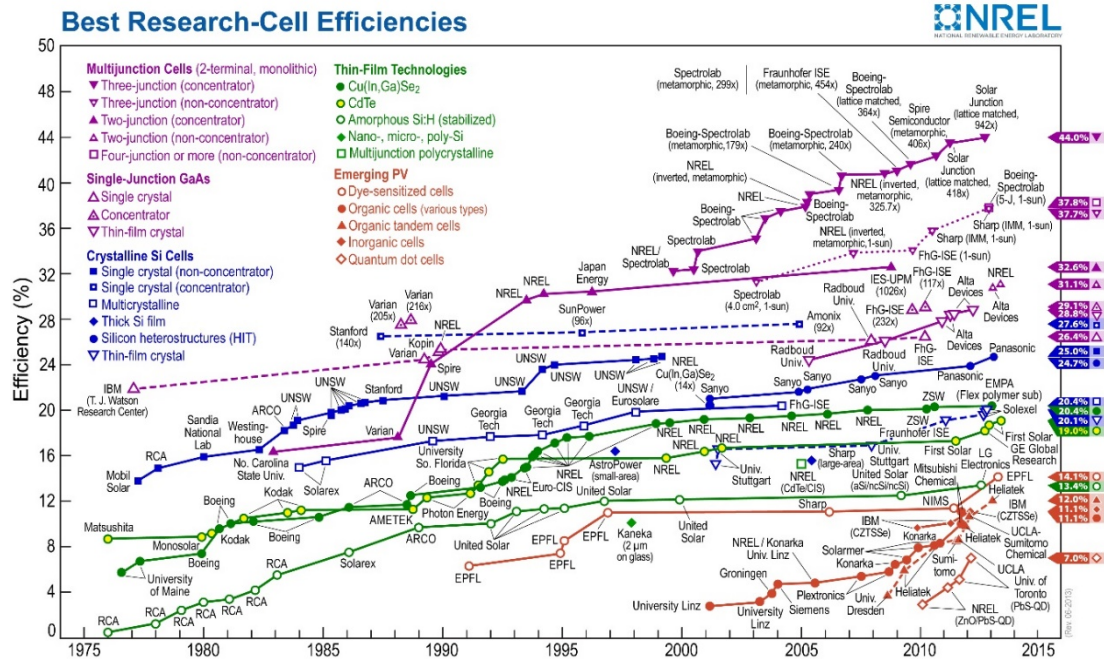


Figure 2.26: Best research solar cell efficiencies [101].

The power electronics efficiency depends on the topology of the PV system. There are two commonly used power electronics topologies: single-stage and two-stage. The PV system uses a single conversion unit (DC/AC inverter) in single-stage topology, whilst it uses a two conversion unit in two-stage - DC/AC inverter and DC/DC converter - to boost the DC PV output voltage and track the maximum power point. The DC/AC inverter in both topologies is used to interface the PV system to the load or grid. However, it is also used as an MPPT in single-stage topology and it delivers the maximum power into the grid with high efficiency, low cost and smaller size. Two-stage PV system topology is less efficient, has a larger size and higher costs due to the need for two conversion units and transformers in some cases. Conversely, higher PV array voltage is not essentially needed in two-stage topology because of the amplification stage. The PV modules are also decoupled from the output power ripple in this stage and allow the system to operate under a wide voltage range.

The relationship between the PV output power and current characteristics are nonlinear and can be affected considerably by temperature and solar irradiance. A Maximum Power

Point Tracker (MPPT) is necessary to solve this problem and ensure the PV system generates the maximum available power. The MPPT technique is significant to PV system overall efficiency, especially during partially shaded conditions. Using a conventional MPPT such as hill-climbing, incremental conductance and ripple correlation during partially shaded conditions can cause considerable loss of photovoltaic output power [102].

2.13.5 Grid Code Requirement for PV

Grid-connected PV installations have grown dramatically in recent years and PV systems from a few kW to multi-MW are now considerably penetrated in distribution systems. This trend makes solar generation based on photovoltaic technology a significant source of Distributed Generation (DG) and a series of standard requirements and regulations should be provided in order to ensure system reliability and safety.

PV design and operation should be compatible with grid requirements and regulations. In power systems with high PV penetration, grid requirements play a significant role to ensure system security and reliability, and frequent updating in PV regulations are highly recommended to enhance the PV technology in power systems. Great efforts have been made globally to impose several standards for PV grid-connection requirements that can be applied by different countries and regions. However, local system operators impose local requirements in most countries.

The IEEE (Institute of Electrical and Electronic Engineers), IEC (International Electrotechnical Commission) and Electronic and Information technologies of DIN and VDE in Germany (the dominant PV market until 2012) are the most relevant international organisations developing and imposing global standards for PV grid-requirements [27]. In recent years, IEEE 1547 and IEC 61727 are the most important and commonly used standards to regulate PV grid-connections in European and US markets. Nowadays, IEEE 1547-2003 [103], the Standard for Interconnecting Distributed Resources with Electric Power Systems, is used as an interconnection standard for all DG technologies. IEEE 1547 deals with the testing and technical specifications for the DG interconnection. The IEEE 1547 standard focuses on general requirements and covers power quality, response to

abnormal conditions, islanding requirements, design and production requirements and other issues. This standard is applicable for interconnection at typical distribution levels (medium voltages) and it also considers low voltage levels of distributed networks. The IEC 61727 standard, called Photovoltaic (PV) Systems-Characteristic of the Utility Interface, published in December 2004, sets requirements for PV systems' standard interconnection to utility distribution systems [104]. The IEC 61727 standard agrees with the IEEE 1547 in the most critical issue of PV connection, which is anti-islanding detection. Table 2.5 gives highlights of the IEEE 1547 and IEC 61727 regulation standards.

Table 2.5: Highlights of IEEE 1547 and IEC 61727 regulation standards.

Standard Requirement	IEEE 1547		IEC 61727	
Voltage Range and Disconnection Time for Voltage Variations	$V < 50\%$	0.16 s	$V < 50\%$	0.1 s
	$50\% \leq V < 88\%$	2.0 s	$50\% \leq V < 85\%$	2.0 s
	$110\% < V < 120\%$	1.0 s	$110\% < V < 135\%$	2.0 s
	$V \geq 120\%$	0.16 s	$V \geq 135\%$	0.05 s
Frequency Range and Disconnection Time for Frequency Variations	$59.3 < f < 60.5$ Hz	0.16 s	$f \pm 1$ Hz	0.2 s
Harmonic Current (order-h) Limits	$h < 11$	4.0%		
	$11 \leq h < 17$	2.0%		
	$17 \leq h < 23$	1.5%		
	$23 \leq h < 35$	0.6%		
	$h \geq 35$	0.3%		
	Note: Even harmonics should be < 25% of the odd harmonic limits listed here. Total Harmonic Distortion (THD) 5.0%			
DC Current Injection	< 0.5% of rated RMS current		< 1.0% of rated RMS current	

In the UK, the Distribution Network Operator (DNO) should agree any connection to local distribution networks to ensure system safety, performance and quality of supply. G59/2 and G83/2 are engineering recommendations for connection. Grid connection regulation standards in the UK are summarised in Table 2.6 [105]. Each PV installation in the UK should be approved by the UK MCS (Microgeneration Certification Scheme), which is the certification mark for on-site sustainable energy technologies.

Table 2.6: UK distributed generation standards guide.

Standard	Description
G83/2	Recommendations for the connection of small scale embedded generators (typically ≤ 16 Ampere per phase) in parallel with public low voltage distribution networks.
G59/2	Recommendations for the connection of generating plant to public electricity suppliers' distribution systems.
G75/1	Recommendations for the connection of embedded generating plant to public distribution systems (> 20 kV) or with outputs (> 5 MW).
ETR113	Notes of guidance for the protection of embedded generating plant up to 5 MW for operation in parallel with public electricity suppliers' distribution systems.

2.13.6 PV Payback Time

PV energy payback time (PV-EPT) is defined as the number of years that the PV system must operate to recover the energy spent in manufacturing. All the energy generated after the payback time is new energy. PV-EPT has dramatically decreased over recent years and studies show that the EPT for crystalline silicon PV systems is between 1.5 and 2.5 years, whilst it is 1 to 1.5 years for thin films [106].

Economic payback time is defined as how long an investment takes to repay the initial outlay. With photovoltaic technology, the sunnier the climate, the quicker the PV system will pay itself back. Local authorities or the government may provide promotions and incentives to encourage investment in PV such as FIT and ROC (Renewable Obligation Certificate) in the UK. As of the end of November 2015, the UK's overall PV cumulative installed capacity exceeded 8.4 GW according to the Department of Energy & Climate Change in the UK. However, the international energy Agency (IEA) said that the future for UK renewables such as solar-PV is less optimistic that it was a year ago because of uncertainty over government policy after their recent announcement about changes to renewable subsidies [107].

Banks may also offer loans with low interest rates to install PV units. The payback time can be calculated using a discount cash flow analysis. In 2010, 10 to 20 years was the economic payback time for an investment in a PV system installation [108]. In recent years, the cost of PV systems based on solar energy has decreased steadily; the average price per watt of a PV module decreased by 65-70% from 2009 to 2013 (IRENA). When the PV installation cost decreases, the economic payback will also decrease.

2.14 Conclusions

In recent years, there has been significant concern regarding increasing the penetration of renewable generation in power systems to reduce greenhouse gas emissions and meet renewable energy portfolio targets. Solar energy based on photovoltaic technology is one of the main renewable resources in distribution networks and there is rapid growth in utilising PV as an alternative power producer. There has been significant development in the photovoltaic industry in the last few years and 140 GW was installed in just the last four years compared to around 40 GW installed beforehand. The year 2014 was a historic year for the PV industry as the total cumulative installed capacity exceeded 178 GW.

This chapter discussed the history of solar energy and the evolution of the photovoltaic industry. The potential and benefits of PV were also discussed and the dramatic increase in photovoltaic installed capacity in Europe and various countries was investigated. Environmental and economic issues related to PV were also discussed in this chapter and compared to conventional power plants. Current photovoltaic technologies were presented and how a PV system works was illustrated. PV cells, modules and arrays were investigated and the differences between them highlighted. The impact of solar irradiance and temperature on PV system operation was discussed in this chapter, as well as the necessity of using a Maximum Power Point Tracker (MPPT) to get the maximum available power. The hill climbing MPPT technique was investigated and its advantages and disadvantages were mentioned. Various challenges and barriers to enhancing photovoltaic technology in power networks were also discussed in this chapter.

CHAPTER 3 Wind Energy

3.1 Introduction

In recent years, demand for electricity has grown yearly due to modernisation, automation and economic growth, and it is expected to double by the year 2050 [73]. It is important to increase power generation capacity to meet this rapid increase in demand and to reduce carbon footprints at the same time. Decreasing greenhouse gases is a global environmental concern and several countries have agreed to the Kyoto Protocol [5], setting reduction targets such as an 80% reduction in greenhouse gas emissions by 2050 in the UK [109]. Low carbon technologies such as wind power will make a significant contribution towards meeting these reduction targets. Many countries have come up with several policies and regulations to increase renewable energy, such as the Renewable Electricity Standard (RES) known as the Renewable Portfolio Standard (RPS). The RPS is designed to increase renewable generation in the power sector and it sets a minimum requirement and percentage for providing electricity from renewable resources by a certain date/year [110].

Among the many renewable resources, wind power is one of the most promising and competitive generating source due to its mature and advanced technologies. Wind power generation has increased substantially in recent years and it has now become a mainstream option for new power generation. More than 90 countries around the world have installed commercial wind power generation, with more than 318 GW of total installed capacity at the end of 2013 which represents around 3% of total power generation globally [111].

The wind power industry has developed dramatically and wind power is now the least costly technology for new capacity in power systems and prices continue to decrease. It is estimated that wind power generation could reach 2 TW by 2030 and this capacity could be doubled by 2050, as illustrated in Figure 3.1. This trend could provide 25-30% of the global power supply [111]. The electricity sector is responsible for around 25% of total greenhouse gases and 40% of total CO₂ emission is produced from burning fossil fuels. It has been shown [111] that wind power could also save more than 3 billion tonnes of CO₂

per year. All these numbers show how important wind power generation is to the power sector.

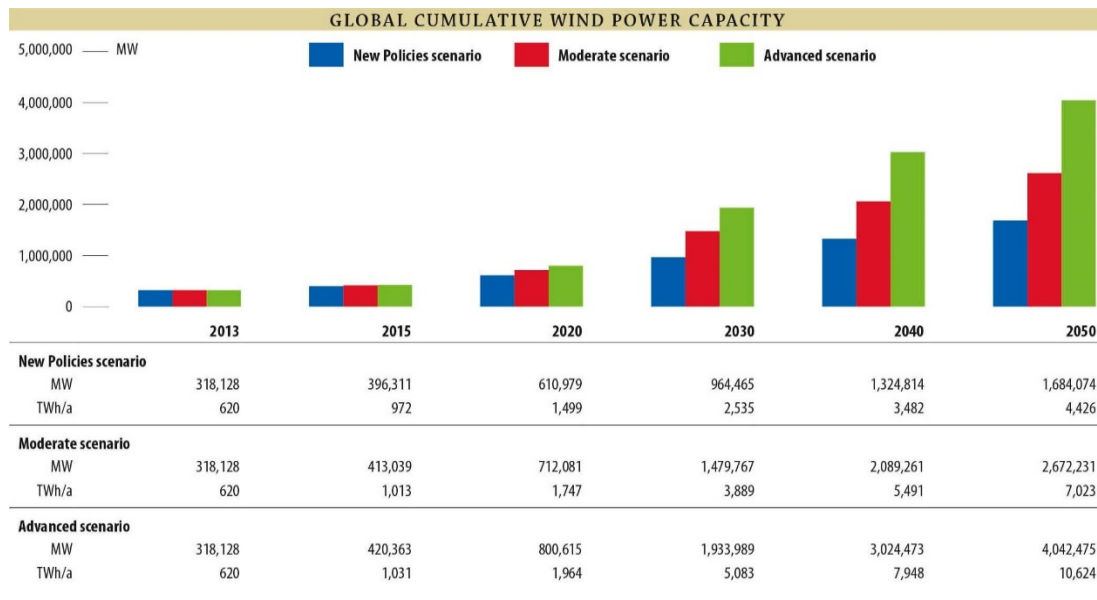


Figure 3.1: Global cumulative wind power capacity [111].

3.2 Wind Energy Background

Wind energy technology is not a new technology and has been used since early recorded history. Windmills were widely used in food production in the Middle East (Arab countries) and the surrounding areas [112]. The use of wind power increased through history and in the 1850s, the US Wind Engine Company was established by Daniel Halladay and John Bumham, who built the Halladay Windmill. James Blyth of Anderson’s College, Glasgow (now known as the University of Strathclyde), built the first windmill used for electricity generation in Scotland in 1887. Danish scientist Poul La Cour built a wind turbine in 1891 to produce electricity and converted his windmill into a prototype power plant to light Askov Village. The dramatic developments in generator, motor and electric appliances designed by Edison, Tesla and others increased the improvement of wind power, especially for remote locations. In 1888, 12 kilowatts of Direct Current (DC) for battery charging at variable speed was produced by the Brush wind turbine in Cleveland [113]. In the late 1890s, windmills became even more efficient due to the invention of steel blades. Total wind power in Denmark reached 30 MW by

1900 and this was a record in that era. The developments in wind power continued and in the 1940s the largest wind turbine was in operation on Vermont Hilltop, generating 1.25 MW to feed a local utility network.

In the 1970s, research was carried out into power generation by wind turbines due to an increase in oil prices. Variable speed wind turbines tied to an AC grid were developed in the early to mid-1970s and became a viable reality [114]. Larry Viterna and Bob Corrigan developed ‘The Viterna Method’ in 1981 and this method became one of the most common methods used to predict wind turbine performance. Since then, wind power technology has continued to develop and several countries have increased their incentives to use this technology for power generation. Nowadays, wind power technology is one of the main electric power resources and it has increased dramatically to ensure sustainable development. The largest wind turbine came online in January 2014. It is known as Vestas V164 and can generate up to 8 MW. The largest onshore wind farm in 2014 was Alta (Oak Creek-Mojave) in the US, with a 1.32 GW capacity, and the largest offshore wind farm is London Array in the UK, with a 630 MW capacity. Figure 3.2 shows the increase in the size of wind turbines since 1985.

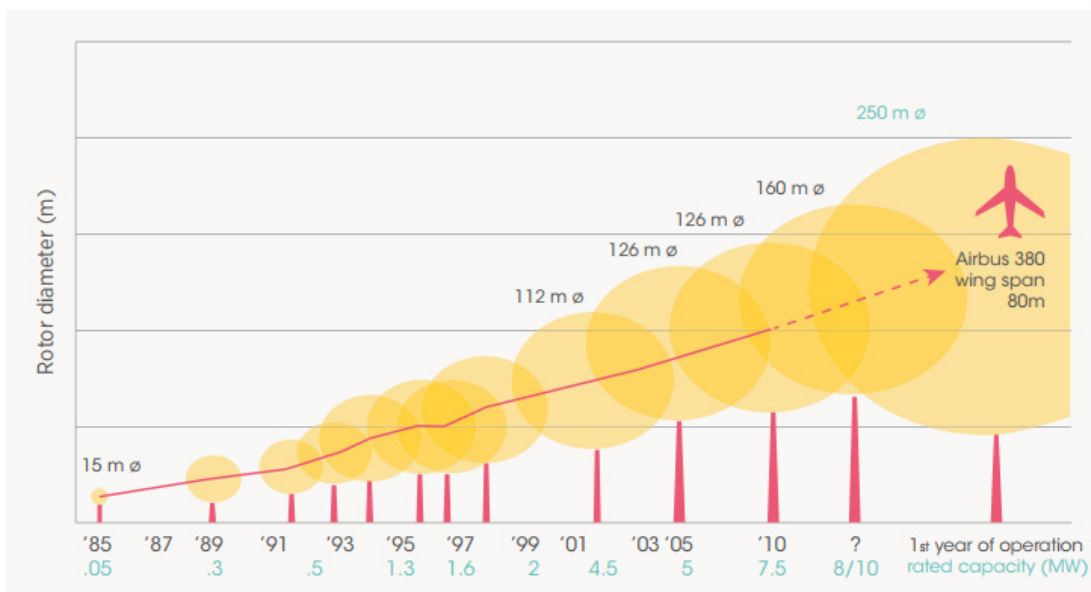


Figure 3.2: The increase in the size of wind turbines since 1985 (Source: UpWind, 2011).

3.3 Wind Power Potential and Benefits

According to the Global Wind Energy Council (GWEC) [115], the number of operating wind turbines globally was 268 thousand at the end of 2014 and there is now around 22 MW installed capacity of wind power per 1000 km of land area in Europe. Wind power has increased rapidly and many people are in favour of it; around 89% of European citizens agree with it according to a 2011 poll. Wind power produces 17–39 times as much energy as it consumes, compared to 11 times for coal and 16 times for nuclear power plants. These benefits and others make wind power promising and a potentially great source of electricity.

Wind energy grown immensely over the last decade and the global cumulative installed capacity in 2014 was approximately 49 times the total capacity of the year 1997 (see Figure 3.3). From 2009 to 2014, the annual installed capacities in the world were at historical records in the wind power industry, at 35–51 GW per year, as shown in Figure 3.4. This wind energy growth trend is expected to continue in the short and long term in many countries around the world (See Figures 3.5 and 3.6 for short and long term growth respectively).

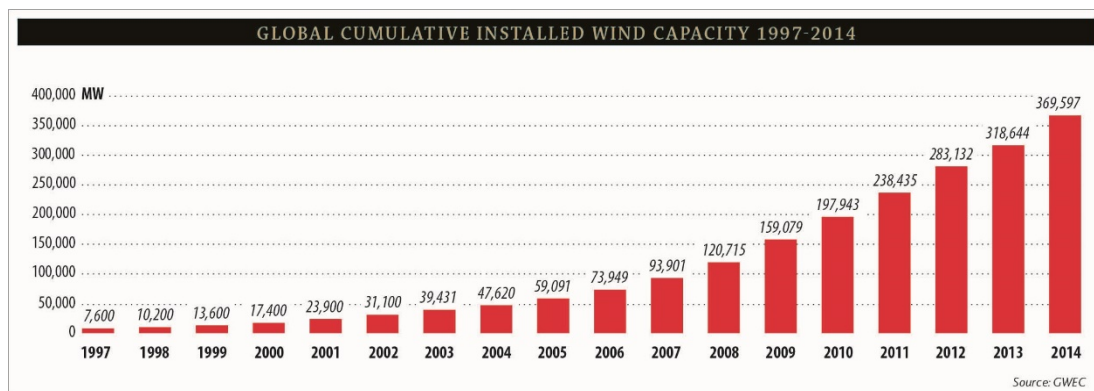


Figure 3.3: Global cumulative installed wind capacity from 1997 to 2014 [116].

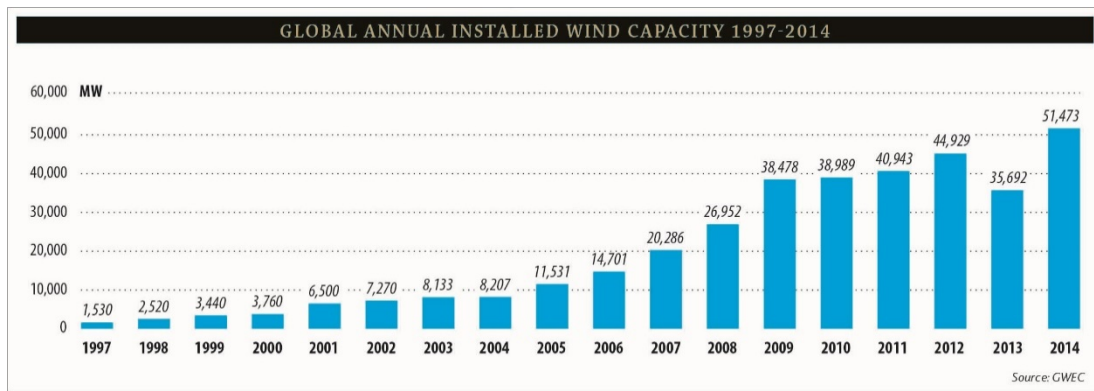


Figure 3.4: Global annual installed wind capacity from 1997 to 2014 [116].

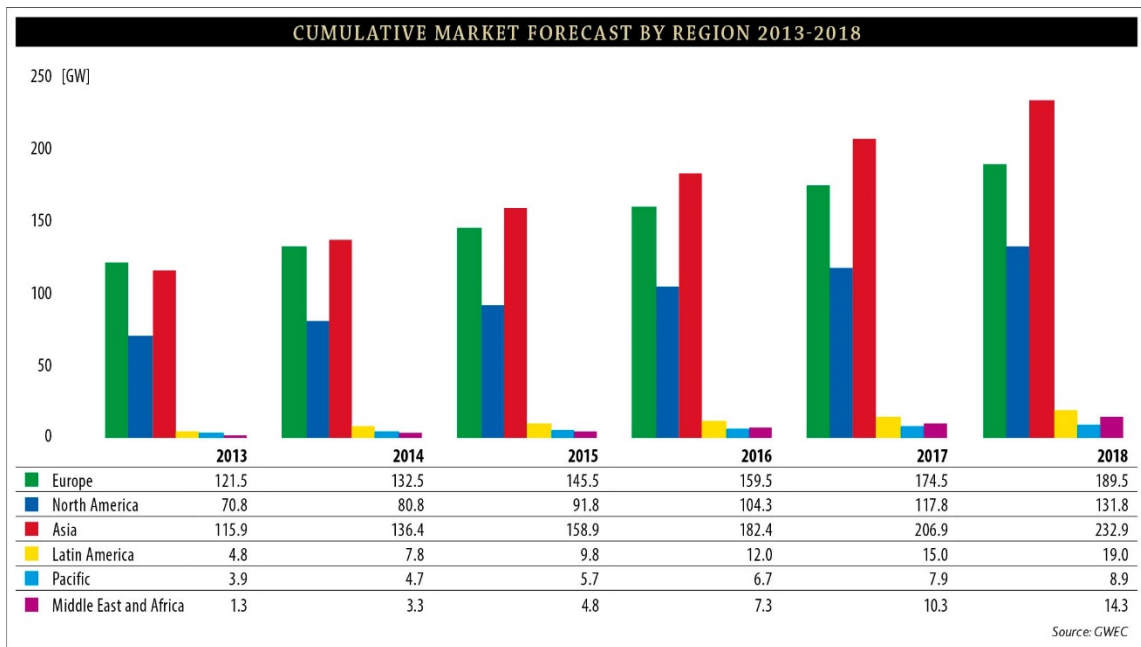


Figure 3.5: Short term expected growth in wind power by region [117].

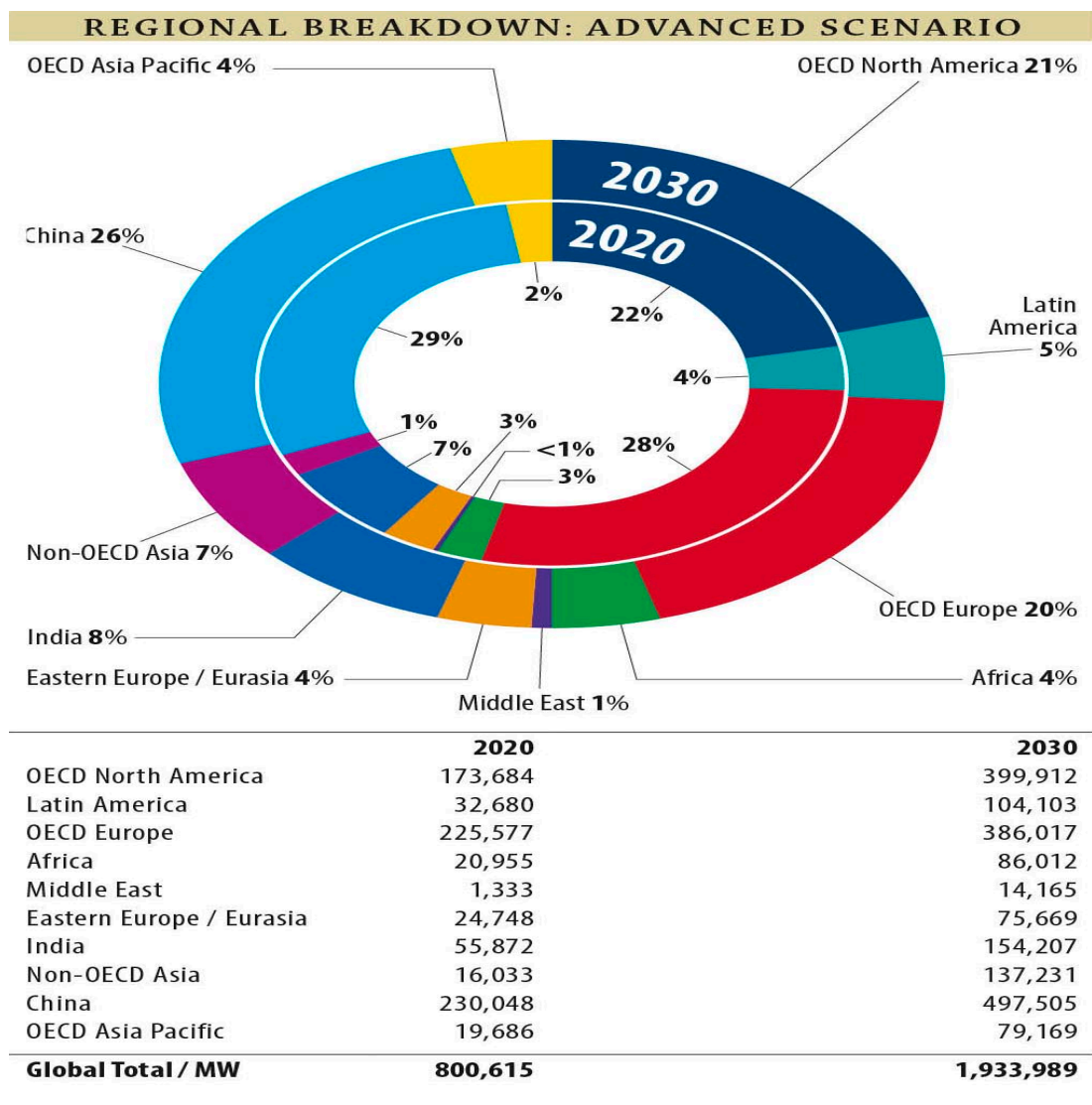


Figure 3.6: Long term expected growth in wind power by region (advanced scenario) [118]; OECD is Organization for Economic Cooperation and Development.

As mentioned, these trends are due to several advantages and according to the International Energy Agency (IEA), wind is the second largest renewable energy source after hydro power. Wind helps in reducing CO₂ emission considerably and it is one of the most abundant forms of renewable energy. Wind energy is a clean and environmentally friendly source of energy and it does not emit undesirable greenhouse gases. Wind power is also an inexhaustible and free source of energy compared to fossil fuels and other conventional sources. The increase in wind energy penetration in power systems is ideally meant to decrease fossil fuel dependency and the risk of rapid increases in fuel prices.

Indeed, wind generating units have become more competitive compared to conventional power plants in recent years. The cost of wind power units is rapidly decreasing and this will continue due to dramatic improvements and developments in the technology. Compared to conventional power plants, wind power has lower operating and maintenance costs. The wind power industry also has another significant benefit, namely it creates new jobs. Around 670,000 people worldwide were employed by the wind power industry in 2011 [119]. The economy in rural areas, where most wind farms are located, can obtain great benefits through the building of wind turbines on existing ranches and farms. Wind turbines on these sites only occupy a small fraction of the land and the rest of the land can be used by farmers. The farmers (land owners) can also get payments for renting this space to wind turbine owners.

3.4 Environmental Impact of Wind Power

Wind power does not produce CO₂ during its operation and thus it is a ‘carbon neutral’ technology. However, it is not a 100% carbon free technology for power generation since it releases CO₂ emissions during its lifecycle, such as during manufacturing, construction, maintenance and decommissioning. Each power generation technology unit has a carbon footprint and this carbon footprint can be described as the total amount of CO₂ and other greenhouse gas emissions produced over the full unit’s lifecycle. It is expressed as the gCO₂eq/kwh grams of CO₂ equivalent per kilowatt hour of power generation. Notwithstanding, wind power has one of the lowest carbon footprints. In recent years, lifecycle assessments indicate that there is a slight difference between the carbon footprints of onshore (4.64 gCO₂eq/kwh) and offshore wind power plants (5.25 gCO₂eq/kwh) [120]. The manufacturing process of onshore and offshore wind units is almost the same but the transportation and foundations are different. The difference between their carbon footprints comes from the larger foundations (concrete) that offshore requires. Conversely, a conventional power plant such as that of coal emits 1000 gCO₂eq/kwh. This means that the emission of carbon dioxide from a coal power plant is around 200 times that emitted from a wind power plant. Therefore, wind power integration in the power sector could help tackle climate change, reduce greenhouse gases and meet

global targets. According to the International Energy Agency (IEA), the Intergovernmental Panel on Climate Change (IPCC) and the American Association for the Advancement of Science (AAAS), CO₂ and other greenhouse gas emissions must be reduced in less than a decade and countries must meet the target of the global mean temperature increasing by 2°C, as signed by 192 member governments of the UNFCCC (United Nations Framework Convention on Climate Change).

3.5 Economic Potential of Wind Energy

The recent technical and technological developments in wind power generation have reduced the cost of wind energy and it is now lower in cost than most new conventional power plants, according to the Wind Energy Foundation (WEF). Wind power has become cost competitive with new natural gas power plants due to governments' renewable energy subsidies and this has promoted wind energy in global power sectors. However, the UK's government plans recently to end new public subsidies for onshore wind generation from 1st of April 2016 by legislating to close the Renewables Obligation to new onshore wind farms [121]. The cost reduction of wind power per kilowatt is expected to continue according to the GWEC, as illustrated in Figure 3.7 [111]. Government support and various financial incentives have been applied to promote renewable energy resources in power systems, such as the Renewable Obligation Certificate (ROC) and Feed in Tariff (FIT) in the UK. According to the International Energy Agency (IEA), there is expected to be a reduction in wind power cost of between 1% and 6% per year until the year 2030 [122].

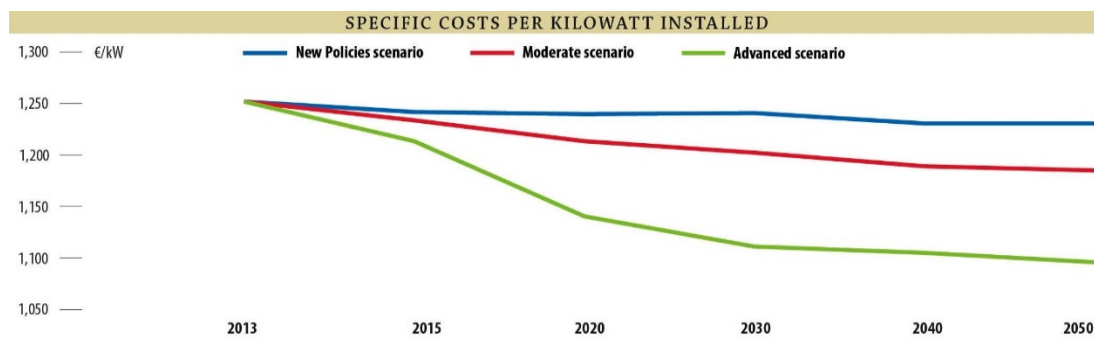


Figure 3.7: Specific cost reductions per kilowatt installed [111].

Wind power prices depend on economic incentives and the wind unit manufacturing process. Manufacturing process costs are related to the costs of raw materials such as iron, steel, copper, glass and fibre, which are the main materials of wind turbine parts such as wind blades, Nacelles, towers and others. Additional costs may include the connection of offshore wind power plants such as HVDC (High Voltage Direct Current) power electronic converters and HVDC cables. Unlike conventional power plants, wind power technology requires almost no operating and maintenance costs. Wind power technology, particularly offshore, requires HVDC links and this encourages new investment in HVDC which is valued at billions of dollars.

3.6 Wind Power Growth

At the end of 1997, the world's total cumulative wind installed capacity was 7.6 GW. Three years later, the growth in wind power capacity was doubled and this was followed by a steady rise until 2005. In 2005, the global cumulative wind capacity was 59 GW and two years later it increased by around 62%. Since 2007 wind power capacity has considerably increased, approaching a historic record of more than 283 GW in 2012. Wind power provides clean and affordable energy to many countries around the world and it is now becoming the second most important renewable source just after hydro power. This growth trend in wind power generation continued in 2014 and the world's cumulative wind installed capacity exceeded 369 GW [116]. Around 51 GW were installed in 2014 and this growth is considerably higher than the installed capacity in 2013, when around 35 GW were installed. The top 10 leading wind power markets in the world at the end of 2014 are shown in Table 3.1. The world's cumulative wind installed capacity shares by the end of 2014 are illustrated in Figure 3.8 and the continental shares according to the GWEC in 2014 are shown in Figure 3.9.

Table 3.1: Leading wind power markets in terms of added capacity in 2014.

Country		Added capacity in 2014 (MW)	Percentage (%)
China		23196	45.1
Germany		5279	10.2
US		4854	9.4
Brazil		2472	4.8
India		2315	4.5
Canada		1871	3.6
United Kingdom		1736	3.4
Sweden		1050	2.0
France		1042	2.0
Turkey		804	1.6
Rest of the World		2042	13.3
Total		51473	100

Total Wind Cumulative Capacity 369.597 GW

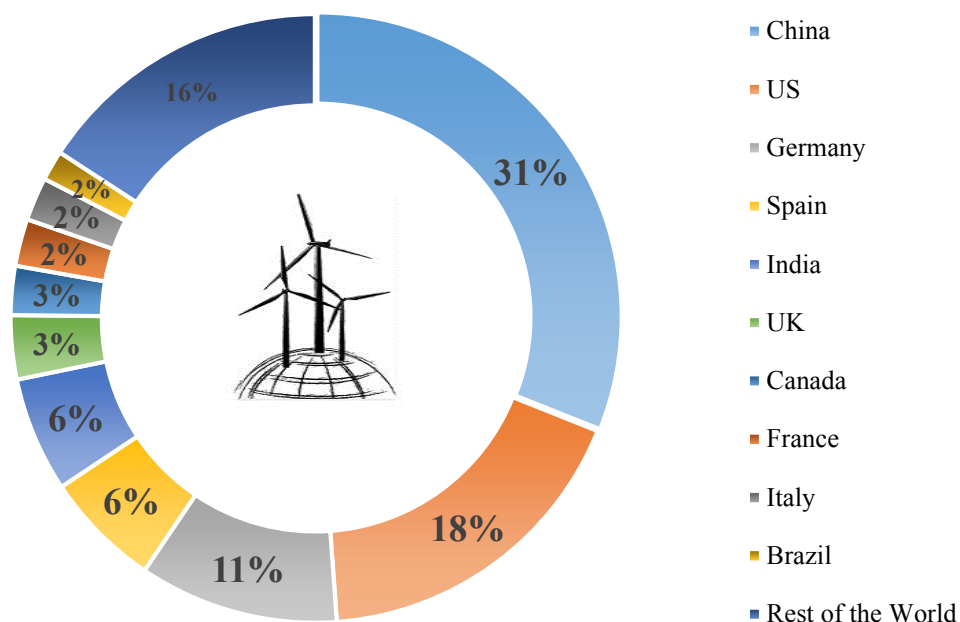


Figure 3.8: The world's cumulative installed wind capacity shares by the end of 2014.

Wind Installed Capacity Continental Shares

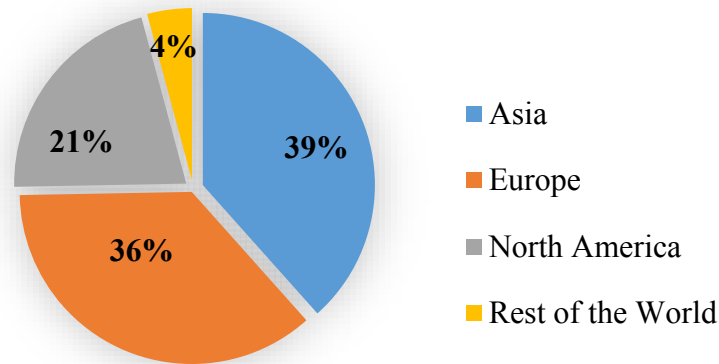


Figure 3.9: The world's cumulative installed wind capacity shares in 2014.

3.7 Wind Energy in Europe and the United Kingdom

Europe was the world's leading region over the past few years in terms of cumulative wind power installed capacity, approaching around 121 GW in 2013. In 2014, wind power evolution in China and the rest of Asia put Asia at the top in terms of total cumulative installed wind capacity with around 142 GW, compared to approximately 134 GW in Europe. Denmark is the top country in wind power generation in terms of the penetration level of wind energy in power systems, at around 33% in 2013. Moreover, Danish wind power generation supplied around 42% of electricity demand in Denmark in 2015 [123]. In recent years, Denmark and other European countries, such as Germany and Spain, have made Europe the leading region in terms of wind participation in the total power generation in their power sectors. Figure 3.10 shows the penetration level of wind power in power systems from 2006 to 2011.

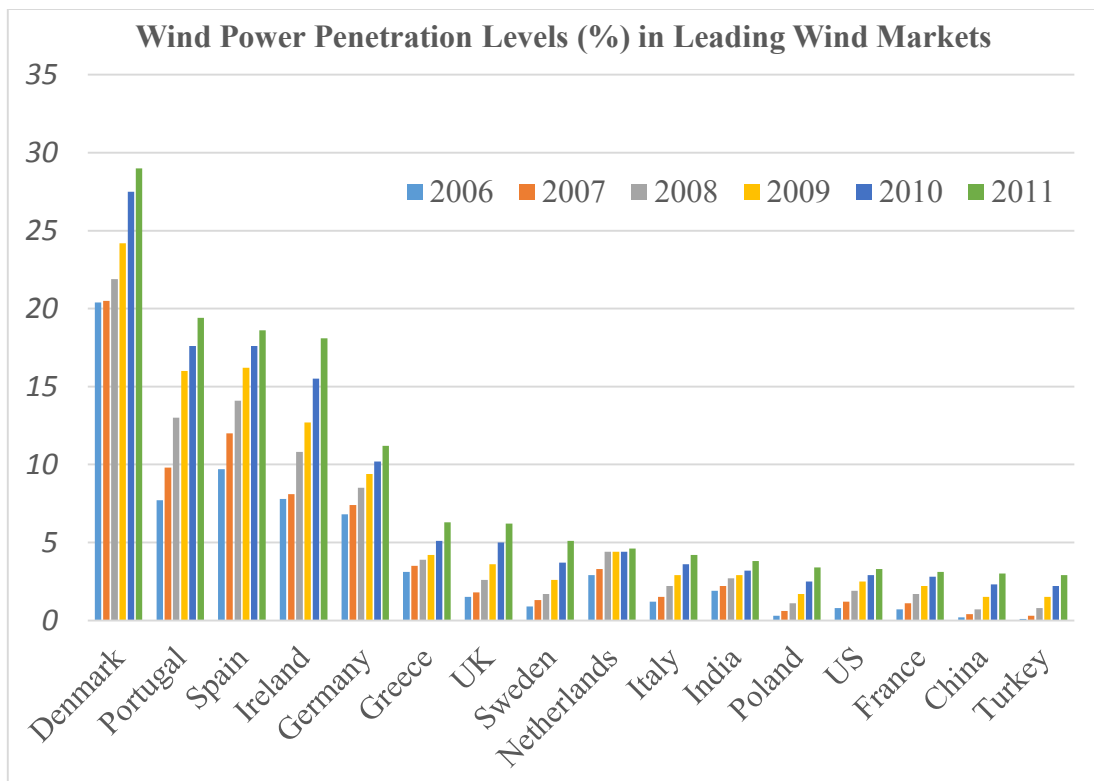


Figure 3.10: Leading countries in terms of wind energy penetration (%) in power systems from 2009 to 2011.

Installation of wind turbines has increased rapidly in the United Kingdom (UK) due to the high availability of wind, as well as government support and investment policy. The total installed capacity in 2008 was around 3 GW and this has increased substantially, reaching more than 12.4 GW in 2014 [116]. The UK is the leading country in terms of cumulative offshore wind installed capacity, with more than 4.4 GW. The UK's cumulative offshore wind installed capacity is shown in Table 3.2. The largest offshore wind farm is also in the UK; known as London Array it has a 630 MW capacity. The offshore wind industry in the UK and the rest of Europe has developed much faster than in other regions. In the UK, the government's subsidises for offshore wind farms are twice than that in onshore.

Table 3.2: The cumulative offshore wind installed capacity in MW from 2011 to 2014.

Position	Country	2014 (MW)	2013 (MW)	2012 (MW)	2011(MW)
1	UK	4494.3	3653	2947.9	1524.6
2	Denmark	1271	1271	921	857.6
3	Germany	1049	914.9	280.3	215.3
4	Belgium	713	571.5	379.5	195
5	China	658	389.6	389.6	222.3
6	Netherlands	249	249	249	249
7	Sweden	212	212	164	164
9	Japan	50	27.3	25.3	25.2
9	Finland	26	26	26	26
10	Ireland	25.2	25.2	25.2	25
11	Spain	5	5	0	0
12	Korea	5	5	0	0
13	Norway	2.3	2.3	2.3	2.3
14	Portugal	2	2	2	2
	Total	8761.8	7357.8	5416.1	3315.0

3.8 Current Wind Power Technologies

In general, wind turbines have two configurations which are the Horizontal Axis Wind Turbine (HAWT) and the Vertical Axis Wind Turbine (VAWT), as illustrated in Figure 3.11. There have been different designs proposed over the years within these configurations. Both the HAWT and the VAWT have similarities in several components, such as gearbox and generator, but with various configurations. The VAWT is cross-flow equipment and it accepts wind from all directions with no need to be oriented into the wind. Therefore a yaw drive mechanism is not required, unlike with the HAWT. This is one of the main advantages of the VAWT as a yaw drive is an expensive component in wind turbine technologies. In addition, the drive train of the VAWT including the gearbox and the generator etc. is installed at the ground of the turbine tower. This reduces the cost of maintenance and makes the maintenance easier. On the other hand, the HAWT is most dominant in the wind industry and commercial applications due to its high power output.

Most modern wind turbines are HAWTs and they are almost all utility scale wind turbines, varying from 100 kilowatts to several megawatts. HAWTs can be installed upwind or downwind, as shown in Figure 3.12.

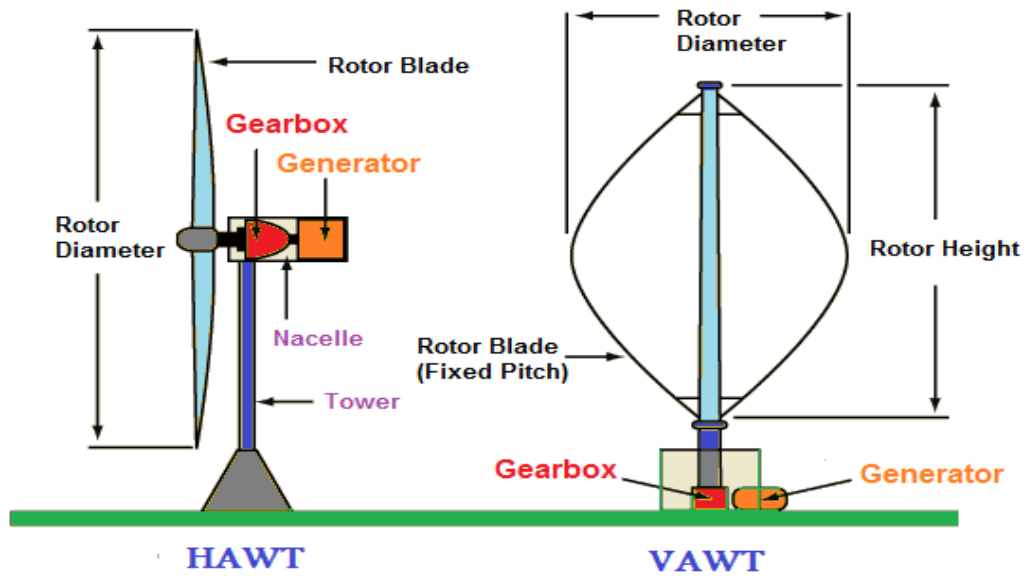


Figure 3.11: Structural differences between HAWT and VAWT.

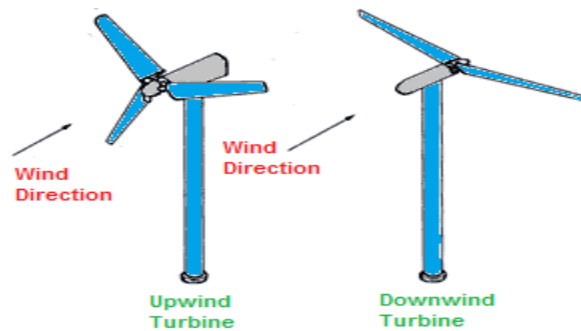


Figure 3.12: Horizontal Axis Wind Turbines (upwind and downwind turbines).

Upwind turbines enable the rotor to face the wind first, while downwind turbines pass the wind to the rotor after the tower and nacelle. The most dominant type in the wind industry is the upwind rotor due to its higher output power, as downwind machines have fluctuated output because the rotor passes through the wing shade of the turbine tower.

Wind power technology has progressed considerably over the last 20 years and this progression has been significantly driven by the increase in physical size of turbines which

has grown their output power. Wind turbines have been developed dramatically in terms of rated capacities and typical wind turbines are rated from a hundred kilowatts to approximately 10 MW. Table 3.3 shows the global top ten wind turbines in terms of rated capacity.

Table 3.3: The global top ten wind turbines in terms of rated capacity [124].

Wind Turbine	Manufacturer	Rated Power (MW)	Hub Height (m)	Rotor Diameter (m)	Swept Area (km ²)	Blade Length (m)
SeaTitan	American Energy Technologies Company	10	125	190	28.353	Not Available
Sway ST10	The Norwegian Technology Company	10	90	164	21.124	67
Areva	French Energy Company Areva	8	90	180	25.446	66
Vestas V164	Danish Wind Turbines Vestas	8	105	164	21	80
Enercon E-126	German Company Enercon	7.58	135	127	12.668	61.5
Samsung S 7.0-171	Samsung Heavy Industries	7	110	171	23	83.5
REpower 6.2M152/ REpower 6.2M/126	Suzlon Group Company REpower	6.2	124	152/216	18.145/36.64	Not Available
Siemens SWT-6.0-154	Siemens	6	120	154	18.6	75
Haliade 150	Alstom Haliade	6	100	150	17.86	73.5
Sinovel SL6000	Chinese Manufacturer Sinovel	6	102	128	12.868	Not Available

3.9 Wind Power Systems

Wind turbines can provide clean energy for small or large scale utilities and they can be installed onshore (on land) or offshore (in water). The main physical components of wind

turbines are described in Table 3.4 with their relative percentage costs [125]. This is an example of a REpower MM92 turbine with a 100 m tower and 45.3 m blade length.

Table 3.4: The main components of wind turbines and their percentage of overall cost [125].

Component	Description	% of cost
Tower	It is made from steel and its length ranges from 40m to more than 100m.	26.3
Rotor Blades	They are made from composite materials. Usually a combination of glass, fibre, epoxy resin and carbon can be added to increase strength and stiffness. Their length can be varied to more than 60 m.	22.2
Rotor Hub	It is made from cast iron. Its function is to hold the blades in position as they turn.	1.37
Rotor Bearings	There are many bearings in the turbine and they should withstand the varying forces and loads produced by the wind.	1.22
Main Shaft	Its function is to transfer the rotational force of the rotor to the gearbox.	1.91
Main Frame	It should be strong enough to support the entire turbine drive train but not too heavy. It is usually made from steel.	2.8
Gearbox	Its function is to increase the low rotational speed of the rotor shaft in several stages to the high speed required to drive the generator.	12.91
Generator	The main function of the generator is to convert the mechanical energy into electrical energy.	3.44
Yaw System	It is a mechanism to rotate the nacelle to face the change in wind direction.	1.25
Pitch System	This system controls the blades' angle to achieve the best performance.	2.66
Power Converters	It converts direct current from the generator into alternating current to be connected to the ac grid.	5.01
Transformer	It converts the electricity from lower voltage at the turbine to higher voltage needed by the ac grid.	3.59
Brake System	Brakes the turbine when needed.	1.32
Nacelle Housing	It is a lightweight glass fibre box that covers the turbine's drive train.	1.35
Cables	It is used for electric connections.	0.96
Screws	They are used to hold the main components in their position and they should be able to withstand extreme loads.	1.04

A wind power system converts kinetic energy from the wind into mechanical energy for power generation. The most modern wind turbines are based on aerodynamic lift and they are known as the lift type, blades or aerofoils. This design uses the aerodynamic properties of the aerofoil profile to produce lift force to rotate the blades when the wind is blown

over them. Most wind turbines have either two or three blades; the blades' rotation causes the rotor to spin. To control the rotor speed, protect the rotor from high wind speed and produce sufficient electricity, a pitch system turns or pitches the turbine blades by several degrees. For effective power control, the required variations in the pitch system are typically from 0° to 35°, and for aerodynamic braking purposes the blades can be pitched up to 90° [126]. A low speed shaft (main shaft) is coupled with the rotor and it rotates at around 30–60 revolutions per minute (rpm). The gearbox connects the low speed shaft to the high speed shaft and increases the rotational speed to around 1000–1800 rpm, as required to drive most generators to generate electricity. The gearbox is a heavy component in the wind power system and it has a relatively high cost. However, it is not required in Direct Drive Generators because they can operate at lower rotational speeds. The generator converts the mechanical energy into electricity; it can be synchronous or asynchronous (induction). The transformer increases the voltage for transmission to a substation and increases again in the substation for transmission over long distances and the ac grid.

3.10 Wind Generation Characteristics

The wind turbine output power (P_w) is a function of the wind speed (v_w) and it is given by the fundamental Equation (3.1).

$$P_w = \frac{1}{2} \rho A C_p v_w^3 \quad (3.1)$$

Where ρ is the air density (1.225 kg/m³), A is the turbine swept area and C_p is the power coefficient which is a function of both tip speed ratio (λ) of the machine and the blade pitch angle (β), as illustrated in Equation (3.2) [127].

$$C_p = \frac{1}{2} (\lambda - 0.022 \beta^2 - 5.6) e^{-0.17\lambda} \quad (3.2)$$

The power coefficient is defined as the ratio between the power extracted from the wind to the total available power, as shown in Equation (3.3).

$$C_p = \frac{\text{Power Extracted from the Wind}}{\text{Total Available Power}} = \frac{\text{Power Extracted}}{\frac{1}{2} \rho A v_w^3} \quad (3.3)$$

The power coefficient is proportional to the ratio of the turbine rotational speed to the wind speed known as tip speed ratio (λ), as shown in Equation (3.4).

$$\lambda = \frac{\omega R}{v_w} \quad (3.4)$$

Where ω is the rotational speed and R is the rotor radius. The relationship between the power coefficient and the tip speed ratio can be varied by a change in the design of the blades. Contrary, Albert Betz found that the maximum possible value for the power coefficient C_p is 0.593, known as ‘Betz Limit’. The relationship between the tip speed ratio and C_p is described by the $C_p - \lambda$ curve and it can be varied by different wind turbine designs. The $C_p - \lambda$ curve under various pitch angles β is illustrated in Figure 3.13. Note that the maximum C_p achieved by this wind turbine is around 0.45 at $\lambda = 6$ and the pitch angle $\beta = 0$. The power coefficient is low at both low and high speed ratios. Therefore, the ideal operation of a wind turbine can be achieved if the turbine operates at all wind speeds at a tip speed ratio λ in which area gives the maximum C_p .

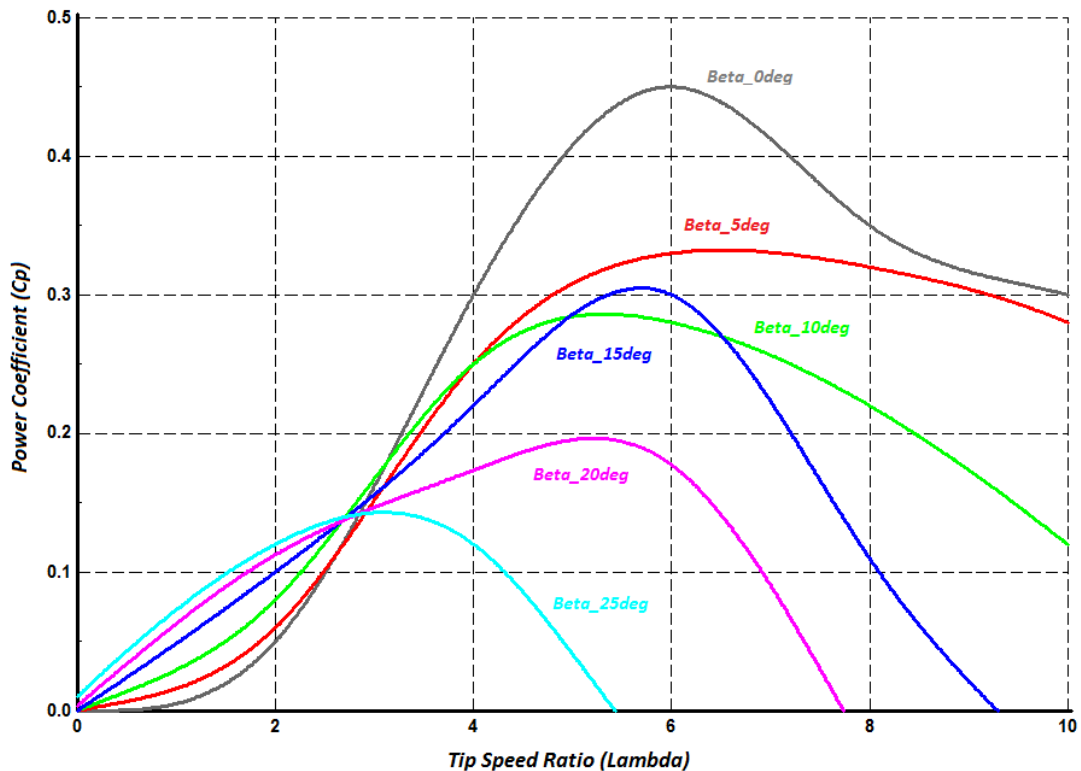


Figure 3.13: The $C_p - \lambda$ curve under various pitch angles β .

The power output of a wind turbine is proportional to the cube of the wind speed v_w and the relationship between them is described by the ‘power curve’ of a wind turbine, as shown in Figure 3.14. The typical values of most wind turbine manufacturers for cut-in, rated and cut-out speeds are 3-5 m/s, 14-15 m/s and 20-25 m/s respectively [128].

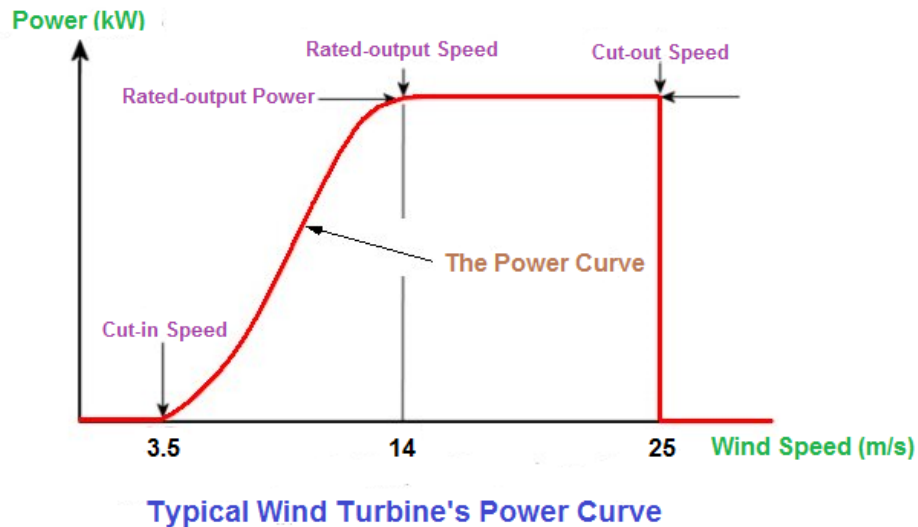


Figure 3.14: The power curve of a typical wind turbine.

Each component of the wind turbine should be designed optimally to extract as much power from the wind as possible. The operation modes of the wind turbine, whether it is constant (fixed) or variable rotational speed, can affect the extracted power. For fixed speed operation mode, the rotational speed is maintained constant but the tip speed ratio λ varies continuously. However, in variable speed operation mode the turbine operates at variable speed and a constant tip speed ratio is maintained, which is needed to obtain the maximum power coefficient. The fixed speed wind turbine is simple and well proven but it has uncontrollable reactive power consumption and limited power quality control. In recent years, the most common operation mode is variable speed because it improves the dynamic behaviour of the wind turbine and the power output of the variable speed wind turbine is much higher than that of fixed speed turbines [129].

In general, a wind turbine goes through two energy conversion stages; the blades and the rotor convert the kinetic energy into mechanical energy and the generator converts the mechanical energy into electrical energy, as shown in Figure 3.15.

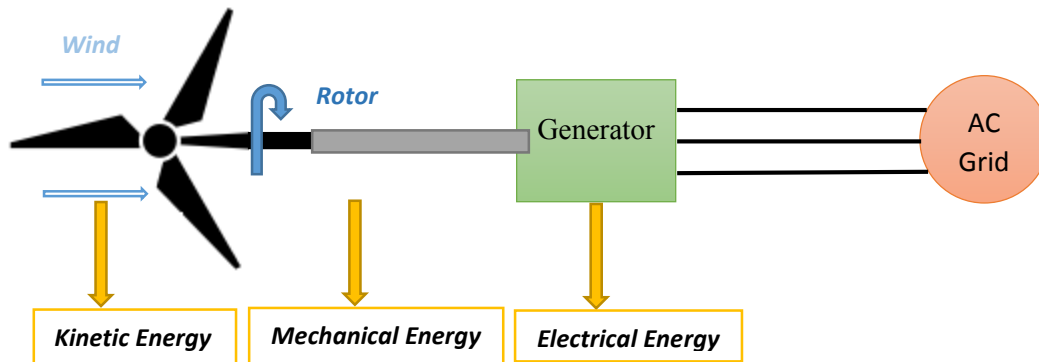


Figure 3.15: Energy conversion stages in wind turbines.

Three different wind generator concepts are currently used in the wind power industry. Early wind turbines used fixed speed induction machines (generators) to generate electricity, for simplicity. However, the induction machines could be used in variable speed mode and Doubly Fed Induction Generators (DFIGs) have been deployed and developed in recent years. DFIGs use a frequency converter to actively control the rotor currents and magnetic field. This allows the wind turbine to operate at variable rotational speed up to 30% [126]. Permanent Magnetic Synchronous Generators (PMSGs) or a synchronous machine with fully rated converters have recently been developed and allow the generator to be completely decoupled from the network frequency. They also have reactive power controllability. This section will highlight the operational theory behind Fixed Speed Induction Generators, Doubly Fed Induction Generators and Synchronous Generators with Fully Rated Converters.

3.10.1 Fixed Speed Generators (Induction Machines)

Induction machines can be classified into two categories: squirrel cage and wound rotor. The squirrel cage induction generator belongs to the fixed speed operation mode field in the wind turbine industry and it was the most dominant generator in the market ten years ago. It has independent rotor winding which is completely isolated from any electrical connection. The currents flowing in the stator windings at start-up produce a magnetic flux that induces a voltage into the rotor winding. This induced voltage results in a current being allowed to flow in the short circuited rotor windings. A second magnetic flux will be produced by the current passing and it opposes the stator magnetic flux. This will produce the generator torque. Since the rotor is driven by the wind turbine rotor (prime

mover), the generator torque acts against the input torque. The generator torque is directly proportional to the active output power of the generator. The required magnetising flux for the rotor windings can be obtained by adding a reactive component to the stator currents. This ensures that a current is always flowing in the rotor windings. The rotational speed of the rotor ω_r must not equal the synchronous speed of the generator ω_s and the relationship between them can be defined by the machine slip, as shown in Equation (3.5). When the slip is negative, i.e. the rotational speed of the rotor is greater than the synchronous speed, the machine operates as a generator, and vice versa for the motor.

$$slip (s) = \frac{\omega_s - \omega_r}{\omega_s} \quad (3.5)$$

The squirrel cage induction generator (SCIG) has been used widely in the wind power industry in the past and it was used in fixed (constant) speed wind turbines. The blades are connected to the turbine hub and it is coupled to the gearbox, and then to the induction generator. The turbine speed is controlled by the torque vs speed characteristics of the squirrel cage induction generator. The SCIG is robust and has a lower cost compared to variable speed wind generators. It also provides stable frequency control due to its fixed speed operation mode. However, the squirrel cage induction generator always requires reactive power support because the field circuit is not separated and there is no direct control for reactive power [126]. The reactive power is usually compensated by capacitor banks and this increases the total cost of the wind turbine. Torque pulsations due to large power variations can also result in gearbox failures, the gearbox being an expensive component in wind turbines. The basic structure of the fixed speed squirrel cage wind generator is illustrated in Figure 3.16.

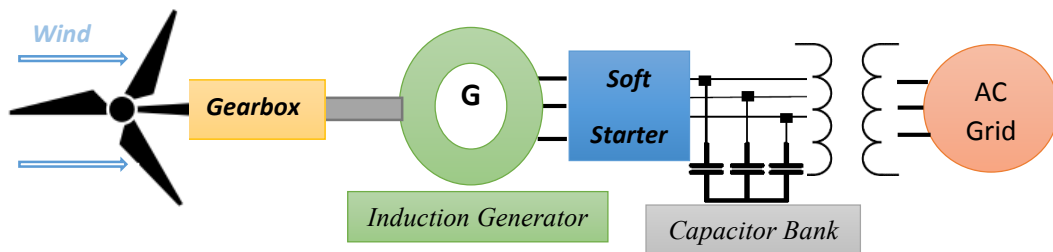


Figure 3.16: Fixed speed wind turbine generator.

3.10.2 Variable Speed Wind Turbine Generators

The main feature of variable speed generators is that the wind turbine operates for a wide range of wind speeds at the optimum tip speed ratio, and hence at the optimum power coefficient. Therefore, the energy captured from the wind is maximised, particularly in wind conditions below the rated wind speed. Variable speed generators have flexible controllability and different parameters can be controlled such as terminal voltages, active reactive powers, torque and frequency. This type of wind turbine generator can also provide reactive power support and frequency regulation, which are necessary in remote locations and offshore wind farms. In addition, power electronic converters which are used in variable speed wind generators to control the generator parameters are becoming cheaper and more reliable. Variable speed wind generators have been used extensively in the last few years for these reasons and they also offer less variations in output power because the larger rotor inertia makes the fluctuations in wind speed smoother and thus reduces voltage flicker problems. This thesis is based on variable speed wind generators for the aforementioned reasons.

Variable speed wind generators are of two types: ac induction generators and ac synchronous generators. Both types use power electronic converters in their control structure. The first type is known as the Doubly Fed Induction Generator (DFIG) and the second is known as the Synchronous Generator with Fully Rated Converters or PMSG.

3.10.2.1 Doubly Fed Induction Generator (DFIG)

The Doubly Fed Induction Generator (DFIG) is one of the most common wind generators based on variable speed operation mode. The induction generator in the DFIG concept is directly connected to the ac grid at the stator terminals. However, the rotor windings are connected to the ac grid via variable frequency AC/DC and DC/AC back to back power electronic converters. These converters are based on insulated gate bipolar transistors (IGBTs). Controlling these converters when the wind speed changes helps in changing the rotor flux rotation from a sub-synchronous to a super-synchronous speed. So the DFIG can generate constant-frequency power by controlling the rotor flux [130]. These power electronic converters which are connected to the rotor terminals only require production of a fraction (typically 25–30%) of the total generated power by the DFIG to achieve full

$$V_{rabc} = R_r i_{rabc} + \frac{d\lambda_{rabc}}{dt} \quad (3.8)$$

The dynamic model of the DFIG can be expressed in terms of two axes (dq axes) known as the synchronous reference frame, as shown in Figures 3.18 and 3.19.

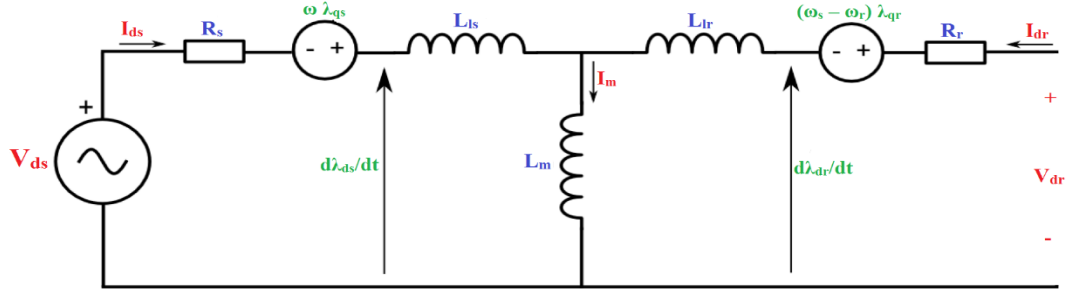


Figure 3.18: d-axis DFIG dynamic model.

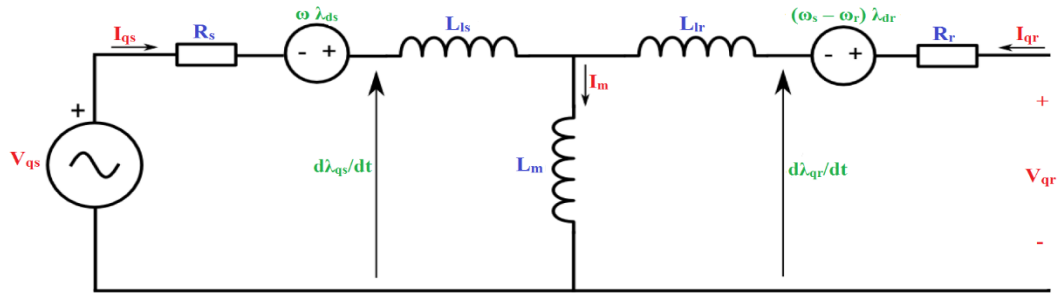


Figure 3.19: q-axis DFIG dynamic model.

The stator voltage equations become:

$$V_{ds} = R_s I_{ds} - \omega \lambda_{qs} + \frac{d\lambda_{ds}}{dt} \quad (3.9)$$

$$V_{qs} = R_s I_{qs} + \omega \lambda_{ds} + \frac{d\lambda_{qs}}{dt} \quad (3.10)$$

The rotor voltage equations are:

$$V_{dr} = R_r I_{dr} - (\omega_s - \omega_r) \lambda_{qr} + \frac{d\lambda_{dr}}{dt} \quad (3.11)$$

$$V_{qr} = R_r I_{qr} + (\omega_s - \omega_r) \lambda_{dr} + \frac{d\lambda_{qr}}{dt} \quad (3.12)$$

Where V_{ds} , I_{ds} and λ_{ds} are the stator voltage, current and flux linkage respectively in the d-axis while V_{qs} , I_{qs} and λ_{qs} are the stator voltage, current and flux linkage respectively in the q-axis. V_{dr} , I_{dr} and λ_{dr} are respectively the rotor voltage, current and flux linkage in the d-axis while V_{qr} , I_{qr} and λ_{qr} are the rotor voltage, current and flux linkage respectively in the q-axis. R_s and R_r are the stator and rotor resistances respectively. The rotor speed is ω_r while ω_s is the rotational speed of the synchronous reference frame.

The flux linkage equations for the stator are:

$$\lambda_{ds} = L_{ls} I_{ds} + L_m(I_{ds} + I_{dr}) = L_s I_{ds} + L_m I_{dr} \quad (3.13)$$

$$\lambda_{qs} = L_{ls} I_{qs} + L_m(I_{qs} + I_{qr}) = L_s I_{qs} + L_m I_{qr} \quad (3.14)$$

While the flux linkage equations for the rotor are:

$$\lambda_{dr} = L_{lr} I_{dr} + L_m(I_{ds} + I_{dr}) = L_m I_{ds} + L_r I_{dr} \quad (3.15)$$

$$\lambda_{qr} = L_{lr} I_{qr} + L_m(I_{qs} + I_{qr}) = L_m I_{qs} + L_r I_{qr} \quad (3.16)$$

Where L_{ls} and L_{lr} are the stator and rotor leakage inductances, and the magnetising (mutual) inductance is L_m . $L_s = L_{ls} + L_m$ is the self-inductance. The frequency of the rotor current ω_{rf} must satisfy the slip frequency constraint in order for the rotor mmf to be in synchronism with the stator mmf.

$$\omega_{rf} = \omega_s - \omega_r = s \omega_s \quad (3.17)$$

The per unit electromagnetic torque (T_e) is given by the following equation:

$$T_e = \lambda_{ds} I_{qs} - \lambda_{qs} I_{ds} = \lambda_{qr} I_{dr} - \lambda_{dr} I_{qr} = L_m (I_{qs} I_{dr} - I_{ds} I_{qr}) \quad (3.18)$$

By neglecting the power losses in the stator and rotor resistances, the active and reactive powers for the stator and the rotor are given by:

$$P_s = \frac{3}{2} (V_{ds} I_{ds} + V_{qs} I_{qs}) \quad (3.19)$$

$$Q_s = \frac{3}{2} (V_{qs} I_{ds} - V_{ds} I_{qs}) \quad (3.20)$$

$$I_{ds} = \frac{L_m}{L_s} (I_{ms} - I_{dr}) \quad (3.24)$$

$$I_{ms} = \frac{V_{qs} - R_s I_{qs}}{\omega_s L_m} \quad (3.25)$$

Then,

$$P_s = -3/2 \omega_s \frac{L_m^2}{L_s} I_{ms} I_{qr} \quad (3.26)$$

$$Q_s = 3/2 \omega_s \frac{L_m^2}{L_s} I_{ms} (I_{ms} - I_{dr}) \quad (3.27)$$

$$V_{dr} = R_r I_{dr} + \sigma L_r \frac{dI_{dr}}{dt} - (\omega_s - \omega_r) \sigma L_r I_{qr} \quad (3.28)$$

$$V_{qr} = R_r I_{qr} + \sigma L_r \frac{dI_{qr}}{dt} + (\omega_s - \omega_r) (\sigma L_r I_{dr} + \frac{L_m^2}{L_s} I_{ms}) \quad (3.29)$$

$$\text{Where } \sigma = 1 - \frac{L_m^2}{L_s L_r} \quad (3.30)$$

Equations (3.26) and (3.27) show that P_s (stator active power) and Q_s (stator reactive power) can be controlled independently by regulating the rotor current d-q components I_{qr} and I_{dr} respectively. The reference values of I_{qr} and I_{dr} can be determined directly from the outer power control loops (P_s and Q_s). The inner current control loops are determined by:

$$V_{dr} = V_{dr1} - V_{dr2} \quad (3.31)$$

$$V_{qr} = V_{qr1} - V_{qr2} \quad (3.32)$$

Where

$$V_{dr1} = R_r I_{dr} + \sigma L_r \frac{dI_{dr}}{dt} \quad (3.33)$$

$$V_{dr2} = (\omega_s - \omega_r) \sigma L_r I_{qr} \quad (3.34)$$

$$V_{qr1} = R_r I_{qr} + \sigma L_r \frac{dI_{qr}}{dt} \quad (3.35)$$

$$V_{qr2} = (\omega_s - \omega_r) (\sigma L_r I_{dr} + \frac{L_m^2}{L_s} I_{ms}) \quad (3.36)$$

Rewriting Equations (3.33) and (3.35) we get:

$$\frac{dI_{dr}}{dt} = \frac{-R_r I_{dr}}{\sigma L_r} + \frac{1}{\sigma L_r} V_{dr1} \quad (3.37)$$

$$\frac{dI_{qr}}{dt} = \frac{-R_r I_{qr}}{\sigma L_r} + \frac{1}{\sigma L_r} V_{qr1} \quad (3.38)$$

Equations (3.37) and (3.38) show that I_{dr} and I_{qr} respond to V_{dr1} and V_{qr1} respectively. It is then possible to design the following Proportional Integral (PI) controllers:

$$V_{dr1} = (k_{pr} + \frac{k_{ir}}{s}) (I_{dr}^* - I_{dr}) \quad (3.39)$$

$$V_{qr1} = (k_{pr} + \frac{k_{ir}}{s}) (I_{qr}^* - I_{qr}) \quad (3.40)$$

Substituting Equations (3.39) and (3.40) into (3.28) and (3.29) we get:

$$V_{dr} = (k_{pr} + \frac{k_{ir}}{s}) (I_{dr}^* - I_{dr}) - s\omega_s \sigma L_r I_{qr} \quad (3.41)$$

$$V_{qr} = (k_{pr} + \frac{k_{ir}}{s}) (I_{qr}^* - I_{qr}) + s\omega_s (\sigma L_r I_{dr} + \frac{L_m^2}{L_s} I_{ms}) \quad (3.42)$$

I_{q}^* and I_{d}^* are the reference signals of the outer control loops which can be determined from the control of the stator active and reactive powers respectively.

2- Modelling of GSC

The control scheme of the GSC of the DFIG consists of two cascaded control loops. The d-axis and the q-axis of the ac side of the GSC I_{dg} and I_{qg} can be controlled independently in the inner current control loops while the reactive power exchanged between the GSC and the ac grid is controlled in the outer control loops. The DC link voltage is also controlled in the outer control loops.

The ac side equations of the GSC can be written as:

$$\frac{dI_{gabc}}{dt} = \frac{-r_g}{L_g} I_{gabc} + \frac{1}{L_g} (V_{gabc} - V_{sabc}) \quad (3.43)$$

Where I_{gabc} and V_{gabc} are the 3 phase ac side of the GSC current and voltage respectively. The ac side of GSC resistance and inductance are r_g and L_g respectively. V_{sabc} is the three phase stator voltage.

Applying the synchronously rotating reference frame transformation to Equation (3.43) with the d-axis aligned to the grid voltage vector (V_s) means $V_s = V_{ds}$ and $V_{qs} = 0$. Then:

$$V_{dg} = r_g I_{dg} + L_g \frac{dI_{dg}}{dt} - \omega_s L_g I_{qg} + V_s \quad (3.44)$$

$$V_{qg} = r_g I_{qg} + L_g \frac{dI_{qg}}{dt} + \omega_s L_g I_{dg} \quad (3.45)$$

The same procedure in the RSC can be used to obtain the Proportional Integral controllers as follows:

$$V_{dg} = (k_{pg} + \frac{k_{ig}}{s}) (I_{dg}^* - I_{dg}) - \omega_s L_g I_{qg} + V_s \quad (3.46)$$

$$V_{qg} = (k_{pg} + \frac{k_{ig}}{s}) (I_{qg}^* - I_{qg}) + \omega_s L_g I_{dg} \quad (3.47)$$

The reference values of I_{dg}^* and I_{qg}^* can be determined from the outer control loop. The DC link voltage V_{DC} can be calculated from:

$$P_r - P_g = V_{DC} I_{DC} \quad (3.48)$$

The feedback loop and the PI controller of I_{dg} is:

$$I_{dg}^* = (k_{pv} + \frac{k_{iv}}{s}) (V_{DC}^* - V_{DC}) \quad (3.49)$$

The reactive power exchanged between the GSC and the ac grid can be controlled by the following equation:

$$Q_g = -\frac{3}{2} V_{ds} I_{qg} = -\frac{3}{2} V_s I_{qg} \quad (3.50)$$

The GSC control scheme is shown in Figure 3.21.

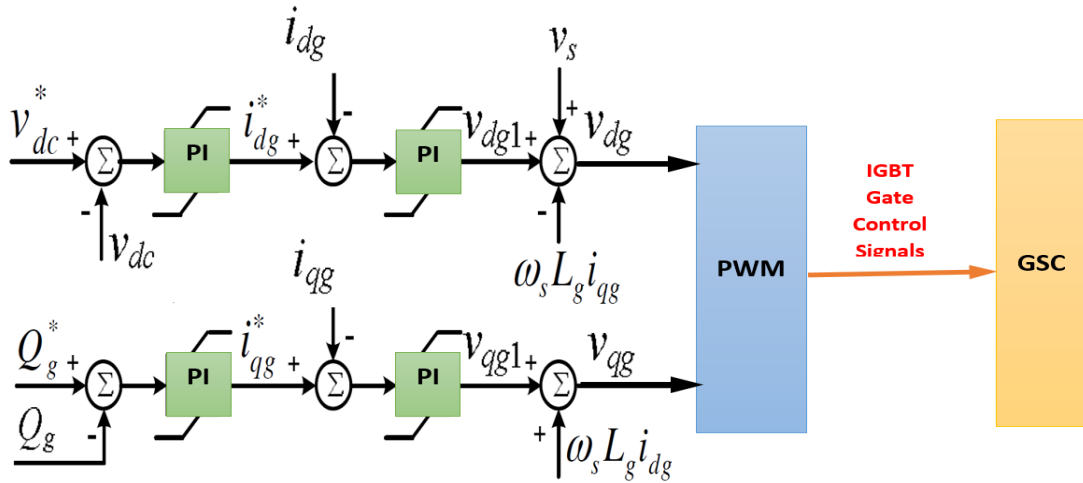


Figure 3.21: Overall vector control scheme of the DFIG grid side converter.

3.10.2.2 Synchronous Machines with Fully Rated Converters (PMSG)

Modern synchronous machines with fully rated converters (FRC) in the wind power industry are either based on direct-drive or geared (with gearbox) turbine generators. The direct-drive wind turbine uses either an electrically excited or Permanent Magnet Synchronous Generator (PMSG) and is characterised by a low rotational speed. The generator needs a high number of poles to generate a high torque and high power. The higher the number of poles, the larger the size of the turbine. However, the direct drive turbine requires less maintenance because it does not need a gearbox. The main advantage of using a PMSG based on a FRC in a wind turbine compared to the DFIG turbine is that the efficiency is higher, there is no need for brushes and fault-ride through capability is less complex [131]. It does not require an external current source for excitation as the rotor magnetic field is naturally created by the rotor magnetic material. Therefore, a PMSG can be defined as a form of synchronous generator where the rotor magnetic field is created by permanent magnets. The operation principle of the PMSG is summarised in the following points:

- The rotation of the generator rotor results in the magnetic field rotation in the machine relative to the stator windings.
- This leads to a changing magnetic flux linking with the stator winding and then inducing voltage.

- The induced voltage causes a current to flow because the stator windings is closed circuit.
- The current produces a second magnetic flux.
- This produces a torque and then electricity.

The characteristics of a synchronous generator with fully rated converters based on wind are shown in Figure 3.22. The wind turbine, with or without a gearbox, is controlled with either an induction generator or a PMSG and connected to the ac grid via fully rated power electronic converters. As shown in Figure 3.22, the generator is completely decoupled from the ac grid, which means the power factor can be corrected by the inverter; this improves the power output quality. This technology can operate under variable wind operation by enabling the Maximum Power Point Tracking (MPPT) such as pitch angle control to track the optimum power, particularly when the wind speed is between the cut-in and rated speeds.

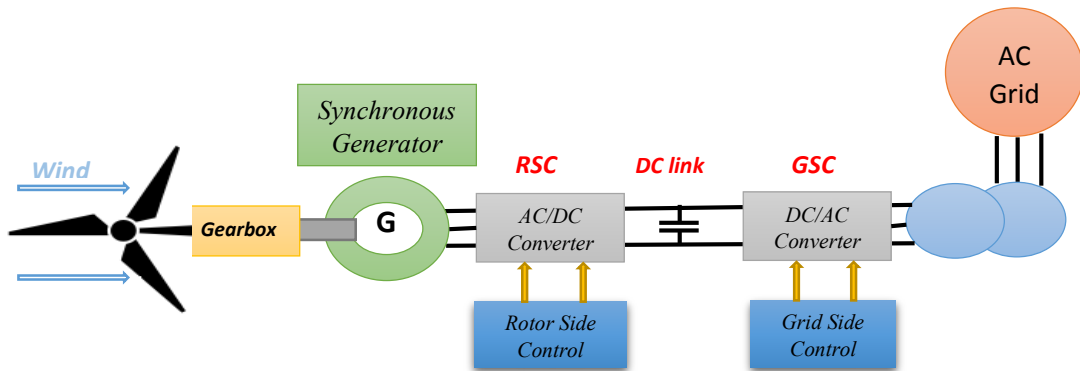


Figure 3.22: Synchronous generator with fully rated converters based on wind energy (general structure).

All electrical machine models are based on voltage and flux equations. Since the PMSG does not have equations for the rotor windings because the excitation is provided from permanent magnets, the dynamic model in a d-q axis frame is represented as shown below, considering the rotor speed ω_r as a reference of the Park Transformation.

The voltage equations:

$$V_{ds} = r_s I_{ds} - \omega_r \lambda_{qs} + \frac{d\lambda_{ds}}{dt} \quad (3.51)$$

$$V_{qs} = r_s I_{qs} + \omega_r \lambda_{ds} + \frac{d\lambda_{qs}}{dt} \quad (3.52)$$

The flux equations:

$$\lambda_{ds} = L_d I_{ds} + \lambda_m, \lambda_m \text{ is the magnetic flux in the rotor.} \quad (3.53)$$

$$\lambda_{qs} = L_q I_{qs} \quad (3.54)$$

From Equations (3.51) – (3.54), the voltage, the current and the torque equations can be defined as:

$$V_d = R_s I_d - \omega_r L_q I_q + \frac{dI_d L_d}{dt} \quad (3.55)$$

$$V_q = R_s I_q + \omega_r L_d I_d + \omega_r \lambda_m + \frac{dI_q L_q}{dt} \quad (3.56)$$

$$\frac{dI_{ds}}{dt} = \frac{V_{ds} + L_{qs} \omega_r I_{qs} - R_{ds} I_{ds}}{L_{ds}} \quad (3.57)$$

$$\frac{dI_{qs}}{dt} = \frac{V_{qs} - L_{ds} \omega_r I_{qs} - R_{qs} I_{qs} - \omega_r \lambda_m}{L_{qs}} \quad (3.58)$$

$$T_e = \frac{3p}{2} [I_{ds} I_{qs} (L_{ds} - L_{qs}) + \lambda_m I_{qs}] \quad (3.59)$$

$$\frac{d\omega_r}{dt} J = (T_e - T_m) \quad (3.60)$$

Where ω_r is the rotor speed in rad/s, and V_d and V_q are the equivalent stator voltages in the d-q axis. The permanent magnet flux linkage is λ_m and I_d and I_q are the equivalent stator currents. L_d and L_q are the equivalent inductances of the stator associated with the d and q axes respectively. T_e and T_m are the electrical and mechanical torques respectively while J is the inertia of the rotating components (kg.m^2). The number of pole pairs is p . The power has to remain invariant when transforming from a three phase system (abc) to a two phase system (dq). Therefore, for a d-q transformation a factor $3/2$ times requires inclusion in the power equations to represent the equivalent power of a three phase system. Hence, the active and reactive power equations in d-q frame are:

$$P_{dq} = \frac{3}{2} [V_q I_q + V_d I_d] \quad (3.61)$$

$$Q_{dq} = \frac{3}{2} [V_q I_d - V_d I_q] \quad (3.62)$$

1- Rotor Side Converter (RSC)

In a fully rated converter wind generator, the RSC is directly connected to the generator, as shown before, to control its operation. The control system is usually based on a synchronous d-q reference frame, where the d-axis is aligned to the rotor flux which is provided by the permanent magnets. The q-axis is 90° ahead of the d-axis in the direction of the rotor rotation. Hence, the q-axis current I_q is proportional to the active power (P). The d-axis is usually assumed to be zero to minimise copper loss.

2- Grid Side Converter (GSC)

The GSC is usually represented in the d-q synchronous reference frame, where the d-axis is aligned to the grid voltage. Hence, the d-axis current controls the active power whilst the q-axis current controls the reactive power and ac voltage. The GSC also controls the DC link voltage through its d-axis current to ensure active power input balances the output power. The control schemes of the RSC and GSC are illustrated in Figures 3.23 and 3.24 respectively [132]. The power electronic converters of this type of wind generator can be arranged in different ways. The RSC can be a diode-based rectifier or a Pulse Width Modulation (PWM) voltage source converter (VSC), while the GSC is typically a PWM (VSC).

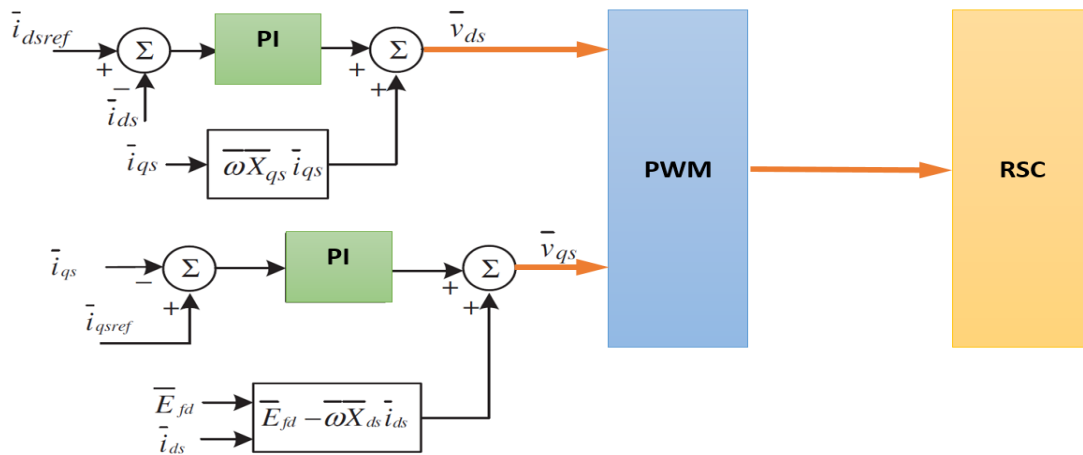


Figure 3.23: Vector control of the rotor side converter (RSC).

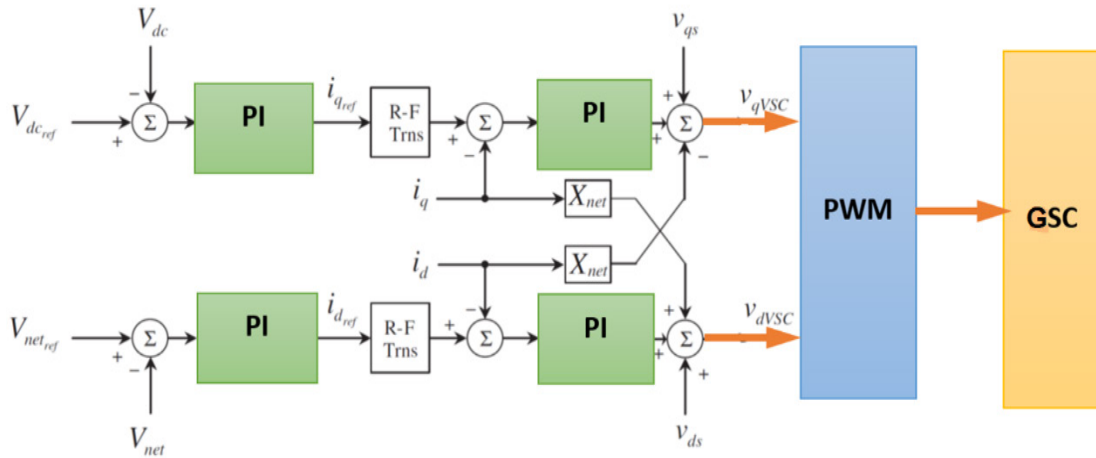


Figure 3.24: Vector control of the grid side converter (GSC).

3.11 Wind Speed

The output power of a wind turbine depends considerably on the wind speed and, as shown in Equation (3.1), the output power is proportional to the cube of the wind speed. This leads to large variations in output power when the wind turbine operates under low and high wind speed conditions at the same period of time. Wind speed variation is a critical aspect in wind power development and industry. The site selection for wind farms and consideration of wind speed fluctuations are significant in any wind farm project. Wind speed fluctuations over long and short timescales can have a significant effect on the design and operation of the wind turbine and the quality of power delivered to the ac grid. Therefore, it is important to study the wind speed at a specific site before installing a wind turbine. There is a number of methods that can be used for wind speed to be modelled in power systems, such as the ARMA (Autoregressive Moving Average) model, MA (Moving Average) model, Mean Observed Wind Speeds, Markov Chain Model, Normal Distribution and Weibull Distribution [133, 134]. The most commonly used method to describe wind speed is Weibull Distribution. Weibull Distribution is a probability density function of a continuous variable whose integral over a region gives the probability that a random variable falls within the region. This function can be used to describe different distribution characteristics by adjusting the parameters c and k . It can be combined with

the Monte Carlo Simulation Method to give better performance in wind speed modelling and its results are similar to the actual wind speed profiles.

The expression of an individual Weibull probability density function is given by:

$$f(v) = \frac{k v^{k-1}}{c^k} e^{-\left(\frac{v}{c}\right)^k} \quad (3.63)$$

Where $f(v)$ is the probability of occurrence of wind speed v ($v \geq 0$), the Weibull scale parameter is c ($c > 0$) and k ($k > 0$) is the shape parameter. The complementary cumulative Weibull distribution function $CF(v)$ gives the probability of the wind speed exceeding the value v and it is expressed as:

$$CF(v) = e^{-\left(\frac{v}{c}\right)^k} \quad (3.64)$$

Therefore, the cumulative probability density function can be calculated as:

$$F(v) = 1 - e^{-\left(\frac{v}{c}\right)^k} \quad (3.65)$$

Figure 3.25 shows the variations in wind speed with a time resolution of 10 minutes over several months. The Weibull probability density for this site with a mean wind speed of ≈ 1.25 m/s is illustrated in Figure 3.26. Figure 3.27 shows the cumulative Weibull probability distribution for this site; the scale parameter c is 1.2903 and the shape parameter k is 1.2980. Figure 3.28 shows real wind speed data for a five month period (1st of April 2009 at 00:00 to 1st of September 2009 at 00:00) with a time resolution of 10 minutes. Figure 3.29 illustrates the Weibull probability distribution for this site with a mean wind speed of ≈ 5.8 m/s. The cumulative Weibull distribution for this particular site is shown in Figure 3.30; the scale parameter c is 7 and the shape parameter k is 1.6748 [135]. From the previous figures, low and high wind speed sites are discussed.

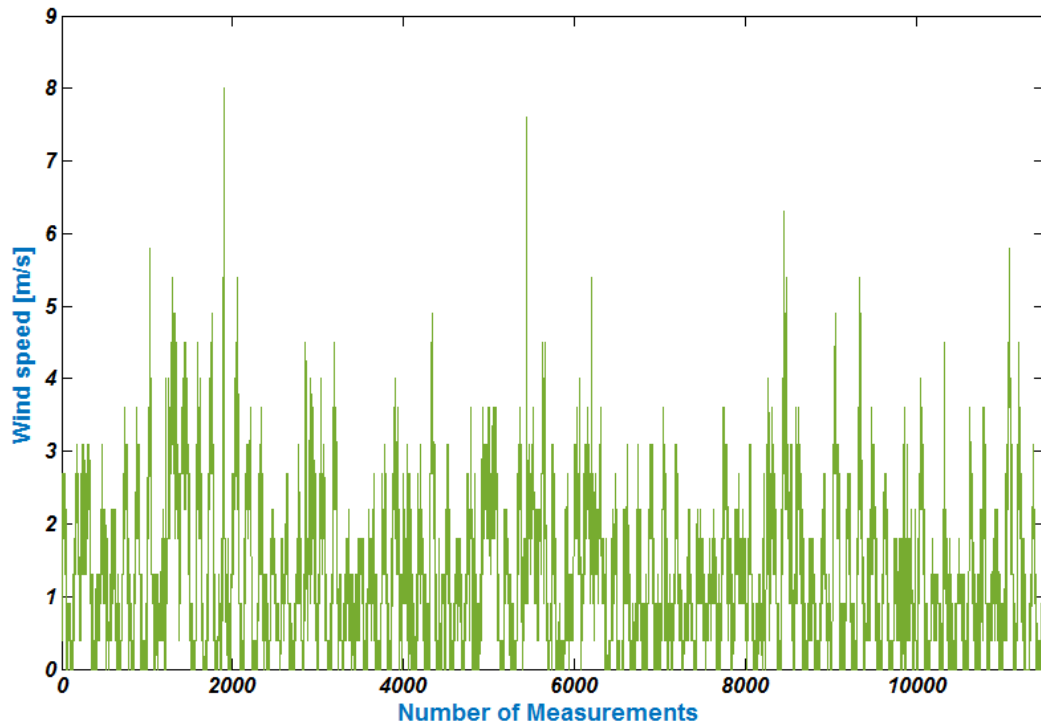


Figure 3.25: Variations in wind speed with a time resolution of 10 minutes over several months for a low wind speed site.

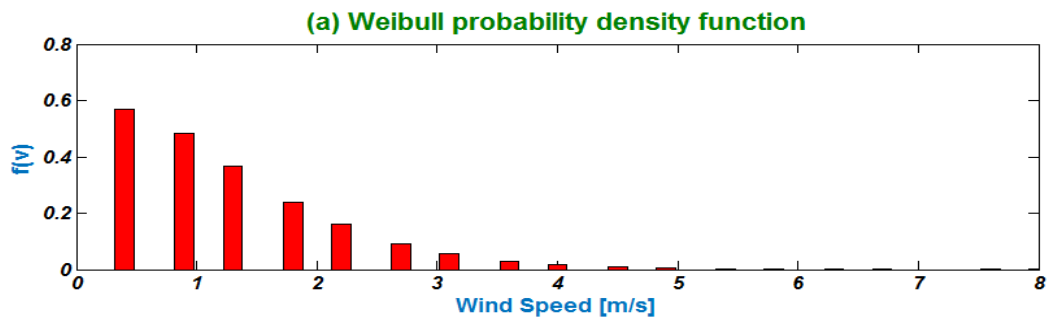


Figure 3.26: Weibull probability density for a low wind speed site.

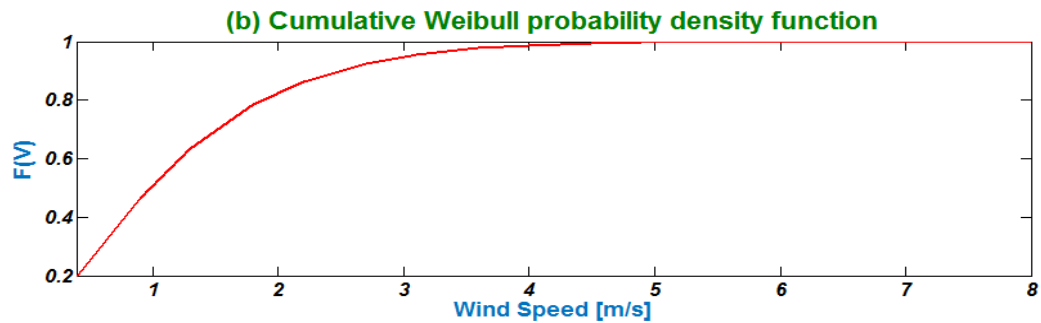


Figure 3.27: Cumulative Weibull probability distribution for a low wind speed site.

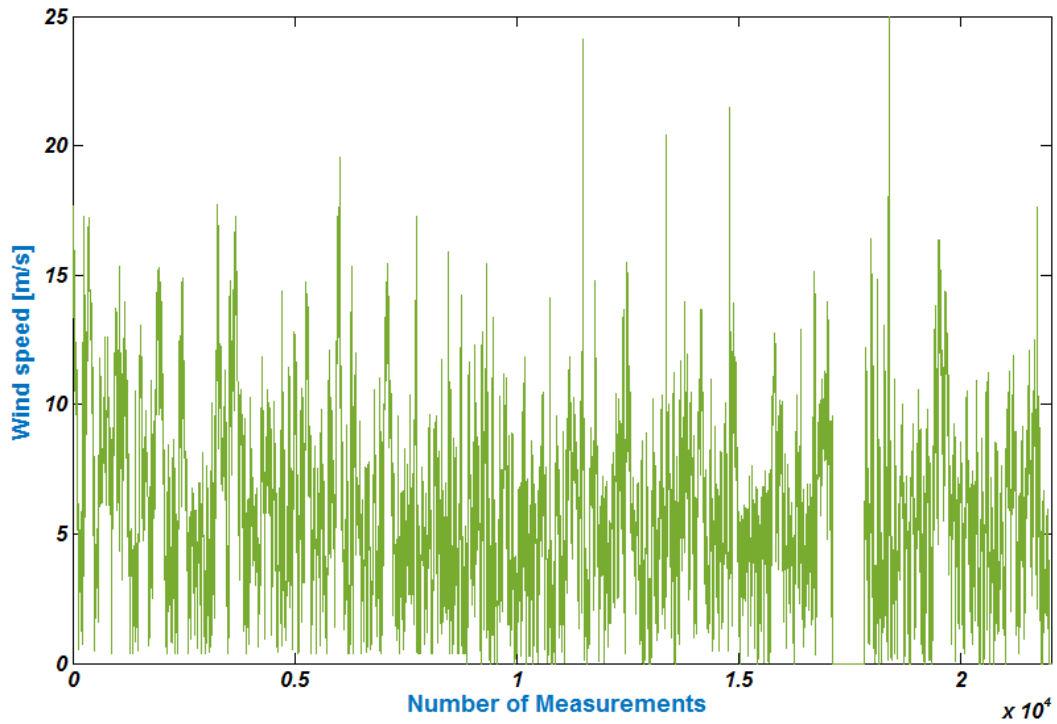


Figure 3.28: Variations in wind speed with a time resolution of 10 minutes over several months for a high wind speed site.

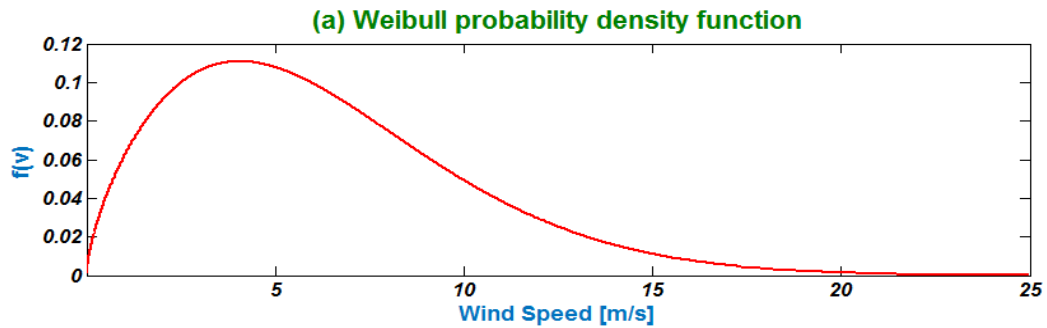


Figure 3.29: Weibull probability density for a high wind speed site.

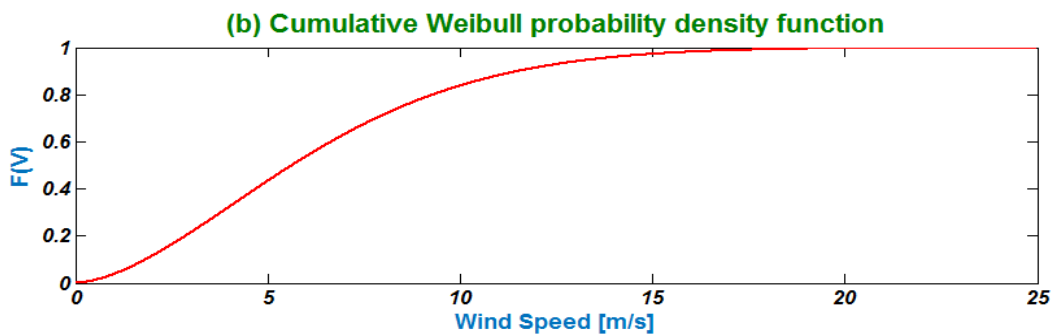


Figure 3.30: Cumulative Weibull probability distribution for a high wind speed site.

3.12 Impact of Wind Speed Variations

Wind power has an intermittent nature because it depends considerably on wind speed, as shown before. This leads to difficulties in predicting the total amount of output power produced by wind turbines and brings great challenges to the integration of large wind power into power systems. Increased penetration of relatively large wind power into power networks has changed the nature and dynamics of these networks. Wind power has an impact on power system reliability and operational security and it is significant to study the consequences of dynamic interaction between wind units and power systems before installing a wind farm into an ac grid.

Wind turbines produce power when the wind is blowing and wind speed cannot be predicted accurately over short periods, minute to minute or hour to hour. Wind speed variations may cause an increase in the operating costs of the power system as a whole because the system must maintain an instantaneous balance at all times between load demand and power generation. In general, the costs associated with maintaining this balance are known as ancillary services costs.

Wind power generation is characterised by variations in all timescales: minutes, hours, days, months and years. The impact of wind power on the power system can be divided into two categories: short term impact and long term impact. Short term refers to balancing the system on the operational timescale from minutes to hours, and long term refers to generating enough power in peak load cases. From the literature it is clear that wind speed variations have an impact on system stability [136, 137], reliability [138, 139], power quality [140, 141] and reserve [142, 143].

A stable and reliable voltage supply for any electricity market customer is a must as connection of wind turbines may cause voltage and frequency stability problems. The intermittent nature of wind power can also affect the quality of the voltage supplied to consumers. This can be worse if wind penetration levels increase. Power system protection is also highly affected by wind power because the integration of wind energy injection may change power flow directions. Thus, conventional protection systems could fail under

fault conditions. In recent years, new requirements for wind turbine operation have been implemented in order to keep power systems stable under disturbances, as described in the grid code requirements section.

3.13 Maximum Power Point Tracking (MPPT)

The wind turbine output power depends on the turbine tip speed ratio (TSR) at a given wind speed. The maximum power extracted from the wind energy can be obtained at a particular TSR for a particular wind speed and blade pitch angle. The turbine's rotor speed should be changed when the wind speed changes to extract the MPP. Figure 3.31 shows the wind turbine power for different wind speeds as a function of rotor speed. As illustrated in this figure, for each wind speed the rotor speed changes to get the maximum power. To determine the optimum rotor speed to get the maximum power at a given wind speed, Maximum Power Point Tracking (MPPT) methods can be used.

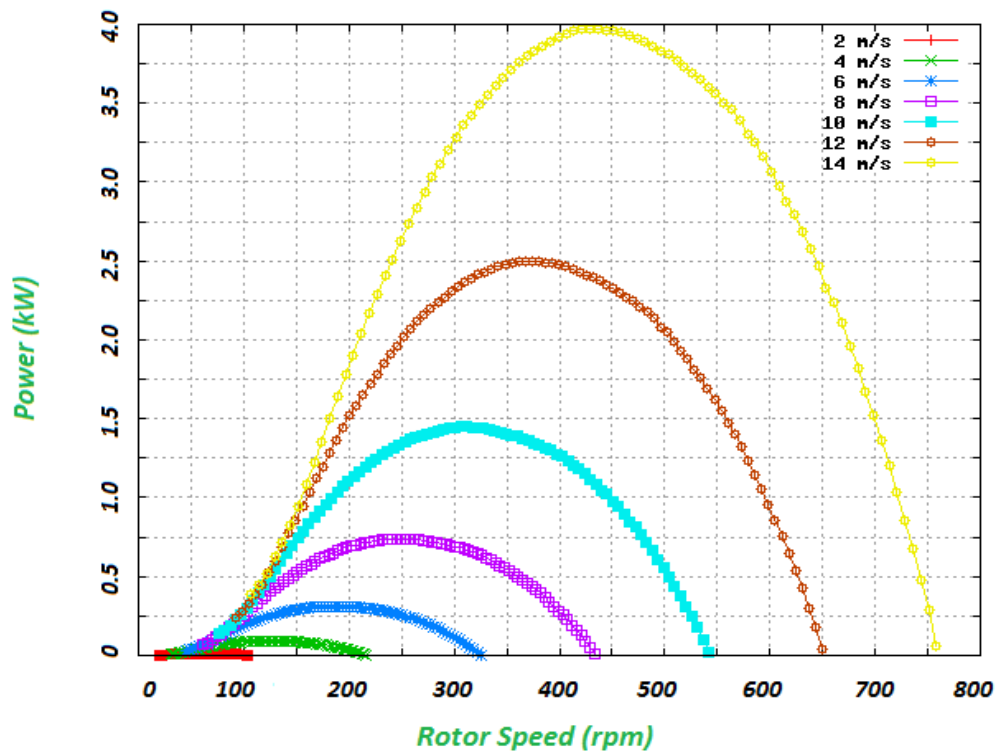


Figure 3.31: The wind turbine power output for different wind speeds as a function of rotor speed.

MPPT algorithms are classified into three categories: tip speed ratio control (TSR), power signal feedback (PSF), and Hill-climb search (HCS) based [144]. There are other MPPTs which have been proposed in recent years, such as look-up table, pitch control, fuzzy logic control and other neural network optimisation techniques. This thesis discusses only the pitch control technique which is the dominant type in newly installed wind turbines. When the rotational speed is constant, pitch angle regulation is necessary, especially if the wind speed is above the rated wind speed. Small changes in pitch angle can lead to a significant change in the output power. Pitch control can be used during low and high wind speed conditions. In low wind speed conditions, pitch control works as an MPPT to extract the maximum available power. However, it works as a speed regulator during high wind speed for de-loading purposes and limits the power capture of the turbine above the rated wind speed. The range of pitch variation needed for effective power control is typically between 0° and 35° . Turbine blades can be pitched up to 90° for aerodynamic braking purposes. Different artificial intelligence techniques, such as fuzzy logic controller, can be used to select the required pitch based on the reference power. Therefore, the pitch angle control can be summarised in the following points:

- Track the maximum available power from the wind turbine when the wind speed is below the rated wind speed by pitching the blades at their optimum to give maximum power.
- When the wind speed is above the rated wind speed, the pitch controller can regulate the aerodynamic power to prevent input mechanical power exceeding the design limits.

3.14 Power Electronics Applications

Power electronics applications are significant parts of the variable speed wind industry and they are essential for fixed speed wind turbines where the system is directly connected to the ac grid, as power electronics switches such as thyristors are used as soft-starters. The main purpose of power electronics in wind turbine operations is to match the characteristics of the wind generator to the grid connection requirements, such as voltage, frequency, control of active and reactive powers, and harmonics. Power electronics in

variable speed wind turbines are divided into two categories: wind generators based on a partial-scale and those based on full-scale power electronic converters. Power electronics applications have been developed considerably in the last three decades. Advancements in semi-conductor devices and microprocessor technology have led to developments in power electronics. These include self-commutated devices such as the insulated gate bipolar transistor (IGBT), the metal oxide silicon field effect transistor (MOSFET), and grid-commutated converters which are based on thyristor converters with high power capacity. Thyristor converters absorb reactive power and do not have the ability to control reactive power. They are mainly used for very high voltage and power applications such as conventional HVDC systems. However, self-commutated devices such as the IGBT with turn-off ability can transfer both active and reactive power in both directions (DC-AC or AC-DC). They usually use pulse width modulation (PWM) control methods and can deliver reactive power.

Power electronic converters are used in the wind industry to improve dynamic and steady-state performances of wind turbines. They can help to control the wind generator and decouple the generator from the ac grid. The generator of the wind turbine is usually connected to the ac grid through power electronics converters. For induction generators with rotor windings, the stator of the generator is connected directly to the grid while the rotor windings are connected to a power electronics controller resistor or to the grid through slip rings and a power electronics converter. For a synchronous generator and induction generator without rotor windings, full rated power electronics converters are used to connect the stator to the ac grid and the full power can be delivered through these converters to the grid.

3.15 Challenges of Wind Power

This section will discuss the requirements and limitations of large scale wind power generation, such as the amount of land needed, the social impact, reliability, wind power efficiency and grid codes.

3.15.1 Land for Wind

This section will discuss how much land wind turbine installation needs, i.e. it will discuss the land area needed for onshore wind turbine installation. In recent years, onshore wind has become more cost effective than offshore. Also, offshore wind farms take longer to develop because the sea is a naturally more hostile environment. However, the investment in onshore wind sector will be uncertain beyond 2016, following changes to onshore subsidy and planning policies in the UK that were announced in June 2015. Onshore wind installations beyond 2016 is under severe threat of cancellation or curtailment due to the subsidy cuts. At least 1.2 GW (more than 50 projects) onshore wind capacity will be installed in 2016 which is more than three times the capacity installed in 2015. This is because onshore wind developers are trying to get these wind projects in operation before current subsidy ends in 2016. For the offshore wind sector, the UK's government has set a long term framework for offshore wind to allow industry to plan ahead and attract investment. Offshore wind developers are set to install more than 4.5 GW of offshore wind capacity in 2016 [145].

The land area of onshore wind farms will be discussed because offshore wind areas are usually not allocated to individual owners. According to the British Wind Energy Association, there are around 4776 onshore wind turbines spread throughout the UK with a total capacity of 7.951 GW [146, 147]. Generation of 10% of the UK's electricity from onshore wind would require the installation of around 12 GW of wind energy capacity. These wind installations need between 80,000 to 120,000 hectares (1 hectare = 0.01 km²) depending on the size of the turbine and this represents 0.3% to 0.5% of the UK's land area. Only around 1% of this area (800 to 1200 hectares) would be used to house the wind turbines, foundations, electrical infrastructure and access roads. The remainder of this area, which represents 99%, would be used for other purposes such as natural habitats or farming. On the other hand, 288,000 to 360,000 hectares are covered by roads in the UK, representing 1.2% to 1.5% of the UK's land area, and agriculture in the UK occupies around 77% of the UK's land area, amounting to around 18.5 million hectares. At present, there is 19.5 MW capacity of wind turbines installed per 1000 km of European land area [148].

As described above, wind turbine installation would occupy only around 1% of the targeted land area (0.3% to 0.5% of the UK’s land area) and 99% of this area could be used for farming, ranching or tourism. This means that wind power installations are not a problem in terms of the land area that they require. They also offer guaranteed income for landowners and farmers.

3.15.2 Social Acceptance of Wind Power

Wind power is becoming a significant source of electricity worldwide and an important contributor to renewable energy and tackling climate change. Although there is opposition to installation of wind units at some regional and local levels, the social acceptance of wind power has increased considerably. According to a 2011 Eurobarometer survey, most European citizens were more favourable about renewable energy than other energy sources, as shown in Figures 3.32.

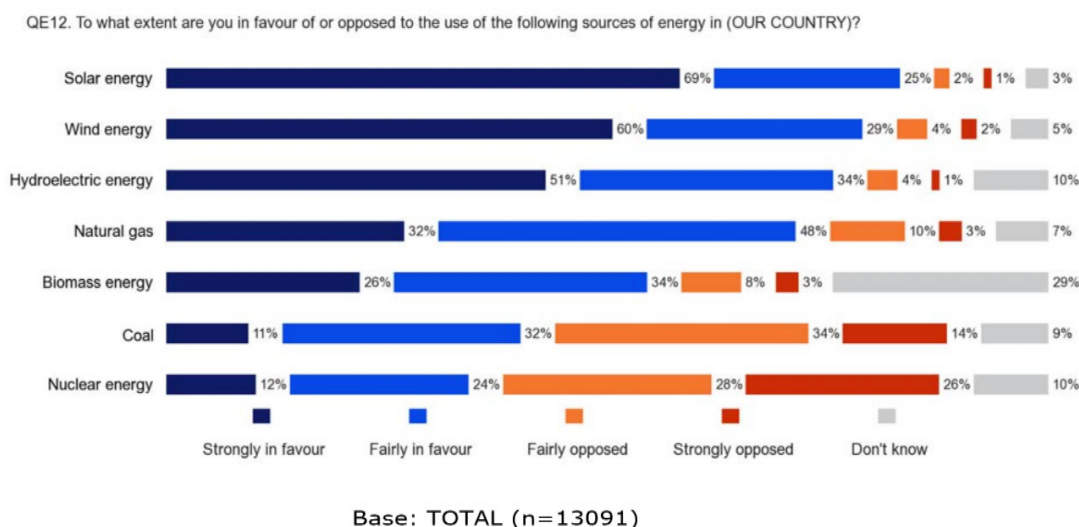


Figure 3.32: Social acceptance for different sources of energy in Europe in 2011 [149].

As shown in Figure 3.32, around 6% of Europe citizens are not in favour of wind power and their opinion is based on several factors, such as wind turbine noise, dislike of wind farms visually, harm they may cause to animals and harm they may cause to human health. The noise of wind turbines has been decreased considerably, especially in three bladed units, and the sound of the blowing wind in rural areas is louder than wind turbines. A Canadian report called ‘the potential health impact of wind turbines’ was released in 2010

and confirmed that the noise level of wind turbines complies with the recommendations of the World Health Organisation (WHO) for residential areas. The look of wind turbines may have been accepted by tourists but some local people found that they distracted from the beauty of nature in several places [150]. Another study was completed by medical professionals from different leading countries in wind power in 2009 called ‘Wind Turbine Sound and Health Effects’. It found that there is no direct evidence that the audible or sub-audible sounds, including infrasound, produced by wind turbines have any significant physiological effects [151]. Many international groups that are interested in the environment and nature conservation support wind energy, such as Birdlife, Greenpeace and Friends of the Earth. Several studies in ecology found that birds’ deaths caused by wind turbines represented only a small fraction of those caused by other human activities, such as buildings and vehicles. They also found that the majority of these animals could live with wind turbines once they were operational [152].

3.15.3 Reliability

Wind power generation has an energy source with an intermittent nature and depends significantly on wind speed. Wind speed fluctuates and depends on several factors, such as the wind turbine’s location. This leads to fluctuating output power from wind turbines which results in reliability problems in power systems. An increase in wind power penetration in power systems causes a negative impact on power generation reliability and the impact increases as the penetration level increases. It is necessary to consider system operator experience and data to study and understand the reliability of wind turbines. It is significant to study the reliability of each of the components of a wind turbine and detect failures in a short amount of time to avoid damaging other components. It is very important to detect a failure in one component and repair it quickly as the cost of repairs can increase significantly if other components get affected. In [153] it was found that faults can be predicted 60 minutes before they occur by using a condition monitoring system. There have been significant improvements in the wind power industry in terms of reliability analysis of wind power [154, 155] and maintenance and repair methods using condition monitoring strategies integrated with supervisory control and data acquisition (SCADA) systems. These fault detection methods have been used to detect faults and

provide early warnings to enable wind turbine operators to take action and carry out predictive maintenance, hence decreasing failure rates [156]. Preventive maintenance actions are required more in large wind turbines than smaller ones. A wind turbine's average lifetime is between 20 and 25 years and can be expressed as a bathtub curve, as shown in Figure 3.33. The failure rate is higher in the infancy period and wear-out as shown, but with lower rates in the middle (useful life period).

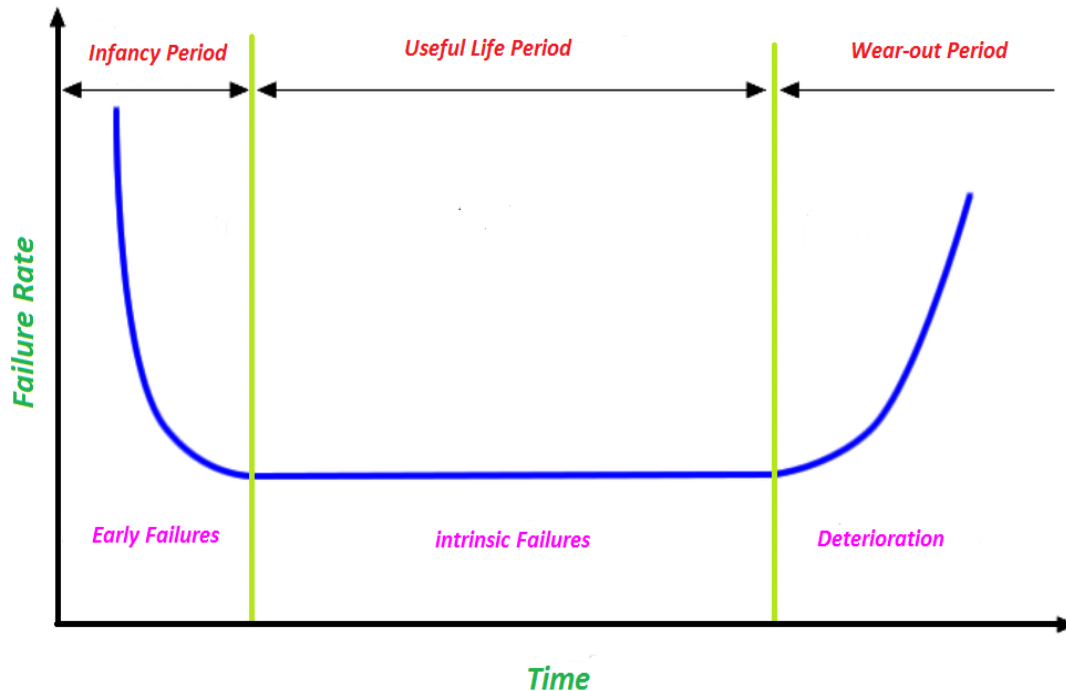


Figure 3.33: Typical bathtub curve for wind turbines.

Historical reliability data for wind turbines is important in wind power reliability analysis and the number of failures for each component can be used as an indication to improve overall wind turbine reliability. Figure 3.34 shows the percentage of required maintenance and repairs for the main components of wind turbines according to the American Wind Energy Association (AWEA).

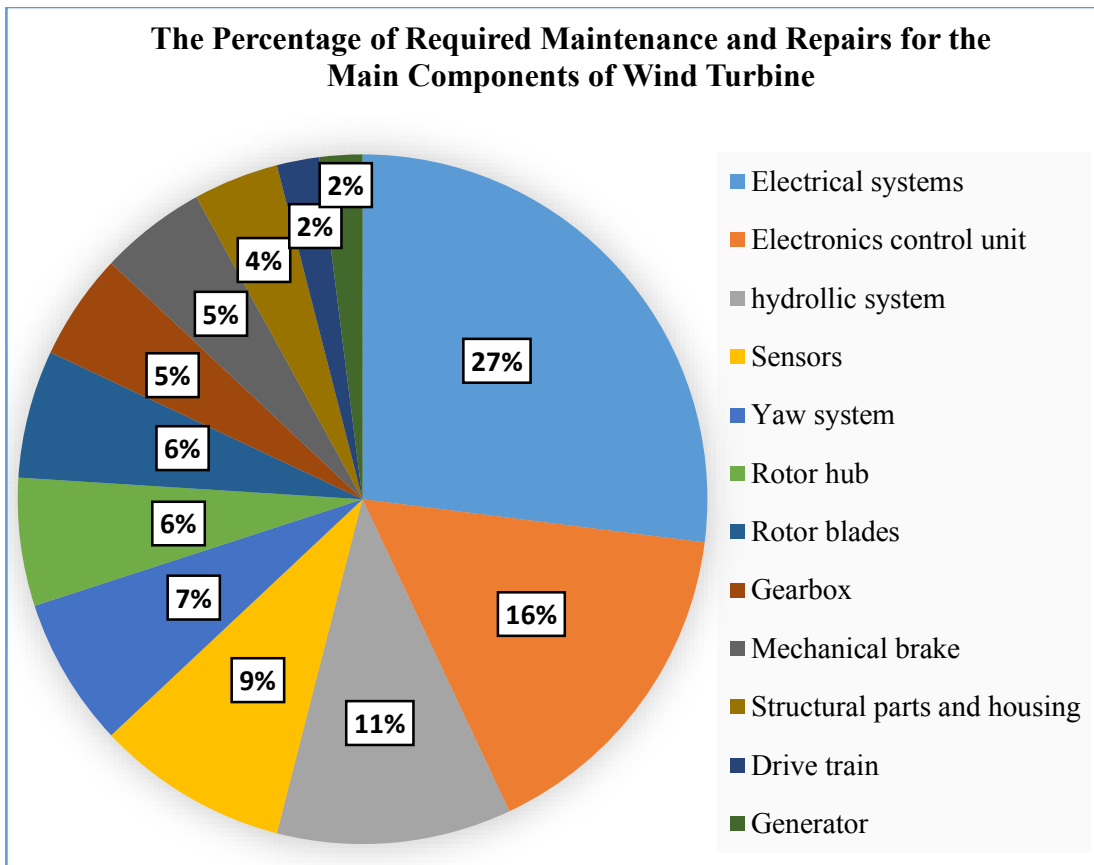


Figure 3.34: Percentage of required maintenance and repairs for the main components of wind turbines according to AWEA [157].

3.15.4 Wind Turbine Efficiency

Wind turbines start operating and producing power at wind speeds of 4 to 5 m/s, known as the cut-in speed, and they generate maximum power at the rated speed, which is 15 m/s. They shut down when the wind speed exceeds 25 m/s, called the cut-off speed. However, they produce different amounts of output power depending on the wind speed. A modern wind turbine generates electricity 70–85% of the time. The efficiency of a wind turbine can be defined as the percentage of the ratio between the input power (kinetic energy of the wind) to the output power (electricity). According to the European Wind Energy Association (EWEA), a typical wind turbine generates around 24% of the theoretical maximum output per year (41% for offshore wind) [148]. This is called the capacity factor (CF). Conventional power plants have a capacity factor between 50% and 80%. On the other hand, the efficiency is determined by how much kinetic energy in the wind is

transformed into electrical energy. The theoretical maximum efficiency of any wind turbine is 0.59, known as the Betz Limit or Betz Law. This means no more than 59% of the energy carried by the wind can be extracted by a wind turbine, i.e. the maximum mechanical energy extracted from the wind that drives the rotor of the turbine is 59% of the kinetic energy. There are also losses in converting mechanical energy into electricity. The real world limit is also below the Betz Limit with values of 0.35–0.45, even for the best designed wind turbines. In practice, wind turbine efficiency is typically between 10% and 30%, because there are mechanical losses in the gearbox, bearing, etc., which mean that only 10% to 30% of the wind energy is actually converted into usable electricity.

3.15.5 Grid Code Requirements for Wind Power

In the past, the capacity and penetration level of wind power in power systems were small compared with the total power generation. No special requirements for wind power integration in power systems were applied because wind farms were connected to the ac grid on a small scale and their impact on power system operation was limited and could be ignored. Under disturbances and abnormal conditions these wind turbines were disconnected. However, the rapid increase in integration and development of wind power has led to a new scenario in terms of operating wind farms properly. The increase in wind power penetration levels has affected the stability of power systems as wind turbines are an intermittent source of energy and depend considerably on the availability of wind. Thus, wind power integration must meet special requirements and considerations before being connected to power systems [158, 159].

Many countries around the world have developed new requirements known as grid codes for wind farm connections. This section highlights the UK grid code requirements for wind farm connection in power systems. These regulations for wind integration require wind turbines to provide additional services and functionality, such as voltage and reactive power control, active power and frequency control and fault ride through capability [160]. Distributed generation connected to distribution networks with a capacity of 100 MW or more in England & Wales, 30 MW or more in Scottish Power Transmission, 10 MW or more in SHETL region, or 10 MW or more in an Offshore Transmission System are

required to comply with the grid code, to have a bilateral connection agreement with National Grid Electricity Transmission and to submit certain data directly [161]. The UK grid code requirements for wind farm connection are summarised in Figures 3.35, 3.36 and 3.37. Figure 3.35 shows the relationship between the wind farm active power and the ac network frequency and this can be summarised in below points:

- When the system frequency is between 49.5 Hz and 50.5 Hz, the wind farm must be able to operate continuously with constant active power.
- When the system frequency changes within a range 49.5 Hz to 47 Hz, the wind farm active power output should not be reduced by more than 5%.
- The wind farm must be able to operate continuously for system frequency between 47 Hz and 52 Hz for periods less than 30 seconds.

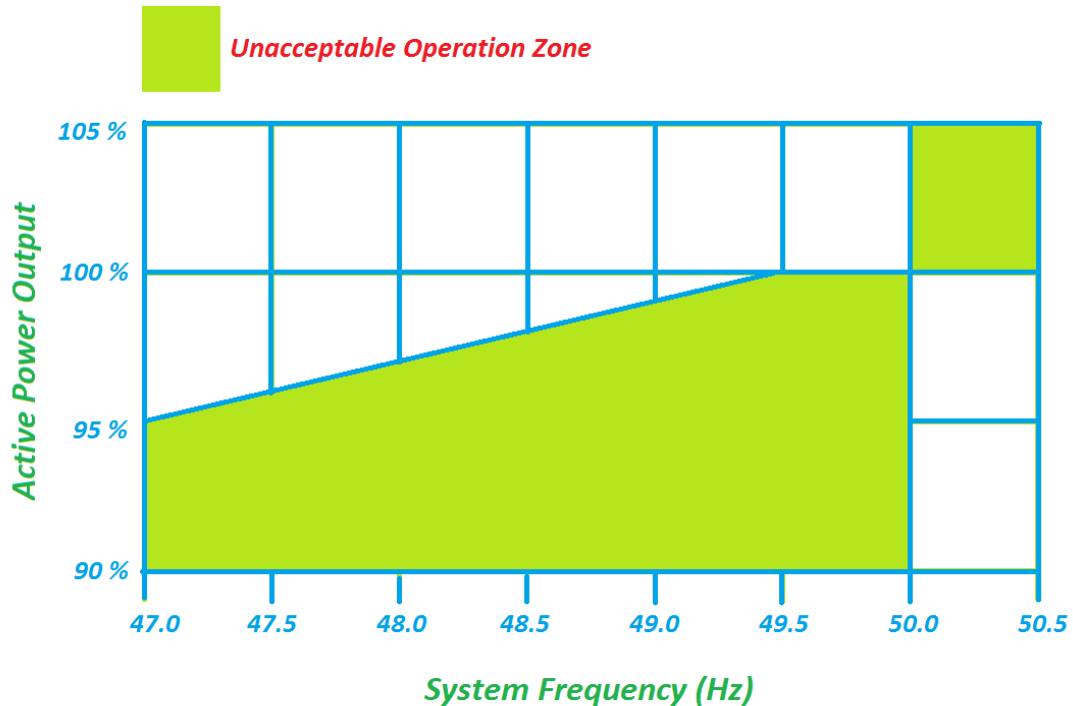


Figure 3.35: Frequency requirements for wind turbines in the UK.

Figure 3.36 shows the ac fault ride through capability requirements for wind turbines in the UK and it can be summarised in the following points:

- A wind farm must remain transiently stable for a closed-up solid short circuit with duration of 140 milliseconds.
- A wind farm should remain connected to the power system for any dip duration on or above the red line shown in Figure 3.36.
- During the fault period, the wind farms and DC converters must generate the maximum reactive power possible without exceeding their thermal ratings.
- The voltage at entry points must be restored to 90% of their pre-fault values within 500 milliseconds as shown in Figure 3.36.
- During the fault period, the terminal voltage of the wind farm should not be < 15% of the nominal voltage.

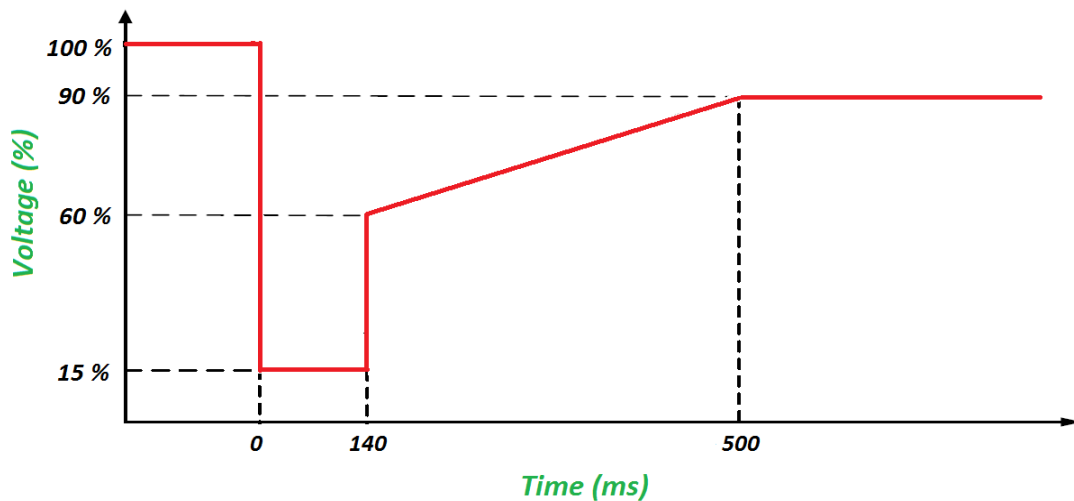


Figure 3.36: AC fault ride-through capability requirements for wind turbines in the UK.

The reactive power requirements for wind turbines in the UK is defined as shown in Figure 3.37. As indicated in the British grid code section CC.6.3.2 [161], all wind farms must be capable of supplying rated MW at the range of power factors from 0.95 lagging to 0.95 leading at the point of common coupling (PCC) with the UK transmission systems. With all plants in service, the reactive power limits defined at rated MW at lagging power factor will apply at all active power transfer levels above 20% of the rated MW output as illustrated in Figure 3.37. With all plants in service, the reactive power limits defined at rated MW at leading power factor will apply to all active power transfer levels above 50% of the rated MW output as shown in Figure 3.37. These reactive power limits shall reduce

linearly below 50% active power output unless the requirement to maintain the reactive power limits defined at the rated MW at leading power factor down to 20% active power transfer.

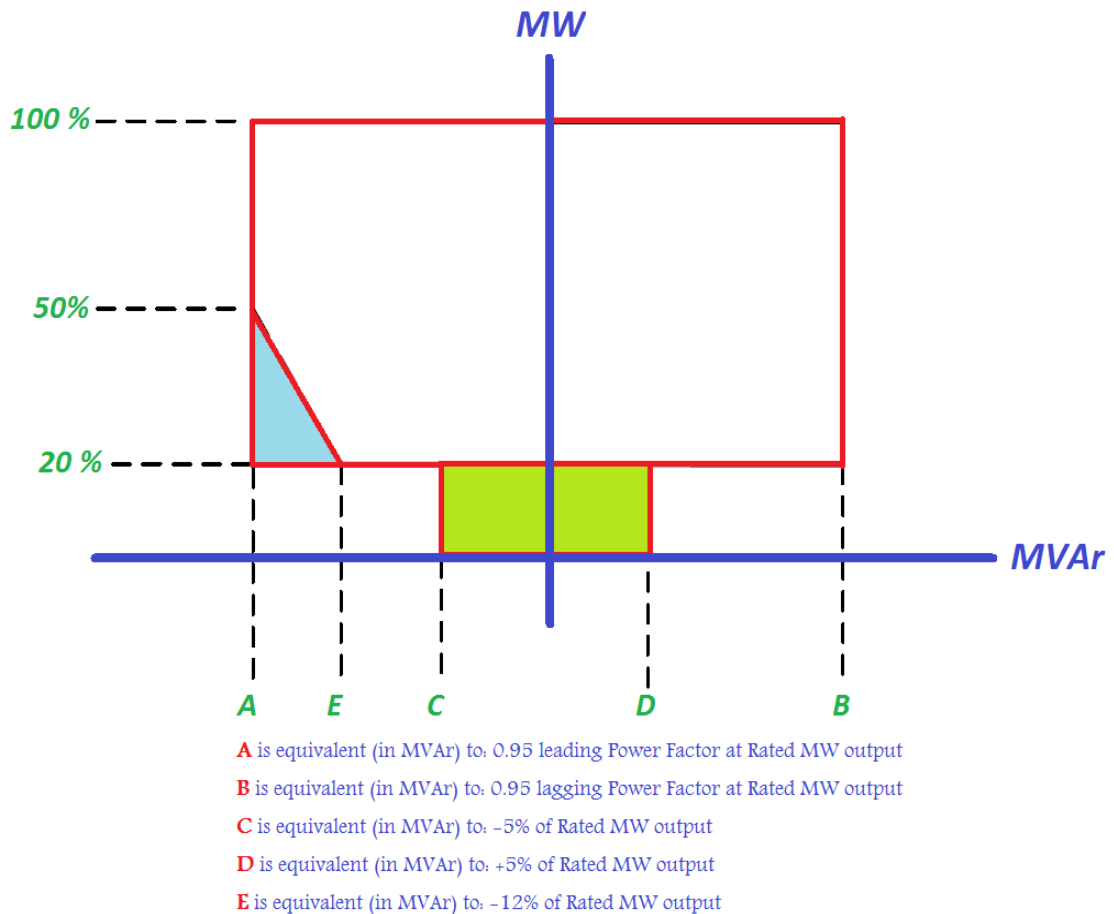


Figure 3.37: Reactive power requirements for wind turbines in the UK.

3.16 Conclusions

Wind energy is one of the most promising renewable energy sources for meeting emission reduction targets and increasing renewable energy portfolios, as set by several countries worldwide to tackle climate change. Wind power has increased dramatically in the last few years and is approaching more than 369 GW installed capacity. This chapter has discussed the potential of wind power and its benefits. These have led to a rapid increase

in the wind capacity installed and this is expected to continue in the short and long term. It has been found that wind power integration in power systems will continue in the future and that many countries around the world set economic incentives to promote wind power. This chapter has also investigated how much CO₂ wind power integration can avoid compared to conventional power plants. Wind power growth in Europe and the UK has been discussed and it has been found that the UK is the leading country in terms of cumulative offshore installed wind capacity, at more than 4.4 GW.

Current wind power technologies and their principles of work have been discussed in this chapter. Different wind generator characteristics have been studied, such as those of the Fixed Speed Squirrel Cage Induction Generator, Doubly Fed Induction Generator (DFIG), and Synchronous Generator with Fully Rated Converters. DFIGs are synchronous generators that are based on variable speed operation mode. They have the controllability to work in different wind speed profiles. They also have power electronics converters in their structure which give them the ability to decouple the generator from the ac grid and control different generator parameters, such as voltage, frequency, active and reactive powers. In addition, this chapter has discussed the relationship between the output power of a wind turbine and wind speed. Wind speed models such as Weibull Distribution have also been investigated and the impact of wind speed variations on power systems has been highlighted. Pitch control and power electronic applications in wind power have also been discussed. Various challenges facing integrating of wind power in power systems, such as how much land is needed, social acceptance, reliability problems, wind turbine efficiency and grid code requirements, have also been studied.

CHAPTER 4 Fault Ride through of Distribution Systems with High Penetration of Renewable Energy

4.1 Introduction

There has been a significant increase in the demand for electricity noticed over the last few years. This has coincided with the growing penetration of renewable energy resources aimed at tackling climate change problems and promoting carbon free technology [162]. Power systems have experienced power quality problems due to heavy loading electronic devices and/or nonlinear loads on system equipment. Meanwhile, distributed generations have contributed towards minimising the burden on several types of system equipment [163, 164]. DGs sized between 50 kW and 1 MW are small when compared with total system generation and load demand. However, they contribute towards system security and reliability when they penetrate different locations with different size units. They are equipped with power electronic devices to interface with distribution networks and mitigate bi-directional power flow [17]. These devices enable DG units to operate in a standalone mode as a voltage source or in a grid connection mode as a current source [165].

Fault ride through (FRT) of distribution systems with high renewable source penetration can be defined as the ability of such systems to remain in operation during and after a wide range of fault scenarios. Due to the rapid increase in renewable power penetration in distribution networks, several countries have set new requirements for renewable energy sources interconnected to utility grids [166]. Some countries e.g. Germany, Denmark and Ireland have specific FRT grid code requirements for distribution systems as well as for transmission ones, however, other countries have only FRT requirements for transmission systems [167, 168]. Distributed generation are required to comply with grid codes, for instance 1 MW or more generation capacity in Germany, 5 MW or more in Ireland and 30 MW or more in Scotland. As the number of renewable energy units increases, loss of a considerable part of these units in the case of network faults is not desirable [169].

Therefore, ride through control for renewable units is necessary for abnormal grid conditions.

4.2 Fault Ride through Background

Grid disturbances such as severe faults can lead to disconnection of generating units such as renewable units. The disconnection of renewable units, especially in high renewable penetration systems, may cause return instability in the power system and may lead to blackouts. To avoid this problem, it is necessary for generating units to continue to operate and to ensure that they can remain connected during and after faults. They should be continuously in operation, even with severe grid disturbances and at very low voltage dips, support the voltage recovery by injecting reactive current and restore active power rapidly after fault clearance with limited ramp values [27]. This is known as the so-called ‘fault ride through’ (FRT) capability and the requirements of FRT vary from one country to another. FRT can also be classified into maximum and minimum voltage ride through (high VRT and low VRT). The main objective of this chapter is to investigate low voltage ride through of different distribution systems with high penetration of renewable energy.

4.3 Grid Code Requirements for FRT

Due to rapid developments in electricity market structures which have led to the separation of ownership of system operators and generation, the relationship between system operators and generating companies should be clearly defined. The rapid integration of renewable generation makes this process more complicated because these generating units have different physical characteristics when compared to the directly connected synchronous generators that are used in large conventional power plants. In order to solve this problem, new grid interconnection requirements called ‘grid codes’ have been developed by Transmission System Operators (TSOs) in several countries worldwide. Electricity regulatory bodies have also set new grid requirements for renewable generating units in different countries [170].

With the increase in penetration levels of renewable energy resources in distribution networks, system operators need to maintain control of overall power generation interconnected to the ac grid. In the past, DG units based on renewable energy were required to be disconnected in all fault conditions, leading to severe voltage and dynamic stability problems at high penetration levels. Disconnection of renewable units in such a system could cause a large imbalance between generation and load, and this jeopardised the security of supply. To prevent the consequences of disconnection of DG units, several DNOs have defined fault ride through requirements. Typically, when a system is under abnormal conditions such as a fault, a short voltage sag will occur. During this short time, FRT requirements ensure that generating units are connected to the system through a temporary fault scenario and need to stay connected to the transmission or distribution systems to help maintain system stability [28, 171].

This chapter will discuss low voltage ride through (LVRT) capability in different generic distribution systems with high penetration levels of DG units based on renewable resources. For this reason, LVRT requirements will be investigated in systems with high penetration levels of DGs, such as German LVRT requirements for distributed generators. In Germany, new low voltage ride through requirements for distributed generation units were released in 2008. The grid code was for the interconnection of DGs at a medium voltage level. This was the first time low voltage ride through requirements were implemented on DGs interconnected at distribution voltage levels. Penetration levels of DGs based on renewable energy are high in German distribution systems and they use Figure 4.1 as a method to address issues related to system stability [172]. Figure 4.1 shows Germany's new LVRT grid code for DGs. The vertical axis represents the nominal voltage per unit and the horizontal axis represents time in milliseconds. When the terminal voltage is above boundary line 1, the DGs are not allowed to disconnect. Between boundary lines 1 and 2, the DG units pass through the fault without disconnecting from the distribution system. The DG units can be disconnected for a short time from the distribution network when the voltage falls below boundary line 2. Below the blue line there is no requirement for the DGs to stay connected to the system [29, 173].

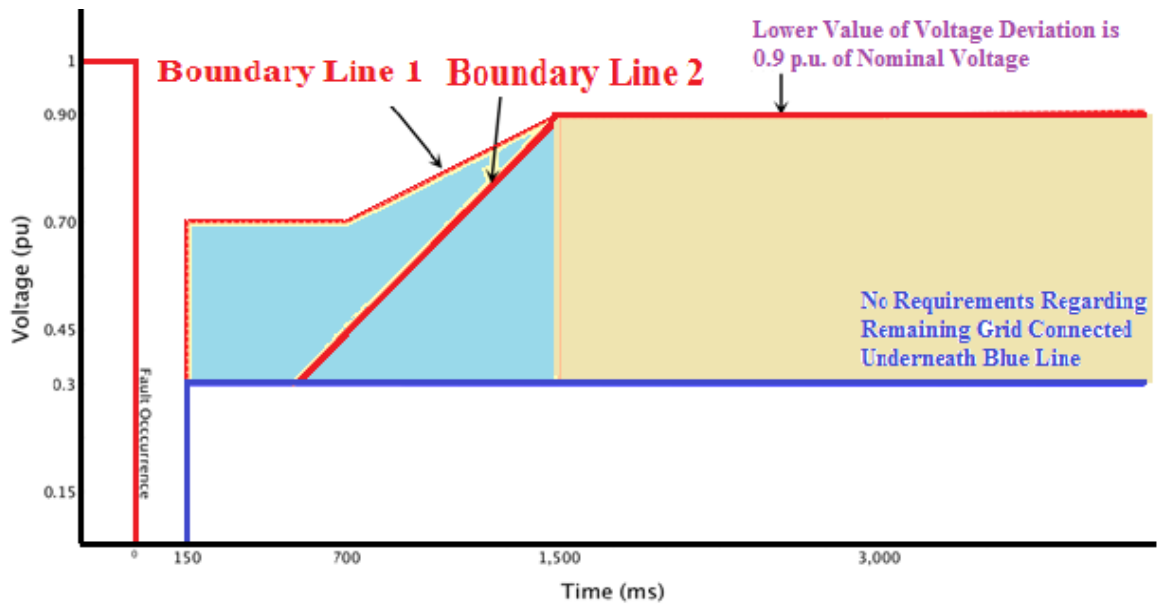


Figure 4.1: German LVRT requirements for distributed generators.

4.4 Wind Generation Impact on FRT Requirements

Short circuit fault occurrence and removal results in voltage sags experienced across an entire power system and so protection devices are usually used to detect and isolate these faults. Any delay in solving fault problems can lead to disconnection of generating units and this can cause loss of synchronism and result in power system collapse. Therefore, it is significant for all generators to remain connected during fault recovery. Conventional synchronous generators (CSGs) connected to transmission systems are able to support the transient stability of a grid by providing reactive power generation, oscillation damping, inertia, resynchronising torque and fault ride through capability. These features make CSGs attractive as they comply with grid connection requirements and help to have a stable grid operation worldwide. In the same manner, generating units based on wind energy should behave, as much as possible, in the same way as CSGs in both steady-state operation and during grid disturbances. It has been a significant challenge for wind turbine manufacturers to constantly follow new grid codes and discover how they can achieve new features required by grid system operators.

The first wind generating units connected to power systems appeared in the 1980s. They were constant speed wind turbines employing squirrel cage induction generators with switched capacitor banks in order to maintain the power factor. The DFIG was introduced in the 1990s and has reactive power controllability. By adding a chopper in the DC link of the DFIG, fault ride through capability can be improved. In the 2000s, generators based on wind energy with full scale converters were introduced. This technology offers fault ride through capability and a wider range of reactive power control.

The main advantage of the DFIG is that the size of the power electronic converter is considerably smaller than a full scale converter. However, the rotor side converter (RSC) in the DFIG is a vulnerable part and has restricted overcurrent limit which requires more attention during grid faults. When the power system experiences a fault which causes voltage sags, the generator magnetic flux cannot change instantaneously. This results in a large change in generator currents. Therefore, the RSC output current should be limited. The RSC may not be able to maintain the current within its limit during severe grid disturbances so it should be protected from overcurrent. The wind turbine converter can be protected by a protection device called a crowbar. There are two types of crowbars, passive and active. An active crowbar allows the generating unit to ride through faults without tripping, whereas a passive crowbar does not have this feature and it will disconnect the unit from the power system. A crowbar consists of a high power resistor and the crowbar system works if the rotor current is too high or when DC link voltage exceeds a given limit; this can happen during severe grid faults.

In fault scenarios close to wind farms, DFIG based wind energy may operate under high risk to its power electronic converters and DC link capacitors due to resulting overvoltages and/or overcurrents. Several researchers have discussed FRT requirements for the DFIG in literature [29-31]. There are two main techniques to solve this problem and avoid power electronic converters being under risk of damage. The first technique that can protect converters is a sustained period of rotor crowbar application [32, 174]. This technique is enabled when a fault is detected to protect the converters and the DC link capacitors from overvoltages or overcurrents while allowing the power electronic converters to resume

control at the earliest possible chance. The crowbar protection technique was developed as a standard rotor circuit protection device a long time before the development of grid code requirements for the DFIG [175]. The technique can be basically described as connecting rotor phases and the RSC together through a resistance [176]. Figure 4.2 shows a crowbar control scheme in the DFIG based on wind energy. The crowbar protection system based on three phase series resistance controlled by power electronic devices is currently used in modern wind turbines. In recent years, FRT performance of the DFIG based on wind energy has been discussed considerably in literature and several schemes have been proposed to ensure the DFIG meets new grid code requirements. This includes the application of controlled crowbar resistance [177], control of the timing of the crowbar protection system [178], and the use of brake resistors [179, 180].

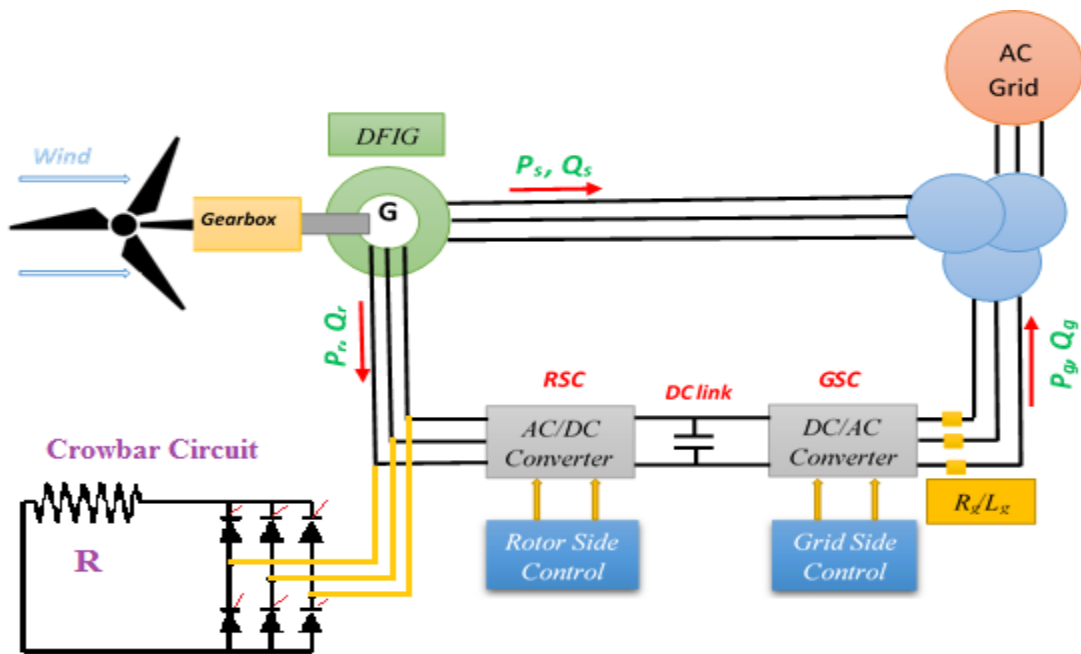


Figure 4.2: The crowbar protection scheme in the DFIG based on wind energy.

The second technique that can protect the power electronic converters of the DFIG is a DC link chopper. A DC chopper circuit with a resistance can be added to the DC link as illustrated in Figure 4.3. The pulse signal used to trigger the IGBT is activated when DC voltage V_{DC} exceeds the maximum limit V_{DCmax} . After that, the chopper is turned on and the energy is dissipated by the internal resistor [33, 181]. Therefore, wind turbines based

on DFIG technology with a DC chopper and crowbar system are capable of handling fault scenarios like voltage sags and swells, short interruptions and rotor over-speed. Thus, with these energy absorbers, the DFIG is able to meet even the most strictest grid FRT requirements [182].

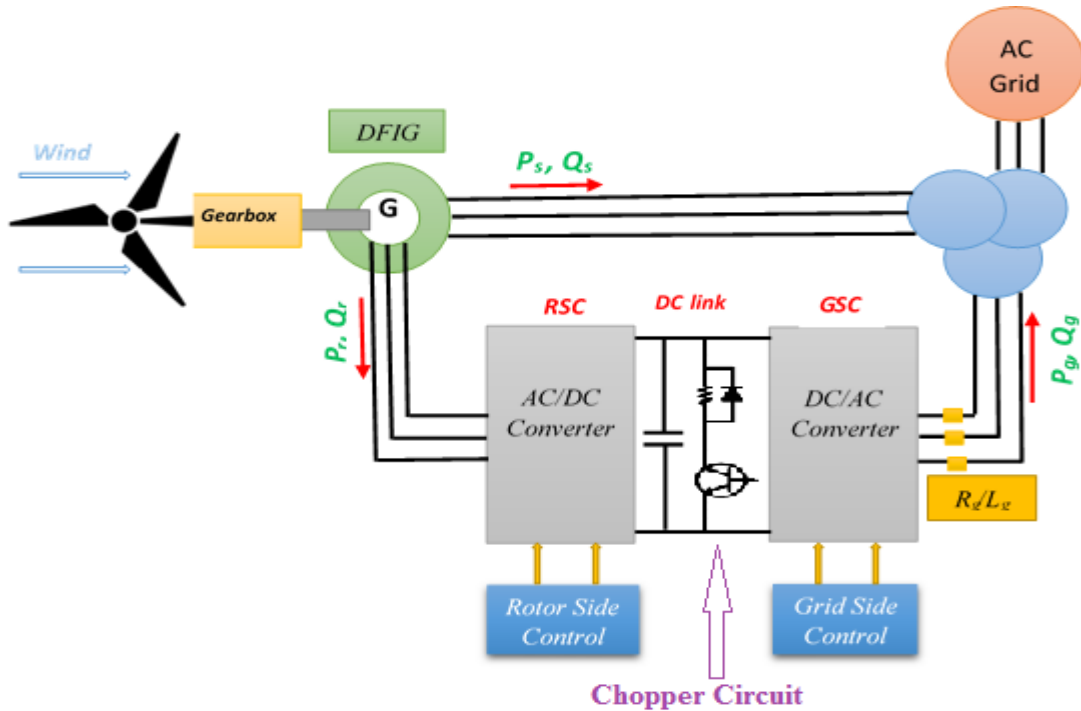


Figure 4.3: The DC chopper protection scheme in the DFIG based on wind energy.

In wind turbines based on fully rated converter technology, there is no induced rotor overcurrent to limit during severe grid disturbances such as faults. However, the DC link needs to be protected. There are several methods to meet FRT requirements in full scale converter wind turbines and they can be classified into those requiring change in their control system to satisfy grid codes and those requiring additional hardware in their control system. The most common methods are crowbar approaches [34], RSC and GSC control [35], a dynamic voltage restorer (DVR) [183], FACTS devices such as SVC and STATCOM [36], energy storage systems in rotor inertia via flywheel [184], super capacitor storage [185] and the use of battery storage [186]. In this thesis, DC chopper and crowbar techniques are used for protection against fault conditions in wind energy generators (DFIG) and synchronous generators with full power electronic converters.

4.5 Photovoltaic Generation Impact on FRT Requirements

Fault ride through capability is significant in large scale grid connected renewable energy systems; however, most research studies have discussed wind power grid connected systems only. This may have been reasonable in the past as photovoltaic generation was small compared to other generating technologies. In recent years, photovoltaic (PV) grid connection has become significant and the penetration level of PV is becoming high in several countries, including Germany. This trend has led to consideration of photovoltaic grid connected generation in new grid code requirements and thus the design of PV inverters will be affected. There is also an ongoing harmonisation of grid codes between European countries in order to achieve European renewable targets. Harmonised grid code requirements for renewables will maximise efficiency of all parties, however, it should be noted that it is not practical to completely harmonise these requirements in one step [187]. At the moment, the PV inverters are disconnected from the grid in many countries worldwide during grid faults for safety purposes. In contrast, with the recent forecasts that expect to see a fast increase in PV grid connections, it is likely that grid code will be updated and require FRT capability from PV grid connected systems in order to stabilise power systems. This could happen to PV systems connected to distribution networks just like wind power systems, as FRT requirements have been introduced after a long time as penetration of wind power systems has become significant.

Fault ride through capability for PV grid connected systems has been investigated in literature [37, 38]. Three single stage photovoltaic grid connections based on a current source inverter (CSI) under grid faults was discussed in [188, 189]. In [190], a proportional resonant (PR) current controller to limit overcurrent was proposed. For a three phase two stage photovoltaic grid connected system, there are few papers that investigate the FRT capability. For this reason, this chapter proposes a three phase two stage PV grid connected system with FRT capability. The main purpose of FRT in a PV system is to protect power electronic converters from overvoltages or overcurrents. The PV system could be disconnected from the grid during faults as the DC link voltage exceeds the limits.

4.6 Modelling and Control of a Renewable Energy System for FRT

Renewable energy source integration into power systems continues to increase, contributing towards a change in large scale wind and PV grid connected units from being simple energy sources to having advanced control to meet new grid code requirements. This section discusses the modelling and control of distributed generation based on wind and solar energy. Three different technologies are investigated to ride through grid faults: a wind turbine based on the DFIG, a wind turbine based on a synchronous generator with fully rated converters, and a solar unit based on photovoltaic. These have been modelled in two types of software, MATLAB/SIMULINK and the commercial package DIGSILENT POWERFACTORY [191, 192]. SIMULINK is used because it is a powerful software to design and control power electronic converters while POWERFACTORY is faster and easier to investigate large-scale power systems. For these reasons both software have been used in this thesis.

4.6.1 DFIG Modelling and Control

DFIG technology is widely used in wind turbines, especially for multi megawatts generation. It is a variable speed wind technology whereby the speed range requirements are modest. It offers adequate performance for the speed range required to exploit typical wind resources. There are two power electronic converters, a rotor side converter (RSC) and a grid side converter (GSC), connected back to back between the rotor windings and the ac grid, as shown in Chapter 3. A DC link is placed between the two converters as energy storage in order to keep the DC voltage variations (ripple) as small as possible. The shaft torque or the speed of the DFIG and the stator terminals power factor can be controlled by the RSC, while the GSC controls the DC link voltage and keeps it within given limits. The GSC works at the grid frequency with a controllable lagging or leading power factor to provide or absorb reactive power, while the RSC changes its output frequency depending on the wind speed. These converters need only be rated to handle the rotor power, which is a fraction of the total generator power, typically 30% of nominal power. In recent developments related to the DFIG, power electronic converters are based on two level six switch voltage source conversion technologies and the switching elements

are IGBTs. Vector control details in dq synchronous frame for DFIG converters were shown in Chapter 3.

4.6.2 Wind Turbine based on Synchronous Generator with Fully Rated Converters

Wind turbines based on a synchronous generator with full scale power converters have been developed in recent years and there are several topologies for this technology. However, this thesis will consider the RSC as a diode rectifier and the GSC as a voltage source inverter, as shown in Figure 4.4. A three phase diode rectifier and boost circuit is used as the RSC and in this topology four variables need to be controlled, namely generator active power, DC link voltage, grid active and reactive powers.

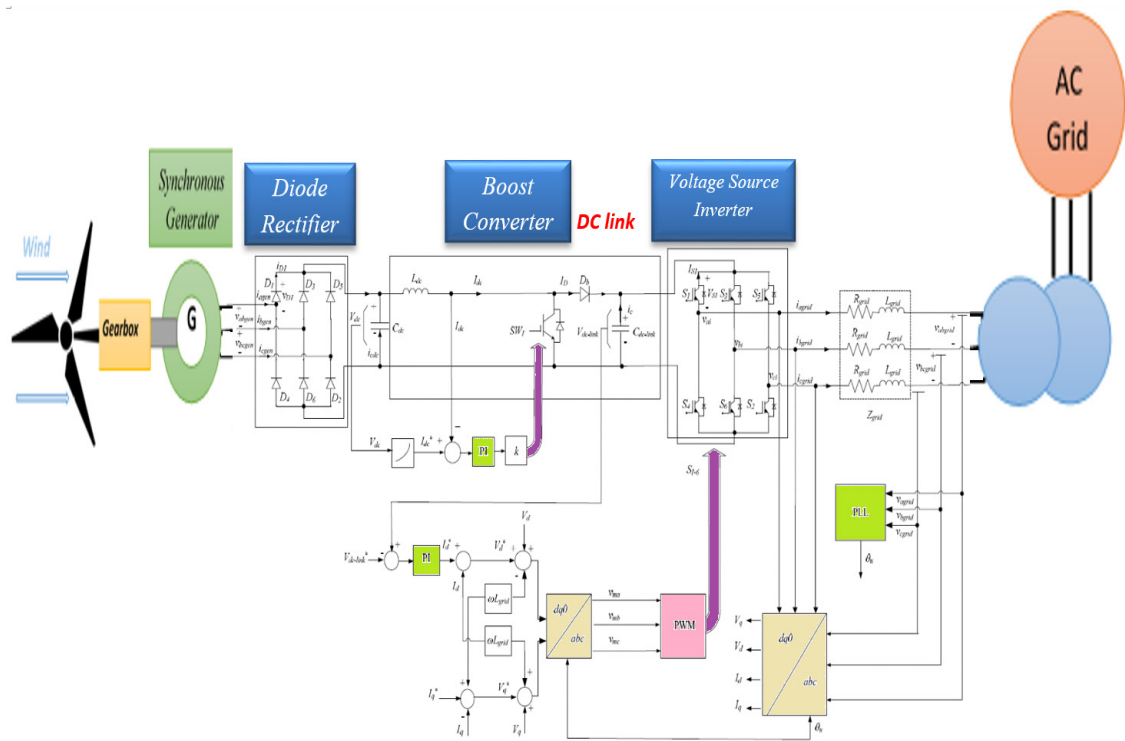


Figure 4.4: Wind turbine based on synchronous generator with fully rated converters and converter control in the dq synchronous frame.

4.6.3 Solar Energy based on Photovoltaic

As mentioned in detail in Chapter 2, a PV system converts solar energy into electricity and there are different topologies. The problem with photovoltaic inverters is that there are many topologies in the market and it is difficult to find standard modules for implementation, unlike wind energy for instance. This thesis uses two main topologies for

the PV system, a three phase two stage transformerless grid connected PV system and a simplified PV model. The three phase two stage grid connected PV system has been discussed in Chapter 2. Three phase PV system will be used throughout this thesis because the PV output power considered in this research is multi MW. A block diagram of the simplified PV model is shown in Figure 4.5. The PV panel and the DC-DC boost converter are neglected and they are represented by the DC voltage source for simplicity to perform simulations and get results for different distribution networks. The DC voltage source is interfaced with the grid through a voltage source inverter (VSI). The PV active and reactive powers can be controlled by modifying the control of the PV inverter. The control of the PV inverter is shown in Figure 4.6 and it is like the control of wind power electronic converters, which depend on the dq synchronous reference frame.

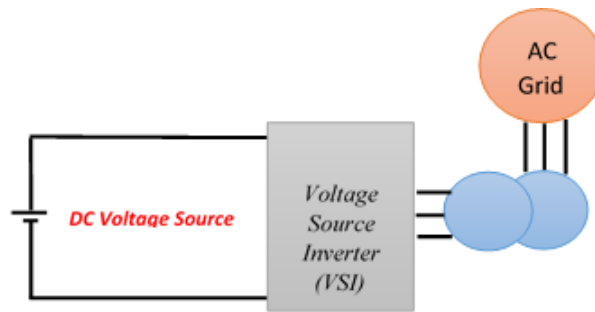


Figure 4.5: Simplified PV model.

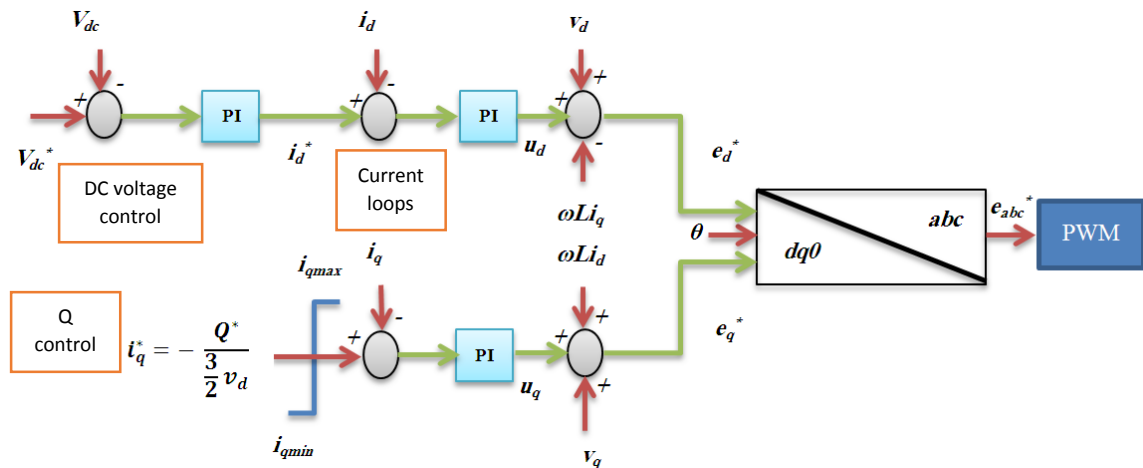


Figure 4.6: Block diagram summarizing the three phase grid connected PV inverter.

To examine the simplified PV model, a simulation test is performed on different PV topologies and the results compared. The test is to observe the dynamic response of the proposed PV system compared to other PV topologies when there is a sudden decrease in irradiance (a 50% decrease). The irradiance changes rapidly from 1000 W/m² at 1.5 seconds to 500 W/m² and returns to its first value at 3 seconds. Figure 4.7 shows the impact of a rapid change in solar irradiance on the PV output power for different PV systems. There are four PV systems that have been selected for examination of the simplified PV model, namely a three phase PV system designed with a commercial package software DIgSILENT POWERFACTORY, a three phase two stage grid connected PV system with Hill-Climbing MPPT, a three phase two stage grid connected PV system with Incremental Conductance MPPT, and a three phase two stage grid connected PV system with Perturb and Observe MPPT. The results show that the simplified PV model is able to operate in dynamic operation and it is fast compared to other PV systems. Figure 4.7 shows that the PV output power of the proposed model is relatively close to the three phase two stage grid connected PV system with Incremental Conductance MPPT.

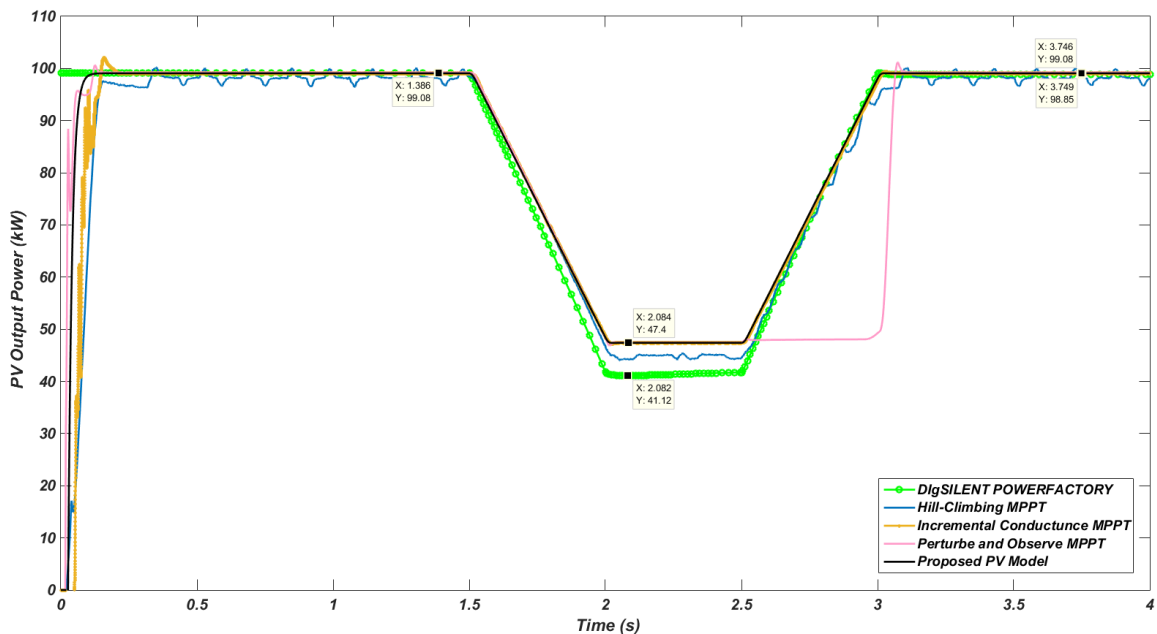


Figure 4.7: The impact of a rapid change in solar irradiance on the PV output power for different PV systems.

4.7 Simulation Scenarios

This chapter investigates different generic distribution networks with high renewable energy penetration subject to different fault conditions. The voltage recovery at renewable buses and at the fault location will be discussed. The voltage recovery will be compared to the grid code requirements that have been shown earlier in section 4.3. The German grid code for FRT will be considered, as Germany released new LVRT requirements for distributed generation connected to the grid in recent years. Three different distributed generation types based on renewable energy are considered, namely a wind turbine based on the DFIG, a wind turbine based on a synchronous generator with fully rated converters, and a solar energy source based on photovoltaic. The voltage recovery is investigated when the distribution systems experience a three phase fault at different locations. Three modified generic distribution networks are considered in this chapter, namely IEEE 13 bus, IEEE 37 bus, and IEEE 123 bus test systems. For each distribution network there are five different cases to investigate the voltage recovery performance of the distribution systems. These include a base case when there is no renewables, 35 % PV penetration of the total generation of the test system, 35 % wind based on DFIG penetration, 35 % penetration of a wind based synchronous generator with fully rated converters, and 35 % wind and PV (mixed renewables) penetration. 35 % of renewable energy penetration was selected to represent a high percentage of renewable energy in a power system which could be reached in the future and this specific percentage was expected as the UK's renewable energy penetration by 2020 [193]. In the third quarter of 2015, 23.5 % of the UK's electricity was provided by renewables [194]. To validate the FRT performance of the selected distribution networks, simulations are performed using two different software programmes, MATLAB/SIMULINK and DIgSILENT POWERFACTORY.

4.7.1 IEEE 13 Bus Distribution System

The IEEE Power Engineering Society published a number of test systems for distribution system analysis, one of them called the IEEE 13 Node Test Feeder [195]. A schematic diagram of this system is shown in Figure 4.8. Detailed data regarding this system are given in Appendix B.1. This system is connected to the ac grid through a two winding ac

transformer. Bus 650 is the bus which interconnects the grid with the test network. This bus has been selected because it is directly connected to the grid through a transformer, which is in effect a substation. Table 4.1 summarises the IEEE 13 bus distribution network data. A conventional distributed generation (CDG) is assumed to be connected at bus number 611, which is one of the farthest nodes from the grid and close to the renewable units' location, to investigate the transient stability of the synchronous generator. Detailed data regarding this CDG are given in Appendix C. The grid is assumed to be an infinite bus. Power flow data of the 13 bus distribution system are given in Appendix B.1, where the grid bus is assumed to be the slack. DG based on renewable resources are connected to the farthest node from the grid, which is bus number 680.

The main objective of this chapter is to investigate the FRT requirements and the voltage recovery of the distribution systems with high renewable energy penetration. Therefore, a three phase fault is applied on two different locations, the first one close to the grid on bus 650 and the second location close to the renewable unit on bus 680.

The duration of the fault is 200 milliseconds (10 cycles for the 50 Hz system) from 3 seconds to 3.2 seconds and the fault impedance is assumed to be zero to observe the worst case scenario. Voltage sag due to faults in the transmission systems are characterised by a short duration, typically up to 100 milliseconds. However, the duration of dips due to faults in distribution networks depend on the type of protection used. By improving protection in these networks, the maximum fault-clearing time may be brought to 200 milliseconds [196]. For these reasons 200 milliseconds was selected as the fault duration in this research work for distribution systems.

Table 4.1: IEEE 13 Bus Network Data.

<i>No. of Buses</i>	<i>No. of Loads</i>	<i>No. of Lines</i>	<i>Total Generation</i>	<i>Total Load</i>	<i>Total Losses</i>
13	9	10	3.62 MW 2.65 MVar	3.47 MW 2.10 MVar	0.15 MW 0.54 MVar

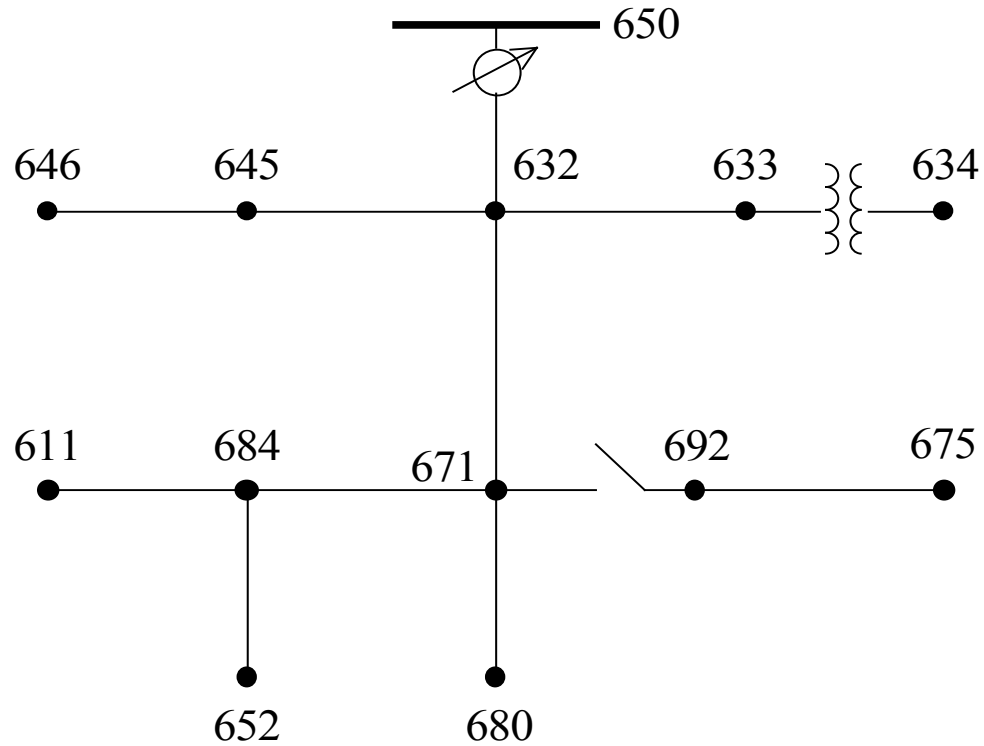


Figure 4.8: IEEE 13 Node Test Feeder

A- Base Case

When a three phase fault is applied on bus 650 for 200 milliseconds at 3 seconds, the voltage dip at this bus falls to zero. Figure 4.9 shows the terminal voltages at bus 650, bus 680 (renewable bus) and the CDG bus (bus 611). It shows that the commercial package DIGSILENT POWERFACTORY gives a relatively close dynamic result compared to MATLAB/SIMULINK. However, after the fault was cleared at 3.2 seconds, the POWERFACTORY gives a higher overshoots. The voltage recovery complies with the FRT grid code requirements, as the voltages recover quickly and return to a nominal value after the fault is cleared.

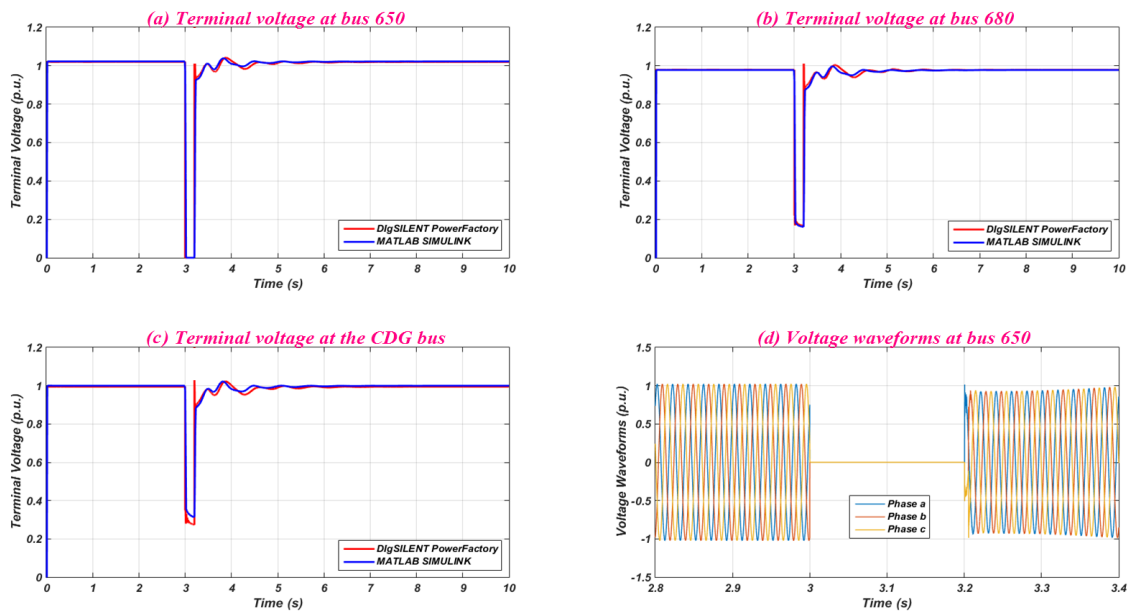


Figure 4.9: Voltage recovery for the base case of the 13 bus system (the fault is applied on bus 650) - (a) Terminal voltage at bus 650, (b) Terminal voltage at bus 680, (c) Terminal voltage at the CDG bus, (d) Voltage waveforms at bus 650.

When the three phase fault is applied on bus 680 with a duration of 200 milliseconds, the voltage recovery at the grid bus and the DG buses is as illustrated in Figure 4.10. It shows also that the terminal voltages return to a nominal value in a few seconds.

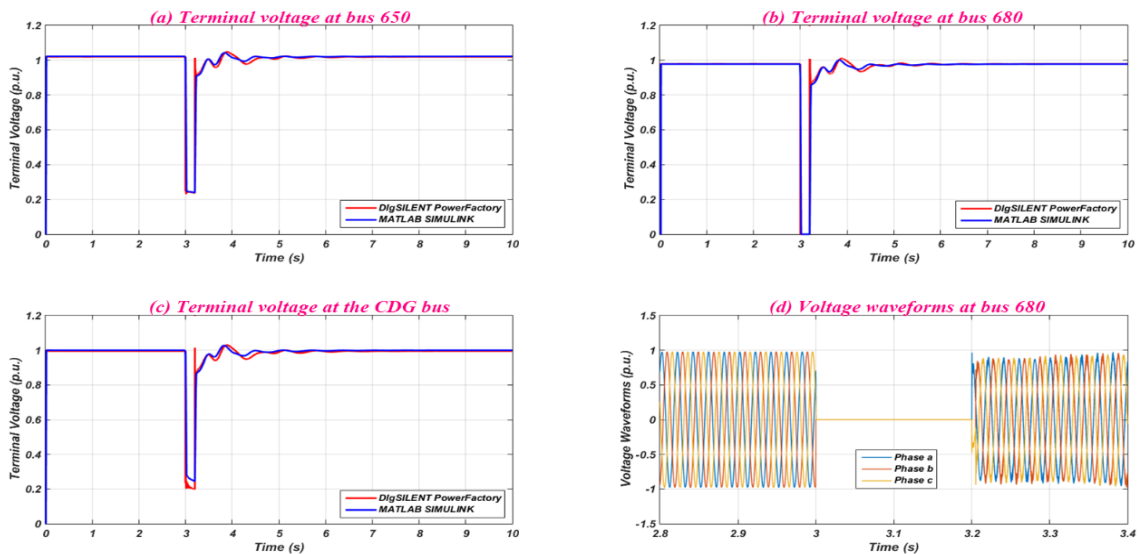


Figure 4.10: Voltage recovery for the base case of the 13 bus system (the fault is applied on bus 680) - (a) Terminal voltage at bus 650, (b) Terminal voltage at bus 680, (c) Terminal voltage at the CDG bus, (d) Voltage waveforms at bus 680.

B- 35 % PV Penetration

A DG based on photovoltaic is installed at bus 680 with 2 MW of output power, which is 35 % of the total generation in the system. This means that small-scale PV installations less than 10 kW are not considered in this work. Detailed data regarding the PV systems are shown in Appendix D. When the distributed generation units based on renewables are injected into the system, an additional load is added to the system at bus 680 which equals the same additional generation 2 MW. This additional load is added to the system to ensure accuracy in the results and the effect of the renewable units on the system. This step ensures the total loading of the grid and the CDG will be the same in the base case and after adding the renewable units to the system. Table 4.2 shows the sources of power generation in the system and their locations.

Table 4.2: Power generation sources' outputs and their locations (PV case).

	<i>Grid</i>	<i>CDG</i>	<i>PV</i>
<i>Total Generation</i>	1.62 MW	2 MW	2 MW
<i>Location</i>	Bus 650	Bus 611	Bus 680

When the three phase fault is applied on bus 650 with the same procedure as in the base case, the voltage recovery of the affected bus and the DG buses is as illustrated in Figure 4.11. The terminal voltage recovers quickly after the fault is cleared at 3.2 seconds and this meets the LVRT requirements that have been discussed earlier. This means the distribution system with high PV penetration could ride through faults and the DGs will stay connected during and after such faults. The DGs' active and reactive powers will be discussed more in the next chapter (Transient Stability). However, to ensure that the PV system stays connected during and after faults, the DC link voltage should be maintained within its acceptable limits, namely between 0.5 p.u. and 1.1 p.u. The photovoltaic system stays connected when the fault is far as in this case; however, when the fault is applied on bus 680 the PV converters will be under risk of overvoltage and this could damage the converters. Figure 4.12 shows the voltage recovery of the PV bus, the CDG bus and the grid bus. The terminal voltages recover and they meet the LVRT requirements because they return to their nominal values in short time.

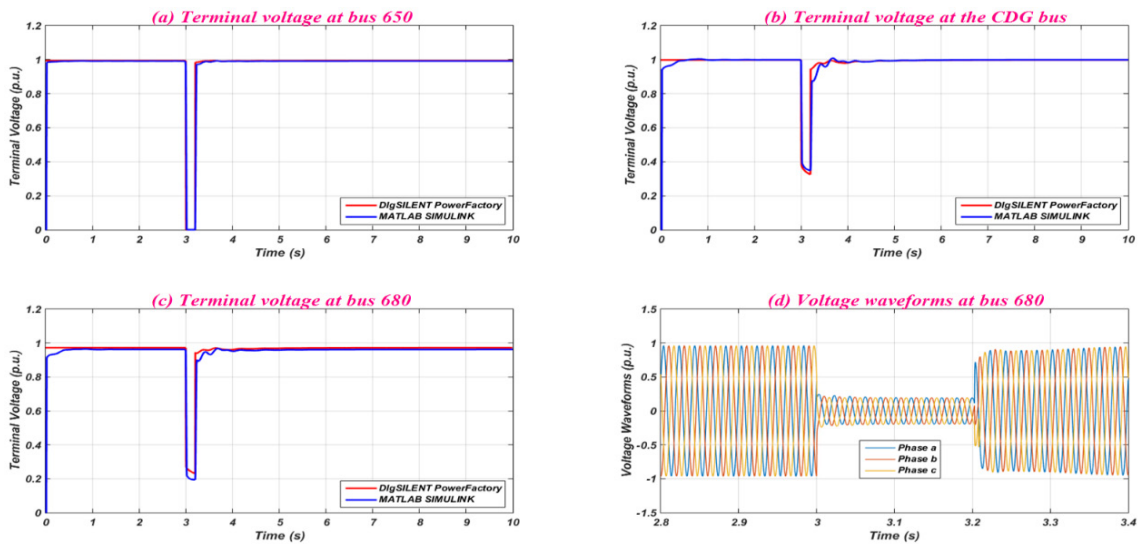


Figure 4.11: Voltage recovery for the 35 % PV penetration case of the 13 bus system (the fault is applied on bus 650) - (a) Terminal voltage at bus 650, (b) Terminal voltage at the CDG bus, (c) Terminal voltage at bus 680, (d) Voltage waveforms at bus 680.

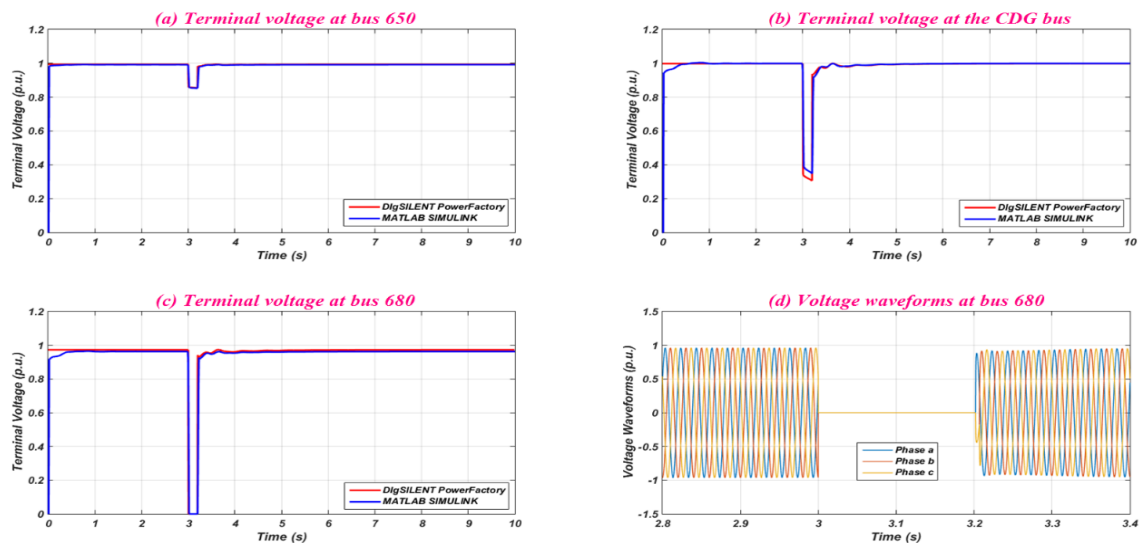


Figure 4.12: Voltage recovery for the 35 % PV penetration case of the 13 bus system (the fault is applied on bus 680) - (a) Terminal voltage at bus 650, (b) Terminal voltage at the CDG bus, (c) Terminal voltage at bus 680, (d) Voltage waveforms at bus 680.

As discussed above, when the fault is applied on the PV bus, the converters should be protected from overvoltages. During a fault, the DC link voltage increases, as explained in this chapter, and it should be maintained within its limits. To protect the DC link and keep the DC link voltage within the given limits, a new technique is proposed in this chapter. A three phase two stage transformerless PV grid connected system with FRT

capability is proposed. There is no need for hardware elements to be added to the control of the PV converter which means no additional costs is needed. However, the DC-DC converter signal which tracks the maximum available power will work during faults to keep the DC voltage within limits and protect the DC converters by using proportional integral (PI) controllers. This method tracks any changes in the DC link voltage as well as the grid current during faults to protect the PV power electronic converters. The proposed control of the PV system is illustrated in Figure 4.13. During the fault, the power output by the DC/AC inverter to the ac grid is reduced. However, power is still being imported from the PV by the DC/DC converter. Thus, the DC voltage continues rising. Due to the fast change of the DC voltage, the imported power from the PV varies due to the imperfect control action on the duty cycle by the DC/DC converter. This results in the ripples on the voltage during the fault. When the AC fault is cleared, the output power by the DC/AC inverter increases rapidly which causes the DC voltage to drop quickly. These are shown in Figure 4.14 and it is shown that the DC voltage has a slow rise during fault because the capacitor size is big. Figure 4.14 shows the DC link voltage with and without DC link protection. After adding the protection circuit shown in Figure 4.13, the DC link voltage is kept within the limits 1.1 p.u. and 0.5 p.u. during and after a fault is cleared. Therefore, the PV system can ride through faults which are close to its terminal connections.

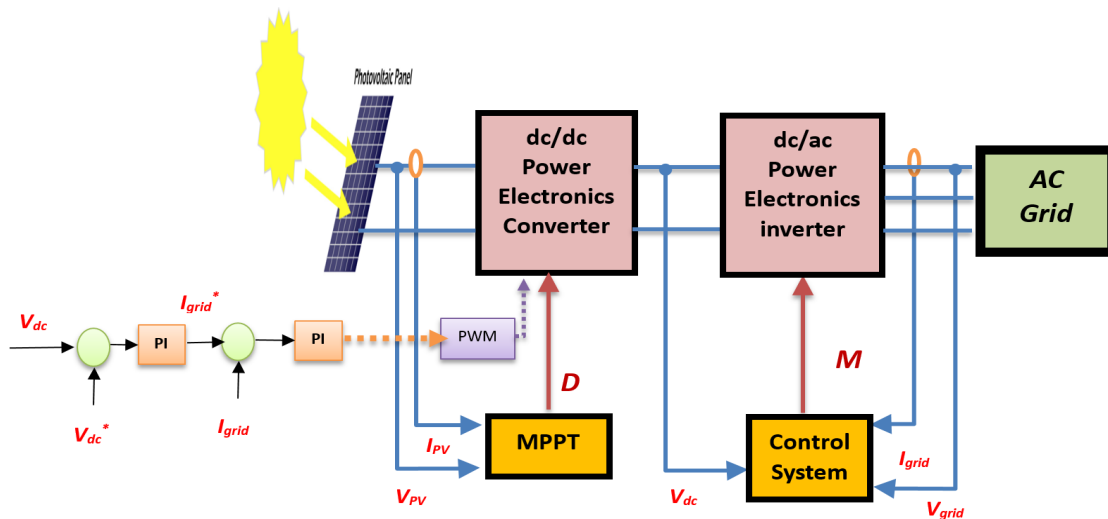


Figure 4.13: Proposed three phase two stage transformerless PV grid connected system with FRT capability.

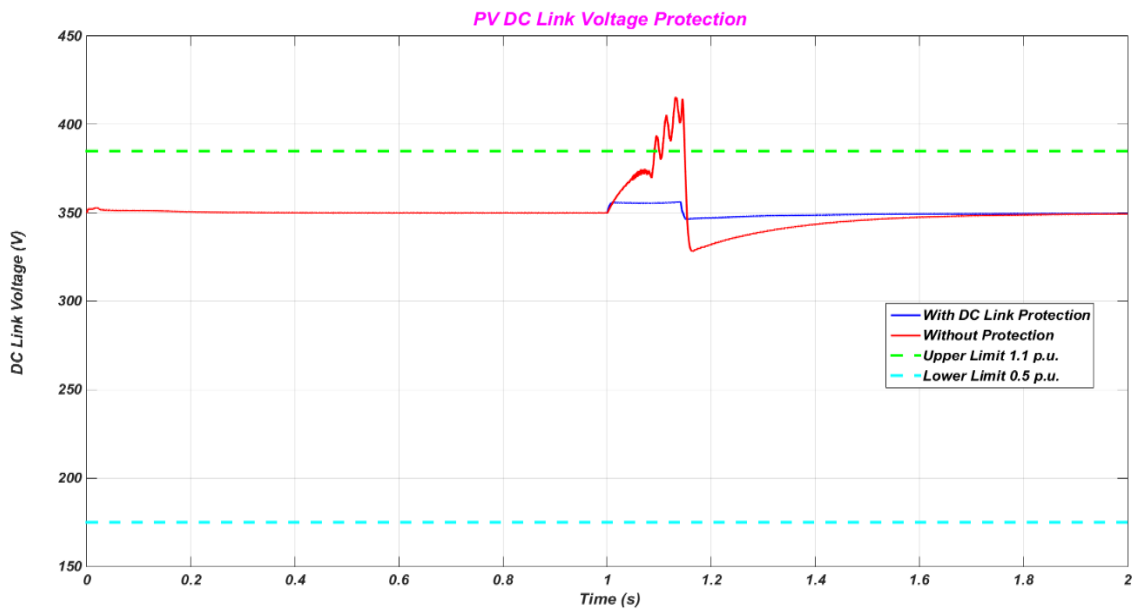


Figure 4.14: PV DC link voltage with and without protection when a fault is applied close to the PV system.

C- 35 % Wind based on DFIG Penetration

A wind turbine based on the DFIG is installed at bus 680 with 2 MW output power, which represents 35 % of the total power generation in the test system. The DFIG parameters and detailed data are given in Appendix D. In the same manner as the PV case, a 2 MW load is added at bus 680 for the same reason. Table 4.3 shows the sources of power generation in the system and their locations.

Table 4.3: Power generation source outputs and their locations (DFIG case).

	Grid	CDG	Wind DFIG
Total Generation	1.62 MW	2 MW	2 MW
Location	Bus 650	Bus 611	Bus 680

When the three phase fault is applied to the grid bus, the voltage recovery of the affected bus and the DG buses is as illustrated in Figure 4.15. The terminal voltage recovers quickly after the fault is cleared at 3.2 seconds and this meets the LVRT requirements that have been discussed earlier. This means the distribution system with high wind energy based on DFIG penetration could ride through faults and the DGs stay connected during and after faults. In contrast, to ensure that the DFIG based on wind remains connected during

and after faults, the DC link voltage should be maintained within its given limits. The DFIG stays connected when the fault location is far as in this case; however, when the fault is applied to its terminal bus the DFIG converters will be under risk of overvoltage, which may cause damage. Figure 4.16 shows the voltage recovery of the DFIG bus, the CDG bus and the grid bus. The terminal voltages recover and they meet the LVRT requirements. However, DFIG converters should be protected from overvoltages and overcurrents which occur during the fault, as shown in Figure 4.16 (e).

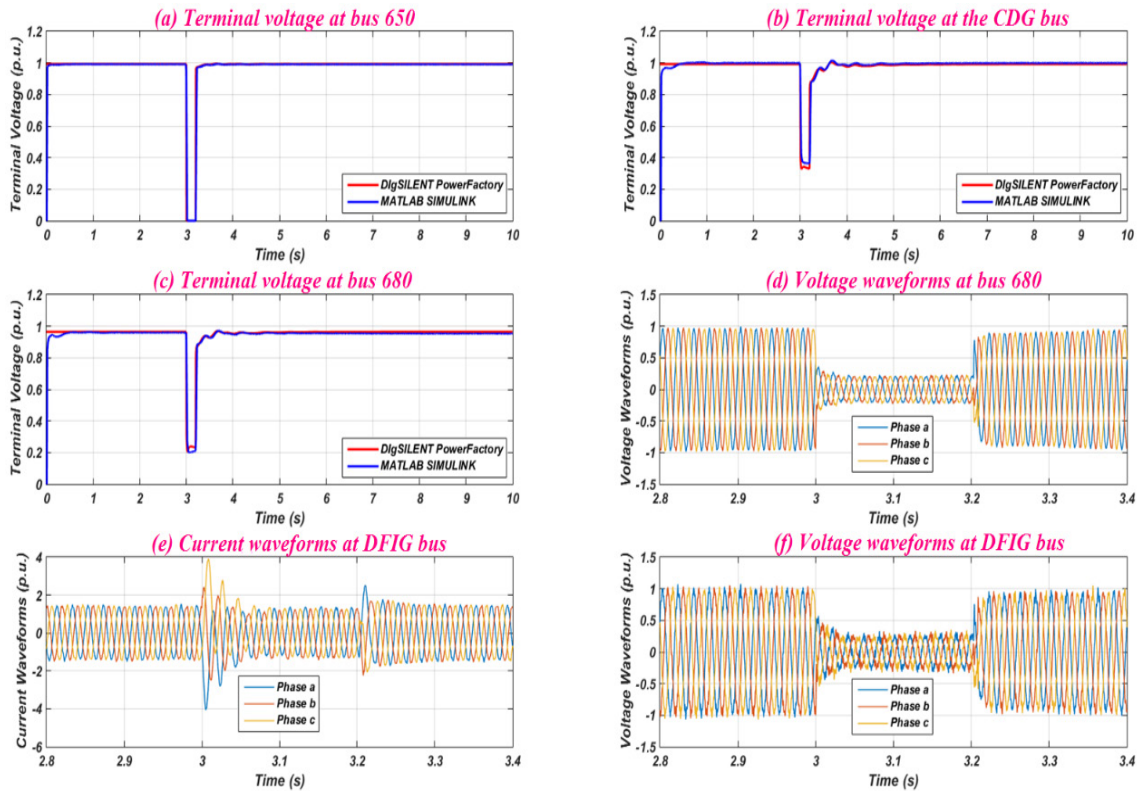


Figure 4.15: Voltage recovery for the case of 35 % wind based on DFIG penetration of the 13 bus system (the fault is applied on bus 650) - (a) Terminal voltage at bus 650, (b) Terminal voltage at the CDG bus, (c) Terminal voltage at bus 680, (d) Voltage waveforms at bus 680, (e) Current waveforms at DFIG bus, (f) Voltage waveforms at DFIG bus.

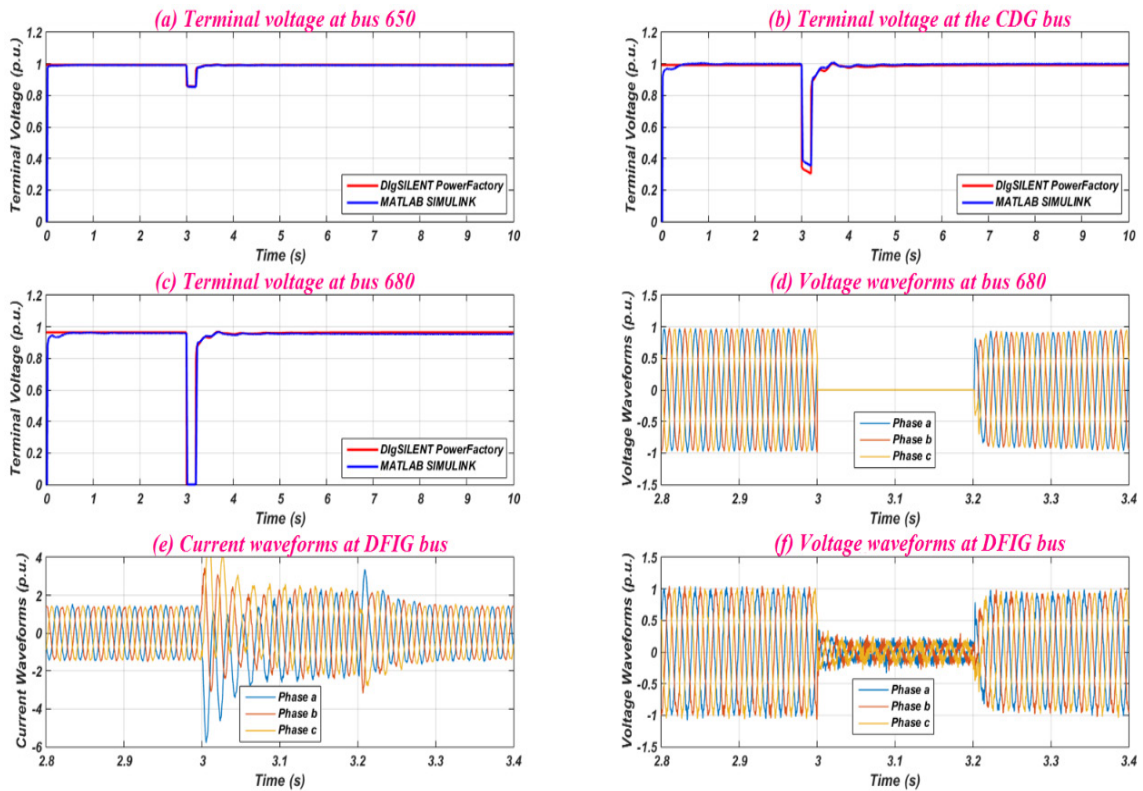


Figure 4.16: Voltage recovery for the case of 35 % wind based on DFIG penetration of the 13 bus system (the fault is applied on bus 680) - (a) Terminal voltage at bus 650, (b) Terminal voltage at the CDG bus, (c) Terminal voltage at bus 680, (d) Voltage waveforms at bus 680, (e) Current waveforms at DFIG bus, (f) Voltage waveforms at DFIG bus.

To protect the DFIG converters, a DC chopper circuit is added to the DC link with a resistance of 0.3 ohm. Figure 4.17 illustrates the difference between the DFIG with a protection circuit and without. After adding the chopper circuit, the DC link voltage is kept within limits during and after faults. Therefore, the DFIG can ride through faults which are close to its ac connection terminals without damaging its converters.

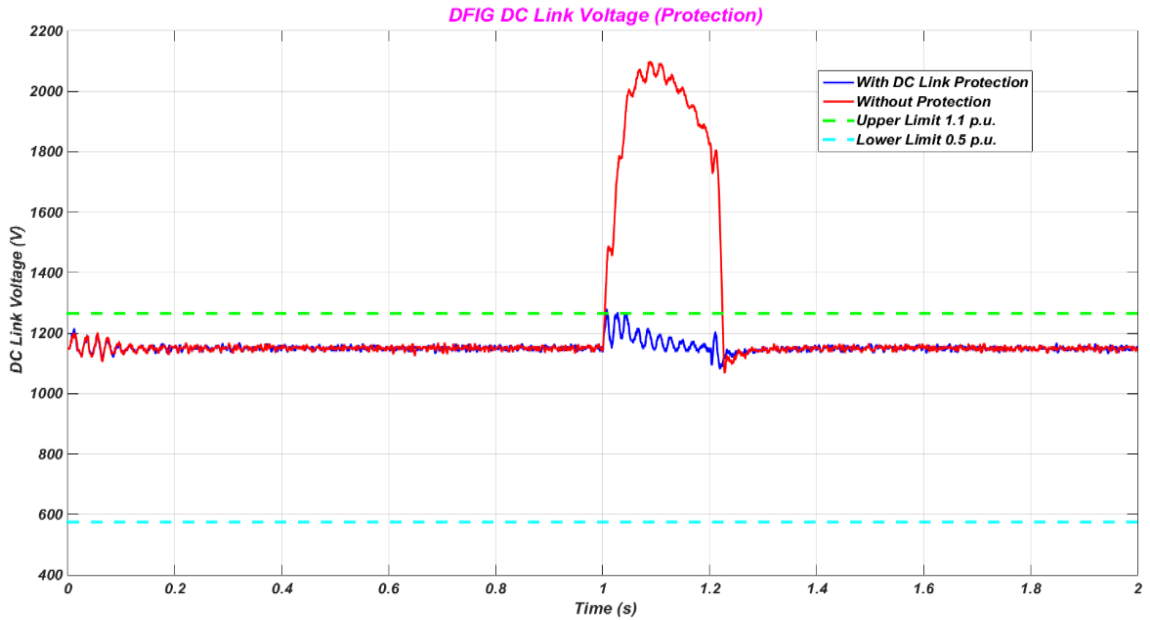


Figure 4.17: DFIG DC link voltage with and without protection when the fault is applied close to the DFIG.

D- 35 % Wind based on a Synchronous Generator with Fully Rated Converters

The same procedure as in cases B and C will be followed to test the wind unit based on a synchronous generator with fully rated converters (FRC) for FRT requirements. A 2 MW wind based on FRC is installed at bus 680 with the addition of a 2 MW load for the same reason mentioned in case B. The wind (FRC) parameters and detailed data are given in Appendix D. Table 4.4 shows the total power generation, which is contributed towards by different sources in the test system.

Table 4.4: Power generation source outputs and their locations (wind FRC case).

	<i>Grid</i>	<i>CDG</i>	<i>Wind FRC</i>
<i>Total Generation</i>	1.62 MW	2 MW	2 MW
<i>Location</i>	Bus 650	Bus 611	Bus 680

When the three phase fault is applied on bus 650, the voltage recovery of the affected bus and the DG buses are as illustrated in Figure 4.18. The terminal voltage recovers quickly after the fault is cleared and this meets the LVRT requirements. Thus, the distribution system with high wind energy based on a synchronous generator with FRC penetration could ride through faults and the DGs will stay connected during and after such faults.

However, to ensure that the wind generator remains connected during and after faults, the DC link voltage should be kept within its limits. The DFIG stays connected when the fault is far as in this case; however, when the fault location is close to the wind generator connection terminals, its converters will be under risk of overvoltage. This happens when the fault duration is more than 150 milliseconds and the system cannot ride through the applied fault. Therefore, the fault duration is changed to 140 milliseconds instead of 200 milliseconds to ensure FRT performance for the system without adding protection to the wind converters. Figure 4.19 shows the terminal voltages of the wind generator based on FRC, the conventional CDG bus and the grid bus. The terminal voltages recover and they meet the LVRT requirements. However, wind converters should be protected from overvoltages, which could damage the power electronic converters as illustrated in Figure 4.19 (f).

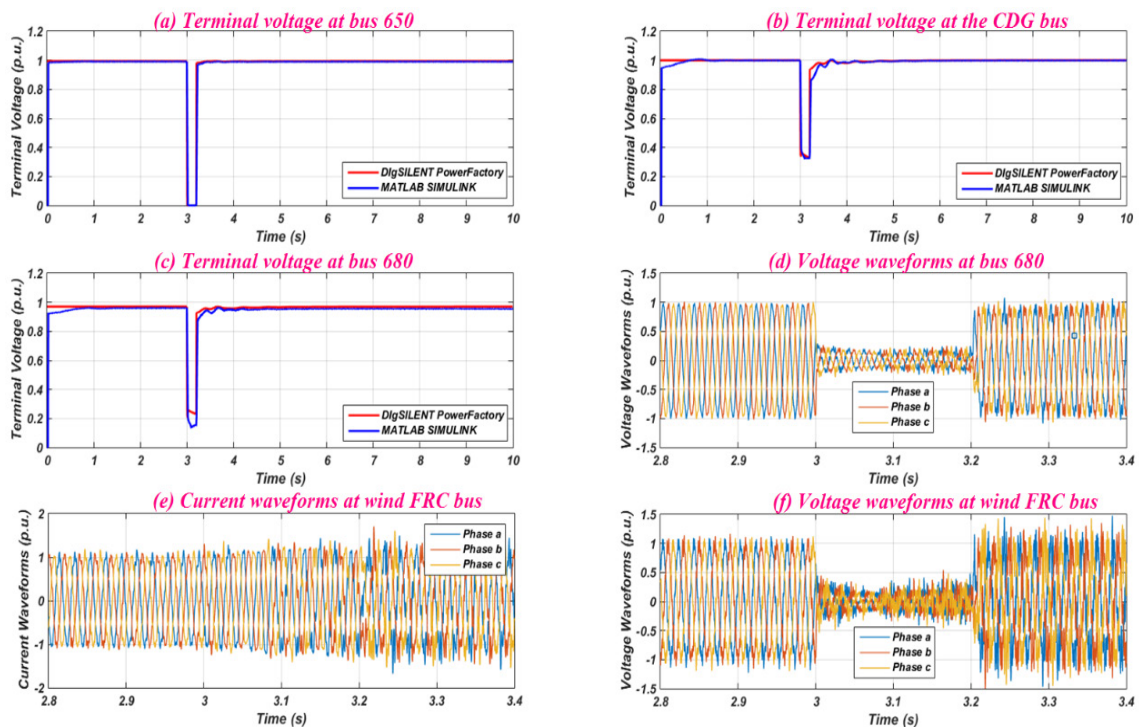


Figure 4.18: Voltage recovery for the case of 35 % wind based on FRC penetration of the 13 bus system (the fault is applied on bus 650) - (a) Terminal voltage at bus 650, (b) Terminal voltage at the CDG bus, (c) Terminal voltage at bus 680, (d) Voltage waveforms at bus 680, (e) Current waveforms at wind FRC bus, (f) Voltage waveforms at wind FRC bus.

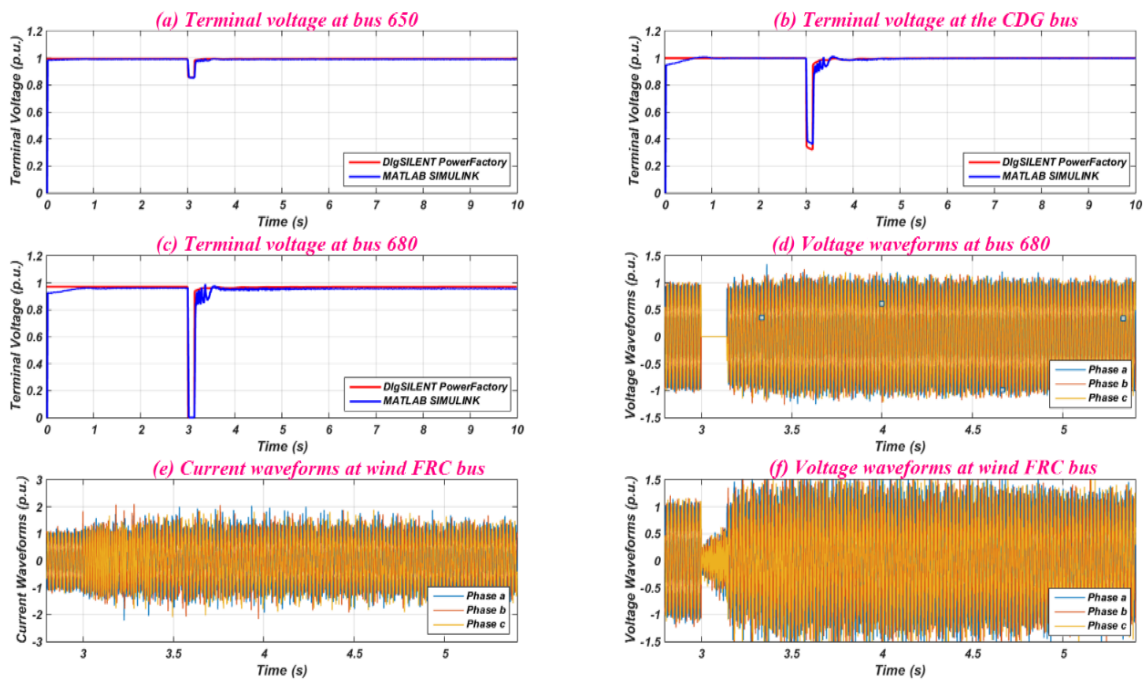


Figure 4.19: Voltage recovery for the case of 35 % wind based on FRC penetration of the 13 bus system (the fault is applied on bus 680) - (a) Terminal voltage at bus 650, (b) Terminal voltage at the CDG bus, (c) Terminal voltage at bus 680, (d) Voltage waveforms at bus 680, (e) Current waveforms at wind FRC bus, (f) Voltage waveforms at wind FRC bus.

A DC chopper circuit is added to the DC link with a resistance of 0.5 ohm to protect the DC link from overvoltages. The higher the DC chopper resistance the better the DC link protection of converters will be because this resistance works as a braking resistance to consume energy during faults. Figure 4.20 shows how the DC link voltage increases to about 4 p.u., which is unacceptable and could damage the converters. In the DFIG case, the DC voltage increased by about 1.8 p.u. during the fault as shown in Figure 4.17. This is because only around 30 % of the DFIG output power goes through the power electronic converters, however, 100 % of the generated power from FRC generator goes through the converters. After adding the chopper circuit, the DC link voltage is maintained within acceptable limits during and after faults. Therefore, the synchronous wind generator with fully rated converters can ride through faults which are located on its ac connection terminals without damaging its converters.

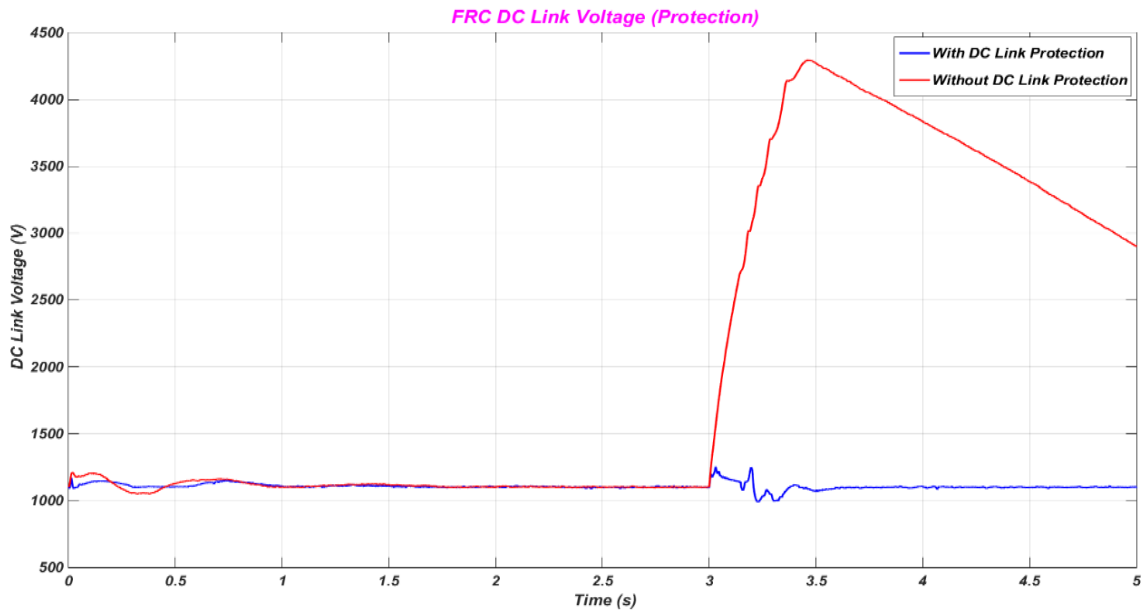


Figure 4.20: DC Link voltage of the wind based on synchronous generator with fully rated converters with and without protection when the fault is applied on bus 680.

E- 35 % Mixed Renewables Penetration

Mixed renewables based on wind and solar energy are installed in this case. 1.5 MW wind based on the DFIG is installed at bus 680 with a 1.5 MW load and 0.5 MW solar based on photovoltaic is installed at bus 652 with a 0.5 MW load. Table 4.5 illustrates the contribution each source in the test system makes to the total power generation.

Table 4.5: Power generation sources outputs and their locations (mixed renewables case).

	<i>Grid</i>	<i>CDG</i>	<i>Wind DFIG</i>	<i>PV</i>
<i>Total Generation</i>	1.62 MW	2 MW	1.5 MW	0.5 MW
<i>Location</i>	Bus 650	Bus 611	Bus 680	Bus 652

The same procedure as in previous cases will be followed to test this distribution system for the LVRT requirements. Two faults are applied, one on bus 650 and the second on bus 680 for 200 milliseconds duration (10 cycles). Figures 4.21 and 4.22 show that the voltage recovery at the buses of the modified test system meets the LVRT grid code requirements, as the terminal voltages return to a nominal value in a short period of time. However, the renewable units' converters should be protected from overcurrents or/and overvoltages.

The protection system for the PV and DFIG converters have been discussed in previous sections.

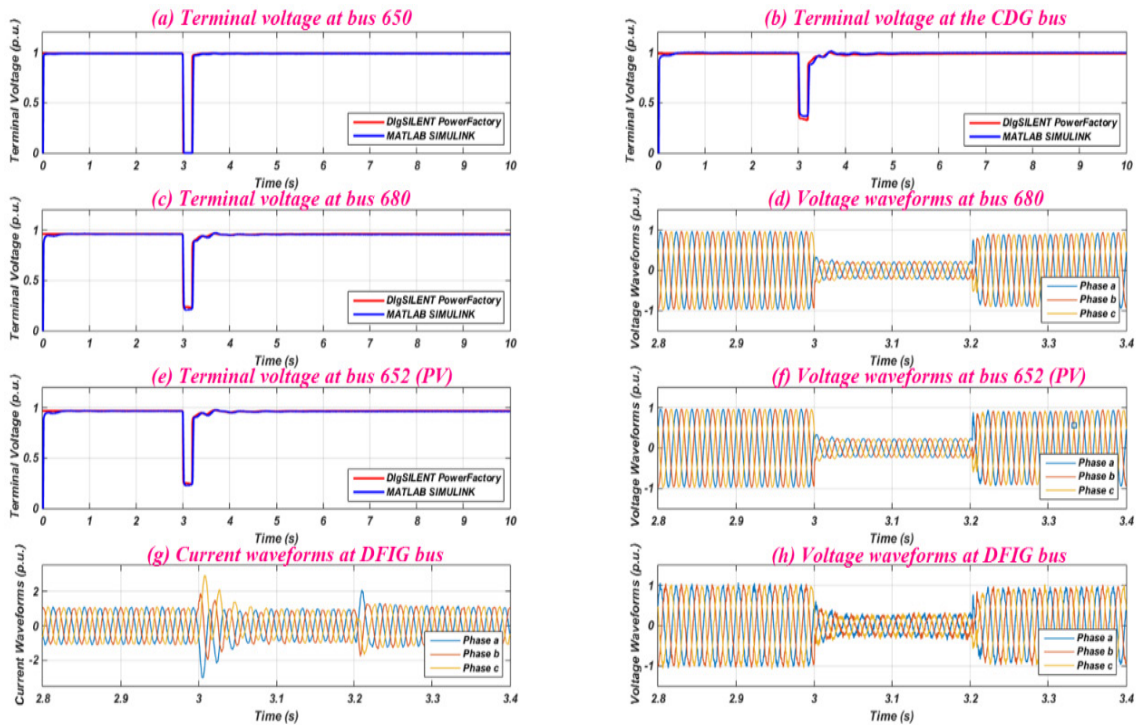


Figure 4.21: Voltage recovery for the 35 % mixed renewables penetration case of the 13 bus system (the fault is applied on bus 650) - (a) Terminal voltage at bus 650, (b) Terminal voltage at the CDG bus, (c) Terminal voltage at bus 680, (d) Voltage waveforms at bus 680, (e) Terminal voltage at bus 652 (PV), (f) Voltage waveforms at bus 652 (PV), (g) Current waveforms at DFIG bus, (h) Voltage waveforms at DFIG bus.

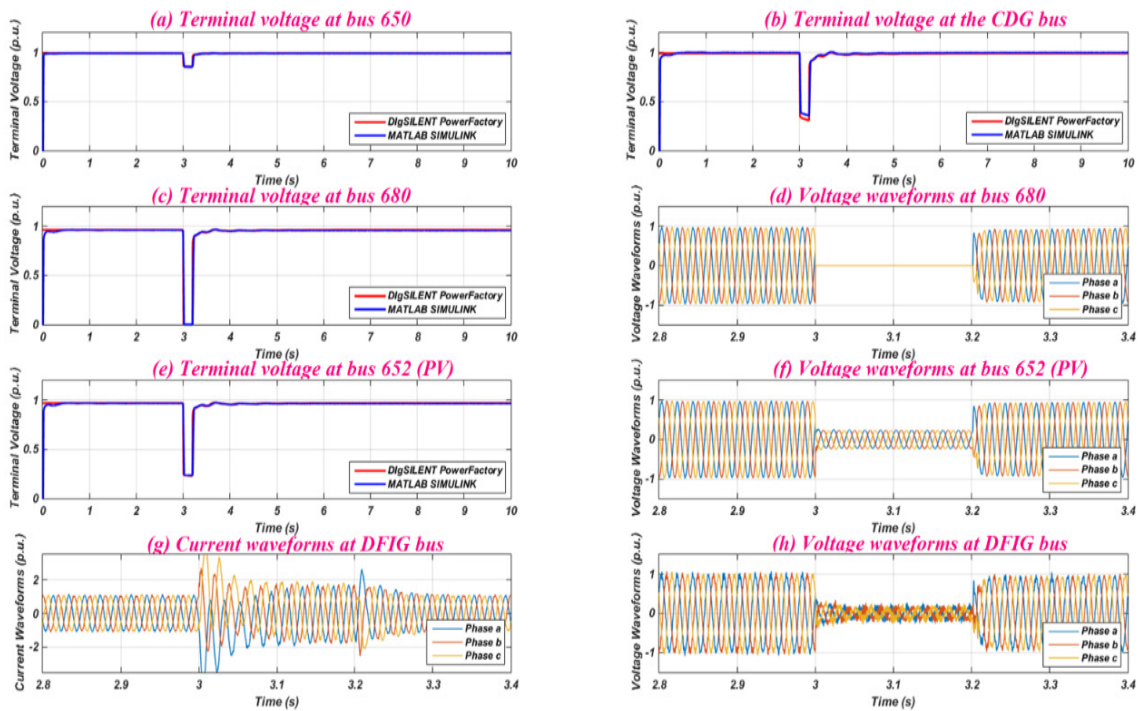


Figure 4.22: Voltage recovery for the 35 % mixed renewables penetration case of the 13 bus system (the fault is applied on bus 680) - (a) Terminal voltage at bus 650, (b) Terminal voltage at the CDG bus, (c) Terminal voltage at bus 680, (d) Voltage waveforms at bus 680, (e) Terminal voltage at bus 652 (PV), (f) Voltage waveforms at bus 652 (PV), (g) Current waveforms at DFIG bus, (h) Voltage waveforms at DFIG bus.

4.7.2 IEEE 37 Bus Distribution System

The IEEE Power Engineering Society published another test system for distribution system analysis called the IEEE 37 Node Test Feeder [195]. A schematic diagram of this system is shown in Figure 4.23. Detailed data regarding this system are given in Appendix B.2. This system is connected to the ac grid through a two winding ac transformer. Bus 799 is the bus which interconnects the grid with the test network. This bus has been selected because it is directly connected to the grid through a transformer, which is in effect a substation. The IEEE 37 bus distribution network data are summarised in Table 4.6. A CDG is assumed to be connected at bus number 740, which is one of the farthest nodes from the grid and close to the renewable units' location, to investigate the transient stability of the synchronous generator. Detailed data regarding this CDG are given in Appendix C. The grid is assumed to be an infinite bus. Power flow data regarding the 37 bus distribution system is given in Appendix B.2, where the grid bus is assumed to be the

slack. The DG based on renewable resources are connected to the farthest node from the grid, which is bus number 741. The same test procedure as for the LVRT grid code requirements which have been discussed in the IEEE 13 bus system will be followed. A three phase fault will be applied on bus 799 for 200 milliseconds and the second test will apply a three phase fault on bus 741 to observe the voltage recovery of the system buses.

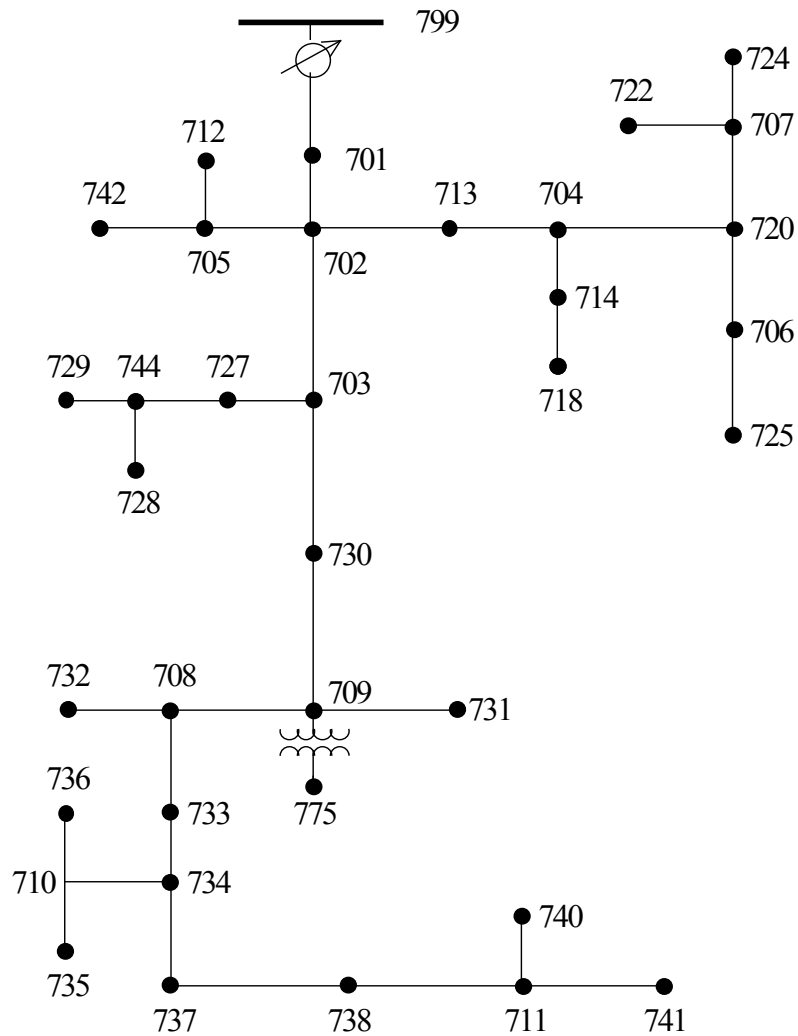


Figure 4.23: IEEE 37 Node Test Feeder.

Table 4.6: IEEE 37 Bus Network Data.

No. of Buses	No. of Loads	No. of Lines	Total Generation	Total Load	Total Losses
37	25	35	2.54 MW 1.34 MVar	2.46 MW 1.20 MVar	0.07 MW 0.13 MVar

A- Base Case

The terminal voltages at the grid bus, the CDG bus and bus 741 are shown in Figure 4.24 for when the three phase fault is applied on bus 799. When the three phase fault is applied on bus 741, the voltage recovery of the system buses is as illustrated in Figure 4.25. Figures 4.24 and 4.25 show that the terminal voltage returns to a nominal value in a short time period after the fault is cleared and this meets the LVRT requirements.

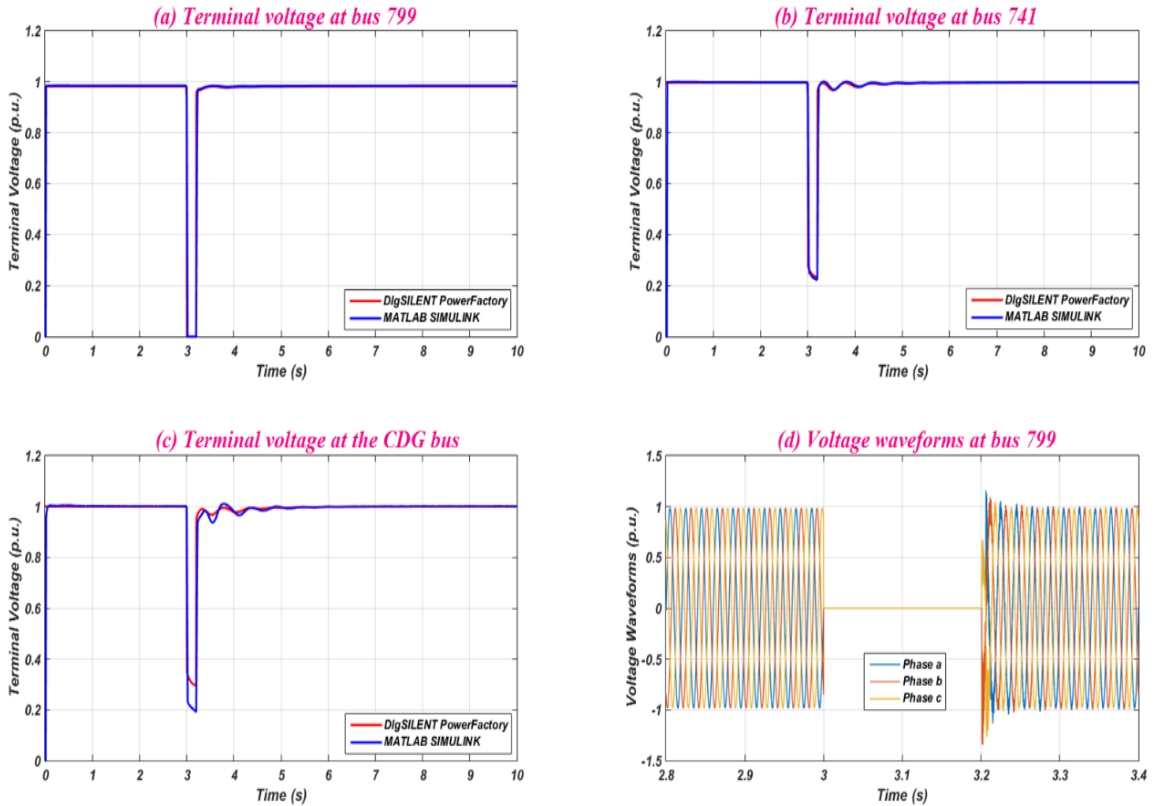


Figure 4.24: Voltage recovery for the base case of the 37 bus system (the fault is applied on bus 799) - (a) Terminal voltage at bus 799, (b) Terminal voltage at bus 741, (c) Terminal voltage at the DG bus, (d) Voltage waveforms at bus 799.

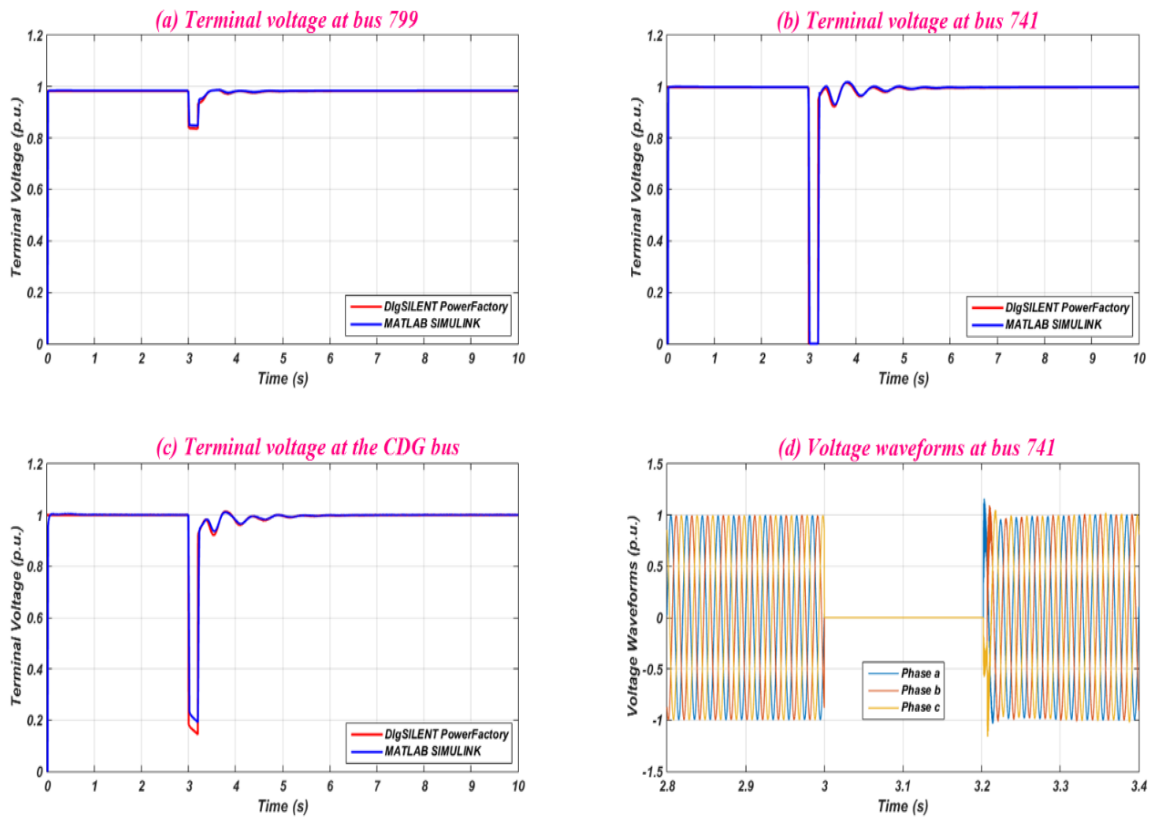


Figure 4.25: Voltage recovery for the base case of the 37 bus system (the fault is applied on bus 741) - (a) Terminal voltage at bus 799, (b) Terminal voltage at bus 741, (c) Terminal voltage at the CDG bus, (d) Voltage waveforms at bus 741.

B- 35 % PV Penetration

A 1.5 MW PV is installed on bus 741, which represents 35 % of the total generation. Table 4.7 shows the contribution of each generating source towards the total power generation of the test system. A 1.5 MW load is also added at bus 741 for the reason mentioned earlier in this chapter. The voltage recovery for this system when the fault is applied on bus 799 is shown in Figure 4.26, while Figure 4.27 illustrates the voltage recovery when the fault is applied on bus 741. From these figures it is clear that the terminal voltages return quickly to nominal values and this meets the LVRT grid code requirements.

Table 4.7: Power generation source outputs and their locations (PV case).

	Grid	CDG	PV
Total Generation	0.54 MW	2 MW	1.5 MW
Location	Bus 799	Bus 740	Bus 741

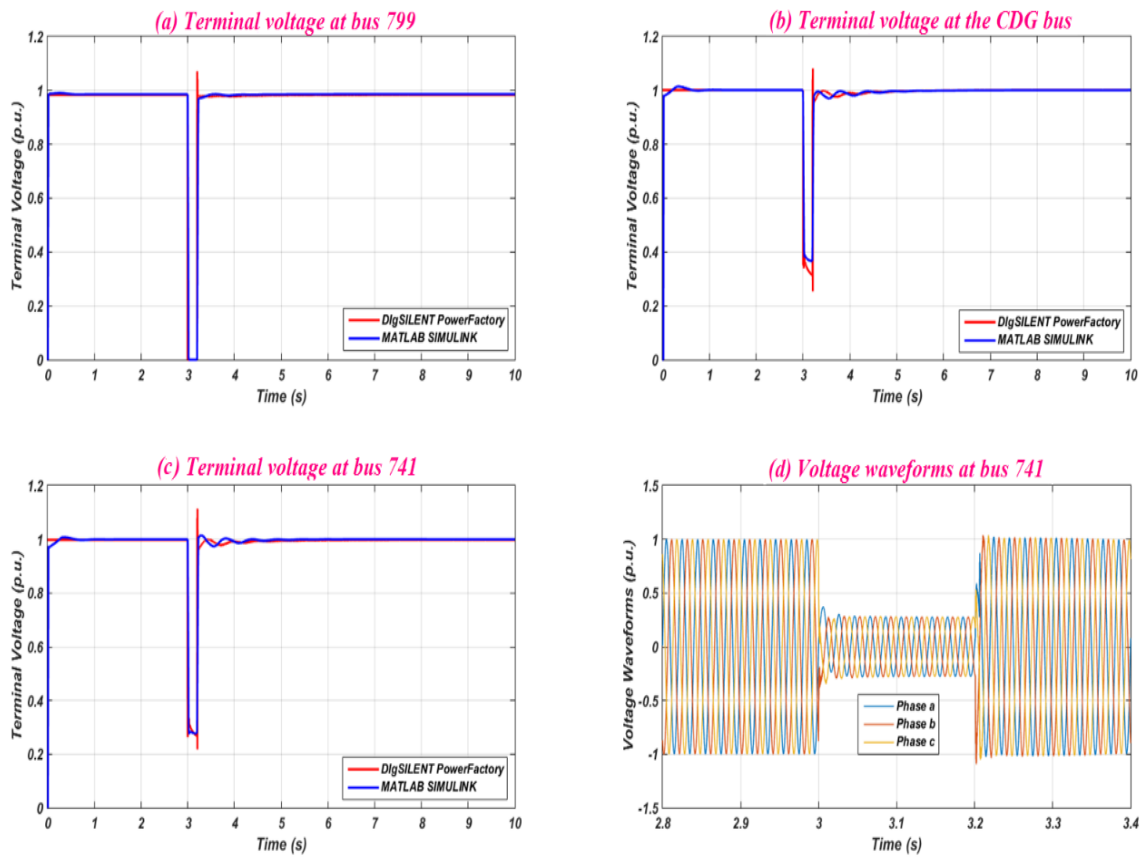


Figure 4.26: Voltage recovery for the PV case of the 37 bus system (the fault is applied on bus 799) - (a) Terminal voltage at bus 799, (b) Terminal voltage at the CDG bus, (c) Terminal voltage at bus 741, (d) Voltage waveforms at bus 741.

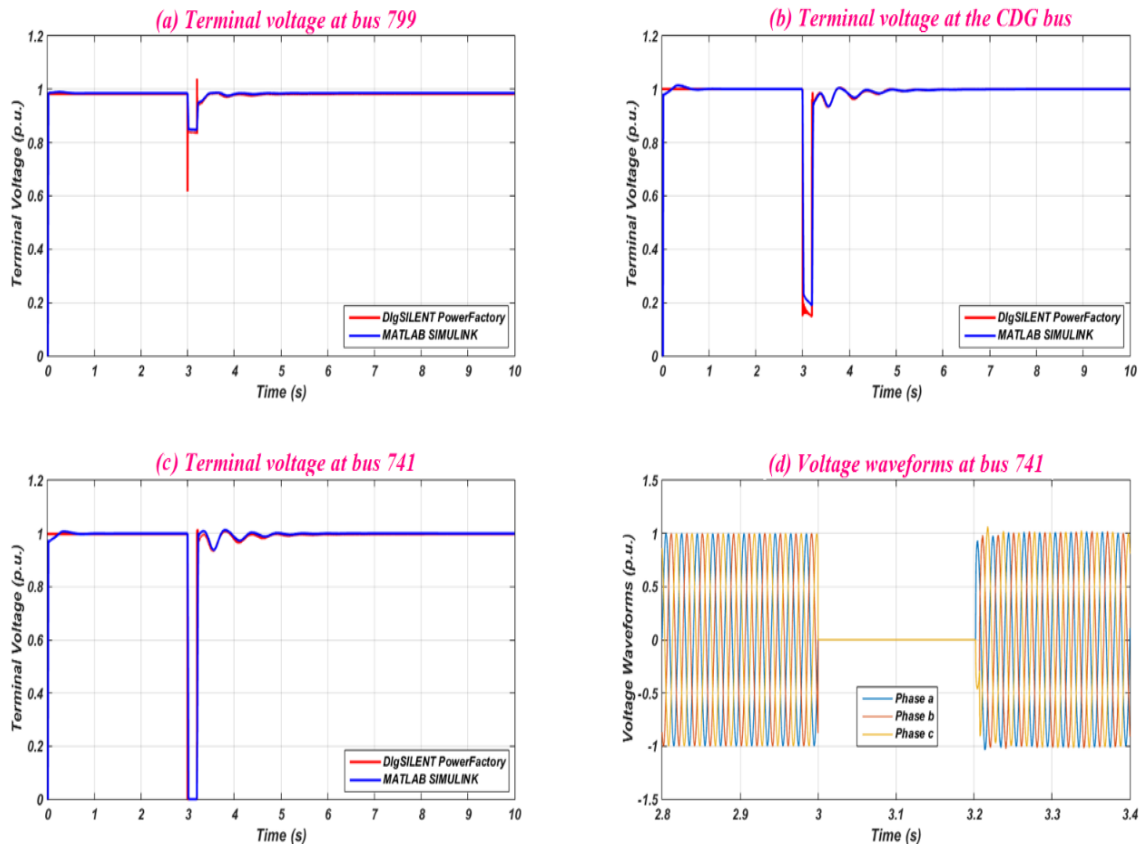


Figure 4.27: Voltage recovery for the PV case of the 37 bus system (the fault is applied on bus 741) - (a) Terminal voltage at bus 799, (b) Terminal voltage at the CDG bus, (c) Terminal voltage at bus 741, (d) Voltage waveforms at bus 741.

C- 35 % Wind based on DFIG Penetration

The wind based on the DFIG is installed at bus 741 with a 1.5 MW power output. A 1.5 MW load is also installed at the same bus. The contribution of generating sources in the test system in this case is shown in Table 4.8. The simulation results of the terminal voltages at the selected buses are given in Figures 4.28 and 4.29 when the fault is applied on bus 799 c and bus 741 respectively. The results show that the system meets the LVRT grid code requirements as the terminal voltages return to nominal values in a short time period.

Table 4.8: Power generation source outputs and their locations (DFIG case).

	Grid	CDG	Wind DFIG
Total Generation	0.54 MW	2 MW	1.5 MW
Location	Bus 799	Bus 740	Bus 741

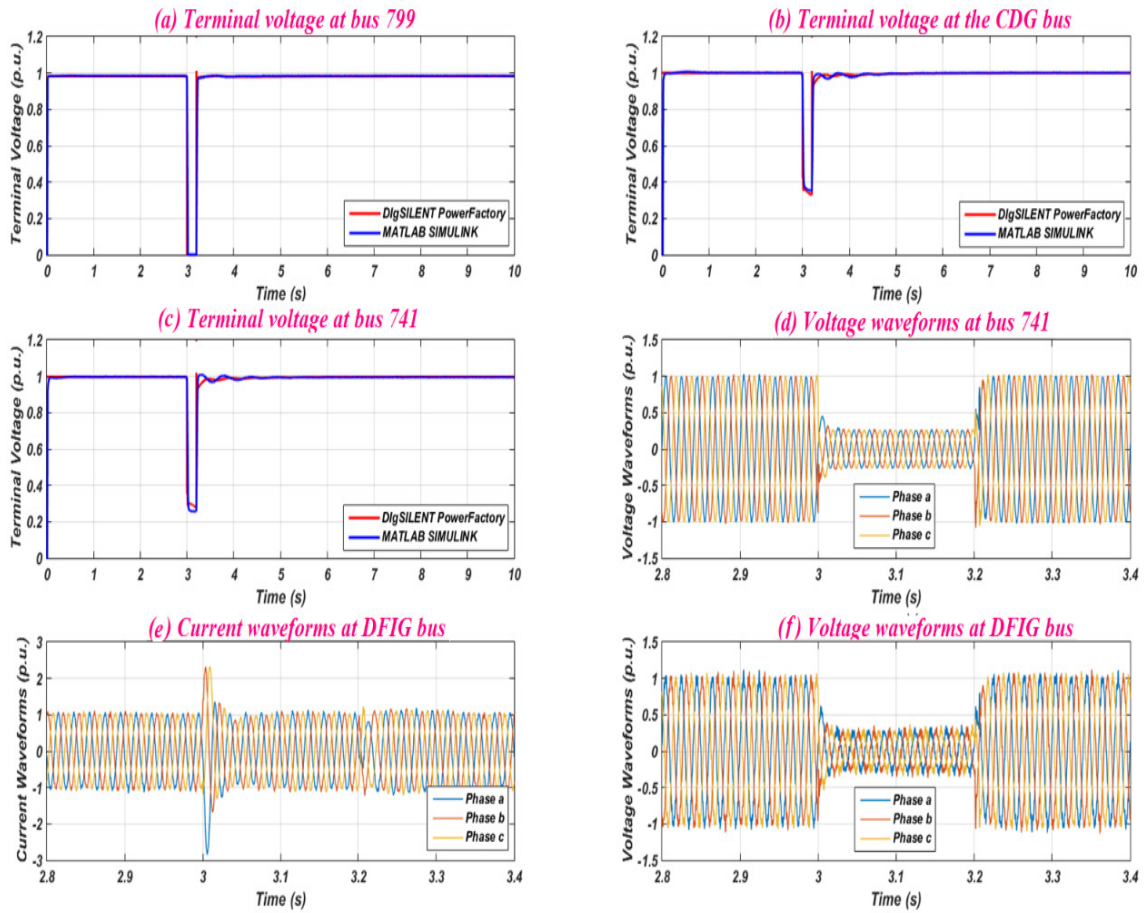


Figure 4.28: Voltage recovery for the 35 % wind based on the DFIG penetration case of the 37 bus system (the fault is applied on bus 799) - (a) Terminal voltage at bus 799, (b) Terminal voltage at the CDG bus, (c) Terminal voltage at bus 741, (d) Voltage waveforms at bus 741, (e) Current waveforms at DFIG bus, (f) Voltage waveforms at DFIG bus.

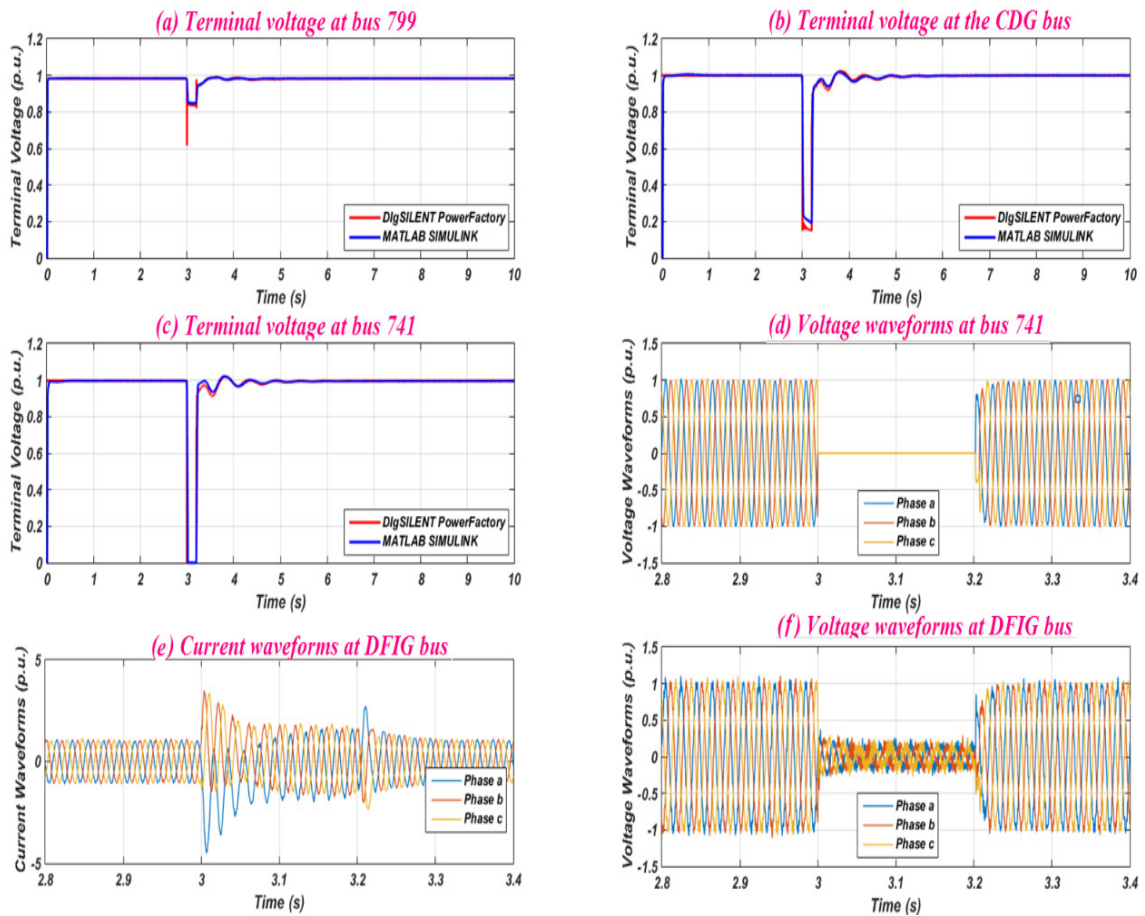


Figure 4.29: Voltage recovery for the 35 % wind based on the DFIG penetration case of 37 bus system (the fault is applied on bus 741) - (a) Terminal voltage at bus 799, (b) Terminal voltage at the CDG bus, (c) Terminal voltage at bus 741, (d) Voltage waveforms at bus 741, (e) Current waveforms at DFIG bus, (f) Voltage waveforms at DFIG bus.

D- 35 % Wind based on Synchronous Generator with Fully Rated Converters

A 1.5 MW wind synchronous generator with fully rated converters is installed on bus 741 with a 1.5 MW load. The contribution of each source of electricity in the test system towards the total power generation is shown in Table 4.9. This system is also investigated when the system experiences faults and simulation results are illustrated in Figures 4.30 and 4.31 when the fault is applied on bus 799 and bus 741 respectively. The results show that the voltage recovery meets the LVRT requirements, as the terminal voltages at the system buses return quickly to nominal values.

Table 4.9: Power generation source outputs and their locations (wind FRC case).

	Grid	CDG	Wind FRC
Total Generation	0.54 MW	2 MW	1.5 MW
Location	Bus 799	Bus 740	Bus 741

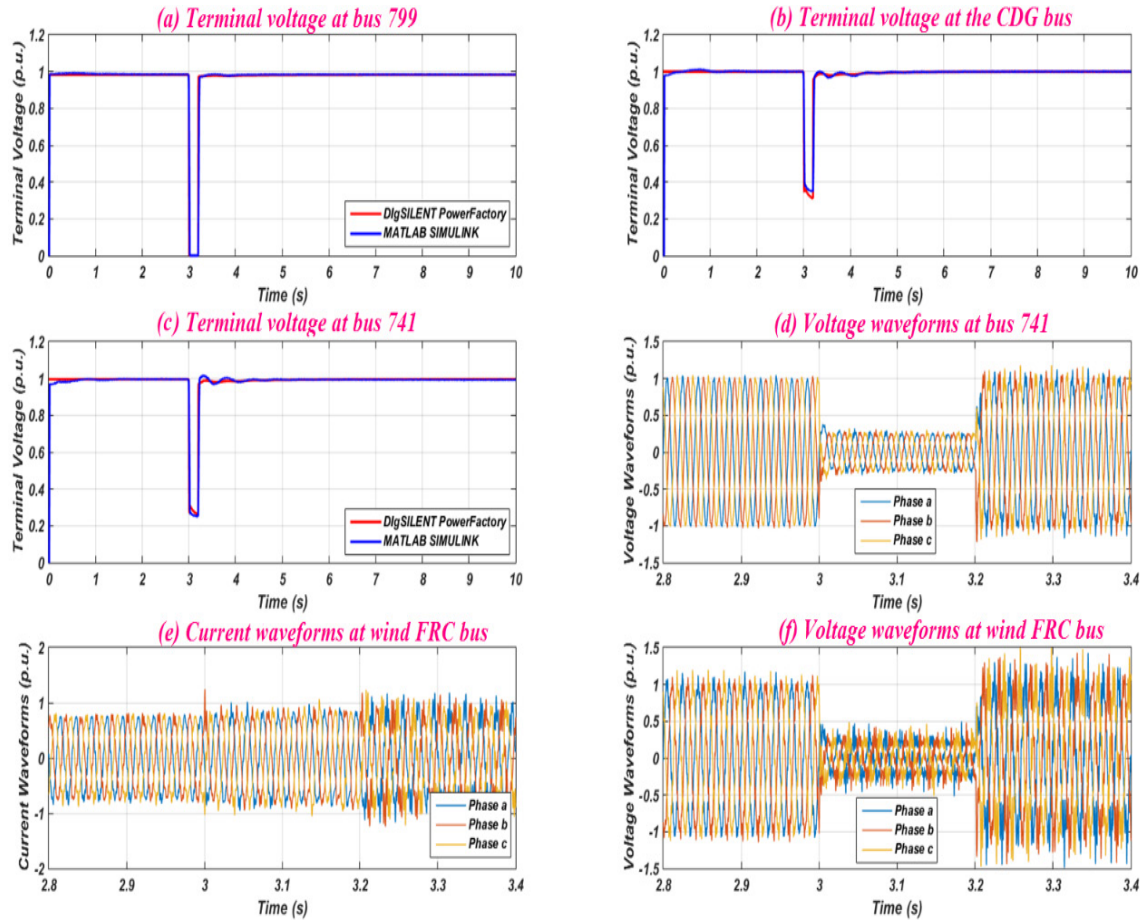


Figure 4.30: Voltage recovery for the 35 % wind based on the FRC penetration case of the 37 bus system (the fault is applied on bus 799) - (a) Terminal voltage at bus 799, (b) Terminal voltage at the CDG bus, (c) Terminal voltage at bus 741, (d) Voltage waveforms at bus 741, (e) Current waveforms at wind FRC bus, (f) Voltage waveforms at wind FRC bus.

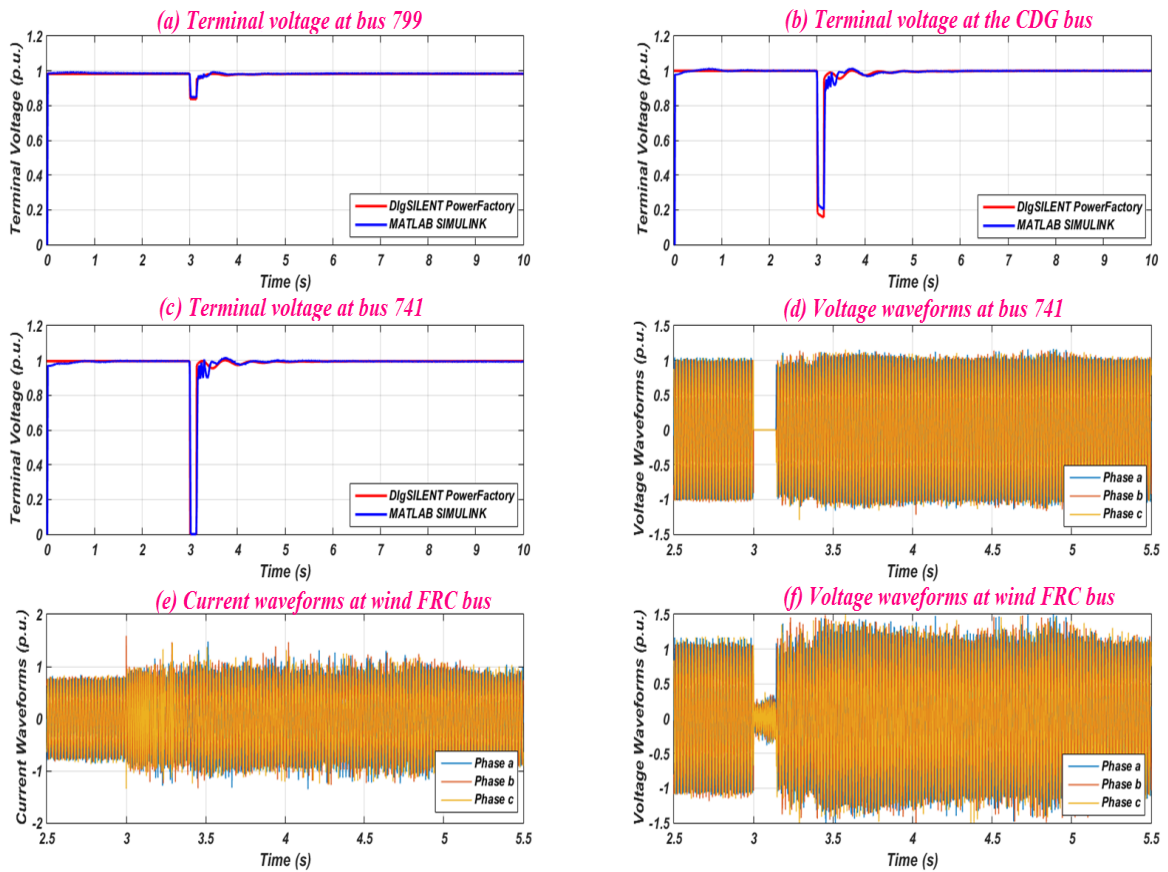


Figure 4.31: Voltage recovery for the 35 % wind based on the FRC penetration case of the 37 bus system (the fault is applied on bus 741) - (a) Terminal voltage at bus 799, (b) Terminal voltage at the CDG bus, (c) Terminal voltage at bus 741, (d) Voltage waveforms at bus 741, (e) Current waveforms at wind FRC bus, (f) Voltage waveforms at wind FRC bus.

E- 35 % Mixed Renewables Penetration

In this case, 1 MW wind based on the DFIG is installed with a 1 MW load at bus 741 and 0.5 MW PV is also installed at bus 737 with a load 0.5 MW. The contribution of each generating unit towards the total power generation in this test system is shown in Table 4.10. The voltage recovery of the test buses is illustrated in Figures 4.32 and 4.33 when the three phase is applied for 200 milliseconds on bus 799 and bus 741 respectively. The simulation results show that the terminal voltages return to nominal values in a short time period and this meets the LVRT requirements of the grid codes.

Table 4.10: Power generation source outputs and their locations (mixed renewables case).

	Grid	CDG	Wind DFIG	PV
Total Generation	0.54 MW	2 MW	1 MW	0.5 MW
Location	Bus 799	Bus 740	Bus 741	Bus 737

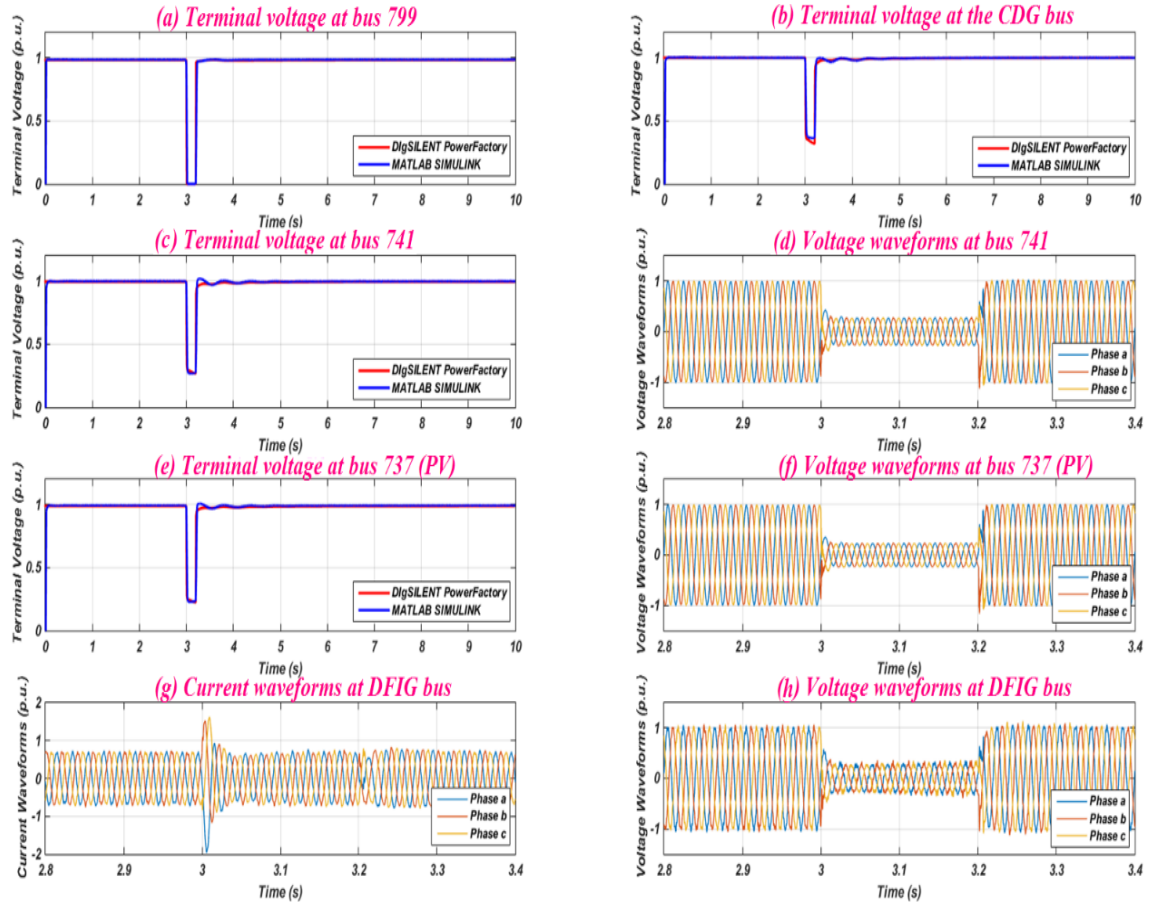


Figure 4.32: Voltage recovery for the 35 % mixed renewables penetration case of the 37 bus system (the fault is applied on bus 799) - (a) Terminal voltage at bus 799, (b) Terminal voltage at the CDG bus, (c) Terminal voltage at bus 741, (d) Voltage waveforms at bus 741, (e) Terminal voltage at bus 737 (PV), (f) Voltage waveforms at bus 737 (PV), (g) Current waveforms at DFIG bus, (h) Voltage waveforms at DFIG bus.

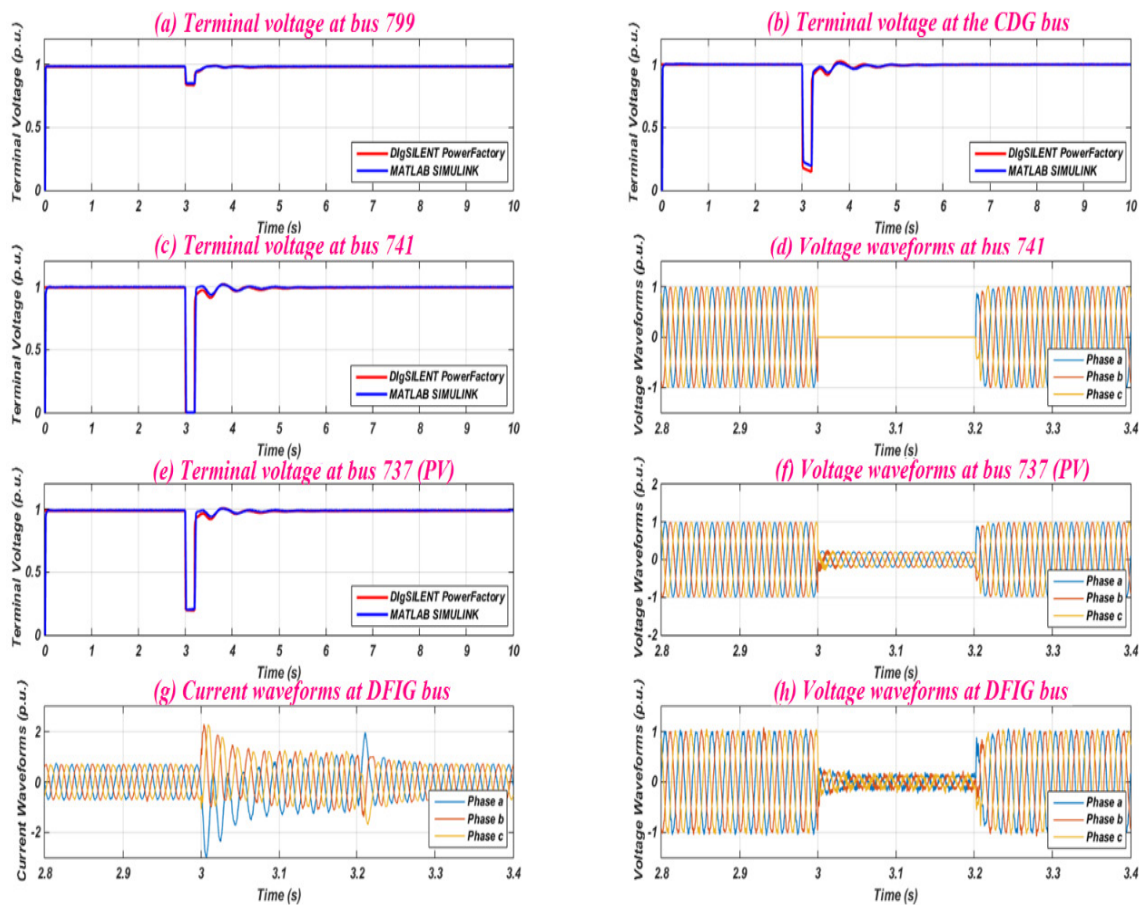


Figure 4.33: Voltage recovery for the 35 % mixed renewables penetration case of the 37 bus system (the fault is applied on bus 741) - (a) Terminal voltage at bus 799, (b) Terminal voltage at the CDG bus, (c) Terminal voltage at bus 741, (d) Voltage waveforms at bus 741, (e) Terminal voltage at bus 737 (PV), (f) Voltage waveforms at bus 737 (PV), (g) Current waveforms at DFIG bus, (h) Voltage waveforms at DFIG bus.

4.7.3 IEEE 123 Bus Distribution System

The IEEE 123 Node Test Feeder is another test system for distribution system analysis, published by the IEEE Power Engineering Society [195]. A schematic diagram of this system is shown in Figure 4.34. Detailed data regarding this system are given in Appendix B.3. This system is connected to the ac grid through a two winding ac transformer. Bus 150 is the bus which interconnects the grid with the test network. This bus has been selected because it is directly connected to the grid through a transformer, which is named a substation. The IEEE 123 bus distribution network data are summarised in Table 4.11. A CDG is assumed to be connected at bus number 96, which is one of the farthest nodes from the grid and close to the renewable units' location, to investigate the transient stability of the synchronous generator. Detailed data regarding this CDG are given in Appendix C. The grid is assumed to be an infinite bus. Power flow data regarding the 123 bus distribution system are given in Appendix B.3, where the grid bus is assumed to be the slack. The DG based on renewable resources are connected to the farthest node from the grid, which is bus number 85. The same test procedure as for the LVRT grid code requirements, which have been discussed in the previous distribution networks, will be followed. A three phase fault will be applied on bus 150 and bus 85 respectively for 200 milliseconds to investigate the voltage recovery of the system buses.

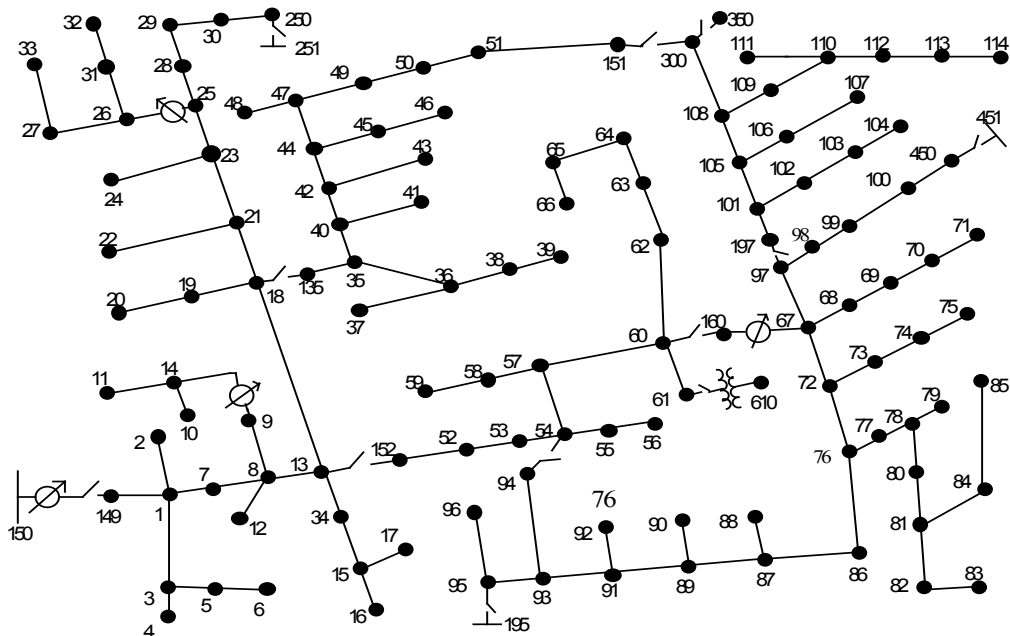


Figure 4.34: IEEE 123 Node Test Feeder.

Table 4.11: IEEE 123 Bus Network Data.

No. of Buses	No. of Loads	No. of Lines	Total Generation	Total Load	Total Losses
123	85	118	3.63 MW 2.27 MVA _r	3.49 MW 1.92 MVA _r	0.13 MW 0.34 MVA _r

A- Base Case

As shown in sections 4.7.1 and 4.7.2, the distribution networks have been investigated for their match with the LVRT requirements. These requirements will also be discussed in this section in regards to the IEEE 123 test distribution system. For this reason, a three phase fault is applied on bus 150 and bus 85 for 200 milliseconds duration. Simulation results for the voltage recovery at system buses are shown in Figures 4.35 and 4.36 respectively. The results show that the system complies with the LVRT grid code requirements, as the terminal voltages return quickly to their nominal values.

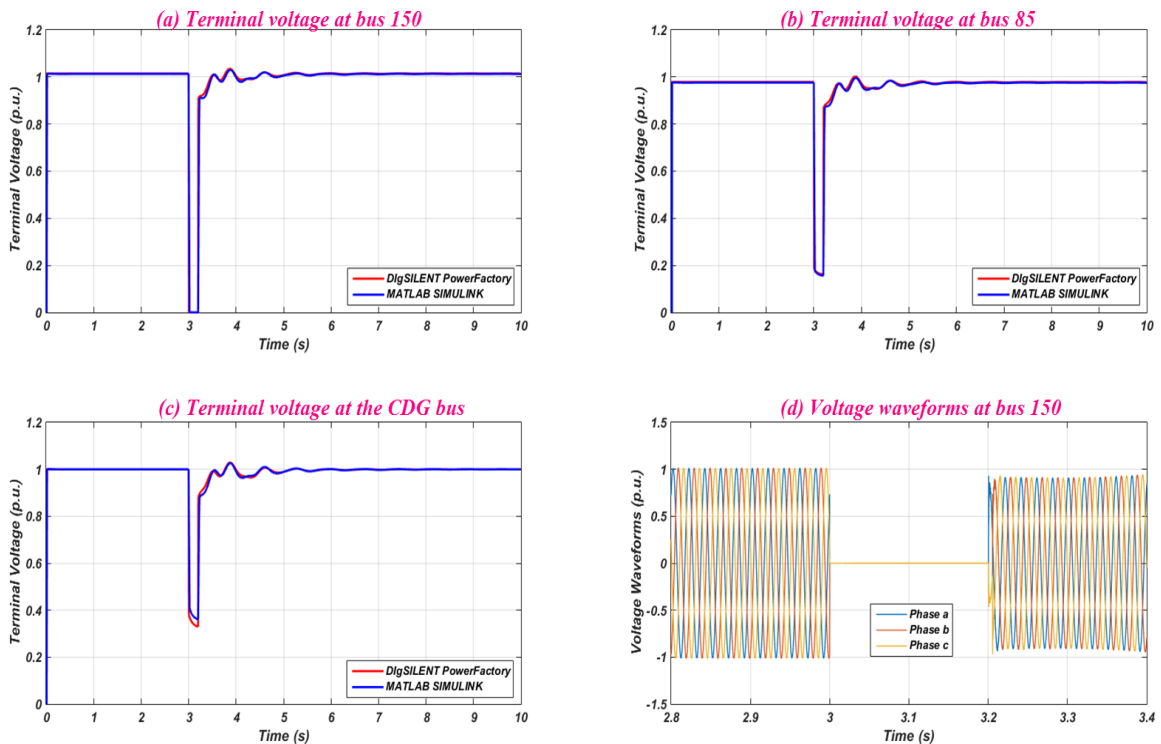


Figure 4.35: Voltage recovery for the base case of the 123 bus system (the fault is applied on bus 150) - (a) Terminal voltage at bus 150, (b) Terminal voltage at bus 85, (c) Terminal voltage at the CDG bus, (d) Voltage waveforms at bus 150.

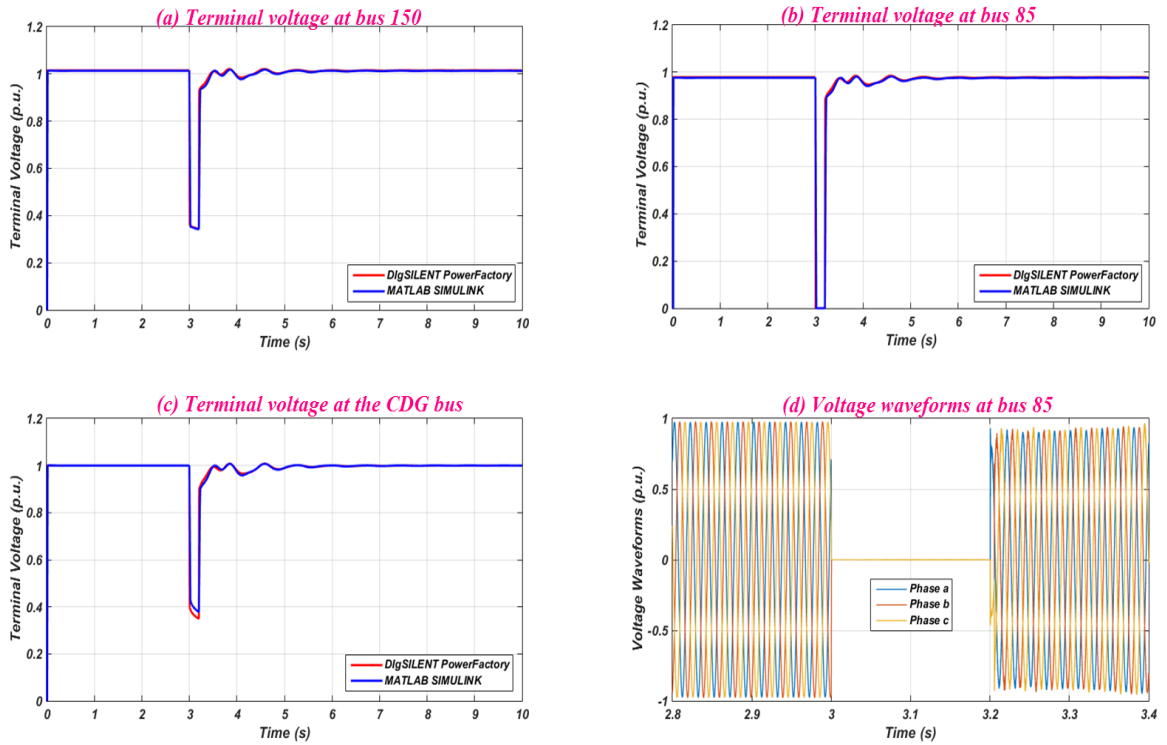


Figure 4.36: Voltage recovery for the base case of the 123 bus system (the fault is applied on bus 85) - (a) Terminal voltage at bus 150, (b) Terminal voltage at bus 85, (c) Terminal voltage at the CDG bus, (d) Voltage waveforms at bus 85.

B- 35 % PV Penetration

Photovoltaic is installed at bus 85 with 2 MW output power and the contribution of each generating unit in the network towards the total power generation is shown in Table 4.12. A 2 MW load is also added at bus number 85 for the reason mentioned in section 3.7.1. The system meets the LVRT requirements as the terminal voltages return to their nominal values in a short time period, as shown in Figures 4.37 and 4.38, when the three phase fault is applied on bus 150 and bus 85 respectively.

Table 4.12: Power generation source outputs and their locations (PV case).

	Grid	CDG	PV
Total Generation	1.63 MW	2 MW	2 MW
Location	Bus 150	Bus 96	Bus 85

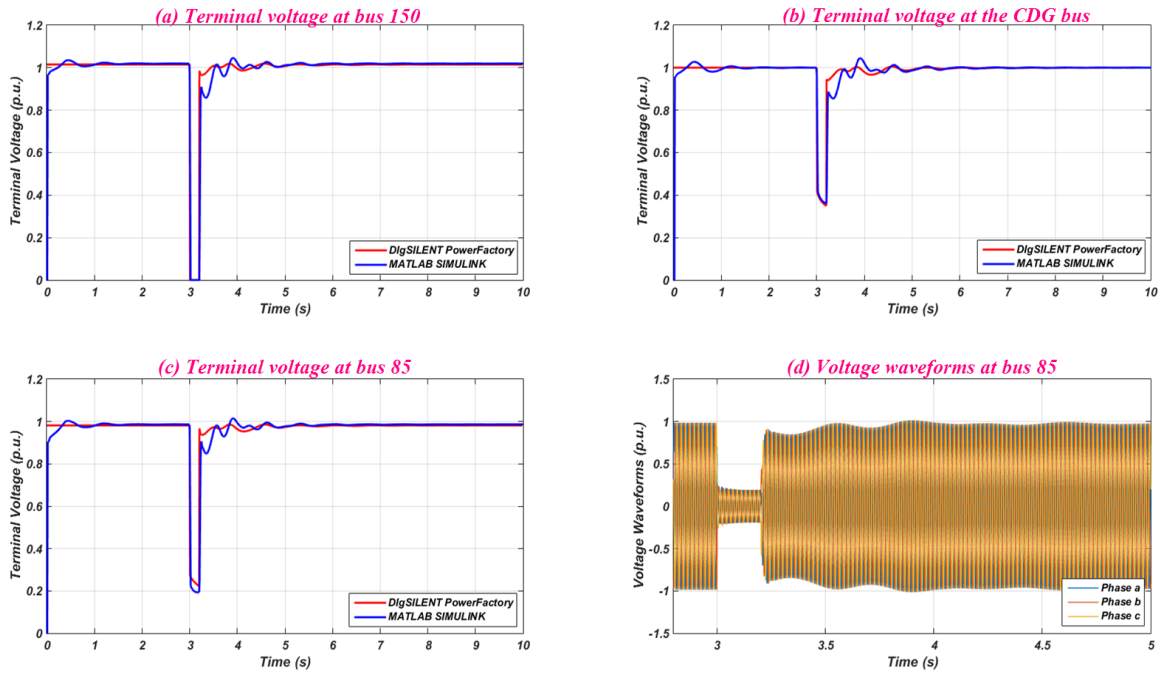


Figure 4.37: Voltage recovery for the PV case of the 123 bus system (the fault is applied on bus 150) - (a) Terminal voltage at bus 150, (b) Terminal voltage at the CDG bus, (c) Terminal voltage at bus 85, (d) Voltage waveforms at bus 85.

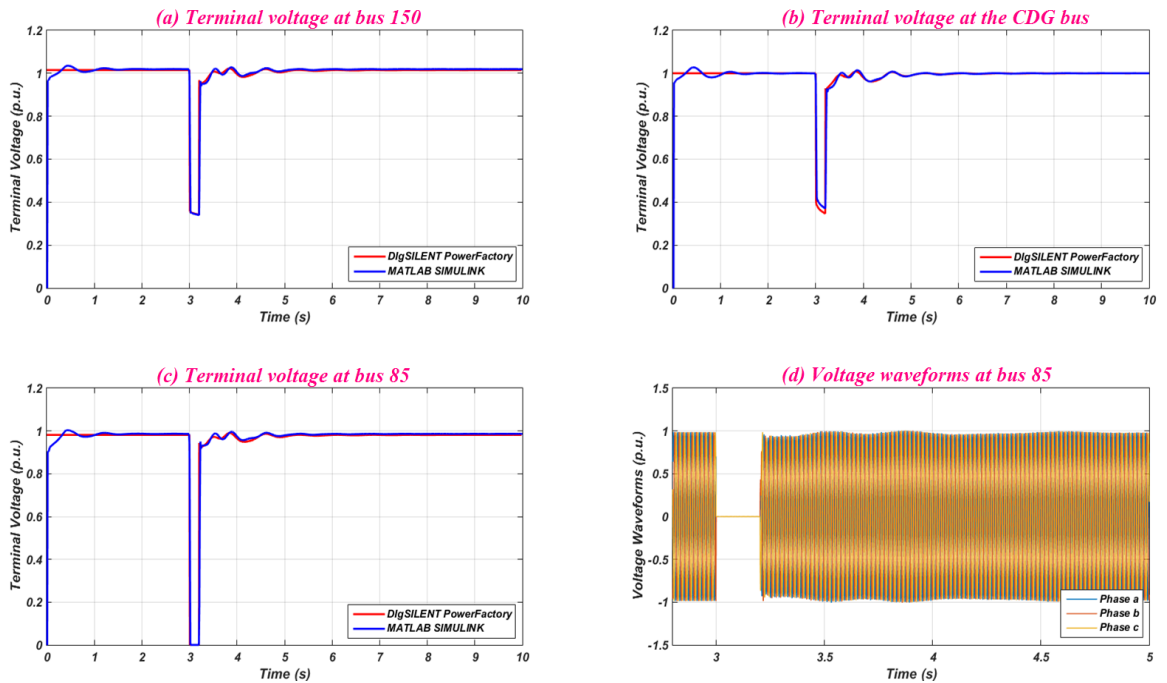


Figure 4.38: Voltage recovery for the PV case of the 123 bus system (the fault is applied on bus 85) - (a) Terminal voltage at bus 150, (b) Terminal voltage at the CDG bus, (c) Terminal voltage at bus 85, (d) Voltage waveforms at bus 85.

C- 35 % Wind based on DFIG Penetration

A wind generator based on DFIG technology is installed at bus 85 with 2 MW output power. The contribution of the generating sources in this test system are illustrated in Table 4.13. A 2 MW load is also added to bus 85. A three phase fault is applied on bus 150 and bus 85 to investigate the voltage recovery of the system buses, as shown in Figures 4.39 and 4.40 respectively. The simulation results show that the system meets the LVRT requirements because the terminal voltages recover quickly after the fault is cleared.

Table 4.13: Power generation source outputs and their locations (DFIG case).

	<i>Grid</i>	<i>CDG</i>	<i>Wind DFIG</i>
<i>Total Generation</i>	1.63 MW	2 MW	2 MW
<i>Location</i>	Bus 150	Bus 96	Bus 85

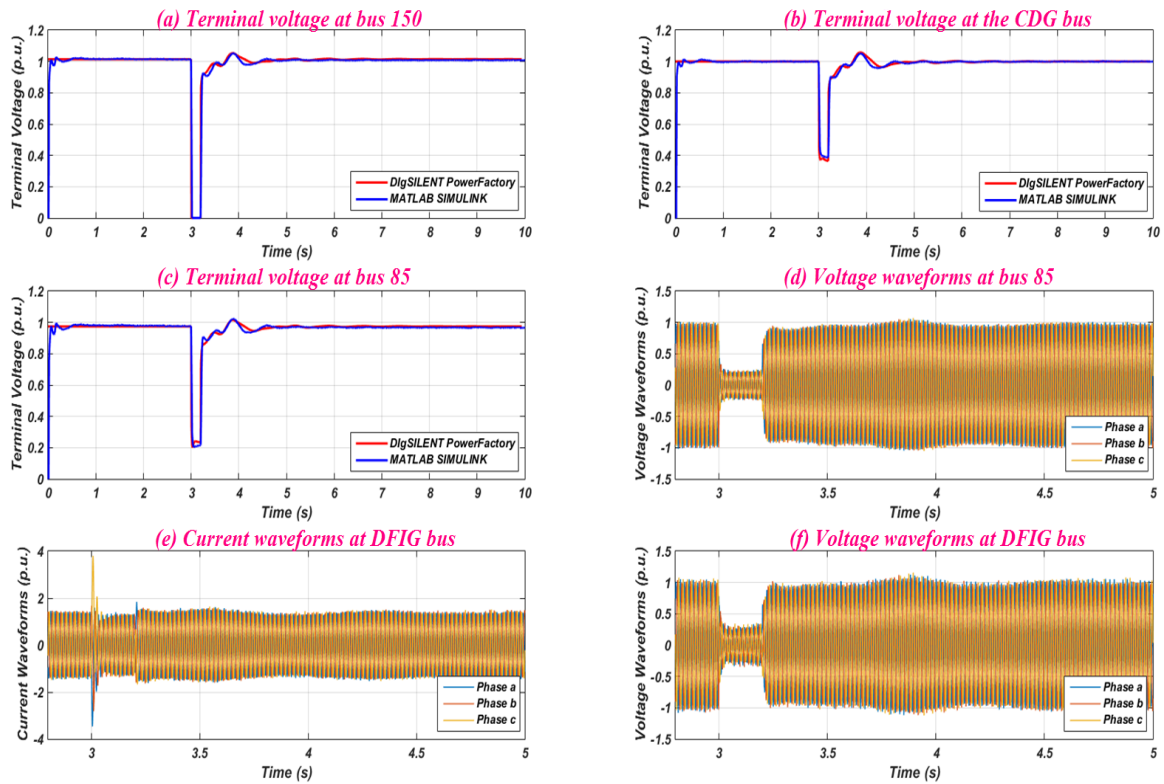


Figure 4.39: Voltage recovery for the 35 % wind based on the DFIG penetration case of the 123 bus system (the fault is applied on bus 150) - (a) Terminal voltage at bus 150, (b) Terminal voltage at the CDG bus, (c) Terminal voltage at bus 85, (d) Voltage waveforms at bus 85, (e) Current waveforms at DFIG bus, (f) Voltage waveforms at DFIG bus.

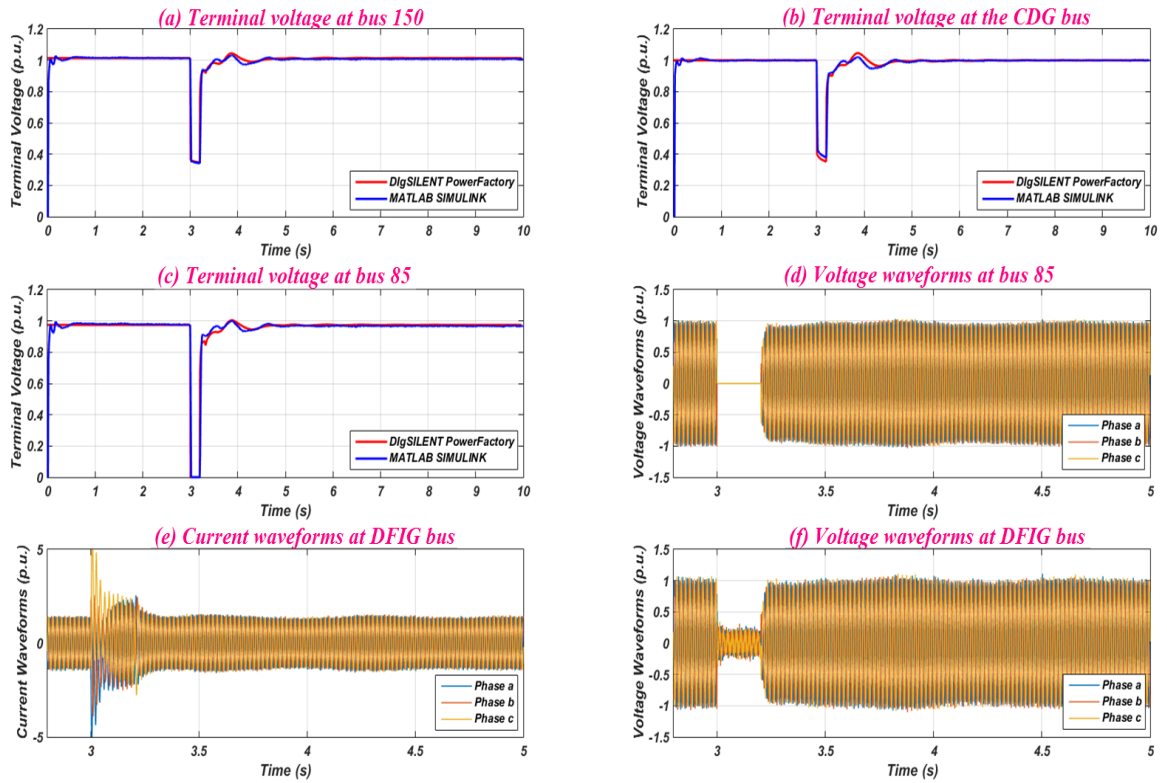


Figure 4.40: Voltage recovery for the 35 % wind based on the DFIG penetration case of the 123 bus system (the fault is applied on bus 85) - (a) Terminal voltage at bus 150, (b) Terminal voltage at the CDG bus, (c) Terminal voltage at bus 85, (d) Voltage waveforms at bus 85, (e) Current waveforms at DFIG bus, (f) Voltage waveforms at DFIG bus.

D- 35 % Wind based on Synchronous Generator with Fully Rated Converters

In this case, a 2 MW wind generator with FRC is installed at bus 85 with 2 MW output power. The generation contribution of each source in the system is illustrated in Table 4.14. The terminal voltages of this system have been investigated when a three phase fault is applied on bus 150 and bus 85 to ensure that the voltage recovery meets the LVRT grid code requirements. Figures 4.41 and 4.42 show that the voltage recovery at the targeted buses meets the LVRT requirements, as the voltages return quickly to their nominal values.

Table 4.14: Power generation source outputs and their locations (wind FRC case).

	Grid	CDG	Wind FRC
Total Generation	1.63 MW	2 MW	2 MW
Location	Bus 150	Bus 96	Bus 85

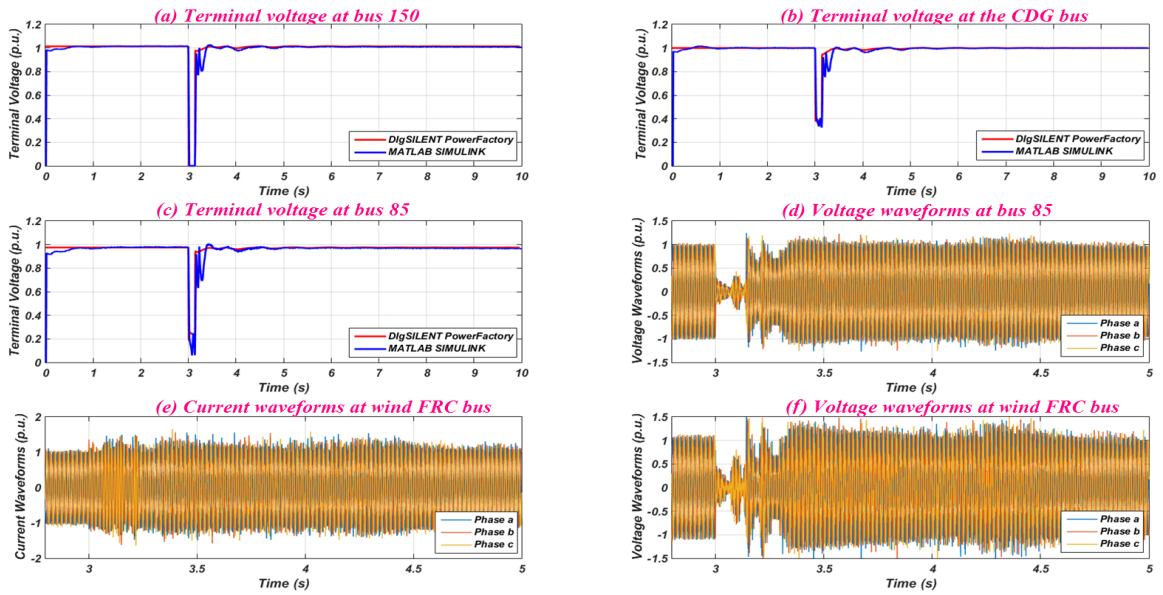


Figure 4.41: Voltage recovery for the 35 % wind based on the FRC penetration case of the 123 bus system (the fault is applied on bus 150) - (a) Terminal voltage at bus 150, (b) Terminal voltage at the CDG bus, (c) Terminal voltage at bus 85, (d) Voltage waveforms at bus 85, (e) Current waveforms at wind FRC bus, (f) Voltage waveforms at wind FRC bus.

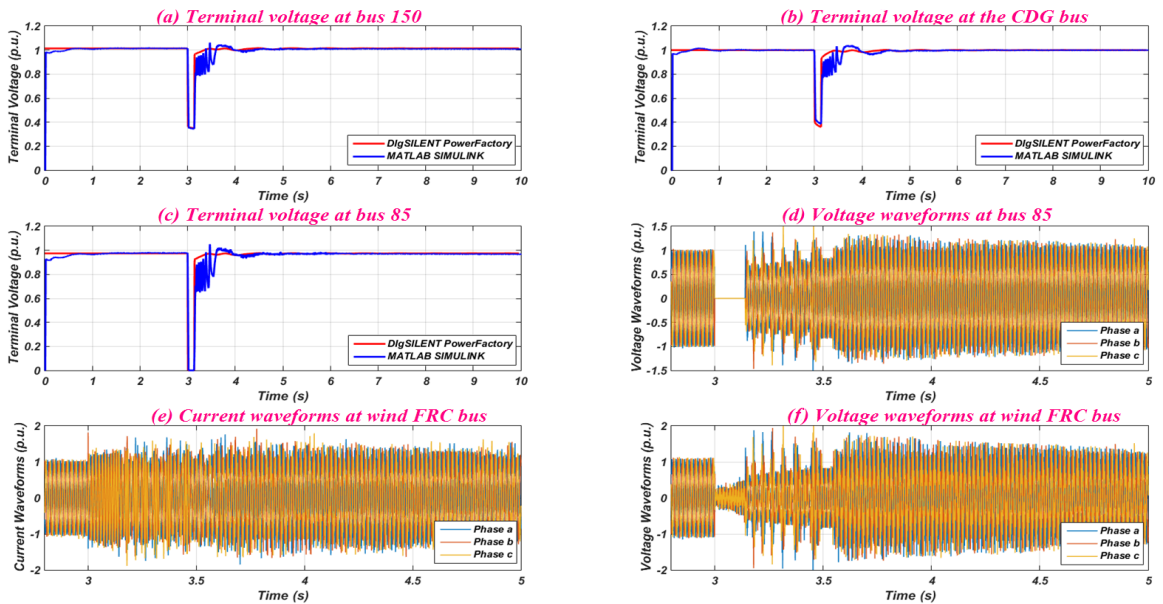


Figure 4.42: Voltage recovery for the 35 % wind based on the FRC penetration case of the 123 bus system (the fault is applied on bus 85) - (a) Terminal voltage at bus 150, (b) Terminal voltage at the CDG bus, (c) Terminal voltage at bus 85, (d) Voltage waveforms at bus 85, (e) Current waveforms at wind FRC bus, (f) Voltage waveforms at wind FRC bus.

E- 35 % Mixed Renewables Penetration

In this case, 1.5 MW wind based on the DFIG is installed at bus 85 with a 1.5 load and 0.5 MW PV is installed with a 0.5 MW load at bus 114. The contribution of the generating units towards the total power generation is shown in Table 4.15. To investigate the LVRT requirements, a three phase fault is applied on bus 150 and bus 85, as illustrated in Figures 4.43 and 4.44 respectively. The voltage recovery of the system buses complies with the LVRT requirements, as the terminal voltages recover to initial values in a short time period.

Table 4.15: Power generation source outputs and their locations (mixed renewables case).

	<i>Grid</i>	<i>CDG</i>	<i>Wind DFIG</i>	<i>PV</i>
<i>Total Generation</i>	1.63 MW	2 MW	1.5 MW	0.5 MW
<i>Location</i>	Bus 150	Bus 96	Bus 85	Bus 114

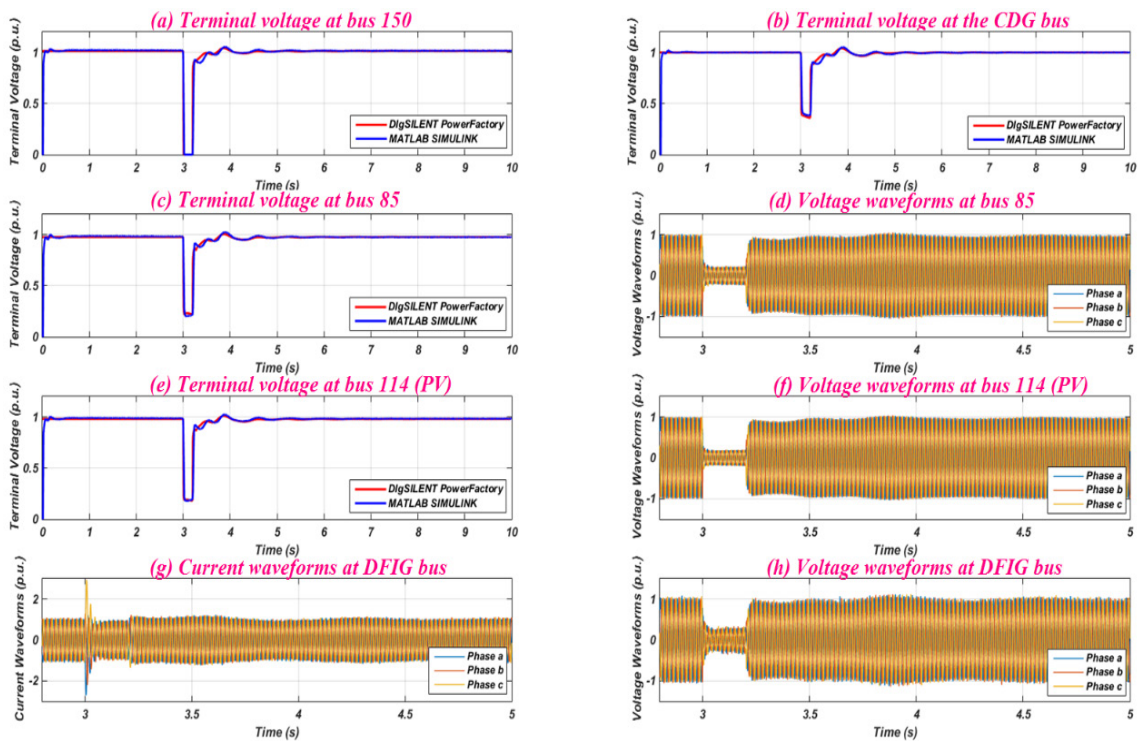


Figure 4.43: Voltage recovery for the 35 % mixed renewables penetration case of the 123 bus system (the fault is applied on bus 150) - (a) Terminal voltage at bus 150, (b) Terminal voltage at the CDG bus, (c) Terminal voltage at bus 85, (d) Voltage waveforms at bus 85, (e) Terminal voltage at bus 114 (PV), (f) Voltage waveforms at PV bus, (g) Current waveforms at DFIG bus, (h) Voltage waveforms at DFIG bus.

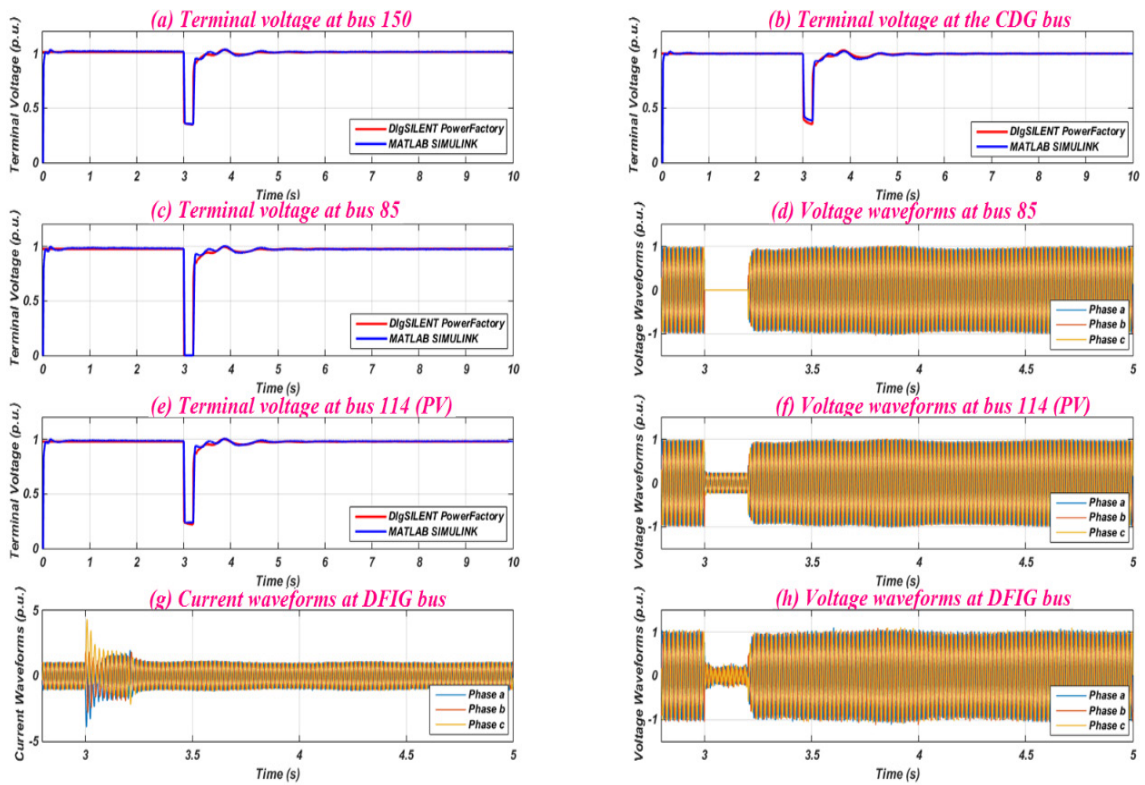


Figure 4.44: Voltage recovery for the 35 % mixed renewables penetration case of the 123 bus system (the fault is applied on bus 85) - (a) Terminal voltage at bus 150, (b) Terminal voltage at the CDG bus, (c) Terminal voltage at bus 85, (d) Voltage waveforms at bus 85, (e) Terminal voltage at bus 114 (PV), (f) Voltage waveforms at PV bus, (g) Current waveforms at DFIG bus, (h) Voltage waveforms at DFIG bus.

4.8 Conclusions

Distributed generation based on wind and photovoltaic energy has increased dramatically in distribution networks due to economic incentives and the need to reduce greenhouse gas emissions. This rapid increase has changed FRT grid requirements and new requirements have been asked from several power system operators worldwide, as the disconnection of large parts of these renewables during fault conditions leads to system instability. The interconnection requirements of renewable energy sources vary from country to country and they are not necessarily depend on the penetration level of renewable energy in power systems. For instance, countries with a weak power system such as Ireland already require FRT capabilities for the interconnected of renewable

sources at a lower renewable penetration [27]. This chapter has discussed the need to ride through grid faults and different generic distribution systems have been investigated while they experience severe fault conditions, such as three phase faults. There are two different locations for the applied fault that have been selected to discuss the FRT performance of the distribution networks. Distributed generation based on renewables could be at risk of overvoltages and/or overcurrents if the fault location is close to the connection terminals.

It has been shown that DC link voltages of DGs based on renewable energy increase during a fault and this could damage the power electronic converters of the DG units. Therefore, the converters should be protected from the impact of such faults. When a DC chopper is added to the DC link of wind generators the results show that the DC link voltages can be kept within acceptable limits. It is important to know that inclusion of FRT capabilities for some renewable sources such as DFIG increases the overall cost of the unit by 5% [27]. For a PV system, a three phase two stage transformerless grid connected has been proposed with a new technique to protect the converters from faults and to maintain the DC link voltage within given limits. The voltage recovery of different distribution systems with high renewable energy penetration has been investigated in this chapter and the simulation results show that they meet the LVRT grid code requirements.

CHAPTER 5 Transient Stability of Distribution Systems with High Renewable Energy Penetration

5.1 Introduction

Increasing concerns over the shortage of fossil fuels and environmental issues have led to acceleration in the development of renewable energy sources. The current renewable portfolios of several countries around the world show that they have set targets to increase the penetration of their renewable sources into their power systems, aimed at addressing the need for clean and sustainable sources of energy. These factors have encouraged the increased penetration of distributed generation based on renewable energy, such as wind and solar energy, into distribution systems. Increased penetration of relatively large distributed generation units based on renewable energy resources into distribution networks in response to the rapid increase in demand for clean energy in recent years has changed the nature and dynamics of distribution systems. Some of these DG units are connected to the grid through a power electronics interface that decouples their dynamics from the grid [40, 197]. As a result they are unable to contribute system inertia. As the proportion of the power generated from such distributed generation units becomes significant and vital to system stability, a new operating regime for these units may be required in order to ensure safe and reliable system operation, especially during operation in small to medium scale, low and medium voltage, micro or smart grids [198]. For a micro grid to be able to operate safely as an independent network or as part of a larger grid, each DG unit must contribute to the power system stability and operation in the same manner as large conventional power plants. Such requirements may force small scale wind power producers to move away from fixed speed induction generators and adopt variable speed wind generators such as the DFIG or synchronous generator with fully rated converters, as they inherently have the ability to participate in ac voltage control. Photovoltaic based solar energy also has the ability to meet such requirements by modifying its control system. Traditionally [39], these renewable units had a small impact

on power system stability as they were deployed on a small scale. However, when the penetration level of renewable sources increases, the dynamic performance of the power system can be affected. This chapter investigates the transient stability of different generic distribution systems with high renewable energy penetration when the systems experience a severe grid disturbance such as faults.

5.2 Power System Stability Background

The importance of power system stability is a concern at the early stage of the development of a power system. The increase in the complexity and dimension of power systems over the years makes the power system stability phenomenon an even more important and challenging issue. Modern power generating plants such as renewables are an example of the stability challenging problem, as these units have a different nature of dynamics which make the control of the power system more complicated [24]. The definition and classification of power system stability are shown in [199]. Power system stability is classified into three main types, as illustrated in Figure 5.1. Among these types, rotor angle stability is one of the most significant phenomena in power system literature. It refers to the ability of synchronous machines (SMs) in a power system to remain in synchronism after being subjected to a disturbance. The synchronous machines of an interconnected power system can remain in synchronism depending on the ability to maintain/restore equilibrium between mechanical torque and electromagnetic torque of each SM in the system. Instability that may result occurs when the angle swings of some generators increase, which results in loss on their synchronism with other generators.

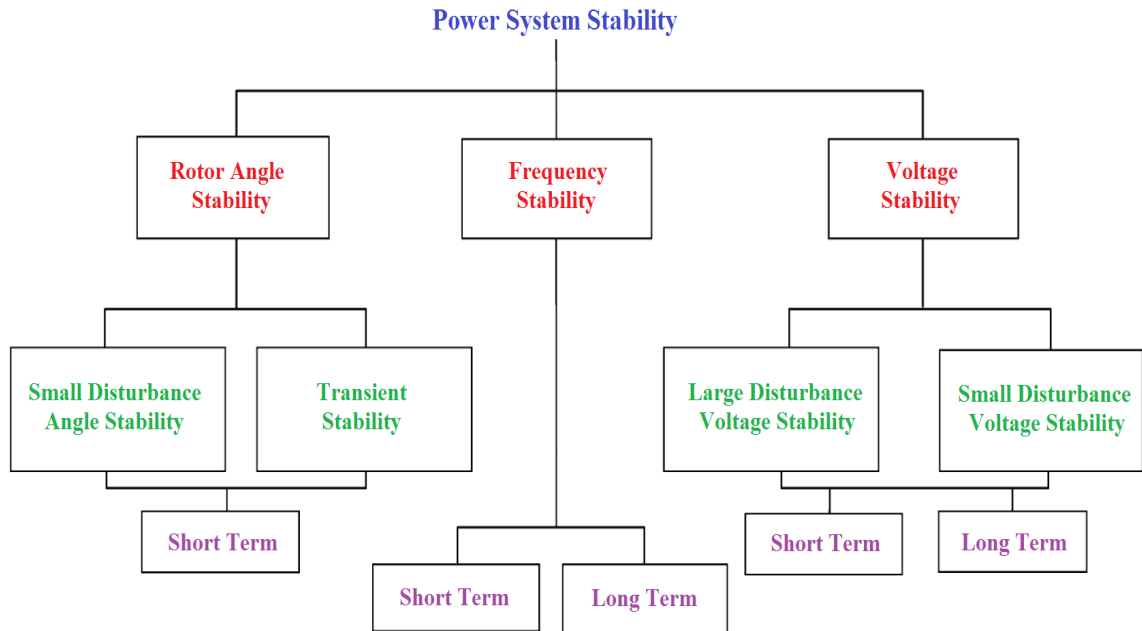


Figure 5.1: Power system stability classification.

Rotor angle stability is divided into two categories, small-disturbance angle stability and large-disturbance angle stability known as Transient Stability. This chapter considers only the transient stability of distribution systems. Transient stability of a distribution system is defined as the ability of the system to maintain synchronism when subjected to a severe transient disturbance, such as faults, loss of a large load or loss of generation [200]. The system's response to such disturbances involves large excursions of generator rotor angles, terminal voltages and other system variables. In most cases, system instability can be avoided by the action of protective devices which can prevent damage to power system components caused by overvoltages and/or overcurrents. The main objective of this chapter is to investigate the transient stability of different generic distribution systems with high renewable energy penetration and whether the systems remain stable or not when a severe disturbance occurs. The severe disturbance which is considered in this chapter is a three phase fault, which is applied at different buses in the system.

5.3 Transient Stability Analysis

The power system has to experience a large disturbance, such as a three phase fault, to conduct the transient stability analysis. One of the parameters used to test the stability of the system is the generator rotor angle measured with respect to a synchronously rotating reference. The Transient Stability Index (TSI) is a method used to assess the severity of a contingency and the trajectory of a power system following a large disturbance, such as faults. The TSI can be calculated based on an angle margin algorithm, as illustrated in equation 5.1 [201].

$$TSI = \frac{360^\circ - \delta_{max}}{360^\circ + \delta_{max}} \times 100 \quad , \text{ where } -100 < TSI < 100 \quad (5.1)$$

Where δ_{max} is the maximum angle separation in degrees between any two generators at the same time in the post-fault response. When the index (TSI) is greater than zero the system is stable; however, if $TSI \leq$ zero, the system is unstable.

In this chapter, the transient stability of a synchronous generator will be investigated in different distribution systems with high renewable energy penetration. Two different fault locations are assumed to study the transient stability, one close to the SG on the renewable bus (as discussed in Chapter 4) and the second on the grid bus. During the fault, the synchronous generator electric torque falls below the mechanical torque and this leads to acceleration of the rotor, causing a higher rotor angle position. For an induction generator such as the DFIG, the physical position of the rotor and the rotor flux vector are not directly connected due to its asynchronous operation. Hence, the dynamic response of this type of generator to grid disturbances is unlike that of synchronous generators [202]. The dynamic response characteristics of other DG units to system disturbance, such as photovoltaic ones, are also different. Therefore, wind based DFIG and photovoltaic grid connected systems are considered in this chapter as renewables sources, as well as a wind based synchronous generator with fully rated converters.

5.4 Wind Generation Impact on Transient Stability

In recent years, renewable energy sources such as wind have obtained worldwide attention due to the significant increase in greenhouse gas emissions and the shortage of fossil fuels. Therefore, wind generating units have been considered as an alternative source of energy to replace fossil fuel power plants and they have increased dramatically due to strong governmental and industrial support. Due to the intermittent nature of wind speed, wind power generation produces variable power. The increase of wind grid connected systems raises a momentous concern about their impact on power system stability [136, 137, 203]. Wind power generation systems based on the DFIG are one of the most common technologies used in recent years, being attractive as they capture more power by implementing variable speed control and can control output power precisely through the power electronics interface.

The impact of integrating wind power based on the DFIG on a power system's transient stability has been discussed in literature. In [41, 204], they show that transient stability can be improved when conventional synchronous generators are replaced by wind ones based on the DFIG with the same capacity. Another research paper concludes that a power system's transient stability can be either enhanced or reduced when a DFIG based wind generator replaces conventional SGs [42]. The inertia of a wind turbine based on the DFIG is decoupled from the system and the power electronic converters control the performance of the units and act as an interface between the generator and the grid. The DFIG is traditionally controlled to capture maximum available power from the wind. Hence, with an increase in the penetration level of wind generating units based on the DFIG, the effective inertia of the system will be decreased. Therefore, power system reliability can be affected when a system experiences large disturbances such as faults. The transient stability of a power system with a high penetration of wind based on the DFIG could not be affected if the power electronic converters of the DFIG are equipped with fault ride through capability [43]. Various researchers have studied system transient stability in transmission systems, such as [205]. However, in this chapter the transient stability of

different distribution networks is investigated when the system has a high penetration of wind based on the DFIG.

A wind power system based on a synchronous generator with fully rated converters (FRC) has been considered as the system with the most potential for the near future, as it can regulate reactive power to a certain degree with decoupled control of active and reactive powers. However, with the increase in the integration of wind energy sources into power systems, the stability of these systems is affected and depends on the dynamic characteristics of the wind energy unit [44]. The transient stability of wind turbines based on a synchronous machine with fully rated converters has been discussed somewhat in literature, such as in [45, 206]. The higher the penetration of wind based on a synchronous generator with FRC in the system, the lower the stability of the system is [46]. However, this chapter will also investigate the impact of high penetration of wind based on a synchronous generator with full scale converters on the transient stability of different systems at the distribution voltage level, where no reactive power supporters or FACTS devices are in the system.

5.5 Photovoltaic Generation Impact on Transient Stability

As shown earlier, transient stability is significant in large scale renewable energy grid connected systems. However, most research studies have investigated wind energy systems. On the other hand, due to the rapid growth in the penetration of photovoltaic systems connected to the grid, their transient stability should be studied. With the increase in the penetration of PV grid connected systems, the transient stability of systems may be influenced, as PV has different characteristics from conventional synchronous generators. In the future, a significant amount of conventional synchronous generators could be replaced by large scale PV grid connected systems and this could lead to a reduction in system inertia. The impact of small photovoltaic systems on the operation of distribution systems has been discussed in [47, 207]. Power system transient stability for systems with high photovoltaic penetration has been assessed in [48, 49, 208]. It has been shown in [50] that system transient stability in high PV grid connected systems can be affected by PV

topologies and fault locations. The appropriate levels of PV penetration in a power system and the presence of fault ride through (FRT) capability can improve transient stability [50, 209]. This chapter investigates the transient stability of different generic distribution systems with high penetration levels of PV grid connected systems.

5.6 Modelling and Control of Renewable Energy Systems

Due to the dramatic increase of renewable energy sources in power systems, large scale wind and PV grid connected systems have changed from being simple energy sources to having advanced control to meet new grid code requirements. This section discusses the modelling and control of distributed generation based on wind and solar energy, which will be used to examine the impact on system transient stability. Three different renewable technologies are used to observe the impact of them on transient stability. They are a wind turbine based on the DFIG, a wind turbine based on a synchronous generator with fully rated converters, and photovoltaic based solar energy. These renewable energy units have been modelled with two types of software, MATLAB/SIMULINK and the commercial package DIGSILENT POWERFACTORY.

5.6.1 DFIG Modelling and Control

In recent years, DFIG based wind energy has become the most widely installed due to its capability to provide reactive power, its relatively small rating of power electronic converters and its high efficiency [210]. With the continuous growth of the penetration of wind based on the DFIG, the impact of wind power on power systems needs to be studied in more depth [211]. As shown in Chapters 3 and 4, DFIG technology has two power converters called the rotor side converter (RSC) and the grid side converter (GSC). They are connected back to back through a DC link. The RSC is connected to the rotor windings while the GSC is linked to the ac grid. The RSC controls the rotor speed by changing its output frequency depending on the wind speed and it also controls the stator terminals power factor. On the other hand, DC link voltage is kept and controlled within limits by the GSC. The grid side converter can be controlled to provide or absorb reactive power. The vector control of the DFIG's power converters in a d-q synchronous frame was shown in Chapter 3.

5.6.2 Wind Turbine based on Synchronous Generator with Fully Rated Converters

A variable speed wind turbine based on a synchronous generator with fully rated converters is a popular option for modern wind turbines. It has two power converters, RSC and GSC, as discussed in Chapter 3. There are several topologies for this technology, such as two level back to back Pulse Width Modulated voltage source converters. However, this thesis uses one of the most popular topologies of wind based on an FRC synchronous generator which considers the RSC as a diode rectifier with a boost converter and the GSC as a voltage source inverter. A schematic diagram of this topology with the converter control in the d-q frame was given in Chapter 4.

5.6.3 Solar Energy based on Photovoltaic

There are different topologies for PV grid connected systems, as discussed in Chapter 2. The problem with PV systems is that there are so many topologies in the market and it is difficult to find standard modules for application, unlike with wind energy for example. In this chapter, the PV grid connected system is simplified to enhance the execution time of the simulations. It consists of a DC voltage source which represents the PV panel and the DC-DC converter, a voltage source inverter. The active and reactive powers of the PV system can be controlled by modifying the control of the PV inverter. The control of the PV inverter depends on the d-q synchronous reference frame like the control in wind power electronic converters as shown in Chapter 4.

5.7 Simulation Scenarios

In this chapter, different generic distribution networks with high renewable energy penetration subject to different fault conditions are investigated. The transient stability is discussed and analysed using the transient stability index method explained earlier to investigate different simulation scenarios. These scenarios are a distribution systems base case when there are no renewables, 35 % penetration of photovoltaic grid connected system, 35 % wind based on DFIG penetration, 35 % wind based on FRC synchronous generator, and 35 % mixed renewables penetration based on wind and solar energy. The transient stability is investigated when the distribution systems experience a three phase fault in different locations. The distribution networks which are considered in this chapter

are the modified IEEE 13 bus, IEEE 37 bus and IEEE 123 bus test systems. To perform the simulations, two types of software have been used to study the transient stability of the selected networks, namely MATLAB/SIMULINK and DIgSILENT POWERFACTORY.

5.7.1 IEEE 13 Bus Distribution System

The IEEE 13 Node Test Feeder is one of the test systems used for distribution system analysis, published by the IEEE Power Engineering Society [195]. A schematic diagram of this system has been shown in Figure 4.8 of Chapter 4. Summarised data regarding the IEEE 13 bus system have been illustrated in Table 4.1 and detailed data are shown in Appendix B.1. The same test procedure as in Chapter 4, section 4.5.1, is used in this chapter; the grid is an infinite bus and is connected to bus 650, and a CDG based on synchronous generator is assumed to be connected at bus 611 to examine the transient stability of the synchronous generator. Detailed data regarding this CDG are given in Appendix C and the power flow data of the IEEE 13 bus system are shown in Appendix B.1, where the grid has been assumed as the slack. Distributed generation based on renewable energy is connected to bus 680. Selection of the locations of the grid, the CDG and the renewable units has been discussed in section 4.7.1.

To investigate the transient stability of the selected distribution systems with high renewable energy penetration is the main objective of this chapter. A large disturbance should be applied to test the systems for study of the transient stability. Therefore, for each simulation scenario a three phase fault is applied on one of the system buses. There are two buses in the IEEE 13 bus system that have been selected as fault locations, bus 650, which is the grid bus, and the renewable sources bus, which is bus number 680. The applied fault starts at 3 seconds in the simulations and it is cleared at 3.2 seconds, which means the duration of the fault is 200 milliseconds. The fault impedance is assumed to be zero to observe the worst case scenario.

A- Base Case

A CDG is installed at bus 611 with 2 MW output power, while the grid generates 1.62 MW in the IEEE 13 bus system. When a three phase fault is applied to bus 650 for 200

milliseconds at 3 seconds, the rotor angle of the CDG will change during the fault duration. Figure 5.2 shows the load angle, the rotor speed, and the active and reactive powers of the CDG. The figure shows that the commercial package DIgSILENT POWERFACTORY gives a relatively close dynamic result compared to MATLAB/SIMULINK. However, there is a slight difference after the fault is cleared between the two software and a considerable difference in the overshoot at 3.2 seconds when the fault is cleared. It also shows that the system remains stable after the system is subjected to the large disturbance. The second fault location is on bus 680 and the response of the CDG to this fault is illustrated in Figure 5.3. The figure shows that the system maintains stability after the fault clears at 3.2 seconds.

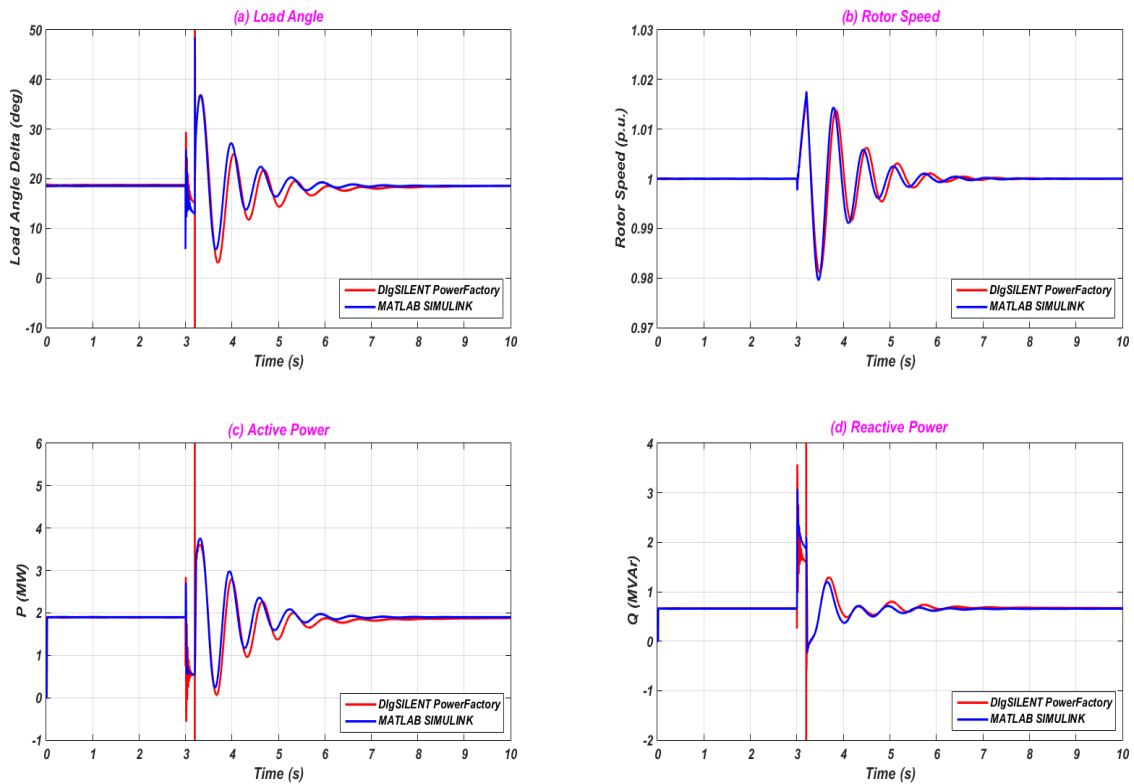


Figure 5.2: CDG responses in 13 bus system to a fault on bus 650 (base case) - (a) load angle, (b) rotor speed, (c) active power, (d) reactive power.

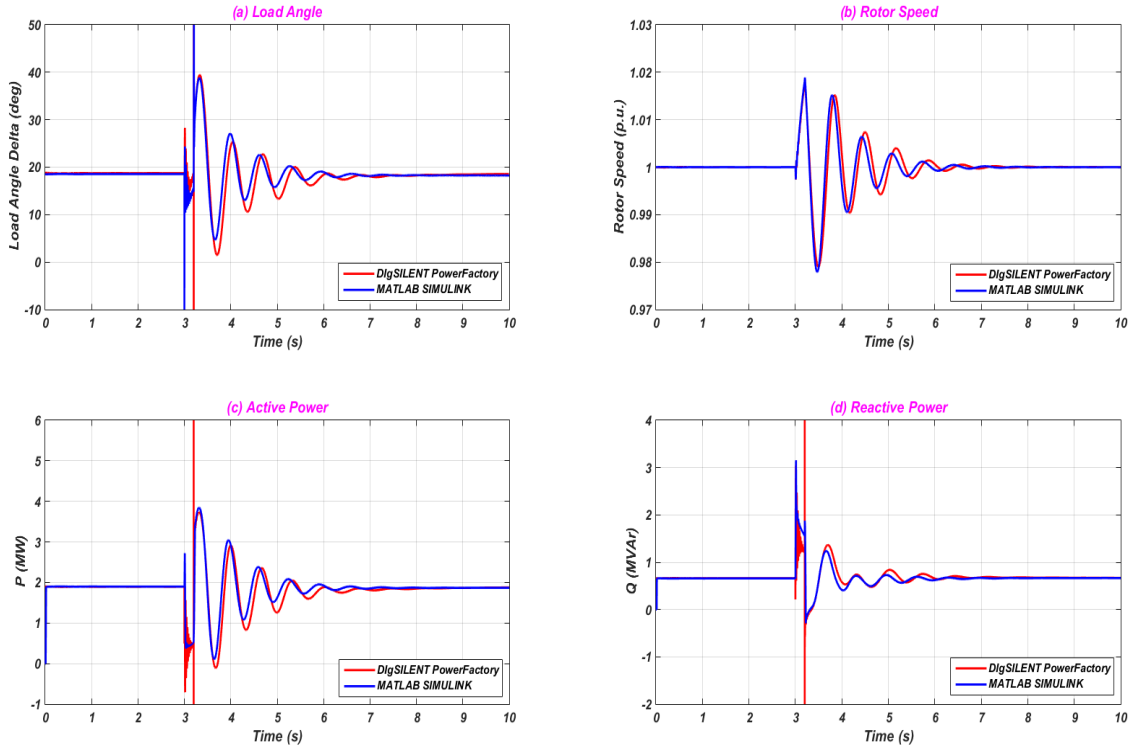


Figure 5.3: CDG responses in 13 bus system to a fault on bus 680 (base case) - (a) load angle (b) rotor speed (c) active power (d) reactive power.

B- 35 % PV Penetration

A photovoltaic grid connected system is installed at bus 680 with 2 MW output power, which represents 35 % of the total generation in the system. Detailed data regarding the PV systems are shown in Appendix D. When the renewable sources are injected into the distribution system, an additional load is added to the system at the same bus (bus 680) which equals the same additional generation 2 MW. The additional load is added to the distribution network to ensure accuracy in the results and the effect of the renewable units on the system. This step ensures that the total loading of the grid and the CDG will be the same in the base case and after adding the renewables to the system. The location and capacity of each generation source in the system are illustrated in Table 5.1.

Table 5.1: Power generation source outputs and their locations (PV case) in the IEEE 13 bus system.

	<i>Grid</i>	<i>CDG</i>	<i>PV</i>
<i>Total Generation</i>	1.62 MW	2 MW	2 MW
<i>Location</i>	Bus 650	Bus 611	Bus 680

The same procedure as in the base case is used here to observe the response of the synchronous generator (CDG) in the system to a transient fault which is applied to the grid bus and the PV bus respectively. Figures 5.4 and 5.5 show the impact of the added PV systems on the transient stability of the synchronous machine. The figures show that the system will remain stable after the fault is cleared. Active and reactive powers of the CDG and PV system are also illustrated. These results are with no fault ride through capability for the PV system. However, some grid codes require renewable units to provide reactive power during system disturbances. It is not the purpose of this chapter to investigate reactive power, rather it considers only the response of the synchronous machine to system disturbances and whether the system remains stable or not. Therefore, the worst case scenario when the DG based renewable without reactive power dynamic support to the grid is used in this chapter. However, the PV converters should be protected from the overvoltages and overcurrents that caused during the fault duration. The protection of the PV converters and FRT have been discussed in Chapter 4. Figure 5.4 shows that when the fault is applied on bus 650 (far away from the CDG), there is a slight difference in the response of the CDG during the fault between the Simulink and the PowerFactory, as the PV model in the PowerFactory detects the fault and the active power of the PV drops to zero, while in the Simulink the power falls to 0.5 MW. However, they have the same performance when the fault is applied on the PV bus at bus 680 (close to the CDG), as shown in Figure 5.5.

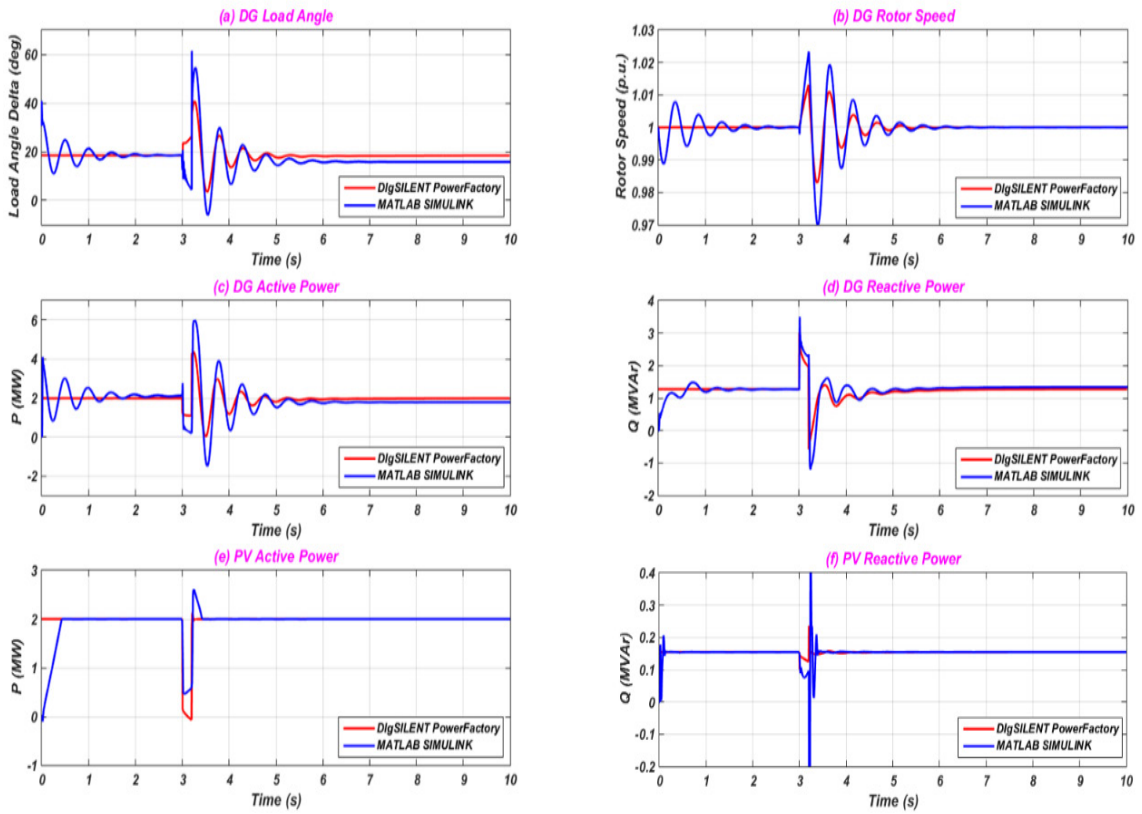


Figure 5.4: Conventional DG and PV responses in 13 bus system to a fault on bus 650 (PV case) - (a) CDG load angle, (b) CDG rotor speed, (c) CDG active power, (d) CDG reactive power, (e) PV active power, (f) PV reactive power.

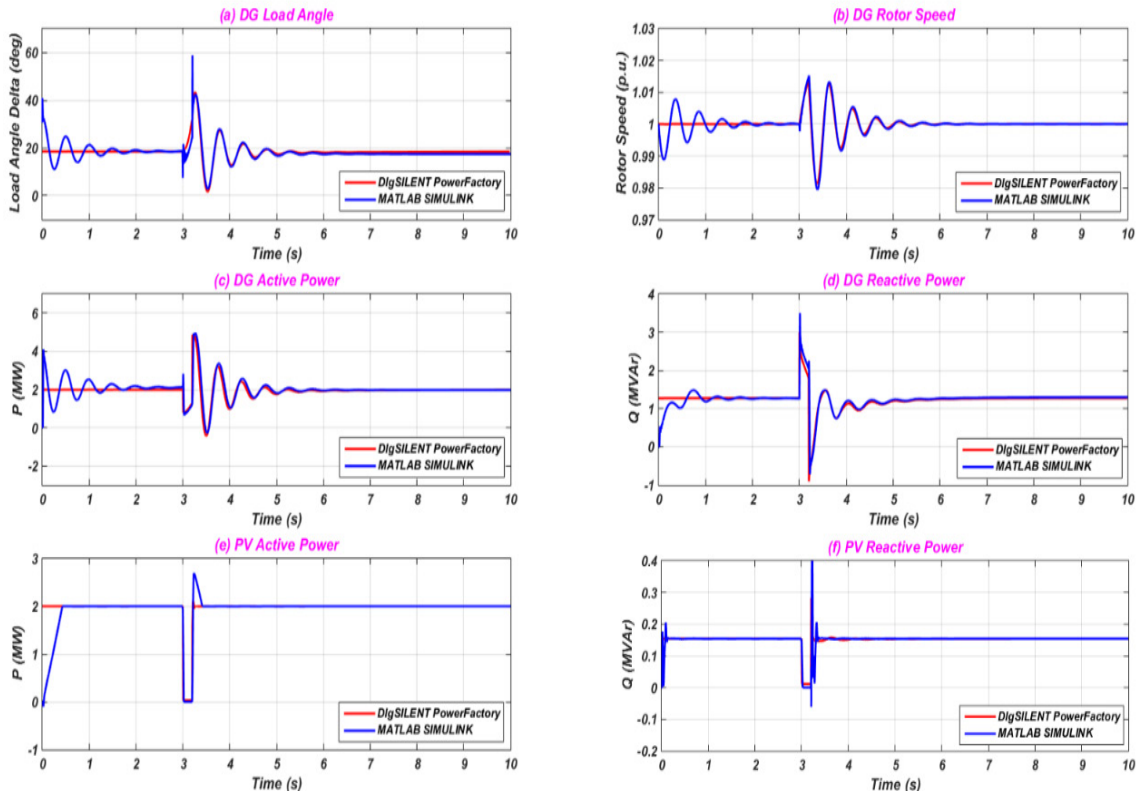


Figure 5.5: Conventional DG and PV responses in 13 bus system to a fault on bus 680 (PV case) - (a) CDG load angle, (b) CDG rotor speed, (c) CDG active power, (d) CDG reactive power, (e) PV active power, (f) PV reactive power.

C- 35 % Wind based on DFIG Penetration

DFIG based wind energy is installed at bus 680 with 2 MW output power, which is 35 % of the total power generation in the test system. The DFIG parameters and detailed data are given in Appendix D. In the same manner as the PV case, a 2 MW load is added at bus 680 for the same reason. Table 5.2 shows the location and capacity of each source of power in the system.

Table 5.2: The capacity of energy sources and their locations (DFIG case).

	Grid	CDG	Wind DFIG
Total Generation	1.62 MW	2 MW	2 MW
Location	Bus 650	Bus 611	Bus 680

For a three phase fault applied on bus 650, the DG based on a conventional synchronous generator and the DFIG based wind energy responses are illustrated in Figures 5.6 and 5.7 respectively. These responses of the CDG and the DFIG are different when the fault location is on bus 680, which is close to the CDG, as shown in Figures 5.8 and 5.9 respectively. The DFIG is modelled without protection in Simulink, as illustrated in Chapter 4, with no FRT capability. However, the DFIG in the PowerFactory has crowbar protection to protect the converters. The simulation results illustrated in these figures show that the system is stable when a large disturbance is applied far away from the CDG at bus 650 and when the fault is applied close to the CDG unit. It has also been shown that the DC link is kept within limits when the fault is far away from the DFIG. However, it will be affected when the fault is on the same bus of the DFIG and it needs protection, which is discussed in detail in Chapter 4.

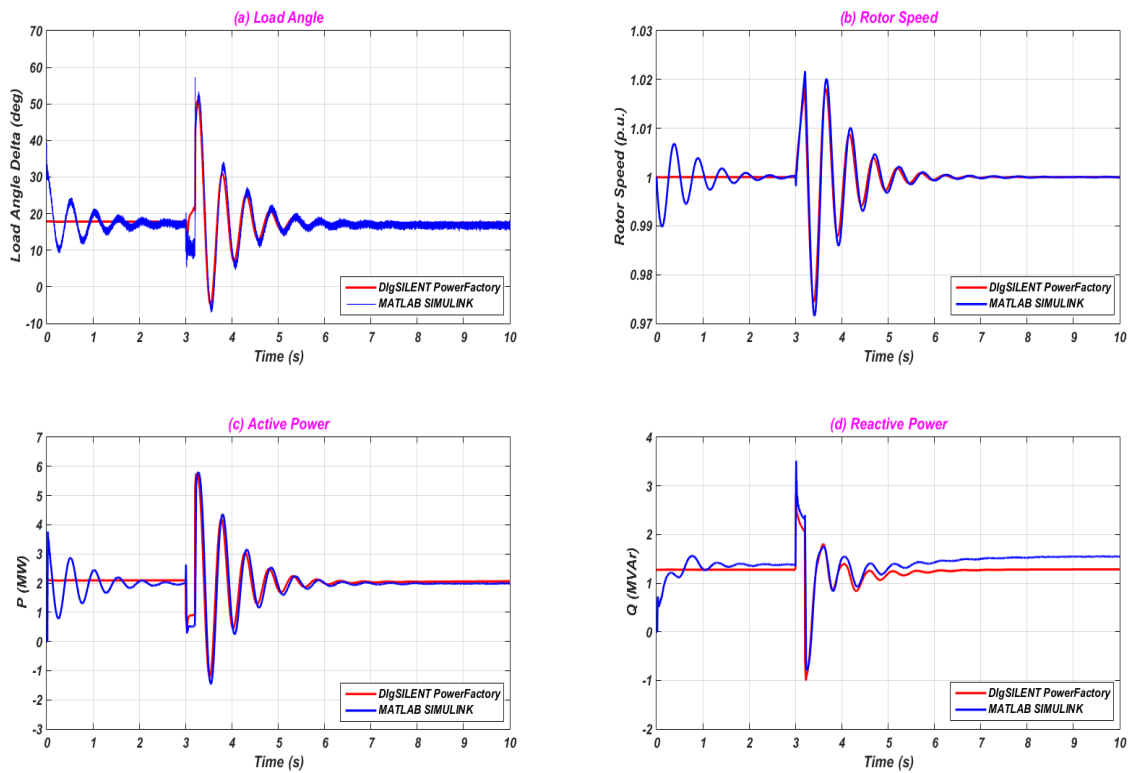


Figure 5.6: CDG responses in the 13 bus system to a fault on bus 650 (DFIG case) - (a) load angle (b) rotor speed (c) active power (d) reactive power.

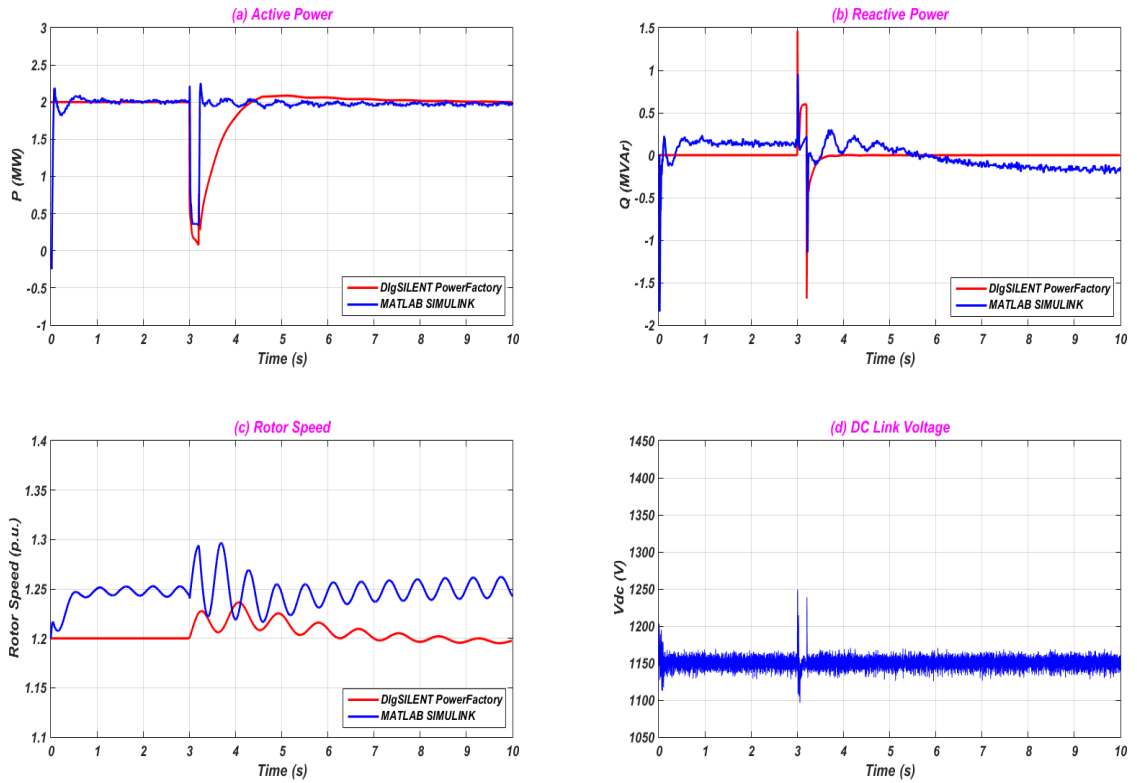


Figure 5.7: DFIG responses in the 13 bus system to a fault on bus 650 (DFIG case) - (a) active power, (b) reactive power, (c) rotor speed, (d) DC link voltage.

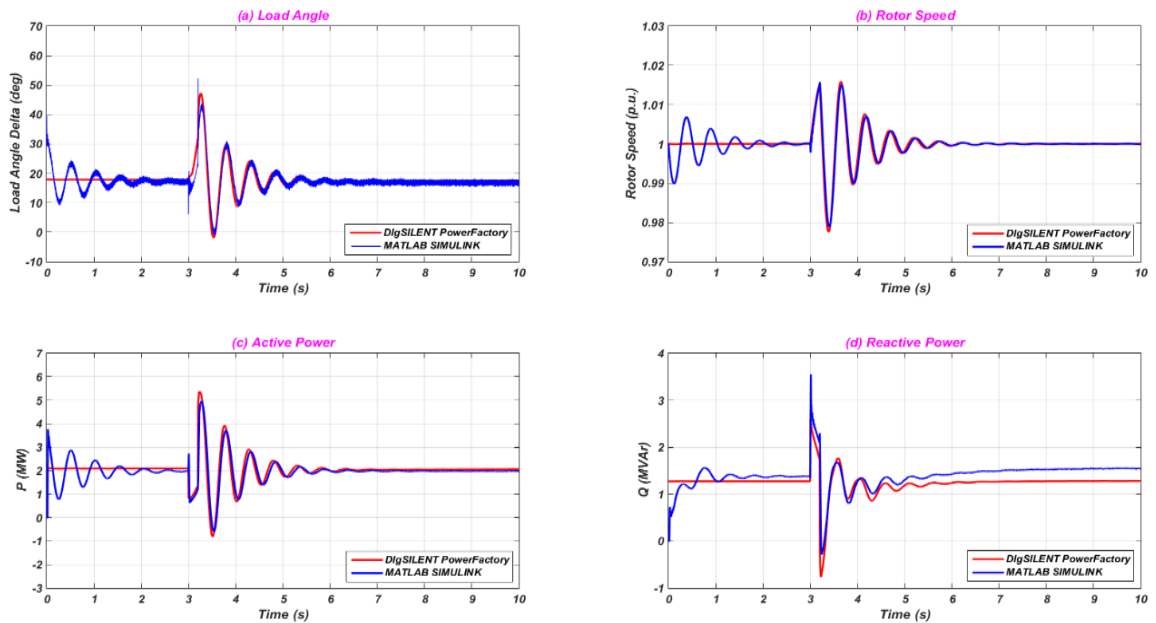


Figure 5.8: CDG responses in the 13 bus system to a fault on bus 680 (DFIG case) - (a) load angle, (b) rotor speed, (c) active power, (d) reactive power.

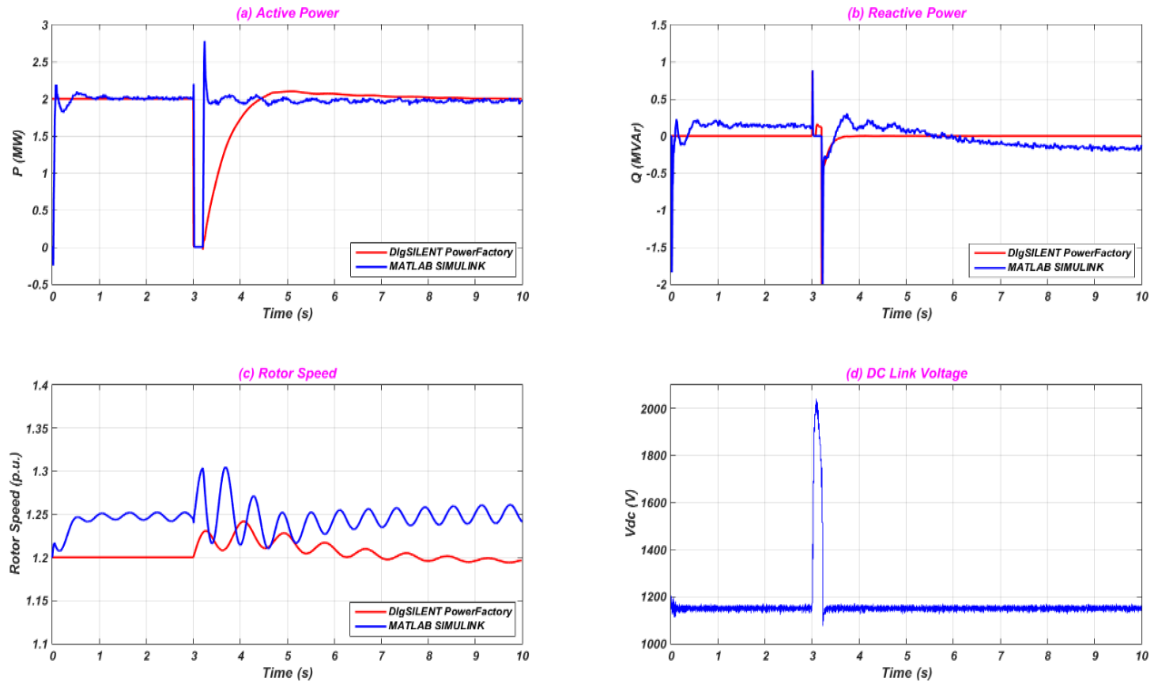


Figure 5.9: DFIG responses in the 13 bus system to a fault on bus 680 (DFIG case) - (a) active power, (b) reactive power, (c) rotor speed, (d) DC link voltage.

D- 35 % Wind based on Synchronous Generator with Fully Rated Converters

The same test procedure as in case B and C will be used to test the wind unit based on a synchronous generator with fully rated converters (FRC) for the transient stability. A 2 MW synchronous generator with FRC is installed at bus 680 with 2 MW added. The wind (FRC) parameters and detailed data are given in Appendix D. The total power generation in the system, which is contributed towards by different sources, is illustrated in Table 5.3.

Table 5.3: The capacity and location of each generation source in the system (wind FRC case).

	Grid	CDG	Wind FRC
Total Generation	1.62 MW	2 MW	2 MW
Location	Bus 650	Bus 611	Bus 680

When a three phase fault is applied on bus 650 (the grid bus) and the renewable bus, which is bus 680, the CDG has different responses to the disturbance, as shown in Figures 5.10 and 5.11 respectively. As shown, the transient stability can be influenced by the location of the disturbance. The responses of the wind generator based on FRC to the applied faults

are illustrated in Figures 5.10 and 5.11 respectively. It is shown in Figure 5.10 that the transient stability can be improved if the wind unit provides dynamic reactive power support during the fault, as the PowerFactory model shows. From these figures it is clear that the system with high wind based FRC penetration remains stable when the system experiences a large disturbance such as faults at different locations.

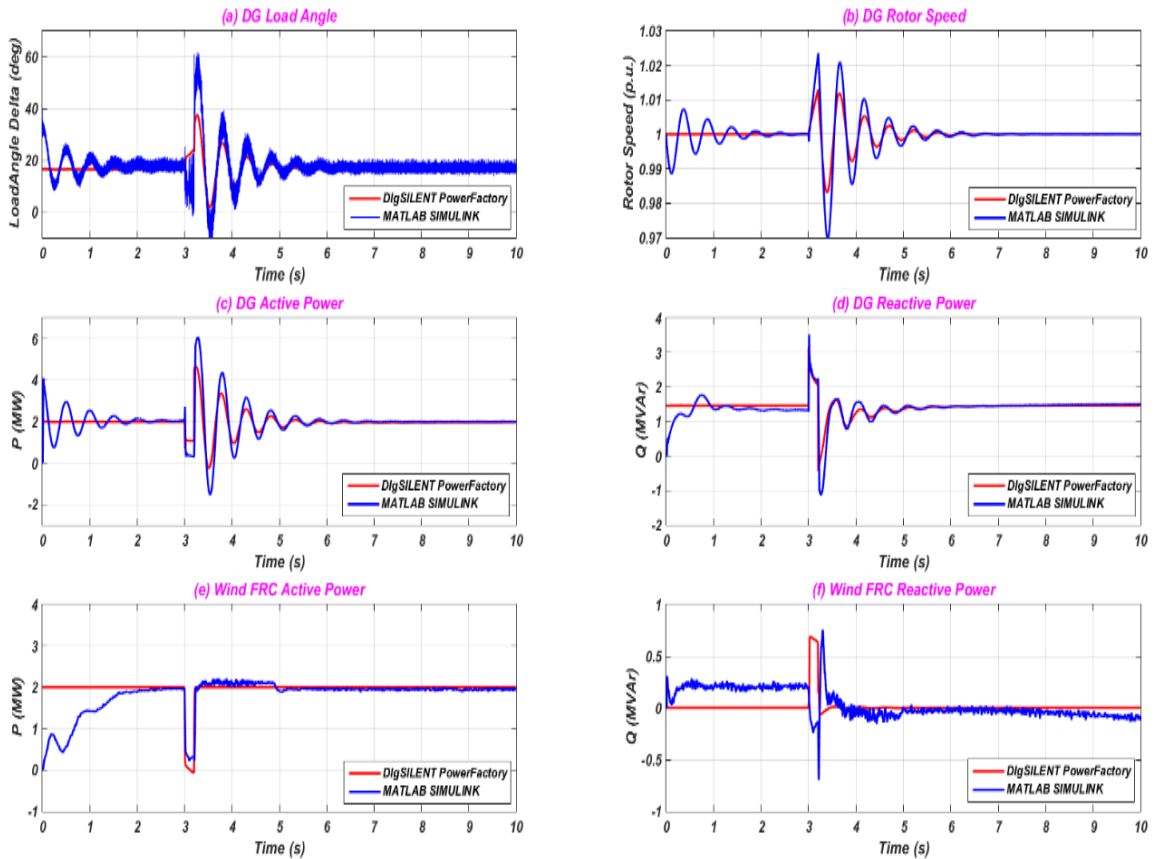


Figure 5.10: CDG and wind based on FRC responses in the 13 bus system to a fault on bus 650 (FRC wind case) - (a) CDG load angle, (b) CDG rotor speed, (c) CDG active power, (d) CDG reactive power, (e) wind FRC active power, (f) wind FRC reactive power.

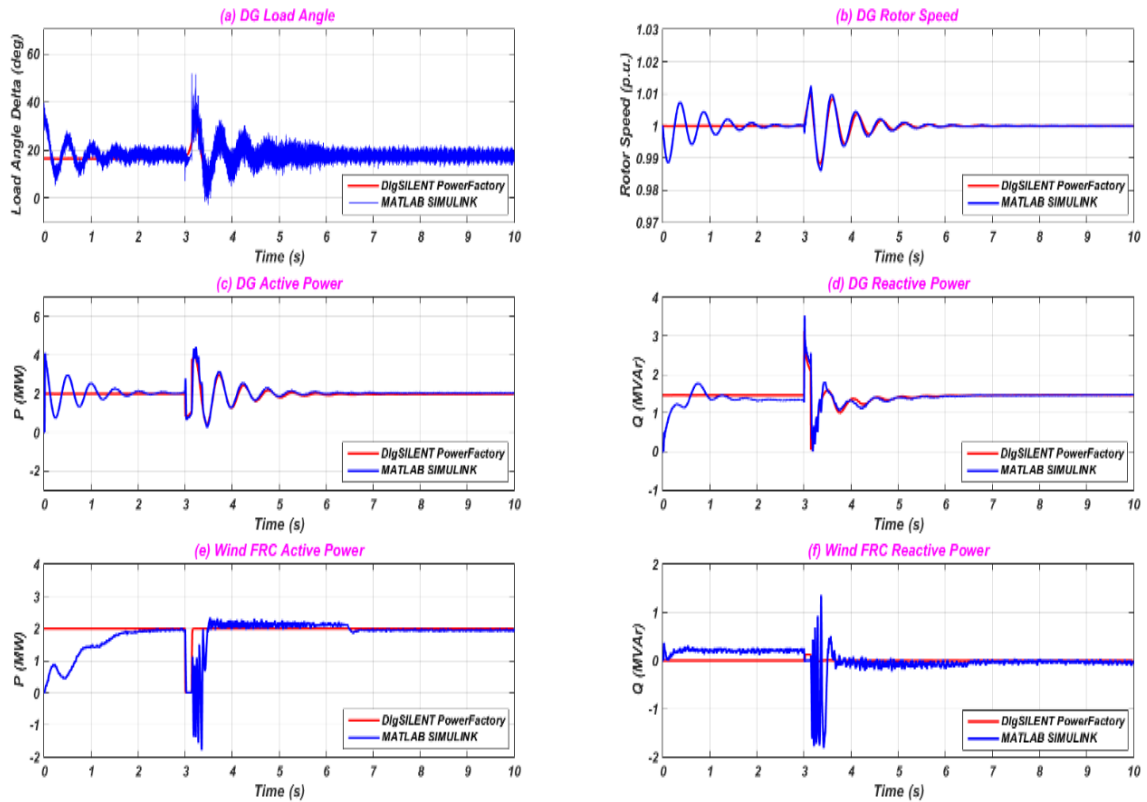


Figure 5.11: CDG and wind based on FRC responses in the 13 bus system to a fault on bus 680 (FRC wind case) - (a) CDG load angle, (b) CDG rotor speed, (c) CDG active power, (d) CDG reactive power, (e) wind FRC active power, (f) wind FRC reactive power.

E- 35 % Mixed Renewables Penetration

This case examines the CDG transient stability when there is high penetration of mixed renewables energy based on solar and wind energy. Mixed renewables based on the DFIG and photovoltaic system are installed in this case; 1.5 MW wind based on the DFIG is installed at bus 680 with a 1.5 MW load and 0.5 MW solar based on photovoltaic is installed at bus 652 with 0.5 MW load. The reason for adding the new loads has been explained in case A. Table 5.4 shows the contribution of each source of energy in the test system to the total power generation.

Table 5.4: Output power of each energy source and locations (mixed renewables case).

	Grid	CDG	Wind DFIG	PV
Total Generation	1.62 MW	2 MW	1.5 MW	0.5 MW
Location	Bus 650	Bus 611	Bus 680	Bus 652

The responses of the CDG based synchronous generator to a three phase fault applied on the grid bus and on the renewable bus are illustrated in Figures 5.12 and 5.14 respectively. Figures 5.13 and 5.15 show the behaviour of the renewable units when the system experiences a large disturbance on bus 650 and bus 680 respectively. From these figures it is clear that the system remains stable. However, the renewable units need to be protected during faults from overvoltages, as discussed in Chapter 4.

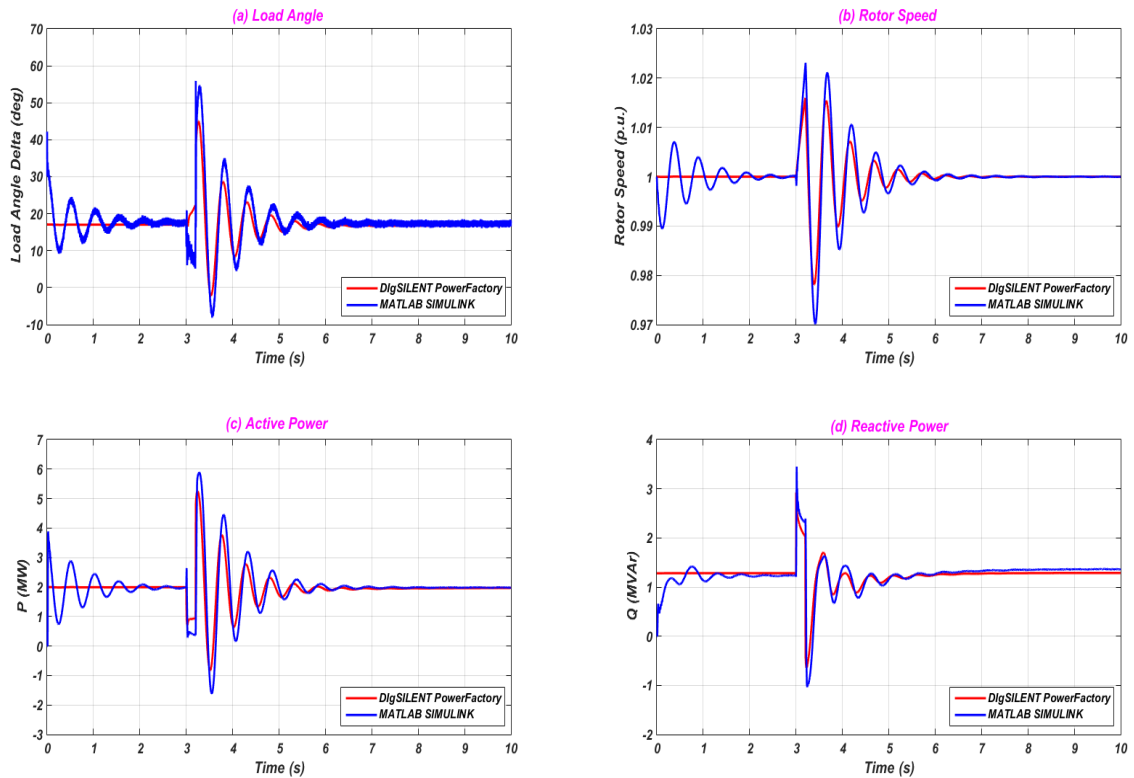


Figure 5.12: CDG responses in 13 bus system to a fault on bus 650 (mixed renewables case) - (a) load angle, (b) rotor speed, (c) active power, (d) reactive power.

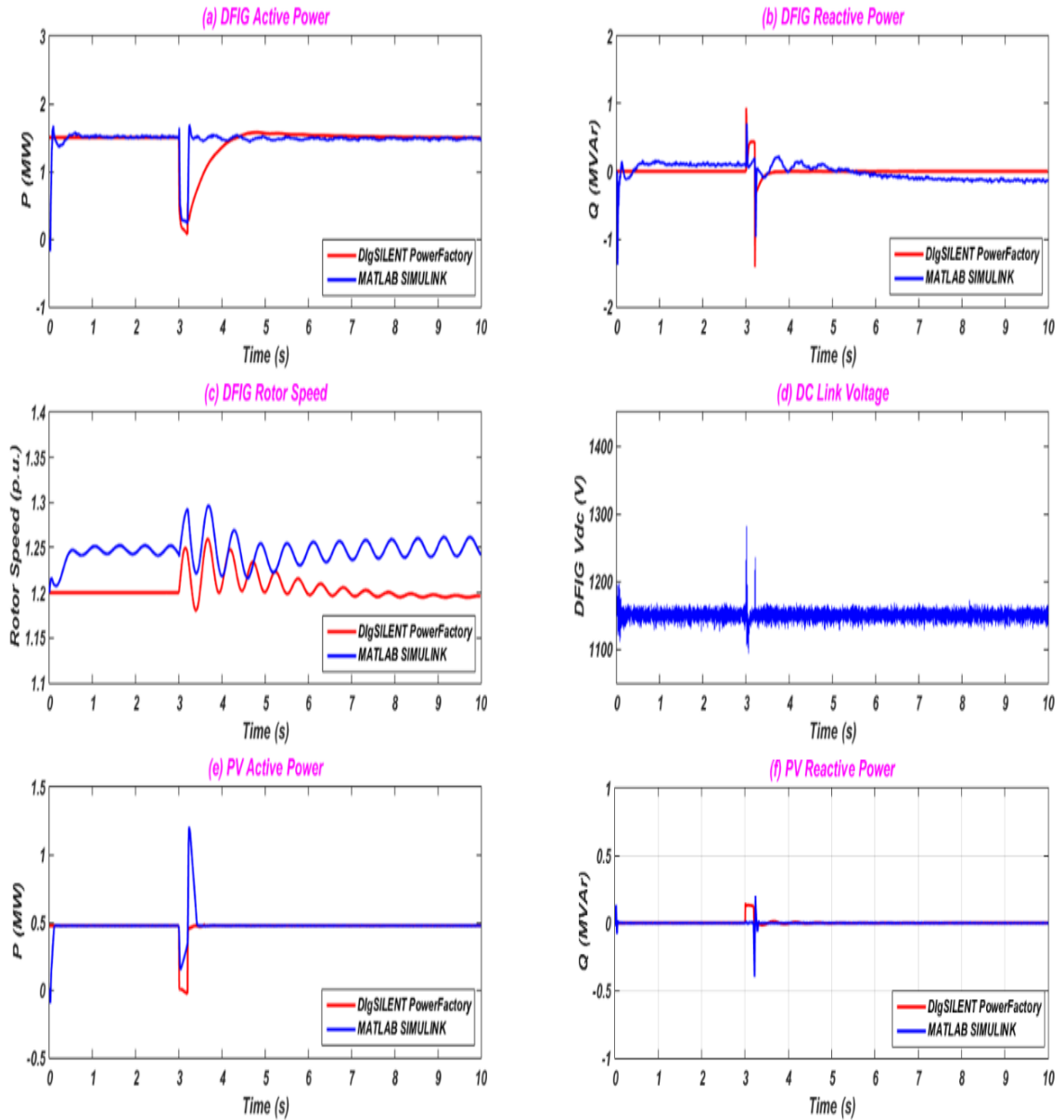


Figure 5.13: Renewable units' responses in 13 bus system to a fault on bus 650 (mixed renewables case) - (a) DFIG active power, (b) DFIG reactive power, (c) DFIG rotor speed, (d) DFIG DC link voltage, (e) PV active power, (f) PV reactive power.

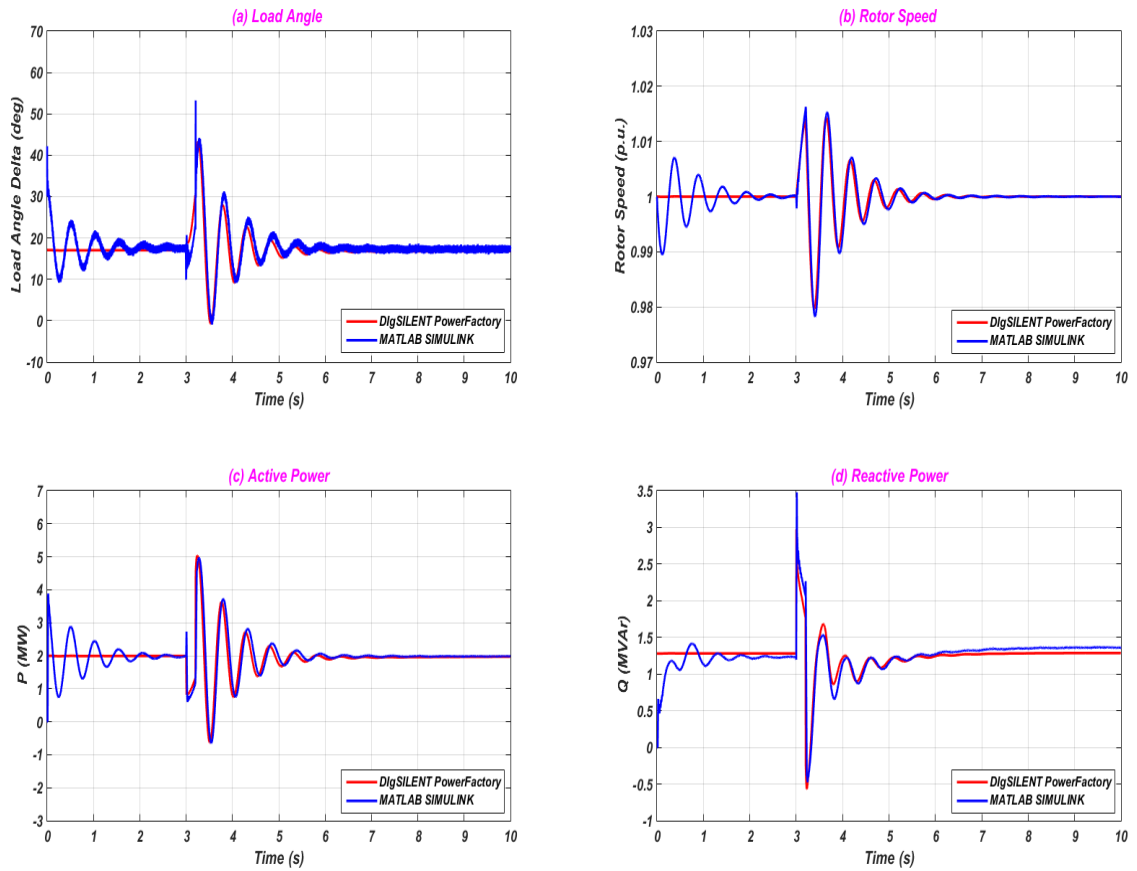


Figure 5.14: CDG responses in 13 bus system to a fault on bus 680 (mixed renewables case) - (a) load angle, (b) rotor speed, (c) active power, (d) reactive power.

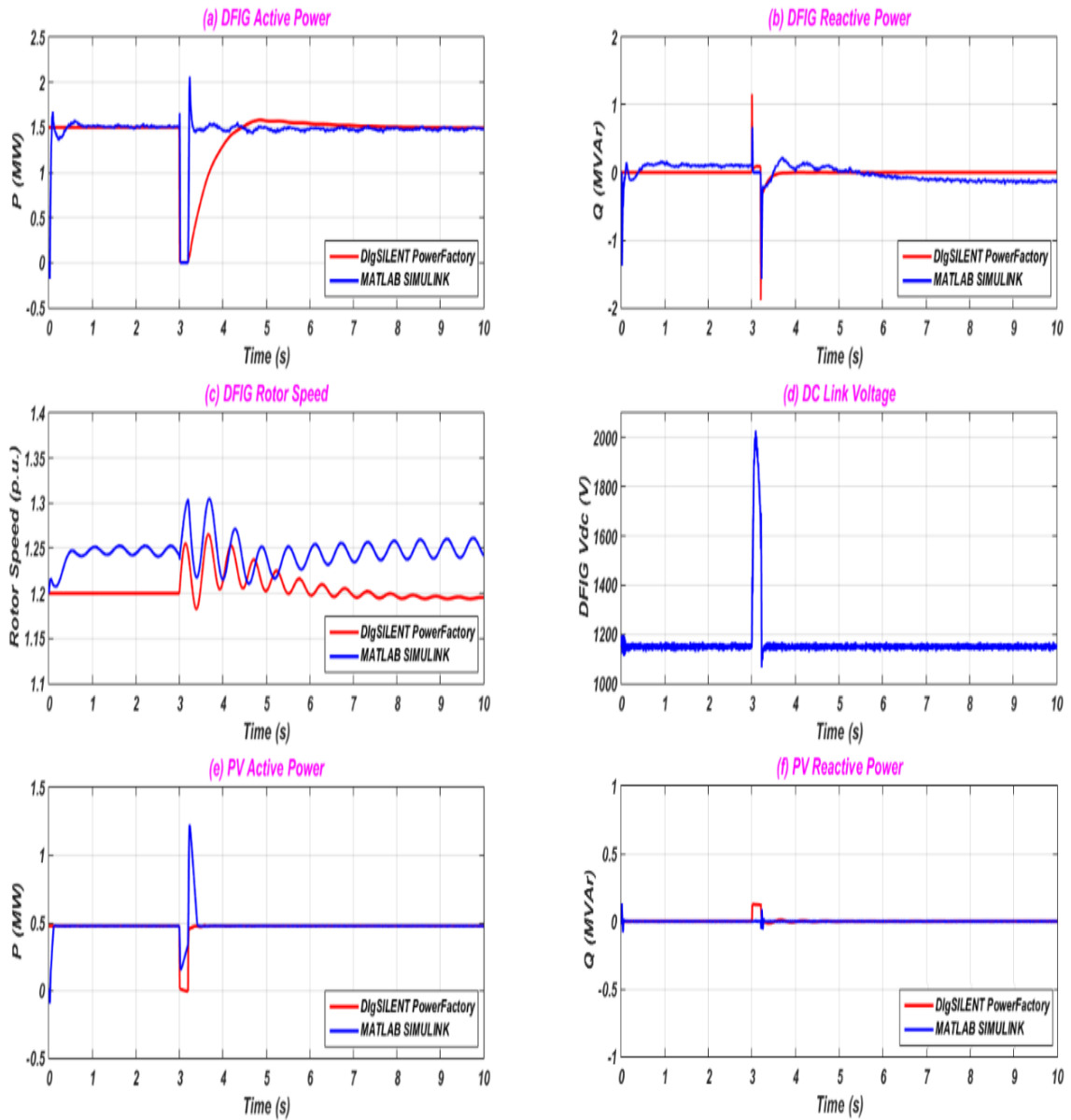


Figure 5.15: Renewable units' responses in 13 bus system to a fault on bus 680 (mixed renewables case), (a) DFIG active power, (b) DFIG reactive power, (c) DFIG rotor speed, (d) DFIG DC link voltage, (e) PV active power, (f) PV reactive power.

Table 5.5 illustrates the transient stability analysis of the IEEE 13 bus system with different case scenarios using the Transient Stability Index (TSI) method, which has been discussed earlier. It shows that the DG units based on renewable energy reduce the transient stability of a system when the system experiences a three phase fault at different locations.

Table 5.5: Transient stability analysis of the IEEE 13 bus system using TSI in %, stable>0, unstable<0.

<i>TSI</i>	<i>Base case</i>	<i>PV case</i>	<i>Wind DFIG case</i>	<i>Wind FRC case</i>	<i>Mixed renewables case</i>
<i>Fault on bus 650</i>	81.36	80	76.47	81.8	78.22
<i>Fault on bus 680</i>	80.22	78.22	76.03	80.90	77.77

5.7.2 IEEE 37 Bus Distribution System

The IEEE 37 Node Test Feeder is another test system used for distribution system analysis, published by the IEEE Power Engineering Society [195]. A schematic diagram of this system is shown in Chapter 4, Figure 4.23. Detailed data regarding this system are given in Appendix B.2. The system is connected to the ac grid through a two winding ac transformer. Bus 799 is the bus which interconnects the grid with the test network. IEEE 37 bus distribution network data are summarised in Chapter 4, Table 4.6. A CDG is assumed to be connected at bus number 740. Detailed data regarding this CDG are given in Appendix C. The grid is assumed to be an infinite bus. Detailed data regarding the power flow of the 37 bus distribution system are given in Appendix B.2, where the grid bus is assumed to be the slack. The DG based on renewable energy is connected to bus 741 and the selection of the locations of each generating unit in the system has been discussed in Chapter 4. The same test procedure as for the IEEE 13 bus system discussed in section 5.7.1 is used here to investigate transient stability.

A- Base Case

The CDG responses to the applied fault on bus 799 and bus 741 are shown in Figures 5.16 and 5.17 respectively. They show that the system remains stable after the applied fault is cleared and returns to pre-fault conditions.

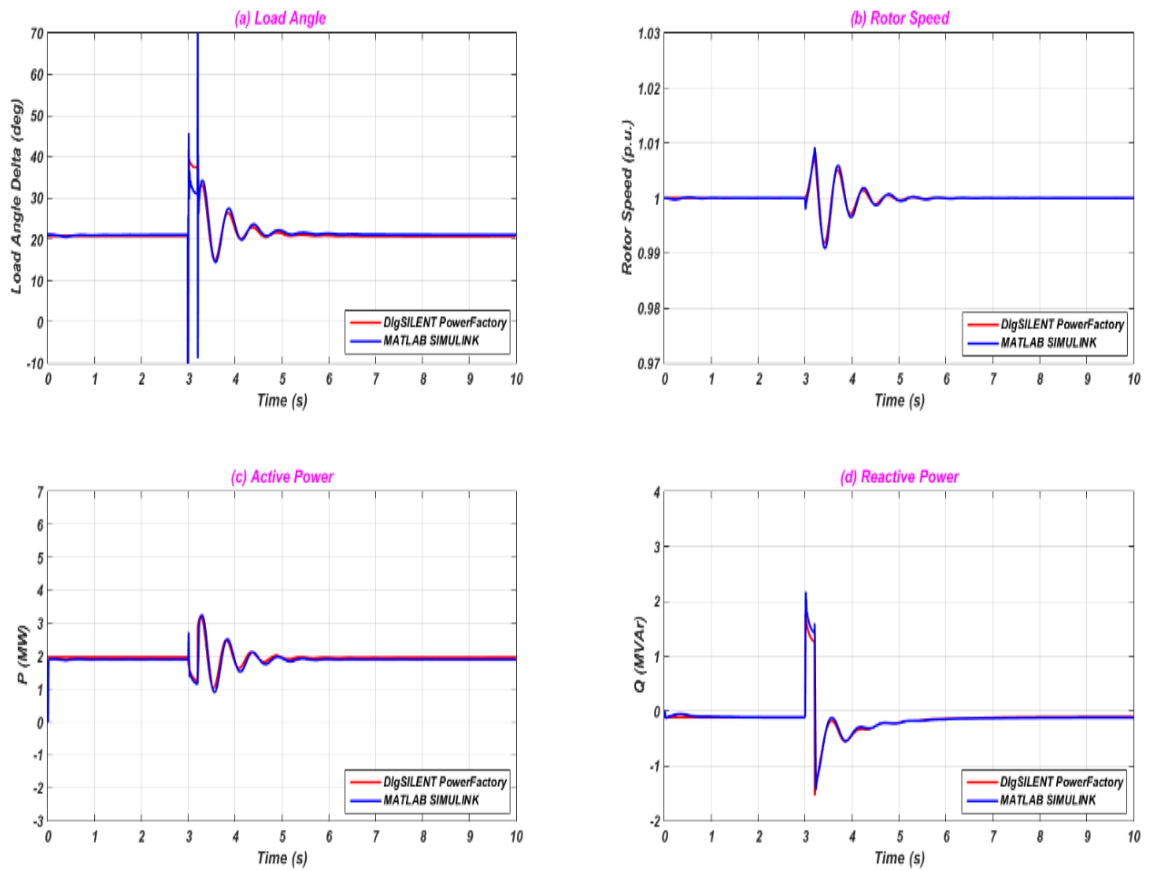


Figure 5.16: CDG responses in 37 bus system to a fault on bus 799 (base case) - (a) load angle, (b) rotor speed, (c) active power, (d) reactive power.

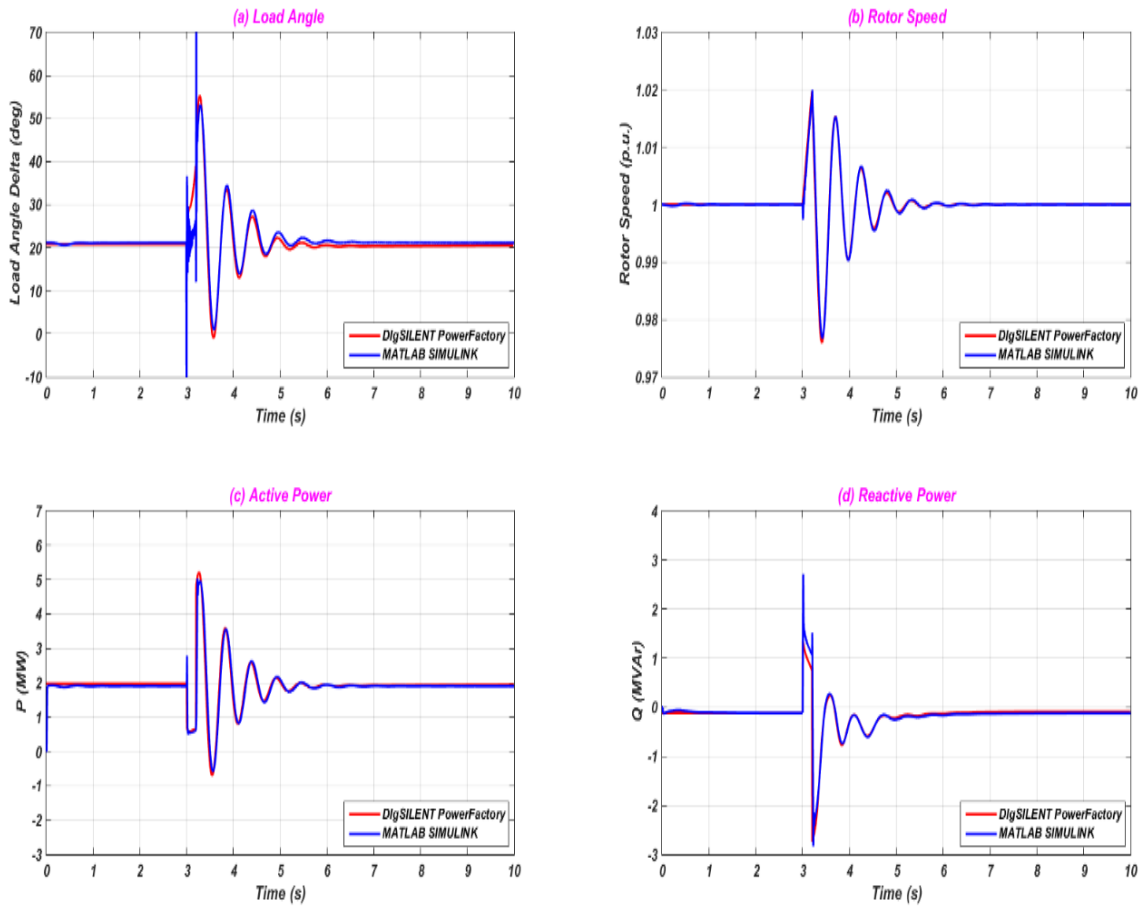


Figure 5.17: CDG responses in 37 bus system to a fault on bus 741 (base case) - (a) load angle, (b) rotor speed, (c) active power, (d) reactive power.

B- 35 % PV Penetration

A 1.5 MW PV system is installed on bus 741, which represents 35 % of the total generation, as illustrated in Table 4.7 in Chapter 4. A 1.5 MW load is installed at the same bus for the same reason as discussed earlier. Figures 5.18 and 5.19 show the generating units' responses to the transient fault applied on bus 799 and bus 741 respectively. As can be seen, the system remains stable after the fault is cleared and returns to pre-fault conditions.

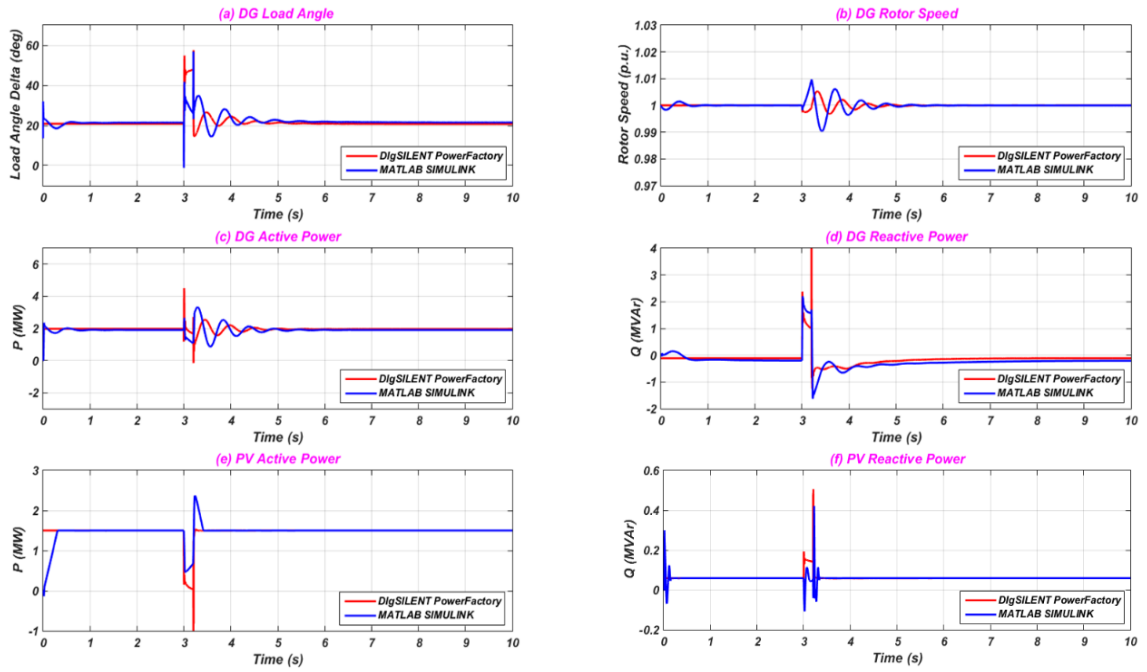


Figure 5.18: CDG and PV responses in 37 bus system to a fault on bus 799 (PV case) - (a) CDG load angle, (b) CDG rotor speed, (c) CDG active power, (d) CDG reactive power, (e) PV active power, (f) PV reactive power.

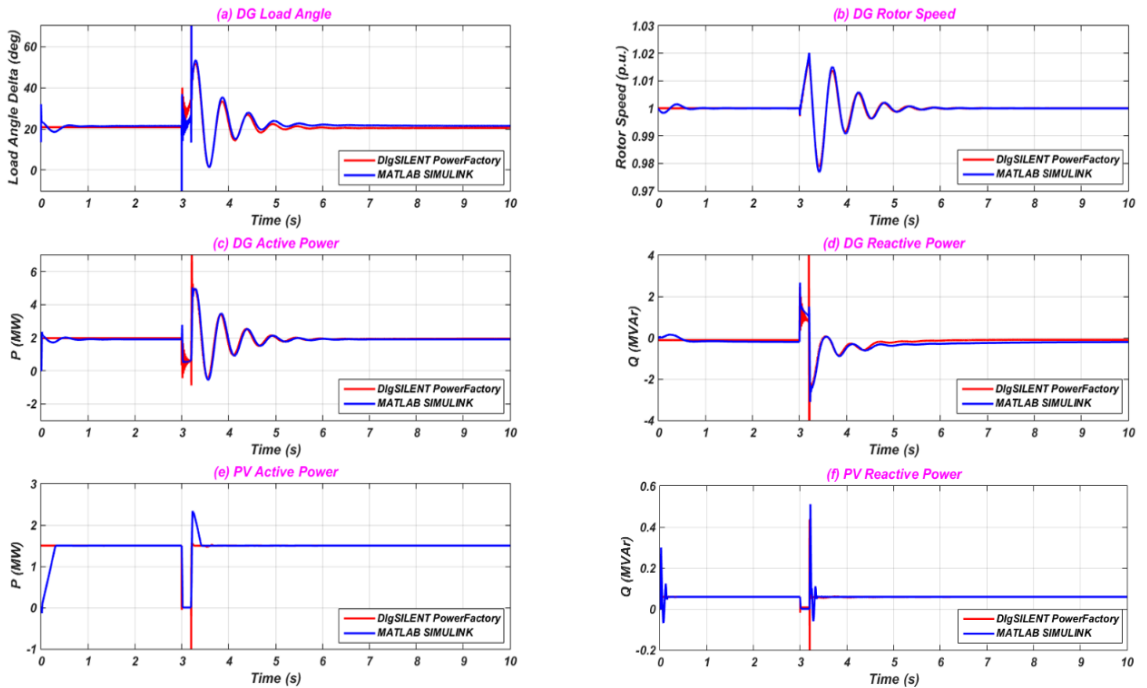


Figure 5.19: CDG and PV responses in 37 bus system to a fault on bus 741 (PV case) - (a) CDG load angle, (b) CDG rotor speed, (c) CDG active power, (d) CDG reactive power, (e) PV active power, (f) PV reactive power.

C- 35 % Wind based on DFIG Penetration

DFIG based wind is installed at bus 741 with 1.5 MW power output. A 1.5 MW load is also installed at the same bus. The CDG based synchronous generator's responses to the applied transient disturbance on bus 799 and 741 are illustrated in Figures 5.20 and 5.22 respectively. They show that the system remains stable and returns to pre-fault status. The DFIG responses are illustrated in Figures 5.21 and 5.23 respectively.

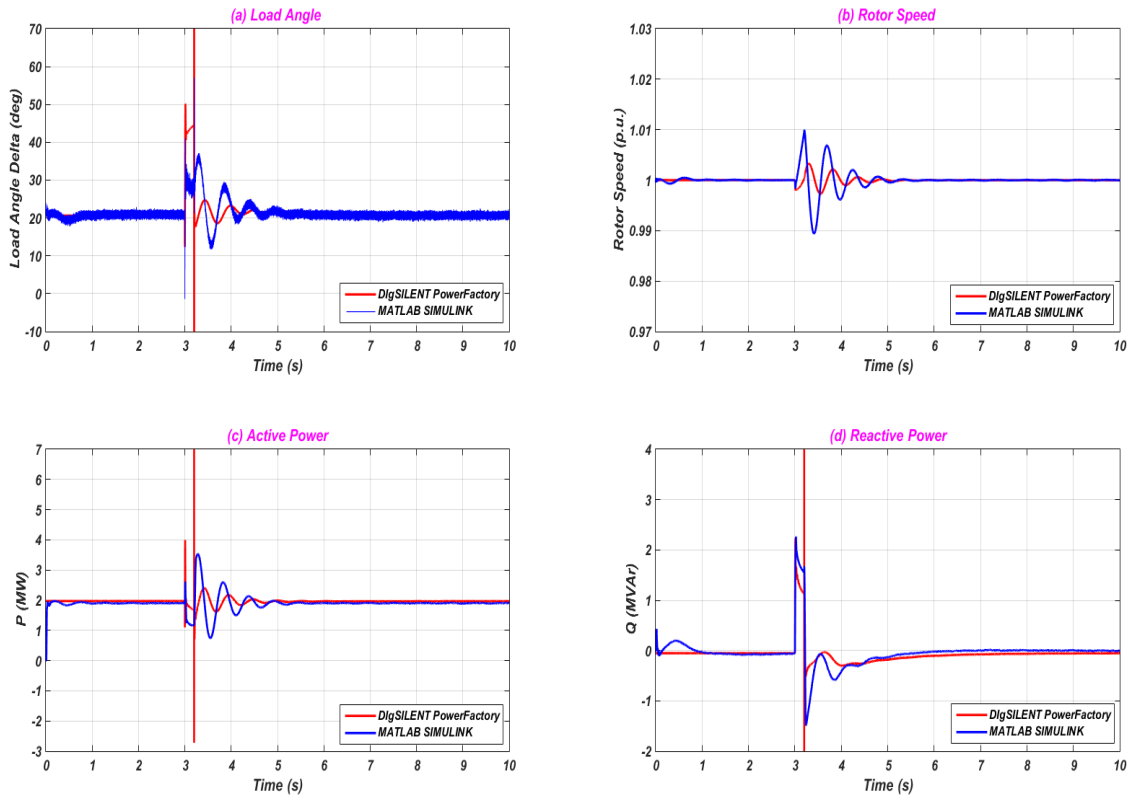


Figure 5.20: CDG responses in 37 bus system to a fault on bus 799 (DFIG case) - (a) load angle, (b) rotor speed, (c) active power, (d) reactive power.

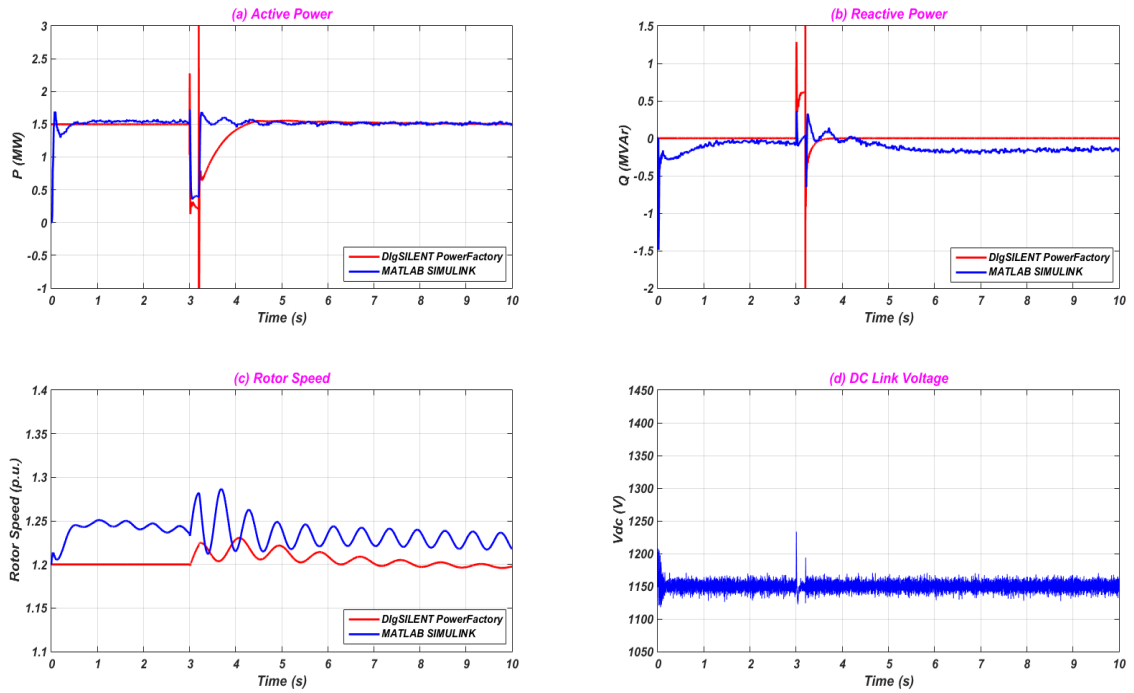


Figure 5.21: DFIG responses in 37 bus system to a fault on bus 799 (DFIG case) - (a) active power, (b) reactive power, (c) rotor speed, (d) DC link voltage.

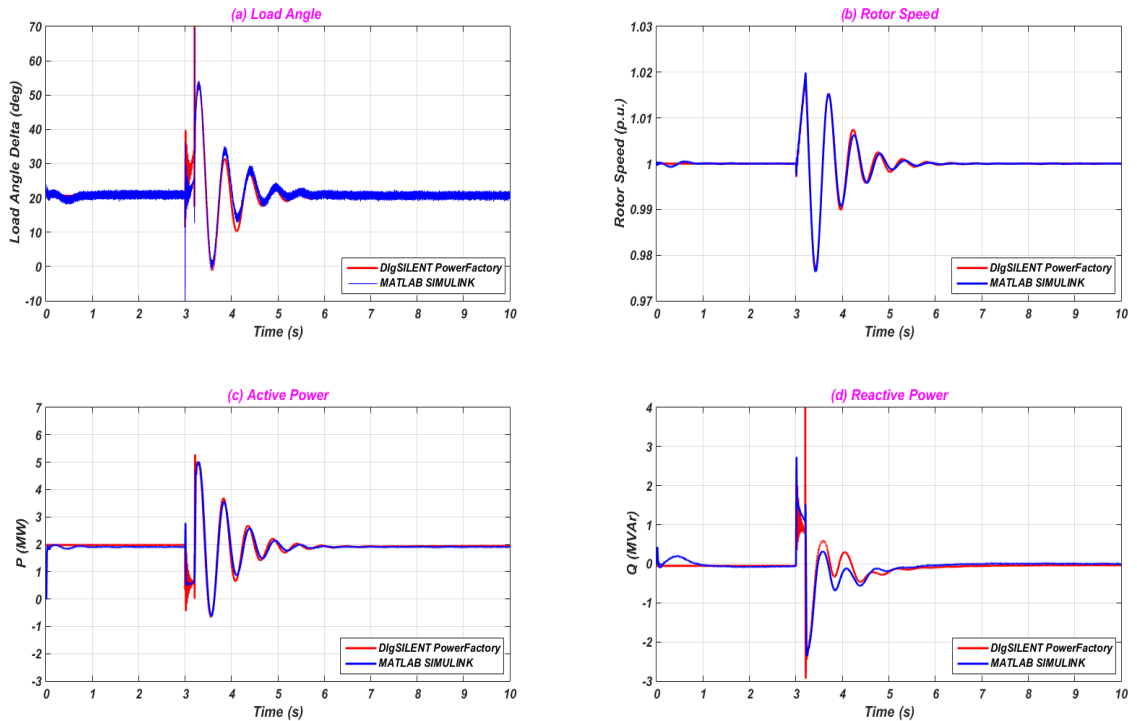


Figure 5.22: CDG responses in 37 bus system to a fault on bus 741 (DFIG case) - (a) load angle, (b) rotor speed, (c) active power, (d) reactive power.

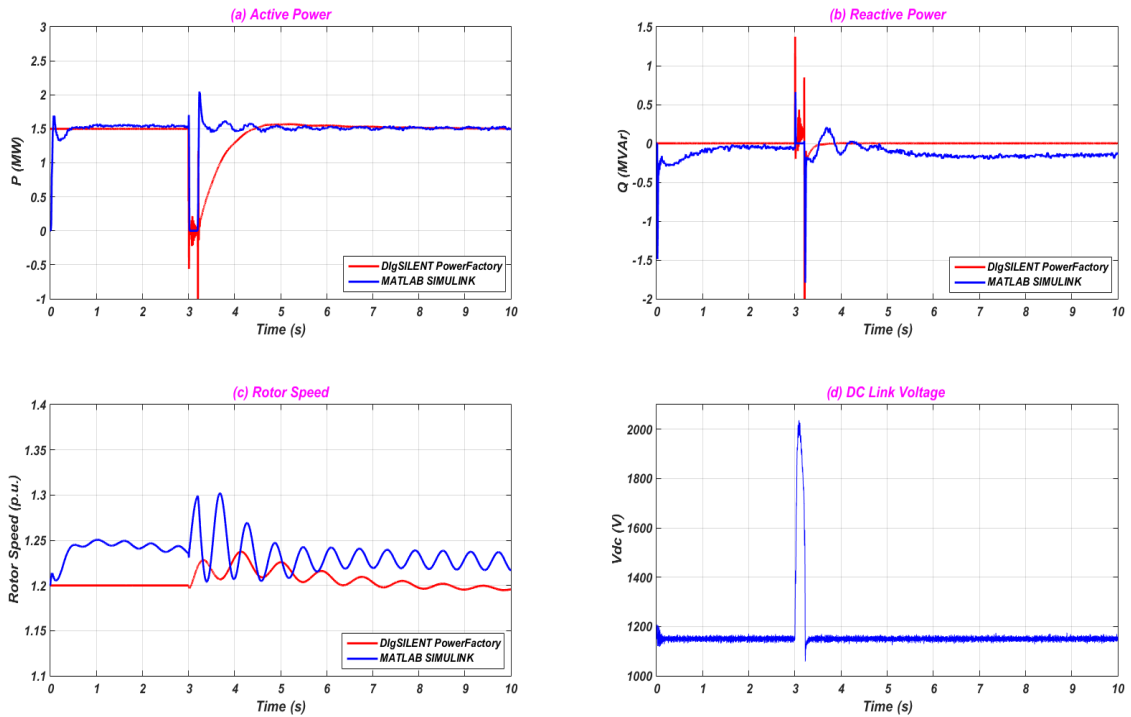


Figure 5.23: DFIG responses in 37 bus system to a fault on bus 741 (DFIG case) - (a) active power, (b) reactive power, (c) rotor speed, (d) DC link voltage.

D- 35 % Wind based on Synchronous Generator with Fully Rated Converters

A 1.5 MW wind synchronous generator with fully rated converters is installed on bus 741 with a 1.5 MW load. This system is also investigated when the system experiences faults and simulation results are illustrated in Figures 5.24 and 5.25 for when a three phase fault is applied on bus 799 and bus 741 respectively. The simulation results show that the system is transiently stable and returns to pre-fault conditions. As shown in Figure 5.24 (f), the POWERFACTORY simulation converges to a stable condition with regard to reactive power flows.

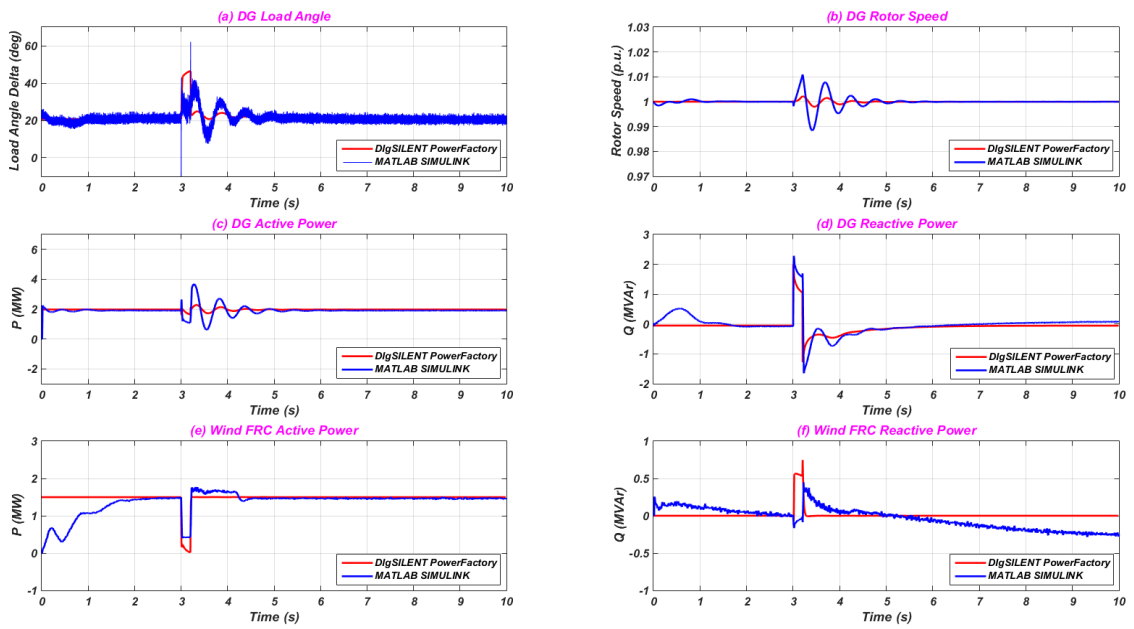


Figure 5.24: CDG and wind based on FRC responses in 37 bus system to a fault on bus 799 (FRC wind case) - (a) CDG load angle, (b) CDG rotor speed, (c) CDG active power, (d) CDG reactive power, (e) wind FRC active power, (f) wind FRC reactive power.

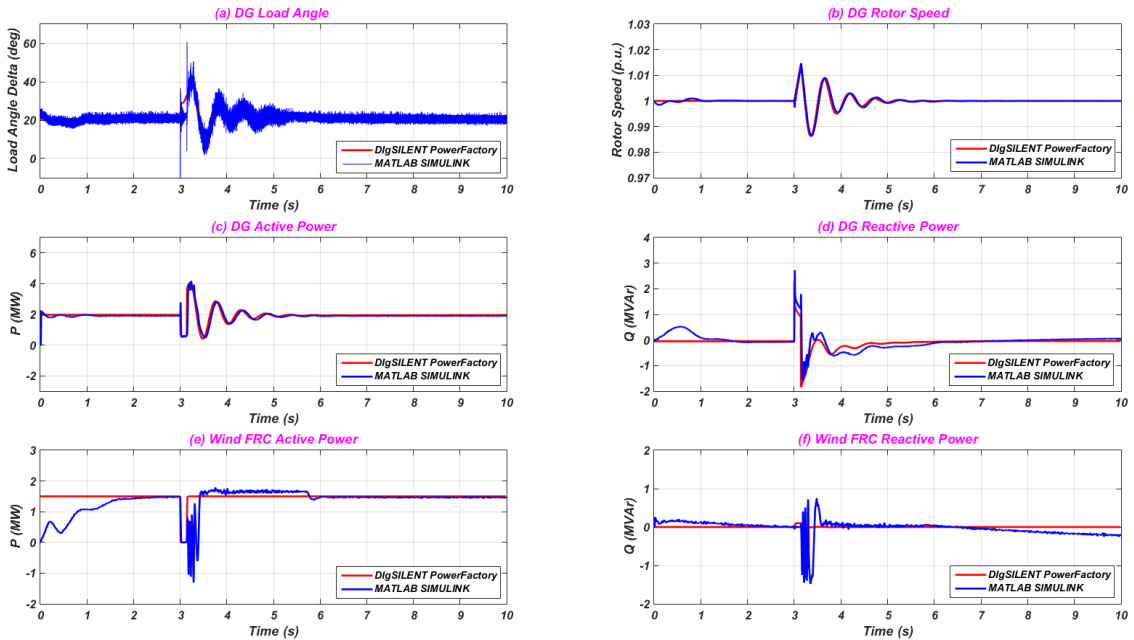


Figure 5.25: CDG and wind based on FRC responses in 37 bus system to a fault on bus 741 (FRC wind case) - (a) CDG load angle, (b) CDG rotor speed, (c) CDG active power, (d) CDG reactive power, (e) wind FRC active power, (f) wind FRC reactive power.

E- 35 % Mixed Renewables Penetration

In this case, 1 MW wind based on the DFIG is installed with a 1 MW load at bus 741, and 0.5 MW PV is also installed at bus 737 with a load 0.5 MW. Figures 5.26 and 5.28 show the CDG responses to the transient stability when a three phase fault is applied on bus 799 and bus 741 respectively. The renewables units' dynamic behaviours are also illustrated in Figures 5.27 and 5.29 respectively. These simulation results show that the system is transiently stable when the distribution system has high renewable energy penetration.

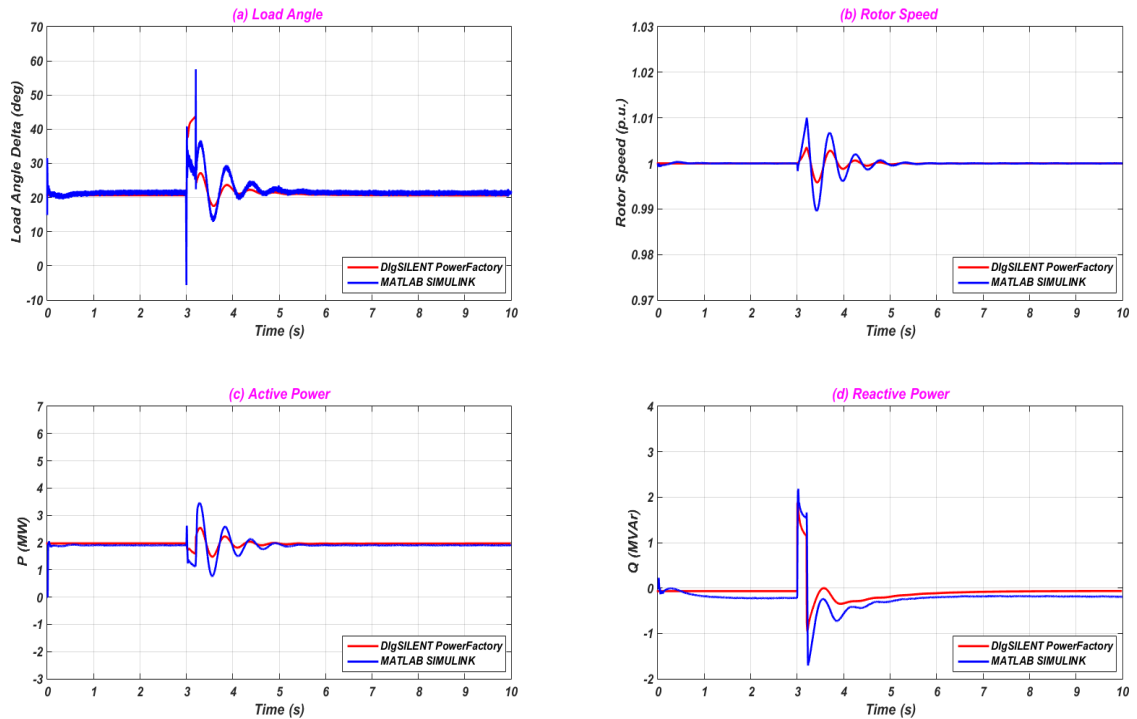


Figure 5.26: CDG responses in 37 bus system to a fault on bus 799 (mixed renewables case) - (a) load angle, (b) rotor speed, (c) active power, (d) reactive power.

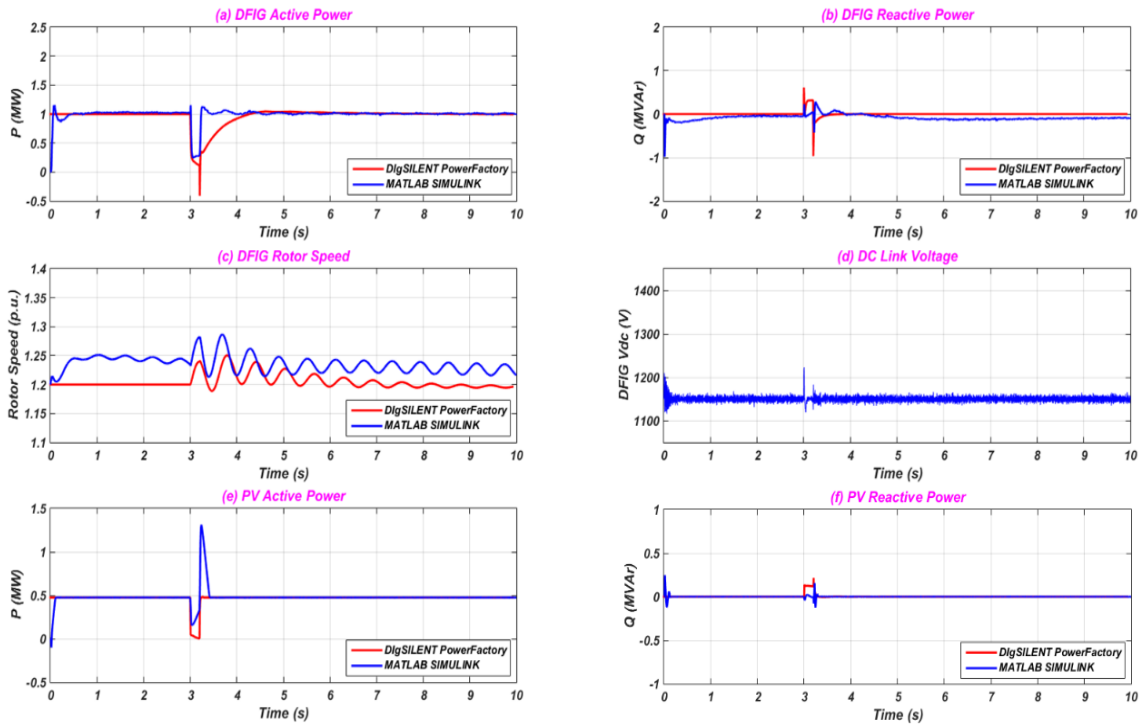


Figure 5.27: Renewable units' responses in 37 bus system to a fault on bus 799 (mixed renewables case) - (a) DFIG active power, (b) DFIG reactive power, (c) DFIG rotor speed, (d) DFIG DC link voltage, (e) PV active power, (f) PV reactive power.

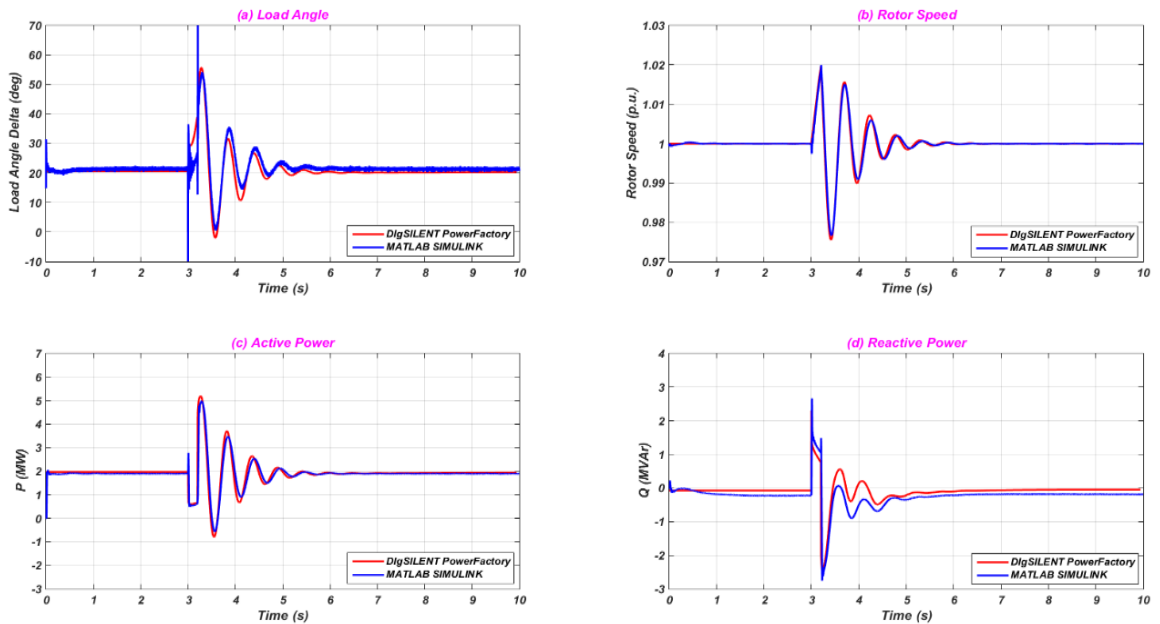


Figure 5.28: CDG responses in 37 bus system to a fault on bus 741 (mixed renewables case) - (a) load angle, (b) rotor speed, (c) active power, (d) reactive power.

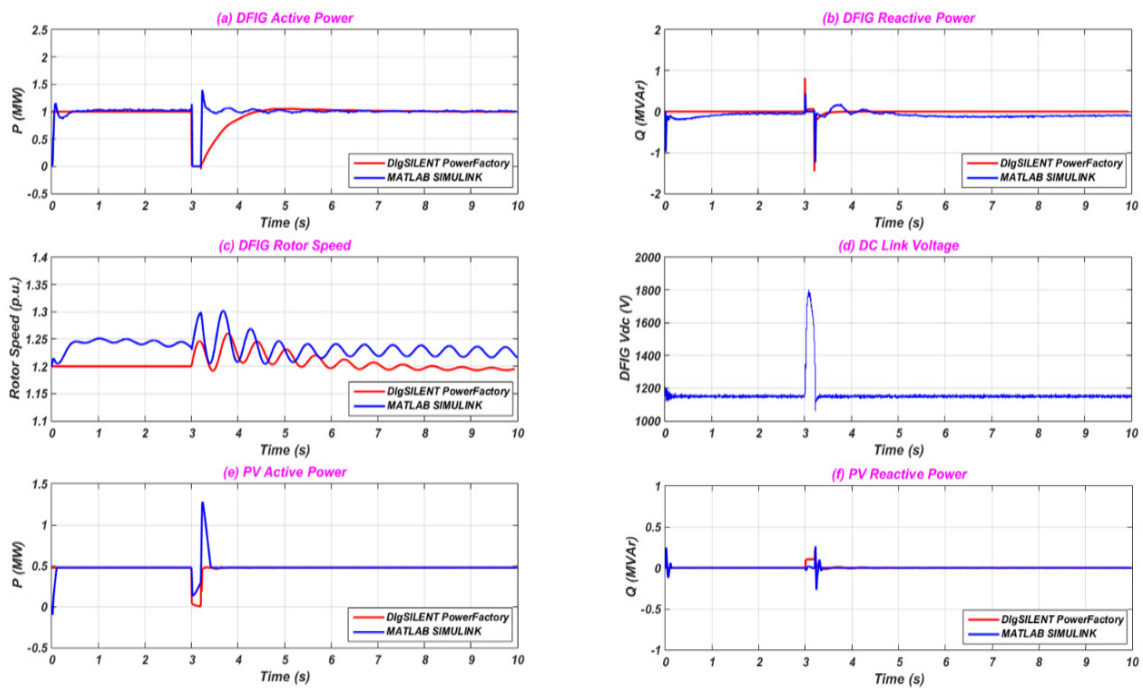


Figure 5.29: Renewable units' responses in 37 bus system to a fault on bus 741 (mixed renewables case) - (a) DFIG active power, (b) DFIG reactive power, (c) DFIG rotor speed, (d) DFIG DC link voltage, (e) PV active power, (f) PV reactive power.

The transient stability analysis of the IEEE 37 bus using the Transient Stability Index (TSI) method is shown in Table 5.6. As can be seen, the DG units based on renewable resources decrease the transient stability of the system when the system experiences a three phase fault at different locations. To improve system transient stability the renewable units should provide reactive power during the transient fault [40]. However, this chapter investigates the impact of DG based on renewable sources on the distribution system transient stability without dynamic reactive power support or reactive power support devices.

Table 5.6: Transient stability analysis of the IEEE 37 bus system using TSI in %, stable>0, unstable<0.

TSI	Base case	PV case	Wind DFIG case	Wind FRC case	Mixed renewables case
Fault on bus 799	82.27	74.33	77.34	78.0	78.21
Fault on bus 741	73.1	73.08	73.0	80.0	73.05

5.7.3 IEEE 123 Bus Distribution System

The IEEE Power Engineering Society has published another system for distribution system analysis called the IEEE 123 Node Test Feeder [195]. A schematic diagram of this system is given in Figure 4.34 of Chapter 4. Detailed data regarding this system are given in Appendix B.3. Bus 150 is the bus which connects the grid with the test network. IEEE 123 bus distribution system data are summarised in Table 4.11. A distributed generator based on fossil fuel (CDG) is assumed to be connected at bus number 96. Detailed data regarding this CDG are given in Appendix C. The grid is assumed to be an infinite bus. Power flow data of the 123 bus distribution system are given in Appendix B.3, where the grid bus is assumed to be the slack. DG based on renewable energy are connected to the farthest node from the grid, which is bus number 85. The same test procedure as the IEEE 13 bus and IEEE 37 bus systems discussed earlier is used here to investigate transient stability.

A- Base Case

Figures 5.30 and 5.31 show the CDG responses to the applied fault on bus 150 and bus 85 respectively. As illustrated in these figures, the system remains stable after the applied fault is cleared and returns to pre-fault conditions.

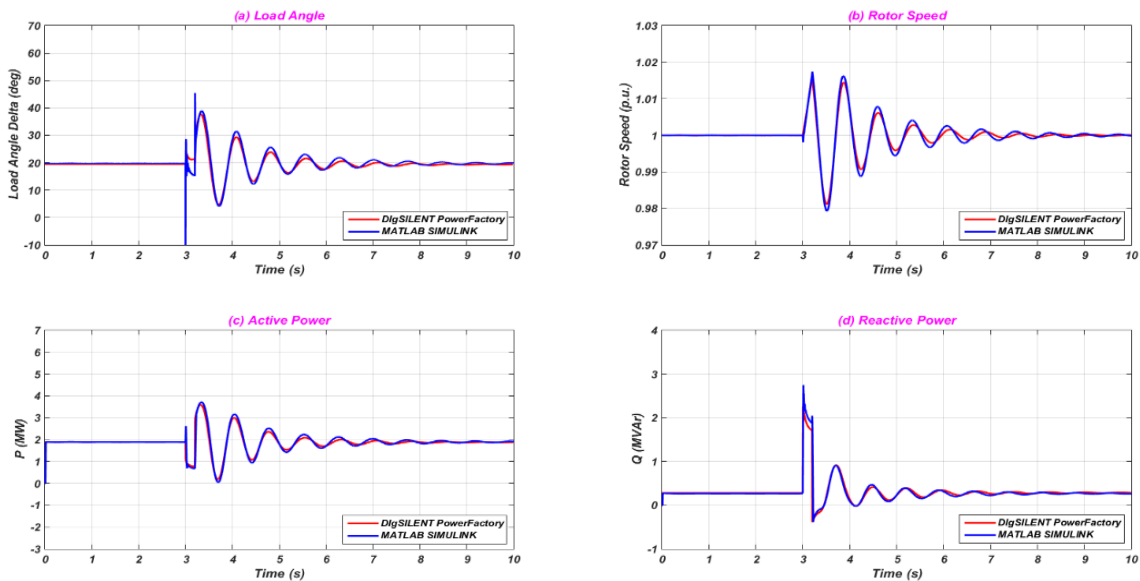


Figure 5.30: CDG responses in 123 bus system to a fault on bus 150 (base case) - (a) load angle, (b) rotor speed, (c) active power, (d) reactive power.

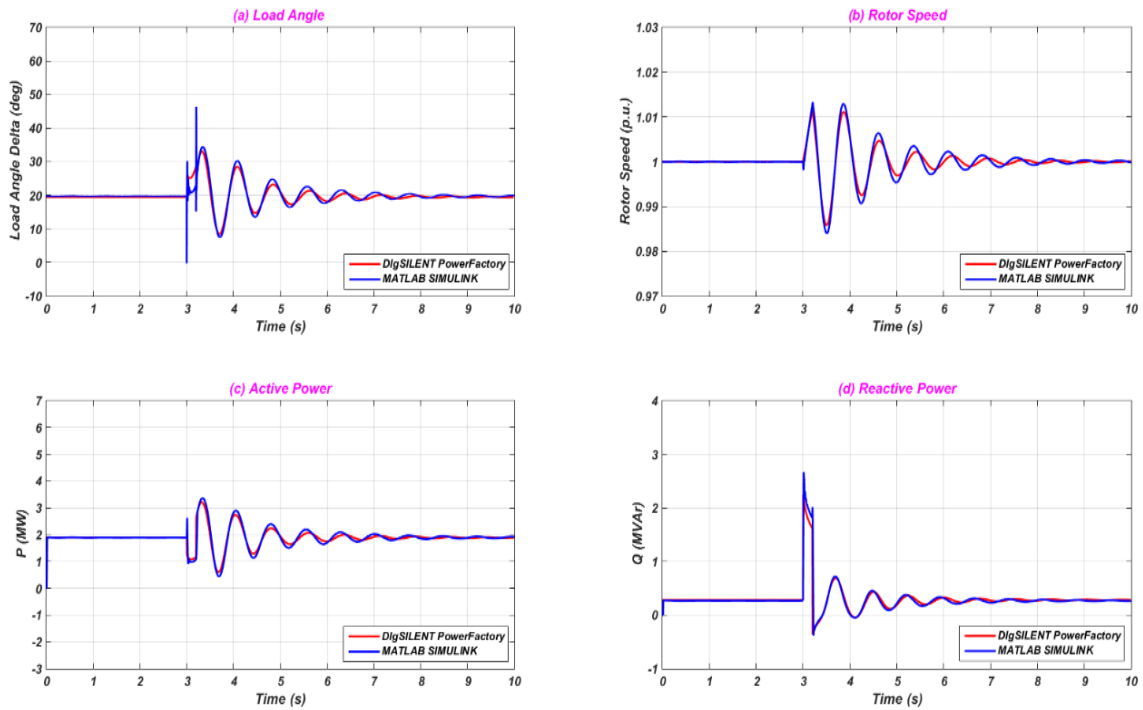


Figure 5.31: CDG responses in 123 bus system to a fault on bus 85 (base case) - (a) load angle, (b) rotor speed, (c) active power, (d) reactive power.

B- 35 % PV Penetration

A 2 MW grid connected PV system, which represents 35 % of total generation in the system, is installed at bus 85 with a 2 MW added load. The system's transient performance is shown in Figures 5.32 and 5.33 when the system is subjected to a three phase fault on bus 150 and 85 respectively. The simulation results show that the system is stable and returns to pre-fault conditions.

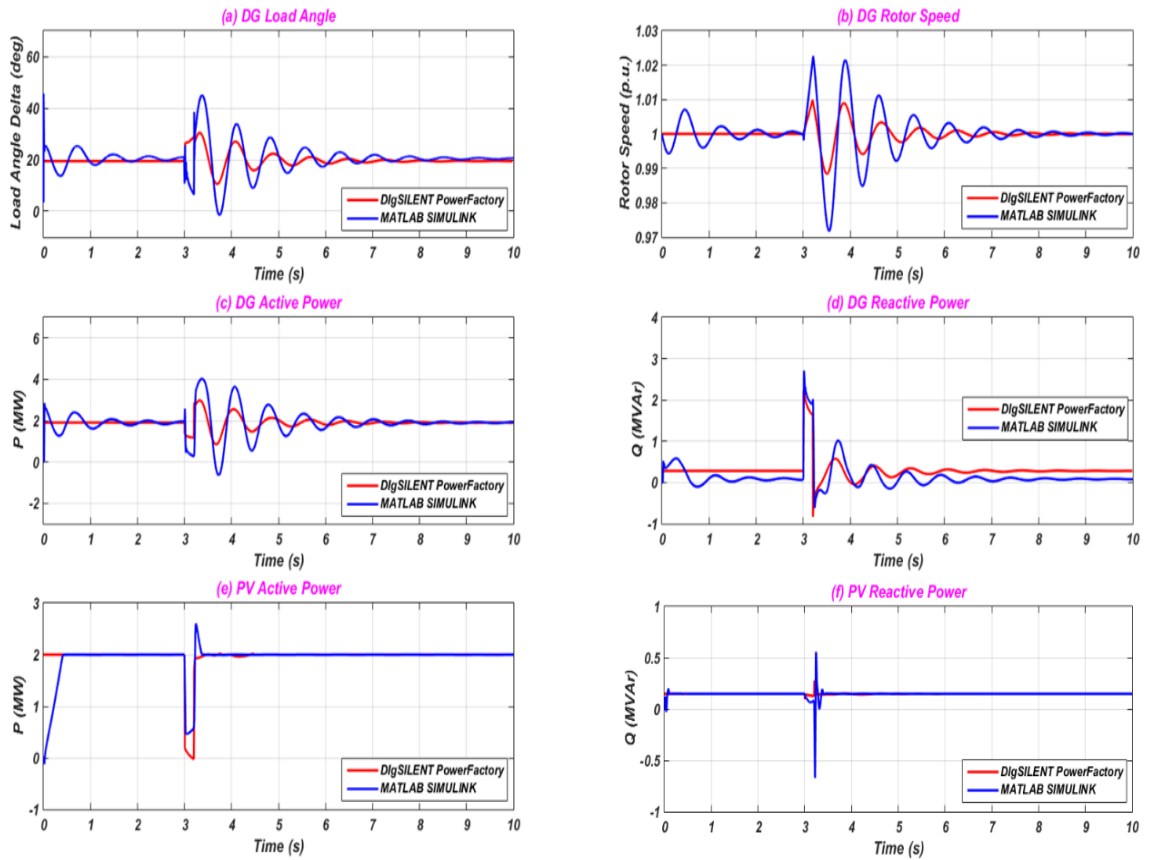


Figure 5.32: CDG and PV responses in the 123 bus system to a fault on bus 150 (PV case) - (a) CDG load angle, (b) CDG rotor speed, (c) CDG active power, (d) CDG reactive power, (e) PV active power, (f) PV reactive power.

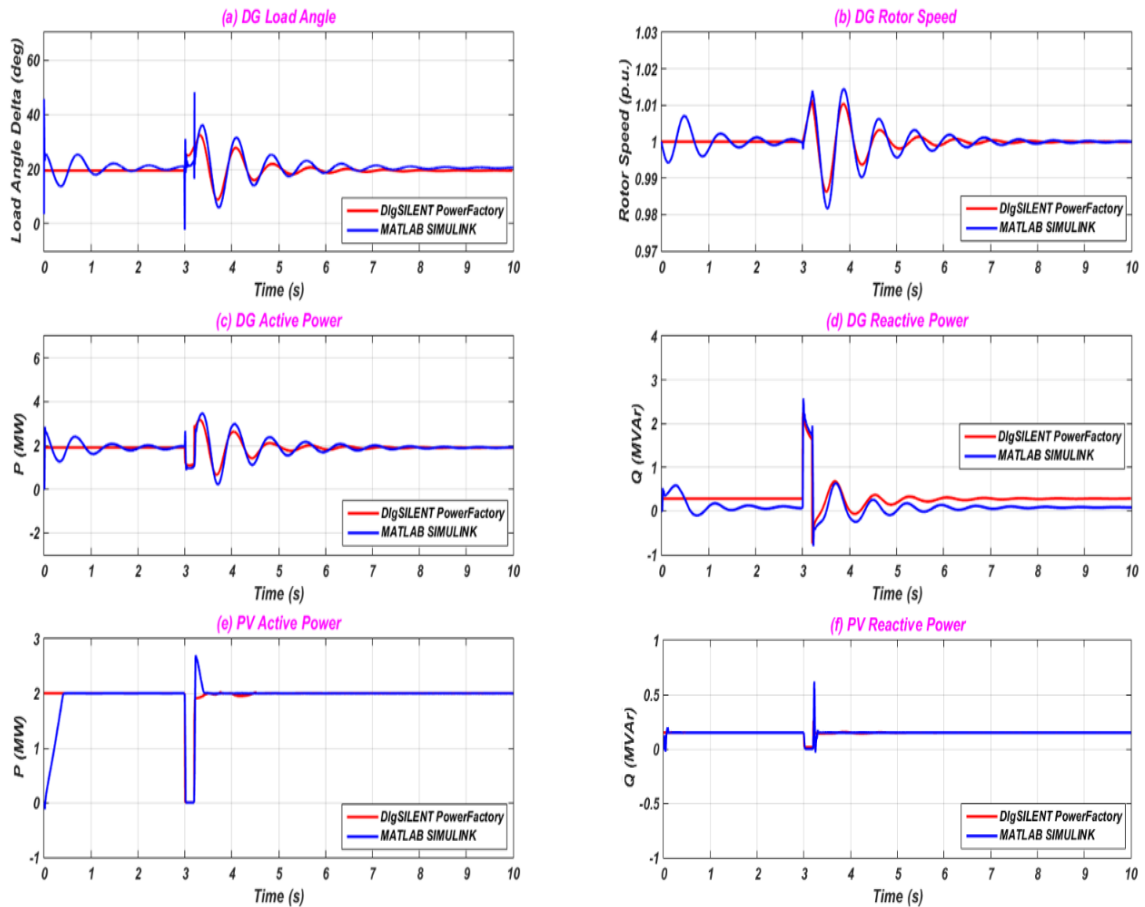


Figure 5.33: CDG and PV responses in the 123 bus system to a fault on bus 85 (PV case) - (a) CDG load angle, (b) CDG rotor speed, (c) CDG active power, (d) CDG reactive power, (e) PV active power, (f) PV reactive power.

C- 35 % Wind based on DFIG Penetration

A wind generator based on DFIG technology is installed at bus 85 with 2 MW output power and a 2 MW load is also added to the same bus. A three phase fault is applied on bus 150 and bus 85 to investigate the system's transient stability. The CDG responses to these disturbances are shown in Figures 5.34 and 5.36 respectively. Figures 5.35 and 5.37 illustrate the dynamic performance of the DG unit based on the DFIG when the system experiences these faults. From the simulation results it is clear that the system remains stable even after adding the renewable energy source based on the DFIG.

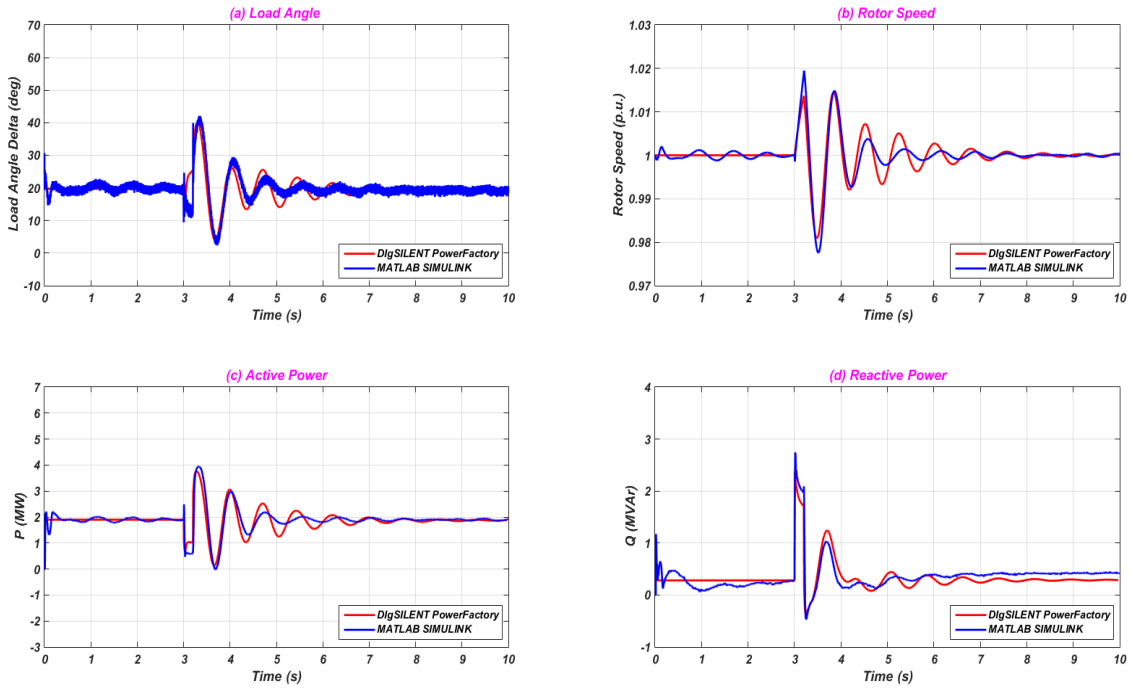


Figure 5.34: CDG responses in the 123 bus system to a fault on bus 150 (DFIG case) - (a) load angle, (b) rotor speed, (c) active power, (d) reactive power.

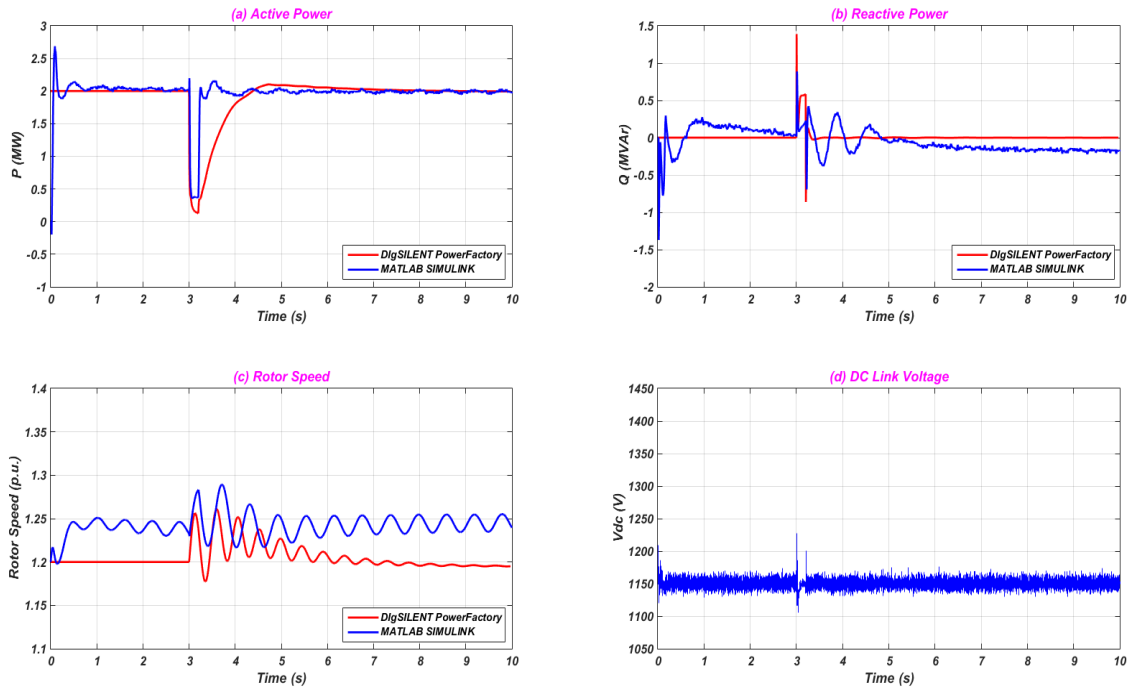


Figure 5.35: DFIG responses in 123 bus system to a fault on bus 150 (DFIG case) - (a) active power, (b) reactive power, (c) rotor speed, (d) DC link voltage.

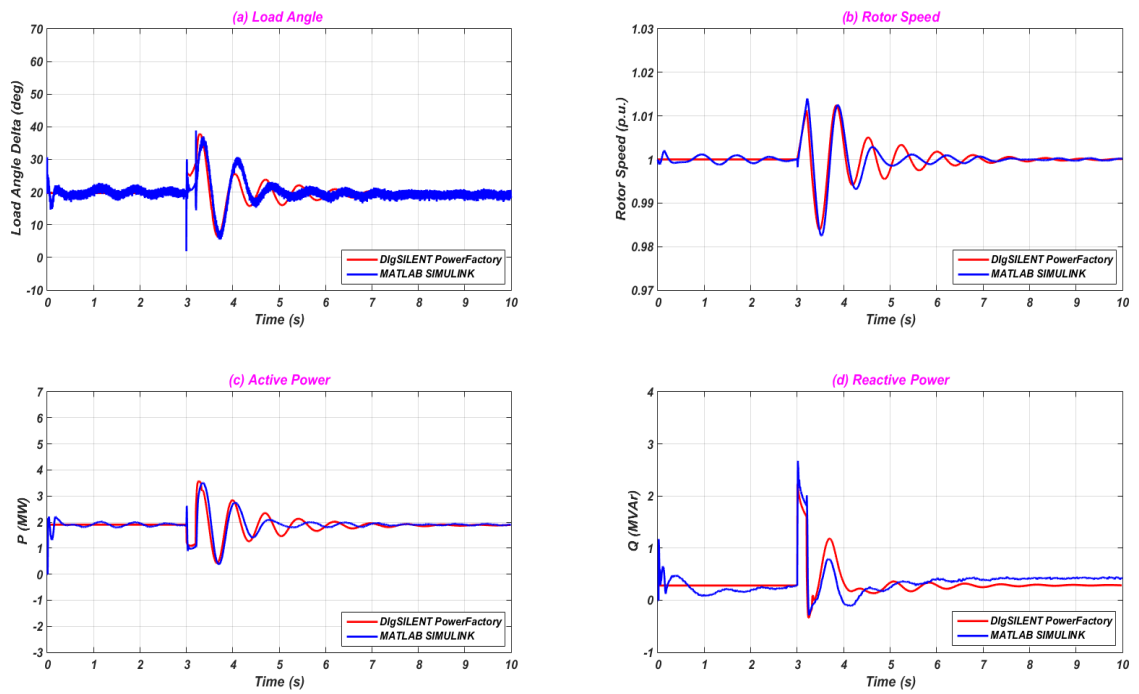


Figure 5.36: CDG responses in the 123 bus system to a fault on bus 85 (DFIG case) - (a) load angle, (b) rotor speed, (c) active power, (d) reactive power.

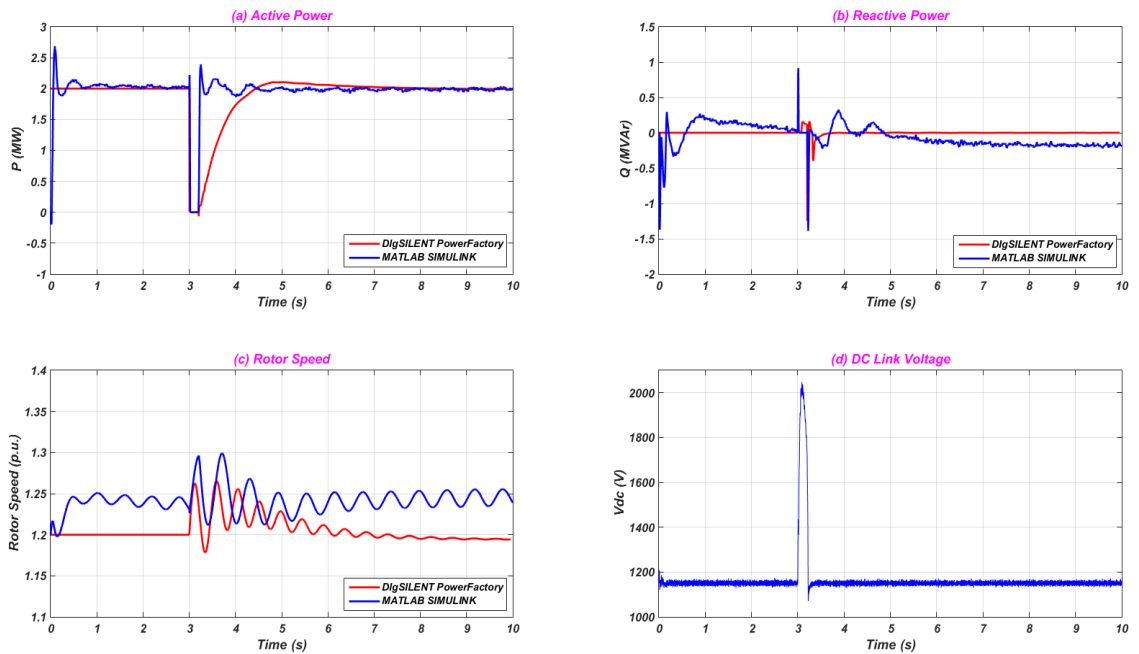


Figure 5.37: DFIG responses in the 123 bus system to a fault on bus 85 (DFIG case) - (a) active power, (b) reactive power, (c) rotor speed, (d) DC link voltage.

D- 35 % Wind base on Synchronous Generator with Fully Rated Converters

In this case, a 2 MW wind generator with fully rated converters is installed at bus 85 with a 2 MW added load. The transient stability of this system is considered when a three phase fault is applied on bus 150 and bus 85 to ensure that the system remains stable. Figures 5.38 and 5.39 show the CDG transient behaviours for the proposed faults on bus 150 and bus 85 respectively. The simulations results show that the system remains stable and returns to pre-fault conditions.

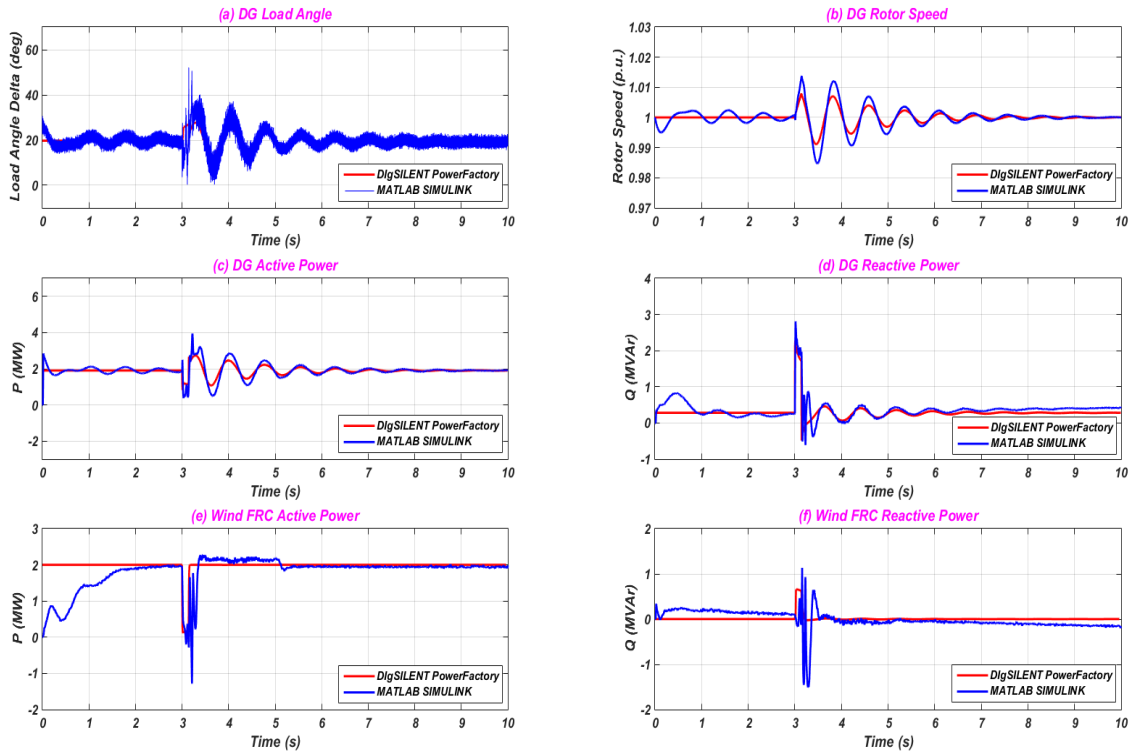


Figure 5.38: CDG and wind based on FRC responses in the 123 bus system to a fault on bus 150 (FRC wind case) - (a) CDG load angle, (b) CDG rotor speed, (c) CDG active power, (d) CDG reactive power, (e) wind FRC active power, (f) wind FRC reactive power.

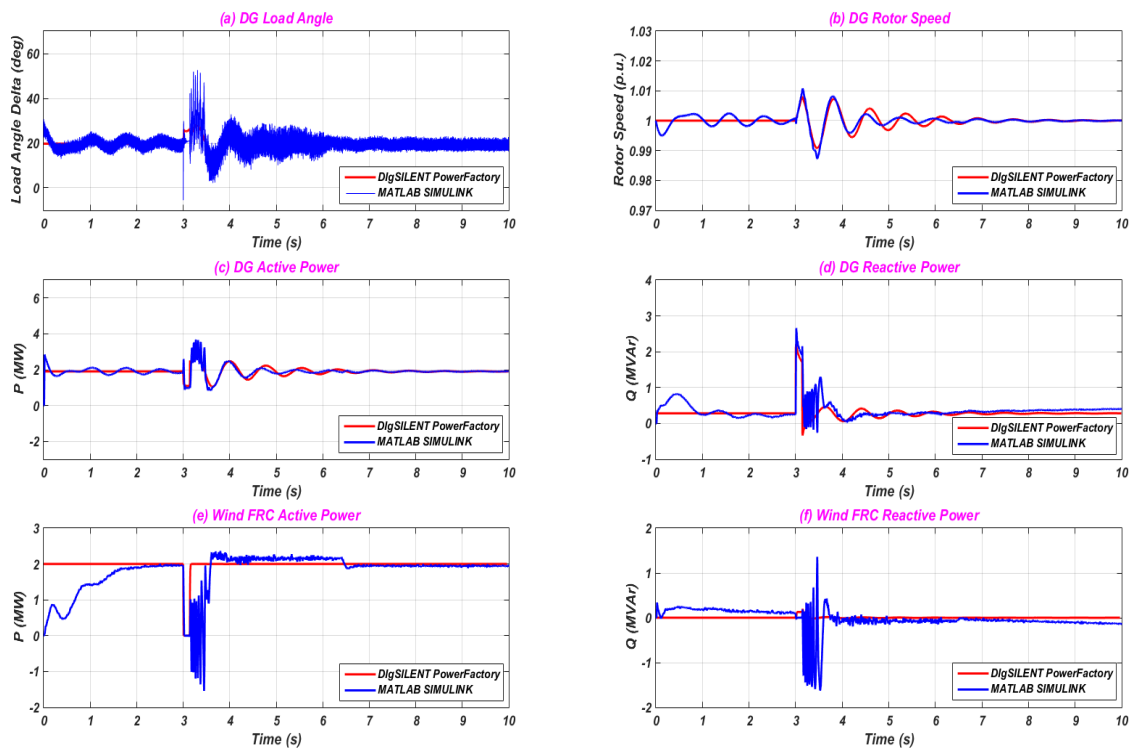


Figure 5.39: CDG and wind based on FRC responses in the 123 bus system to a fault on bus 85 (FRC wind case) - (a) CDG load angle, (b) CDG rotor speed, (c) CDG active power, (d) CDG reactive power, (e) wind FRC active power, (f) wind FRC reactive power.

E- 35 % Mixed Renewables Penetration

In this case, 1.5 MW DFIG based wind energy is installed at bus 85 with a 1.5 MW load and 0.5 MW grid connected PV is installed with a 0.5 MW load at bus 114. The CDG responses to a three phase fault applied on bus 150 and bus 85 are shown in Figures 5.40 and 5.42 respectively. Figures 5.41 and 5.43 illustrate the renewable units' performance during these faults respectively. The system remains stable and returns to pre-fault conditions.

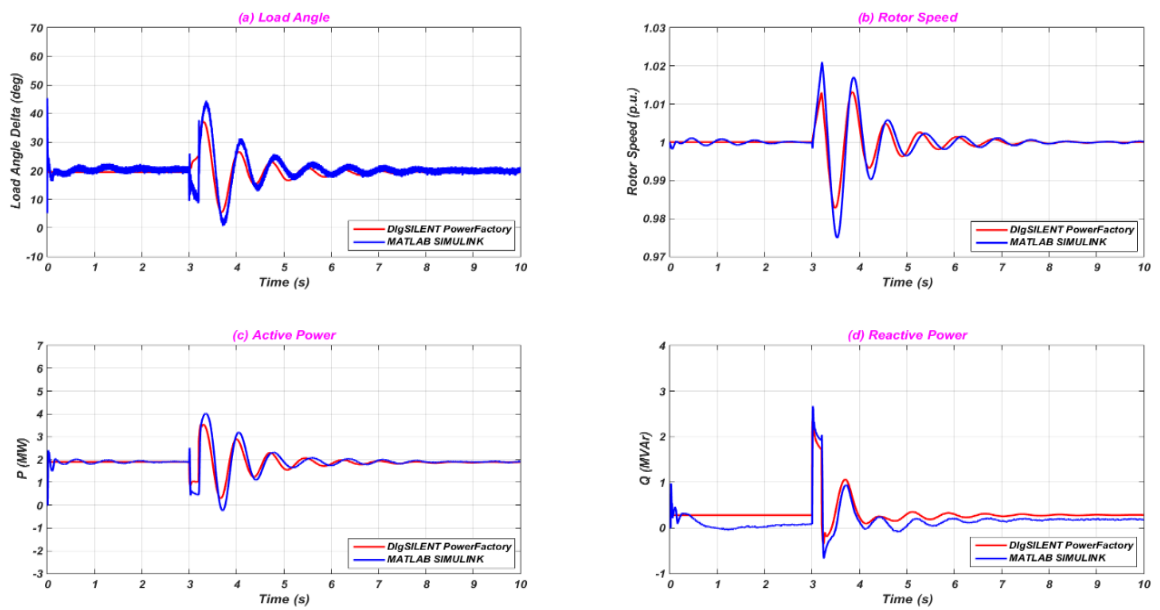


Figure 5.40: CDG responses in the 123 bus system to a fault on bus 150 (mixed renewables case) - (a) load angle, (b) rotor speed, (c) active power, (d) reactive power.

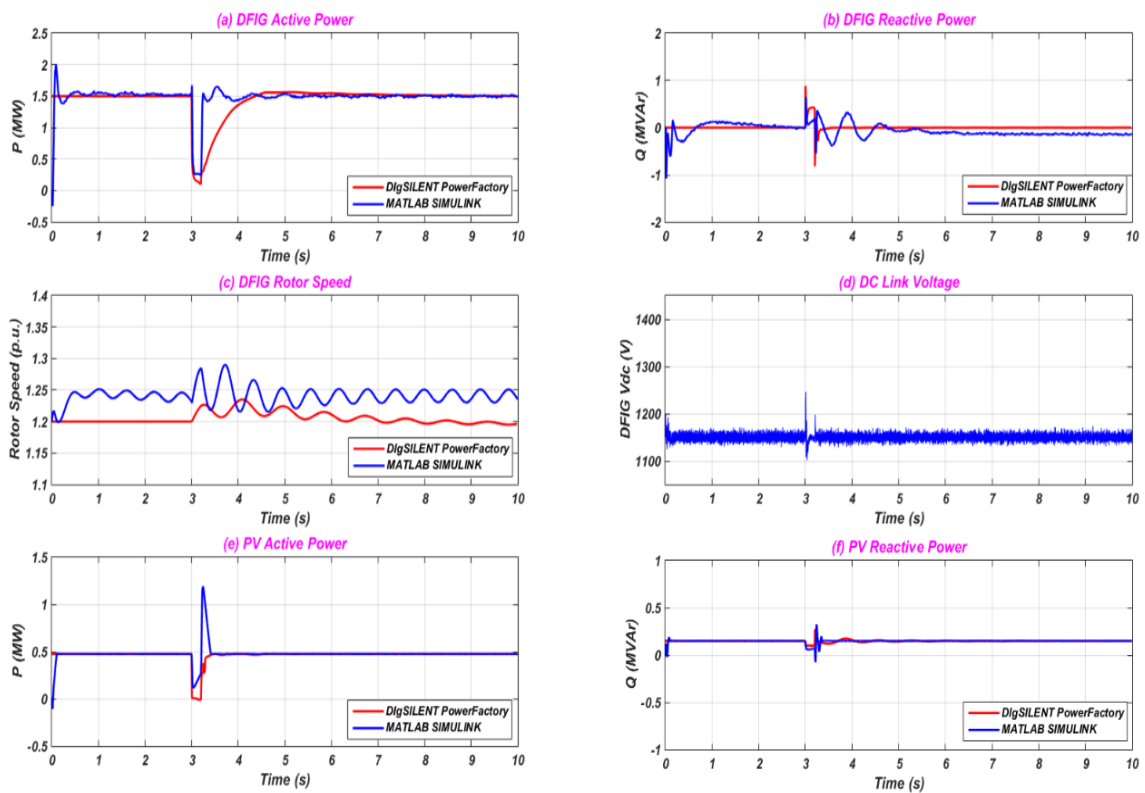


Figure 5.41: Renewable units' responses in the 123 bus system to a fault on bus 150 (mixed renewables case) - (a) DFIG active power, (b) DFIG reactive power, (c) DFIG rotor speed, (d) DFIG DC link voltage, (e) PV active power, (f) PV reactive power.

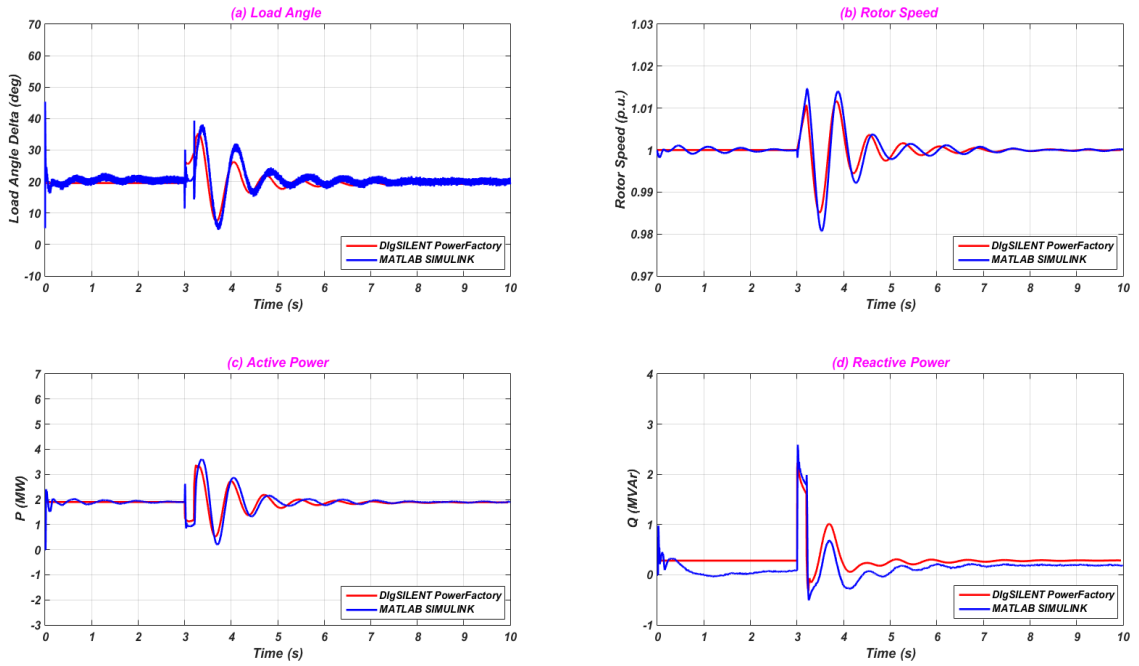


Figure 5.42: CDG responses in the 123 bus system to a fault on bus 85 (mixed renewables case), (a) load angle, (b) rotor speed, (c) active power, (d) reactive power.

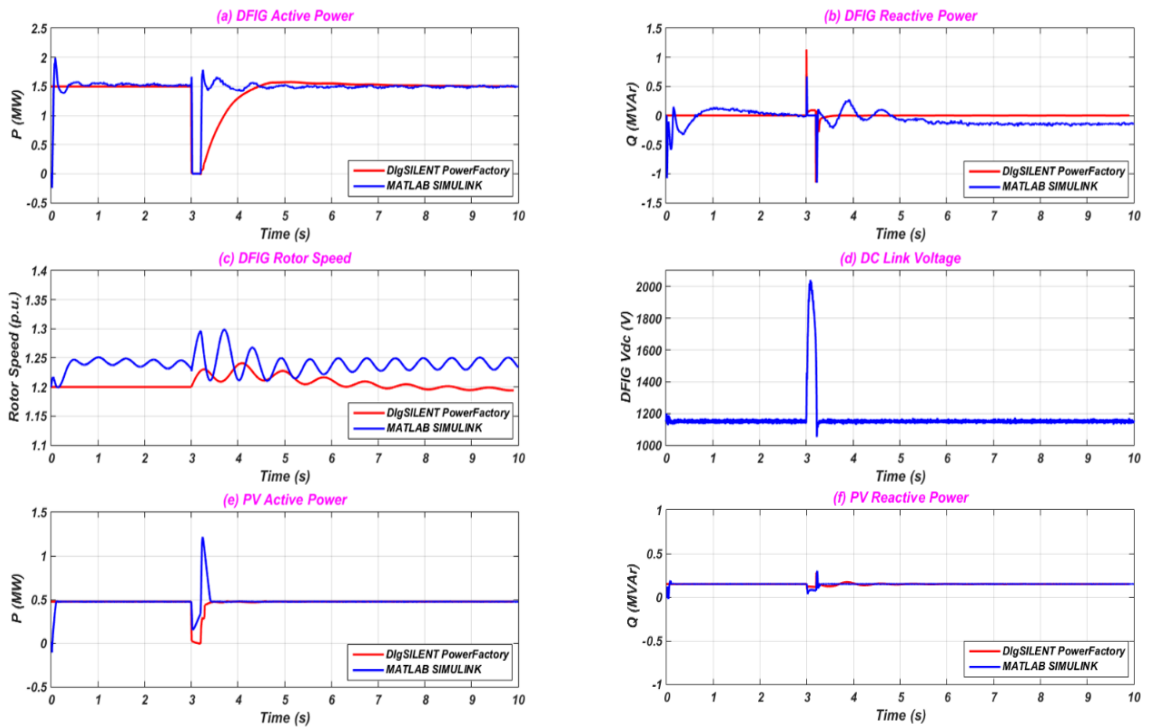


Figure 5.43: Renewable units' responses in the 123 bus system to a fault on bus 85 (mixed renewables case) - (a) DFIG active power, (b) DFIG reactive power, (c) DFIG rotor speed, (d) DFIG DC link voltage, (e) PV active power, (f) PV reactive power.

The Transient Stability Index (TSI) method can be used to assess the transient stability of the IEEE 123 bus, as illustrated in Table 5.7. The table shows that the increased penetration of renewable resources reduces the transient stability of the system when the system is subjected to a three phase fault at different locations.

Table 5.7: Transient stability analysis of the IEEE 123 bus system using TSI in %, stable>0, unstable<0.

<i>TSI</i>	<i>Base case</i>	<i>PV case</i>	<i>Wind DFIG case</i>	<i>Wind FRC case</i>	<i>Mixed renewables case</i>
<i>Fault on bus 150</i>	80.45	77.34	79.55	82.27	78.22
<i>Fault on bus 85</i>	82.74	81.82	81.82	83.67	81.36

5.8 Conclusions

Due to the dramatic increase in distributed generation based on renewable sources, the issue of distribution system stability is significant. It has been shown in this chapter that the higher the penetration of renewable energy the lower the stability of the system will be. The transient stability of distribution networks has been assessed using the Transient Stability Index method. Simulation results show that system transient stability is reduced when the system has high renewable energy penetration. It has also been discussed how different fault locations in a system affect the transient stability. Three generic IEEE distribution systems with high renewable source penetration have been examined when these systems are subjected to a three phase fault. The simulation results illustrate that the systems remain stable and return to pre-fault conditions. This chapter has investigated various distribution systems with high renewable energy penetration (35 % of the total power generation in the system) in terms of the systems' transient stability. The renewables include different technologies, namely wind turbines based on the DFIG, a wind based synchronous generator with fully rated converters, and a photovoltaic system based on solar energy. To improve the impact of renewable units on system transient stability, FRT capability and reactive power dynamic support during a fault are required.

CHAPTER 6 Frequency Response of Distributed Generation based on Renewable Energy

6.1 Introduction

Demand for electricity is growing at a significant rate, more than ever before. This rise in demand has led to the emergence of many distributed generation units in power systems under new restructuring and deregulation regimes. For this reason, DGs based on renewable energy are increasing and set to rise even faster in the future [212, 213]. This is not the only reason for the considerable rate of renewable energy penetration in power systems, as tackling climate change, reducing operating costs and reducing the dependency on fossil fuels to be prepared for fuel shortages in the future are several other advantages of using renewable energy resources. Several countries around the world have set renewable portfolio targets; 20 % of total power generation from renewable resources by the year 2020 in the UK, 22 % of installed capacity from DGs by the year 2020 in the US, and Japan has planned to generate around 60 % of its electricity from renewable resources by 2050 [214-216].

The new electricity market structure and smart grids have significantly increased the penetration of distributed generation based on renewable resources in distribution systems. In several cases, the contribution towards dynamic system operation from DGs rather than conventional generation plants has become more feasible because the opportunity costs of DGs are much less due to their small generation capacity. Also, DGs are usually located close to the load centre. This leads to a significant reduction in energy consumption costs due to the long transmission distances of conventional power units. However, DG units could change the dynamics and nature of distribution systems and bring about undesirable system operation, such as bi-directional power flows. They may also increase system fault current levels. As a result, DG units based on renewable resources are normally equipped with power electronic interfaces to decouple their dynamics from the main system and avoid any undesirable system operation. A more reliable power operation may need small scale wind power owners to replace fixed speed

induction generators with variable speed wind generators such as the Doubly Fed Induction Generator (DFIG) or synchronous generator with fully rated converters, as they have the ability to contribute towards ac voltage control. They can also contribute towards ac network frequency and damping support by modifying their control systems. Solar energy based on photovoltaic technology can also be controlled in the same manner as wind generators.

The frequency of a power system is continuously varying and to enhance the power system's security, the frequency should remain within acceptable limits, as defined by the power system operators. A sudden loss of generation or load demand could lead to a frequency deviation from the nominal value (50 Hz in this thesis) because the system frequency is directly proportional to the balance between load and generation. High renewable energy penetration in power systems can affect frequency stability and this issue has become a significant concern for Transmission System Operators (TSOs). It is an issue in power dynamic operations, as some renewable energy sources have different characteristics from conventional synchronous generators in several respects. For instance, some renewable sources are connected to the grid via power electronic converters and this leads to decoupling of the inertia of their generators from power system inertia, such as in variable speed wind turbines based on the DFIG or synchronous generator with fully rated converters. In addition, some other renewable resources, such as solar based on photovoltaics, do not contribute towards system inertia as there is no machine in the construction to contribute towards power system inertia.

Traditionally, grid connected renewable systems operate to provide the maximum available power and they have not been required to participate in power system operation. Therefore, this chapter investigates the frequency response of different renewable resources in different distribution systems when these systems are subjected to a frequency disturbance such as a sudden increase or decrease in load demand. In literature, a transmission system is usually selected to study frequency response as small generating units have a small impact on power system frequency. However, enhancing system security in distribution systems could contribute towards increasing system security of a

transmission system and many renewable units are usually connected close to the load demand in distribution systems. Therefore, this chapter takes distribution systems into consideration and studies frequency response.

6.2 Frequency Control Background

The electrical frequency f in (Hz) of a power system is the same across the entire area and all generator rotors rotate at the same angular speed ω in (rad/sec), times a factor that is a function of their number of poles p , as illustrated in equation 6.1 [200, 217].

$$f = \frac{p}{2} \times \frac{\omega}{2\pi} \quad (6.1)$$

$$\omega = \frac{4\pi f}{p} \quad (6.2)$$

$$n = \frac{60}{2\pi} \omega \quad (6.3)$$

Then,

$$n = \frac{120f}{p} \quad (6.4)$$

The prime mover which can be driven by various energy sources (including steam, gas or wind) drives the rotor, produces mechanical power (P_m) and creates a mechanical torque (T_m). In contrast, the generator delivers electrical power (P_e) and creates an opposite torque called an electrical torque (T_e). Neglecting losses, the rotor speed will not change if equation 6.5 is satisfied.

$$T_m = T_e \quad (6.5)$$

However, if $T_m > T_e$ then the rotor will accelerate, and if $T_m < T_e$ then the rotor will decelerate.

These relationships, including losses, can be modelled mathematically with the so-called swing equation, as shown in equation 6.6.

$$J\omega \frac{d^2\delta}{dt^2} = P_m - P_e - P_l \quad (6.6)$$

Where, J is the total moment of inertia of the rotor masses in (kg.m^2), $d^2\delta/dt^2$ represents the rotor acceleration in (rad/sec^2) and P_l is the power losses in the process in (W).

Equation 6.1 to 6.6 show that the system frequency depends on the speed and the speed depends on the active power. To conclude, the active power withdrawn or injected into the power system inherently affects the system frequency. If P_e increases, the speed will decrease and therefore the P_m should be increased to maintain the same speed, and vice versa [218].

Loss of generation or load can cause a sudden and undesirable change in system frequency. Uncertainties in demand forecasting or an inability of generators to cope with load variations may increase the possibility of imbalance between load demand and generation. Any mismatch between load and generation causes frequency deviations and if large enough, it may lead to system collapse. Under the new restructured environment, several questions arise about which generator or equipment should provide balancing services.

An effective frequency response is defined as an automatic corrective frequency response procedure provided towards balancing generation and load demand. After a disturbance, it is the responsibility of generator governors to arrest the system frequency change. There is a significant relationship between the rate of change of frequency and system inertia constant (H), as illustrated in equation (6.7).

$$\frac{df}{dt} = \frac{\Delta P}{2H} \times f_o \quad (6.7)$$

Where, df/dt is rate of change of frequency (Hz/sec), $\Delta P = (PL-PG)/PG$ power change in (p.u.), PL is load power in (W), PG is generation power in (W), H is system inertia constant in (sec) and f_o is frequency at disturbance time in (Hz).

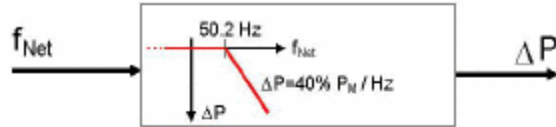
This chapter will investigate primary frequency response and will find out how distribution systems respond after adding DG units based on renewable resources, as well as whether they can improve frequency response or not. The primary frequency response is the instantaneous proportional increase or decrease in the generation units' active power output in response to a deviation in system frequency within 10 to 15 seconds.

6.3 Grid Code Requirements for Frequency Response

As discussed earlier, frequency stability is an important concern in power systems, as a considerable fall in frequency can lead to an increase in magnetising currents which may

damage power transformers and induction motors, such as water pumps [200]. Power system operators have to ensure that system frequency is kept within limits and as close to the nominal frequency value as possible. Various international grid codes worldwide have imposed frequency requirements that generating units in power systems should provide. Generally, all large generating units should have the technical capability to participate in system frequency control. At the moment, thermal power plants with high inertia constants are the most reliable units to provide primary and secondary frequency responses during frequency disturbances. Grid code requirements for frequency response have been introduced over the years in various European countries, such as Germany and the United Kingdom.

In Germany, it is required that every generator should have the capability to decrease its output power to allow constant active power control of 1 % of its rated power per minute. In addition, it is required that all generating units with ≥ 100 MW rating power should provide a primary frequency response. It is also not allowed to disconnect any generator from the grid when the system frequency is changing between 47.5 and 51.5 Hz [28, 219]. Outside this range, disconnection of these generating units without delay may be required. Germany's new grid codes have imposed new frequency requirements for wind turbines and they are required to reduce turbine output power when system frequency is above 50.2 Hz, as shown in Figure 6.1 [63]. As illustrated in Figure 6.1, all renewable generating units have to decrease their output power when the system frequency is greater than 50.2 Hz and the output power should be decreased with a gradient of 40 %/Hz of the instantaneously available power. When the frequency is below 50.05 Hz, the output powers of these generating units are allowed to increase again. These requirements can be applied to grid connected distributed generation based on wind and solar energy, as will be discussed in the simulation results section.



$$\Delta P = 20 P_M \frac{50.2 \text{ Hz} - f_{\text{Netz}}}{50 \text{ Hz}} \quad \text{at } 50,2 \text{ Hz} \leq f_{\text{Netz}} \leq 51,5 \text{ Hz}$$

P_M Available power

ΔP Power reduction

f_{Netz} Frequency

Between $47.5 \text{ Hz} \leq f_{\text{Netz}} \leq 50.2 \text{ Hz}$ no limitation

At $f_{\text{Netz}} \leq 47.5 \text{ Hz}$ and $f_{\text{Netz}} \geq 51.5 \text{ Hz}$ separation from grid

Figure 6.1: Germany's grid code requirements for renewable generators [63].

The National Grid in the United Kingdom, which is the power system operator, has a license obligation to control system frequency within certain boundaries $\pm 1\%$ of nominal frequency (50 Hz), as specified in the Electricity Supply Regulations. The National Grid operates the system shown in Figure 6.2 [220]. As can be seen, under normal operation conditions, the system frequency is between 50.2 and 49.8 Hz (called operational limits) which means the maximum frequency deviation is within 0.4% of nominal frequency. The statutory steady state limits of ± 0.5 Hz represents the maximum frequency deviation after a normal infeed loss. After infrequent infeed loss, ± 0.8 Hz is the maximum deviation in frequency. Generating units can start tripping when the system frequency exceeds 52 Hz, while for under frequency conditions load starts shedding when the frequency is below 48.8 Hz. The National Grid also requires that any frequency deviation outside the limits of $\pm 1\%$ of nominal frequency must not exceed 60 seconds in duration. These grid code requirements are for all transmission connected generation types; however, all distributed generation types connected to distribution systems with a capacity less than 50 MW in England and Wales, and 30 MW in Scottish Power Transmission respectively, will be required to meet the relevant Distribution Code and Engineering Recommendation G75

and G59/1 respectively. These recommendations, G75 and G59/1 respectively, recommend a low frequency threshold of 47 Hz [221].

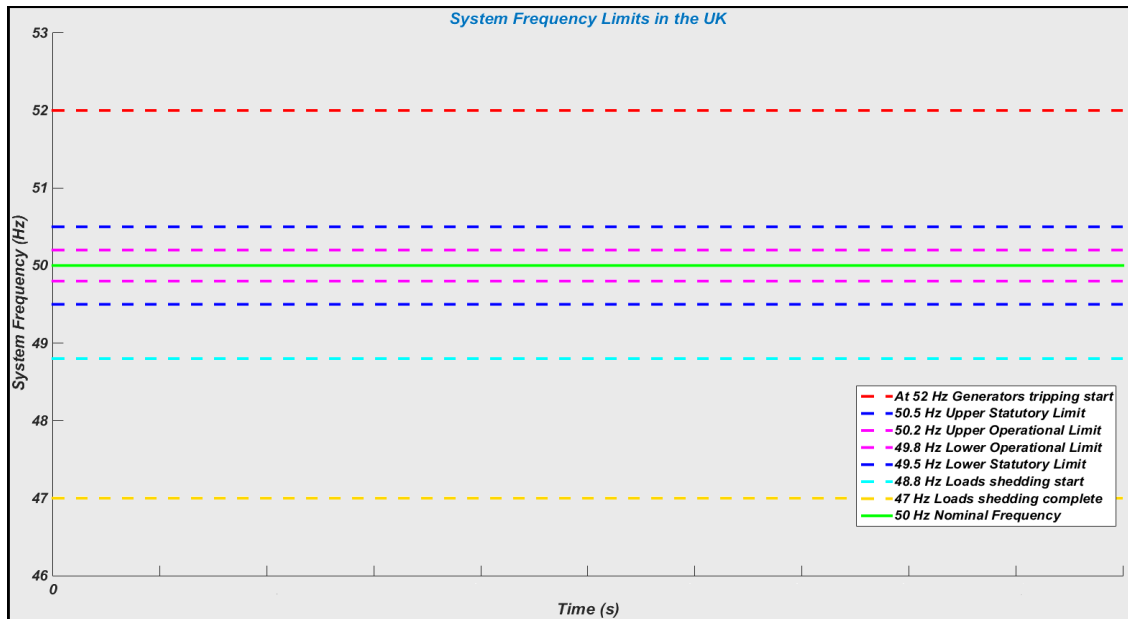


Figure 6.2: UK operational and statutory limits of power system frequency.

In the UK, frequency response can be classified as a dynamic response and a non-dynamic frequency response. A dynamic response is continuous frequency control second by second, while non-dynamic frequency response is a service at a defined frequency deviation, as shown in Figure 6.3 [222].

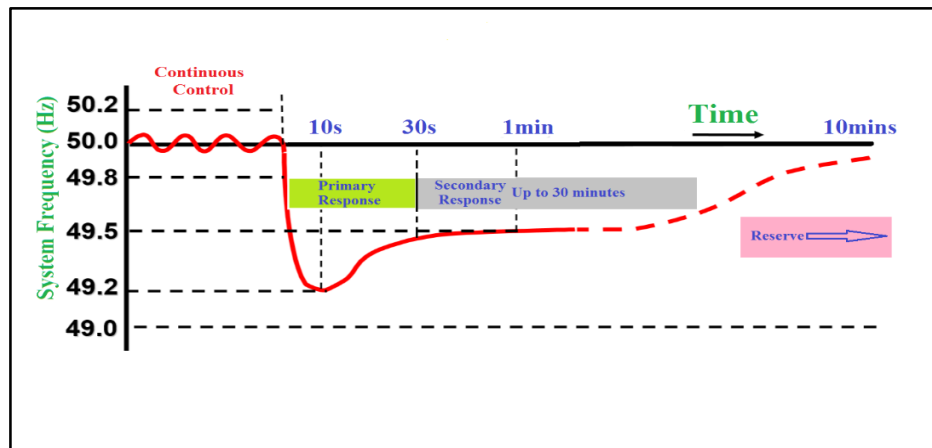


Figure 6.3: Frequency response in the UK's power system.

6.4 Wind Generation Impact on System Frequency

Due to the rapid increase in wind energy penetration in power systems, different technical, economic and regulatory concerns have arisen involving the interaction between large wind turbines and power systems. Unlike conventional power plants based on synchronous generators, wind power systems have different dynamic and operation characteristics. Nowadays, several countries around the world have set technical requirements called grid codes for wind farms which include the participation of wind systems in frequency control [223]. These grid codes are typically for large wind farms connected to transmission systems, rather than smaller generating units connected to distribution systems.

In recent years, system operator requirements for wind turbines have become one of the major drivers in developing wind power technology. They have led wind power from being a simple technology to an advanced control technology. Frequency control requirements are one of the most challenging issues for wind system owners, as they require that wind turbines should regulate power output to a defined level, which is called active power curtailment. It is also required that wind turbines participate in the frequency response of systems and control their output power according to the frequency deviation. Several European countries, such as Germany, the United Kingdom and Ireland, have set frequency control requirements for wind farms. In the UK, it is required that wind farms should have a frequency control device to provide primary and secondary frequency responses [223].

Typically, wind turbines based on fixed speed induction generators provide a better frequency response to power systems because their rotors are directly connected to the grid and this means their inertia contributes towards overall power system inertia. Unlike fixed speed induction generators, variable speed wind turbines' inertia is decoupled by power electronic converters from the power system inertia. Therefore, wind turbines based on variable wind speed should be controlled in such a way to participate in frequency response. Modern wind turbines are based on variable speed and they have been developed considerably, as discussed in Chapter 3. Thus, variable speed wind turbines based on the

DFIG and synchronous generator with fully rated converters (FRC) are considered in this thesis. The inertia response of variable speed wind turbines such as the DFIG could be provided by manipulating the set-torque of the controller and the inertia control gain. Wind power based on the DFIG was discussed in terms of primary and secondary frequency response in [53, 224]. DFIG based wind energy has also been controlled in [55, 56, 225] to provide an active contribution towards frequency response. DFIG controllers for inertia response were proposed in [56, 225], and in [55] a drop frequency control was added to inertia response controllers. In literature, pitch angle control has been used to enhance the frequency response of the DFIG, as shown in [54]. However, these models were based on constant wind speed and wind turbines connected to large power systems. In this chapter, the frequency response of wind power based on the DFIG is investigated for smaller power systems, i.e. distribution systems where the penetration of wind is significant. Different frequency responses for the DFIG are discussed to meet new grid code requirements, including active power reduction, inertia response and a proposed frequency control model to enhance the frequency response of the Doubly Fed Induction Generator based on wind energy.

In wind turbines based on a synchronous generator with fully rated converters, the rotor is not connected to the grid so the inertia response is minimal. In contrast, the power electronic converters of the FRC synchronous generator based on wind can be controlled in such a way as to provide frequency response. The frequency control in a FRC wind generator has not been considered much in literature and there are few papers discussing this issue. Several research papers have investigated the frequency response of FRC wind systems, such as [58]. In [58], a control scheme for a synchronous generator based on wind energy has been developed to improve frequency control performance. In [57], the coordinated frequency control for the DFIG, which was applied in [226], has been used for a wind turbine based on a synchronous generator with full-scale converters. It has been shown in [226], that the proposed control scheme for the frequency response in FRC wind generators can be used for different wind speed conditions, such as low wind. In this chapter, active power curtailment for over-frequency conditions according to Germany's

grid codes is used to give a frequency response to wind turbines based on a synchronous generator with fully rated converters.

6.5 Photovoltaic Generation Impact on System Frequency

Solar energy based on photovoltaics has become one of the major contributors towards power system generation from a renewable source in recent years. This technology has been developed considerably and the growth of installed PV grid connected systems raises technical and economic challenges that need to be solved to enhance the penetration level of PV in the near future. Due to the rapid increase of installed PV systems in power systems, power mismatches introduced by solar energy are no longer negligible. In the past, small scale PV grid connected systems were not obliged to provide frequency responses to power systems. They were disconnected from the grid during network disturbances. However, with the increase in penetration of PV grid connected systems, their impact on overall system control will be significant.

Several grid code requirements worldwide request frequency control from large scale renewable energy systems to contribute towards system frequency stability. In Germany, it is required that each renewable energy source reduces its output power to a defined level in over-frequency scenarios. This is usually called de-loading of the generating units. In order to provide frequency control, PV grid connected systems should be able to control their output power with system frequency changes. Photovoltaics is fully interfaced by power electronic converters which can be controlled to provide frequency response controllability. In literature, there are three different approaches to provide frequency responses from PV grid connected systems: keep PV systems in the MPPT mode and install an energy storage system, as illustrated in [59, 60], install a dump load to absorb surplus energy and the PV active power curtailment approach [61]. The power curtailment approach is more cost effective than the other two approaches for providing frequency control via a PV system, as shown in [62]. In this chapter, the power curtailment approach is used for PV grid connected systems to provide a frequency response to different generic distribution systems. The active power reduction approach is based on the new German grid code requirements which have been discussed in detail in section 6.3.

6.6 Modelling and Control of Renewable Energy Systems for

Frequency Response

The rapid increase in renewable energy penetration into power systems has led to the defining of new grid code requirements for generating units based on renewables. In order to meet these new grid code requirements, generating units based on renewables should be controlled in a particular way. One of these requirements is frequency control, which has been discussed earlier. The modelling and control of distributed generation based on wind and solar energy are discussed in this section in relation to complying with frequency control grid code requirements. Wind turbines based on the DFIG, wind turbines based on a synchronous generator with fully rated converters, and a solar generating unit based on photovoltaics are investigated in terms of the frequency response to various generic distribution systems. Two types of software have been used to model the test systems and the renewable generating units, namely MATLAB/SIMULINK and the commercial package DIGSILENT POWERFACTORY.

6.6.1 DFIG Modelling and Control

Wind turbines based on the DFIG have been rapidly developed and their use in power systems has increased due to their high efficiency. The DFIG consists of a wound rotor induction generator with slip-rings to transfer current between rotor windings and the rotor side converter (RSC), while the stator windings are connected to the ac grid. The RSC is connected to the grid side converter (GSC) through a DC link. The GSC is connected to the ac grid through a transformer, as was shown in Chapter 3. When the DFIG is operating above synchronous speed, the generator rotor can provide power to the grid, which represents around 30 % of total power generation from the DFIG unit and 70% from the stator. However, the generator rotor will consume power from the grid when the rotor operates below the synchronous speed. The RSC and the GSC are capable of allowing active and reactive powers to be transferred in both directions, which is called four quadrant operation. The Power electronic converters can be controlled by vector control which decouples the active and reactive power control and allows fast regulation action, typically within milliseconds. The active and reactive power delivered to the ac network

is controlled by the RSC, while DC link voltage can be regulated by the GSC. Cascaded loops are used in the controller structure, as discussed in Chapter 3, as fast inner current controller loops which control currents to the reference values specified by external power control loops.

This chapter discusses frequency control provision by the DFIG based on wind energy controlled by three different techniques. The traditional inertia response from the DFIG discussed earlier in literature, active power reduction, and a proposed frequency control technique aimed at improving the frequency response of the DFIG. The inertia response control is defined by adding another torque term to the generator torque; the extra torque is defined in equation 6.8 and illustrated in Figure 6.4.

$$T_{inertia} = K_i \frac{df}{dt} \quad (6.8)$$

Where K_i is the gain and df/dt is the change in frequency. Controlled detailed of this method is explained in literature and it will not be implemented in this chapter. The active power reduction technique is required from renewable units in distribution systems according to Germany's grid codes explained earlier in section 6.3. Active power reduction is used in this chapter to provide frequency responses from distributed generation based on wind and solar energy according to the German grid code requirements discussed in section 6.3. Figure 6.5 shows the frequency controlled by the active power reduction method. Active power can be reduced to zero and this method is effective for over-frequency conditions. Table 6.1 shows active power reduction requirements from DFIG based wind for the frequency response applied in this chapter.

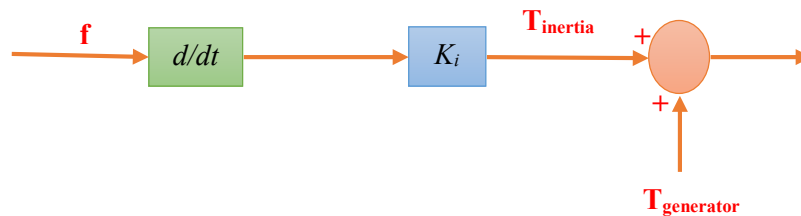


Figure 6.4: Inertia response control from DFIG.

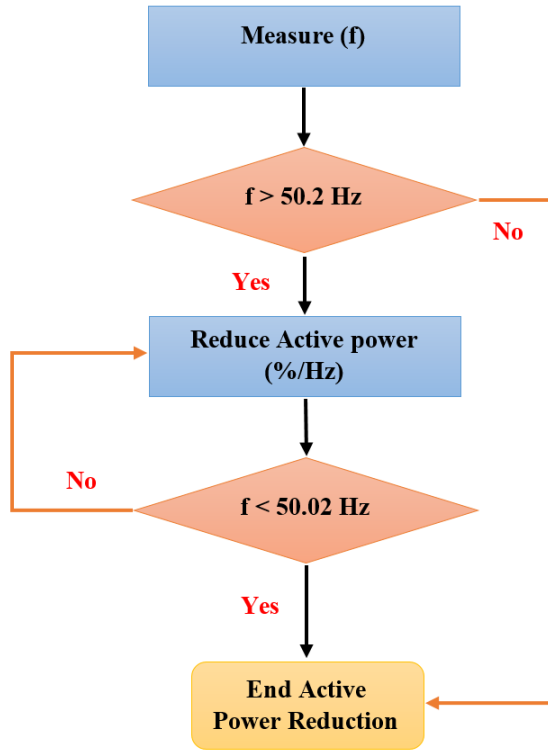


Figure 6.5: Active power reduction technique for frequency response control from renewable generating units.

Table 6.1: DFIG active power reduction parameters.

Starting active power reduction	50.2 Hz
Ending active power reduction	50.02 Hz
Gradient active power reduction	50 %/Hz
Minimal active power	0
Negative gradient for power change	-0.1
Positive gradient for power change	0.1

A proposed frequency control is used to provide a frequency response from DFIG based wind and ensure that the frequency is within obligated limits which, for instance, is $\pm 1\%$ of the nominal frequency for the UK's power system. The proposed technique is aimed at controlling the system frequency of different generic distribution systems by giving second by second responses from the DFIG. In the proposed control technique, the RSC controls the electromagnetic torque of the machine, as explained in the following. The

DFIG equations in the d-q reference frame have been discussed in Chapter 3, equations 3.9 to 3.12. The relationship between the rotor speed ω_r and the rotational speed of the synchronous reference frame ω_s is given in equation 6.9.

$$\omega_s = \left(\frac{2}{p}\right) \omega_r \quad (6.9)$$

Where p is the number of machine poles. Then, from equations 3.9 to 3.12, the delivered electromagnetic torque of the DFIG T_{em} is given in equation 6.10.

$$T_{em} = \left(\frac{3}{2}\right) \left(\frac{p}{2}\right) (I_{qs} \lambda_{ds} - I_{ds} \lambda_{qs}) \quad (6.10)$$

Where I_{ds} and λ_{ds} are the stator current and flux in the d-axis respectively, while I_{qs} and λ_{qs} are the current and flux in the q-axis respectively. The relationship between the electromagnetic torque of the DFIG and the rotational speed is given in equation 6.11, which also shows the relationship between the torque and the machine inertia.

$$J \frac{d\omega_s}{dt} = T_{mech} - T_{em} \quad (6.11)$$

Where J is the moment of inertia of the machine, T_{mech} is the mechanical torque which is the input to the generator and T_{em} is the electromagnetic torque which is the output of the generator. By rewriting equation 6.10 in rotor reference using equations 3.9 to 3.22, the electromagnetic torque can be given by equation 6.12.

$$T_{em} = \left(\frac{3}{2}\right) \left(\frac{p}{2}\right) \frac{L_m}{L_s} (I_{dr} \lambda_{qs} - I_{qr} \lambda_{ds}) \quad (6.12)$$

Where L_m and L_s are the magnetising mutual inductance and the self-inductance respectively. In order to control the electromagnetic torque T_{em} , it is desirable to assume $\lambda_{ds} = 0$, so the electromagnetic torque can be calculated from equation 6.13.

$$T_{em} = \left(\frac{3}{2}\right) \left(\frac{p}{2}\right) \frac{L_m}{L_s} I_{dr} \lambda_{qs} \quad (6.13)$$

The proposed technique to control frequency in the DFIG is shown in Figure 6.6. The gain parameters K_f and K_p are assumed to be 30 and 1 respectively for all simulation scenarios.

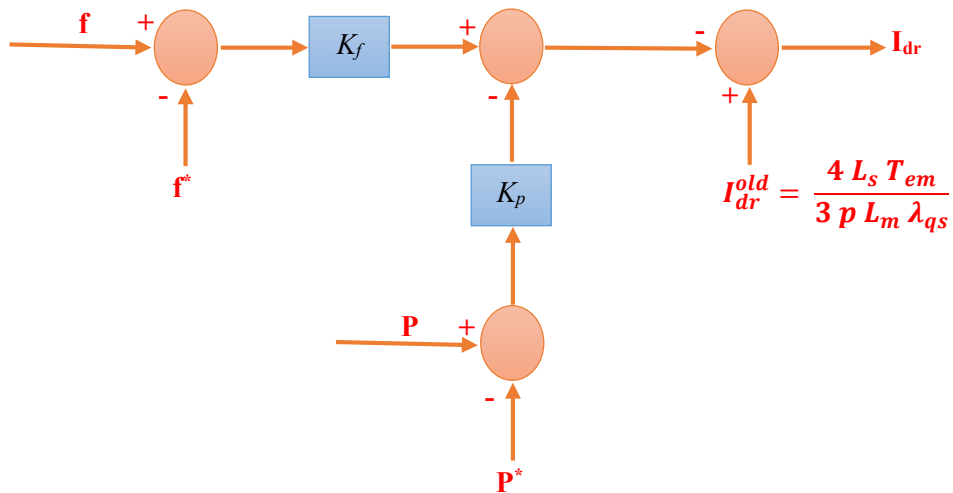


Figure 6.6: Proposed frequency control in DFIG.

6.6.2 Wind Turbine based on Synchronous Generator with Fully Rated Converters

In recent years, wind turbines based on synchronous generator with full-scale converters technology have been developed. The configuration of this technology is shown in Chapter 3. There are two back-to-back power electronic converters in this technology and each converter can control different parameters, as explained in Chapter 3. The frequency response from a wind based FRC generator is provided by the active power reduction method explained in Figure 6.5, based on Germany’s grid code requirements. Table 6.2 shows the FRC active power reduction requirements to provide the frequency response in various distribution test systems.

Table 6.2: FRC active power reduction parameters.

Starting active power reduction	50.2 Hz
Ending active power reduction	50.05 Hz
Gradient active power reduction	40 %/Hz
Minimal active power	0
Negative gradient for power change	-0.25
Positive gradient for power change	0.25

6.6.3 Solar Energy based on Photovoltaics

Photovoltaic technology converts solar energy into electricity and there are various different topologies, as discussed in Chapter 2. Frequency control from PV grid connected

systems will be discussed in this chapter based on de-loading PV units, which reduces their active power, to control system frequency for various generic distribution systems. This method is shown in Figure 6.5. PV active power reduction can be given in the same manner as FRC shown in Table 6.3, based on the new grid code requirements of Germany explained earlier.

Table 6.3: PV active power reduction parameters.

Starting active power reduction	50.2 Hz
Ending active power reduction	50.05 Hz
Gradient active power reduction	40 %/Hz
Minimal active power	0

6.7 Simulation Scenarios

This chapter investigates various generic distribution networks with high renewable energy penetration subject to over-frequency and under-frequency conditions. The frequency response of these systems will be discussed according to Germany's new grid code requirements discussed in section 6.3. The frequency should be within certain specified limits ($\pm 1\%$), as discussed earlier in this chapter. The German grid code for frequency response will be considered, as Germany has released new requirements for distributed generation connected to the grid. Three different distributed generation types based on renewable energy are considered, namely a wind turbine based on the DFIG, a wind turbine based on a synchronous generator with fully rated converters, and a solar energy source based on photovoltaics. The frequency response is investigated when the distribution systems experience a frequency disturbance, a sudden increase in load for under-frequency conditions and a sudden loss of load for over-frequency conditions. Three modified generic distribution networks are considered in this chapter, namely the IEEE 13 bus, IEEE 37 bus and IEEE 123 bus test systems. For each distribution network there are three different cases to control the frequency, as has been investigated earlier: inertia response, active power reduction and the proposed technique. To validate the frequency response of the selected distribution networks, simulations are performed using

two different types of software, MATLAB/SIMULINK and DIGSILENT POWERFACTORY.

6.7.1 IEEE 13 Bus Distribution System

The IEEE Power Engineering Society has published a number of test systems for distribution system analysis, one of which is called the IEEE 13 Node Test Feeder [195]. A schematic diagram of this system is shown in Figure 4.8. Detailed data regarding this system are given in Appendix B.1. The system is connected to the ac grid through a two winding ac transformer. Bus 650 is the bus which interconnects the grid with the test network. A summary of the IEEE 13 bus distribution network is shown in Chapter 4, Table 4.1. A CDG is assumed to be connected at bus number 611, which is one of the farthest nodes from the grid. Detailed data regarding this CDG are shown in Appendix C. The grid is assumed to be a synchronous generator based on fossil fuels and has the same parameters as the CDG. It is assumed to be the slack generator in the system. The DG based on renewable resources is connected to the farthest node from the grid, which is bus number 680.

The main objective of this chapter is to investigate the frequency control requirements of DGs based on renewable energy and the frequency response of distribution systems with high renewable energy penetration. Therefore, an under-frequency disturbance and an over-frequency disturbance are applied to investigate the frequency response of the test systems.

A- Traditional Frequency Response

In 13 bus distribution systems, under-frequency conditions are represented as a sudden increase in load at bus 680 (adding a 2 MW load) from 3 seconds to 3.5 seconds, while for over-frequency conditions a removal of loads equal to 2 MW which means disconnecting of load at buses 671 and 675 from the systems for 500 milliseconds between 3 seconds to 3.5 seconds. The frequency responses of the system without renewables for under-frequency and over-frequency conditions are shown in Figures 6.7 and 6.8 respectively. They show that the frequency exceeds the limits which are defined earlier between 50.5 Hz and 49.5 Hz.

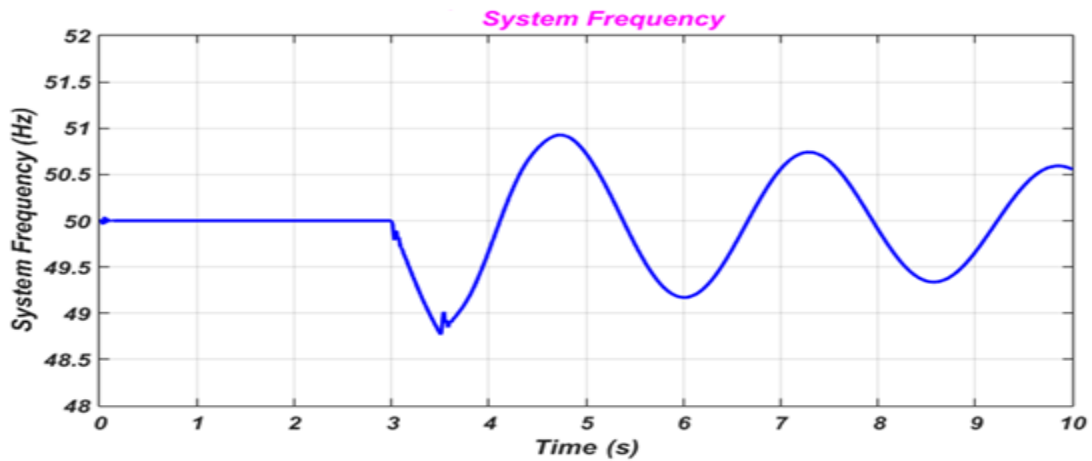


Figure 6.7: IEEE 13 bus system without renewable energy frequency response for under-frequency condition.

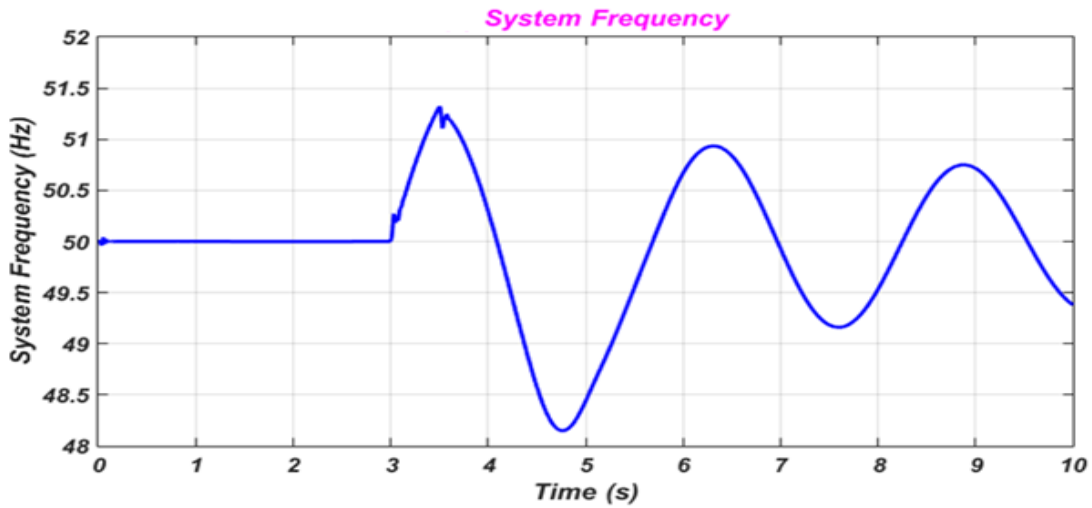


Figure 6.8: IEEE 13 bus system without renewable energy frequency response for over-frequency condition.

Adding a wind turbine based on the DFIG to bus 680 as a renewable source and adding an additional load with the same capacity on the same bus to ensure accuracy in the results are performed for the same reasons as mentioned in Chapters 4 and 5. DFIG control and parameters are given in Appendix D. The frequency response of the IEEE 13 bus system with renewable energy penetration for the defined under-frequency disturbance is illustrated in Figure 6.9. It shows that the increase in penetration of renewable energy based on the DFIG leads to a better frequency response and means the higher the renewable energy penetration the better the frequency response is. Figure 6.10 shows the

DFIG behaviour during and after the under-frequency condition. The frequency response of this test system with renewable energy penetration for the defined over-frequency condition is shown in Figure 6.11. In the same manner as the under-frequency case, the higher the renewable penetration the better the frequency response. The DFIG performance during and after the defined frequency disturbance is illustrated in Figure 6.12.

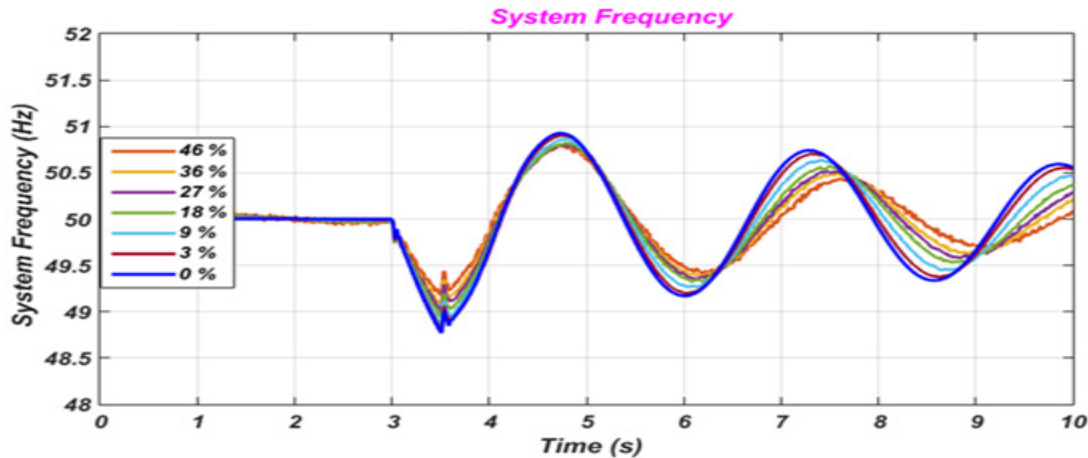


Figure 6.9: IEEE 13 bus system with renewable energy frequency response for under-frequency condition with different wind power penetration.

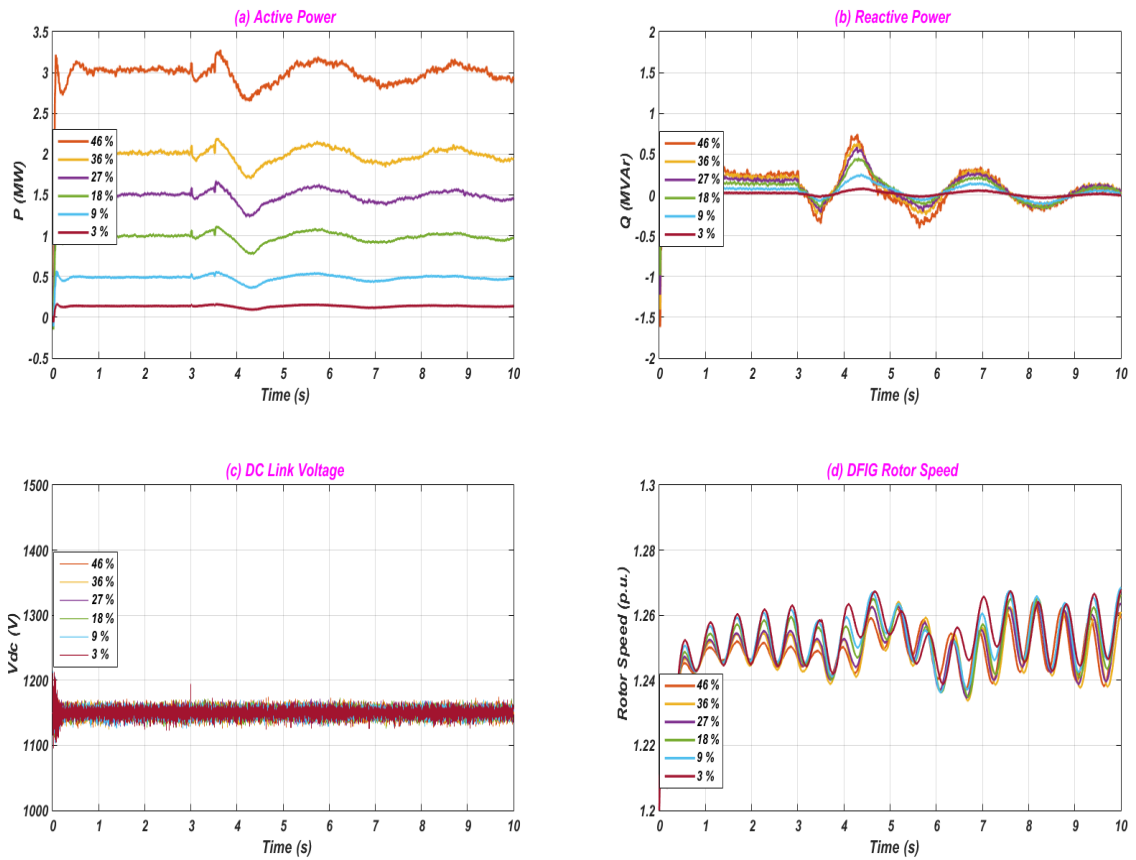


Figure 6.10: DFIG based wind energy performance during and after under-frequency condition with different wind power penetration - (a) active power, (b) reactive power, (c) DC link voltage, (d) rotor speed.

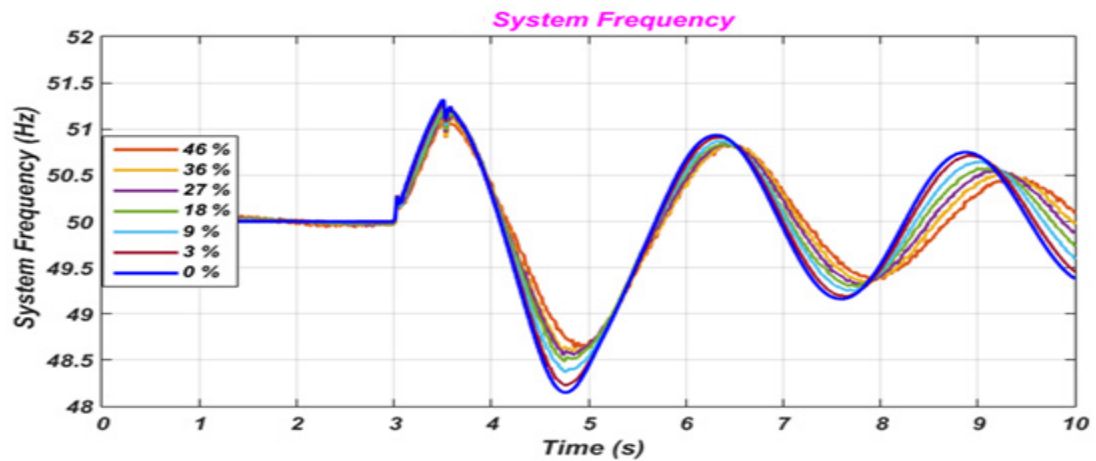


Figure 6.11: IEEE 13 bus system with renewable energy frequency response for over-frequency condition with different wind power penetration.

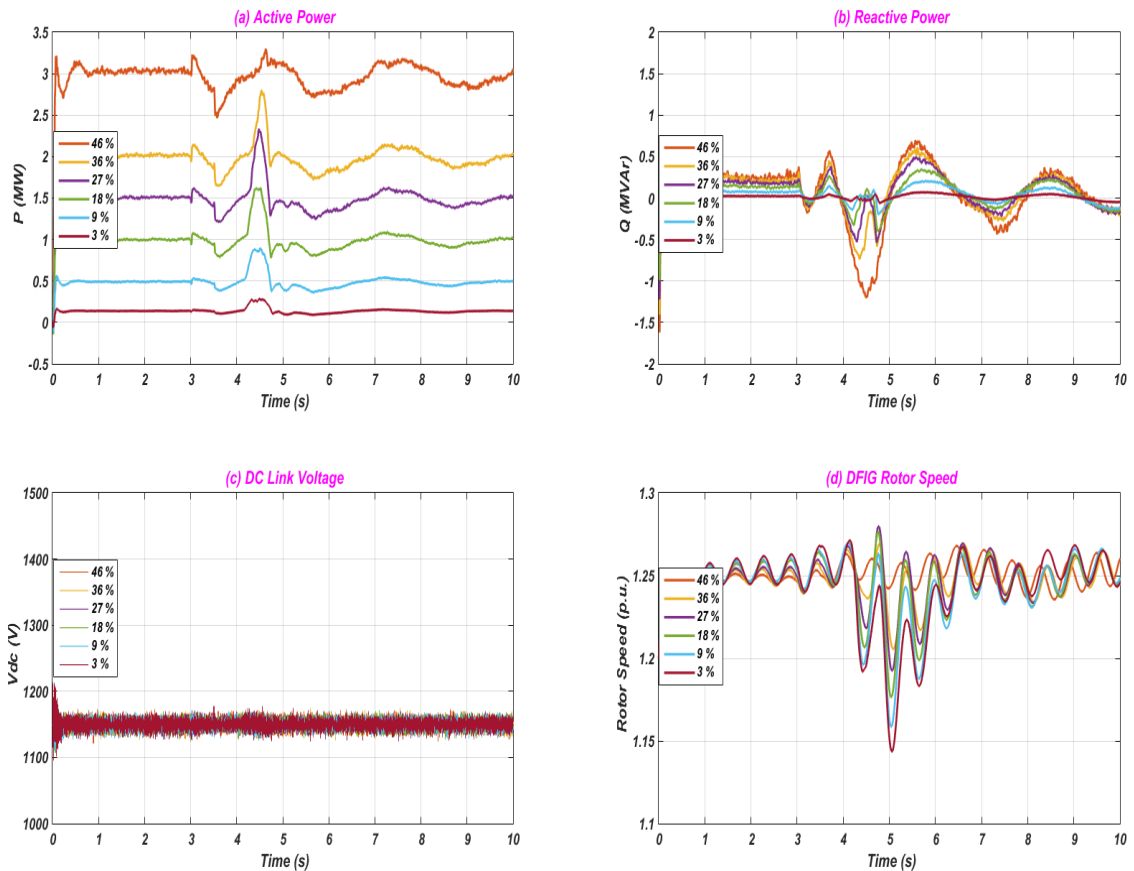


Figure 6.12: DFIG based wind energy performance during and after over-frequency condition with different wind power penetration - (a) active power, (b) reactive power, (c) DC link voltage, (d) rotor speed.

B- Active power reduction

In this method various distributed generations based on renewable energy will be considered. Renewable generating units are connected at bus 680 with a power output of 3.6 MW, representing 50 % of the total power generation in the IEEE 13 bus distribution systems. This percentage represents a high renewable energy penetration and it has been selected based on available data of the renewable generating units. There are five simulation cases, namely a base case without renewable energy, 50 % DFIG based wind penetration, 50 % wind FRC penetration, 50 % PV penetration, and 50 % mixed renewable energy sources, which represents 1.5 MW DFIG, 1.1 MW PV and 1 MW FRC. The active power reduction technique discussed earlier will be used to observe the frequency response when the distribution systems experience a frequency disturbance. An under-frequency condition is assumed in this case by increasing all load demands in the test

system by 100 % from 3 seconds to 3.5 seconds, while a sudden decrease in demand by 100 % represents the over-frequency condition. The frequency responses of the IEEE 13 bus system for different renewable energy scenarios are shown in Figure 6.13 for the under-frequency condition and in Figure 6.14 for the over-frequency condition. These figures show that the frequency response of the system with renewable energy penetration is better; however, it varies from one technology to another according to the defined active power gradient limiters shown in section 6.6.

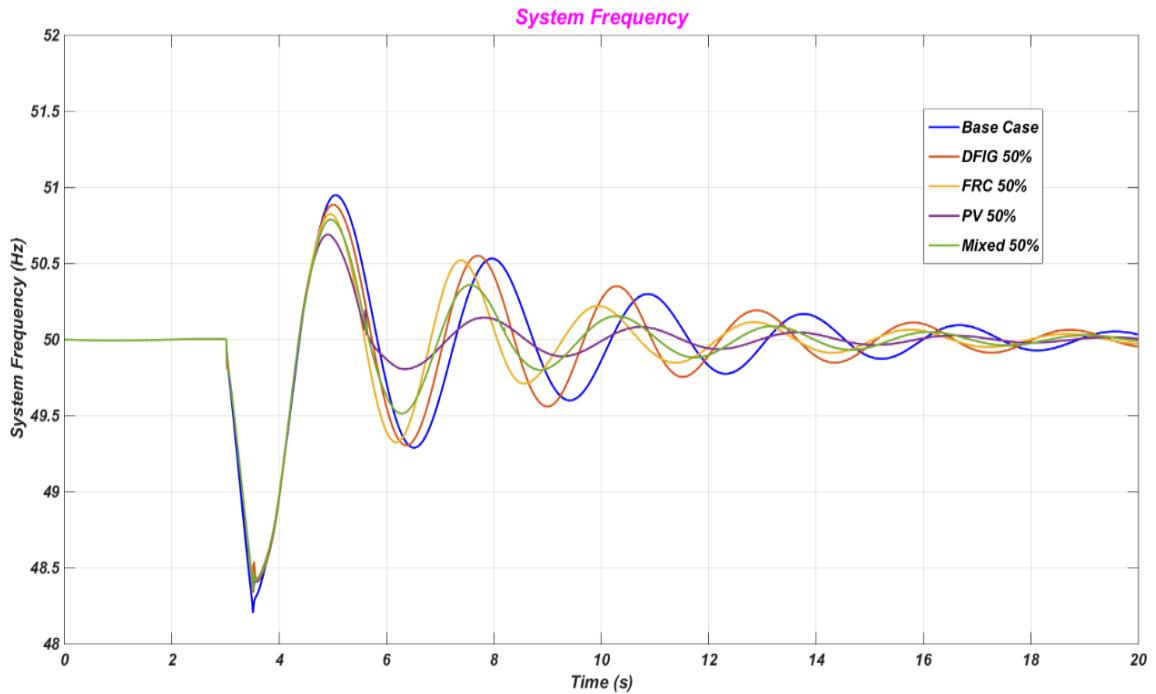


Figure 6.13: The frequency response of the IEEE 13 bus system with high renewable energy penetration using the active power reduction method for the under-frequency condition.

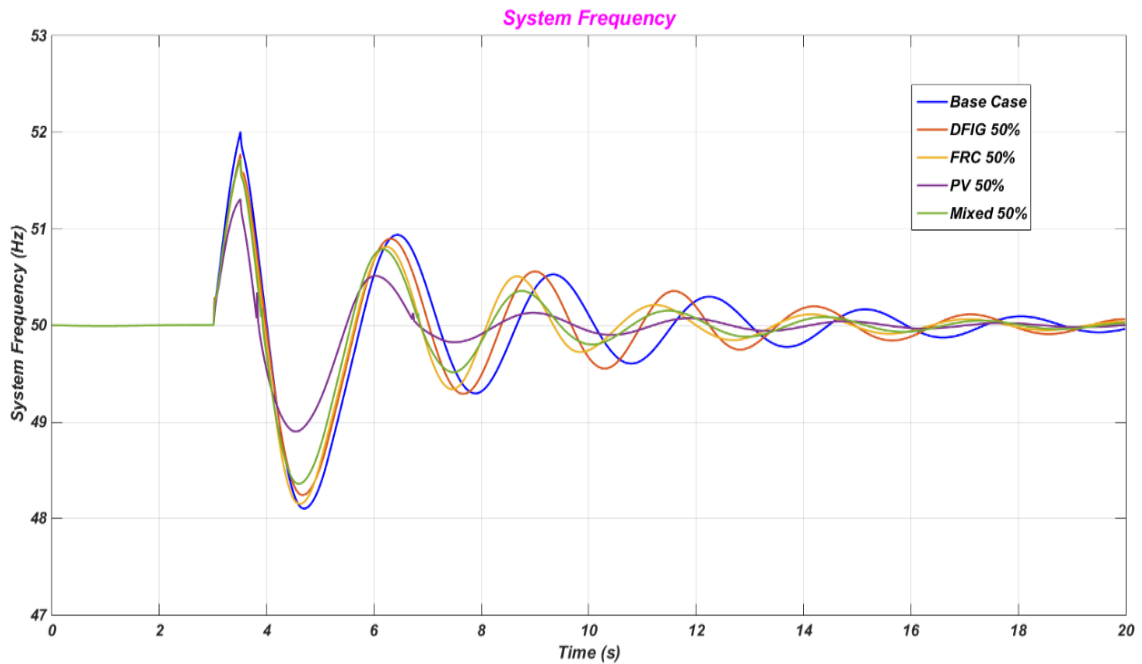


Figure 6.14: The frequency response of the IEEE 13 bus system with high renewable energy penetration using the active power reduction method for the over-frequency condition.

C- A proposed new frequency control technique

As shown earlier, the proposed technique will be applied on a wind turbine based on the DFIG. In this section the simulation results obtained in section A will be compared to the frequency response controlled by the new frequency control applied to the DFIG unit. The penetration percentage will be fixed in this section. The frequency response of the test system at certain penetrations in section A will be compared to the same penetration level of the DFIG in this section. The penetration level which has been selected for the renewable energy based on the DFIG is 27 %. The same frequency disturbances as in section A are used here to investigate the frequency response of the test systems with the proposed frequency control for the DFIG. The frequency responses for the IEEE 13 bus system with 27 % penetration of wind based on the DFIG for under-frequency and over-frequency conditions are shown in Figures 6.15 and 6.16 respectively. They show that the proposed frequency control of the DFIG is effective and improves the frequency of the system considerably. They also show that the system frequency returns to acceptable limits in a short period of time.

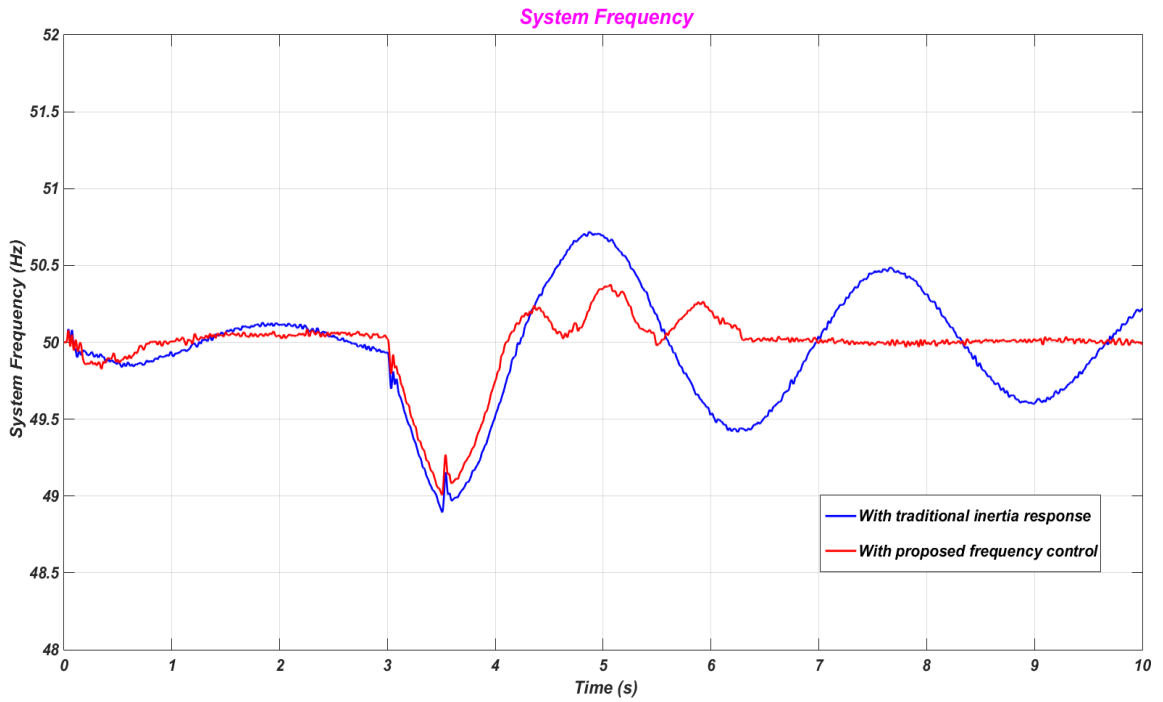


Figure 6.15: The proposed frequency response of the IEEE 13 bus system with high DFIG penetration for the under-frequency condition.

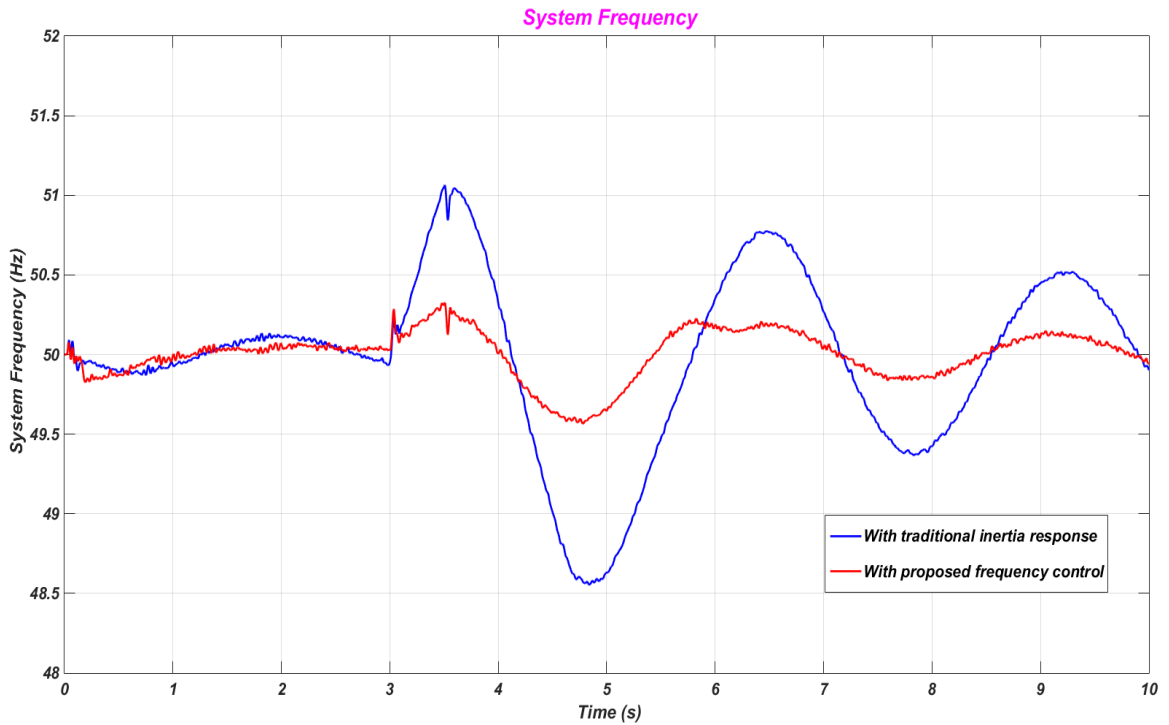


Figure 6.16: The proposed frequency response of the IEEE 13 bus system with high DFIG penetration for the over-frequency condition.

6.7.2 IEEE 37 Bus Distribution System

The IEEE 37 Node Test Feeder is another system published by the IEEE Power Engineering Society for distribution system analysis [195]. A schematic diagram of this system is shown in Chapter 4, Figure 4.23. Detailed data regarding this system are given in Appendix B.2. The system is connected to the ac grid through a two winding ac transformer. Bus 799 is the bus which interconnects the grid with the test network. This bus has been selected because it is directly connected to the grid through a transformer, which is named the substation. A summary of the data for the IEEE 37 bus distribution system is given in Table 4.6. A CDG is assumed to be connected at bus number 740, which is one of the farthest nodes from the grid. Detailed data regarding this CDG are shown in Appendix C. The grid is assumed to be a synchronous generator based on fossil fuels with the same parameters as the CDG. However, it is assumed to be a slack generator. The DG based on renewable resources is connected to the farthest node from the grid, which is bus number 741. The same test procedure used in section 6.7.1 for the IEEE 13 bus system is used in this section for the IEEE 37 bus network. Therefore, the system frequency responses will be investigated when the system experiences different frequency disturbances, namely under- and over-frequency disturbances.

A- Traditional Frequency Response

A sudden increase in load at bus 711 (adding a 1.034 MW load) from 3 seconds to 3.5 seconds and a sudden removal of loads equal to 1.034 MW, which means disconnection of load at buses 729, 730, 731, 732, 733, 734, 735, 736, 737, 738, 740, 741, 742, and 744 from the systems for 500 milliseconds from 3 seconds to 3.5 seconds are the under-frequency and over-frequency conditions used to study the frequency responses of the IEEE 37 bus distribution system. The frequency responses of the 37 bus system without renewable energy penetration for under-frequency and over-frequency conditions are illustrated in Figures 6.17 and 6.18 respectively. They show that the system frequency exceeds the limits, which have been defined earlier as between 50.5 Hz and 49.5 Hz during and after the frequency disturbance.

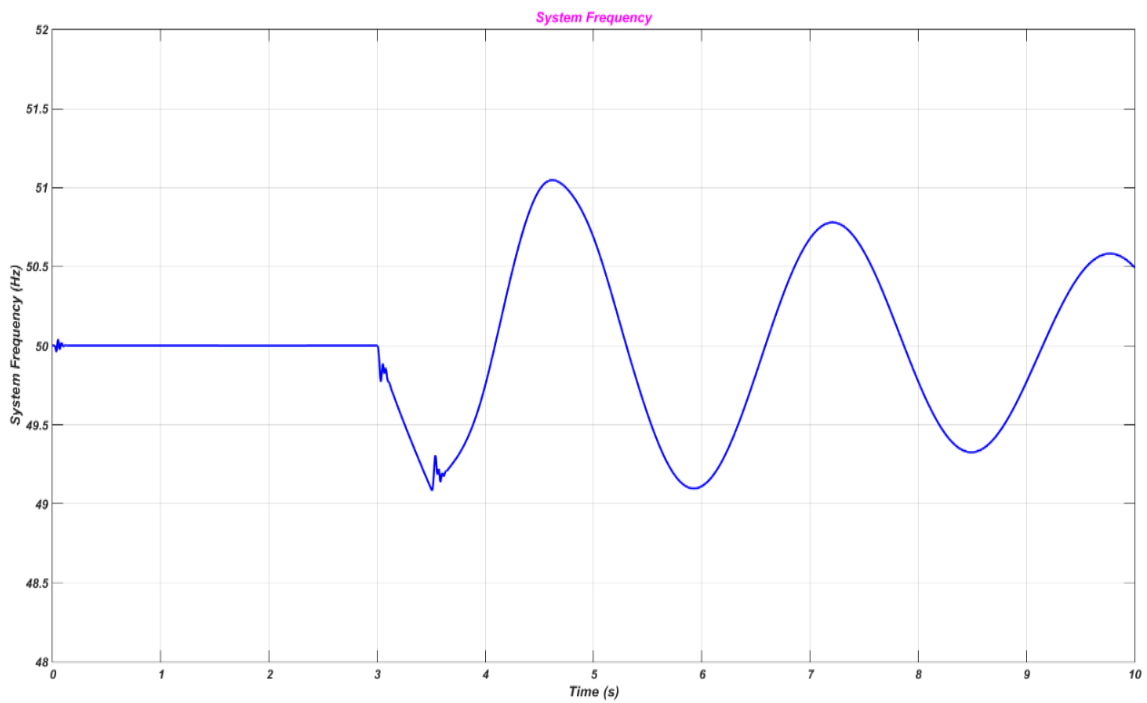


Figure 6.17: IEEE 37 bus system without renewable energy frequency response for under-frequency condition.

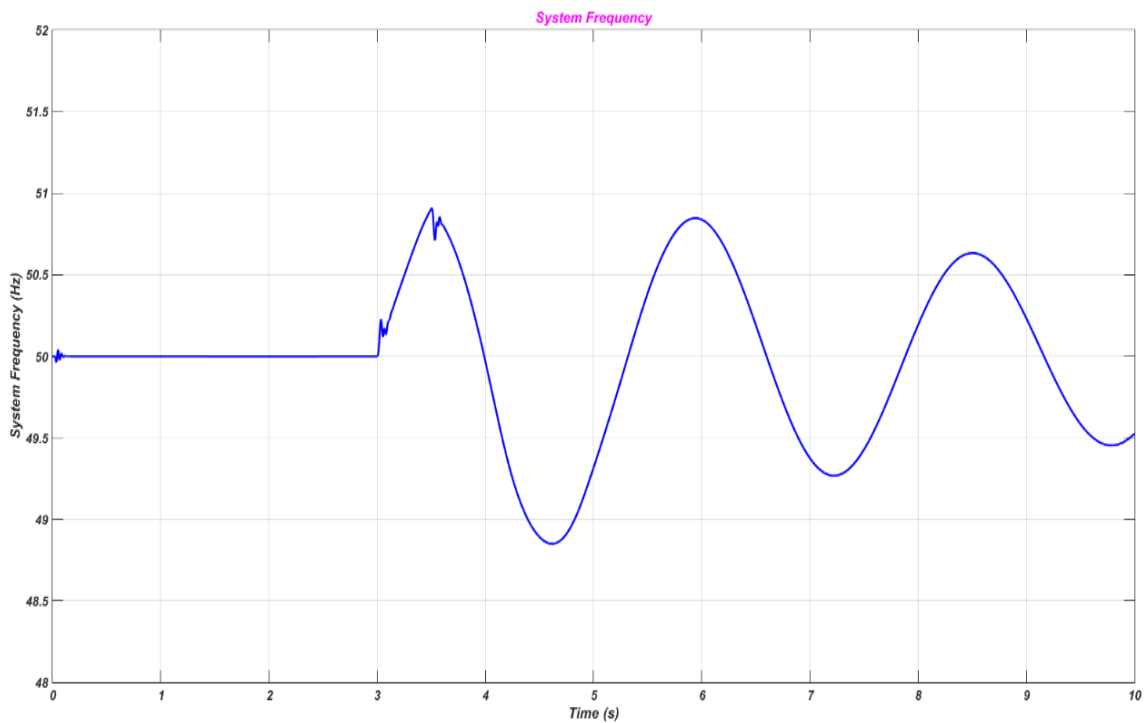


Figure 6.18: IEEE 37 bus system without renewable energy frequency response for over-frequency condition.

Similar to the approach used in the IEEE 13 bus system, after adding a wind source based on the DFIG to the IEEE 37 bus system at bus 741, the frequency response will be changed from the case of no renewable penetration in the system. A new load is added at the same bus equal to the installed DFIG output power to ensure accuracy in the simulation results for the reason as mentioned in Chapters 4 and 5. The frequency response of the IEEE 37 bus system with wind energy penetration for the defined under-frequency disturbance is shown in Figure 6.19. It shows that the increase in penetration of wind energy provides an improved frequency response. Figure 6.19 also shows the DFIG behaviour during and after the under-frequency condition. The frequency response of the test system with the DFIG based wind penetration for the defined over-frequency condition is shown in Figure 6.20. It also shows that the frequency response of the IEEE 37 bus system is improved after increasing the penetration of the wind energy based on the DFIG during and after the over-frequency condition. The DFIG performance during and after the defined over-frequency disturbance is also illustrated in Figure 6.20.

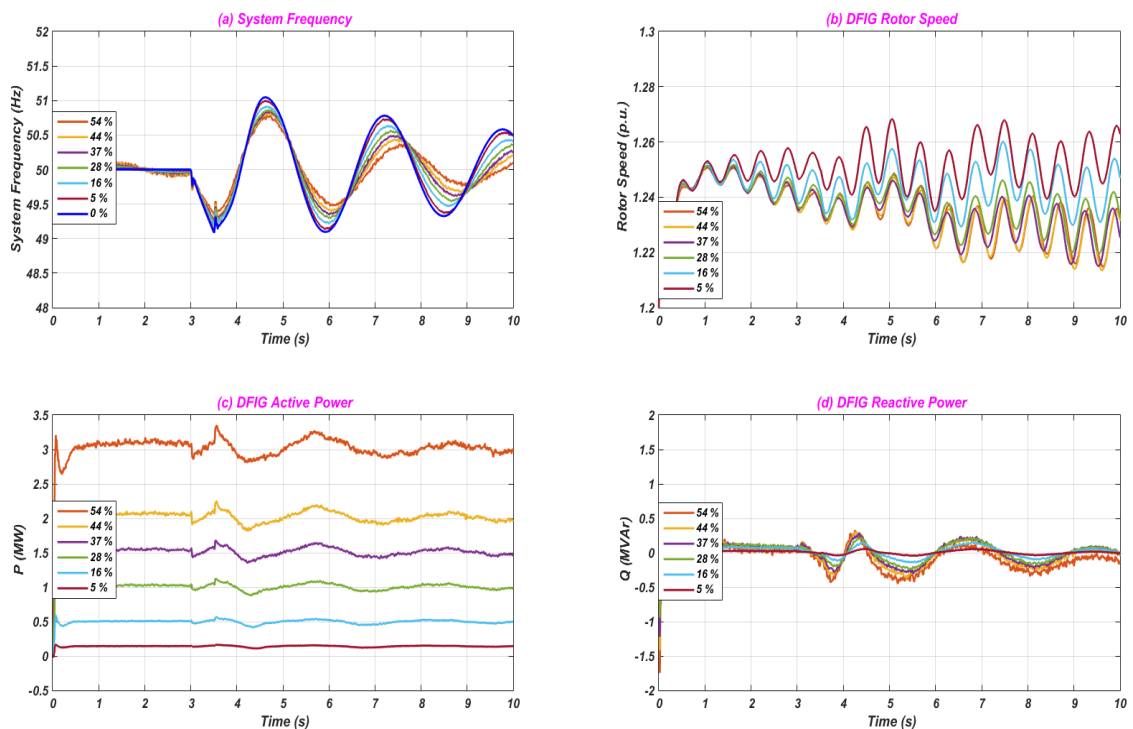


Figure 6.19: IEEE 37 bus system with renewable energy frequency response for under-frequency condition with different wind power penetration - (a) system frequency, (b) DFIG rotor speed, (c) DFIG active power, (d) DFIG reactive power.

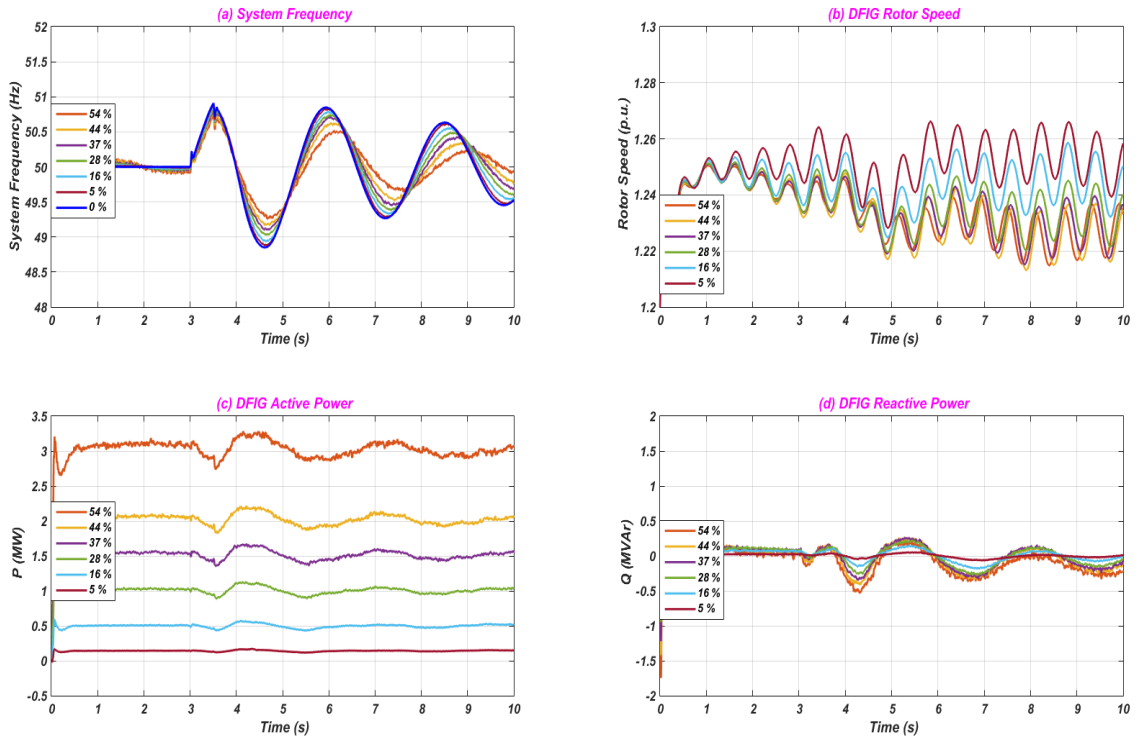


Figure 6.20: IEEE 37 bus system with renewable energy frequency response for over-frequency condition with different wind power penetration - (a) system frequency, (b) DFIG rotor speed, (c) DFIG active power, (d) DFIG reactive power.

B- Active power reduction

The same test procedure used for the IEEE 13 bus system in section 6.7.1 for the active power reduction scenario is implemented in this section to study the frequency response of the IEEE 37 bus distribution system. An under-frequency condition is assumed in this case to be an increase in load demand in the test system by 100 % from 3 seconds to 3.5 seconds, while a sudden decrease in demand by 100 % represents the over-frequency condition. The frequency responses of the IEEE 37 bus system for various renewable energy scenarios are shown in Figure 6.21 for the under-frequency condition and in Figure 6.22 for the over-frequency condition. It is shown in these figures that the frequency response of the IEEE 37 bus distribution system with renewable energy sources is better; however, it is different from one technology to another according to the defined active power gradient limiters shown in section 6.6.

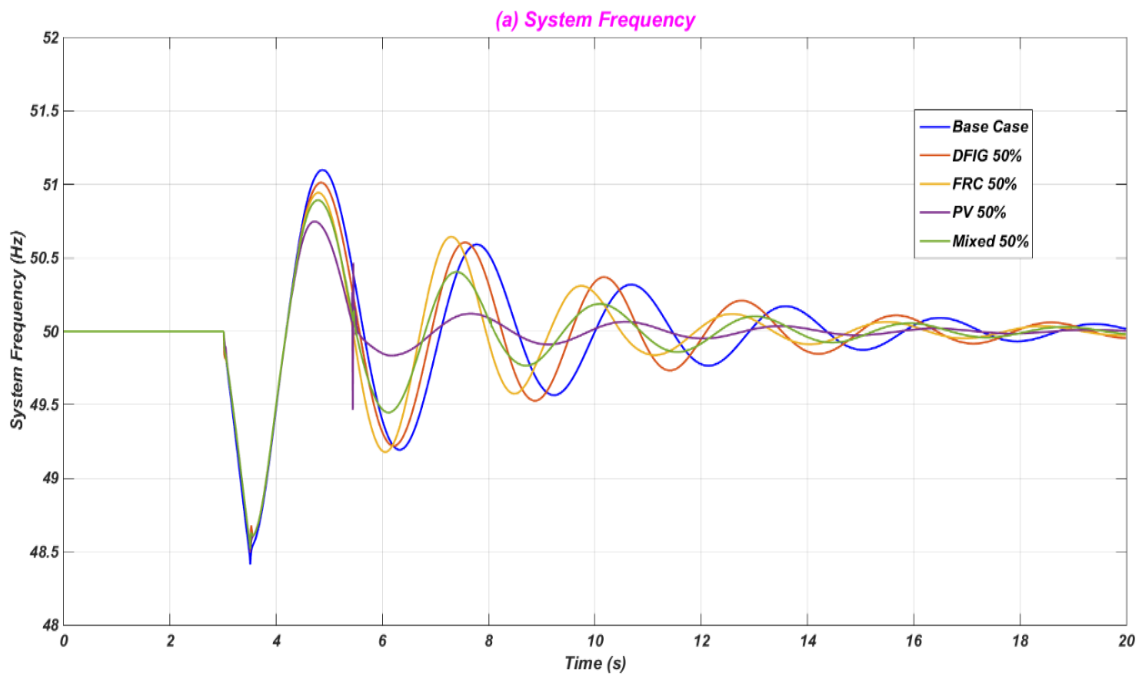


Figure 6.21: The frequency response of the IEEE 37 bus system with high renewable energy penetration using the active power reduction method for the under-frequency condition.

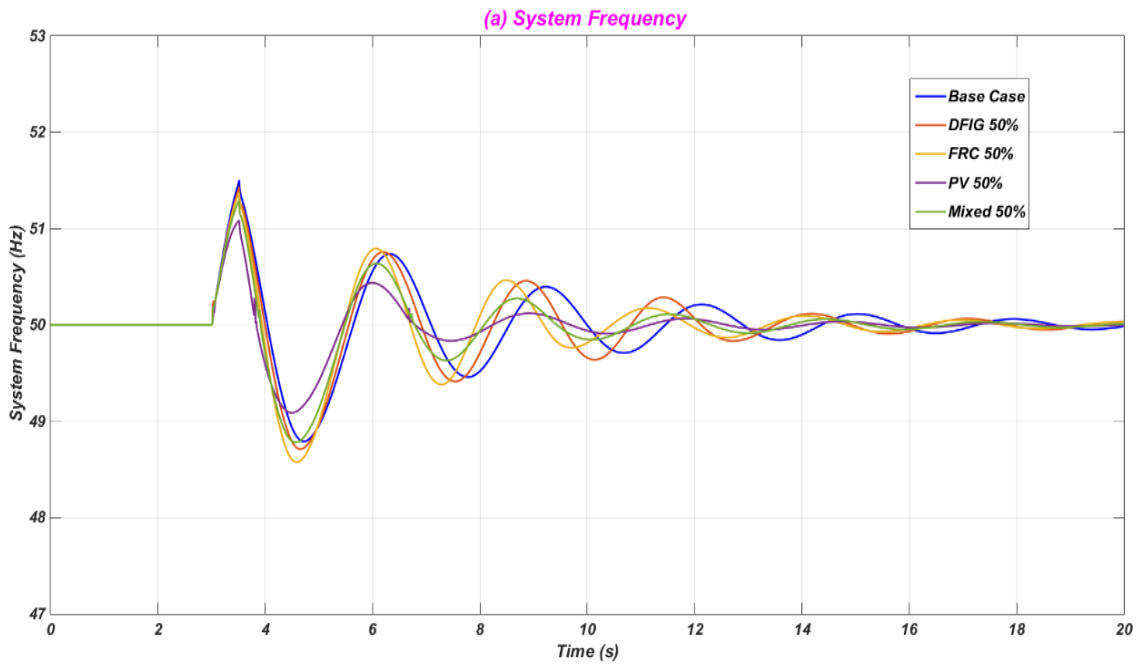


Figure 6.22: The frequency response of the IEEE 37 bus system with high renewable energy penetration using the active power reduction method for the over-frequency condition.

C- A proposed new frequency control technique

As shown in the IEEE 13 bus system, the proposed technique will be applied on a wind turbine based on the DFIG. In this section, the simulation results for the frequency response of the IEEE 37 bus system obtained in section A will be compared with the frequency response obtained after applying the new frequency control of the DFIG unit. The penetration level which has been selected for the wind energy based on the DFIG is 37 % in both cases with a traditional frequency response and with the proposed frequency control technique. The same frequency disturbances as in section A are applied here to study the frequency response of the 37 test system with the proposed frequency control for the DFIG. The frequency responses of the IEEE 37 bus distribution system with 37 % wind energy penetration for under-frequency and over-frequency conditions are illustrated in Figures 6.23 and 6.24 respectively. From these figures it is clear that the proposed frequency control for the DFIG based wind energy is effective and enhances the frequency of the system considerably. The system frequency also returns to acceptable limits in a short period of time.

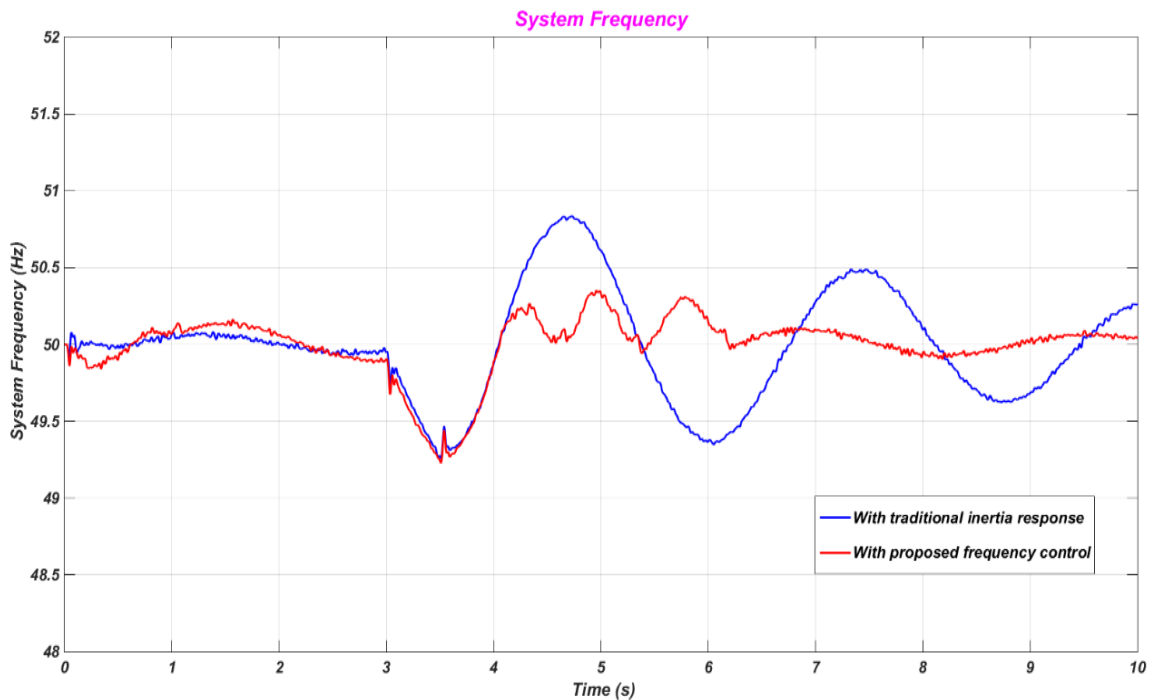


Figure 6.23: The proposed frequency response of the IEEE 37 bus system with high DFIG penetration for the under-frequency condition.

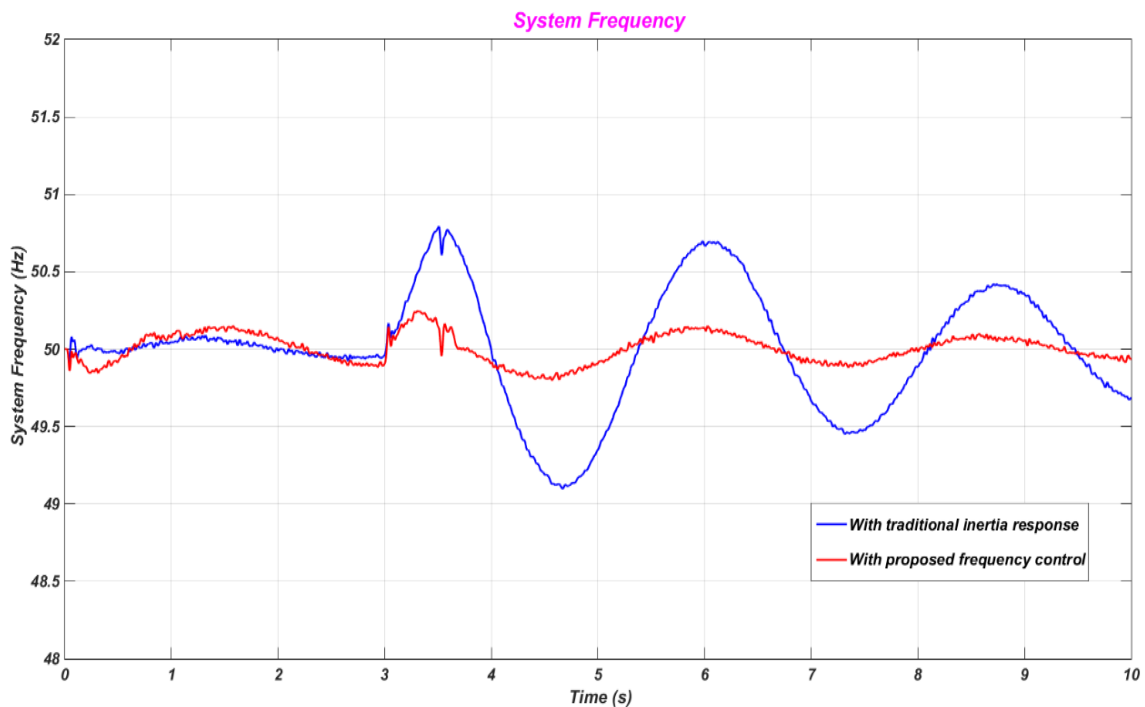


Figure 6.24: The proposed frequency response of the IEEE 37 bus system with high DFIG penetration for the over-frequency condition.

6.7.3 IEEE 123 Bus Distribution System

The IEEE 123 Node Test Feeder is a test system published by the IEEE Power Engineering Society for distribution system analysis [195]. A schematic diagram of this system is shown in Chapter 4, Figure 4.34. Detailed data regarding this system are given in Appendix B.3. The system is connected to the ac grid through a two winding ac transformer. Bus 150 is the bus which interconnects the grid with the test network. A summary of data regarding the IEEE 123 bus distribution system is given in Table 4.11. A CDG is assumed to be connected at bus number 96, which is one of the farthest nodes from the grid. Detailed data regarding this CDG are illustrated in Appendix C. The grid is assumed to be a synchronous generator based on fossil fuel, with the same parameters as the CDG. However, it is assumed to be a slack generator. The distributed generation based on renewable resources is connected to one of the farthest nodes from the grid, namely bus 114. The same test procedure used in section 6.7.1 for the IEEE 13 bus system and in section 6.7.2 for the IEEE 37 bus system is used in this section for the IEEE 123 bus

distribution system. The system frequency response will be studied when the system is subjected to different frequency disturbances, under- and over-frequency disturbances.

A- Traditional Frequency Response

A sudden increase in load at bus 108 (adding a 1.99 MW load) from 3 seconds to 3.5 seconds and a sudden removal of load equal to 1.99 MW, which means disconnection of load at buses 1, 4, 6, 9, 11, 16, 19, 20, 22, 24, 28, 29, 30, 33, 34, 35, 37, 43, 50, 52, 53, 62, 63, 69, 71, 47, 48, 49, 64, 65, 66, and 76 from the systems for 500 milliseconds from 3 seconds to 3.5 seconds are the under-frequency and over-frequency conditions used to study the frequency responses of the IEEE 123 bus network. The frequency responses of the 123 bus system without wind energy penetration for under-frequency and over-frequency conditions are shown in Figures 6.25 and 6.26 respectively. They show that the system frequency exceeds the acceptable limits, which are defined by the grid codes, between 50.5 Hz and 49.5 Hz during and after the frequency disturbance.

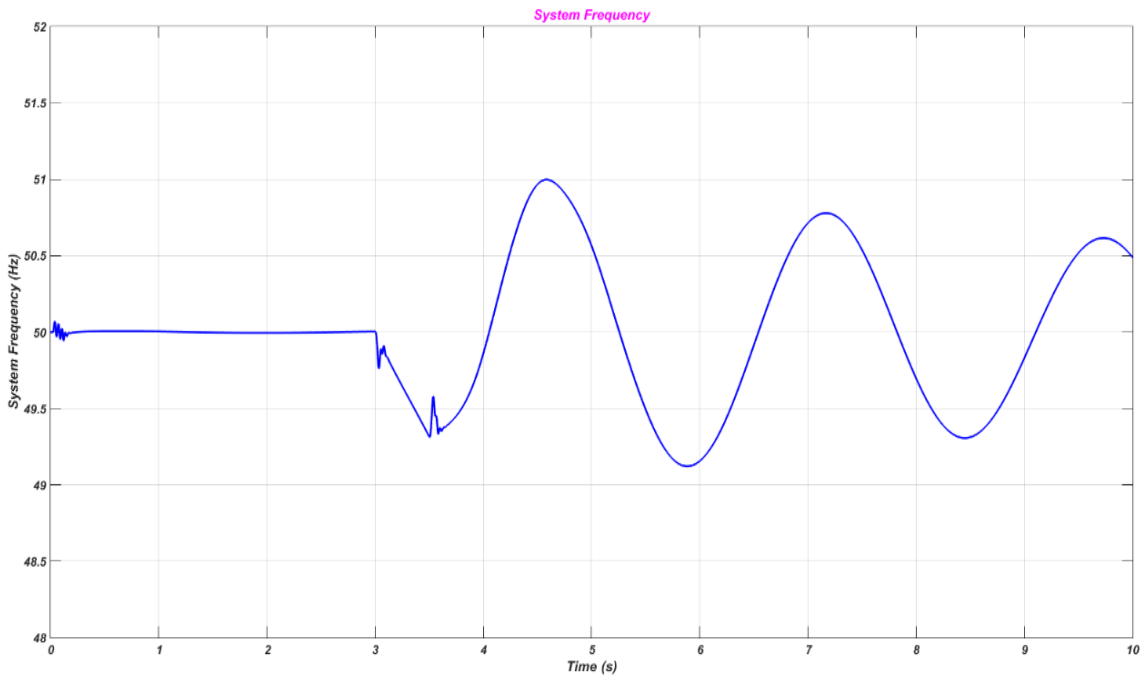


Figure 6.25: IEEE 123 bus system without renewable energy frequency response for under-frequency condition.

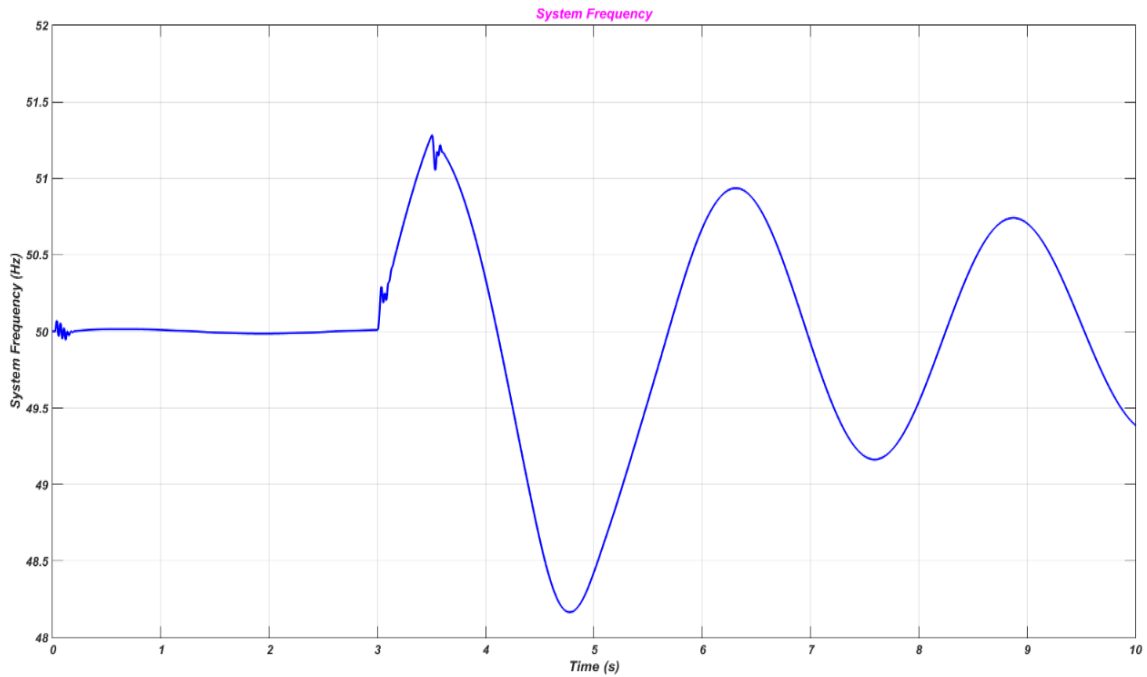


Figure 6.26: IEEE 123 bus system without renewable energy frequency response for over-frequency condition.

After adding a wind energy source based on the DFIG to the IEEE 123 bus system at bus 114, the frequency response will be changed from having no wind penetration in the distribution system. A new load is added at the same bus equal to the installed wind source output power to ensure accuracy in the simulation results for the reason mentioned in Chapters 4 and 5. The frequency response of the IEEE 123 bus distribution system with different wind penetration for the defined under-frequency disturbance is shown in Figure 6.27. It shows that the increase in penetration of renewable energy based on the DFIG improves the frequency response. Figure 6.27 also shows the DFIG performance during and after the under-frequency condition. The frequency response of this distribution system with DFIG penetration for the defined over-frequency condition is shown in Figure 6.28. It also shows that the frequency response of the IEEE 123 bus distribution system is enhanced after increasing the penetration of wind based on the DFIG during and after the over-frequency condition. The DFIG behaviour during and after the defined over-frequency disturbance is also illustrated in Figure 6.28.

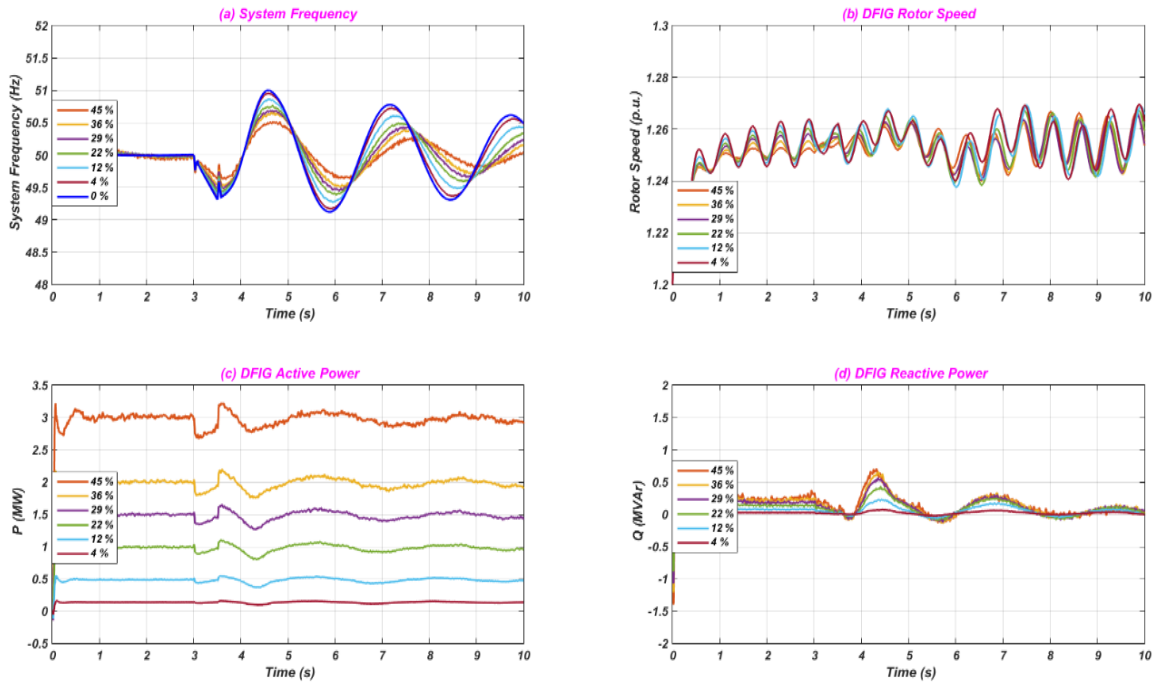


Figure 6.27: IEEE 123 bus system with renewable energy frequency response for under-frequency condition with different wind power penetration - (a) system frequency, (b) DFIG rotor speed, (c) DFIG active power, (d) DFIG reactive power.

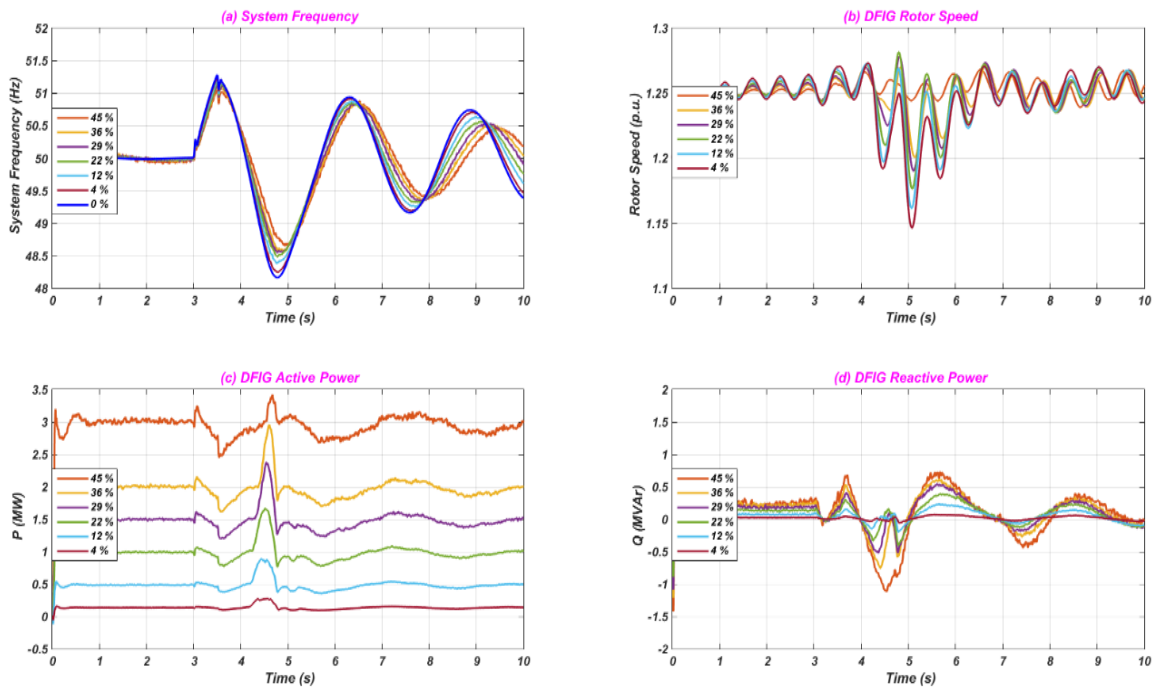


Figure 6.28: IEEE 123 bus system with renewable energy frequency response for over-frequency condition with different wind power penetration - (a) system frequency, (b) DFIG rotor speed, (c) DFIG active power, (d) DFIG reactive power.

B- Active power reduction

The same test procedure used for both the IEEE 13 bus and IEEE 37 bus distribution systems for the active power reduction case is used in this section to study the frequency response of the IEEE 123 bus network. An under-frequency condition is assumed in this case to be an increase in load demand in the test system by 100 % from 3 seconds to 3.5 seconds, while a sudden decrease in demand by 100 % represents the over-frequency condition. The frequency responses of the IEEE 123 bus system for various renewable energy cases are shown in Figure 6.29 for the under-frequency condition and in Figure 6.30 for the over-frequency condition. It can be seen in these figures that the frequency response of the IEEE 123 bus system with high renewable energy penetration is improved. However, the behaviour is different from one technology to another based on the defined active power gradient limiters shown in section 6.6.

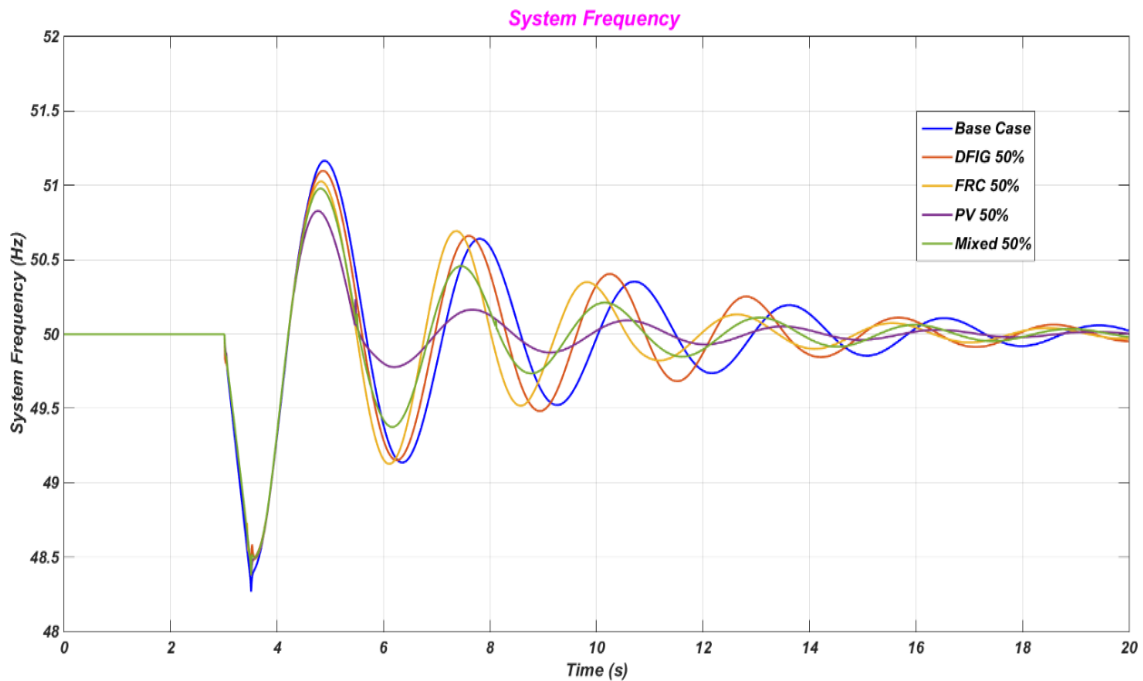


Figure 6.29: The frequency response of the IEEE 123 bus system with high renewable energy penetration using the active power reduction method for the under-frequency condition.

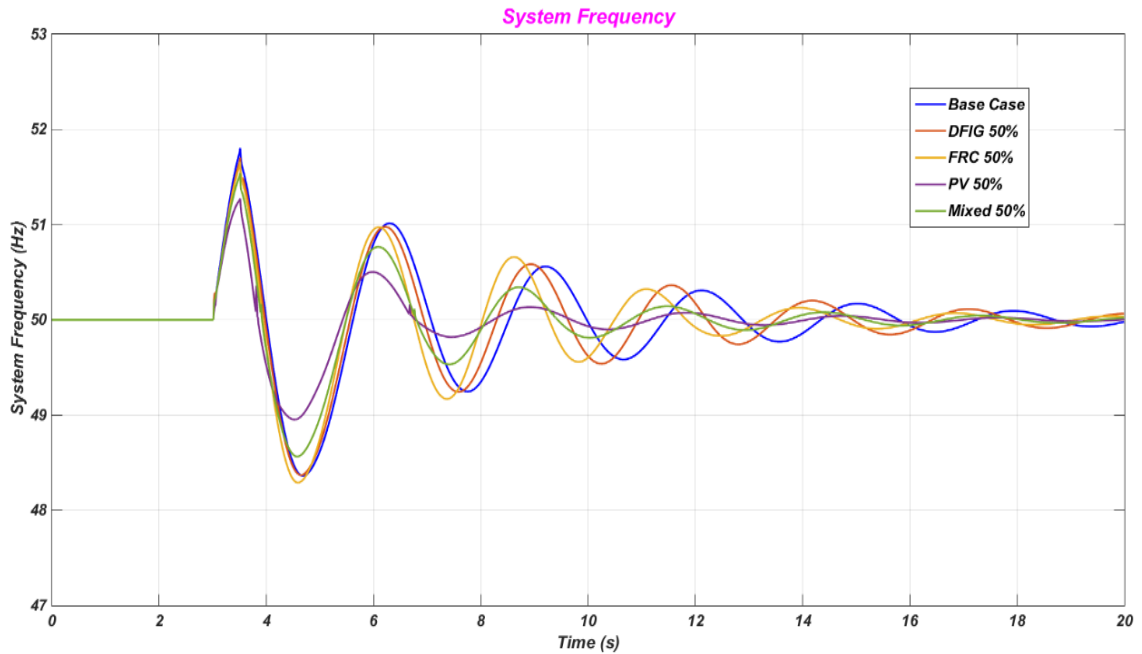


Figure 6.30: The frequency response of the IEEE 123 bus system with high renewable energy penetration using the active power reduction method for the over-frequency condition.

C- A proposed new frequency control technique

As with the previous test systems, the IEEE 13 bus and the IEEE 37 bus, the proposed technique will be applied on a wind turbine based on the DFIG. In this section, the simulation results for the system frequency response of the IEEE 123 bus system obtained in section A will be compared with the system frequency response obtained after applying the new controller for the DFIG unit frequency. The penetration level which has been used for the DFIG based wind is 29 % for both cases with a traditional frequency response and with the proposed frequency control method. The same frequency disturbances as in section A are applied in this section to investigate the frequency response of the 123 distribution system with the proposed frequency method for the DFIG. The frequency responses of the IEEE 123 bus network with 29 % penetration of the DFIG based on wind for under-frequency and over-frequency conditions are shown in Figures 6.31 and 6.32 respectively. From these figures it is clear that the proposed frequency method for the wind turbine based on the DFIG is effective and improves the frequency of the test system considerably. The system frequency also returns to its given limits in a short period of time.

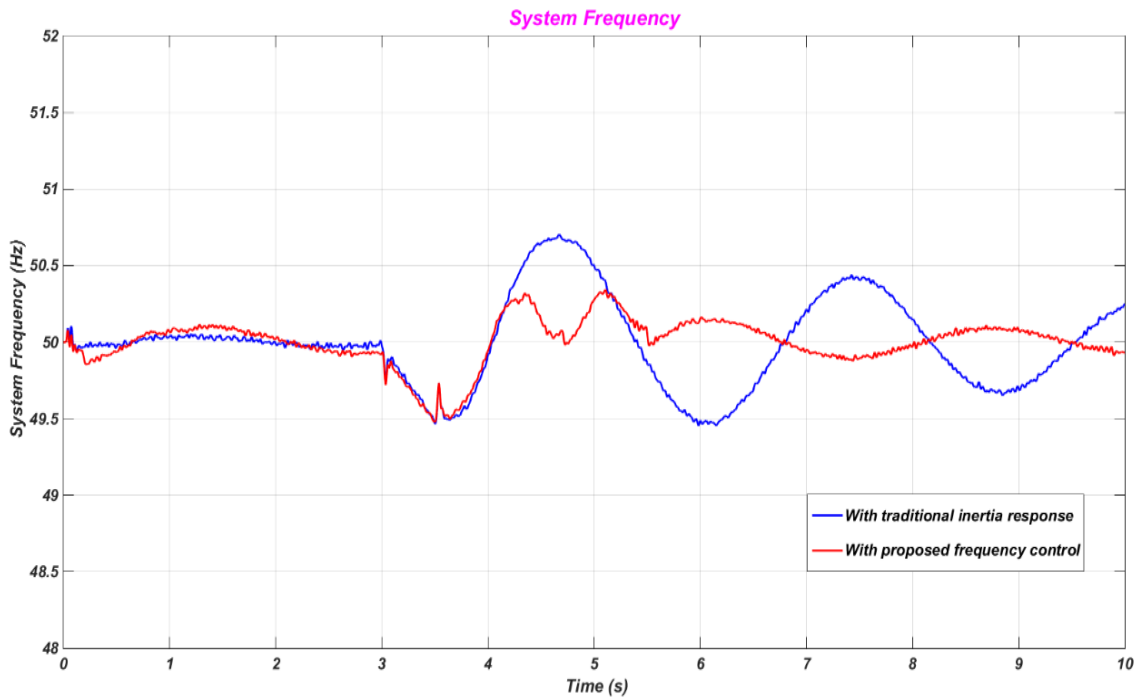


Figure 6.31: The proposed frequency response of the IEEE 123 bus system with high DFIG penetration for the under-frequency condition.

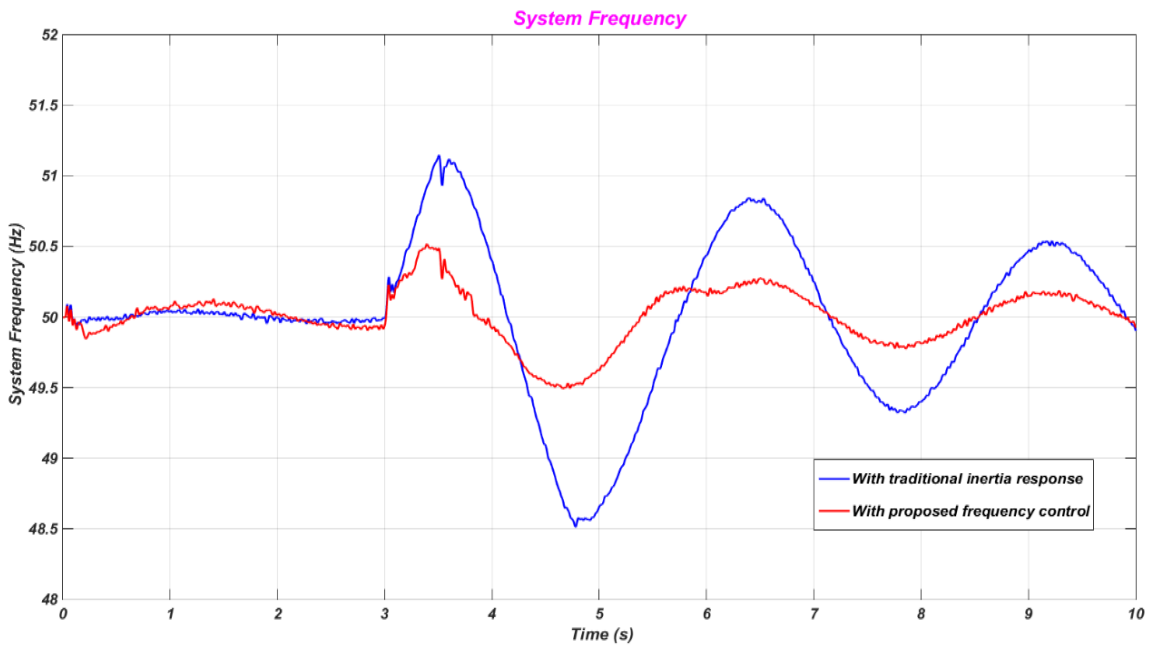


Figure 6.32: The proposed frequency response of the IEEE 123 bus system with high DFIG penetration for the over-frequency condition.

6.8 Conclusions

The rapid increase in renewable energy penetration in power systems has led to various technical, economic and regulatory concerns. Due to the dramatic growth in renewable energy sources in power systems, several countries have released grid code requirements for renewable energy sources. A frequency response requirement is one such grid codes which has been introduced in recent years. This chapter has discussed the frequency response of different renewable energy sources based on wind and solar energy. It has been shown how different frequency controls have been proposed in literature, including inertia response, active power curtailment and the frequency droop control technique. All these control methods have been implemented on large power systems. However, due to the dramatic increase in the penetration of distributed generation based on wind and solar energy in distribution systems, it is significant to investigate the frequency response of such systems. This chapter has studied the frequency responses of various generic distribution systems with high renewable energy penetration. Active power reduction and traditional inertia control techniques have been discussed in relation to these systems for various renewable energy technologies, namely a wind turbine based on the DFIG, a wind turbine based on a synchronous generator with fully rated converters, and solar energy based on photovoltaics. A proposed frequency control technique for DFIG based wind energy has been discussed in relation to various distribution systems. The simulation results show that the proposed frequency control improves the system frequency response when the test systems experience under- and over-frequency conditions.

CHAPTER 7 Effect of Renewable Generation in Distribution Networks on Grid Power Factor

7.1 Introduction

The development of renewable energy technologies has been significant in tackling the rapid increase in greenhouse gas emissions, such as carbon dioxide (CO₂). To reduce carbon footprints and help solve climate change problems, various solutions should be considered, such as promoting renewable energy resources in power systems. In the last few years, there has been substantial growth in the development and utilization of renewable energy sources such as wind power, solar energy based on photovoltaics (PV), fuel cells, biomass and geothermal energy. Among these renewable resources, wind and solar technologies have attracted the attention of researchers and investors due to their great potential and features. They are potentially abundant sources of energy and they are sustainable, clean (pollution free) and environmentally friendly.

Notwithstanding, increasing the penetration of renewable units in distribution systems has led to voltage variations due to an increase in active power generation. Nowadays, wind and solar units are commonly connected to distribution systems at unity power factors, which means the injection of real power can affect voltages around the point of common coupling (PCC). Therefore, DGs based on renewable energy can be used to mitigate overvoltages, which means absorbing or injecting reactive power to regulate voltages within acceptable limits. Voltage support equipment, such as capacitor banks and static var compensators (SVC), can also be used; however, the renewables' intermittent nature can cause frequent tap changes which may increase the stress on such equipment and require extra maintenance costs.

High penetration levels of renewable units in distribution systems also brings about several challenges for distribution network operators (DNOs). Frequent changes in solar irradiance and wind speed may cause disturbances to the grid, such as voltage sags and swells. These issues cannot be solved by slow responding equipment such as capacitor

banks, which may result in power quality problems. Fast responding equipment such as D-STATCOM is considered an alternative solution; however, it is expensive for owners of small wind and solar units. Renewable generating units with a VAR injection and consumption capability can provide the required reactive power to maintain voltage regulation within acceptable limits of $\pm 5\%$ [227]. Providing voltage control and reactive power supported by local distributed generators such as wind and solar can minimize thermal losses and optimize the operation and management of distribution networks, as well as reduce the cost of installing reactive power compensation equipment in local grids, by utilizing the available reactive power of renewable generating units. This chapter investigates the reactive power support of various renewable resources in different distribution systems and studies the impact of high renewable energy penetration on the grid system power factor.

7.2 Reactive Power Background

Reactive power is essential to maintain the voltage profile within acceptable operation limits, adequate reactive power availability is necessary. Power system equipment as well as customer electric devices are designed to operate at a certain voltage rating and any considerable changes in voltages across power systems can damage such equipment.

Traditionally, several reactive power compensation techniques have been used in power system operation and control to compensate reactive power and thus enhance the power security and quality of the system. These technologies include conventional synchronous generators, capacitor banks and static var compensators (SVCs). In this section, a brief review is given of the latest technologies for reactive power compensation, such as D-STATCOM. Also, end user reactive power compensation will be discussed in the following subsections.

7.2.1 Conventional Synchronous Generators

Large synchronous generators have been typically used as a reactive power supporter to stabilize transmission systems by injecting reactive power into systems. These generators control their terminal voltages within acceptable boundaries via their excitation systems, which may include dc or ac exciters. The main components of a synchronous generator

are shown in the block diagram in Figure 7.1. In addition, synchronous generators may inject or absorb reactive power depending on their excitation systems; under-excitation represents the absorption condition and over-excitation represents the injection condition. They are usually equipped with Automatic Voltage Regulators (AVRs) to control the excitation systems continuously, as their ability to provide or absorb reactive power continually is limited by armature and field currents, as well as other heating restrictions [200].

These synchronous generators are located far away from load centres and distribution systems and this limits the impact of these conventional synchronous generators on reactive power support and voltage control in distribution networks. As a result, additional reactive power supporters are essential to ensure power security and quality in urban and rural areas of distribution networks.

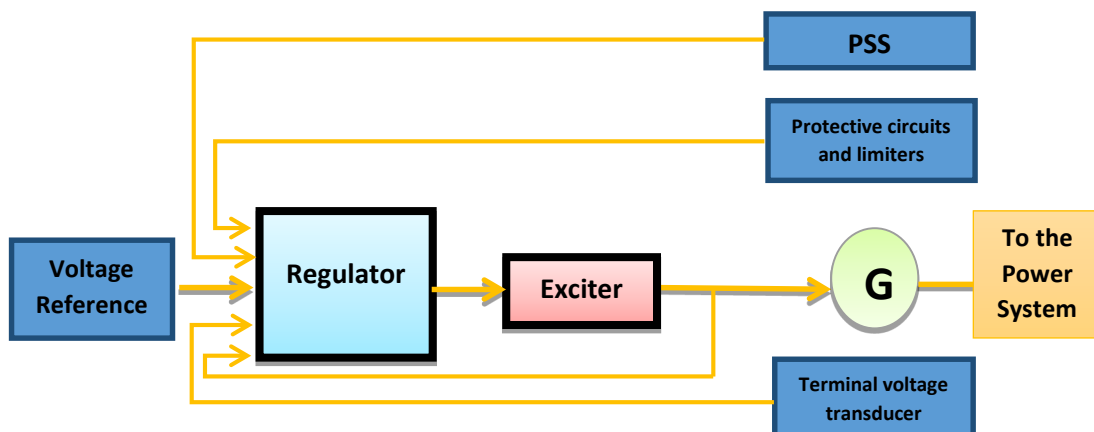


Figure 7.1: Synchronous generator block diagram.

7.2.2 Capacitor Banks

Capacitor banks basically involve several large capacitors which may be connected to or disconnected from a distribution system by switches. They are installed and controlled by local system operators. The operators install these banks in specific locations to provide the required amount of reactive power to the local system. Several research studies have been conducted recently to study and investigate the optimal location and size of capacitor banks [228-230]. The use of capacitor banks can improve power quality by meeting the $\pm 5\%$ of voltage variation standard and reducing thermal losses in distribution feeders.

However, there are several disadvantages to using capacitor banks, such as the fact that they can produce higher order harmonics and that frequent switching (ON/OFF) of the individual capacitors leads to adverse switching transients which may damage equipment.

The response of capacitor banks is also slow compared to other smarter network devices and cannot accommodate a sudden change in the output of local distributed generation based on renewable resources. Therefore, more flexible, fast and reliable control systems should be applied to these capacitor banks in order to achieve reactive power requirements in local distribution networks which may involve high penetration of distributed generation based on renewable energy.

7.2.3 Static Var Compensator (SVC)

The SVC can be a combined system that consists of a Thyristor Switched Capacitor (TSC) or a Thyristor Controlled Reactor (TCR) or a combination of both, as illustrated in Figure 7.2. It is the most commonly used thyristor controlled reactive power compensator and can contain capacitor banks. Unlike a synchronous generator, the SVC is a passive device and its operation depends on the change in its admittances. SVC reactive power output limits can be obtained from its maximum and minimum admittances. Hence, the SVC can provide or absorb reactive power and this can be controlled by the thyristor's firing angles. There are a number of disadvantages in using the SVC as a reactive power compensator. Using TSC as a VAR compensation device gives variable reactive power compensation (not continuous) and each of its capacitor banks needs a separate thyristor switch. Also, each thyristor should be protected against fault currents and line voltage transients by protection devices and this increases the overall unit cost. Using TCR configuration as a reactive power compensation device can also produce lower order harmonics and can cause higher losses in cases where this device is used in absorbing VAR [231]. Using a combined system of TSC and TCR solves the previous drawbacks, although this is expensive [232].

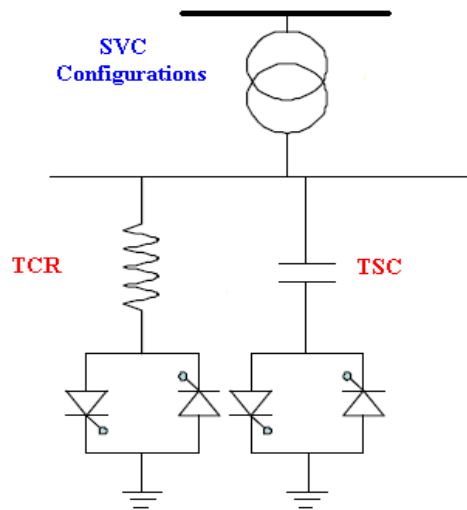


Figure 7.2: SVC configurations.

7.2.4 STATCOM (D-STATCOM)

The Static Synchronous Compensator (STATCOM) is a contemporary reactive power compensation device which is based on a solid-state voltage source converter, as shown in Figure 7.3. It is structured from power electronic elements in the same manner as basic elements of a SVC; however, its response and behaviour are similar to the synchronous generator. It is a fully controlled VAR compensation device and it operates as a controllable voltage source to control terminal voltages and maintain them within acceptable limits. The STATCOM is also a shunt controller which can produce or absorb reactive power, and it can be used at transmission or distribution levels [233].

Using the STATCOM in distribution systems has been investigated and implemented recently, such as in offshore wind farms connected through an HVDC system to regulate terminal voltages and improve power factor [234, 235]. Using the STATCOM at distribution levels or close to load centres has been called Distribution STATCOM or D-STATCOM. The basic components of D-STATCOM are a DC voltage source implemented inverter using IGBT and connected in parallel to the distribution bus through a coupling reactor [236-239]. Using D-STATCOM is a reliable way to provide/absorb reactive power and it has a fast response; however, it is not economical to use it in distribution networks and micro-grids due to its considerably high cost.

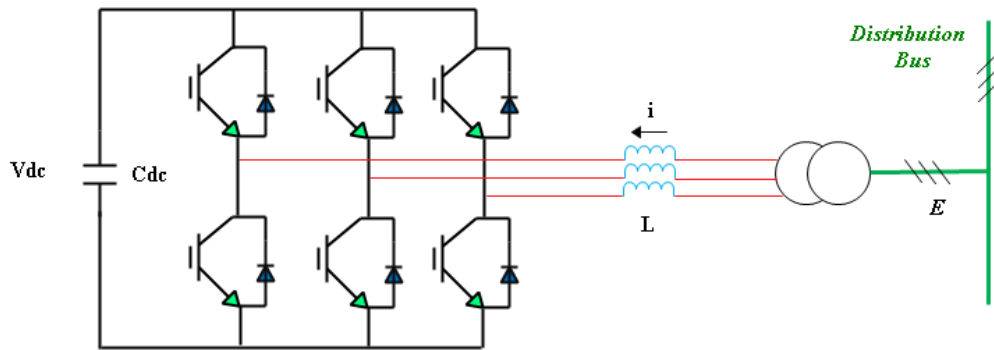


Figure 7.3: STATCOM structure.

7.2.5 End User or Distributed Generation Owner

Distributed generation (DG) based on inverter technologies such as wind and solar represents end user reactive power compensation in distribution systems. This kind of compensation is not yet extensively deployed. There are several reasons for encouraging the deployment of this technology and for it being extraordinarily promising. Providing reactive power compensation from DGs based on wind and solar energy is flexible, i.e., the rapid increase in using distributed generation based on renewables in residential areas results in increasing the opportunity to enable a large number of individual inverter based compensators to participate in reactive power support, along with other local compensators. Reducing the risk of using capacitor banks which need a reliable coordination control between themselves and any new renewable generators is another reason to upgrade to inverter based technology. Sections 7.4 and 7.5 review recent works in this area.

7.3 Grid Code Requirements for Reactive Power Support

The evolution of mixed power generation technologies has changed the nature and dynamics of power systems due to the intermittent nature of some renewable units, such as wind and solar units. Renewable generating units have been operated to maximize output power in the past without considering the possibility of using the available reactive power to improve system performance. It is a matter of conflict between revenue return and system security, since a renewable unit's owner usually prefers to sell the maximum available output power regardless of the potential to improve system performance.

Therefore, several transmission and distribution system operators (TSO and DSO) have introduced specific requirements in their grid codes for renewable energy grid connected units to control reactive power and contribute to voltage regulation, such as in the Germany regulations [219]. In the United Kingdom, wind turbines are required to have technical capability to regulate reactive power at their connection terminals to control the voltage at the point of common coupling (PCC). Reactive power requirements from wind farms have been defined in Chapter 3, Figure 3.37.

The increase in renewable systems without reactive power controllability in distribution networks has also had a negative impact on the power factor (p.f.) of utility grids, as illustrated in Figures 7.4 and 7.5. Figure 7.5 shows a grid working on a 0.9 p.f. to supply a load where there is 10 % renewable energy penetration, as illustrated in equation 7.1. The grid power factor will be affected if the renewable unit works at the unity power factor (without reactive power controllability). It is shown in Figures 7.4 and 7.5 that the power factor at the utility grid without renewable energy penetration is 0.9 and with 10 % renewable penetration the power factor at the utility deteriorates to become 0.878. Therefore, the renewable energy unit should contribute towards correcting the power factor and avoiding any negative impact on the utility. The example that has been shown in Figures 7.4 and 7.5 raises an important question: what is the reactive power value that the renewable unit should provide to correct the power factor at the utility grid?

The conventional power factor correction method that has been used in literature to estimate the value of a capacitor to correct the power factor can be used here. By using equations 7.2, 7.3 and 7.4 we can calculate the reactive power (Q_{add}) that the renewable unit should provide to the system, which is 48.44 VAR in this example. This means the renewable energy units should operate at a 0.87 lagging power factor. For the case of leading power factor it can be estimated in the same manner.

$$\%Renewable\ Energy\ Penetration = \frac{Renewable\ Unit\ Total\ Power}{System\ Total\ Power} \times 100\% \quad (7.1)$$

$$Q = P \times \tan(\phi) \quad (7.2)$$

$$\phi = \cos^{-1}(p.f.) \quad (7.3)$$

$$Q_{add} = Q_{old} - Q_{new} \quad (7.4)$$

Where Q is the reactive power in VAr, P is the active power in watts and Φ is the phase shift angle between the terminal voltage and current. Q_{old} is the grid supplied reactive power at 0.878 p.f. and Q_{new} is the total reactive power needed to maintain a 0.9 lagging power factor. Finally, Q_{add} is the additional reactive power required to correct the power factor at the utility grid in this case ($Q_{Renewable}$).

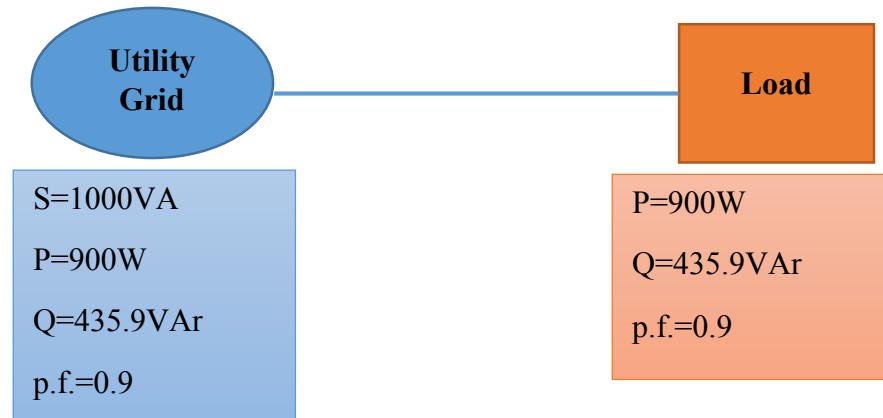


Figure 7.4: Utility grid supplies a load with 0.9 p.f. lagging.

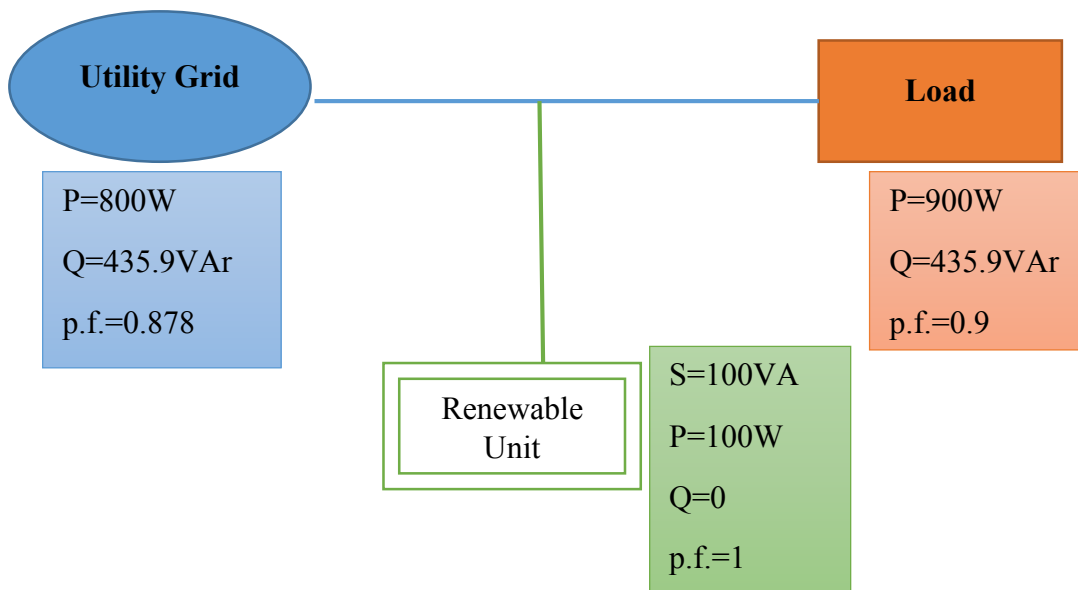


Figure 7.5: Utility grid and renewable unit supply a load with 0.9 p.f. lagging.

7.4 Wind Generation Impact on Grid System Power Factor

In power systems, voltage control is directly related to the regulation of reactive power, and due to the rapid increase of wind energy penetration in power systems, new grid code requirements have been set demanding reactive power provision from wind farms as much as with conventional power plants. Reactive power requirements can be defined by the power system operator requiring a set-point value for the voltage or power factor or reactive power at the wind farm's connection terminals. In recent years, wind turbines based on the Doubly Fed Induction Generator (DFIG) have been installed extensively in power systems. The reactive power capability of wind parks based on the DFIG was discussed in [64]. The fast response of the control of DFIG power electronic converters enhances the voltage control and reactive power regulation, as illustrated in [240]. There are two reactive power regulations that have been discussed in literature for the DFIG known as voltage control mode and power factor mode [241]. The dynamic limits of the reactive power capability of wind turbines based on the DFIG was investigated in [66]. The paper also discussed the reactive power regulation of wind energy based on the DFIG to support the grid and improve local voltage stability. In [65], the steady-state reactive power loading capability of wind turbines based on the DFIG was investigated by considering an active-reactive power capability curve.

Modern wind turbines based on a synchronous generator with fully rated converters have increased in power systems. In the same manner as the DFIG, FRC based wind energy can also provide reactive power to a system by controlling the power electronic converters [205]. There are few papers that have investigated the reactive power capability of wind based synchronous generators with fully rated converters in literature. However, in [67], reactive power provision technical and economic limitations from an FRC wind unit were discussed. The majority of research papers have studied the reactive power capability of large-scale wind turbines in large power systems. In contrast, this chapter investigates the impact of high wind energy penetration based on the DFIG and a synchronous generator with fully rated converters on the grid power factor and the possibility of providing reactive power in various generic distribution systems.

7.5 Photovoltaic Generation Impact on Grid System Power Factor

The impact of photovoltaic generation on distribution networks has been the target of several research studies [47, 50, 242-245]. In [242], an actual PV case study was investigated with historical data for solar irradiance and temperature to provide a reference of PV generation selling price in such an area. The required incentives were discussed to promote the new PV installation in this particular area. The impact of photovoltaic generation on possible power loss and voltage variation of the distribution feeder was also highlighted. The effects of increased PV penetration on a power system's stability were analysed in [50, 243] and the impact of PV power generation with high penetration on voltage regulation and line losses was studied in [245]. UK data were used in [47] to investigate the effects of widespread photovoltaic power generation on real distribution systems and the simulation results proved that even with high PV penetration, voltage rises were small and did not cause problems. Due to the intermittent nature of PV output, [244] investigated the dynamic performance of PV units under dramatic change in solar irradiance and different voltage control techniques were suggested to reduce the associated impact.

Recently, several manufacturers have released PV inverters with reactive power control into the market, such as SUNNY MINI CENTRAL 9000TL/10000TL/11000TL with reactive power control by the SMA Company, and the Solaron 500 250 and 500 kW PV inverter by ADVANCED ENERGY. Notwithstanding, these PV opportunities should not increase the burden on PV units by either limiting PV real power generation or boundless dispatch of reactive power.

To increase system security and reliability in micro-grids and rural systems, extra investment is required for reactive power compensation. As a result, it is necessary to find useful technical and economical solutions to provide/absorb reactive power in these distribution networks. Capacitor banks are a useful option; however, the DSO needs a complicated procedure to coordinate and control their operations individually. The total system cost will also be increased as new hardware is required, in this case multiple capacitor banks in different locations. Other traditional reactive power compensators are

more expensive than capacitor banks. The DSO needs to investigate the best technical and economical option to provide/absorb reactive power in these micro-grids.

Photovoltaic units and other types of distributed generation are competitive options for reactive power compensation, as they have a fast response when compared to traditional methods. PV penetration is increasing rapidly in distributed networks so there is no extra cost in using PV units as a reactive power supporter. There is promising potential to use photovoltaic inverters as reactive power supporters for local utility grids. Therefore, PV inverters with reactive power control capability have become essential in recent years in power systems with high PV penetration [68, 69]. This chapter discusses the impact of high solar energy penetration based on photovoltaics on the grid power factor and the capability to provide reactive power in different generic distribution systems.

7.6 Modelling and Control of Renewable Energy Systems for Reactive Power Support

This section investigates the modelling and control of distributed generation based on wind and solar energy. Three different technologies are considered to provide reactive power support to the grid, namely a wind turbine based on the DFIG, a wind turbine based on a synchronous generator with fully rated converters, and a solar unit based on photovoltaics. These have been modelled in MATLAB/SIMULINK to study their impact on the grid power factor when they provide reactive power or do not.

7.6.1 DFIG Modelling and Control

Wind turbines based on the DFIG have reactive power capability, as discussed in literature. The DFIG has two power electronic converters in its structure and these converters are connected back-to-back through a DC link. They are known as the rotor side converter (RSC) and the grid side converter (GSC). The RSC is responsible for controlling the stator side active and reactive power independently. The GSC controls the DC link voltage within limits and it can also regulate the reactive power exchanged with the grid, called reactive power support [246]. The GSC vector control scheme of the DFIG

implemented in this chapter and more detailed information about DFIG based wind energy control were discussed in Chapter 3.

7.6.2 Wind Turbine based on Synchronous Generator with Fully Rated Converters

There are several topologies for an FRC synchronous generator based on wind energy. However, this thesis will consider the RSC as a diode rectifier and the GSC as a voltage source inverter, as shown in Chapter 4.

7.6.3 Solar Energy based on Photovoltaics

The problem with solar based on photovoltaic systems is that there are so many topologies in the market it is difficult to find standard modules for implementation, unlike with wind energy for example. This thesis uses two main topologies for the PV system: a three phase two stage transformerless grid connected PV system and a proposed PV model. The three phase two stage grid connected PV system was discussed in detail in Chapter 2. A block diagram of the simplified PV model is shown in Chapter 4. The PV panel and the DC-DC boost converter are neglected and they are represented by the DC voltage source for simplicity to perform simulations and get results for different distribution networks. The DC voltage source is interfaced with the grid through a voltage source inverter (VSI). The PV active and reactive powers can be regulated by modifying the control of the PV inverter. The PV inverter can be controlled in the same manner as the control of power electronic converters in wind systems, which depends on the d-q synchronous reference frame.

7.6.4 Proposed Technique for PV Reactive Power Controllability

Many photovoltaic inverters have been investigated with active power generation only. With high PV penetration in distribution networks, it is essential to consider the possibility of a photovoltaic system to contribute towards reactive power compensation and power factor correction of the utility system. The standard VDE-AR-N 4105 was introduced in Germany in August 2011 due to the rapid increase in PV generation and a stricter requirement for newly installed PV inverters to operate at 0.9 leading to 0.9 lagging power factor. This chapter investigates three different power factor settings to fulfil future PV operations in smart grids, as illustrated in the P-Q capability curve in Figure 7.6. These settings include unity power factor (traditional inverter operation), 0.9 p.f. which

represents the German grid code requirement, and 0.8 p.f. which represents current inverter technology by SMA, an international inverters manufacturer. There are also three main scenarios to test the proposed PV system, as follows:

- 1) Sunny day conditions
- 2) Cloudy weather
- 3) Night operation

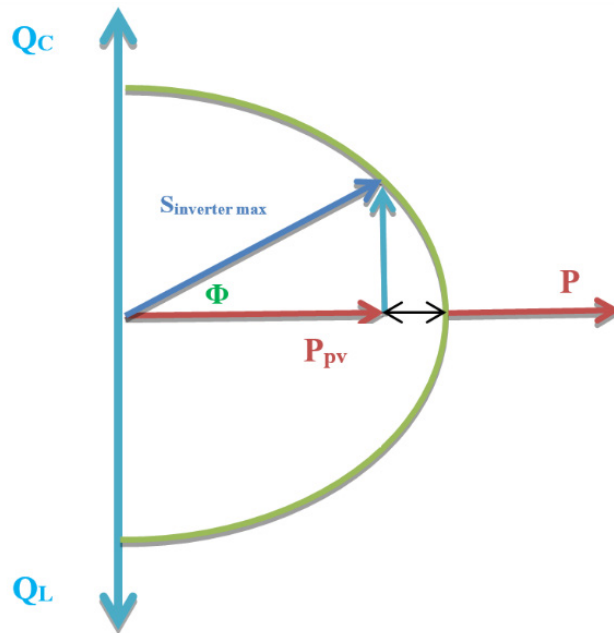


Figure 7.6: PV inverter P-Q capability curve.

A three phase two stages grid connected PV system with reactive power capability is proposed. A control block diagram of the PV inverter was shown in Chapter 4, Figure 4.6. The control systems for the three phase inverter are in a d-q synchronous reference frame. The d-axis loop is utilized for the dc link voltage control and the q-axis is utilized for the voltage support or reactive power control. It should be noted that the control structures have theoretical basis or justification.

Conventional control approaches in PV systems assumes there is no reactive power control by setting (i_q^*) equal to zero. In recent PV control approaches, ac bus voltage is compared to a reference voltage value, e.g. 1 p.u., to control the PV reactive power. However, in this chapter the reactive power controller is basically designed depending on

the calculation of the reference current (i_q^*), as illustrated in equations 7.5 and 7.6. Other controller terms are calculated using equations 7.7 – 7.10. Classical cascaded control loops with internal current loops are used in this chapter. The design and modelling of the current loops and dc link voltage control have been studied in literature [247].

$$i_q^* = -\frac{2Q^*}{3v_d} \quad (7.5)$$

$$Q^* = S_{pv} \times \sin(\cos^{-1} p.f.^*) \quad (7.6)$$

$$u_d = k_p (i_d^* - i_d) + k_i \int (i_d^* - i_d) dt \quad (7.7)$$

$$u_q = k_p (i_q^* - i_q) + k_i \int (i_q^* - i_q) dt \quad (7.8)$$

$$e_d = u_d + v_d - \omega L i_q \quad (7.9)$$

$$e_q = u_q + v_q + \omega L i_d \quad (7.10)$$

Where Q^* is the reference reactive power that the PV should provide and p.f.* is the reference power factor that the system operator demands the PV owner to operate at. S_{pv} is the inverter maximum apparent power, as illustrated in Figure 7.6.

7.7 Simulation Scenarios

This chapter investigates the impact of a three phase two stage transformerless PV grid connected system with various power factor settings on the grid power factor. The PV system is directly connected to an infinite bus voltage source representing the utility grid. Simulation results are obtained using MATLAB/SIMULINK. In addition, the impact of high renewable energy penetration on the grid power factor of various generic distribution systems is discussed. Three different distributed generations based on renewable energy are considered, namely a wind turbine based on the DFIG, a wind turbine based on a synchronous generator with fully rated converters, and a solar energy source based on a proposed photovoltaic system, as discussed in section 7.6.3. The impact of these distributed generation units on the grid power factor is investigated when the DG units operate under various power factor settings, unity, 0.9 lagging and 0.8 lagging. Three modified generic distribution networks are considered in this chapter, namely the IEEE

13 bus, IEEE 37 bus and IEEE 123 bus test systems. To validate the impact of DGs based on renewable energy on the grid power factor of the selected distribution networks, simulations are performed using MATLAB/SIMULINK.

7.7.1 Proposed Technique for PV Reactive Power Controllability

The tested PV system consists of ten parallel arrays with a total rated power of 800 VA; the design circuit parameters and design specification are listed in Table 7.1. Three main cases are considered in the proposed PV system at different power factor settings and simulations are performed using MATLAB.

Table 7.1: Design circuit parameters and design specification

PV array rated power	800 W
PV modules	SHELL Ultra-80-P
Smoothing capacitor, C	4 mF
Boost inductor, L	0.3 mH
DC output voltage, V_{dc}	350 V
Switching frequency, f_s	4000 Hz

A- Sunny day conditions

During a sunny day the solar irradiance is set at the typical radiation under STC, which is 1000W/m². The PV system will produce the maximum available power at 1000 W/m² solar irradiance and the system can track the maximum power point (MPP) by using the hill climbing method discussed in Chapter 3. As demonstrated in Figure 7.7 (a), the PV system generates around 800 W and no reactive power output. When the inverter works at unity power factor there is no phase shift between the grid voltage and current. There is a 25.80° phase shift between the voltage and the current when the PV inverter operates at 0.9 p.f. lag and the PV inverter can also provide around 380 VAR (reactive power) while the active power output drops to about 760 W, as shown in Figure 7.7 (b). The voltage leads the current by 36.90° of phase shift to provide about 480 VAR reactive power when the PV system operates at 0.8 power factor lagging (see Figure 7.7 (c)). Note the voltage curve is divided by a factor of 20 to observe the phase shift between the grid voltage and current.

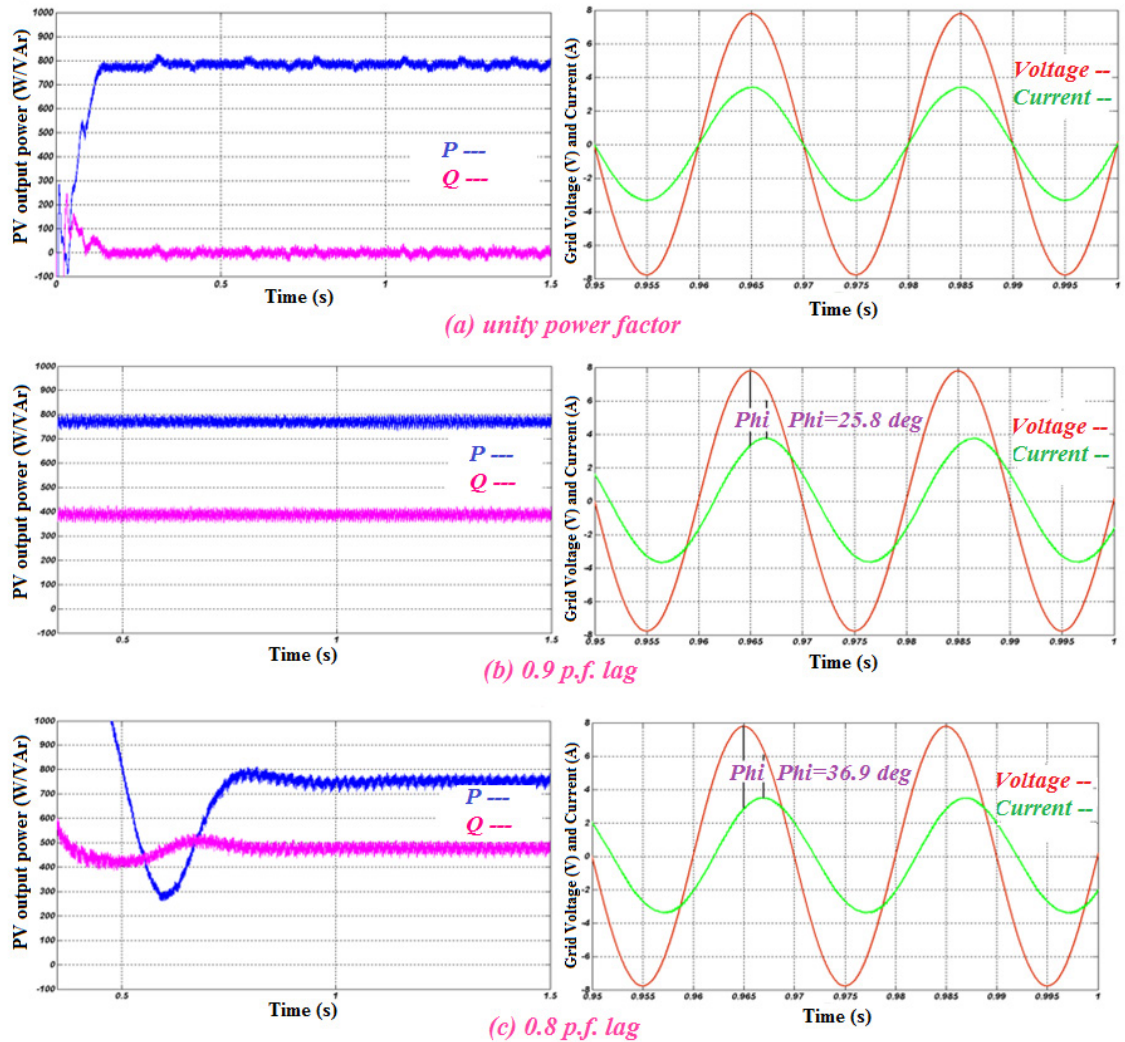


Figure 7.7: PV output power in (W & VAr) and grid voltage in (V) and current in (A) during sunny day conditions under different power factor settings - (a) unity p.f., (b) 0.9 p.f. lag, (c) 0.8 p.f. lag.

B- Cloudy weather

Cloudy weather operation is an important consideration when designing and testing a PV system. This chapter considers a worst case scenario for solar irradiance of $<500 \text{ W/m}^2$. The solar radiation (G) is set at 400 W/m^2 and the maximum available power will be around 280 W , as shown in Figure 7.8. For unity power factor operation there is no reactive power provision; however, the PV inverter can provide around 140 VAr and 200 VAr for 0.9 p.f. lagging and 0.8 p.f. lagging operation respectively (see Figure 7.8 (b) and (c)).

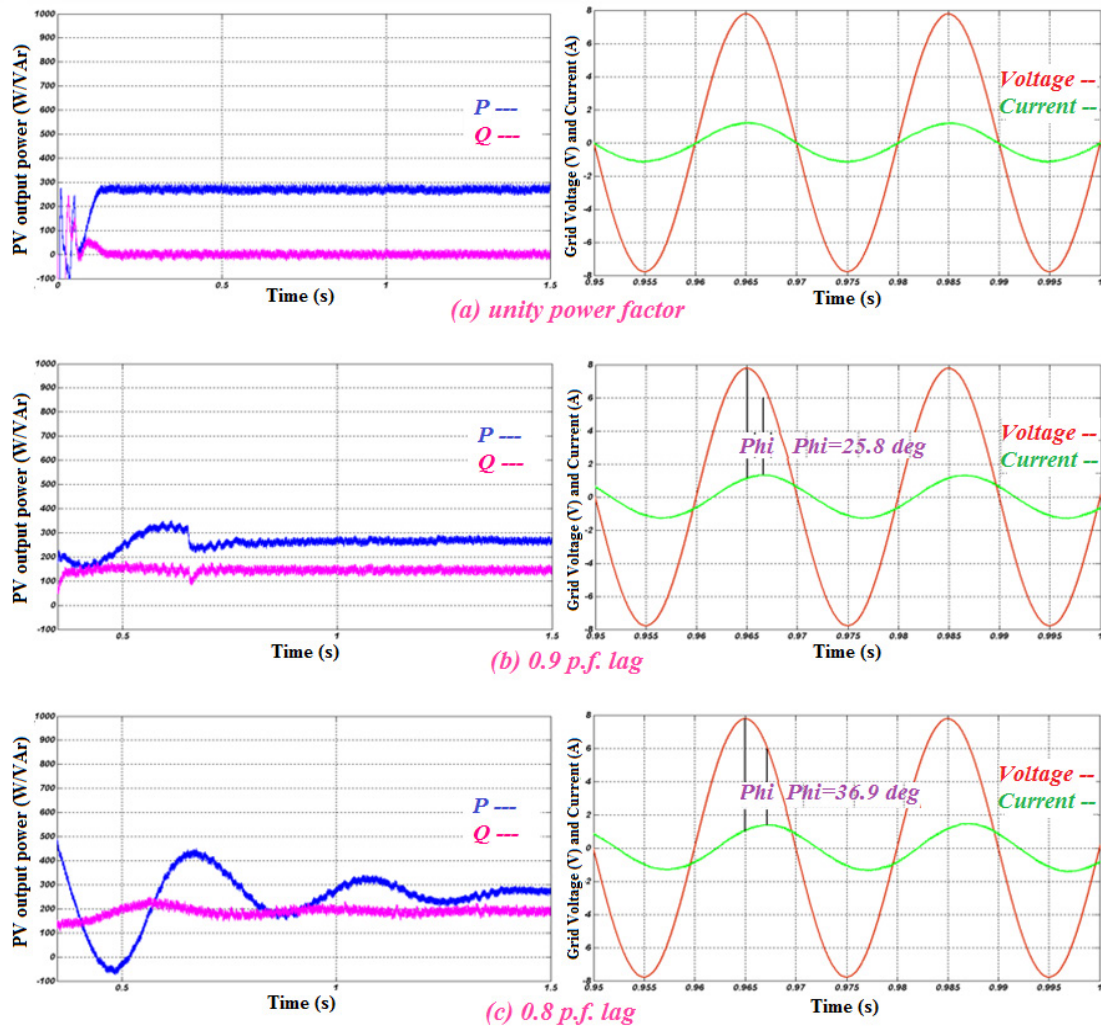


Figure 7.8: PV output power in (W & VAr) and grid voltage in (V) and current in (A) during cloudy weather under different power factor settings - (a) unity p.f., (b) 0.9 p.f. lag, (c) 0.8 p.f. lag.

C- Night operation

Traditionally, a PV system is used for a grid system during daytime by generating real power and increasing the generation mix to increase security and supply load demands. A PV system is a passive device conventionally as it cannot contribute to power system operation and it cannot give solutions to the system operator. It can generate active power when there is sufficient solar irradiance and it should be disconnected when there is a disturbance in the network. Various studies have been carried out to make PV systems active and contribute towards operation by providing different services such as reactive

power, especially during night operation. A PV inverter like the one proposed in this chapter can convert a PV system into being an active device, and it can support the utility grid with reactive power and improve the utility power factor. As a result, the proposed PV inverter can also provide reactive power during the night or when there is insufficient solar irradiance. As illustrated in Figure 7.9, the PV inverter can support the utility grid by around 130VAr.

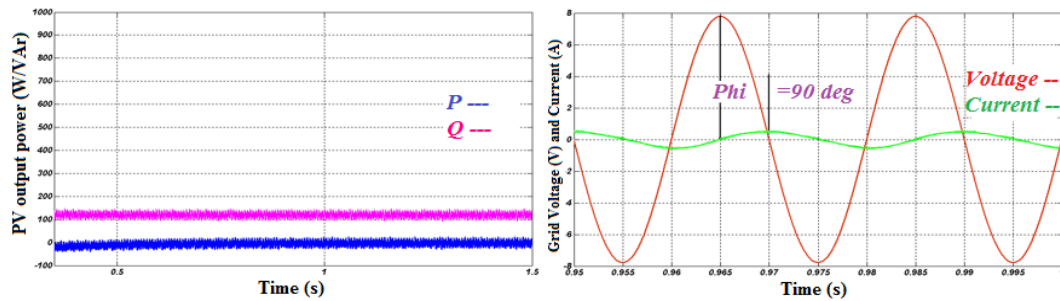


Figure 7.9: PV output power in (W & VAr), grid voltage in (V) and current in (A) for night operation.

7.7.2 IEEE 13 Bus Distribution System

The IEEE 13 bus system is a test system used for distribution system analysis published by the IEEE Power Engineering Society [195]. A schematic diagram of this system is illustrated in Chapter 4, Figure 4.8. Detailed data regarding this system are given in Appendix B.1. The system is connected to the ac grid through a two winding ac transformer. Bus 650 is the bus which interconnects the grid with the test network. Table 4.1 in Chapter 4 summarises the IEEE 13 bus distribution network data. The grid is assumed to be an infinite bus. The distributed generation based on renewable sources are connected to the farthest node from the grid, which is bus number 680.

The main objective of this chapter is to investigate the impact of different renewable energy sources on the grid power factor. These renewable sources are the DFIG based on wind energy, an FRC synchronous generator based on wind energy, and a solar energy unit based on the proposed simplified PV system mentioned in section 7.6.3. The grid power factor without adding renewable sources is 0.81 lag, as shown in Figure 7.10.

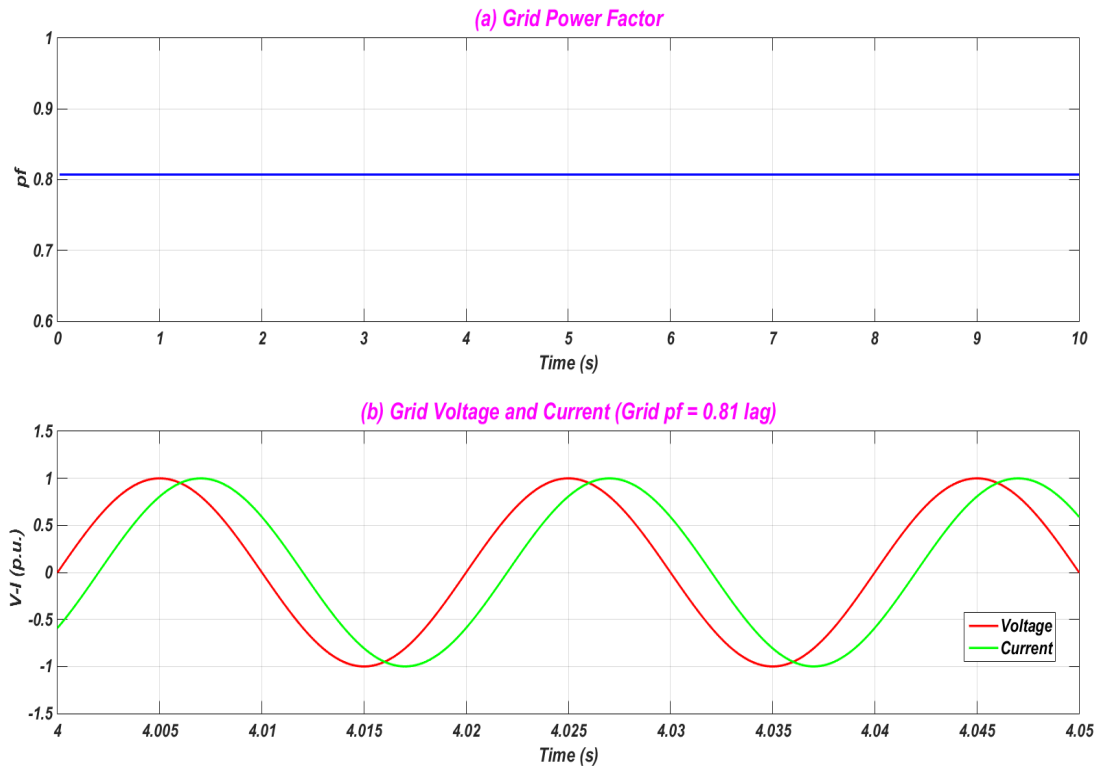


Figure 7.10: IEEE 13 bus system without renewables - (a) grid power factor, (b) grid voltage and current.

A- With PV Penetration

A DG based on photovoltaics is installed at bus 680 with 1 MW output power, which is 28 % of the total generation in the system. Detailed data regarding the PV system are shown in Appendix D. Table 7.2 shows the contribution of each source of energy to the total power generation in the system and the locations. The impact of the installed PV system on the grid power factor is illustrated in Figures 7.11, 7.12 and 7.13 for various power factor settings, unity, 0.9 lag and 0.8 lag respectively. Figure 7.14 shows a comparison between various PV power factor settings on the grid power factor. It shows that the grid power factor is improved when the PV provides reactive power and operates at non unity power factors.

Table 7.2: IEEE 13 bus system, power generation source outputs and their locations (PV case).

	Grid	PV
Total Generation	2.62 MW	1 MW
Location	Bus 650	Bus 680

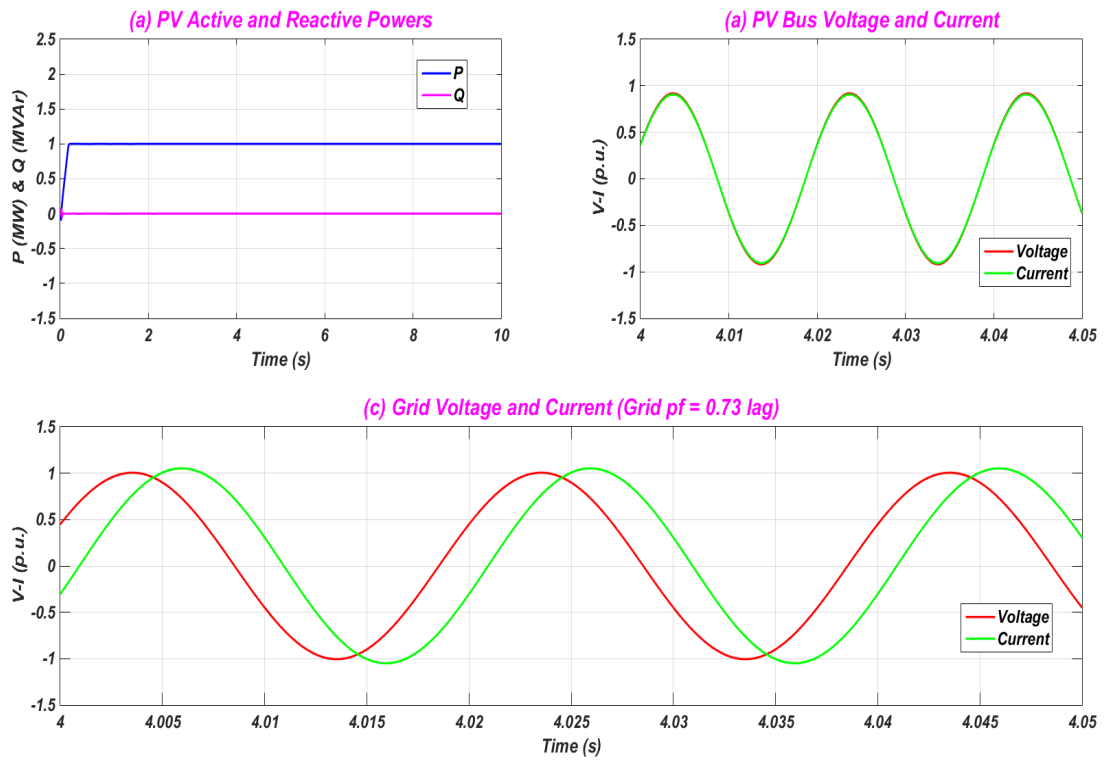


Figure 7.11: IEEE 13 bus system, PV with unity power factor impact on grid power factor - (a) PV active and reactive power, (b) PV bus voltage and current, (c) grid voltage and current.

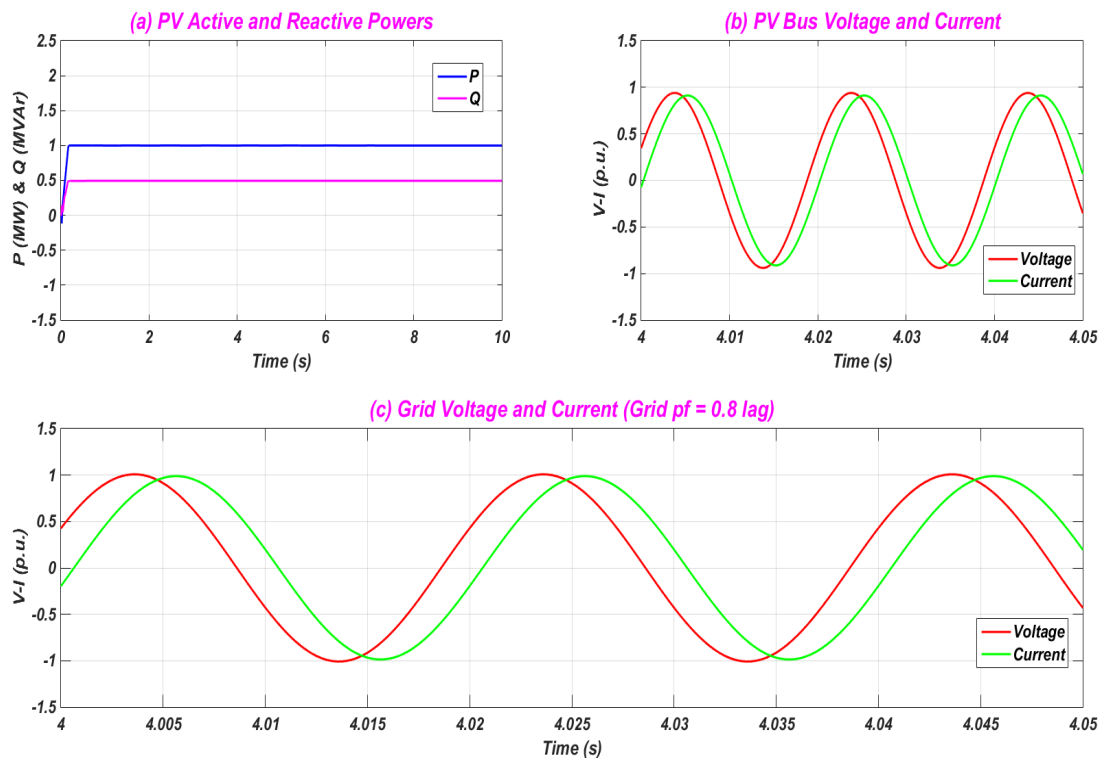


Figure 7.12: IEEE 13 bus system, PV with 0.9 lag power factor impact on grid power factor - (a) PV active and reactive power, (b) PV bus voltage and current, (c) grid voltage and current.

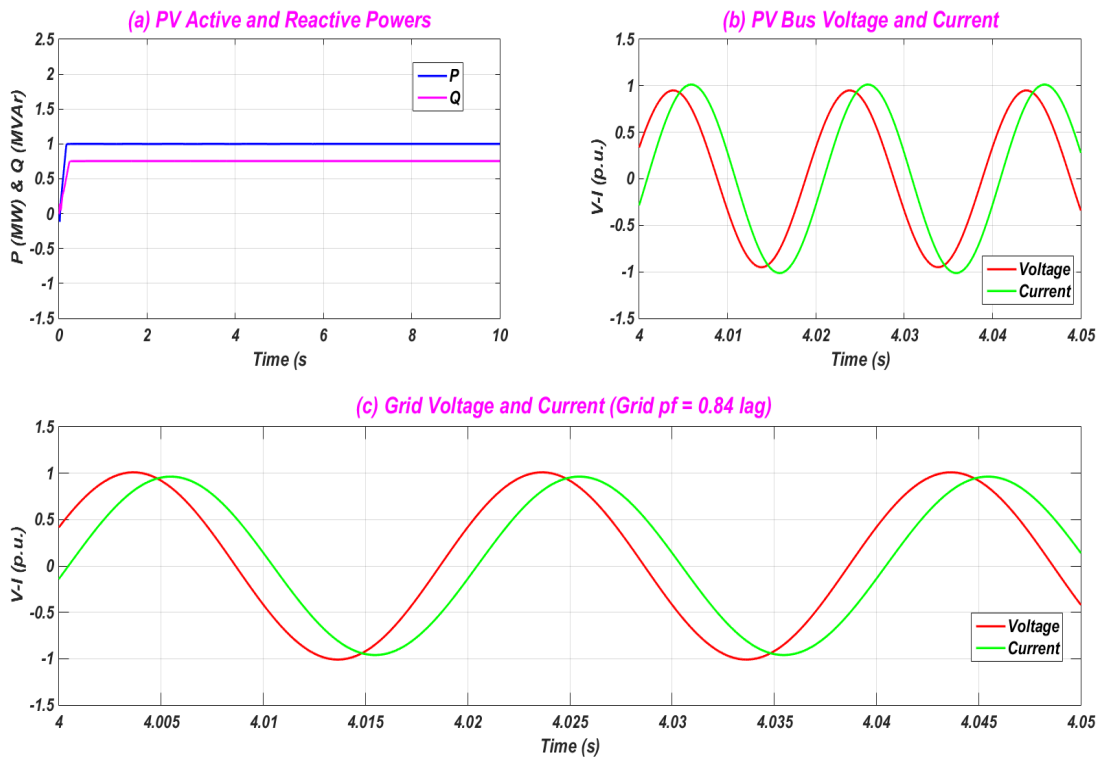


Figure 7.13: IEEE 13 bus system, PV with 0.8 lag power factor impact on grid power factor - (a) PV active and reactive power, (b) PV bus voltage and current, (c) grid voltage and current.

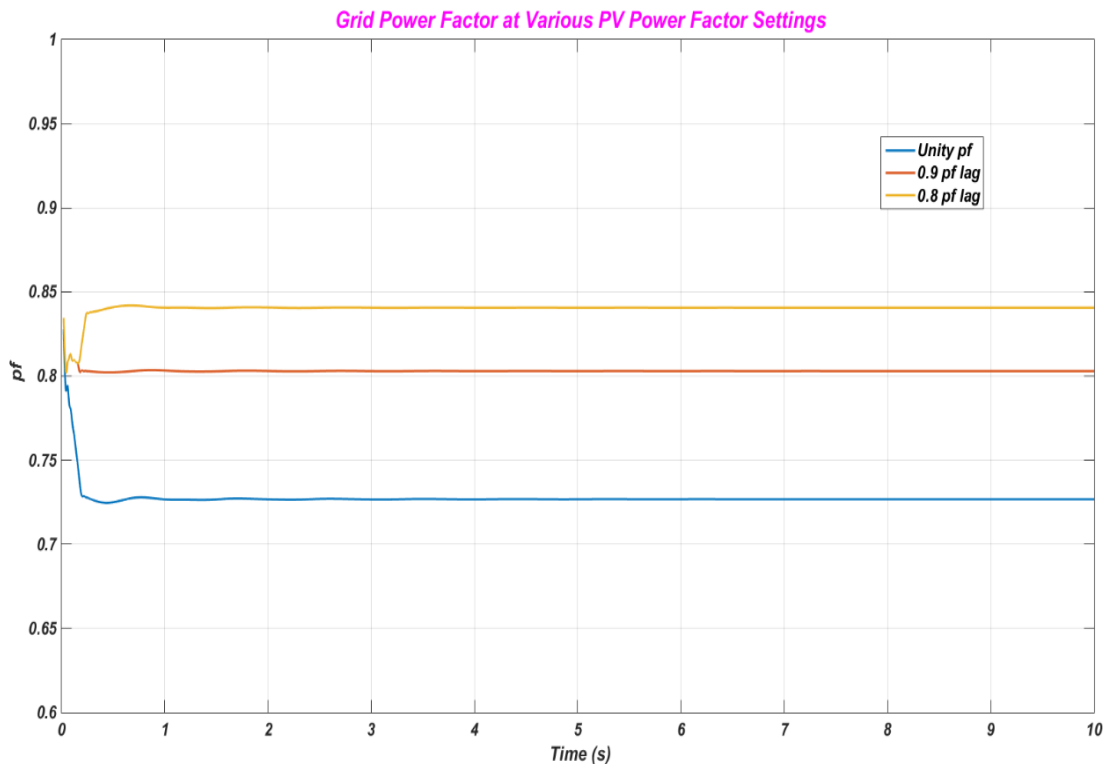


Figure 7.14: IEEE 13 bus system with PV penetration, grid power factor at various PV power factor settings.

B- With Wind based on DFIG Penetration

A DG based on the DFIG is installed at bus 680 with 1.5 MW output power, which is 41 % of the total generation in the system. Detailed data regarding the DFIG system are shown in Appendix D. The contribution of each power source to the total power generation in the system and the locations are given in Table 7.3. The impact of the installed DFIG based on wind energy on the grid power factor is shown in Figures 7.15, 7.16 and 7.17 for various power factor settings, unity, 0.9 lag and 0.8 lag respectively. Figure 7.18 shows a comparison between different DFIG power factor settings on the grid power factor. From this figure it is clear that the grid power factor is enhanced when the DFIG provides reactive power and operates at non unity power factors.

Table 7.3: IEEE 13 bus system, power generation source outputs and their locations (DFIG case).

	<i>Grid</i>	<i>DFIG</i>
<i>Total Generation</i>	2.12 MW	1.5 MW
<i>Location</i>	Bus 650	Bus 680

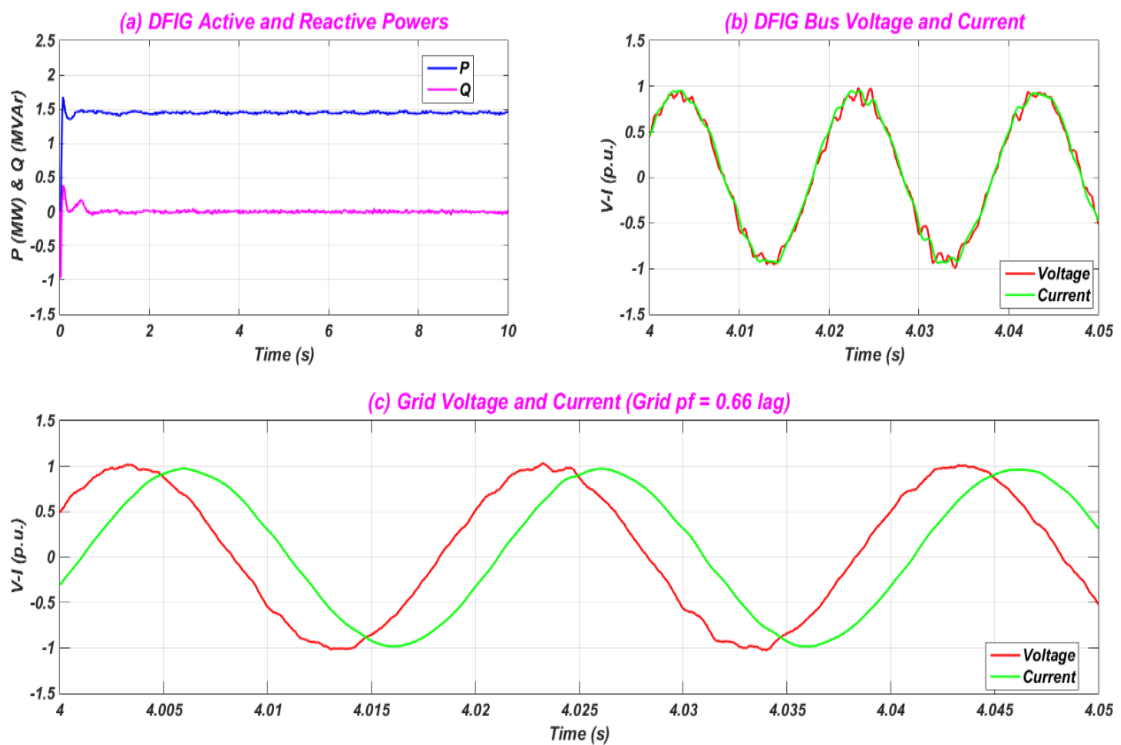


Figure 7.15: IEEE 13 bus system, DFIG based wind with unity power factor impact on grid power factor - (a) DFIG active and reactive power, (b) DFIG bus voltage and current, (c) grid voltage and current.

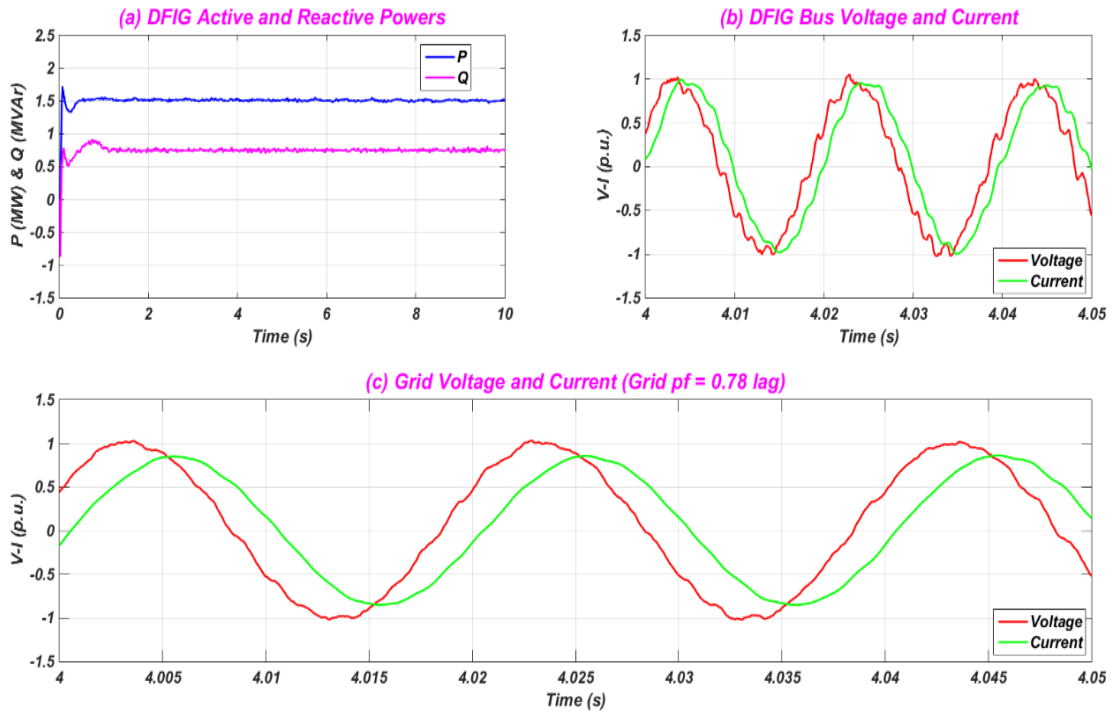


Figure 7.16: IEEE 13 bus system, DFIG based wind with 0.9 lag power factor impact on grid power factor - (a) DFIG active and reactive power, (b) DFIG bus voltage and current, (c) grid voltage and current.

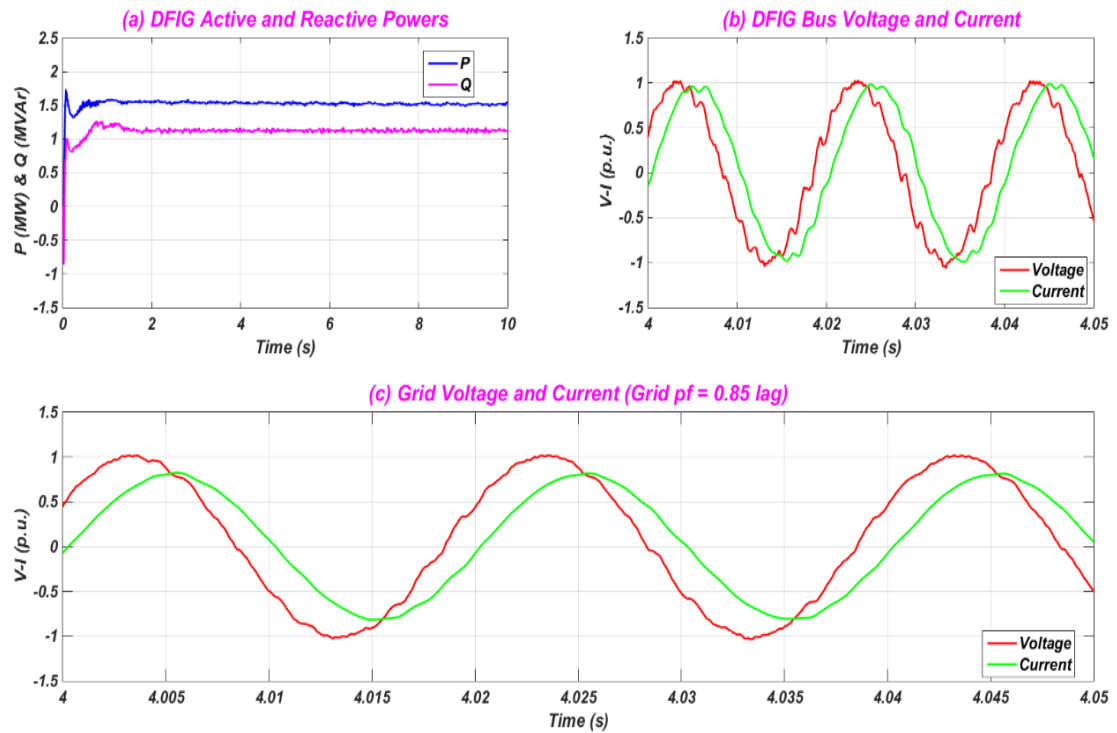


Figure 7.17: IEEE 13 bus system, DFIG based wind with 0.8 lag power factor impact on grid power factor - (a) DFIG active and reactive power, (b) DFIG bus voltage and current, (c) grid voltage and current.

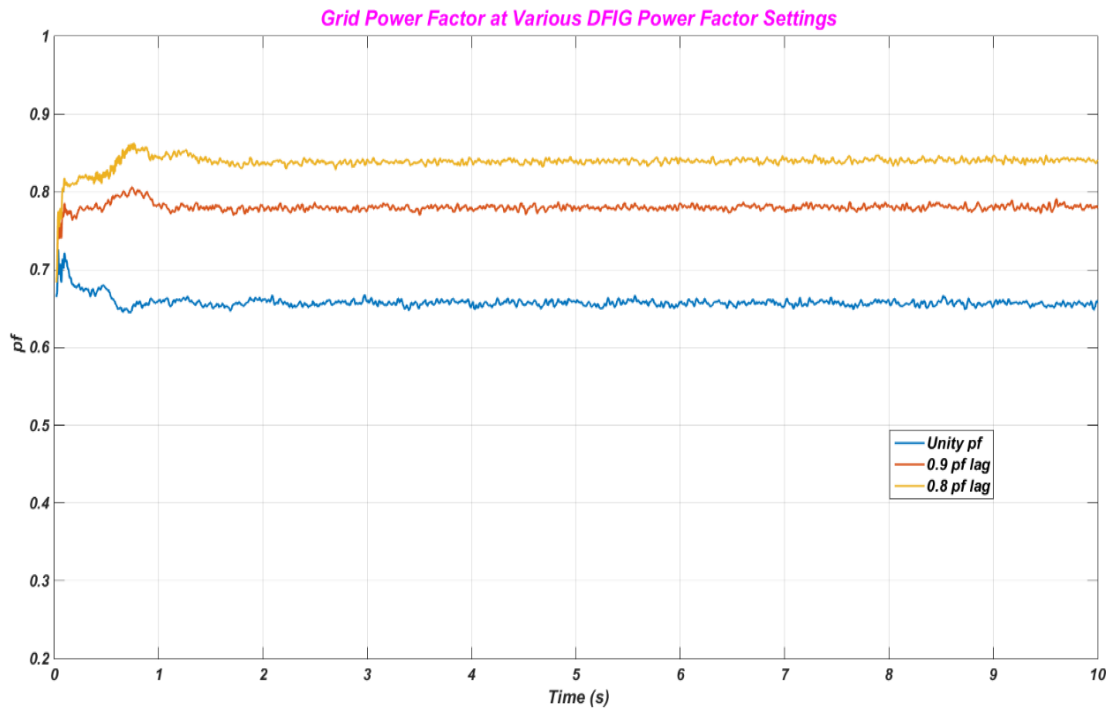


Figure 7.18: IEEE 13 bus system with DFIG penetration, grid power factor at various DFIG power factor settings.

C- Wind based on Synchronous Generator with Fully Rated Converters Penetration

A 2 MW distributed generation based on a wind FRC synchronous generator is installed at bus 680, which is 55 % of the total generation in the system. Detailed data regarding the FRC synchronous generator based on wind are shown in Appendix D. The contribution of each power source to the total power generation in the distribution system and the locations are given in Table 7.4. The impact of the installed DG based on a wind FRC synchronous generator on the grid power factor is illustrated in Figures 7.19, 7.20 and 7.21 for various power factor settings, unity, 0.9 lag and 0.8 lag respectively. A comparison between different installed DG power factor settings on the grid power factor is shown in Figure 7.22. As shown in the figure, the grid power factor is enhanced by around 55% when the FRC unit provides reactive power and operates at non unity power factors.

Table 7.4: IEEE 13 bus system, power generation source outputs and their locations (FRC case).

	Grid	wind FRC
Total Generation	1.62 MW	2 MW
Location	Bus 650	Bus 680

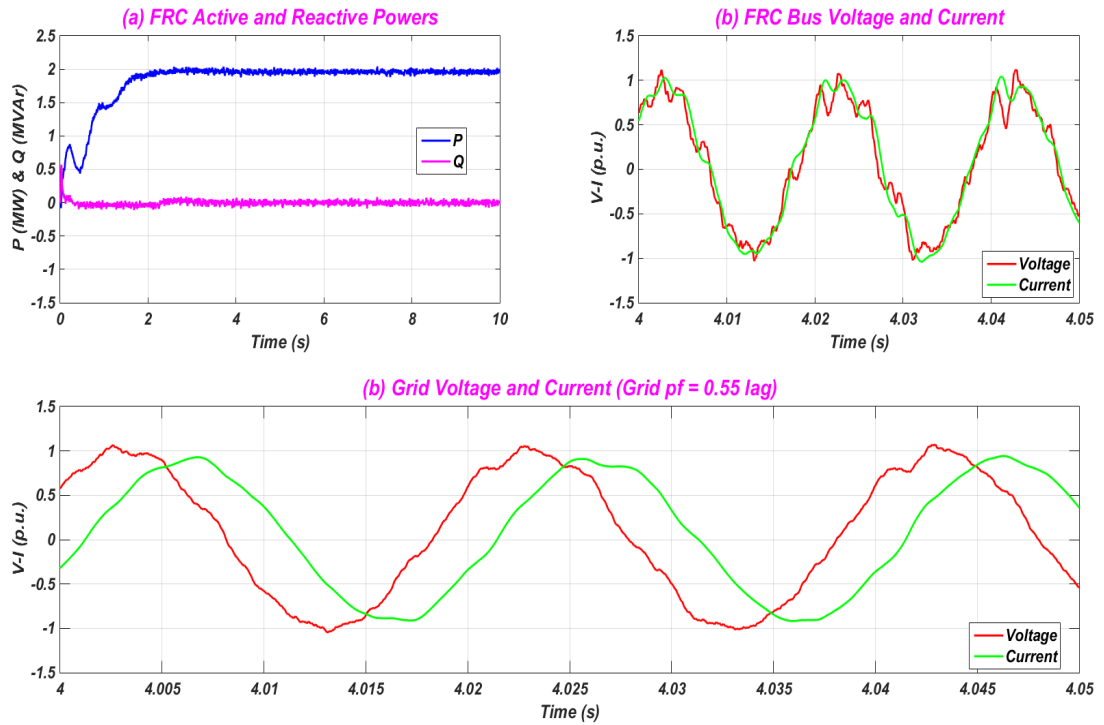


Figure 7.19: IEEE 13 bus system, FRC based wind with unity power factor impact on grid power factor - (a) FRC active and reactive power, (b) FRC bus voltage and current, (c) grid voltage and current.

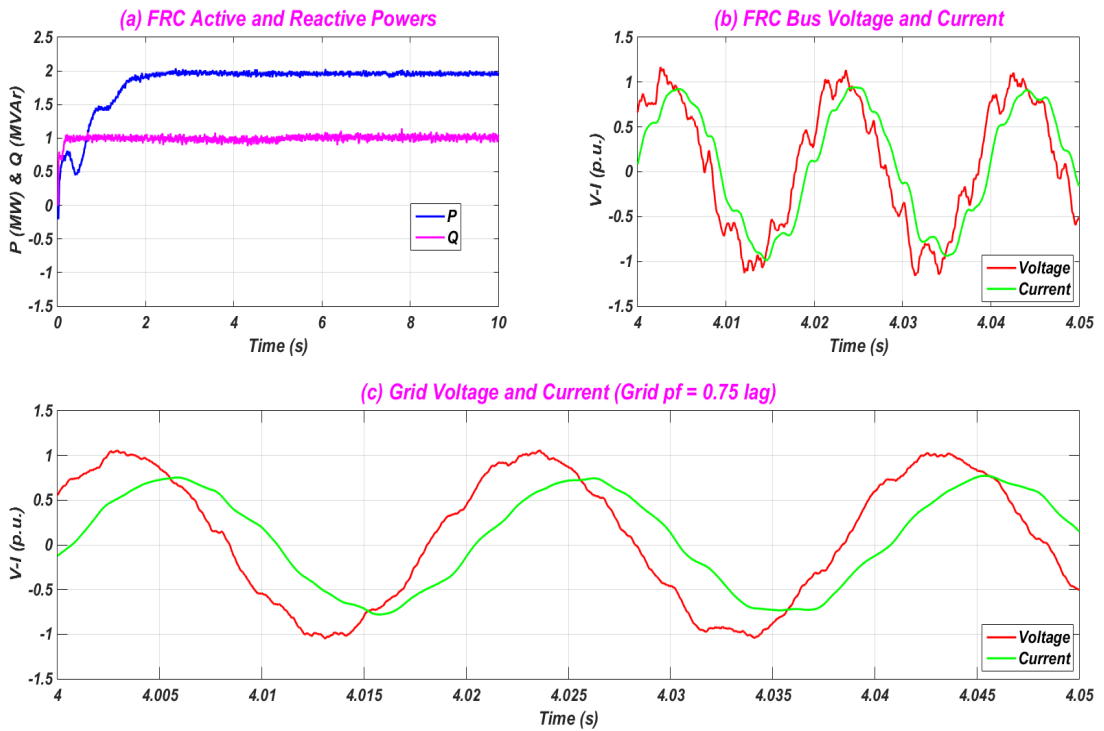


Figure 7.20: IEEE 13 bus system, FRC based wind with 0.9 lag power factor impact on grid power factor - (a) FRC active and reactive power, (b) FRC bus voltage and current, (c) grid voltage and current.

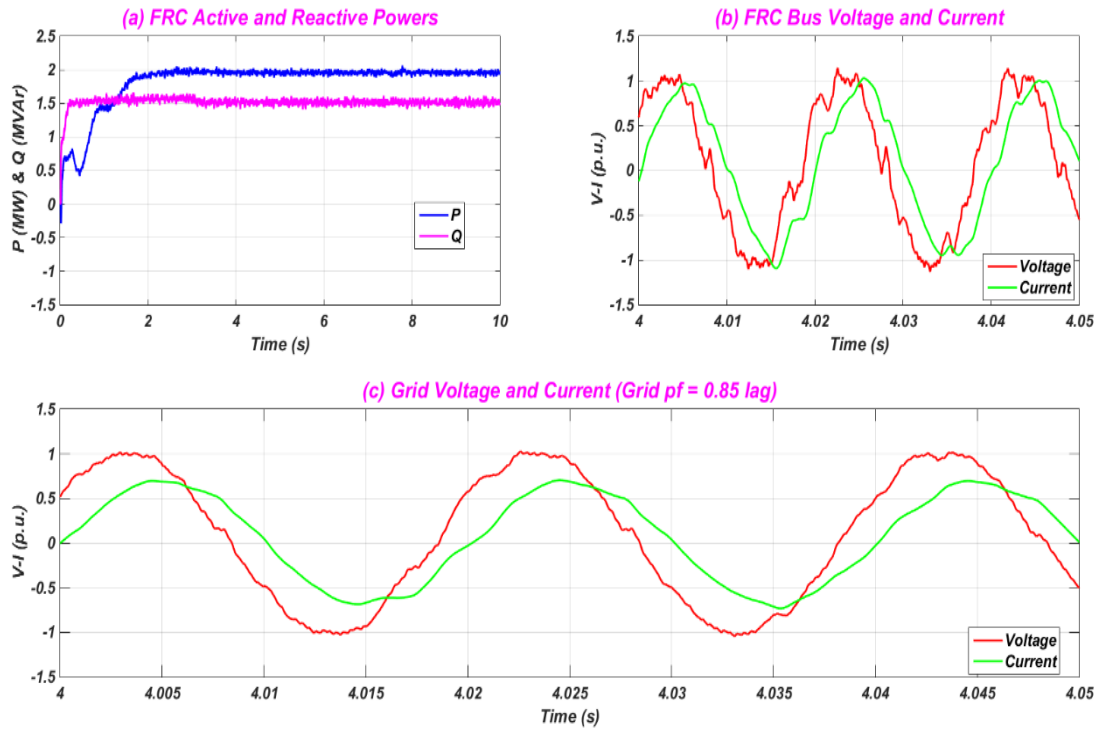


Figure 7.21: IEEE 13 bus system, FRC based wind with 0.8 lag power factor impact on grid power factor - (a) FRC active and reactive power, (b) FRC bus voltage and current, (c) grid voltage and current.

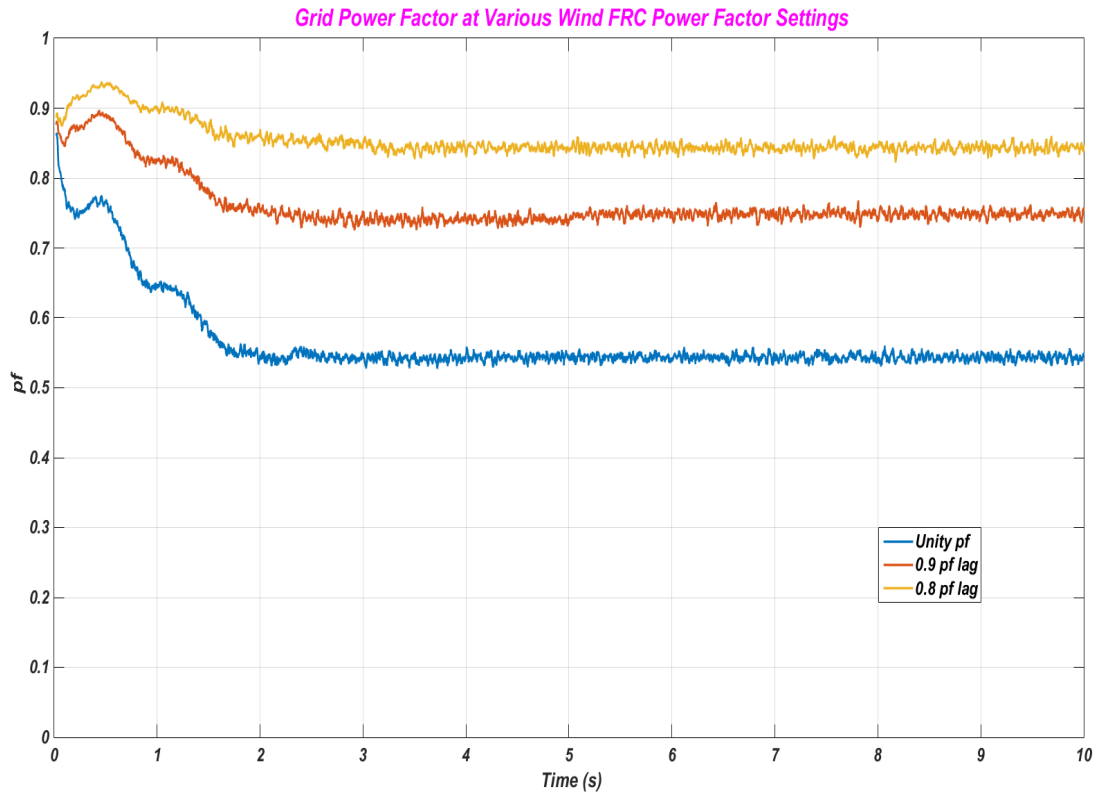


Figure 7.22: IEEE 13 bus system with wind FRC penetration, grid power factor at various FRC power factor settings.

7.7.3 IEEE 37 Bus Distribution System

The IEEE Power Engineering Society has published another test system for distribution system analysis called the IEEE 37 Node Test Feeder [195]. A schematic diagram of this system is illustrated in Chapter 4, Figure 4.23. Detailed data regarding this system are given in Appendix B.2. The system is connected to the ac grid through a two winding ac transformer. Bus 799 is the bus which interconnects the grid with the test network. Table 4.6 in Chapter 4 summarizes the IEEE 37 bus distribution network data. The grid is assumed to be an infinite bus. The renewable resources are connected to the farthest node from the grid, which is bus number 741. The main objective of this chapter is to investigate the impact of different renewable energy sources on the grid power factor and the same test procedure discussed for the IEEE 13 bus system in section 7.7.2 is used. The grid power factor without adding the renewable sources in the 37 bus system is 0.88 lag, as shown in Figure 7.23.

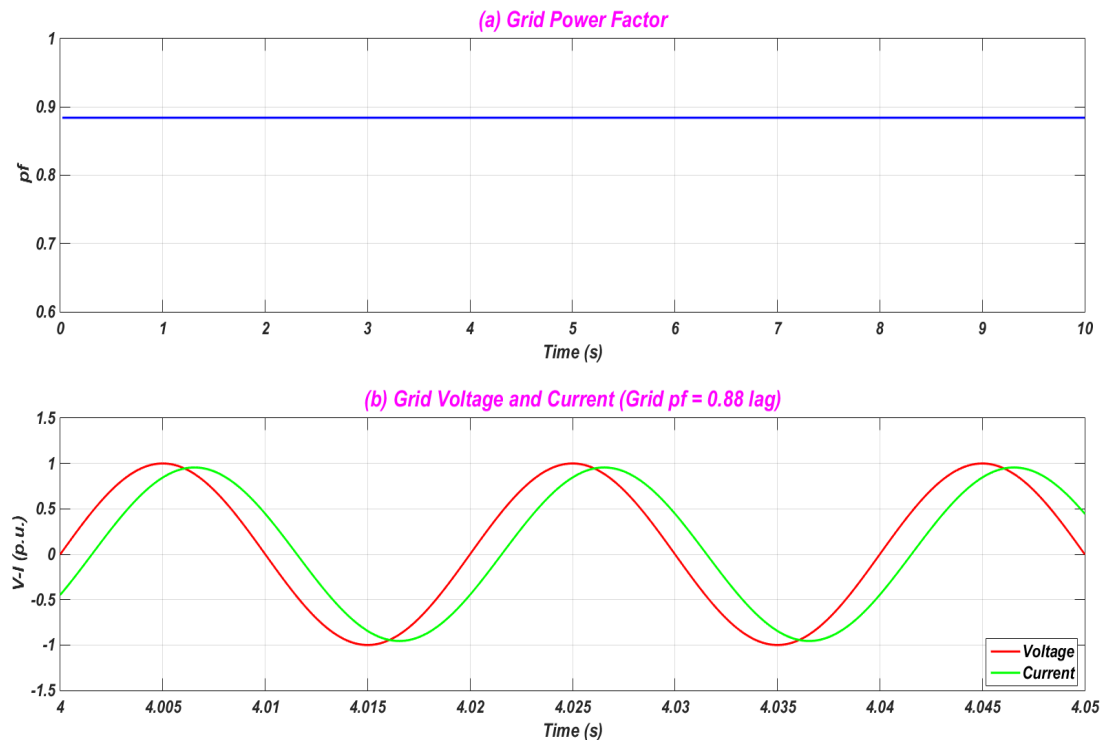


Figure 7.23: IEEE 37 bus system without renewables - (a) grid power factor, (b) grid voltage and current.

A- With PV Penetration

A 1 MW photovoltaics unit is installed at bus 741, which represents 39 % of the total generation in the system. The contribution of each power source to the total power generation in the 37 bus system and the locations are given in Table 7.5. The impact

of the installed photovoltaic unit on the grid power factor is shown in Figures 7.24, 7.25 and 7.26 for various power factor settings, unity, 0.9 lag and 0.8 lag respectively. Figure 7.27 gives a comparison between various power factor settings of PV on the grid power factor. It also shows that the grid power factor is enhanced when the PV unit provides reactive power and operates at non unity power factors.

Table 7.5: IEEE 37 bus system, power generation source outputs and their locations (PV case).

	Grid	PV
Total Generation	1.54 MW	1 MW
Location	Bus 799	Bus 741

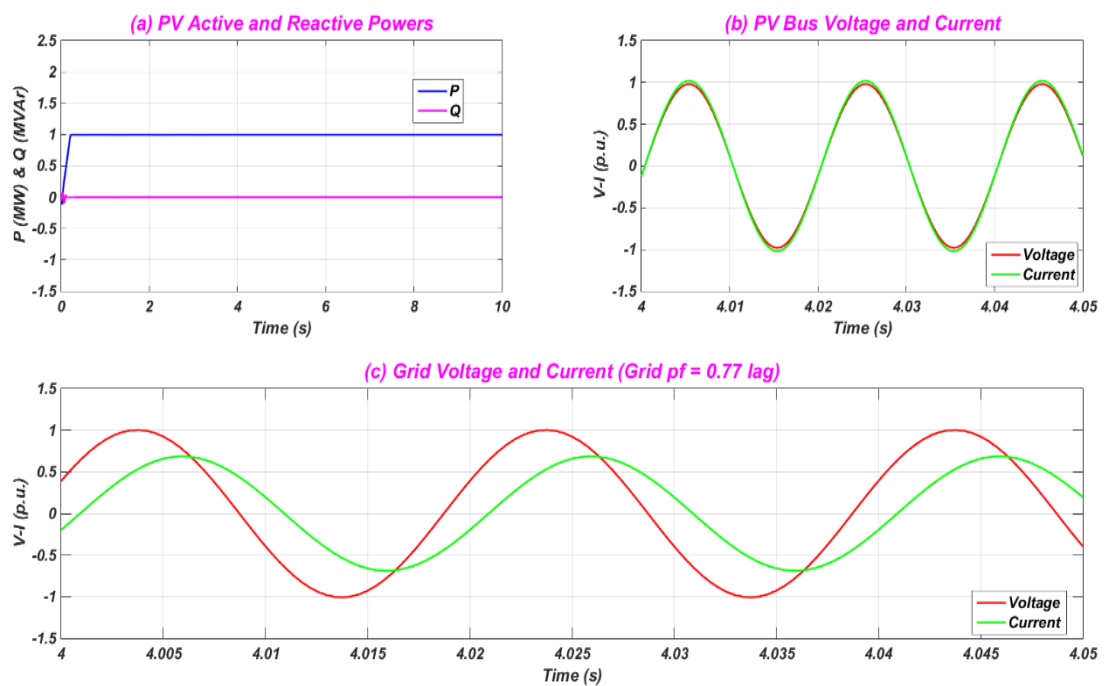


Figure 7.24: IEEE 37 bus system, PV with unity power factor impact on grid power factor - (a) PV active and reactive power, (b) PV bus voltage and current, (c) grid voltage and current.

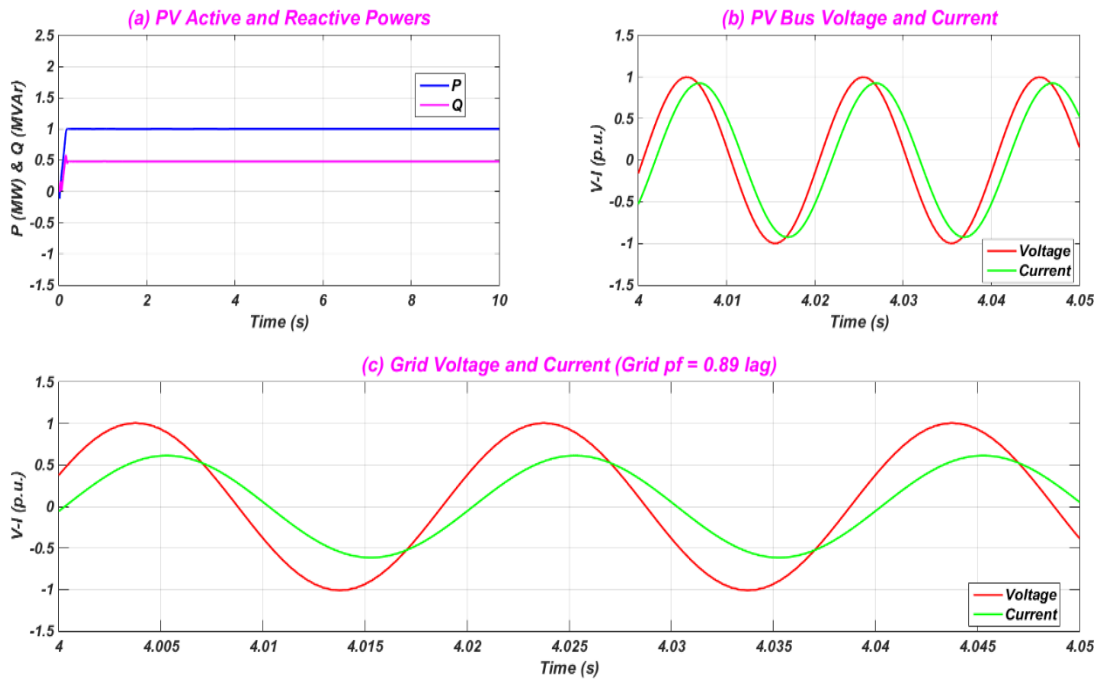


Figure 7.25: IEEE 37 bus system, PV with 0.9 lag power factor impact on grid power factor - (a) PV active and reactive power, (b) PV bus voltage and current, (c) grid voltage and current.

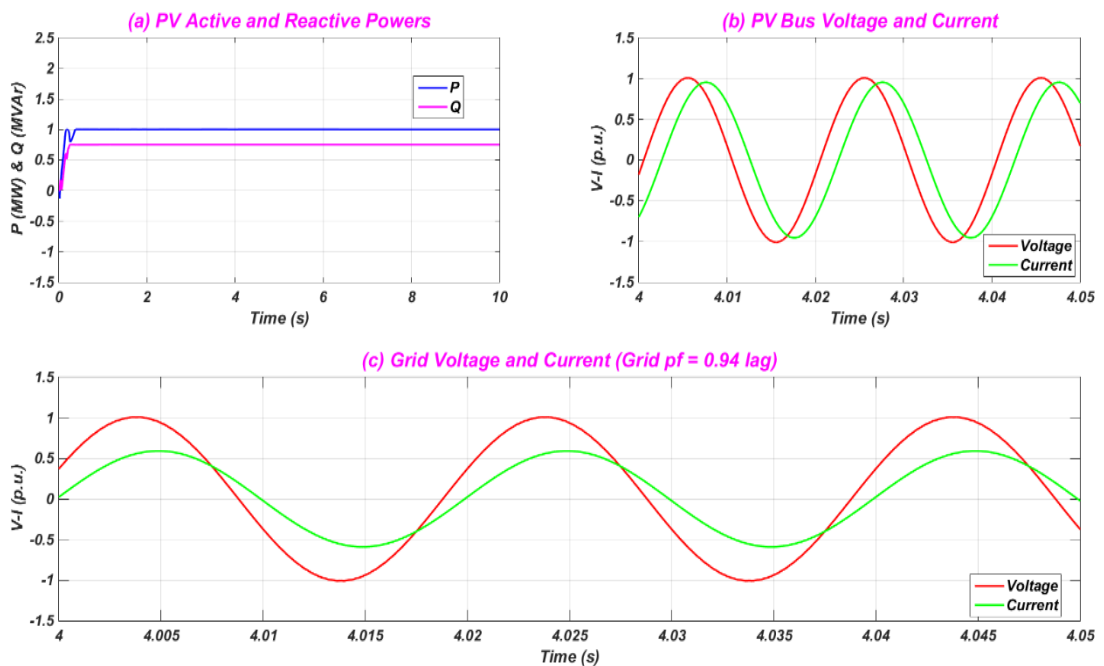


Figure 7.26: IEEE 37 bus system, PV with 0.8 lag power factor impact on grid power factor - (a) PV active and reactive power, (b) PV bus voltage and current, (c) grid voltage and current.

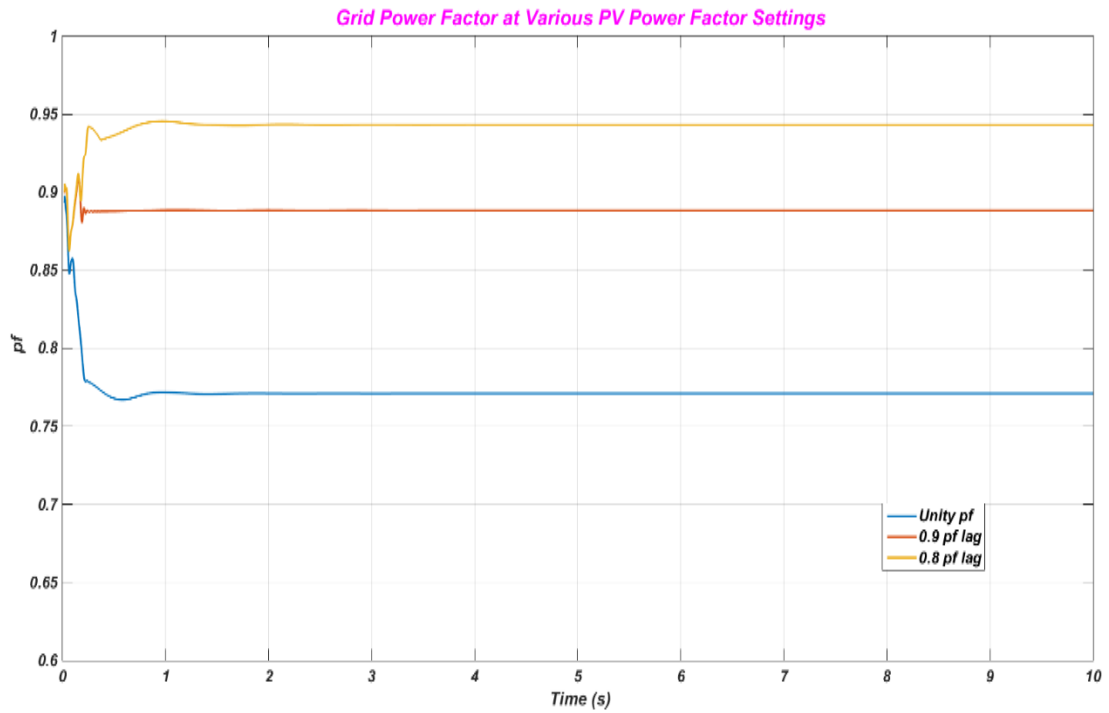


Figure 7.27: IEEE 37 bus system with PV penetration, grid power factor at various PV power factor settings.

B- With Wind based on DFIG Penetration

A DFIG based on wind energy is installed at bus 741 with 1.5 MW output power, which is 59 % of the total generation in the 37 bus system. Table 7.6 shows the contribution of each power source in the 37 bus system to the total power generation and the locations. The impact of the installed DFIG on the grid power factor is shown in Figures 7.28, 7.29 and 7.30 for various power factor settings, unity, 0.9 lag and 0.8 lag respectively. Figure 7.31 shows a comparison between different power factor settings of the installed DFIG on the grid power factor. As shown in this figure, the grid power factor is improved when the DFIG offers reactive power and operates at non unity power factors.

Table 7.6: IEEE 37 bus system, power generation source outputs and their locations (DFIG case).

	<i>Grid</i>	<i>DFIG</i>
<i>Total Generation</i>	1.04 MW	1.5 MW
<i>Location</i>	Bus 799	Bus 741

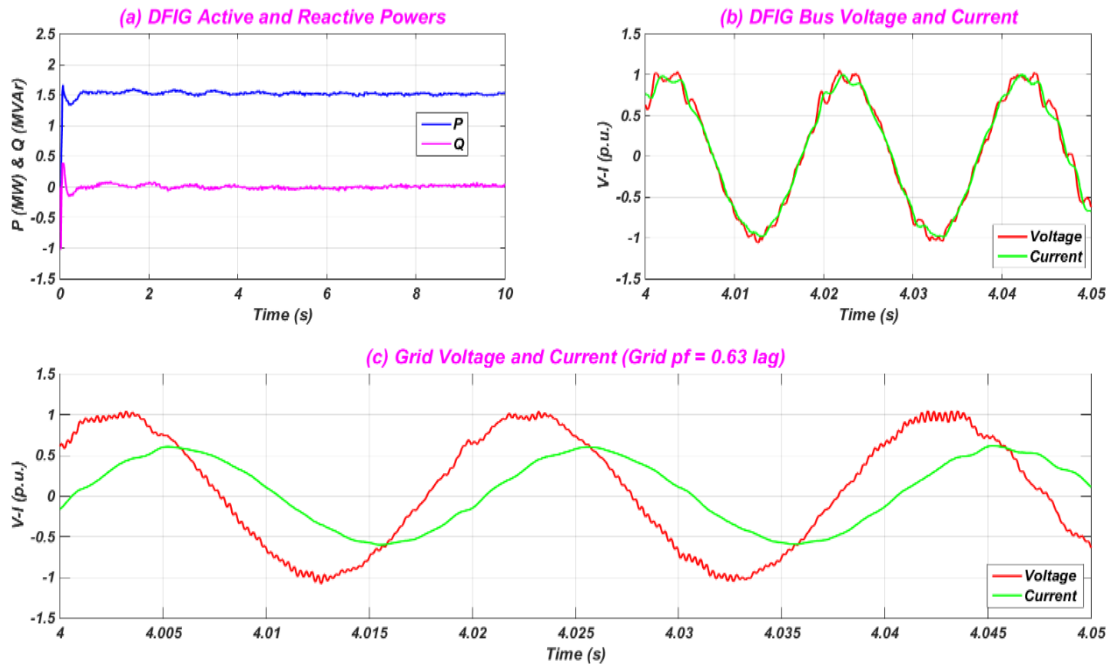


Figure 7.28: IEEE 37 bus system, DFIG based wind with unity power factor impact on grid power factor - (a) DFIG active and reactive power, (b) DFIG bus voltage and current, (c) grid voltage and current.

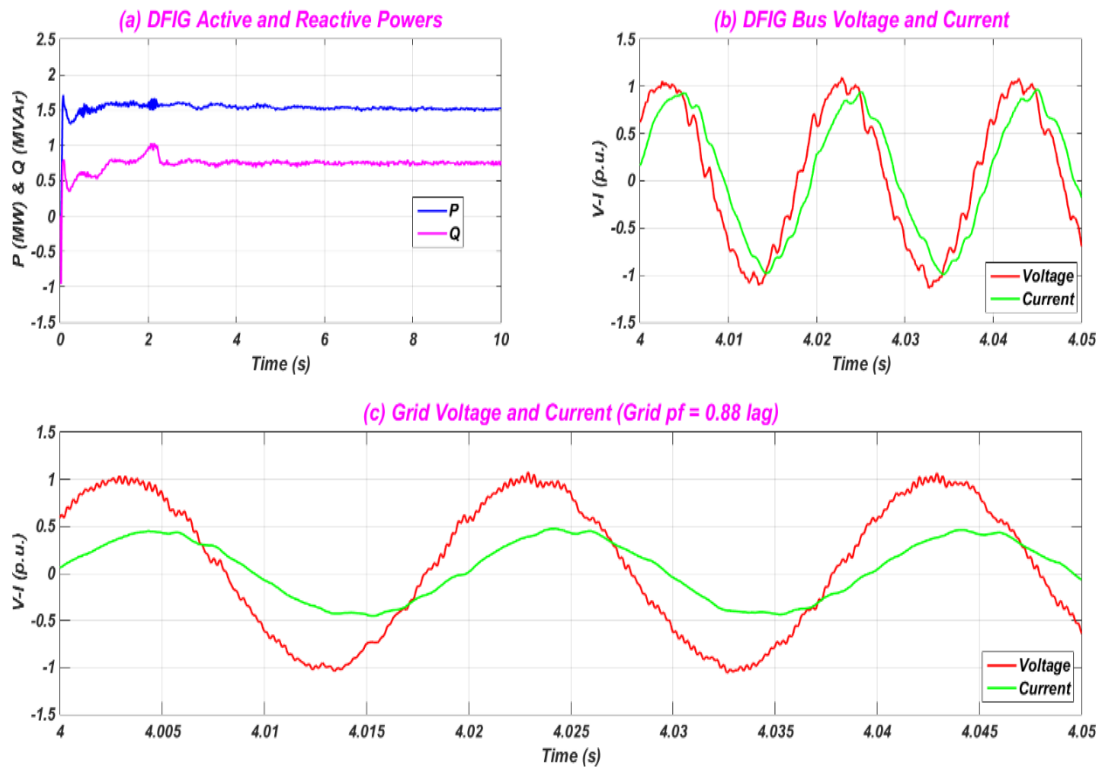


Figure 7.29: IEEE 37 bus system, DFIG based wind with 0.9 lag power factor impact on grid power factor - (a) DFIG active and reactive power, (b) DFIG bus voltage and current, (c) grid voltage and current.

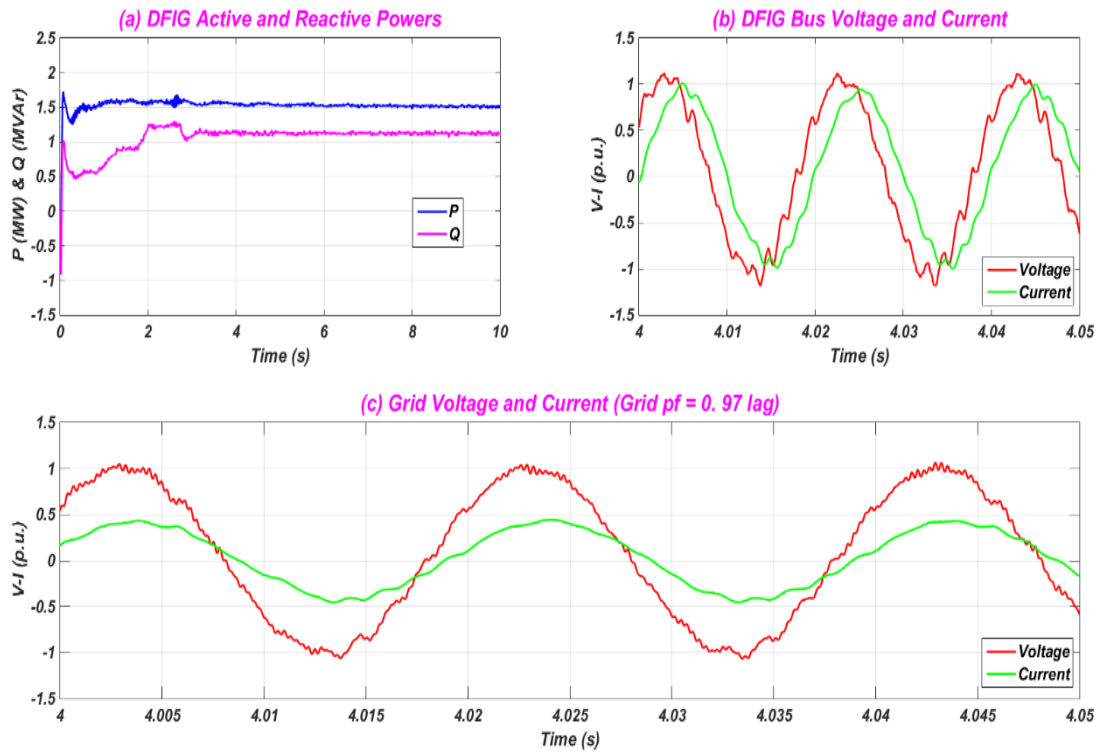


Figure 7.30: IEEE 37 bus system, DFIG based wind with 0.8 lag power factor impact on grid power factor - (a) DFIG active and reactive power, (b) DFIG bus voltage and current, (c) grid voltage and current.

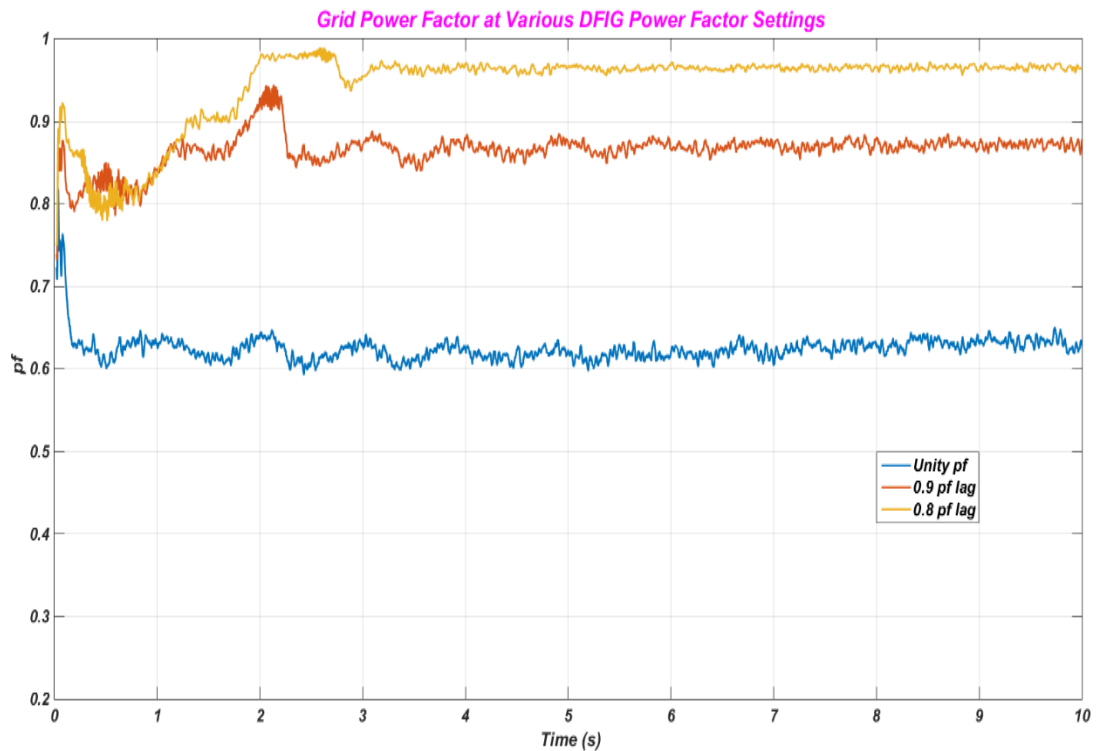


Figure 7.31: IEEE 37 bus system with DFIG penetration, grid power factor at various DFIG power factor settings.

C- Wind based on Synchronous Generator with Fully Rated Converters Penetration

A DG based on a wind FRC synchronous generator is installed at bus 680 with 2 MW output power, which represents 79 % of the total generation in the 37 bus system. The participation of each power source in the 37 bus system to the total power generation and the locations are given in Table 7.7. The impact of the installed FRC wind unit on the grid power factor is shown in Figures 7.32, 7.33 and 7.34 for various power factor settings, unity, 0.9 lag and 0.8 lag respectively. Figure 7.35 shows a comparison between different power factor settings of the installed wind FRC on the grid power factor. It shows that the grid power factor is improved when the FRC unit provides reactive power and operates at non unity power factors.

Table 7.7: IEEE 37 bus system, power generation source outputs and their locations (FRC case).

	<i>Grid</i>	<i>wind FRC</i>
<i>Total Generation</i>	0.54 MW	2 MW
<i>Location</i>	Bus 799	Bus 741

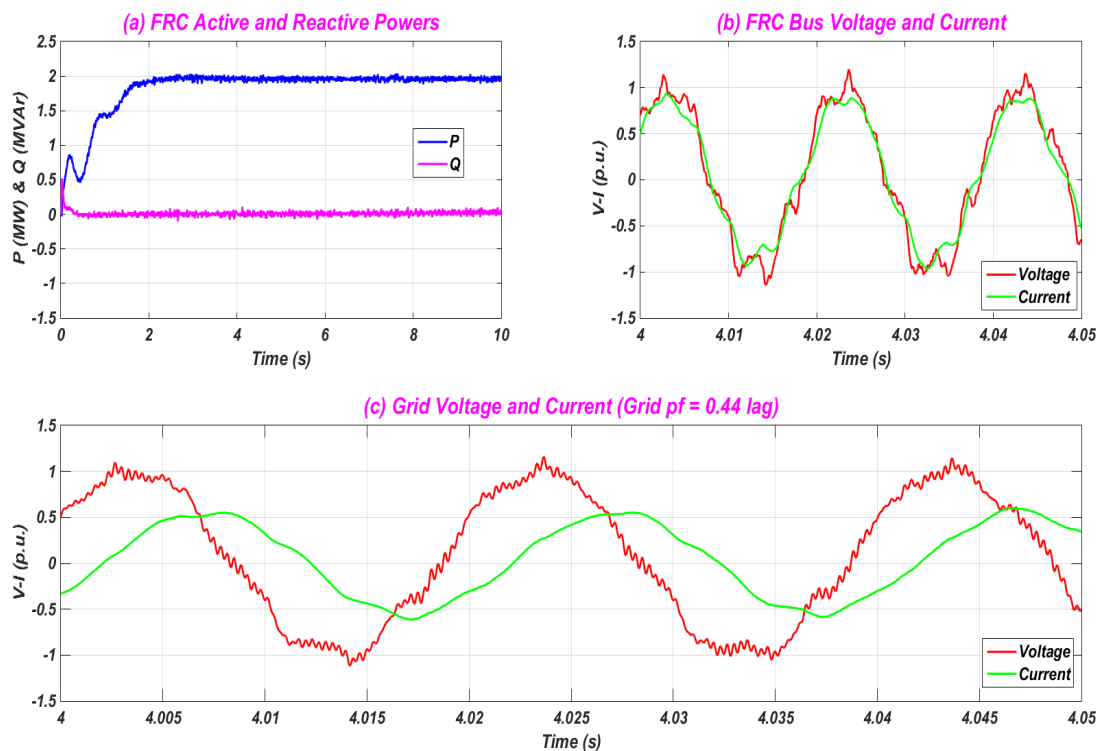


Figure 7.32: IEEE 37 bus system, FRC based wind with unity power factor impact on grid power factor - (a) FRC active and reactive power, (b) FRC bus voltage and current, (c) grid voltage and current.

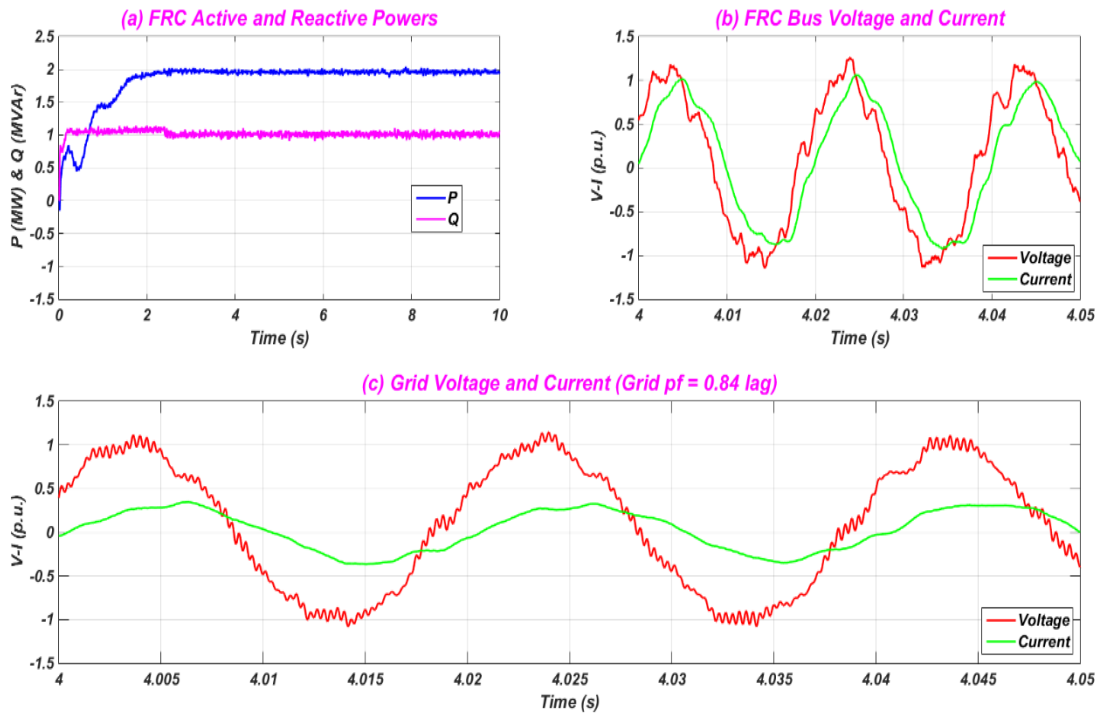


Figure 7.33: IEEE 37 bus system, FRC based wind with 0.9 lag power factor impact on grid power factor - (a) FRC active and reactive power, (b) FRC bus voltage and current, (c) grid voltage and current.

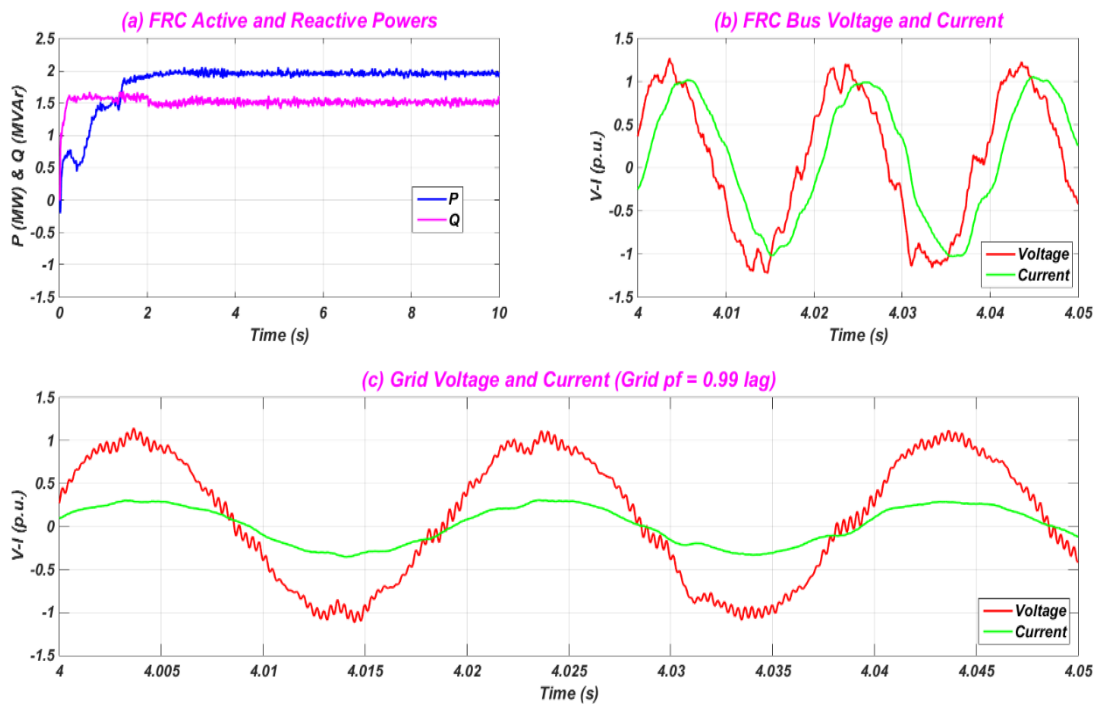


Figure 7.34: IEEE 37 bus system, FRC based wind with 0.8 lag power factor impact on grid power factor - (a) FRC active and reactive power, (b) FRC bus voltage and current, (c) grid voltage and current.

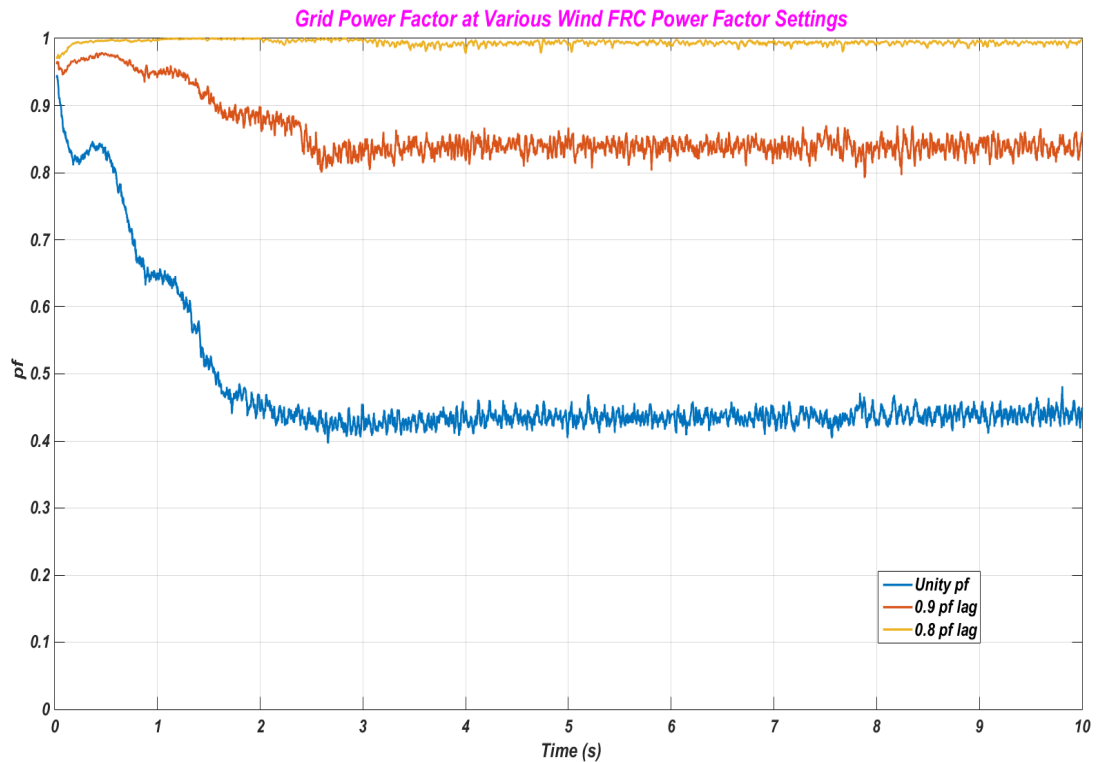


Figure 7.35: IEEE 37 bus system with wind FRC penetration, grid power factor at various FRC power factor settings.

7.7.4 IEEE 123 Bus Distribution System

The IEEE 123 Node Test Feeder is another test system for distribution system analysis released by the IEEE Power Engineering Society [195]. A schematic diagram of this system is illustrated in Chapter 4, Figure 4.34. Detailed data regarding this system are given in Appendix B.3. The system is connected to the ac grid through a two winding ac transformer. Bus 150 is the bus which interconnects the grid with the test network. Table 4.11 in Chapter 4 summarizes the IEEE 123 bus distribution network data. The grid is assumed to be an infinite bus. The DG based on renewable energy resources is connected to the farthest node from the grid, which is bus 85. In this chapter, the impact of different renewable energy sources on the grid power factor is investigated and the same test procedure discussed for the IEEE 13 bus and IEEE 37 bus systems, in sections 7.7.2 and 7.7.3, is used. The grid power factor of the 123 bus system without adding the renewable energy sources is 0.85 lag, as shown in Figure 7.36.

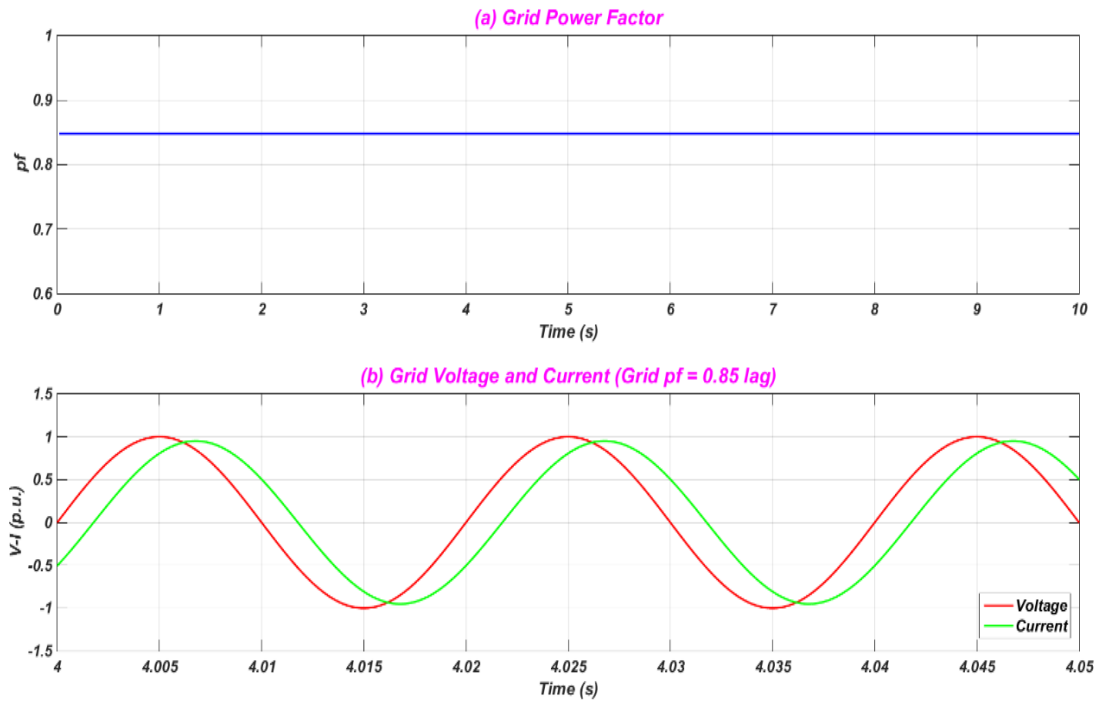


Figure 7.36: IEEE 123 bus system without renewables - (a) grid power factor, (b) grid voltage and current.

A- With PV Penetration

A 1 MW DG based on a PV grid connected system is installed at bus 85, which represents 27 % of the total generation in the 123 bus system. The contribution of each power source to the total power generation in the 123 bus distribution system and the locations are given in Table 7.8. The impact of the installed grid connected PV system on the grid power factor is illustrated in Figures 7.37, 7.38 and 7.39 for various power factor settings, unity, 0.9 lag and 0.8 lag respectively. A comparison between various power factor settings of the photovoltaic unit on the grid power factor is shown in Figure 7.40. It illustrates that the grid power factor is improved when the photovoltaic unit offers reactive power and operates at non unity power factors.

Table 7.8: IEEE 123 bus system, power generation source outputs and their locations (PV case).

	<i>Grid</i>	<i>PV</i>
<i>Total Generation</i>	2.63 MW	1 MW
<i>Location</i>	Bus 150	Bus 85

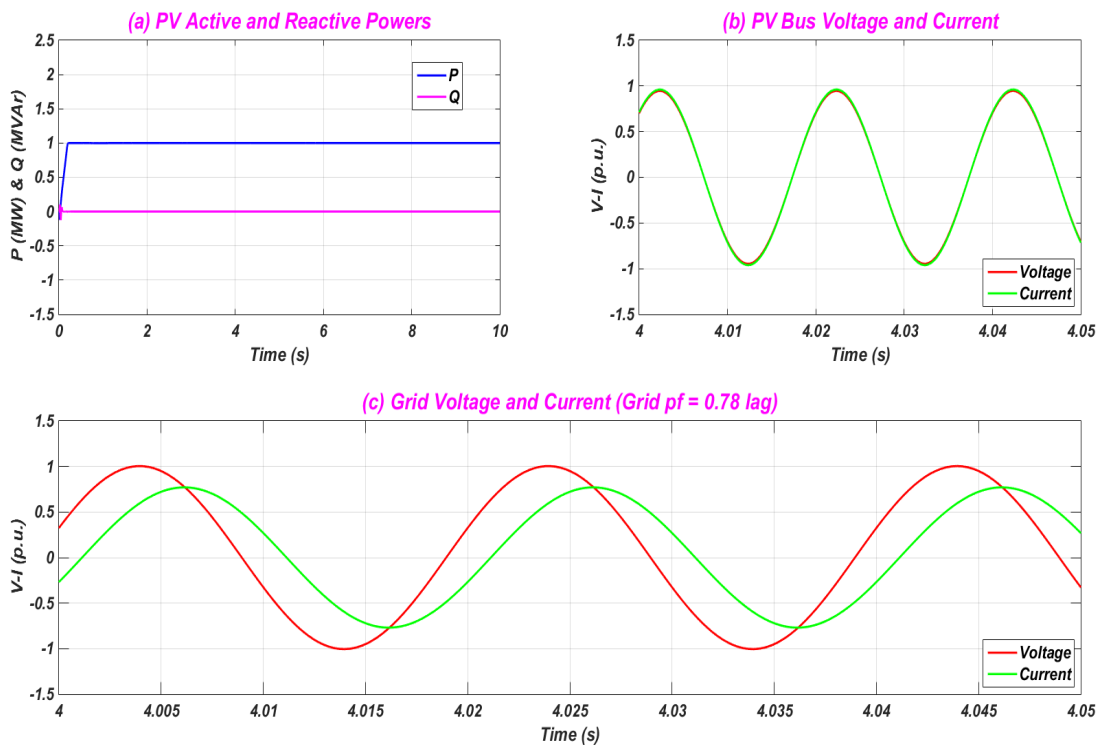


Figure 7.37: IEEE 123 bus system, PV with unity power factor impact on grid power factor - (a) PV active and reactive power, (b) PV bus voltage and current, (c) grid voltage and current.

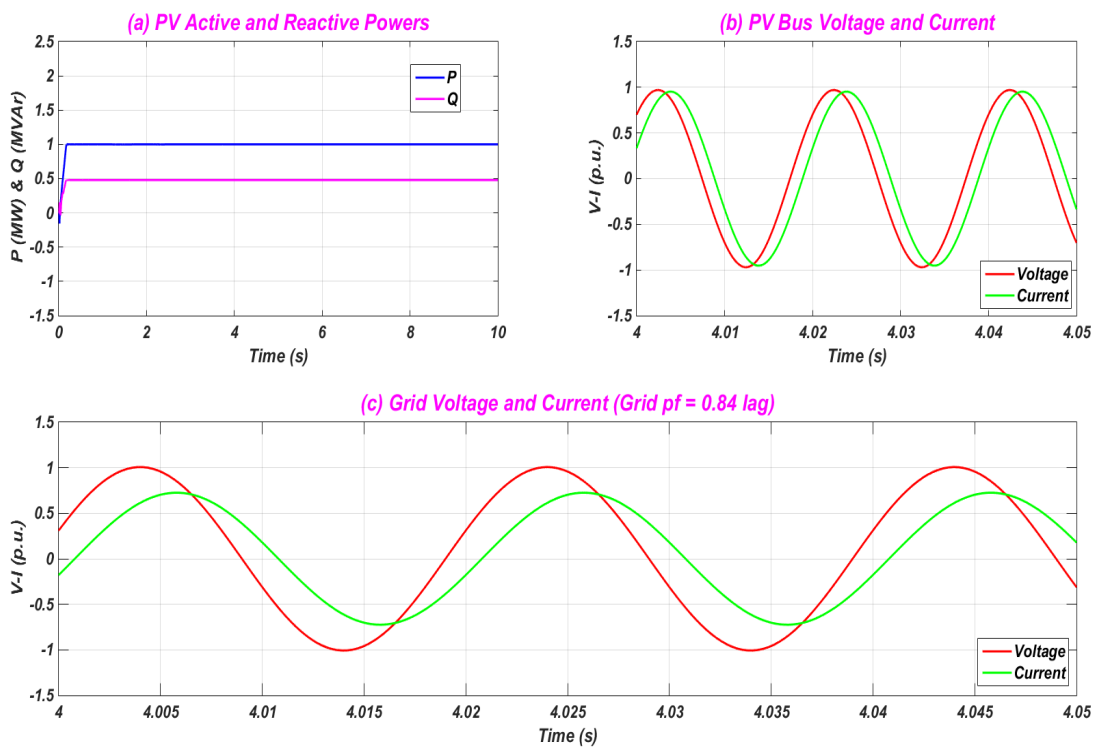


Figure 7.38: IEEE 123 bus system, PV with 0.9 lag power factor impact on grid power factor - (a) PV active and reactive power, (b) PV bus voltage and current, (c) grid voltage and current.

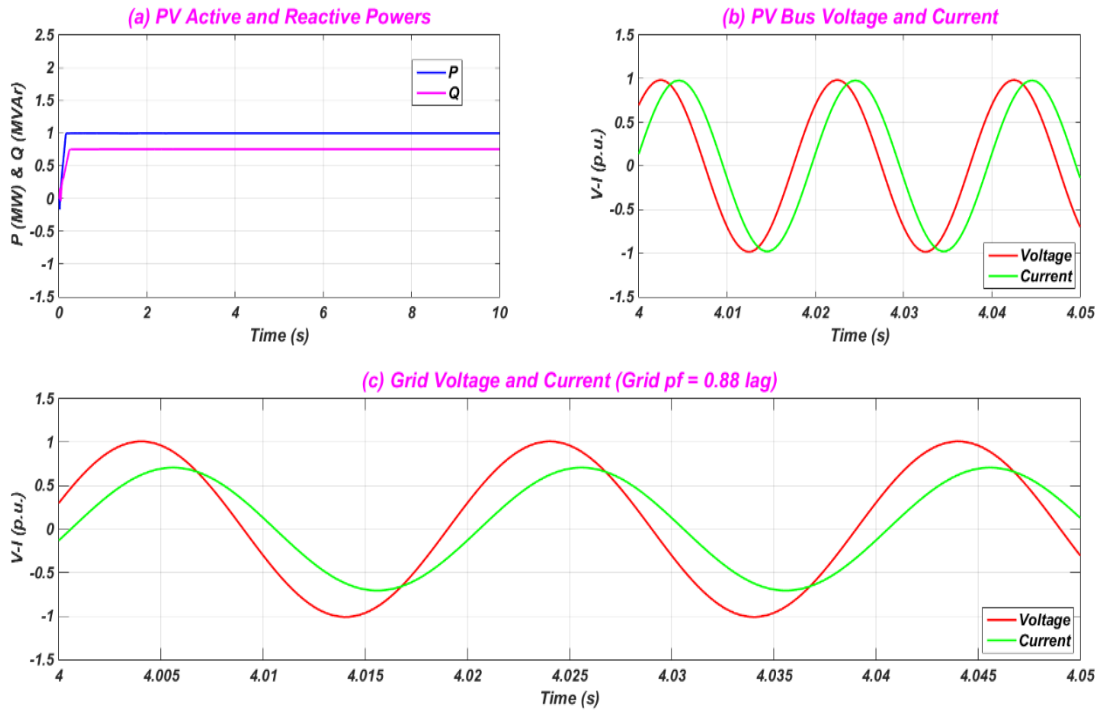


Figure 7.39: IEEE 123 bus system, PV with 0.8 lag power factor impact on grid power factor - (a) PV active and reactive power, (b) PV bus voltage and current, (c) grid voltage and current.

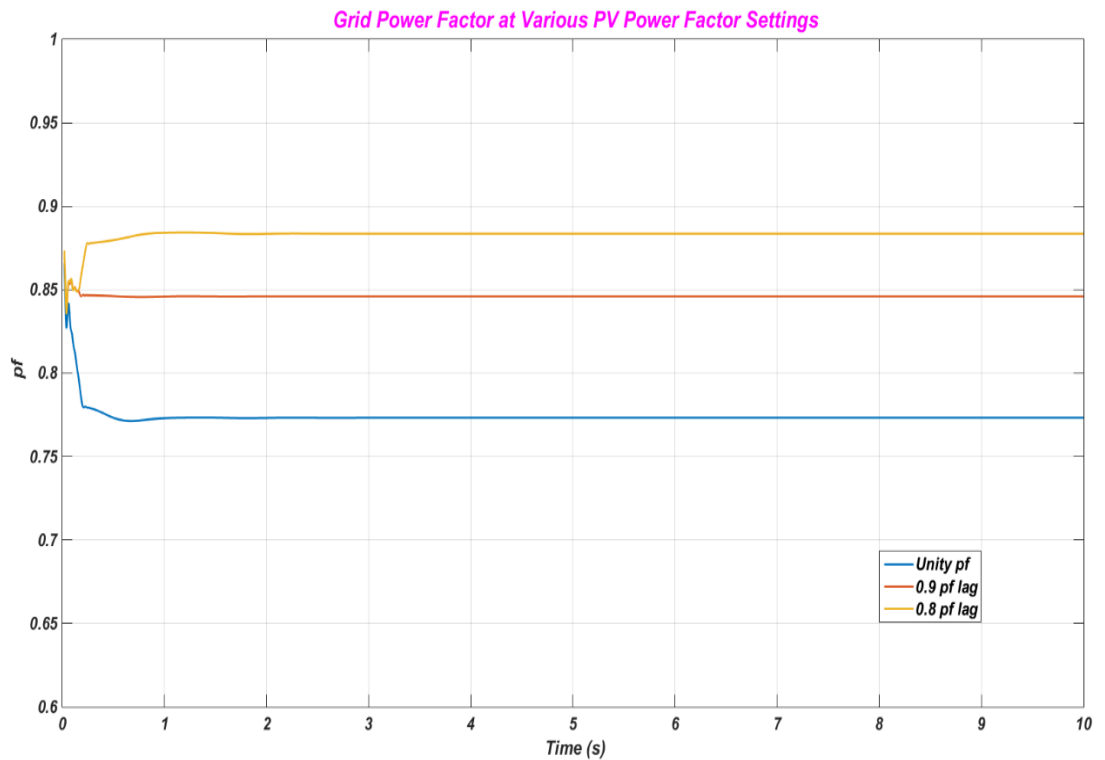


Figure 7.40: IEEE 123 bus system with PV penetration, grid power factor at various PV power factor settings.

B- With Wind based on DFIG Penetration

A 1.5 DFIG based on wind is installed at bus 85, which is 41 % of the total generation in the 123 bus distribution system. The contribution of each power source in the 123 bus distribution system to the total power generation and the locations are given in Table 7.9. The impact of the installed renewable unit based on the DFIG on the grid power factor is illustrated in Figures 7.41, 7.42 and 7.43 for various power factor settings, unity, 0.9 lag and 0.8 lag respectively. A comparison between different power factor settings of the installed wind turbine based on the DFIG on the grid power factor is shown in Figure 7.44. From the figure it is clear that the grid power factor is enhanced when the DFIG based on wind energy provides reactive power and operates at non unity power factors.

Table 7.9: IEEE 123 bus system, power generation source outputs and their locations (DFIG case).

	<i>Grid</i>	<i>DFIG</i>
<i>Total Generation</i>	2.13 MW	1.5 MW
<i>Location</i>	Bus 150	Bus 85

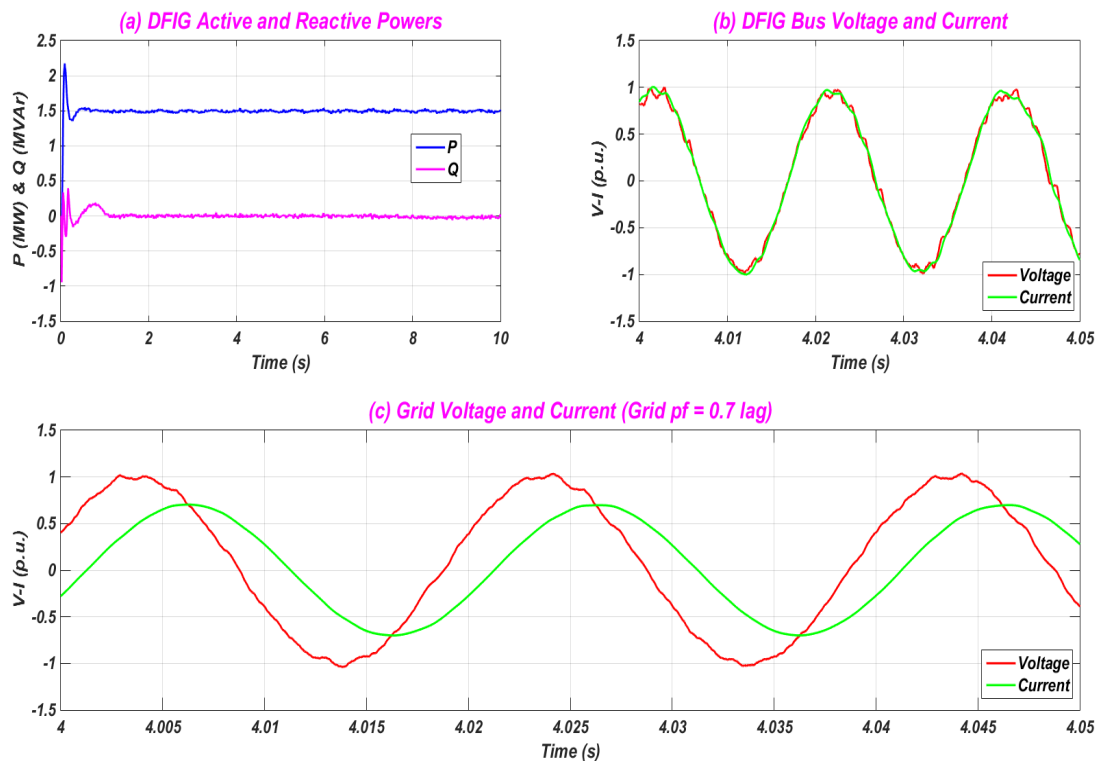


Figure 7.41: IEEE 123 bus system, DFIG based wind with unity power factor impact on grid power factor - (a) DFIG active and reactive power, (b) DFIG bus voltage and current, (c) grid voltage and current.

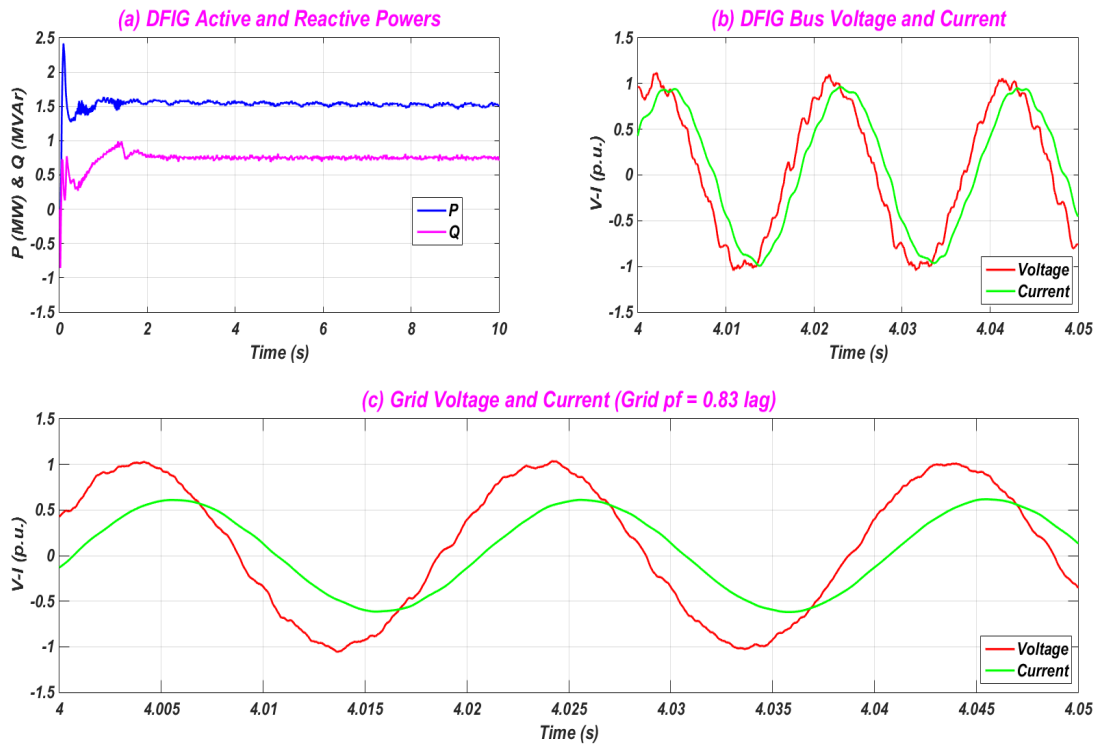


Figure 7.42: IEEE 123 bus system, DFIG based wind with 0.9 lag power factor impact on grid power factor - (a) DFIG active and reactive power, (b) DFIG bus voltage and current, (c) grid voltage and current.

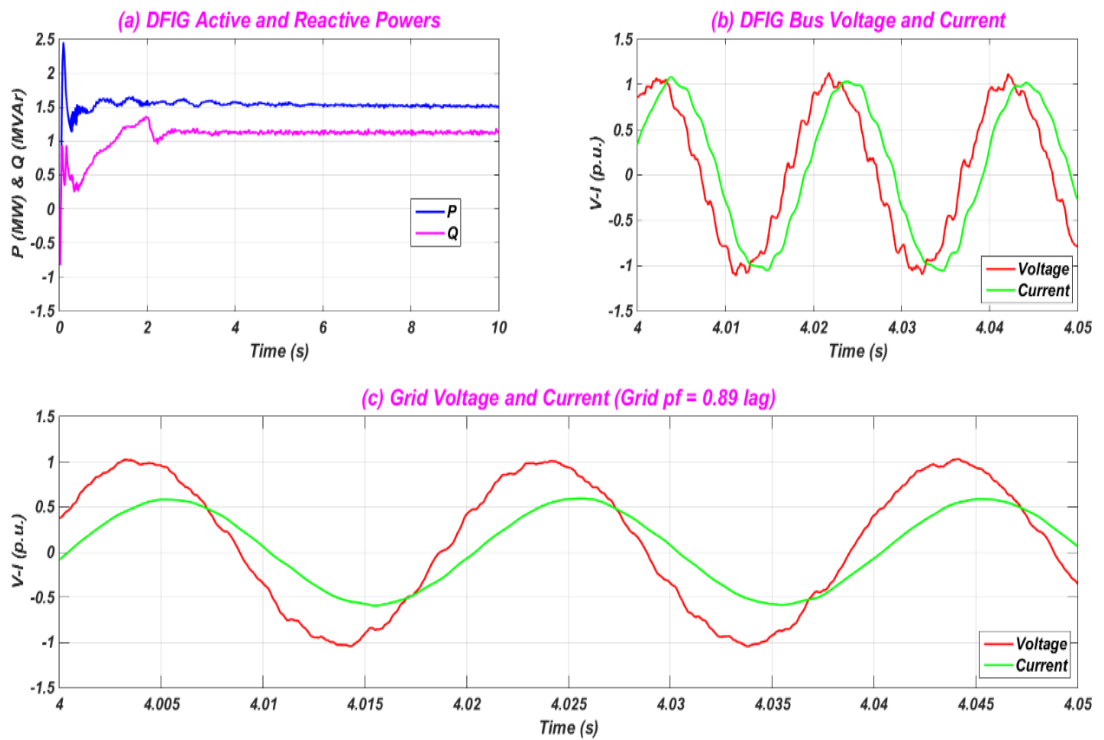


Figure 7.43: IEEE 123 bus system, DFIG based wind with 0.8 lag power factor impact on grid power factor - (a) DFIG active and reactive power, (b) DFIG bus voltage and current, (c) grid voltage and current.

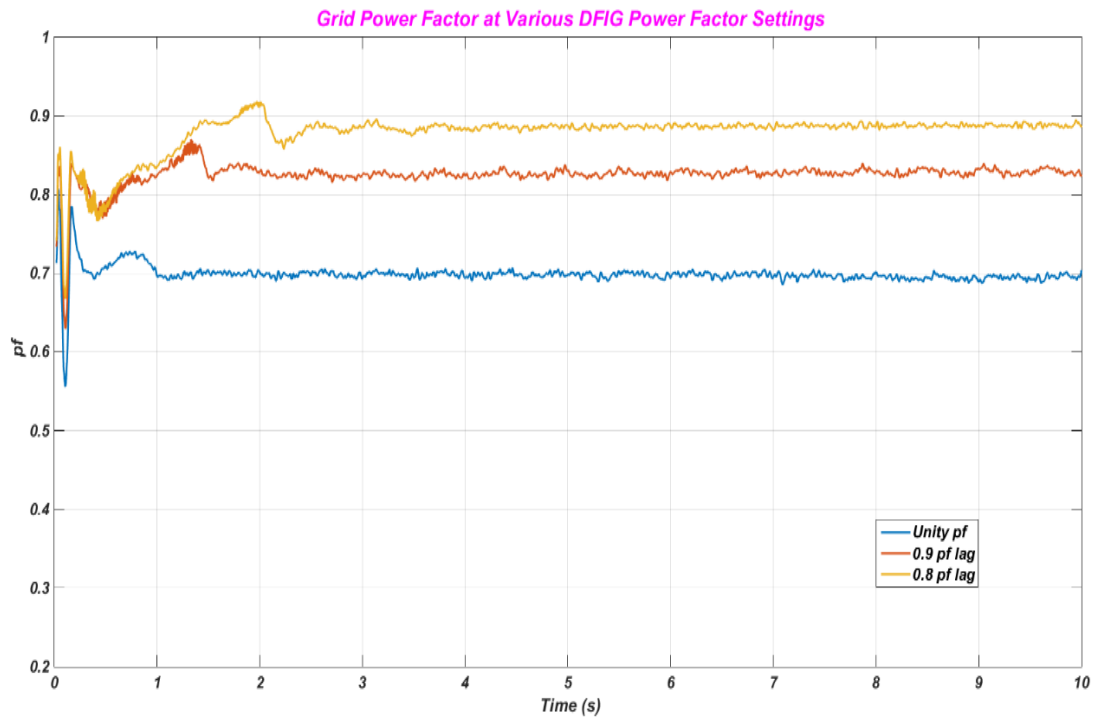


Figure 7.44: IEEE 123 bus system with DFIG penetration, grid power factor at various DFIG power factor settings.

C- Wind based on Synchronous Generator with Fully Rated Converters Penetration

A 2 MW distributed generation based on a wind FRC synchronous generator is installed at bus 85, which represents 55 % of the total generation in the 123 bus distribution system. The contribution of each power source in the 123 bus distribution system to the total power generation and the locations are given in Table 7.10. The impact of the installed DG unit on the grid power factor is illustrated in Figures 7.45, 7.46 and 7.47 for various power factor settings, unity, 0.9 lag and 0.8 lag respectively. A comparison between different power factor settings of the installed FRC unit based on wind energy on the grid power factor is shown in Figure 7.48. From this figure it is clear that the grid power factor is enhanced when the FRC unit offers reactive power and operates at non unity power factors.

Table 7.10: IEEE 123 bus system, power generation source outputs and their locations (FRC case).

	Grid	wind FRC
Total Generation	1.63 MW	2 MW
Location	Bus 150	Bus 85

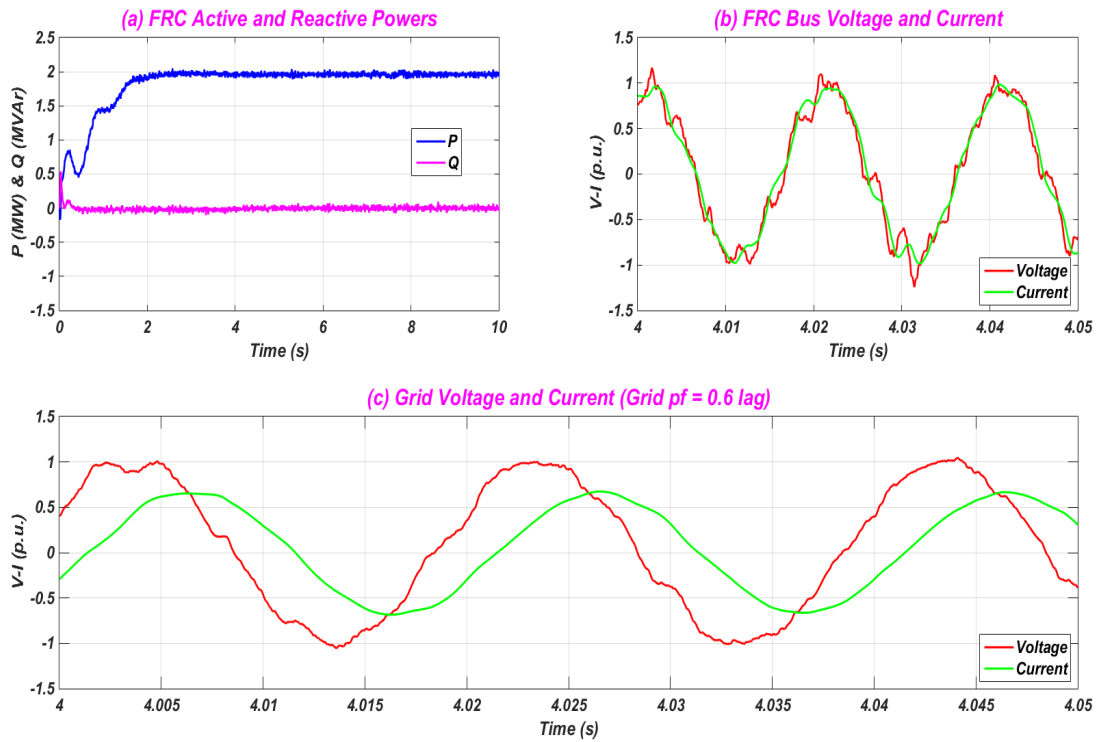


Figure 7.45: IEEE 123 bus system, FRC based wind with unity power factor impact on grid power factor - (a) FRC active and reactive power, (b) FRC bus voltage and current, (c) grid voltage and current.

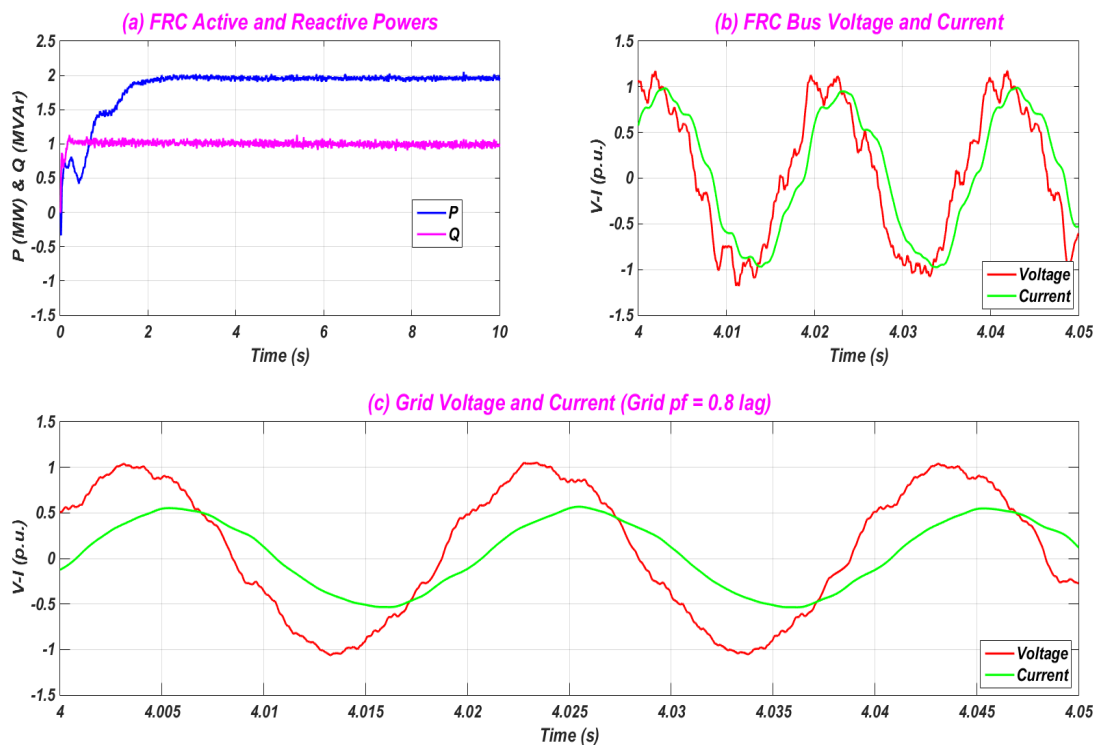


Figure 7.46: IEEE 123 bus system, FRC based wind with 0.9 lag power factor impact on grid power factor - (a) FRC active and reactive power, (b) FRC bus voltage and current, (c) grid voltage and current.

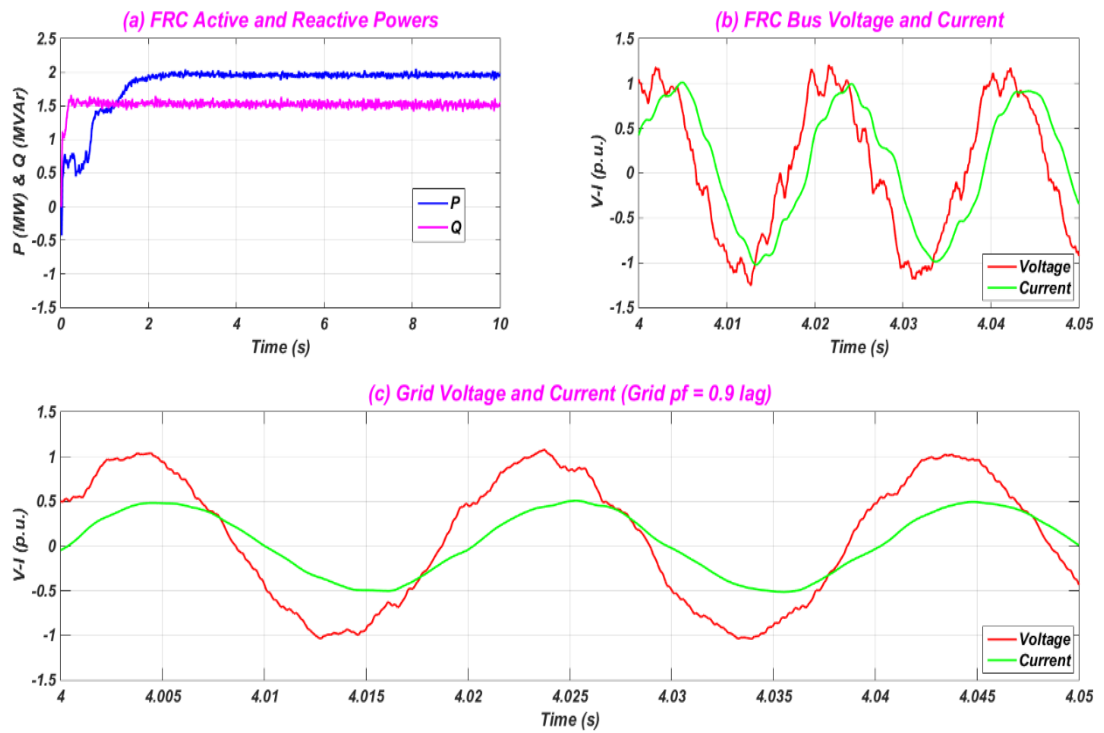


Figure 7.47: IEEE 123 bus system, FRC based wind with 0.8 lag power factor impact on grid power factor - (a) FRC active and reactive power, (b) FRC bus voltage and current, (c) grid voltage and current.

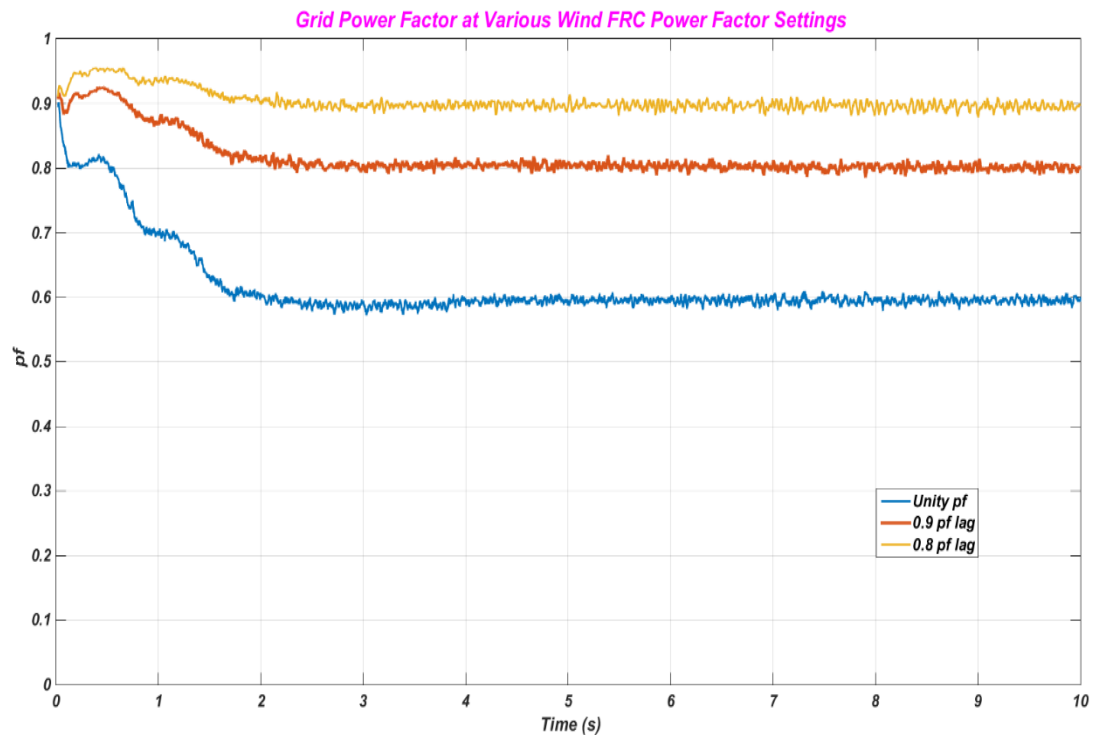


Figure 7.48: IEEE 123 bus system with wind FRC penetration, grid power factor at various FRC power factor settings.

7.8 Conclusions

The presence of renewable energy sources based on wind and solar energy has increased considerably in distribution systems due to governmental support and the need to tackle climate change. However, the increase in renewable energy penetration has led to various technical challenges to power systems, such as renewable units without reactive power controllability experiencing a rise in system voltages. In addition, the grid power factor can be affected, as discussed in this chapter. Providing reactive power from renewable energy resources can improve this. This chapter has investigated the need for reactive power support from renewable units in power systems. It has also discussed various renewable energy technologies. A wind turbine based on the DFIG, a wind turbine based on a synchronous generator with fully rated converters, and solar energy based on photovoltaics have all been discussed in this chapter and they have been used as distributed generation units.

A three phase two stage transformerless PV grid connected system has been proposed in this chapter with reactive power capability. The simulation results have illustrated how a PV system can provide reactive power under different solar irradiance conditions. The grid power factor of various distribution systems have been investigated with and without renewable energy penetration. DG units based on wind energy DFIG, FRC wind, and photovoltaics have been shown to affect the grid power factor when these units operate at unity power factor for the selected distribution systems. When these generating units operate at different power factor settings, the power factor of the grid is improved, as shown in the simulation results.

CHAPTER 8 Conclusions

8.1 General Conclusions

This thesis presented a general review of renewable energy generating units based on wind and solar-photovoltaics, focusing on the relevant technologies in use today for wind power generation and PV grid connected systems. The evolution of the wind and photovoltaic industry and the potential and benefits of such renewable energy sources were discussed. The aim was to put forward an understanding of the dramatic increase and developments of wind power and PV generation systems around the world and the likely consequences this will have on power systems operation. It was shown that the PV industry has been developed considerably in the last few years, with 140 GW being installed in just the last four years compared to around 40 GW installed beforehand. Wind power has increased rapidly in the last few years and is approaching more than 369 GW cumulative installed capacity. The main reasons for the rapid development in wind and PV generation in power systems are environmental, economic (governments' economic incentives such as cost subsidies) and related to the security of supply. However, solar and wind power generation have intermittent nature and their output power can be affected by solar irradiance and wind speed respectively which may have a negative impact on power systems operation. Various challenges facing the integration of PV systems and wind generators in power networks were also discussed, such as how much land is needed, raw material availability, reliability problems, PV and wind generating units' efficiency and grid code requirements.

Distributed generation units based on renewable energy including wind and PV units have been required to be disconnected in the past for all fault conditions. This may have led to severe voltage and dynamic stability problems at high renewable penetration levels. The security of supply can be jeopardised by disconnection of renewable energy units in such a system as this leads to a large imbalance between generation and load. Therefore, due to the increase in the use of renewable energy sources for power generation in distribution networks, fault ride through (FRT) grid requirements have been changed in several countries worldwide because the disconnection of large parts of these renewable generating units during fault conditions may cause system instability. This thesis discussed the need to ride through grid faults,

as the distributed generation based on renewable energy could also be at risk of overvoltages and/or overcurrents when the fault location is close to connection terminals. Wind turbines based on the DFIG, wind turbines based on a synchronous generator with fully rated converters, and photovoltaics based on solar energy were investigated as renewable energy sources. These wind and solar units have power electronic converters in their structures. The DC link voltages of these renewable generating units increase during faults and this can damage the power electronic converters. As a result, the power electronic converters should be protected from the effects of such fault conditions. DC choppers were added to the DC link of wind generating units and the simulation results showed that DC link voltages can be maintained within acceptable limits. The fault ride through issues for wind power in transmission systems were investigated in the past, however, this research investigated the fault ride through requirements of such renewable sources in distribution systems. For a photovoltaic based solar energy system, a three phase two stage transformerless PV grid connected was proposed with a new technique to protect the PV converters from faults and to keep the DC link voltage within given limits. There is no need for hardware elements to be added to the control of the PV converter which means no additional costs is needed. However, the DC-DC converter signal which tracks the maximum available power will work during faults to keep the DC voltage within limits and protect the PV converters by using proportional integral (PI) controllers. The simulation results showed that the proposed PV system can ride through faults and the DC link voltage was kept within limits. Various modified generic distribution systems were investigated while experiencing severe fault conditions such as three phase faults. Two different locations for the applied faults were selected to discuss the FRT performance of the distribution networks, one close to the grid and the other close to the renewable generating units. The simulation results showed that the voltage recovery of these distribution systems with high renewable energy penetration based on wind and PV meet the German's LVRT requirements for distributed generators.

The higher the penetration levels of renewable energy sources in distribution systems the lower the stability of the systems will be, as illustrated in this thesis. Unlike the works done in literature which considered large power systems (transmission systems), the transient stability of various distribution networks with high wind and solar power

penetration was investigated in this research. The transient stability was assessed by using the Transient Stability Index method and the simulation results showed that the transient stability of the distribution systems is reduced when these systems have high renewable energy penetration based on wind and PV. The transient stability of these systems was studied when these systems were subjected to a three phase fault and different fault locations affected the transient stability. Wind turbines based on the DFIG, a synchronous generator with fully rated converters based on wind energy, and solar energy based on photovoltaic technology were the renewable energy sources used in this thesis to investigate the transient stability. The simulation results showed that the distribution systems remain stable and return to pre-fault conditions when these systems experience transient fault conditions. However, to improve the impact of renewable sources on system transient stability, fault ride through capability and reactive power dynamic support during fault conditions are required from these generating units.

Due to the rapid increase in renewable energy sources in power systems, several countries have released grid code requirements for renewable energy generating units. A frequency response requirement is one such grid code requirement which has been introduced in recent years. It is an issue in power dynamic operations, as some renewable energy sources have different characteristics from conventional synchronous generators in several respects. One significant difference is that, some renewable generators are connected to the grid via power electronic converters and this causes decoupling of the inertia of their generators from power system inertia, such as in variable speed wind turbines based on the DFIG or a synchronous generator with fully rated converters. Some other renewable energy units, such as photovoltaics do not contribute towards system inertia as there is no machine in their structures to contribute towards power system inertia. Therefore, this thesis discussed system frequency response with high penetration of such renewable technologies when a system is subjected to under- or over-frequency conditions. Various different frequency controls published in literature, including inertia response, active power curtailment and the frequency droop control technique were implemented on large power systems; however, due to the dramatic growth in penetration of renewable sources in distribution systems, it has been important to study the frequency response

of such systems. Various modified generic distribution networks with high renewable energy penetration based on wind and PV were discussed in this research in terms of frequency response. Inertia control and active power reduction methods were investigated in relation to these test systems for different renewable energy technologies based on wind and solar energy. A new frequency control for a wind turbine based on the DFIG was also proposed in this research and was discussed in relation to different distribution systems. The proposed technique to control frequency in the DFIG is aimed at controlling the system frequency by giving second by second responses from the DFIG. The DFIG was modelled in the d-q synchronous frame and the frequency was controlled by added a signal of the frequency and active power changing to the nominal values (1 p.u.) during the frequency disturbance conditions to the rotor current in the d-axis. The proposed frequency control for the DFIG improved the distribution systems' frequency responses, as shown in the simulation results, when these systems experienced under- and over-frequency conditions.

Finally, the grid power factor can be affected when the distributed generation based on renewable sources does not have reactive power control and when they operate at the unity power factor as discussed in this thesis. High renewable energy penetration without reactive power controllability can also lead to a rise in system voltages. Providing reactive power from these generating units can help to solve these problems. The majority of research publications in literature have discussed the reactive power capability of large-scale wind turbines in transmission systems. However, this research investigated the impact of high wind power penetration based on DFIG and synchronous generator with fully rated converters on the grid power factor and the possibility of providing reactive power and operating at non-unity power factor in various generic distribution systems. The grid power factor of various distribution systems was discussed with and without such renewable energy sources. The simulation results of these distribution systems showed that the renewable energy generating units affected the grid power factor when these units operated at the unity power factor. When these renewable generating units operated at different power factor settings, the grid power factor was improved. A three phase two stage transformerless PV grid connected system with reactive power capability was also proposed in this thesis. The proposed model of the PV system was achieved by

controlling the PV inverter and the inverter was controlled in the d-q reference frame. The PV inverter reactive power was controlled in the q-axis. The simulation results showed how a photovoltaic system can provide reactive power and operate at non-unity power factor under different solar irradiance conditions.

8.2 Suggestions for Future Research

The research undertaken in this thesis has addressed some issues related to the integration of distributed generation based on wind and photovoltaics in distribution systems. These issues included fault ride through, transient stability, frequency response and the impact on the grid power factor. However, there are several issues that need further investigation in the future, as identified in the following points:

- **Voltage stability of distribution systems with high renewable energy penetration**

It would be interesting to study the voltage stability of various distribution systems with different renewable energy technologies, such as wind turbines based on the DFIG, a synchronous generator with fully rated converters based on wind energy, and solar energy based on photovoltaics. The impact of these renewable generating units with and without reactive power controllability and using reactive power compensators such as SVC and DSTATCOM on the voltage stability can be investigated.

- **Further research on the transient stability of distribution systems with high renewable energy penetration**

The transient fault duration applied in this thesis was 200 milliseconds (10 cycles, 50 Hz system). In future research the fault duration could be extended to, for instance, 500 milliseconds, and consideration could be given to the protection devices settings of distribution systems. The impact of renewable energy generating units with reactive power controllability on distribution system transient stability is another interesting research topic.

- **Investigating the impact of high renewable energy penetration in distribution systems on protection systems**

It would be useful to study the effects of different renewable energy technologies, such as wind and solar technologies, on the protection devices of distribution systems.

- **Investigating renewable energy sources with storage devices**

Technical issues were investigated in this thesis in relation to renewable energy sources that do not include storage devices. It would be useful to study these issues when storage devices such as batteries are included.

- **Economic analysis of increasing renewable energy penetration in distribution systems**

It would be useful to analyse the integration of renewable generation from an economic point of view, with and without, for instance, fault ride through capability and reactive power controllability.

REFERENCES

- [1] U.S. Energy Information Administration. (2009, Accessed: 20th January 2016). *Annual Energy Outlook 2009 With Projections to 2030*. Available: <http://www.eia.gov/oiaf/aeo/pdf/0383%282009%29.pdf>
- [2] U.S. Energy Information Administration. (2013, Accessed: 2nd August 2015). *International Energy Outlook 2013*. Available: <http://www.eia.gov/forecasts/ieo/pdf/0484%282013%29.pdf>
- [3] M. Azhar Khan, M. Zahir Khan, K. Zaman, and L. Naz, "Global estimates of energy consumption and greenhouse gas emissions," *Renewable and Sustainable Energy Reviews*, vol. 29, pp. 336-344, 2014.
- [4] Z. M. Chen and G. Q. Chen, "An overview of energy consumption of the globalized world economy," *Energy Policy*, vol. 39, pp. 5920-5928, 2011.
- [5] UNITED NATIONS. (1998, Accessed: 4th November 2015). KYOTO PROTOCOL TO THE UNITED NATIONS FRAMEWORK CONVENTION ON CLIMATE CHANGE Available: <http://unfccc.int/resource/docs/convkp/kpeng.pdf>
- [6] EWEA. (2011, Accessed: 29th September 2015). *EU Energy Policy to 2050, Achieving 80-95% emissions reductions*. Available: http://www.ewea.org/fileadmin/files/library/publications/reports/EWEA_EU_Energy_Policy_to_2050.pdf
- [7] X. Xia and J. Xia, "Evaluation of Potential for Developing Renewable Sources of Energy to Facilitate Development in Developing Countries," in *Power and Energy Engineering Conference (APPEEC), 2010 Asia-Pacific*, 2010, pp. 1-3.
- [8] A. Y. Saber and G. K. Venayagamoorthy, "Plug-in Vehicles and Renewable Energy Sources for Cost and Emission Reductions," *Industrial Electronics, IEEE Transactions on*, vol. 58, pp. 1229-1238, 2011.
- [9] G. Z. Liu, C. W. Yu, X. R. Li, and F. S. Wen, "Impacts of emission trading and renewable energy support schemes on electricity market operation," *Generation, Transmission & Distribution, IET*, vol. 5, pp. 650-655, 2011.
- [10] K. Sakurai, K. Matsubara, and K. Sakuta, "Energy payback and GHG emissions of renewable power generation systems in Japan: A review," in *Photovoltaic Specialists Conference (PVSC), 2011 37th IEEE*, 2011, pp. 003277-003279.
- [11] IEA. (2013, Accessed: 8th August 2015). Technology Roadmap, Wind Energy. Available: https://www.iea.org/publications/freepublications/publication/Wind_2013_Roadmap.pdf
- [12] EURELECTRIC. (2013, Accessed: 5th August 2015). Power Statistics & Trends 2013. Available: http://www2.warwick.ac.uk/fac/soc/csgr/green/foresight/energyenvironment/2013_eurelectric_power_statistics_trends_2013.pdf
- [13] Department of Energy & Climate Change UK Government. (2014, Accessed: 10th August 2015). Renewable electricity in Scotland, Wales, Northern Ireland and the regions of England in 2013 Available: https://www.gov.uk/government/uploads/system/uploads/attachment_data/file/357539/Renewable_electricity_2013.pdf
- [14] L. L. Lai, *Power System Restructuring and Deregulation*. West Sussex, England: John Wiley & Sons Ltd, 2001.
- [15] D. Kirschen and G. Strbac, *Fundamentals of Power System Economics*. Chichester, UK: John Wiley & Sons Ltd, 2004.
- [16] IEA. (2014, Accessed: 12th August 2015). Energy Technology Perspectives 2014. Available: <http://www.iea.org/Textbase/npsum/ETP2014SUM.pdf>
- [17] B. Meyer, "Distributed Generation: towards an effective contribution to power system security," in *Power Engineering Society General Meeting, 2007. IEEE*, 2007, pp. 1-6.
- [18] S. Martel and D. Turcotte, "Review of Distributed Generation Product and Interconnection Standards for Canada," in *Electrical Power Conference, 2007. EPC 2007. IEEE Canada*, 2007, pp. 242-247.
- [19] G. Pepermans, J. Driesen, D. Haeseldonckx, R. Belmans, and W. D'haeseleer, "Distributed generation: definition, benefits and issues," *Energy Policy*, vol. 33, pp. 787-798, 2005.
- [20] K. Purchala, R. Belmans, L. Exarchakos, and A. D. Hawkes, "Distributed generation and the grid integration issues," EU-SUSTEL Project (European Sustainable Electricity)2007.

- [21] P. Dondi, D. Bayoumi, C. Haederli, D. Julian, and M. Suter, "Network integration of distributed power generation," *Journal of Power Sources*, vol. 106, pp. 1-9, 2002.
- [22] T. Ackermann, G. Andersson, and L. Söder, "Distributed generation: a definition1," *Electric Power Systems Research*, vol. 57, pp. 195-204, 2001.
- [23] A. F. Zobaa and R. C. Bansal, *Handbook of Renewable Energy Technology*. Singapore: World Scientific, 2011.
- [24] F. Alsokhry, G. P. Adam, and K. L. Lo, "Contribution of distributed generation to ancillary services," in *Universities Power Engineering Conference (UPEC), 2012 47th International*, 2012, pp. 1-5.
- [25] European_Photovoltaic_Industry_Association. (2012, Accessed: 20th July 2015). *Global Market Outlook for Photovoltaics until 2016* [Report]. Available: http://www.pv-magazine.com/fileadmin/uploads/PDFs/Global_Market_Outlook_2016.pdf
- [26] IEA. (2002, Accessed: 15th August 2015). Distributed Generation in Liberalised Electricity Markets. Available: <http://library.umac.mo/ebooks/b13623175.pdf>
- [27] R. Teodorescu, M. Liserre, and P. Rodriguez, *Grid Converters for Photovoltaic and Wind Power Systems*: John Wiley & Sons, Ltd, 2011.
- [28] I. Erlich and U. Bachmann, "Grid code requirements concerning connection and operation of wind turbines in Germany," in *Power Engineering Society General Meeting, 2005. IEEE*, 2005, pp. 1253-1257 Vol. 2.
- [29] G. Hua, L. Cong, and Y. Geng, "LVRT Capability of DFIG-Based WECS Under Asymmetrical Grid Fault Condition," *Industrial Electronics, IEEE Transactions on*, vol. 60, pp. 2495-2509, 2013.
- [30] L. G. Meegahapola, T. Littler, and D. Flynn, "Decoupled-DFIG Fault Ride-Through Strategy for Enhanced Stability Performance During Grid Faults," *Sustainable Energy, IEEE Transactions on*, vol. 1, pp. 152-162, 2010.
- [31] Y. Lihui, X. Zhao, J. Ostergaard, D. Zhao Yang, and W. Kit Po, "Advanced Control Strategy of DFIG Wind Turbines for Power System Fault Ride Through," *Power Systems, IEEE Transactions on*, vol. 27, pp. 713-722, 2012.
- [32] S. Seman, J. Niiranen, S. Kanerva, A. Arkkio, and J. Saitz, "Performance Study of a Doubly Fed Wind-Power Induction Generator Under Network Disturbances," *Energy Conversion, IEEE Transactions on*, vol. 21, pp. 883-890, 2006.
- [33] K. E. Okedu, S. M. Muyeen, R. Takahashi, and J. Tamura, "Comparative study between two protection schemes for DFIG-based wind generator," in *Electrical Machines and Systems (ICEMS), 2010 International Conference on*, 2010, pp. 62-67.
- [34] M. Rizo, A. Rodriguez, E. Bueno, F. J. Rodriguez, Giro, x, and C. n, "Low voltage ride-through of wind turbine based on interior Permanent Magnet Synchronous Generators sensorless vector controlled," in *Energy Conversion Congress and Exposition (ECCE), 2010 IEEE*, 2010, pp. 2507-2514.
- [35] D. Fujin and C. Zhe, "Low-voltage ride-through of variable speed wind turbines with permanent magnet synchronous generator," in *Industrial Electronics, 2009. IECON '09. 35th Annual Conference of IEEE*, 2009, pp. 621-626.
- [36] M. Singh, V. Khadkikar, and A. Chandra, "Grid synchronisation with harmonics and reactive power compensation capability of a permanent magnet synchronous generator-based variable speed wind energy conversion system," *Power Electronics, IET*, vol. 4, pp. 122-130, 2011.
- [37] G. M. S. Islam, A. Al-Durra, S. M. Muyeen, and J. Tamura, "Low voltage ride through capability enhancement of grid connected large scale photovoltaic system," in *IECON 2011 - 37th Annual Conference on IEEE Industrial Electronics Society*, 2011, pp. 884-889.
- [38] A. Marinopoulos, F. Papandrea, M. Reza, S. Norrga, F. Spertino, and R. Napoli, "Grid integration aspects of large solar PV installations: LVRT capability and reactive power/voltage support requirements," in *PowerTech, 2011 IEEE Trondheim*, 2011, pp. 1-8.
- [39] X. Y. Bian, Y. Geng, K. L. Lo, Y. Fu, and Q. B. Zhou, "Coordination of PSSs and SVC Damping Controller to Improve Probabilistic Small-Signal Stability of Power System With Wind Farm Integration," *Power Systems, IEEE Transactions on*, vol. PP, pp. 1-12, 2015.
- [40] M. Edrah, K. L. Lo, and O. Anaya-Lara, "Impacts of High Penetration of DFIG Wind Turbines on Rotor Angle Stability of Power Systems," *Sustainable Energy, IEEE Transactions on*, vol. 6, pp. 759-766, 2015.
- [41] M. V. Nunes, J. A. P. Lopes, U. H. Bezerra, H. H. Zurn, and R. Almeida, "Influence of the variable speed wind generators in transient stability margin of the conventional generators

- integrated in electrical grids," in *Power Engineering Society General Meeting, 2004. IEEE*, 2004, p. 1734 Vol.2.
- [42] C. Samarasinghe and G. Ancell, "Effects of large scale wind generation on transient stability of the New Zealand power system," in *Power and Energy Society General Meeting - Conversion and Delivery of Electrical Energy in the 21st Century, 2008 IEEE*, 2008, pp. 1-8.
- [43] E. Muljadi, C. P. Butterfield, B. Parsons, and A. Ellis, "Effect of Variable Speed Wind Turbine Generator on Stability of a Weak Grid," *Energy Conversion, IEEE Transactions on*, vol. 22, pp. 29-36, 2007.
- [44] S. M. Mueen, R. Takahashi, T. Murata, J. Tamura, and M. H. Ali, "Transient stability analysis of permanent magnet variable speed synchronous wind generator," in *Electrical Machines and Systems, 2007. ICEMS. International Conference on*, 2007, pp. 288-293.
- [45] S. Nanou, G. Tsourakis, and C. D. Vournas, "Full-converter wind generator modelling for transient stability studies," in *PowerTech, 2011 IEEE Trondheim*, 2011, pp. 1-7.
- [46] G. Hua, D. Xu, W. Bin, and Y. Geng, "Active Damping for PMSG-Based WECS With DC-Link Current Estimation," *Industrial Electronics, IEEE Transactions on*, vol. 58, pp. 1110-1119, 2011.
- [47] M. Thomson and D. G. Infield, "Impact of widespread photovoltaics generation on distribution systems," *Renewable Power Generation, IET*, vol. 1, pp. 33-40, 2007.
- [48] M. Yagami, N. Kimura, M. Tsuchimoto, and J. Tamura, "Power system transient stability analysis in the case of high-penetration photovoltaics," in *PowerTech (POWERTECH), 2013 IEEE Grenoble*, 2013, pp. 1-6.
- [49] M. Yagami, T. Hasegawa, and J. Tamura, "Transient stability assessment of synchronous generator in power system with high-penetration photovoltaics," in *Electrical Machines and Systems (ICEMS), 2012 15th International Conference on*, 2012, pp. 1-6.
- [50] S. Eftekharijad, V. Vittal, G. T. Heydt, B. Keel, and J. Loehr, "Impact of increased penetration of photovoltaic generation on power systems," *Power Systems, IEEE Transactions on*, vol. 28, pp. 893-901, 2013.
- [51] Z. Changhong, U. Topcu, and S. H. Low, "Frequency-based load control in power systems," in *American Control Conference (ACC), 2012*, 2012, pp. 4423-4430.
- [52] L. Mei and J. D. McCalley, "Influence of renewable integration on frequency dynamics," in *Power and Energy Society General Meeting, 2012 IEEE*, 2012, pp. 1-7.
- [53] L. Holdsworth, J. B. Ekanayake, and N. Jenkins, "Power system frequency response from fixed speed and doubly fed induction generator-based wind turbines," *Wind Energy*, vol. 7, pp. 21-35, 2004.
- [54] R. G. de Almeida and J. A. Peas Lopes, "Participation of Doubly Fed Induction Wind Generators in System Frequency Regulation," *Power Systems, IEEE Transactions on*, vol. 22, pp. 944-950, 2007.
- [55] G. Ramtharan, J. B. Ekanayake, and N. Jenkins, "Frequency support from doubly fed induction generator wind turbines," *Renewable Power Generation, IET*, vol. 1, pp. 3-9, 2007.
- [56] J. Morren, J. Pierik, and S. W. H. de Haan, "Inertial response of variable speed wind turbines," *Electric Power Systems Research*, vol. 76, pp. 980-987, 2006.
- [57] W. Ziping, G. Wenzhong, W. Jianhui, and G. Shusheng, "A coordinated primary frequency regulation from Permanent Magnet Synchronous Wind Turbine Generation," in *Power Electronics and Machines in Wind Applications (PEMWA), 2012 IEEE*, 2012, pp. 1-6.
- [58] J. F. Conroy and R. Watson, "Frequency Response Capability of Full Converter Wind Turbine Generators in Comparison to Conventional Generation," *Power Systems, IEEE Transactions on*, vol. 23, pp. 649-656, 2008.
- [59] N. Kakimoto, S. Takayama, H. Satoh, and K. Nakamura, "Power Modulation of Photovoltaic Generator for Frequency Control of Power System," *Energy Conversion, IEEE Transactions on*, vol. 24, pp. 943-949, 2009.
- [60] C. A. Hill, M. C. Such, C. Dongmei, J. Gonzalez, and W. M. Grady, "Battery Energy Storage for Enabling Integration of Distributed Solar Power Generation," *Smart Grid, IEEE Transactions on*, vol. 3, pp. 850-857, 2012.
- [61] R. Tonkoski, L. A. C. Lopes, and D. Turcotte, "Active power curtailment of PV inverters in diesel hybrid mini-grids," in *Electrical Power & Energy Conference (EPEC), 2009 IEEE*, 2009, pp. 1-6.

- [62] W. A. Omran, M. Kazerani, and M. M. A. Salama, "Investigation of Methods for Reduction of Power Fluctuations Generated From Large Grid-Connected Photovoltaic Systems," *Energy Conversion, IEEE Transactions on*, vol. 26, pp. 318-327, 2011.
- [63] I. Erlich and F. Shewarega, "Interaction of Large Wind Power Generation Plants with the Power System," in *Power and Energy Conference, 2006. PECon '06. IEEE International*, 2006, pp. 12-18.
- [64] X. Lie and P. Cartwright, "Direct active and reactive power control of DFIG for wind energy generation," *Energy Conversion, IEEE Transactions on*, vol. 21, pp. 750-758, 2006.
- [65] S. Engelhardt, I. Erlich, C. Feltes, J. Kretschmann, and F. Shewarega, "Reactive Power Capability of Wind Turbines Based on Doubly Fed Induction Generators," *Energy Conversion, IEEE Transactions on*, vol. 26, pp. 364-372, 2011.
- [66] M. Kayikci and J. V. Milanovic, "Reactive Power Control Strategies for DFIG-Based Plants," *Energy Conversion, IEEE Transactions on*, vol. 22, pp. 389-396, 2007.
- [67] N. R. Ullah, K. Bhattacharya, and T. Thiringer, "Wind Farms as Reactive Power Ancillary Service Providers; Technical and Economic Issues," *Energy Conversion, IEEE Transactions on*, vol. 24, pp. 661-672, 2009.
- [68] A. Cagnano, E. De Tuglie, M. Liserre, and R. A. Mastromauro, "Online Optimal Reactive Power Control Strategy of PV Inverters," *Industrial Electronics, IEEE Transactions on*, vol. 58, pp. 4549-4558, 2011.
- [69] C. Chia-Hsi, L. Yu-Hui, C. Yaow-Ming, and C. Yung-Ruei, "Simplified Reactive Power Control for Single-Phase Grid-Connected Photovoltaic Inverters," *Industrial Electronics, IEEE Transactions on*, vol. 61, pp. 2286-2296, 2014.
- [70] Department_of_Energy_& Climate_Change. (2008, Accessed: 13th March 2015). Climate Change Act 2008, CHAPTER 27. Available: http://www.legislation.gov.uk/ukpga/2008/27/pdfs/ukpga_20080027_en.pdf
- [71] Department_of_Energy_& Climate_Change_UK_Government. (2013, Accessed: 20th August 2015). UK Renewable Energy Roadmap Update 2013. Available: https://www.gov.uk/government/uploads/system/uploads/attachment_data/file/255182/UK_Renewable_Energy_Roadmap_-_5_November_-_FINAL_DOCUMENT_FOR_PUBLICATION_.pdf
- [72] E. Ares. (2011, Accessed: 1st April 2015). Renewable Electricity: Feed-in Tariffs and The Renewables Obligation. Available: http://www.fitariffs.co.uk/library/regulation/110623hoc_fits_ro.pdf
- [73] World_Energy_Council. (2013, Accessed: 30th January 2016). 2013 World Energy Issues Monitor. Available: <http://www.worldenergy.org/wp-content/uploads/2013/02/2013-World-Energy-Issues-Monitor-Report-Feb2013.pdf>
- [74] U.S._Energy_Information_Administration. (2013, Accessed: 30th January 2016). Annual Energy Outlook 2013 With Projections to 2040. Available: <http://www.eia.gov/forecasts/aeo/pdf/0383%282013%29.pdf>
- [75] B. K. Bose, "Global Warming: Energy, Environmental Pollution, and the Impact of Power Electronics," *Industrial Electronics Magazine, IEEE*, vol. 4, pp. 6-17, 2010.
- [76] SolarPowerEurope. (2015, Accessed: 20th January 2016). Global Market Outlook For Solar Power/ 2015 - 2019. Available: http://helapco.gr/pdf/Global_Market_Outlook_2015_-_2019_lr_v23.pdf
- [77] A. Luque and S. Hegedus, *handbook of photovoltaic science and engineering*, second ed. West Sussex, United Kingdom: John Wiley & Sons, Ltd, 2011.
- [78] F. Dimroth. (2013, Accessed: 25th January 2016). World Record Solar Cell with 44.7% Efficiency. Available: <http://www.ise.fraunhofer.de/en/press-and-media/pdfs-zu-presseinfos-englisch/2013/press-release-world-record-solar-cell-with-44-7-efficiency.pdf>
- [79] European_Photovoltaic_Industry_Association and Greenpeace International. (2011, Accessed: 21st January 2016). Solar Generation 6, Solar Photovoltaic Electricity Empowering the World. Available: <http://www.greenpeace.org/international/Global/international/publications/climate/2011/Final%20SolarGeneration%20VI%20full%20report%20lr.pdf>
- [80] National_Renewable_Energy_Laboratory. (2012, Accessed: 22nd January 2016). Life Cycle Greenhouse Gas Emissions from Solar Photovoltaics. Available: <http://www.nrel.gov/docs/fy13osti/56487.pdf>

- [81] E. Meza. (2014, Accessed: 16th January 2016). IRENA: PV prices have declined 80% since 2008. Available: http://www.pv-magazine.com/news/details/beitrag/irena-pv-prices-have-declined-80-since-2008_100016383/#ixzz3DVitSgJQ
- [82] IEA_PVPS. (2015, Accessed: 21st January 2016). A Snapshot of Global PV Markets 2014. Available: [http://iea-pvps.org/index.php?id=92&no_cache=1&tx_damfrontend_pi1\[showUid\]=2430&tx_damfrontend_pi1\[backPid\]=92](http://iea-pvps.org/index.php?id=92&no_cache=1&tx_damfrontend_pi1[showUid]=2430&tx_damfrontend_pi1[backPid]=92)
- [83] Department_of_Energy_&_Climate_Change. (2014, Accessed: 21st January 2016). Weekly solar PV installation & capacity based on registration date. Available: <https://www.gov.uk/government/statistical-data-sets/weekly-solar-pv-installation-and-capacity-based-on-registration-date>
- [84] A. Kay. (2013, Accessed: 25th January 2016). FIT Data Analysis April 2010 to March 2013. Available: <http://greenbusinesswatch.co.uk/fit-data-analysis>
- [85] NPD_Solarbuzz. (2014, Accessed: 2nd September 2015). UK Deal Tracker and European PV Markets Quarterly reports. Available: <http://www.solarbuzz.com/reports/european-pv-markets-quarterly>
- [86] Department_of_Energy_&_Climate_Change. (2015, Accessed: 21st January 2016). Solar Photovoltaics Deployment in the UK November 2015. Available: https://www.gov.uk/government/uploads/system/uploads/attachment_data/file/488141/Solar_photovoltaics_deployment_December_2015.xlsx
- [87] "IEEE Recommended Practice for Testing the Performance of Stand-Alone Photovoltaic Systems," *IEEE Std 1526-2003*, pp. 0_1-18, 2004.
- [88] A. N. A. Ali, M. H. Saied, M. Z. Mostafa, and T. M. Abdel-Moneim, "A survey of maximum PPT techniques of PV systems," in *Energytech, 2012 IEEE*, 2012, pp. 1-17.
- [89] T. Eswam and P. L. Chapman, "Comparison of Photovoltaic Array Maximum Power Point Tracking Techniques," *Energy Conversion, IEEE Transactions on*, vol. 22, pp. 439-449, 2007.
- [90] K. L. Lian, J. H. Jhang, and I. S. Tian, "A Maximum Power Point Tracking Method Based on Perturb-and-Observe Combined With Particle Swarm Optimization," *Photovoltaics, IEEE Journal of*, vol. 4, pp. 626-633, 2014.
- [91] maxima_integrated. (2012, Accessed: 21st January 2016). How to Design an Efficient DC-DC Converter Using the DS1875 PWM Controller. Available: <http://pdfserv.maximintegrated.com/en/an/AN4332.pdf>
- [92] RenewableUK. (2015, Accessed: 1st December 2015). UKWED Figures explained. Available: <http://www.renewableuk.com/en/renewable-energy/wind-energy/uk-wind-energy-database/figures-explained.cfm>
- [93] Department_of_Energy_&_Climate_Change. (2013, Accessed: 1st September 2015). ENERGY TRENDS. Available: https://www.gov.uk/government/uploads/system/uploads/attachment_data/file/266403/et_dec_13.pdf
- [94] Department_of_Energy_&_Climate_Change. (2014, Accessed: 20th January 2016). Renewable sources of energy: chapter 6, Digest of United Kingdom energy statistics (DUKES). Available: <https://www.gov.uk/government/statistics/renewable-sources-of-energy-chapter-6-digest-of-united-kingdom-energy-statistics-dukes>
- [95] G. Petrone, G. Spagnuolo, R. Teodorescu, M. Veerachary, and M. Vitelli, "Reliability Issues in Photovoltaic Power Processing Systems," *Industrial Electronics, IEEE Transactions on*, vol. 55, pp. 2569-2580, 2008.
- [96] N. G. Dhere, "Reliability of PV modules and balance-of-system components," in *Photovoltaic Specialists Conference, 2005. Conference Record of the Thirty-first IEEE*, 2005, pp. 1570-1576.
- [97] H. Laukamp. (2002, Accessed: 22nd January 2016). Reliability Study of Grid Connected PV Systems Field Experience and Recommended Design Practice. Available: http://www.solelprogrammet.se/Global/Projekteringsverktyg/PDF/herman%20laukamp%20fin_rep.pdf?epslanguage=sv
- [98] K. Mitchell, J. Rizk, and M. Nagrial, "Balanced renewable energy system," in *Power Electronics and Motion Control Conference, 2000. Proceedings. IPEMC 2000. The Third International*, 2000, pp. 857-861 vol.2.

- [99] A. D. Dhass, E. Natarajan, and L. Ponnusamy, "Influence of shunt resistance on the performance of solar photovoltaic cell," in *Emerging Trends in Electrical Engineering and Energy Management (ICETEEEM), 2012 International Conference on*, 2012, pp. 382-386.
- [100] G. M. Wilson. (2013, Accessed: 15th January 2016). Building on 35 Years of Progress – The Next 10 Years of Photovoltaic Research at NREL. Available: <https://www.purdue.edu/discoverypark/energy/assets/pdfs/pdf/Pioneer%20in%20Energy%20Greg%20Wilson%20Presentation%207.17.13.pdf>
- [101] G. Wilson and K. Emery. (2014, Accessed: 17th January 2016). *Best Research Cell Efficiencies* Available: http://www.nrel.gov/ncpv/images/efficiency_chart.jpg
- [102] H. Patel and V. Agarwal, "MATLAB-Based Modeling to Study the Effects of Partial Shading on PV Array Characteristics," *Energy Conversion, IEEE Transactions on*, vol. 23, pp. 302-310, 2008.
- [103] "IEEE Standard for Interconnecting Distributed Resources with Electric Power Systems," *IEEE Std 1547-2003*, pp. 1-28, 2003.
- [104] IEC61727, "Photovoltaic (PV) Systems – Characteristics of the Utility Interface," ed, 2004.
- [105] Energy_Networks_Association. (2013, Accessed: 1st October 2015). Distributed Generation Connection Guide. Available: <http://www.energynetworks.org/electricity/engineering/distributed-generation/distributed-generation.html>
- [106] V. Fthenakis and E. Alsema, "Photovoltaics energy payback times, greenhouse gas emissions and external costs: 2004–early 2005 status," *Progress in photovoltaics: research and applications*, vol. 14, pp. 275-280, 2006.
- [107] CaplorEnergy. (2015, Accessed: 22nd January 2016). IEA scales back UK renewables forecast, citing policy uncertainty. Available: <http://www.caplor.co.uk/caplor-blog/iea-scales-back-uk-renewables-forecast-citing-policy-uncertainty/>
- [108] K. Harrison. (2010, Accessed: 17th January 2016). It's payback time for home generation. Available: <http://news.bbc.co.uk/1/hi/sci/tech/8751862.stm>
- [109] Department_of_Energy_&_Climate_Change_UK_Government. (2013, Accessed: 4th December 2015). Reducing the UK's greenhouse gas emissions by 80% by 2050. Available: <https://www.gov.uk/government/policies/reducing-the-uk-s-greenhouse-gas-emissions-by-80-by-2050>
- [110] R. Wiser, C. Namovicz, M. Gielecki, and R. Smith, "Renewables Portfolio Standards: A Factual Introduction to Experience from the United States " 2007.
- [111] Global_Wind_Energy_Council. (2014, Accessed: 15th January 2016). GLOBAL WIND ENERGY OUTLOOK 2014. Available: <http://www.greenpeace.org/international/Global/international/briefings/climate/2014/GWEO-2014-final.pdf>
- [112] S. Heier, *Grid Integration of Wind Energy Conversion Systems*, Second ed. England: John Wiley & Sons Ltd, 2006.
- [113] P. W. Carlin, A. S. Laxson, and E. B. Muljadi. (2001, Accessed: 16th January 2016). The History and State of the Art of Variable-Speed Wind Turbine Technology. Available: <http://www.nrel.gov/docs/fy01osti/28607.pdf>
- [114] J. K. Kaldellis and D. Zafirakis, "The wind energy (r)evolution: A short review of a long history," *Renewable Energy*, vol. 36, pp. 1887-1901, 2011.
- [115] GWEC. (2015, Accessed: 22nd January 2016). Wind in numbers. Available: <http://www.gwec.net/global-figures/wind-in-numbers/>
- [116] GWEC. (2015, Accessed: 22nd January 2016). Global statistics. Available: <http://www.gwec.net/global-figures/graphs/>
- [117] GWEC. (2014, Accessed: 20th January 2016). THE EUROPEAN UNION GLOBAL WIND REPORT ANNUAL MARKET UPDATE 2013. Available: http://www.gwec.net/wp-content/uploads/2014/04/GWEC-Global-Wind-Report_9-April-2014.pdf
- [118] GWEC. (2014, Accessed: 21st January 2016). Global Wind Energy Outlook: 2000 gigawatts by 2030. Available: <http://www.gwec.net/publications/global-wind-energy-outlook/global-wind-energy-outlook-2014/>
- [119] GWEC. (2013, Accessed: 22nd June 2015). Wind in numbers. Available: <http://www.gwec.net/global-figures/wind-in-numbers/>

- [120] Parliament_Office_of_Science_and_Technology. (2006, Accessed: 22nd January 2016). CARBON FOOTPRINT OF ELECTRICITY GENERATION Available: <http://www.parliament.uk/documents/post/postpn268.pdf>
- [121] Department_of_Energy_&_Climate_Change. (2015, Accessed: 30th September 2015). Changes to onshore wind subsidies protect investment and get the best deal for bill payers. Available: <https://www.gov.uk/government/news/changes-to-onshore-wind-subsidies-protect-investment-and-get-the-best-deal-for-bill-payers>
- [122] E. Lantz, R. Wiser, and M. Hand. (2012, Accessed: 23rd January 2016). IEA Wind Task 26 The Past and Future Cost of Wind Energy. Available: https://www.ieawind.org/index_page_postings/WP2_task26.pdf
- [123] A. Neslen. (2016, Accessed: 23rd January 2016). Denmark broke world record for wind power in 2015. Available: <http://www.theguardian.com/environment/2016/jan/18/denmark-broke-world-record-for-wind-power-in-2015>
- [124] power-technology. (2014, Accessed: 5th February 2016). The world's 10 biggest wind turbines. Available: <http://www.power-technology.com/features/featurethe-worlds-biggest-wind-turbines-4154395/>
- [125] EWEA. (2009, Accessed: 6th February 2016). The Economics of Wind Energy. Available: http://www.ewea.org/fileadmin/files/library/publications/reports/Economics_of_Wind_Energy.pdf
- [126] T. Burton, N. Jenkins, D. Sharpe, and E. Bossanyi, *Wind Energy Handbook*: John Wiley & Sons Ltd, 2011.
- [127] I. S. Naser, "The Impact of Wind Generation on Power System Voltage Stability," PhD, Electronic and Electrical Engineering Department, University of Strathclyde, Glasgow, United Kingdom, 2013.
- [128] I. Dinçer and C. Zamfirescu, *Sustainable Energy Systems and Applications*. New York Springer Science+Business Media, 2012.
- [129] P. Shi, "Effect of Intermittent Generation on Conventional Generators in Power Systems," PhD, Electronic and Electrical Engineering Department, University of Strathclyde, Glasgow, United Kingdom, 2010.
- [130] J. Zhenhua and Y. Xunwei, "Modeling and control of an integrated wind power generation and energy storage system," in *Power & Energy Society General Meeting, 2009. PES '09. IEEE*, 2009, pp. 1-8.
- [131] H. Li and Z. Chen, "Overview of different wind generator systems and their comparisons," *Renewable Power Generation, IET*, vol. 2, pp. 123-138, 2008.
- [132] O. Anaya-Lara, N. Jenkins, J. Ekanayake, P. Cartwright, and M. Hughes, *WIND ENERGY GENERATION Modelling and Control*. United Kingdom: John Wiley & Sons Ltd, 2009.
- [133] R. Billinton and H. Dange, "Incorporating Wind Power in Generating Capacity Reliability Evaluation Using Different Models," *Power Systems, IEEE Transactions on*, vol. 26, pp. 2509-2517, 2011.
- [134] R. Billinton, R. Karki, G. Yi, H. Dange, H. Po, and W. Wangdee, "Adequacy Assessment Considerations in Wind Integrated Power Systems," *Power Systems, IEEE Transactions on*, vol. 27, pp. 2297-2305, 2012.
- [135] M. West. (2009, Accessed: 1st March 2015). Wind Data Analysis. Available: www.inl.gov/wind
- [136] M. J. Hossain, H. R. Pota, M. A. Mahmud, and R. A. Ramos, "Investigation of the Impacts of Large-Scale Wind Power Penetration on the Angle and Voltage Stability of Power Systems," *Systems Journal, IEEE*, vol. 6, pp. 76-84, 2012.
- [137] D. Gautam, V. Vittal, and T. Harbour, "Impact of Increased Penetration of DFIG-Based Wind Turbine Generators on Transient and Small Signal Stability of Power Systems," *Power Systems, IEEE Transactions on*, vol. 24, pp. 1426-1434, 2009.
- [138] Z. Yi, A. A. Chowdhury, and D. O. Koval, "Probabilistic Wind Energy Modeling in Electric Generation System Reliability Assessment," *Industry Applications, IEEE Transactions on*, vol. 47, pp. 1507-1514, 2011.
- [139] R. Karki, H. Po, and R. Billinton, "Reliability Evaluation Considering Wind and Hydro Power Coordination," *Power Systems, IEEE Transactions on*, vol. 25, pp. 685-693, 2010.
- [140] L. Kai, X. Hongbing, M. Qian, and Z. Ji, "Hierarchy control of power quality for wind - battery energy storage system," *Power Electronics, IET*, vol. 7, pp. 2123-2132, 2014.

- [141] T. Thiringer, T. Petru, and C. Liljegren, "Power quality impact of a sea located hybrid wind park," *Energy Conversion, IEEE Transactions on*, vol. 16, pp. 123-127, 2001.
- [142] K. De Vos, J. Morbee, J. Driesen, and R. Belmans, "Impact of wind power on sizing and allocation of reserve requirements," *Renewable Power Generation, IET*, vol. 7, pp. 1-9, 2013.
- [143] D. A. Halamay, T. K. A. Brekken, A. Simmons, and S. McArthur, "Reserve Requirement Impacts of Large-Scale Integration of Wind, Solar, and Ocean Wave Power Generation," *Sustainable Energy, IEEE Transactions on*, vol. 2, pp. 321-328, 2011.
- [144] S. Musunuri and H. L. Ginn, "Comprehensive review of wind energy maximum power extraction algorithms," in *Power and Energy Society General Meeting, 2011 IEEE*, 2011, pp. 1-8.
- [145] RenewableUK. (2015, Accessed: 23rd January 2016). Busy year of construction activity ahead for British wind industry but onshore wind faces uncertain future. Available: <http://www.renewableuk.com/en/news/renewableuk-news.cfm/23-12-2015-busy-year-of-construction-activity-ahead-for-british-wind-industry-but-onshore-wind-faces-uncertain-future>
- [146] RenewableUK. (2013, Accessed: 15th January 2016). Small and Medium Wind UK Market Report. Available: <http://www.renewableuk.com/en/publications/reports.cfm>
- [147] P. Denholm, M. Hand, M. Jackson, and S. Ong. (2009, Accessed: 16th January 2016). Land-Use Requirements of Modern Wind Power Plants in the United States. Available: <http://www.nrel.gov/docs/fy09osti/45834.pdf>
- [148] EWEA. (2014, Accessed: 25th January 2016). *Wind energy's frequently asked questions (FAQ)*. Available: <http://www.ewea.org/wind-energy-basics/faq/>
- [149] European Commission Special Eurobarometer. (2011, Accessed: 25th January 2016). SPECIAL EUROBAROMETER 364 Public Awareness and Acceptance of CO2 capture and storage. Available: http://ec.europa.eu/public_opinion/archives/ebs/ebs_364_en.pdf
- [150] Scottish Natural Heritage. (2014, Accessed: 28th January 2016). *Visual representation*. Available: <http://www.snh.gov.uk/planning-and-development/renewable-energy/visual-representation/>
- [151] W. D. Colby, R. Dobie, G. Leventhall, D. M. Lipscomb, R. J. McCunney, M. T. Seilo, and B. Søndergaard. (2009, Accessed: 21st January 2016). Wind Turbine Sound and Health Effects An Expert Panel Review Executive Summary. Available: http://canwea.ca/pdf/talkwind/Wind_Turbine_Sound_and_Health_Effects-Executive_Summary.pdf
- [152] J. W. Pearce-Higgins, L. Stephen, A. Douse, and R. H. W. Langston, "Greater impacts of wind farms on bird populations during construction than subsequent operation: results of a multi-site and multi-species analysis," *Journal of Applied Ecology*, vol. 49, pp. 386-394, 2012.
- [153] A. Kusiak and W. Li, "The prediction and diagnosis of wind turbine faults," *Renewable Energy*, vol. 36, pp. 16-23, 2011.
- [154] J. M. Pinar Pérez, F. P. García Márquez, A. Tobias, and M. Papaelias, "Wind turbine reliability analysis," *Renewable and Sustainable Energy Reviews*, vol. 23, pp. 463-472, 2013.
- [155] S. Shi, "Operation and Assessment of Wind Energy on Power System Reliability Evaluation," PhD, Electronic and Electrical Engineering Department, University of Strathclyde, Glasgow, United Kingdom, 2014.
- [156] F. P. García Márquez, A. M. Tobias, J. M. Pinar Pérez, and M. Papaelias, "Condition monitoring of wind turbines: Techniques and methods," *Renewable Energy*, vol. 46, pp. 169-178, 2012.
- [157] A. Ragheb and M. Ragheb. (2011, Accessed: 7th February 2016). *Wind Turbine Gearbox Technologies, Fundamental and Advanced Topics in Wind Power*. Available: <http://www.intechopen.com/books/fundamental-and-advanced-topics-in-wind-power/wind-turbine-gearbox-technologies>
- [158] A. Causebrook and B. Fox, "Modernising Grid Codes to Accommodate Diverse Generation Technologies, Especially Modern Windfarms," *Wind Engineering*, vol. 28, pp. 75-86, 2004.
- [159] I. M. de Alegría, J. Andreu, J. L. Martín, P. Ibañez, J. L. Villate, and H. Camblong, "Connection requirements for wind farms: A survey on technical requirements and regulation," *Renewable and Sustainable Energy Reviews*, vol. 11, pp. 1858-1872, 2007.
- [160] A. Johnson and N. Tleis, "The development of grid code requirements for new and renewable forms of generation in Great Britain," *Wind Engineering*, vol. 29, pp. 201-216, 2005.

- [161] National_Grid_UK. (2015, Accessed: 15th September 2015). THE GRID CODE, ISSUE 5, REVISION 14, 26 August 2015. Available: <http://www2.nationalgrid.com/UK/Industry-information/Electricity-codes/Grid-code/The-Grid-code/>
- [162] D. Kundu, "An Overview of the Distributed Generation (DG) Connected to the GRID," in *Power System Technology and IEEE Power India Conference, 2008. POWERCON 2008. Joint International Conference on*, 2008, pp. 1-8.
- [163] J. A. Momoh, X. Yan, and G. D. Boswell, "An approach to determine Distributed Generation (DG) benefits in power networks," in *Power Symposium, 2008. NAPS '08. 40th North American*, 2008, pp. 1-7.
- [164] G. Joos, B. T. Ooi, D. McGillis, F. D. Galiana, and R. Marceau, "The potential of distributed generation to provide ancillary services," in *Power Engineering Society Summer Meeting, 2000. IEEE*, 2000, pp. 1762-1767 vol. 3.
- [165] F. Alsokhry and K. L. Lo, "Effect of distributed generations based on renewable energy on the transient fault - Ride through," in *Renewable Energy Research and Applications (ICRERA), 2013 International Conference on*, 2013, pp. 1102-1106.
- [166] K. Ki-Hong, J. Yoon-Cheul, L. Dong-Choon, and K. Heung-Geun, "LVRT Scheme of PMSG Wind Power Systems Based on Feedback Linearization," *Power Electronics, IEEE Transactions on*, vol. 27, pp. 2376-2384, 2012.
- [167] F. Iov, A. D. Hansen, P. Sørensen, and N. A. Cutululis. (2007, Accessed: 1st September 2015). Mapping of grid faults and grid codes. Available: http://orbit.dtu.dk/files/7703139/ris_r_1617.pdf
- [168] K. Corfee, D. Korinek, W. Cassel, C. Hewicker, J. Zillmer, M. P. Morgado, H. Ziegler, N. Tong, D. Hawkins, and J. Cernadas. (2011, Accessed: 5th September 2015). Distributed Generation in Europe -Network Planning and Operational Impacts. Available: http://www.energy.ca.gov/2011_energypolicy/documents/2011-05-09_workshop/documents/Memo%20%20DG%20Network%20Planning%20and%20Operational%20Impacts.pdf
- [169] F. Tang, X. Jin, Z. Xiao, X. Wu, and L. Ma, "A novel LVRT strategy for direct-drive wind turbines based on permanent magnet synchronous generator," in *Power Electronics and Motion Control Conference (IPEMC), 2012 7th International*, 2012, pp. 2228-2233.
- [170] R. A. E. Ibrahim, "Low Voltage Ride-Through of Permanent Magnet Synchronous Generator Wind Energy Systems," PhD, Electronic and Electrical Engineering Department, University of Strathclyde, Glasgow, United Kingdom, 2014.
- [171] E. J. Coster, J. M. A. Myrzik, and W. L. Kling, "Effect of grid disturbances on fault-ride-through behaviour of MV-connected DG-units, in especially CHP-plants," in *Integration of Wide-Scale Renewable Resources Into the Power Delivery System, 2009 CIGRE/IEEE PES Joint Symposium*, 2009, pp. 1-11.
- [172] R. Piwko, E. Camm, A. Ellis, E. Muljadi, R. Zavadil, R. Walling, M. O'Malley, G. Irwin, and S. Saylor, "A Promising Outlook.," *Power and Energy Magazine, IEEE*, vol. 7, 2009.
- [173] BDEW. (2008, Accessed: 1st July 2015). Technical Guideline Generating Plants Connected to the Medium-Voltage Network Available: [https://www.bdew.de/internet.nsf/id/A2A0475F2FAE8F44C12578300047C92F/\\$file/BDEW_RL_EA-am-MS-Netz_engl.pdf](https://www.bdew.de/internet.nsf/id/A2A0475F2FAE8F44C12578300047C92F/$file/BDEW_RL_EA-am-MS-Netz_engl.pdf)
- [174] O. Gomis-Bellmunt, A. Junyent-Ferre, A. Sumper, and J. Bergas-Jan, "Ride-Through Control of a Doubly Fed Induction Generator Under Unbalanced Voltage Sags," *Energy Conversion, IEEE Transactions on*, vol. 23, pp. 1036-1045, 2008.
- [175] J. Morren and S. W. H. de Haan, "Short-Circuit Current of Wind Turbines With Doubly Fed Induction Generator," *Energy Conversion, IEEE Transactions on*, vol. 22, pp. 174-180, 2007.
- [176] M. Salles, J. R. Cardoso, A. P. Grilo, C. Rahmann, and K. Hameyer, "Control strategies of doubly fed induction generators to support grid voltage," in *Electric Machines and Drives Conference, 2009. IEMDC '09. IEEE International*, 2009, pp. 1551-1556.
- [177] R. Yuan and Z. Wei, "A novel control strategy of an active crowbar for DFIG-based wind turbine during grid faults," in *Electric Machines & Drives Conference (IEMDC), 2011 IEEE International*, 2011, pp. 1137-1142.
- [178] G. Pannell, D. J. Atkinson, and B. Zahawi, "Minimum-Threshold Crowbar for a Fault-Ride-Through Grid-Code-Compliant DFIG Wind Turbine," *Energy Conversion, IEEE Transactions on*, vol. 25, pp. 750-759, 2010.

- [179] Y. Jin, J. E. Fletcher, and J. O'Reilly, "A Series-Dynamic-Resistor-Based Converter Protection Scheme for Doubly-Fed Induction Generator During Various Fault Conditions," *Energy Conversion, IEEE Transactions on*, vol. 25, pp. 422-432, 2010.
- [180] Y. Xiangwu, G. Venkataramanan, W. Yang, D. Qing, and Z. Bo, "Grid-Fault Tolerant Operation of a DFIG Wind Turbine Generator Using a Passive Resistance Network," *Power Electronics, IEEE Transactions on*, vol. 26, pp. 2896-2905, 2011.
- [181] R. Takahashi, M. Nakatani, J. Tamura, S. M. Muyeen, M. Sugimasa, A. Komura, M. Futami, M. Ichinose, and K. Ide, "Smoothing control of wind farm output fluctuation by new scheme with energy storage system," in *Power Electronics and Applications (EPE 2011), Proceedings of the 2011-14th European Conference on*, 2011, pp. 1-9.
- [182] ABB. (2011, Accessed: 5th July 2015). System description and start-up guide ACS800-67 wind turbine converters. Available: https://library.e.abb.com/public/57bac11129b6e563c1257b7f004b19cb/EN_ACS800-67_System_descr_A.pdf
- [183] G. Nicolaescu, H. Andrei, and S. Radulescu, "Dynamic voltage restorer response analysis for voltage sags mitigation in MV networks with secondary distribution configuration," in *Environment and Electrical Engineering (EEEIC), 2014 14th International Conference on*, 2014, pp. 40-45.
- [184] R. S. Weissbach, G. G. Karady, and R. G. Farmer, "Dynamic voltage compensation on distribution feeders using flywheel energy storage," *Power Delivery, IEEE Transactions on*, vol. 14, pp. 465-471, 1999.
- [185] L. Qicheng and L. Yuping, "An Integration of Super Capacitor Storage Research for Improving Low-Voltage-Ride-Through in Power Grid with Wind Turbine," in *Power and Energy Engineering Conference (APPEEC), 2012 Asia-Pacific*, 2012, pp. 1-4.
- [186] W. Wenliang, G. Baoming, B. Daqiang, Q. Ming, and L. Wei, "Energy storage based LVRT and stabilizing power control for direct-drive wind power system," in *Power System Technology (POWERCON), 2010 International Conference on*, 2010, pp. 1-6.
- [187] EWEA. (2009, Accessed: 28th January 2016). Harmonising Europe's Grid Codes for the Connection of Wind Power Plants to the Electricity Network. Available: http://www.ewea.org/fileadmin/ewea_documents/documents/publications/position_papers/091210_EWEA_Harmonising_Europes_GC_for_the_Connection_of_Wind_Power_Plants.pdf
- [188] A. Yazdani, A. R. Di Fazio, H. Ghoddami, M. Russo, M. Kazerani, J. Jatskevich, K. Strunz, S. Leva, and J. A. Martinez, "Modeling Guidelines and a Benchmark for Power System Simulation Studies of Three-Phase Single-Stage Photovoltaic Systems," *Power Delivery, IEEE Transactions on*, vol. 26, pp. 1247-1264, 2011.
- [189] A. A. A. Radwan and Y. A. R. I. Mohamed, "Analysis and Active Suppression of AC- and DC-Side Instabilities in Grid-Connected Current-Source Converter-Based Photovoltaic System," *Sustainable Energy, IEEE Transactions on*, vol. 4, pp. 630-642, 2013.
- [190] G. M. S. Azevedo, P. Rodriguez, M. C. Cavalcanti, G. Vazquez, and F. A. S. Neves, "New control strategy to allow the photovoltaic systems operation under grid faults," in *Power Electronics Conference, 2009. COBEP '09. Brazilian*, 2009, pp. 196-201.
- [191] MATLAB/SIMULINK. (2015, R2014b). Available: <http://uk.mathworks.com/products/simulink/>
- [192] DIgSILENT/PowerFactory. (2015, PowerFactory 15.1). Available: <http://www.digsilent.de/index.php/products-powerfactory.html>
- [193] M. Brown. (2011, Accessed: 24th May 2015). Renewable sources could provide 35 percent of UK energy by 2020. Available: <http://www.wired.co.uk/news/archive/2011-06/14/35-percent-renewable-energy-in-2020>
- [194] RenewableUK. (2015, Accessed: 15th January 2016). Big leap in clean electricity generated by wind Available: <http://www.renewableuk.com/en/news/press-releases.cfm/22-12-15-big-leap-in-clean-electricity-generated-by-wind>
- [195] IEEE_PES. (2001, Accessed: 1st May 2015). Distributed Test Feeders. Available: <http://ewh.ieee.org/soc/pes/dsacom/testfeeders/index.html>
- [196] K. Bhattacharya, M. Bollen, and J. E. Daalder, *Operation of Restructured Power Systems*. New York: Springer Science & Business Media, 2001.

- [197] X. Y. Bian, X. X. Huang, K. C. Wong, K. L. Lo, Y. Fu, and S. H. Xuan, "Improvement on probabilistic small-signal stability of power system with large-scale wind farm integration," *International Journal of Electrical Power & Energy Systems*, vol. 61, pp. 482-488, 2014.
- [198] A. S. Emhemed, R. M. Tumilty, N. K. Singh, G. M. Burt, and J. R. McDonald, "Analysis of Transient Stability Enhancement of LV-Connected Induction Microgenerators by Using Resistive-Type Fault Current Limiters," *Power Systems, IEEE Transactions on*, vol. 25, pp. 885-893, 2010.
- [199] P. Kundur, J. Paserba, V. Ajjarapu, G. Andersson, A. Bose, C. Canizares, N. Hatziargyriou, D. Hill, A. Stankovic, C. Taylor, T. Van Cutsem, and V. Vittal, "Definition and classification of power system stability IEEE/CIGRE joint task force on stability terms and definitions," *Power Systems, IEEE Transactions on*, vol. 19, pp. 1387-1401, 2004.
- [200] P. Kundur, *Power System Stability and Control*: McGraw-Hill 1994.
- [201] S. Libao, D. Shiqiang, N. Yixin, Y. Liangzhong, and M. Bazargan, "Transient stability of power systems with high penetration of DFIG based wind farms," in *Power & Energy Society General Meeting, 2009. PES '09. IEEE*, 2009, pp. 1-6.
- [202] F. M. Hughes, O. Anaya-Lara, N. Jenkins, and G. Strbac, "Control of DFIG-based wind generation for power network support," *Power Systems, IEEE Transactions on*, vol. 20, pp. 1958-1966, 2005.
- [203] A. Mitra and D. Chatterjee, "Stability enhancement of wind farm connected power system using superconducting magnetic energy storage unit," in *Power Systems Conference (NPSC), 2014 Eighteenth National*, 2014, pp. 1-6.
- [204] L. Li, H. Hongjing, L. Wenxia, and J. Sheng, "Simulation and comparison of transient stability of power system including DFIGs wind farm based on detailed model," in *Sustainable Power Generation and Supply, 2009. SUPERGEN '09. International Conference on*, 2009, pp. 1-6.
- [205] N. R. Ullah and T. Thiringer, "Variable Speed Wind Turbines for Power System Stability Enhancement," *Energy Conversion, IEEE Transactions on*, vol. 22, pp. 52-60, 2007.
- [206] A. D. Hansen and G. Michalke, "Multi-pole permanent magnet synchronous generator wind turbines' grid support capability in uninterrupted operation during grid faults," *Renewable Power Generation, IET*, vol. 3, pp. 333-348, 2009.
- [207] M. Thomson and D. G. Infield, "Network Power-Flow Analysis for a High Penetration of Distributed Generation," *Power Systems, IEEE Transactions on*, vol. 22, pp. 1157-1162, 2007.
- [208] V. Nguyen Hoang and A. Yokoyama, "Impact of fault ride-through characteristics of high-penetration photovoltaic generation on transient stability," in *Power System Technology (POWERCON), 2010 International Conference on*, 2010, pp. 1-7.
- [209] M. Yagami, S. Ishikawa, Y. Ichinohe, K. Misawa, and J. Tamura, "Transient stability analysis of power system with photovoltaic systems installed," in *Renewable Power Generation Conference (RPG 2014), 3rd*, 2014, pp. 1-6.
- [210] S. Muller, M. Deicke, and R. W. De Doncker, "Doubly fed induction generator systems for wind turbines," *Industry Applications Magazine, IEEE*, vol. 8, pp. 26-33, 2002.
- [211] M. Liserre, R. Cardenas, M. Molinas, and J. Rodriguez, "Overview of Multi-MW Wind Turbines and Wind Parks," *Industrial Electronics, IEEE Transactions on*, vol. 58, pp. 1081-1095, 2011.
- [212] D. E. Newman, B. A. Carreras, M. Kirchner, and I. Dobson, "The Impact of Distributed Generation on Power Transmission Grid Dynamics," in *System Sciences (HICSS), 2011 44th Hawaii International Conference on*, 2011, pp. 1-8.
- [213] D. Jinxu and A. Somani, "A Long-Term Investment Planning Model for Mixed Energy Infrastructure Integrated with Renewable Energy," in *Green Technologies Conference, 2010 IEEE*, 2010, pp. 1-10.
- [214] N. Nimpitiwan, "Inverter-based photovoltaic distributed generations: Modeling and dynamic simulations," in *TENCON 2010 - 2010 IEEE Region 10 Conference*, 2010, pp. 7-12.
- [215] E. Espinosa-Juarez, J. Lucio, and A. Hernandez, "Analysis of Distributed Generation Impact on the Optimal Location of Voltage Sag Monitors by Applying Genetic Algorithms," in *Electronics, Robotics and Automotive Mechanics Conference, 2009. CERMA '09.*, 2009, pp. 107-112.
- [216] A. H. Parsaeifard, M. Manbachi, M. B. A. Kopayi, and M. R. Haghifam, "A market-based generation expansion planning in deregulated environment based on distributed generations development," in *Probabilistic Methods Applied to Power Systems (PMAPS), 2010 IEEE 11th International Conference on*, 2010, pp. 677-684.

- [217] John J. Grainger and W. D. Stevenson, *Power System Analysis*. New York: Mc Graw Hill, 1994.
- [218] F. Alsokhiry and K. L. Lo, "Distributed generation based on renewable energy providing frequency response ancillary services," in *Power Engineering, Energy and Electrical Drives (POWERENG), 2013 Fourth International Conference on*, 2013, pp. 1200-1205.
- [219] BDWE. (June 2008, Accessed: 21st December 2015). *Technical Guidelines, Generating Plants Connected to the Medium Voltage Network* [Report]. Available: [http://www.bdew.de/internet.nsf/id/A2A0475F2FAE8F44C12578300047C92F/\\$file/BDEW_RL_EA-am-MS-Netz_engl.pdf](http://www.bdew.de/internet.nsf/id/A2A0475F2FAE8F44C12578300047C92F/$file/BDEW_RL_EA-am-MS-Netz_engl.pdf)
- [220] National_Grid_UK. (2008, Accessed: 2nd July 2015). Report of the investigation into the automatic demand disconnection following multiple generation losses and the demand control response that occurred on the 27th May 2008 Available: <http://www2.nationalgrid.com/assets/0/745/746/3464/3466/3488/3475/623fcd6f-31e3-416a-bfb7-c4edbfd763d2.pdf>
- [221] National_Grid_UK. (2009, Accessed: 4th July 2015). Report of the National Grid Investigation into the Frequency Deviation and Automatic Demand Disconnection that occurred on the 27th May 2008 Available: <http://www2.nationalgrid.com/assets/0/745/746/3464/3466/3488/3475/745fc2acd57e-4df7-b619-4c68f2821e8d.pdf>
- [222] Leon Freris and D. Infield, *Renewable Energy in Power Systems*. United Kingdom: John Wiley, 2008.
- [223] M. Tsili and S. Papathanassiou, "A review of grid code technical requirements for wind farms," *Renewable Power Generation, IET*, vol. 3, pp. 308-332, 2009.
- [224] A. Mullane and M. O'Malley, "The Inertial Response of Induction-Machine-Based Wind Turbines," *Power Systems, IEEE Transactions on*, vol. 20, pp. 1496-1503, 2005.
- [225] G. Lalor, A. Mullane, and M. O'Malley, "Frequency control and wind turbine technologies," *Power Systems, IEEE Transactions on*, vol. 20, pp. 1905-1913, 2005.
- [226] Z. S. Zhang, Y. Z. Sun, J. Lin, and G. J. Li, "Coordinated frequency regulation by doubly fed induction generator-based wind power plants," *Renewable Power Generation, IET*, vol. 6, pp. 38-47, 2012.
- [227] F. Alsokhiry and K. L. Lo, "Provision of reactive power support ancillary services from distributed generation based on renewable energy," in *Renewable Energy Research and Applications (ICRERA), 2013 International Conference on*, 2013, pp. 1018-1023.
- [228] G. W. Chang, C. Wen-Chang, C. Ching-Sheng, and S. Dong-Yeen, "Fuzzy Logic and Immune-Based Algorithm for Placement and Sizing of Shunt Capacitor Banks in a Distorted Power Network," *Power Delivery, IEEE Transactions on*, vol. 26, pp. 2145-2153, 2011.
- [229] H. Khani, M. Moallem, S. Sadri, and M. Dolatshahi, "A New Method for Online Determination of the Location of Switched Capacitor Banks in Distribution Systems," *Power Delivery, IEEE Transactions on*, vol. 26, pp. 341-351, 2011.
- [230] X. Yan, D. Zhao Yang, W. Kit Po, E. Liu, and B. Yue, "Optimal Capacitor Placement to Distribution Transformers for Power Loss Reduction in Radial Distribution Systems," *Power Systems, IEEE Transactions on*, vol. 28, pp. 4072-4079, 2013.
- [231] S. Torseng, "Shunt-connected reactors and capacitors controlled by thyristors," *Generation, Transmission and Distribution, IEE Proceedings C*, vol. 128, pp. 366-373, 1981.
- [232] J. Dixon, L. Moran, J. Rodriguez, and R. Domke, "Reactive Power Compensation Technologies: State-of-the-Art Review," *Proceedings of the IEEE*, vol. 93, pp. 2144-2164, 2005.
- [233] J. J. Shea, "Understanding FACTS-concepts and technology of flexible AC transmission systems [Book Review]," *Electrical Insulation Magazine, IEEE*, vol. 18, pp. 46-46, 2002.
- [234] S. V. Bozhko, R. Blasco-Gimenez, L. Risheng, J. C. Clare, and G. M. Asher, "Control of Offshore DFIG-Based Wind Farm Grid With Line-Commutated HVDC Connection," *Energy Conversion, IEEE Transactions on*, vol. 22, pp. 71-78, 2007.
- [235] W. Li and T. Dinh-Nhon, "Stability Enhancement of DFIG-Based Offshore Wind Farm Fed to a Multi-Machine System Using a STATCOM," *Power Systems, IEEE Transactions on*, vol. 28, pp. 2882-2889, 2013.
- [236] H. Gaztanaga, I. Etxeberria-Otadui, D. Ocnasu, and S. Bacha, "Real-Time Analysis of the Transient Response Improvement of Fixed-Speed Wind Farms by Using a Reduced-Scale STATCOM Prototype," *Power Systems, IEEE Transactions on*, vol. 22, pp. 658-666, 2007.

- [237] S. D. G. Jayasingha, D. M. Vilathgamuwa, and U. K. Madawala, "Cascade multilevel static synchronous compensator configuration for wind farms," *Power Electronics, IET*, vol. 4, pp. 548-556, 2011.
- [238] S. Rajendran, U. Govindarajan, A. B. Reuben, and A. Srinivasan, "Shunt reactive VAR compensator for grid-connected induction generator in wind energy conversion systems," *Power Electronics, IET*, vol. 6, pp. 1872-1883, 2013.
- [239] L. Tzung-Lin, H. Shang-Hung, and C. Yu-Hung, "D-STATCOM With Positive-Sequence Admittance and Negative-Sequence Conductance to Mitigate Voltage Fluctuations in High-Level Penetration of Distributed-Generation Systems," *Industrial Electronics, IEEE Transactions on*, vol. 60, pp. 1417-1428, 2013.
- [240] G. Tapia, A. Tapia, and J. X. Ostolaza, "Proportional–Integral Regulator-Based Approach to Wind Farm Reactive Power Management for Secondary Voltage Control," *Energy Conversion, IEEE Transactions on*, vol. 22, pp. 488-498, 2007.
- [241] M. El Moursi, C. Abbey, and G. Joos, "Optimal tracking secondary voltage control for the DFIG wind turbines," in *Power Engineering Society General Meeting, 2006. IEEE, 2006*, p. 6 pp.
- [242] L. Chia-Hung, H. Wei-Lin, C. Chao-Shun, H. Cheng-Ting, K. Te-Tien, and T. Cheng-Ta, "Financial Analysis of a Large-Scale Photovoltaic System and Its Impact on Distribution Feeders," *Industry Applications, IEEE Transactions on*, vol. 47, pp. 1884-1891, 2011.
- [243] S. Eftekharijad, V. Vittal, G. T. Heydt, B. Keel, and J. Loehr, "Small Signal Stability Assessment of Power Systems With Increased Penetration of Photovoltaic Generation: A Case Study," *Sustainable Energy, IEEE Transactions on*, vol. 4, pp. 960-967, 2013.
- [244] T. Yun Tiam and D. S. Kirschen, "Impact on the Power System of a Large Penetration of Photovoltaic Generation," in *Power Engineering Society General Meeting, 2007. IEEE, 2007*, pp. 1-8.
- [245] P. Mitra, G. T. Heydt, and V. Vittal, "The impact of distributed photovoltaic generation on residential distribution systems," in *North American Power Symposium (NAPS), 2012, 2012*, pp. 1-6.
- [246] Y. Jun, L. Hui, C. Zhe, X. Xianfeng, C. Xiyin, L. Qing, and L. Yong, "Enhanced Control of a DFIG-Based Wind-Power Generation System With Series Grid-Side Converter Under Unbalanced Grid Voltage Conditions," *Power Electronics, IEEE Transactions on*, vol. 28, pp. 3167-3181, 2013.
- [247] E. Figueres, G. Garcera, J. Sandia, F. Gonzalez-Espin, and J. C. Rubio, "Sensitivity Study of the Dynamics of Three-Phase Photovoltaic Inverters With an LCL Grid Filter," *Industrial Electronics, IEEE Transactions on*, vol. 56, pp. 706-717, 2009.

Appendices

Appendix A: Commonly PV Modules in the UK Market

Manufacturer	Product	Technology	Efficiency %	Width (mm)	Height (mm)	Area (Metre Squared)	Watts per metre squared	Peak Voltage (Volts)	Peak Current (Amps)	Peak Output (Watts)	Maximum System Voltage (Volts)
SunPower	315 Solar Panel	Monocrystalline	19.32	1559	1046	1.63	193.17	54.7	5.76	315	600
SunPower	230 Solar Panel	Monocrystalline	18.49	1559	798	1.24	184.88	41	5.61	230	600
SunPower	225 Solar Panel	Monocrystalline	18.09	1559	798	1.24	180.86	41	5.49	225	600
SunPower	215 Solar Panel	Monocrystalline	17.28	1559	798	1.24	172.82	39.8	5.4	215	600
SunPower	210 Solar Panel	Monocrystalline	16.88	1559	798	1.24	168.8	40	5.25	210	600
Mitsubishi	PV-TD175MF5	Polycrystalline	12.66	1658	834	1.38	126.56	23.9	7.32	175	1000
Mitsubishi	PV-TD180MF5	Polycrystalline	13.02	1658	834	1.38	130.17	24.2	7.45	180	1000
Mitsubishi	PV-TD185MF5	Polycrystalline	13.38	1658	834	1.38	133.79	24.4	7.58	185	1000
Mitsubishi	PV-TD190MF5	Polycrystalline	13.74	1658	834	1.38	137.41	24.7	7.71	190	1000
Mitsubishi	PV-TE130MF5N	Polycrystalline	12.9	1495	674	1.01	129.02	17.4	7.47	130	1000
Mitsubishi	PV-TE125MF5N	Polycrystalline	12.41	1495	674	1.01	124.05	17.3	7.23	125	1000
Mitsubishi	PV-TE120MF5N	Polycrystalline	11.91	1495	674	1.01	119.09	17.2	6.99	120	1000
Mitsubishi	PV-TE115MF5N	Polycrystalline	11.41	1495	674	1.01	114.13	17.1	6.75	115	1000
Mitsubishi	PV-MF185TD4	Polycrystalline	13.38	1658	834	1.38	133.79	24.4	7.58	185	780
Mitsubishi	PV-MF180TD4	Polycrystalline	13.02	1658	834	1.38	130.17	24.2	7.45	180	780
Mitsubishi	PV-MF175TD4	Polycrystalline	12.66	1658	834	1.38	126.56	23.9	7.32	175	780
Mitsubishi	PV-MF170TD4	Polycrystalline	12.29	1658	834	1.38	122.94	23.7	7.19	170	780
Mitsubishi	PV-MF130TE4N	Polycrystalline	12.9	1495	674	1.01	129.02	17.4	7.47	130	780
Mitsubishi	PV-MF125TE4N	Polycrystalline	12.41	1495	674	1.01	124.05	17.3	7.23	125	780
Mitsubishi	PV-MF120TE4N	Polycrystalline	11.91	1495	674	1.01	119.09	17.2	6.99	120	780
Mitsubishi	PV-MF115TE4N	Polycrystalline	11.41	1495	674	1.01	114.13	17.1	6.75	115	780

Manufacturer	Product	Technology	Efficiency %	Width (mm)	Height (mm)	Area (Metre Squared)	Watts per metre squared	Peak Voltage (Volts)	Peak Current (Amps)	Peak Output (Watts)	Maximum System Voltage (Volts)
Mitsubishi	PV-AD190MF5	Polycrystalline	13.74	1658	834	1.38	137.41	24.7	7.71	190	1000
Mitsubishi	PV-AD185MF5	Polycrystalline	13.38	1658	834	1.38	133.79	24.4	7.58	185	1000
Mitsubishi	PV-AD180MF5	Polycrystalline	13.02	1658	834	1.38	130.17	24.2	7.45	180	1000
Mitsubishi	PV-AD175MF5	Polycrystalline	12.66	1658	834	1.38	126.56	23.9	7.32	175	1000
Mitsubishi	PV-AE130MF5N	Polycrystalline	12.9	1495	674	1.01	129.02	17.4	8.05	130	1000
Mitsubishi	PV-AE125MF5N	Polycrystalline	12.41	1495	674	1.01	124.05	17.3	7.9	125	1000
Mitsubishi	PV-AE120MF5N	Polycrystalline	11.91	1495	674	1.01	119.09	17.2	7.75	120	1000
Mitsubishi	PV-AE115MF5N	Polycrystalline	11.41	1495	674	1.01	114.13	17.1	7.6	115	1000
Mitsubishi	PV-MF170EB4	Polycrystalline	13.45	1580	800	1.26	134.49	24.6	6.93	170	780
Mitsubishi	PV-MF165EB4	Polycrystalline	13.05	1580	800	1.26	130.54	24.2	7.36	165	780
Mitsubishi	PV-MF125EA4	Polycrystalline	12.47	1248	803	1	124.73	18.8	6.63	125	600
Mitsubishi	PV-MF120EC4	Polycrystalline	13.04	1425	646	0.92	130.36	17.6	6.84	120	780
Mitsubishi	PV-MF110EC4	Polycrystalline	11.95	1425	646	0.92	119.49	17.1	6.43	110	780
Mitsubishi	PV-MF160EB4	Polycrystalline	12.66	1580	800	1.26	126.58	23.8	6.72	160	780
Mitsubishi	PV-MF130EA4	Polycrystalline	12.97	1248	803	1	129.72	19.2	6.79	130	600
Sanyo	HIT-240HDE4	HIT	17.31	1610	861	1.39	173.13	35.5	6.77	240	1000
Sanyo	HIT-235HDE4	HIT	16.95	1610	861	1.39	169.53	35.1	6.7	235	1000
Sanyo	HIT-205DNKHE1	HIT	14.59	1630	862	1.41	145.9	41.3	4.97	205	1000
Sanyo	HIT-200DNKHE1	HIT	14.23	1630	862	1.41	142.34	40.7	4.92	200	1000
Sanyo	HIT-N220E01	HIT	17.45	1580	798	1.26	174.49	41.6	5.31	220	1000
Sanyo	HIT-N215E01	HIT	17.05	1580	798	1.26	170.52	40.9	5.27	215	1000
Sharp	NE-80EJEA	Polycrystalline	12.41	1200	537	0.64	124.15	21.6	4.63	80	600
Sharp	NE-165UC1	Polycrystalline	12.68	1575	826	1.3	126.83	34.6	4.77	165	600
Sharp	NE-170UC1	Polycrystalline	13.07	1575	826	1.3	130.67	34.8	4.9	170	600
Sharp	ND-123UJF	Polycrystalline	12.39	1499	662	0.99	123.95	17.2	7.15	123	600

Manufacturer	Product	Technology	Efficiency %	Width (mm)	Height (mm)	Area (Metre Squared)	Watts per metre squared	Peak Voltage (Volts)	Peak Current (Amps)	Peak Output (Watts)	Maximum System Voltage (Volts)
Sharp	ND-130UJF	Polycrystalline	13.1	1499	662	0.99	131	17.4	7.5	130	600
Sharp	ND-176UC1	Polycrystalline	13.33	1328	994	1.32	133.33	23.42	7.52	176	600
Sharp	ND-198UC1	Polycrystalline	13.36	1491	994	1.48	133.6	26.3	7.52	198	600
Sharp	ND-224UC1	Polycrystalline	13.74	1640	994	1.63	137.41	29.3	7.66	224	600
Sharp	NU-U230F3	Monocrystalline	14.11	1640	994	1.63	141.09	30	7.67	230	600
Sharp	NU-U235F1	Monocrystalline	14.42	1640	994	1.63	144.16	30	8.4	235	600
Sharp	NA-V115H5	Thin Film	8.09	1409	1009	1.42	80.89	174	0.661	115	1000
Sharp	NA-V121H5	Thin Film	8.51	1409	1009	1.42	85.11	180	0.673	121	1000
Sharp	NA-V128H5	Thin Film	9	1409	1009	1.42	90.03	186	0.688	128	1000
Sharp	NA-V142H5	Thin Film	9.99	1409	1009	1.42	99.88	188	0.72	142	1000
Sharp	NA-V135H5	Thin Film	9.5	1409	1009	1.42	94.96	192	0.74	135	1000
Yingli	YL 165 P-23b	Polycrystalline	12.72	1310	990	1.3	127.23	23	7.17	165	1000
Yingli	YL 170 P-23b	Polycrystalline	13.11	1310	990	1.3	131.08	23	7.39	170	1000
Yingli	YL 175 P-23b	Polycrystalline	13.49	1310	990	1.3	134.94	23	7.61	175	1000
Yingli	YL 180 P-23b	Polycrystalline	13.88	1310	990	1.3	138.79	23	7.83	180	1000
Yingli	YL 185 P-23b	Polycrystalline	14.26	1310	990	1.3	142.65	23.5	7.87	185	1000
Yingli	YL 260 P-35b	Polycrystalline	13.33	1970	990	1.95	133.31	35	7.43	260	1000
Yingli	YL 265 P-35b	Polycrystalline	13.59	1970	990	1.95	135.88	35.3	7.5	265	1000
Yingli	YL 270 P-35b	Polycrystalline	13.84	1970	990	1.95	138.44	35.3	7.65	270	1000
Yingli	YL 275 P-35b	Polycrystalline	14.1	1970	990	1.95	141	35.5	7.75	275	1000
Yingli	YL 280 P-35b	Polycrystalline	14.36	1970	990	1.95	143.57	35.5	7.89	280	1000
Yingli	YL 235 P-32b	Polycrystalline	13.11	1810	990	1.79	131.15	32	7.34	235	1000
Yingli	YL 240 P-32b	Polycrystalline	13.39	1810	990	1.79	133.94	32.2	7.45	240	1000
Yingli	YL 245 P-32b	Polycrystalline	13.67	1810	990	1.79	136.73	32.2	7.61	245	1000
Yingli	YL 250 P-32b	Polycrystalline	13.95	1810	990	1.79	139.52	32.3	7.74	250	1000
Yingli	YL 255 P-32b	Polycrystalline	14.23	1810	990	1.79	142.31	32.5	7.85	255	1000
Yingli	YL 210 P-29b	Polycrystalline	12.86	1650	990	1.63	128.56	28.5	7.37	210	1000

Manufacturer	Product	Technology	Efficiency %	Width (mm)	Height (mm)	Area (Metre Squared)	Watts per metre squared	Peak Voltage (Volts)	Peak Current (Amps)	Peak Output (Watts)	Maximum System Voltage (Volts)
Yingli	YL 215 P-29b	Polycrystalline	13.16	1650	990	1.63	131.62	29	7.41	215	1000
Yingli	YL 220 P-29b	Polycrystalline	13.47	1650	990	1.63	134.68	29	7.59	220	1000
Yingli	YL 225 P-29b	Polycrystalline	13.77	1650	990	1.63	137.74	29	7.63	225	1000
Yingli	YL 230 P-29b	Polycrystalline	14.08	1650	990	1.63	140.8	29.5	7.8	230	1000
Yingli	YL 235 P-29b	Polycrystalline	14.39	1650	990	1.63	143.86	29.5	7.97	235	1000
Yingli	YL 190 P-26b	Polycrystalline	12.84	1495	990	1.48	128.37	25.8	7.36	190	1000
Yingli	YL 195 P-26b	Polycrystalline	13.18	1495	990	1.48	131.75	26	7.5	195	1000
Yingli	YL 200 P-26b	Polycrystalline	13.51	1495	990	1.48	135.13	26.3	7.6	200	1000
Yingli	YL 205 P-26b	Polycrystalline	13.85	1495	990	1.48	138.51	26.5	7.74	205	1000
Yingli	YL 210 P-26b	Polycrystalline	14.19	1495	990	1.48	141.89	26.6	7.9	210	1000
Yingli	YL175Wp	Polycrystalline	13.49	1310	990	1.3	134.94	23.5	7.5	175	1000
Yingli	YL180Wp	Polycrystalline	13.88	1310	990	1.3	138.79	23	7.8	180	1000
Yingli	YL210Wp	Polycrystalline	12.86	1650	990	1.63	128.56	29.5	7.2	210	1000
Yingli	YL230Wp	Polycrystalline	14.08	1650	990	1.63	140.8	30	7.66	230	1000
Yingli	YL260P-35b	Polycrystalline	13.33	1970	990	1.95	133.31	35	7.43	260	1000
Yingli	YL265P-35b	Polycrystalline	13.59	1970	990	1.95	135.88	35.3	7.5	265	1000
Yingli	YL270-35b	Polycrystalline	13.84	1970	990	1.95	138.44	35.3	7.65	270	1000
Yingli	YL275-35b	Polycrystalline	14.1	1970	990	1.95	141	35.5	7.75	275	1000
Yingli	YL280-35b	Polycrystalline	14.36	1970	990	1.95	143.57	35.5	7.89	280	1000
Suntech	STP210-18/Ud	Polycrystalline	14.28	1482	992	1.47	142.84	26.4	7.95	210	1000
Suntech	STP205-18/Ud	Polycrystalline	14.62	1482	992	1.47	146.24	26.3	7.8	215	1000
Suntech	STP225-20-Wd	Polycrystalline	13.64	1665	991	1.65	136.36	29.6	7.61	225	1000
Suntech	STP220-20-Wd	Polycrystalline	13.33	1665	991	1.65	133.33	29.5	7.46	220	1000
Suntech	STP195S-24-Ad+	Polycrystalline	15.27	1580	808	1.28	152.74	36.6	5.33	195	1000
Suntech	STP190S-24-Ad+	Polycrystalline	14.88	1580	808	1.28	148.83	36.5	5.2	190	1000
Suntech	STP090Ts-AA	Thinfilim	6.29	1300	1100	1.43	62.94	73.2	1.23	90	1000
Suntech	STP086Ts-AA	Thinfilim	6.01	1300	1100	1.43	60.14	72.3	1.19	86	1000

Manufacturer	Product	Technology	Efficiency %	Width (mm)	Height (mm)	Area (Metre Squared)	Watts per metre squared	Peak Voltage (Volts)	Peak Current (Amps)	Peak Output (Watts)	Maximum System Voltage (Volts)
Suntech	STP082s-AA	Thinfilm	5.73	1300	1100	1.43	57.34	71.3	1.15	82	1000
Suntech	STP380Ts-DA	Thinfilm	6.64	2600	2200	5.72	66.43	148.4	2.56	380	1000
Suntech	STP370Ts-DA	Thinfilm	6.47	2600	2200	5.72	64.69	147.4	2.51	370	1000
Suntech	STP360Ts-DA	Thinfilm	6.29	2600	2200	5.72	62.94	146.3	2.46	360	1000
Suntech	STP350Ts-DA	Thinfilm	6.12	2600	2200	5.72	61.19	145.2	2.41	350	1000
Suntech	STP185Ts-BA	Thinfilm	6.47	2200	1300	2.86	64.69	147.4	1.26	185	1000
Suntech	STP180s-BA	Thinfilm	6.29	2200	1300	2.86	62.94	146.4	1.23	180	1000
Suntech	STP175s-BA	Thinfilm	6.12	2200	1300	2.86	61.19	145.2	1.21	175	1000
Suntech	STP170s-BA	Thinfilm	5.94	2200	1300	2.86	59.44	144.1	1.18	170	1000
Suntech	STP090Ts-AC	Thinfilm	6.2	1309	1109	1.45	62	73.2	1.23	90	1000
Suntech	STP086Ts-AC	Thinfilm	5.92	1309	1109	1.45	59.24	72.3	1.19	86	1000
Suntech	STP082Ts-AC	Thinfilm	5.65	1309	1109	1.45	56.49	71.3	1.15	82	1000
Suntech	STP185Ts-CA	Thinfilm	6.47	2600	1100	2.86	64.69	73.7	2.51	185	1000
Suntech	STP180Ts-CA	Thinfilm	6.29	2600	1100	2.86	62.94	73.2	2.46	180	1000
Suntech	STP175Ts-CA	Thinfilm	6.12	2600	1100	2.86	61.19	72.6	2.41	175	1000
Suntech	STP170Ts-CA	Thinfilm	5.94	2600	1100	2.86	59.44	72	2.36	170	1000
Suntech	STP185S-24-Ad	Monocrystalline	14.49	1580	808	1.28	144.91	36.4	5.09	185	1000
Suntech	STP180S-24-Ad	Monocrystalline	14.1	1580	808	1.28	141	36	5	180	1000
Suntech	STP280-24-Vd	Monocrystalline	14.43	1956	992	1.94	144.3	35.2	7.95	280	1000
Suntech	STP275-24-Vd	Monocrystalline	14.17	1956	992	1.94	141.73	35.1	7.84	275	1000
Romag	PowerGlaz RG-SMT5(36)M	Monocrystalline	13.08	1197	530	0.63	130.83	18.1	4.6	83	1000
Romag	PowerGlaz RG-SMT6(48)P 648185	Polycrystalline	14.12	1318	994	1.31	141.21	24.5	7.7	185	1000
Romag	PowerGlaz RG-SMT6(48)P 648180	Polycrystalline	13.74	1318	994	1.31	137.39	23.9	7.6	180	1000

Manufacturer	Product	Technology	Efficiency %	Width (mm)	Height (mm)	Area (Metre Squared)	Watts per metre squared	Peak Voltage (Volts)	Peak Current (Amps)	Peak Output (Watts)	Maximum System Voltage (Volts)
Romag	PowerGlaz RG-SMT6(48)P 648175	Polycrystalline	13.36	1318	994	1.31	133.58	23.5	7.5	175	1000
Romag	PowerGlaz RG-SMT6(48)P 648170	Polycrystalline	12.98	1318	994	1.31	129.76	23.1	7.4	170	1000
Romag	PowerGlaz RG-SMT6(48)P 648165	Polycrystalline	12.59	1318	994	1.31	125.95	22.5	7.4	165	1000
Romag	PowerGlaz RG-SMT6(48)P 648160	Polycrystalline	12.21	1318	994	1.31	122.13	21.9	7.31	160	1000
Romag	PowerGlaz RG-SMT6(54)P 654210	Polycrystalline	14.26	1482	994	1.47	142.56	27.54	7.6	210	1000
Romag	PowerGlaz RG-SMT6(54)P 654200	Polycrystalline	13.58	1482	994	1.47	135.77	26.91	7.5	200	1000
Romag	PowerGlaz RG-SMT6(54)P 654195	Polycrystalline	13.24	1482	994	1.47	132.37	26.35	7.4	195	1000
Romag	PowerGlaz RG-SMT6(54)P 654190	Polycrystalline	12.9	1482	994	1.47	128.98	26.03	7.3	190	1000
Romag	PowerGlaz RG-SMT6(60)P 660235	Polycrystalline	14.42	1640	994	1.63	144.16	30.6	7.7	235	1000
Romag	PowerGlaz RG-SMT6(60)P 660230	Polycrystalline	14.11	1640	994	1.63	141.09	30.3	7.6	230	1000

Manufacturer	Product	Technology	Efficiency %	Width (mm)	Height (mm)	Area (Metre Squared)	Watts per metre squared	Peak Voltage (Volts)	Peak Current (Amps)	Peak Output (Watts)	Maximum System Voltage (Volts)
Romag	PowerGlaz RG-SMT6(60)P 660225	Polycrystalline	13.8	1640	994	1.63	138.02	29.9	7.5	225	1000
Romag	PowerGlaz RG-SMT6(60)P 660220	Polycrystalline	13.5	1640	994	1.63	134.96	29.4	7.5	220	1000
Romag	PowerGlaz RG-SMT6(60)P 660210	Polycrystalline	12.88	1640	994	1.63	128.82	28.4	7.4	210	1000
Romag	PowerGlaz RG-SMT6(60)P 660205	Polycrystalline	12.58	1640	994	1.63	125.75	27.9	7.3	205	1000
Kyocera	KD210GH-2PU	Polycrystalline	14.14	1500	990	1.49	141.41	26.6	7.9	210	1000
Kyocera	KD185GH-2PU	Polycrystalline	13.97	1338	990	1.32	139.66	23.6	7.84	185	1000
Kyocera	KD135GH-2PU	Polycrystalline	13.47	1500	668	1	134.73	17.7	7.63	135	1000
Kyocera	KD135SX-1PU	Polycrystalline	13.47	1500	668	1	134.73	17.7	7.63	135	750
Kyocera	KD95SX-1P	Polycrystalline	13.8	1043	660	0.69	138.01	17.9	5.31	95	750
Kyocera	KD70SX-1P	Polycrystalline	13.63	778	660	0.51	136.32	17.9	3.92	70	750
Kyocera	KD50SE-1P	Polycrystalline	9.52	706	744	0.53	95.19	17.9	2.8	50	750
Kyocera	KC16T	Polycrystalline	11.05	517	280	0.14	110.53	17.4	0.93	16	50
Kyocera	KC21T	Polycrystalline	11.18	367	512	0.19	111.76	17.4	1.12	21	50
Kyocera	KC32T	Polycrystalline	12.09	517	512	0.26	120.89	17.4	1.84	32	50
Schott	SCHOTT POLY 225	Polycrystalline	13.45	1685	993	1.67	134.47	29.8	7.55	225	600
Schott	SCHOTT POLY 220	Polycrystalline	13.15	1685	993	1.67	131.48	29.7	7.41	220	600
Schott	SCHOTT POLY 217	Polycrystalline	12.97	1685	993	1.67	129.69	29.6	7.33	217	600

Manufacturer	Product	Technology	Efficiency %	Width (mm)	Height (mm)	Area (Metre Squared)	Watts per metre squared	Peak Voltage (Volts)	Peak Current (Amps)	Peak Output (Watts)	Maximum System Voltage (Volts)
Schott	SCHOTT POLY 210	Polycrystalline	12.55	1685	993	1.67	125.51	29.3	7.16	210	600
BP Solar	BP350J	Polycrystalline	11.1	839	537	0.45	110.98	17.5	2.9	50	600
BP Solar	BP380J	Polycrystalline	12.32	1209	537	0.65	123.22	17.6	4.6	80	600
BP Solar	BP3160N	Polycrystalline	12.71	1593	790	1.26	127.14	35.1	4.55	160	1000
BP Solar	BP3170N	Polycrystalline	13.51	1593	790	1.26	135.08	35.5	4.8	170	1000
BP Solar	BP4175N	Polycrystalline	13.91	1593	790	1.26	139.06	35.4	4.9	175	1000
BP Solar	BP4175T	Polycrystalline	13.96	1587	790	1.25	139.58	35.4	4.9	175	1000
BP Solar	SX-305M	Polycrystalline	7.41	269	251	0.07	74.05	16.5	0.27	5	50
BP Solar	SX-310J	Polycrystalline	8.62	425	273	0.12	86.19	16.8	0.59	10	50
BP Solar	SX-320U	Polycrystalline	9.37	502	425	0.21	93.74	16.8	1.19	20	50
BP Solar	SX-330U	Polycrystalline	10.04	595	502	0.3	100.44	16.8	1.78	30	50

Appendix B: IEEE Distribution Systems Detailed Data

B1. IEEE 13 Bus Distribution System

B1.1 Bus Data and Load Flow Results

Bus No.	Terminal Voltage		Generation		Load	
	Magnitude (p.u.)	Angle (deg)	Active (MW)	Reactive (MVar)	Active (MW)	Reactive (MVar)
611	0.899	24.73	0.00	0.00	0.17	0.08
632	0.934	26.56	0.00	0.00	0.20	0.12
633	0.931	26.51	0.00	0.00	0.00	0.00
634	0.908	25.04	0.00	0.00	0.40	0.29
645	0.931	26.53	0.00	0.00	0.17	0.125
646	0.930	26.51	0.00	0.00	0.23	0.132
650	0.981	28.86	0.00	0.00	0.00	0.00
652	0.899	24.75	0.00	0.00	0.128	0.086
671	0.901	24.76	0.00	0.00	1.155	0.66
675	0.898	24.71	0.00	0.00	0.843	0.462
680	0.901	24.76	0.00	0.00	0.00	0.00
684	0.900	24.74	0.00	0.00	0.00	0.00
692	0.901	24.76	0.00	0.00	0.17	0.151
B (Grid)	1.000	0.00	3.62	2.65	0.00	0.00

B1.2 Transformers Data

Transformer	Between Buses	MVA	kV-high	kV-low	R -%	X -%
Substation	B (Grid) - 650	5	115 - D	4.16 Gr. Y	1	8
XFM -1	633-634	0.5	4.16 - Gr.W	0.48 - Gr.W	1.1	2

B1.3 Lines Data

Node A	Node B	Length (km)	R1 (ohm/km)	X1 (ohm/km)	B1 (microS/km)	R0 (ohm/km)	X0 (ohm/km)	B0 (microS/km)
632	645	0.152	0.507	0.465	2.128	0.635	0.750	1.569
632	633	0.152	0.368	0.472	4.237	0.658	1.286	1.657
633	634	0.000	0.000	0.000	0.000	0.000	0.000	0.000
645	646	0.091	0.507	0.465	2.128	0.635	0.750	1.569
650	632	0.610	0.116	0.371	4.535	0.406	1.185	2.051
684	652	0.244	0.278	0.106	18.432	0.278	0.106	18.432
632	671	0.610	0.116	0.371	4.535	0.406	1.185	2.051
671	684	0.091	0.507	0.465	2.128	0.635	0.750	1.569
671	680	0.305	0.116	0.371	4.535	0.406	1.185	2.051
671	692	0.000	0.000	0.000	0.000	0.000	0.000	0.000
684	611	0.091	0.275	0.279	0.936	0.275	0.279	0.936
692	675	0.152	0.303	0.258	60.204	0.877	0.290	60.204

B1.4 Distances between each bus and the grid

Bus	650	632	633	634	645	646	671	692	675	684	611	652	680
Distance (km)	0.000	0.610	0.762	0.762	0.762	0.853	1.219	1.219	1.372	1.311	1.402	1.554	1.524

B2. IEEE 37 Bus Distribution System

B2.1 Bus Data and Load Flow Results

Bus No.	Terminal Voltage		Generation		Load	
	Magnitude (p.u.)	Angle (deg)	Active (MW)	Reactive (MVar)	Active (MW)	Reactive (MVar)
701	0.970	-1.65	0.00	0.00	0.63	0.315
702	0.963	-1.81	0.00	0.00	0.00	0.00
703	0.957	-1.94	0.00	0.00	0.00	0.00
704	0.959	-1.82	0.00	0.00	0.00	0.00
705	0.962	-1.80	0.00	0.00	0.00	0.00
706	0.957	-1.83	0.00	0.00	0.00	0.00
707	0.954	-1.80	0.00	0.00	0.00	0.00
708	0.949	-1.97	0.00	0.00	0.00	0.00
709	0.951	-1.96	0.00	0.00	0.00	0.00
710	0.943	-1.98	0.00	0.00	0.00	0.00
711	0.940	-2.01	0.00	0.00	0.00	0.00
712	0.962	-1.79	0.00	0.00	0.085	0.04
713	0.961	-1.81	0.00	0.00	0.085	0.04
714	0.959	-1.82	0.00	0.00	0.038	0.018
718	0.958	-1.82	0.00	0.00	0.085	0.04
720	0.957	-1.83	0.00	0.00	0.085	0.04
722	0.953	-1.80	0.00	0.00	0.161	0.08
724	0.953	-1.80	0.00	0.00	0.042	0.021
725	0.956	-1.83	0.00	0.00	0.042	0.021
727	0.956	-1.93	0.00	0.00	0.042	0.021
728	0.955	-1.93	0.00	0.00	0.126	0.063
729	0.955	-1.93	0.00	0.00	0.042	0.021
730	0.952	-1.96	0.00	0.00	0.085	0.04
731	0.950	-1.97	0.00	0.00	0.085	0.04
732	0.949	-1.97	0.00	0.00	0.042	0.021
733	0.947	-1.98	0.00	0.00	0.085	0.04
734	0.944	-1.99	0.00	0.00	0.042	0.021
735	0.943	-1.98	0.00	0.00	0.085	0.04
736	0.942	-1.97	0.00	0.00	0.042	0.021
737	0.942	-2.00	0.00	0.00	0.14	0.07
738	0.941	-2.00	0.00	0.00	0.126	0.062
740	0.940	-2.00	0.00	0.00	0.085	0.04
741	0.940	-2.01	0.00	0.00	0.042	0.021
742	0.961	-1.79	0.00	0.00	0.093	0.044
744	0.955	-1.93	0.00	0.00	0.042	0.021
775	0.950	-1.98	0.00	0.00	0.00	0.00
799	0.984	-1.37	0.00	0.00	0.00	0.00
B	1.000	0.00	2.54	1.34	0.00	0.00

B2.2 Transformers Data

Transformer	Between Buses	MVA	kV-high	kV-low	R -%	X -%
Substation	B (Grid) - 799	2.5	230 - D	4.8 - D	2	8
XFM -1	709-775	0.5	4.8 - D	0.48 - D	0.09	1.81

B2.3 Lines Data

Node A	Node B	Length (km)	R1 (ohm/km)	X1 (ohm/km)	B1 (microS/km)	R0 (ohm/km)	X0 (ohm/km)	B0 (microS/km)
701	702	0.293	0.197	0.205	79.430	0.476	0.126	79.430
702	705	0.122	0.987	0.317	37.437	1.940	0.789	37.437
702	713	0.110	0.509	0.290	46.504	1.399	0.647	46.504
702	703	0.402	0.197	0.205	0.000	0.476	0.126	0.000
703	727	0.073	0.987	0.317	37.437	1.940	0.789	37.437
703	730	0.183	0.509	0.290	46.504	1.399	0.647	46.504
704	714	0.024	0.987	0.317	37.437	1.940	0.789	37.437
704	720	0.244	0.509	0.290	46.504	1.399	0.647	46.504
705	742	0.098	0.987	0.317	37.437	1.940	0.789	37.437
705	712	0.073	0.987	0.317	37.437	1.940	0.789	37.437

Node A	Node B	Length (km)	R1 (ohm/km)	X1 (ohm/km)	B1 (microS/km)	R0 (ohm/km)	X0 (ohm/km)	B0 (microS/km)
706	725	0.085	0.987	0.317	37.437	1.940	0.789	37.437
707	724	0.232	0.987	0.317	37.437	1.940	0.789	37.437
707	722	0.037	0.987	0.317	37.437	1.940	0.789	37.437
708	733	0.098	0.509	0.290	46.504	1.399	0.647	46.504
708	732	0.098	0.987	0.317	37.437	1.940	0.789	37.437
709	731	0.183	0.509	0.290	46.504	1.399	0.647	46.504
709	708	0.098	0.509	0.290	46.504	1.399	0.647	46.504
710	735	0.061	0.987	0.317	37.437	1.940	0.789	37.437
710	736	0.390	0.987	0.317	37.437	1.940	0.789	37.437
711	741	0.122	0.509	0.290	46.504	1.399	0.647	46.504
711	740	0.061	0.987	0.317	37.437	1.940	0.789	37.437
713	704	0.158	0.509	0.290	46.504	1.399	0.647	46.504
714	718	0.158	0.987	0.317	37.437	1.940	0.789	37.437
720	707	0.280	0.987	0.317	37.437	1.940	0.789	37.437
720	706	0.183	0.509	0.290	46.504	1.399	0.647	46.504
727	744	0.085	0.509	0.290	46.504	1.399	0.647	46.504
730	709	0.061	0.509	0.290	46.504	1.399	0.647	46.504
733	734	0.171	0.509	0.290	46.504	1.399	0.647	46.504

Node A	Node B	Length (km)	R1 (ohm/km)	X1 (ohm/km)	B1 (microS/km)	R0 (ohm/km)	X0 (ohm/km)	B0 (microS/km)
734	737	0.195	0.509	0.290	46.504	1.399	0.647	46.504
734	710	0.158	0.987	0.317	37.437	1.940	0.789	37.437
737	738	0.122	0.509	0.290	46.504	1.399	0.647	46.504
738	711	0.122	0.509	0.290	46.504	1.399	0.647	46.504
744	728	0.061	0.987	0.317	37.437	1.940	0.789	37.437
744	729	0.085	0.987	0.317	37.437	1.940	0.789	37.437
775	709	0.000	0.000	0.000	0.000	0.000	0.000	0.000
799	701	0.564	0.141	0.145	99.290	0.737	0.220	99.290

B2.4 Distances between each bus and the grid

Bus	799	701	702	703	704	705	706	707	708	709	710	711	712	713	714	718	720	724	725
Distance (km)	0.00	0.56	0.86	1.26	1.12	0.98	1.55	1.65	1.60	1.50	2.03	2.31	1.05	0.97	1.15	1.31	1.37	1.88	1.64
Bus	742	727	744	728	729	730	731	732	733	734	735	736	737	738	740	741	775	722	
Distance (km)	1.08	1.33	1.42	1.48	1.50	1.44	1.69	1.70	1.70	1.87	2.09	2.42	2.06	2.19	2.37	2.43	1.50	1.69	

B3. IEEE 123 Bus Distribution System

B3.1 Bus Data and Load Flow Results

Bus No.	Terminal Voltage		Generation		Load	
	Magnitude (p.u.)	Angle (deg)	Active (MW)	Reactive (MVar)	Active (MW)	Reactive (MVar)
1	0.973	28.42	0.00	0.00	0.04	0.02
10	0.959	27.90	0.00	0.00	0.02	0.01
100	0.921	26.25	0.00	0.00	0.04	0.02
101	0.921	26.25	0.00	0.00	0.00	0.00
102	0.920	26.25	0.00	0.00	0.02	0.01
103	0.920	26.24	0.00	0.00	0.04	0.02
104	0.920	26.24	0.00	0.00	0.04	0.02
105	0.920	26.23	0.00	0.00	0.00	0.00
106	0.920	26.23	0.00	0.00	0.04	0.02
107	0.920	26.22	0.00	0.00	0.04	0.02
108	0.920	26.21	0.00	0.00	0.00	0.00
109	0.919	26.20	0.00	0.00	0.04	0.02
11	0.959	27.90	0.00	0.00	0.04	0.02
110	0.919	26.20	0.00	0.00	0.00	0.00
111	0.919	26.20	0.00	0.00	0.02	0.01
112	0.919	26.20	0.00	0.00	0.02	0.01
113	0.919	26.19	0.00	0.00	0.04	0.02
114	0.919	26.19	0.00	0.00	0.02	0.01
12	0.960	27.91	0.00	0.00	0.02	0.01
13	0.952	27.61	0.00	0.00	0.00	0.00
14	0.960	27.90	0.00	0.00	0.00	0.00
15	0.952	27.61	0.00	0.00	0.00	0.00
150	0.984	28.84	0.00	0.00	0.00	0.00
151	0.944	27.31	0.00	0.00	0.00	0.00
16	0.952	27.60	0.00	0.00	0.04	0.02
17	0.952	27.60	0.00	0.00	0.02	0.01
18	0.952	27.58	0.00	0.00	0.00	0.00
19	0.952	27.58	0.00	0.00	0.04	0.02
2	0.973	28.42	0.00	0.00	0.02	0.01
20	0.951	27.57	0.00	0.00	0.04	0.02
21	0.951	27.55	0.00	0.00	0.00	0.00
22	0.951	27.55	0.00	0.00	0.04	0.02
23	0.951	27.53	0.00	0.00	0.00	0.00
24	0.950	27.50	0.00	0.00	0.04	0.02
25	0.950	27.51	0.00	0.00	0.00	0.00
250	0.950	27.49	0.00	0.00	0.00	0.00
26	0.950	27.51	0.00	0.00	0.00	0.00
27	0.950	27.50	0.00	0.00	0.00	0.00
28	0.950	27.51	0.00	0.00	0.04	0.02
29	0.950	27.50	0.00	0.00	0.04	0.02
3	0.973	28.42	0.00	0.00	0.00	0.00
30	0.950	27.49	0.00	0.00	0.04	0.02
300	0.920	26.21	0.00	0.00	0.00	0.00
31	0.950	27.50	0.00	0.00	0.02	0.01
32	0.950	27.50	0.00	0.00	0.02	0.01
33	0.950	27.50	0.00	0.00	0.04	0.02
34	0.952	27.61	0.00	0.00	0.04	0.02

Bus No.	Terminal Voltage		Generation		Load	
	Magnitude (p.u.)	Angle (deg)	Active (MW)	Reactive (MVar)	Active (MW)	Reactive (MVar)
35	0.949	27.49	0.00	0.00	0.04	0.02
36	0.949	27.48	0.00	0.00	0.00	0.00
37	0.949	27.48	0.00	0.00	0.04	0.02
38	0.947	27.53	0.00	0.00	0.02	0.01
39	0.947	27.53	0.00	0.00	0.02	0.01
4	0.973	28.41	0.00	0.00	0.04	0.02
40	0.948	27.45	0.00	0.00	0.00	0.00
41	0.948	27.45	0.00	0.00	0.02	0.01
42	0.947	27.40	0.00	0.00	0.02	0.01
43	0.947	27.40	0.00	0.00	0.04	0.02
44	0.946	27.37	0.00	0.00	0.00	0.00
45	0.946	27.37	0.00	0.00	0.02	0.01
450	0.921	26.25	0.00	0.00	0.00	0.00
46	0.946	27.37	0.00	0.00	0.02	0.01
47	0.945	27.33	0.00	0.00	0.105	0.075
48	0.945	27.32	0.00	0.00	0.21	0.15
49	0.944	27.31	0.00	0.00	0.14	0.095
5	0.973	28.41	0.00	0.00	0.02	0.01
50	0.944	27.31	0.00	0.00	0.04	0.02
51	0.944	27.31	0.00	0.00	0.02	0.01
52	0.946	27.35	0.00	0.00	0.04	0.02
53	0.943	27.23	0.00	0.00	0.04	0.02
54	0.941	27.15	0.00	0.00	0.00	0.00
55	0.941	27.15	0.00	0.00	0.02	0.01
56	0.941	27.15	0.00	0.00	0.02	0.01
57	0.936	26.94	0.00	0.00	0.00	0.00
58	0.936	26.94	0.00	0.00	0.02	0.01
59	0.936	26.94	0.00	0.00	0.02	0.01
6	0.972	28.41	0.00	0.00	0.04	0.02
60	0.926	26.49	0.00	0.00	0.02	0.01
61	0.926	26.49	0.00	0.00	0.00	0.00
610	0.926	26.48	0.00	0.00	0.00	0.00
62	0.924	26.49	0.00	0.00	0.04	0.02
63	0.924	26.50	0.00	0.00	0.04	0.02
64	0.922	26.50	0.00	0.00	0.075	0.035
65	0.921	26.51	0.00	0.00	0.14	0.10
66	0.920	26.51	0.00	0.00	0.075	0.035
67	0.922	26.32	0.00	0.00	0.00	0.00
68	0.922	26.31	0.00	0.00	0.02	0.01
69	0.922	26.31	0.00	0.00	0.04	0.02
7	0.965	28.11	0.00	0.00	0.02	0.01
70	0.921	26.30	0.00	0.00	0.02	0.01
71	0.921	26.30	0.00	0.00	0.04	0.02
72	0.920	26.24	0.00	0.00	0.00	0.00
73	0.920	26.23	0.00	0.00	0.04	0.02
74	0.920	26.23	0.00	0.00	0.04	0.02
75	0.920	26.22	0.00	0.00	0.04	0.02
76	0.919	26.19	0.00	0.00	0.245	0.18
77	0.918	26.15	0.00	0.00	0.04	0.02
78	0.918	26.15	0.00	0.00	0.00	0.00
79	0.918	26.14	0.00	0.00	0.04	0.02
8	0.960	27.91	0.00	0.00	0.00	0.00

Bus No.	Terminal Voltage		Generation		Load	
	Magnitude (p.u.)	Angle (deg)	Active (MW)	Reactive (MVA _r)	Active (MW)	Reactive (MVA _r)
80	0.918	26.12	0.00	0.00	0.04	0.02
81	0.917	26.10	0.00	0.00	0.00	0.00
82	0.917	26.09	0.00	0.00	0.04	0.02
83	0.917	26.09	0.00	0.00	0.02	0.01
84	0.917	26.09	0.00	0.00	0.02	0.01
85	0.917	26.09	0.00	0.00	0.04	0.02
86	0.918	26.12	0.00	0.00	0.02	0.01
87	0.917	26.08	0.00	0.00	0.04	0.02
88	0.917	26.08	0.00	0.00	0.04	0.02
89	0.916	26.07	0.00	0.00	0.00	0.00
9	0.960	27.91	0.00	0.00	0.04	0.02
90	0.916	26.07	0.00	0.00	0.04	0.02
91	0.916	26.06	0.00	0.00	0.00	0.00
92	0.916	26.06	0.00	0.00	0.04	0.02
93	0.916	26.05	0.00	0.00	0.00	0.00
94	0.916	26.05	0.00	0.00	0.04	0.02
95	0.916	26.05	0.00	0.00	0.02	0.01
96	0.916	26.05	0.00	0.00	0.02	0.01
97	0.921	26.28	0.00	0.00	0.00	0.00
98	0.921	26.27	0.00	0.00	0.04	0.02
99	0.921	26.25	0.00	0.00	0.04	0.02
B	1.000	0.00	3.63	2.27	0.00	0.00

B3.2 Transformers Data

Transformer	Between Buses	MVA	kV-high	kV-low	R -%	X -%
Substation	B (Grid) - 150	5	115 - D	4.16 – Gr-W	1	8
XFM -1	61-610	0.15	4.16 - D	0.48 - D	1.27	2.72

B3.3 Lines Data

Node A	Node B	Length (km)	R1 (ohm/km)	X1 (ohm/km)	B1 (microS/km)	R0 (ohm/km)	X0 (ohm/km)	B0 (microS/km)
1	2	0.053	0.275	0.279	0.936	0.275	0.279	0.936
1	3	0.076	0.275	0.279	0.936	0.275	0.279	0.936
1	7	0.091	0.190	0.390	2.767	0.481	1.204	5.063
3	4	0.061	0.275	0.279	0.936	0.275	0.279	0.936
3	5	0.099	0.275	0.279	0.936	0.275	0.279	0.936
5	6	0.076	0.275	0.279	0.936	0.275	0.279	0.936
7	8	0.061	0.190	0.390	2.767	0.481	1.204	5.063
8	12	0.069	0.275	0.279	0.936	0.275	0.279	0.936
8	9	0.069	0.275	0.279	0.936	0.275	0.279	0.936
8	13	0.091	0.190	0.390	2.767	0.481	1.204	5.063
9	14	0.130	0.275	0.279	0.936	0.275	0.279	0.936
13	34	0.046	0.275	0.279	0.936	0.275	0.279	0.936
13	18	0.251	0.190	0.390	2.767	0.481	1.204	5.063
14	11	0.076	0.275	0.279	0.936	0.275	0.279	0.936
14	10	0.076	0.275	0.279	0.936	0.275	0.279	0.936
15	16	0.114	0.275	0.279	0.936	0.275	0.279	0.936
15	17	0.107	0.275	0.279	0.936	0.275	0.279	0.936

Node A	Node B	Length (km)	R1 (ohm/km)	X1 (ohm/km)	B1 (microS/km)	R0 (ohm/km)	X0 (ohm/km)	B0 (microS/km)
18	19	0.076	0.275	0.279	0.936	0.275	0.279	0.936
18	21	0.091	0.190	0.390	2.767	0.481	1.204	5.063
19	20	0.099	0.275	0.279	0.936	0.275	0.279	0.936
21	22	0.160	0.275	0.279	0.936	0.275	0.279	0.936
21	23	0.076	0.190	0.390	2.767	0.481	1.204	5.063
23	24	0.168	0.275	0.279	0.936	0.275	0.279	0.936
23	25	0.084	0.190	0.390	2.767	0.481	1.204	5.063
25	26	0.107	0.159	0.364	1.912	0.254	0.603	2.567
25	28	0.061	0.190	0.390	2.767	0.481	1.204	5.063
26	27	0.084	0.159	0.364	1.912	0.254	0.603	2.567
26	31	0.069	0.275	0.279	0.936	0.275	0.279	0.936
27	33	0.152	0.275	0.279	0.936	0.275	0.279	0.936
28	29	0.091	0.190	0.390	2.767	0.481	1.204	5.063
29	30	0.107	0.190	0.390	2.767	0.481	1.204	5.063
30	250	0.061	0.190	0.390	2.767	0.481	1.204	5.063
31	32	0.091	0.275	0.279	0.936	0.275	0.279	0.936
34	15	0.030	0.275	0.279	0.936	0.275	0.279	0.936
35	36	0.198	0.159	0.364	1.912	0.254	0.603	2.567

Node A	Node B	Length (km)	R1 (ohm/km)	X1 (ohm/km)	B1 (microS/km)	R0 (ohm/km)	X0 (ohm/km)	B0 (microS/km)
35	40	0.076	0.190	0.390	2.767	0.481	1.204	5.063
36	37	0.091	0.275	0.279	0.936	0.275	0.279	0.936
36	38	0.076	0.275	0.279	0.936	0.275	0.279	0.936
38	39	0.099	0.275	0.279	0.936	0.275	0.279	0.936
40	41	0.099	0.275	0.279	0.936	0.275	0.279	0.936
40	42	0.076	0.190	0.390	2.767	0.481	1.204	5.063
42	43	0.152	0.275	0.279	0.936	0.275	0.279	0.936
42	44	0.061	0.190	0.390	2.767	0.481	1.204	5.063
44	45	0.061	0.275	0.279	0.936	0.275	0.279	0.936
44	47	0.076	0.190	0.390	2.767	0.481	1.204	5.063
45	46	0.091	0.275	0.279	0.936	0.275	0.279	0.936
47	48	0.046	0.190	0.390	2.767	0.481	1.204	5.063
47	49	0.076	0.190	0.390	2.767	0.481	1.204	5.063
49	50	0.076	0.190	0.390	2.767	0.481	1.204	5.063
50	51	0.076	0.190	0.390	2.767	0.481	1.204	5.063
51	151	0.152	0.190	0.390	2.767	0.481	1.204	5.063
52	53	0.061	0.190	0.390	2.767	0.481	1.204	5.063
53	54	0.038	0.190	0.390	2.767	0.481	1.204	5.063

Node A	Node B	Length (km)	R1 (ohm/km)	X1 (ohm/km)	B1 (microS/km)	R0 (ohm/km)	X0 (ohm/km)	B0 (microS/km)
54	55	0.084	0.190	0.390	2.767	0.481	1.204	5.063
54	57	0.107	0.190	0.390	2.767	0.481	1.204	5.063
55	56	0.084	0.190	0.390	2.767	0.481	1.204	5.063
57	58	0.076	0.275	0.279	0.936	0.275	0.279	0.936
57	60	0.229	0.190	0.390	2.767	0.481	1.204	5.063
58	59	0.076	0.275	0.279	0.936	0.275	0.279	0.936
60	61	0.168	0.190	0.390	2.767	0.481	1.204	5.063
60	62	0.076	0.630	0.300	41.771	1.582	0.779	41.771
62	63	0.053	0.630	0.300	41.771	1.582	0.779	41.771
63	64	0.107	0.630	0.300	41.771	1.582	0.779	41.771
64	65	0.130	0.630	0.300	41.771	1.582	0.779	41.771
65	66	0.099	0.630	0.300	41.771	1.582	0.779	41.771
67	68	0.061	0.275	0.279	0.936	0.275	0.279	0.936
67	72	0.084	0.190	0.390	2.767	0.481	1.204	5.063
67	97	0.076	0.190	0.390	2.767	0.481	1.204	5.063
68	69	0.084	0.275	0.279	0.936	0.275	0.279	0.936
69	70	0.099	0.275	0.279	0.936	0.275	0.279	0.936
70	71	0.084	0.275	0.279	0.936	0.275	0.279	0.936

Node A	Node B	Length (km)	R1 (ohm/km)	X1 (ohm/km)	B1 (microS/km)	R0 (ohm/km)	X0 (ohm/km)	B0 (microS/km)
72	73	0.084	0.275	0.279	0.936	0.275	0.279	0.936
72	76	0.061	0.190	0.390	2.767	0.481	1.204	5.063
73	74	0.107	0.275	0.279	0.936	0.275	0.279	0.936
74	75	0.122	0.275	0.279	0.936	0.275	0.279	0.936
76	77	0.122	0.190	0.390	2.767	0.481	1.204	5.063
76	86	0.213	0.190	0.390	2.767	0.481	1.204	5.063
77	78	0.030	0.190	0.390	2.767	0.481	1.204	5.063
78	79	0.069	0.190	0.390	2.767	0.481	1.204	5.063
78	80	0.145	0.190	0.390	2.767	0.481	1.204	5.063
80	81	0.145	0.190	0.390	2.767	0.481	1.204	5.063
81	82	0.076	0.190	0.390	2.767	0.481	1.204	5.063
81	84	0.206	0.275	0.279	0.936	0.275	0.279	0.936
82	83	0.076	0.190	0.390	2.767	0.481	1.204	5.063
84	85	0.145	0.275	0.279	0.936	0.275	0.279	0.936
86	87	0.137	0.190	0.390	2.767	0.481	1.204	5.063
87	88	0.053	0.275	0.279	0.936	0.275	0.279	0.936
87	89	0.084	0.190	0.390	2.767	0.481	1.204	5.063
89	90	0.069	0.275	0.279	0.936	0.275	0.279	0.936

Node A	Node B	Length (km)	R1 (ohm/km)	X1 (ohm/km)	B1 (microS/km)	R0 (ohm/km)	X0 (ohm/km)	B0 (microS/km)
89	91	0.069	0.190	0.390	2.767	0.481	1.204	5.063
91	92	0.091	0.275	0.279	0.936	0.275	0.279	0.936
91	93	0.069	0.190	0.390	2.767	0.481	1.204	5.063
93	94	0.084	0.275	0.279	0.936	0.275	0.279	0.936
93	95	0.091	0.190	0.390	2.767	0.481	1.204	5.063
95	96	0.061	0.275	0.279	0.936	0.275	0.279	0.936
97	98	0.084	0.190	0.390	2.767	0.481	1.204	5.063
98	99	0.168	0.190	0.390	2.767	0.481	1.204	5.063
99	100	0.091	0.190	0.390	2.767	0.481	1.204	5.063
100	450	0.244	0.190	0.390	2.767	0.481	1.204	5.063
101	102	0.069	0.275	0.279	0.936	0.275	0.279	0.936
101	105	0.084	0.190	0.390	2.767	0.481	1.204	5.063
102	103	0.099	0.275	0.279	0.936	0.275	0.279	0.936
103	104	0.213	0.275	0.279	0.936	0.275	0.279	0.936
105	106	0.069	0.275	0.279	0.936	0.275	0.279	0.936
105	108	0.099	0.190	0.390	2.767	0.481	1.204	5.063
106	107	0.175	0.275	0.279	0.936	0.275	0.279	0.936
108	109	0.137	0.275	0.279	0.936	0.275	0.279	0.936

Node A	Node B	Length (km)	R1 (ohm/km)	X1 (ohm/km)	B1 (microS/km)	R0 (ohm/km)	X0 (ohm/km)	B0 (microS/km)
108	300	0.305	0.190	0.390	2.767	0.481	1.204	5.063
109	110	0.091	0.275	0.279	0.936	0.275	0.279	0.936
110	111	0.175	0.275	0.279	0.936	0.275	0.279	0.936
110	112	0.038	0.275	0.279	0.936	0.275	0.279	0.936
112	113	0.160	0.275	0.279	0.936	0.275	0.279	0.936
113	114	0.099	0.275	0.279	0.936	0.275	0.279	0.936
135	35	0.114	0.190	0.390	2.767	0.481	1.204	5.063
149	1	0.122	0.190	0.390	2.767	0.481	1.204	5.063
152	52	0.122	0.190	0.390	2.767	0.481	1.204	5.063
160	67	0.107	0.190	0.390	2.767	0.481	1.204	5.063
197	101	0.076	0.190	0.390	2.767	0.481	1.204	5.063

B3.4 Distances between each bus and the grid

Bus	150	149	1	2	3	4	5	6	7	8	9	10	11	12	13	14	
Distance (km)	0.000	0.000	0.122	0.175	0.198	0.259	0.297	0.373	0.213	0.274	0.343	0.549	0.549	0.343	0.366	0.472	
Bus	34	15	17	16	18	19	20	21	22	23	24	25	26	27	28	29	
Distance (km)	0.411	0.442	0.549	0.556	0.617	0.693	0.792	0.709	0.869	0.785	0.953	0.869	0.975	1.059	0.930	1.021	
Bus	30	32	31	33	250	251	135	35	36	37	38	39	40	41	42	43	
Distance (km)	1.128	1.135	1.044	1.212	1.189	1.189	0.617	0.732	0.930	1.021	1.006	1.105	0.808	0.907	0.884	1.036	
Bus	44	45	46	47	48	49	50	51	151	152	52	53	54	55	56	57	
Distance (km)	0.945	1.006	1.097	1.021	1.067	1.097	1.173	1.250	1.402	0.366	0.488	0.549	0.587	0.671	0.754	0.693	
Bus	58	59	60	61	610	62	63	64	65	66	160	67	68	69	70	71	
Distance (km)	0.770	0.846	0.922	1.090	1.090	0.998	1.052	1.158	1.288	1.387	0.922	1.029	1.090	1.173	1.242	1.356	
Bus	72	73	74	75	76	77	78	79	80	81	82	83	84	85	86	87	
Distance (km)	1.113	1.196	1.303	1.425	1.173	1.295	1.326	1.394	1.471	1.615	1.692	1.768	1.821	1.966	1.387	1.524	
Bus	88	89	90	91	92	93	94	95	96	195	97	98	99	100	450	451	
Distance (km)	1.577	1.608	1.676	1.676	1.768	1.745	1.829	1.836	1.897	1.836	1.105	1.189	1.356	1.448	1.692	1.692	
Bus	101	102	103	104	105	106	107	108	109	110	111	112	113	114	300	350	197
Distance (km)	1.181	1.250	1.349	1.562	1.265	1.334	1.509	1.364	1.501	1.593	1.768	1.631	1.791	1.890	1.669	1.669	1.105

Appendix C: Conventional Distributed Generation (CDG) Data

C1. Synchronous generator parameter (salient pole rotor)

Nominal Power S_n (MVA)	Line to Line Voltage $V_{L-L, rms}$ (kV)	Frequency f_n (Hz)	Reactances (p.u.)					
			X_d	X_d'	X_d''	X_q	X_q'	X_q''
2.5	11	50	1.305	0.296	0.252	0.474	0.243	0.18
Stator Resistance R_{st} (p.u.)	Inertia Coefficient H (s)	No. of Pole-pairs	Time Constants (s)					
			T_d'	T_d''	T_q''			
0.003	2.5	1	1.01	0.053	0.051266			

C2. Automatic Voltage Regulator (AVR)

AVR Type	Type	IEEEX1
Low-pass-filter time constant (s)	T_r	0.005
Regulator gain	K_a	500
Regulator time constant (s)	T_a	0.001
Exciter gain	K_e	1
Exciter time constant (s)	T_e	0.6
Transient gain reduction (s)	T_b	0.8
	T_c	1
Damping filter gain	K_f	0.005
Damping filter time constant (s)	T_f	0.7
Regulator minimum output limit (p.u.)	V_{min}	-5
Regulator maximum output limit (p.u.)	V_{max}	5

C3. CDG Governor (Diesel Engine Governor)

Governor Type	Type	DEGOV1
Regulator gain	K	30
Regulator time constants (s)	T_1	0.002
	T_2	0.003
	T_3	0.005
Actuator time constants (s)	T_4	0.1
	T_5	0.01
	T_6	0.02
Torque limits (p.u.)	T_{min}	-0.05
	T_{max}	1
Engine delay time (s)	T_d	0.001
Droop (p.u.)		0.006

Appendix D: Renewable Energy Generating Units Modelling

Parameters

D1. Three phase two stage transformerless PV grid connected system

Design circuit parameters and design specification

PV array rated power	850 W
PV modules	SHELL Ultra-80-P
PV modules number	10
Short circuit current	5.54 A
Open circuit voltage	22.2 V
Current at Pmax	4.95 A
Voltage at Pmax	17.2 V
Smoothing capacitor, C	4 mF
Boost inductor, L	0.3 mH
DC output voltage, V_{dc}	350 V
Switching frequency, f_s	4000 Hz

Hill climbing MPPT codes

```
function A =hill_climbing1(u)
p=u(1);p1=u(2);D=u(3);D1=u(4);
dp=p-p1;
dD=(D-D1);
c=0.00035;
e=0.000001;
if D<=0
    i=0.35;
elseif D>=0.9
    i=0.9;
else
if dp > e
    if dD > e
        i=D+c;
    else
        i=D-c;
    end
elseif dp<e
    if dD>e
        i=D-c;
    else
        i=D+c;
    end
else
    i=D;
end
end
[A] = i ;
```

D2. DFIG modelling parameters

Generator parameters

Rotor Type	Line to Line Voltage $V_{L-L_{rms}}$ (kV)	Frequency f_n (hz)	Stator Resistance and Inductance (p.u.)	
			R_s	L_s
Wound	575	50	0.023	0.18
Inertia Coefficient H (s)	No. of Pole-pairs	Magnetizing inductance (p.u.) L_m	Rotor Resistance and Inductance (p.u.)	
			R_r	L_r
0.685	3	2.9	0.016	0.16

Control parameters

Grid side coupling inductor (p.u.)	R	0.003
	L	0.3
Nominal DC bus voltage (V)	V _{dc}	1150
DC bus capacitor (mF)	C	10
Line filter capacitor (kVAr)	Q _c	120
DC bus voltage regulator gains	K _p	8
	K _i	400
Grid side converter current regulator gains	K _p	0.83
	K _i	5
Rotor side converter current regulator gains	K _p	0.6
	K _i	8
Speed regulator gains	K _p	3
	K _i	0.6
Pitch controller gain	K _p	150
Pitch compensation gains	K _p	3
	K _i	30
Frequency of the grid side PWM carrier (Hz)	f _{gc}	2700
Frequency of the rotor side PWM carrier (Hz)	f _{rc}	1620
Maximum pitch angle (degree)	β_{max}	27
Maximum rate of change of pitch angle (deg/sec)	d β_{max} /dt	10

D3. Synchronous generator with fully rated converter modelling parameters

Generator parameters

Rotor Type	Line to Line Voltage $V_{L-L_{rms}}$ (kV)	Frequency f_n (hz)	Reactances (p.u.)					
			X_d	X_d'	X_d''	X_q	X_q'	X_q''
Salient pole	730	50	1.305	0.296	0.252	0.474	0.243	0.18
Stator Resistance R_{st} (p.u.)	Inertia Coefficient H (s)	No. of Pole-pairs	Time Constants (s)					
			T_d'	T_d''	T_q''			
0.006	0.62	1	4.49	0.0681	0.0513			

Control parameters

Grid side coupling inductor (p.u.)	R	0.003
	L	0.15
Nominal DC bus voltage (V)	Vdc	1100
DC bus capacitor (mF)	C	90
Line filter capacitor (kVAr)	Qc	150
Boost converter inductance	R (ohm)	0.005
	L (H)	0.0012
DC bus voltage regulator gains	Kp	1.1
	Ki	27.5
Grid side converter current regulator gains	Kp	1
	Ki	50
Speed regulator gains	Kp	5
	Ki	1
Pitch controller gain	Kp	15
Pitch compensation gains	Kp	1.5
	Ki	6
Boost converter current regulator gains	Kp	0.025
	Ki	100
Frequency of the grid side PWM carrier (Hz)	f _{gc}	3000